

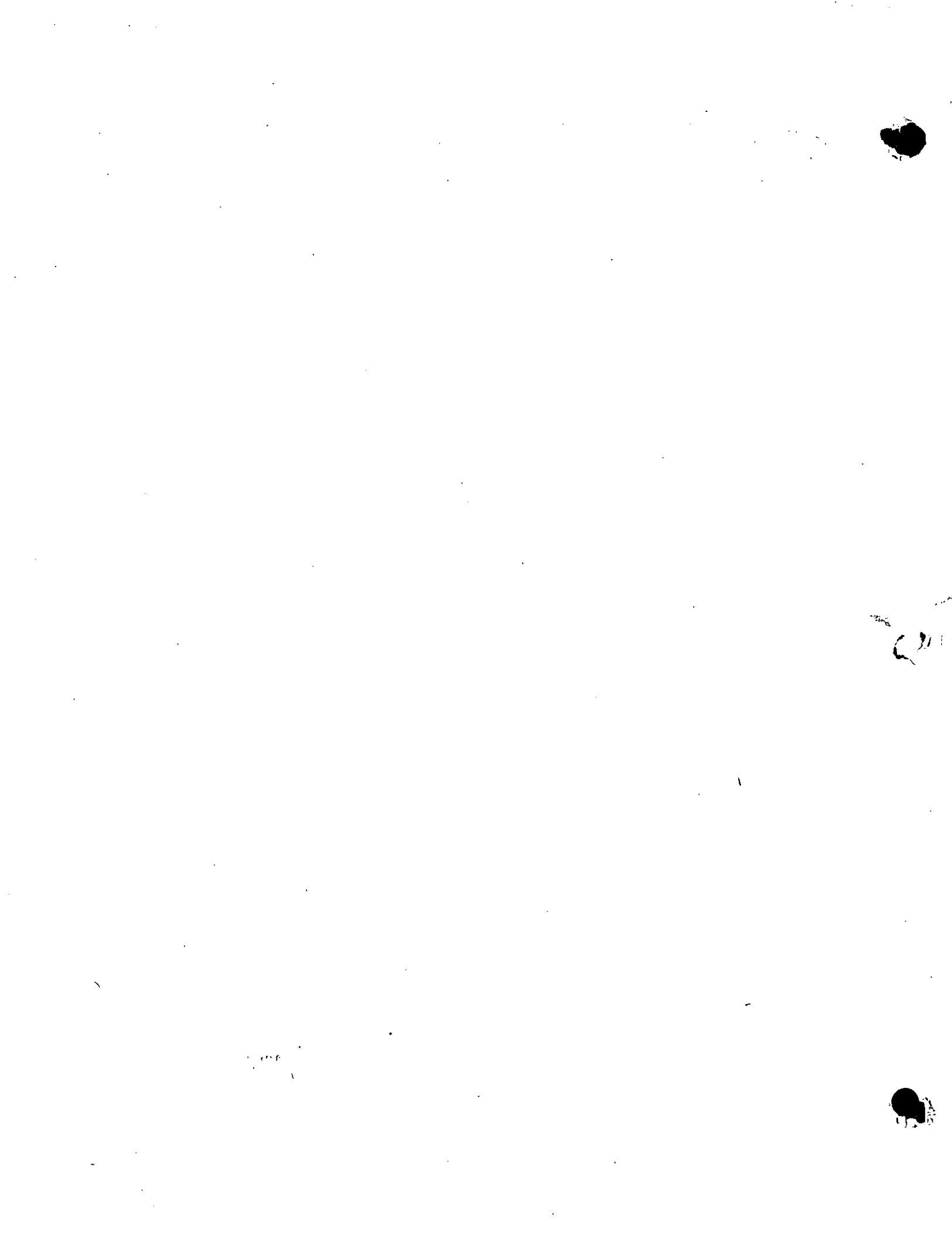


**DIVISION DE EDUCACION CONTINUA  
FACULTAD DE INGENIERIA U.N.A.M.**

**CURSO: "INGENIERIA DE YACIMIENTOS GEOTERMICOS"  
13 DE MARZO AL 18 DE MAYO DE 1984**

**FLUJO DE FLUIDOS Y CALOR EN  
YACIMIENTOS**

**PROF. DR. HEBER CINCO LEY  
26-30 de marzo**



THIS PRESENTATION IS SUBJECT TO CORRECTION

## Two-Phase, Two-Dimensional Simulation of a Geothermal Reservoir and the Wellbore System

By

Robert M. Toronyi, Member SPE-AIME, Scientific Software Corp. and S. M. Farouq Ali, Member SPE-AIME, Pennsylvania State U.

© Copyright 1975

American Institute of Mining, Metallurgical, and Petroleum Engineers, Inc.

This paper was prepared for the 50th Annual Fall Meeting of the Society of Petroleum Engineers of AIME, to be held in Dallas, Texas, Sept. 28-Oct. 1, 1975. Permission to copy is restricted to an abstract of not more than 300 words. Illustrations may not be copied. The abstract should contain conspicuous acknowledgment of where and by whom the paper is presented. Publication elsewhere after publication in the JOURNAL OF PETROLEUM TECHNOLOGY or the SOCIETY OF PETROLEUM ENGINEERS JOURNAL is usually granted upon request to the Editor of the appropriate journal provided agreement to give proper credit is made.

Discussion of this paper is invited. Three copies of any discussion should be sent to the Society of Petroleum Engineers office. Such discussions may be presented at the above meeting and, with the paper, may be considered for publication in one of the two SPE magazines.

### ABSTRACT

A numerical mathematical model for simulating production from a two-phase geothermal reservoir was developed and tested. The simulation is rather unique, in that it consists of two coupled models, a reservoir model and a wellbore model. The reservoir model was a two-dimensional areal or cross-sectional, unsteady state description of the flow of mass and heat within an anisotropic, heterogeneous porous medium, containing a single component, two-phase fluid. The wellbore model was a one-dimensional, steady state description of the flow of a homogeneous, two-phase mixture. A totally implicit solution scheme was employed.

The simulator was used to investigate the effects of various levels of porosity, permeability, and initial pressure and liquid phase saturation distributions upon production.

The numerical simulator was tested for a wide variety of conditions, and was found to be stable for large time steps.

Based upon the numerical results, the behavior of two-phase geothermal reservoir was classified into three types, depending

on the initial liquid saturation. Wellhead steam quality was higher than the bottomhole quality, in the runs conducted. It was found that superheated regions formed more readily in reservoirs of low porosity and permeability.

### INTRODUCTION

A geothermal system occurs as a heat anomaly, which can be explained as follows. The earth's interior is hotter than its surface, and this difference produces a temperature gradient which in turn provides a measure of the heat flow rate. The average heat flux for the earth is  $1.5 \text{ cal/cm}^2 \text{ - sec}$  (1). A geothermal system involves a flux which is one and one-half to five times higher than the average (2). Consequently, a geothermal system occurs as an anomaly in terms of heat flow. A high heat flux, along with surface seeps, is indicative of a geothermal system.

Since the main mode of heat transfer within a geothermal fluid reservoir is convection, the reservoir itself is called a hydrothermal convection system. Hydrothermal convection systems have been classified into two types based upon the physical state of the dominant pressure-controlling

phase, i.e. hot water systems and vapor-dominated systems (1). In hot water systems, fluids exist within the reservoir mostly in the liquid state and generally produce from 70 to 90% of their total mass as water at the surface.

Vapor dominated systems generally produce dry to superheated steam, and fluids exist within the reservoir mostly in the vapor state. Surface manifestations will usually take the form of fumaroles, mud pots, mud volcanoes, turbid pools, and acid leached ground. Only three known areas in the world exist as this type of system. These are the Geysers field in California, the Larderello field in Italy, and the Matsukawa field in Japan. The pressures of vapor dominated systems are below hydrostatic. Also, the initial pressures and temperatures in vapor dominated systems are very close to the temperature and pressure relating to the maximum enthalpy of saturated steam, i.e., 236°C and 31.8 kg/cm<sup>2</sup>. An explanation for this behavior has been given by James (3) and White, Muffler, and Truesdell (4).

Only during the last decade have reservoir engineering principles been used to study production aspects of geothermal systems. In that time relatively few models have been developed that simulate the production from a geothermal reservoir containing both a liquid and a vapor phase.

In fact, only three models have assumed the presence of a two-phase fluid within a geothermal reservoir. One of these models, developed by Donaldson (5) was a steady state, one-dimensional description of two-phase flow within porous media, but did not simulate production. The other two models, that of Whiting and Ramey (6) and that of Brigham and Morrow (7), were lumped parameter formulations. Thus, the objective of this work is to develop a model that simulates production from a two-phase geothermal reservoir in greater detail than has previously been done. Specifically, the simulation consists of two models, one for the reservoir and the other for the wellbore. The reservoir model is a two-dimensional areal or cross-sectional, unsteady state description of the flow of mass and heat within an anisotropic, heterogeneous porous medium containing a single component, two-phase fluid; while the wellbore model is a one-dimensional, steady state description of the flow of a homogeneous, two-phase mixture. The two models are then coupled together by treating the wellbore block as a point sink within the reservoir and by viewing the reservoir pressure and quality as inlet conditions for the wellbore.

## MATHEMATICAL MODELS OF GEOTHERMAL SYSTEMS

Models of geothermal systems can be thought of as being concerned either with the formation and stability of a geothermal system or with the production of fluids from a geothermal reservoir. Shown in Figure 1 is a diagrammatic representation of models relating to geothermal systems.

The fundamental formulation of a free convection problem in porous media, henceforth called the Fundamental Problem, is given in the AGU monograph on terrestrial heat flow, by Elder (8). Laboratory models and theoretical studies dealing with the physical processes of geothermal systems derive from this formulation in varying degrees of complexity. Constant temperature as well as no-flow boundary conditions, are employed in this formulation. For scaled model studies, Prandtl and Rayleigh numbers, and the aspect ratio can be used to define the system. Additionally, heat and fluid discharge can be characterized by the Nusselt and discharge numbers, respectively.

Wooding (9) first related the Fundamental Problem to a geothermal system, using classical perturbation methods.

Donaldson (10) carried out a mathematical study of the Fundamental Problem, but instead used finite difference techniques for its solution. He also solved a variation of the Fundamental Problem where the planar region was a two-layer system consisting of an upper permeable layer and an underlying impermeable layer. In a more complex formulation (11), he represented the planar region by three permeable channels, surrounded by impermeable rock. The model was studied further (12), taking account of the various permeabilities upon the Nusselt and discharge numbers.

The Fundamental Problem and the studies resulting from it consider only a single phase fluid. The only study that has been done that considers a two-phase fluid is by Donaldson (12). In the study a mathematical treatment was undertaken of the steady flow of water within a one-dimensional vertical channel (heated from below). A most interesting finding of Donaldson from a reservoir engineering standpoint was the sudden change in fluid saturations at interfaces of permeability reduction and at points of flow rate change. Donaldson's formulation in a sense is a specific case of a more general model considered in this paper.

Model studies relating to the production of fluids from geothermal reservoirs center



on fluid flow in the reservoir and in the wellbore. Thus, a further breakdown of model studies can be based on whether the model concerns itself with fluid flow in the reservoir or with fluid flow in the wellbore.

### Reservoir Mechanics

Ramey, Kruger, and Raghavan (13) have pointed out factors which affect boiling in porous media. They state that vapor pressure data obtained from flat interfaces may not be appropriate in porous media due to the effect of capillarity which bends an interface between two phases. Works by Cady (14) and Bilhartz (15) have tried to validate this effect under conditions similar to geothermal reservoirs.

Evaporation and condensation of a liquid and its vapor within a porous medium greatly increase the heat transfer capacity of the rock. This behavior, first introduced by Grover, Cotter, and Erickson (16), has been called the heat pipe concept. White, Muffler, and Truesdell (4) suggested a vapor dominated reservoir exists as a heat pipe, i.e., it transfers heat at high rates by evaporating the liquid in warm parts and condensing the vapors in the cooler parts of the reservoir. Goman and Somerton (17) have studied the effect of vapor saturation on thermal conductivity of rock and have confirmed the heat pipe phenomenon.

Reservoir models of thermal processes are based upon a mass balance and an energy balance. The most detailed of these reservoir models is a distributed parameter system, i.e., the independent variables are parameterized with respect to both spatial and temporal variables. Models offering less detail but which have wider use are lumped parameter systems, i.e., the independent variables are parameterized only with respect to time.

The conservation of mass can be applied to the phases making up the system, or to the components making up the phases. In the former case, an interphase mass transfer term is to be included. The energy balance is made upon the entire system, but it has been based either upon internal energies or enthalpies. Coats (18) has formulated the energy balance for a steamflooding model in terms of internal energies, while Shutler (19) has formulated the energy balance for a steamflooding model in terms of enthalpies. Differing solution methods validate the need for these two formulations.

All but one of the reservoir models of geothermal systems that have been published in the literature are lumped parameter formulations. The most wellknown is by Whiting

and Ramey (6). Their model consists of a conservation of mass balance upon the single component, water, and a conservation of energy balance using internal energies.

Brigham and Morrow (7), in an attempt to take into account the large spatial variation of the independent variables, found by Cady (14) for vapor-containing reservoirs, developed three lumped parameter models based on vapor liquid distribution. For each model it was assumed that there was no influx of mass into the reservoir. The resulting equations developed for each model were solved in a trial-and-error process for a given increment of depletion.

The only distributed parameter model that has been published is by Mercer (20). This model was developed for an areal study of a hot-water dominated field. The model consists of a single phase mass balance and the energy balance. The time term was approximated by finite difference techniques, while spatial terms were approximated by mixing isoparametric quadrilateral elements in a finite element technique. The model was successfully used to match temperature and pressure distributions in a hot water field in Wairakei, New Zealand.

### Wellbore Models

Wellbore models used in reservoir studies have as their basis the steady state, one-dimensional balances of mass, momentum, and energy. Wallis (21) gives these equations for homogeneous equilibrium flow. In the petroleum literature these same equations have been solved assuming the two-phase to be homogeneous for steam injection down a wellbore by Pacheco and Farouq Ali (22), and others.

James (23) has developed one of three wellbore models published in the literature where flashing is assumed to occur within the wellbore. For this type of flow James has split up the wellbore into two sections. From the sandface up to the point where the pressure drops below the saturation pressure, the flashpoint, James solves the mass and momentum equations for a single phase fluid. From the flashpoint up to the wellhead, James solves the mass balance and the momentum balance under a homogeneity assumption for two-phase flow, along with a third empirical equation which couples the sandface enthalpy with the wellhead pressure. The empirical equation was derived from a bean (or choke) performance on flowing geothermal wells in the Wairakei field in New Zealand and is functionally identical to equations used on oil field wellbores.

The second wellbore model where flashing is assumed to occur in the wellbore, originally

done by Elder (8), was later modified by Mathenson (24). Again they split the wellbore into two sections.

The third and most detailed wellbore model has been developed by Gould (25). Gould's two-phase flow model differs from the homogeneous models discussed previously in that it considers the flow of each phase separately. This means that instead of solving the momentum balance for average viscosities and densities, empirical approximations based upon the morphology of flow are used for the acceleration, frictional, and gravitational terms.

Rumi (26) has proposed a wellbore model for the single phase flow of steam vapor. He formulates his problem in terms of a conservation of energy equation neglecting the potential energy term, a conservation of momentum equation neglecting gravity, a mass balance, an equation of state, and an equation for entropy production. By assuming isothermal flow, these equations are reduced to a single equation which relates flow rate with pressure.

MATHEMATICAL DEVELOPMENT

The production of fluids from a two-phase geothermal system is envisioned as follows. A two-phase, single component mixture of steam and water is assumed to be contained within a porous reservoir. The reservoir is closed to flow of mass and heat. Specifically, the no-flow mass boundary condition corresponds to a reservoir which is not surrounded by an aquifer and thus is not subject to a water drive. The no-flow heat boundary condition corresponds to the case where the heat gain and the heat loss for the reservoir is small compared to the forced convective heat transfer generated by production. A well is assumed to be drilled into the reservoir from the surface of the earth and thus serves as a conduit for the flow of fluids from the reservoir up to the surface. Production is then accomplished by expansion of the fluids within the reservoir at the wellbore. The wellbore model herein developed assumes the flow of a homogeneous mixture of steam and water. This assumption has proven to be adequate for the high flow rates encountered in geothermal reservoirs.

Reservoir Model

The physical system representing the reservoir is considered to be a two-dimensional, anisotropic, heterogeneous porous rock of rectilinear geometry. The rock is saturated with a single component fluid, water, existing either in the liquid state or the vapor state. The capillary pressure

existing between these two phases is neglected. It is recognized that in cross-sectional simulations in particular, capillary pressure would influence fluid saturation distributions.

The conservation of mass with a point sink term applied to the single component, water, over a differential volumetric element of the reservoir yields:

$$-\nabla \cdot (\eta_w \rho_w \hat{v}_w + \eta_g \rho_g \hat{v}_g) - Q = \frac{\partial}{\partial t} (\phi \eta_w \rho_w S_w + \phi \eta_g \rho_g S_g) \quad (1)$$

The relative permeabilities are assumed to be independent of the direction of the medium and to be unique functions of the liquid phase saturation; they are assumed to be independent of temperature. Thus the extension of Darcy's Law for multiphase flow is given as:

$$\hat{v}_w = \frac{-\bar{k} k_{rw}}{\mu_w} (\nabla P - \gamma_w \nabla \xi) \quad (2)$$

and

$$\hat{v}_g = \frac{-\bar{k} k_{rg}}{\mu_g} (\nabla P - \gamma_g \nabla \xi) \quad (3)$$

where

$$\bar{k} = \begin{pmatrix} k_x & 0 \\ 0 & k_y \end{pmatrix}$$

The relative permeabilities assumed in this study are variations of a functional form proposed by Corey (30) for a drainage displacement process. The drainage assumption implies that the wetting phase saturation is decreasing. For a two-phase, single component fluid this means that the process of vaporization will predominate condensation.

$$k_{rw} = \frac{(S_w - S_{wi})^4}{(1 - S_{wi})^4} \quad (4)$$

$$k_{rg} = \left[ 1 - \frac{(S_w - S_{wi})}{(S_{wm} - S_{wi})} \right]^2 \left[ 1 - \frac{(S_w - S_{wi})^2}{(S_{wi} - 1)^2} \right] \quad (5)$$

where

$$S_{wi} = .05 \text{ and } S_{wm} = .95$$

Since a single component fluid is assumed to exist within the rock, the mass fraction of water in each phase is taken to be one, that is

$$\begin{aligned} \eta_w &= 1 \\ \eta_g &= 1 \end{aligned} \quad (6)$$

Substitution of Equations (2) and (3) and (6) into Equation (1) results in:

$$\begin{aligned} \hat{\nabla} \cdot \left[ \frac{\bar{k} k_{rw} \rho_w}{\mu_w} (\hat{\nabla} P - \gamma_w \hat{\nabla} \xi) \right. \\ \left. + \frac{\bar{k} k_{rg} \rho_g}{\mu_g} (\hat{\nabla} P - \gamma_g \hat{\nabla} \xi) \right] \\ - Q = \frac{\partial}{\partial t} (\phi \rho_w S_w + \phi \rho_g S_g) \end{aligned} \quad (7)$$

The conservations of energy with a heat sink made over a differential volumetric reservoir element based on enthalpies yields:

$$\begin{aligned} \hat{\nabla} \cdot (\bar{\kappa} \hat{\nabla} T) - \hat{\nabla} \cdot (\eta_w \rho_w h_w \hat{\nabla} w + \eta_g \rho_g h_g \hat{\nabla} g) - Q_h = \\ \frac{\partial}{\partial t} \left[ \phi (\eta_w \rho_w h_w S_w + \eta_g \rho_g h_g S_g) + (1 - \phi) \rho_r h_r \right] \end{aligned} \quad (8)$$

This equation assumes constant rock density, constant specific heat of rock, instantaneous thermal equilibrium between the reservoir rock and the two fluid phases, and anisotropic behavior of thermal conductivity similar to that of permeability, i.e., orthogonal principal axes are congruent with the coordinate axis.

Again by assuming a single component fluid and Darcy's Law, substitution of Equations (2), (3) and (6) into Equation (8) yields:

$$\begin{aligned} \hat{\nabla} \cdot (\bar{\kappa} \hat{\nabla} T) - \hat{\nabla} \cdot \left[ \frac{\bar{k} k_{rw} \rho_w h_w}{\mu_w} (\hat{\nabla} P - \gamma_w \hat{\nabla} \xi) \right. \\ \left. + \frac{\bar{k} k_{rg} \rho_g h_g}{\mu_g} (\hat{\nabla} P - \gamma_g \hat{\nabla} \xi) \right] - Q_h \\ = \frac{\partial}{\partial t} \left[ (\phi \rho_w h_w S_w + \phi \rho_g h_g S_g) + (1 - \phi) \rho_r h_r \right] \end{aligned} \quad (9)$$

The temperatures and pressures within the reservoir are then connected by the saturated pressure relationship for steam:

$$T = 115.1 P^{.225} \quad (10)$$

Substituting Equation (10) into Equation (9) results in:

$$\begin{aligned} \hat{\nabla} \cdot (\bar{\kappa} \frac{\partial T}{\partial P} \hat{\nabla} P) - \hat{\nabla} \cdot \left[ \frac{\bar{k} k_{rw} \rho_w h_w}{\mu_w} (\hat{\nabla} P - \right. \\ \left. \gamma_w \hat{\nabla} \xi) + \frac{\bar{k} k_{rg} \rho_g h_g}{\mu_g} (\hat{\nabla} P - \gamma_g \hat{\nabla} \xi) \right] - Q_h = \\ \frac{\partial}{\partial t} \left[ (\phi \rho_w h_w S_w + \phi \rho_g h_g S_g) + (1 - \phi) \rho_r h_r \right] \end{aligned} \quad (11)$$

#### Auxiliary Relations

The vapor and liquid phase saturations are related by

$$S_g + S_w = 1 \quad (12)$$

The density, viscosity, and enthalpy for both water and steam are assumed to be functionally dependent on pressure and temperature at saturated conditions as follows:

$$\mu_g = 10^{-4} [82.2516 + .17815 T + 6.59 \cdot 10^{-5} T^2 - \rho_g (31.45 - .05253 T)] \quad (13)$$

$$\mu_w = 2.185 / (0.04012 T + 5.154 \cdot 10^{-6} T^2 - 1.0) \quad (14)$$

$$h_w = 91.0 P^{.2574} \quad (15)$$

$$h_g = 1119 P^{.01267} \quad (16)$$

$$f_w = 1.0 / (.0158682 + 7475 \cdot 10^{-6} T + 15.111 \cdot 10^{-9} T^2) \quad (17)$$

$$\rho_g = .002473007 P^{.9588} \quad (18)$$

The porosity of the rock is assumed to be a function of both space and pressure. The functional form assumed separates the effects of space and pressure in the following manner:

$$\phi = \phi_r(x, y) \cdot \phi_p(P) \quad (19)$$

where

$$\phi_p = [1 + C_r (P - P_o)]$$

$P_o$  = pressure at assumed reference point

$C_r$  = rock compressibility

### Wellbore Model

The wellbore (as shown in Figure 2) is considered to be a one-dimensional, vertical duct of constant diameter, through which a two-phase mixture of steam and water undergoes steady flow. The two-phase fluid is assumed to be a homogeneous mixture in which the phases are in thermal equilibrium with each other. In particular the frictional pressure drop of the two-phase mixture is determined by Martinelli-Nelson (27) two-phase multipliers. The Martinelli correlation balances frictional shear stresses versus pressure drop under a separated flow hypothesis. This correlation was made on the horizontal flow of boiling water. In a geothermal wellbore, vertical, flashing flow of water occurs. This then implies that the body forces and inertial forces are assumed small compared to frictional forces.

The equations describing a homogeneous, two-phase fluid undergoing steady, one-dimensional equilibrium flow over a differential element are a conservation of mass

$$\omega = \rho_m u a = \text{constant}, \quad (20)$$

a conservation of momentum

$$\frac{\omega}{g_c} \frac{du}{dz} = 144 a \frac{dP}{dz} - P \tau_w - a \rho_m \frac{g}{g_c}, \quad (21)$$

and an energy balance

$$\frac{dq_e}{dz} - \frac{1}{J_c} \frac{dW_e}{dz} = \omega \frac{d}{dz} \left[ h_m + \frac{u^2}{2g_c J_c} + \frac{gZ}{g_c J_c} \right] \quad (22)$$

Here Z is taken in the direction of the flow and is thus positive upwards.

The rate of work of viscous and pressure forces is neglected, thus

$$\frac{dW_e}{dz} = 0$$

So rearranging Equation (22) results in:

$$\frac{1}{\omega} \frac{dq_e}{dZ} = \frac{d}{dZ} \left[ h_m + \frac{u^2}{2g_c J_c} + \frac{gZ}{g_c J_c} \right] \quad (23)$$

Equations (20), (21), and (23) are the equations that Pacheco and Farouq Ali (22) used in their study of steam injection. The treatment employed in this work is similar to their work except for the handling of friction and heat loss. The method consists of eliminating the mass balance equation by substituting it into the momentum and energy balances. Further algebraic and functional relations are then applied to the resulting two balances in order to produce a pair of differential equations in pressure and quality, which are as follows:

$$\frac{1}{\omega} \frac{dq_e}{dZ} - \frac{g}{J_c g_c} = \left[ \frac{\partial h_m}{\partial P} + \frac{\Gamma^2 v_m}{J_c g_c} \frac{\partial v_m}{\partial P} \right] \frac{dP}{dZ} +$$

$$\left[ \frac{\partial h_m}{\partial X} + \frac{\Gamma^2 v_m}{J_c g_c} \frac{\partial v_m}{\partial X} \right] \frac{dX}{dZ} \quad (24)$$

$$\left[ \frac{\Gamma^2 v_m}{g_c} \frac{\partial v_m}{\partial P} + 144 v_m \right] \frac{dP}{dZ} +$$

$$\frac{\Gamma^2 v_m}{g_c} \frac{\partial v_m}{\partial X} \frac{dX}{dZ} = \frac{2 \theta_f f v_m^2 \Gamma^2}{D g_c} - \frac{g}{g_c} \quad (25)$$

#### Auxiliary Relations

In order to solve these differential equations, auxiliary relations are needed for the friction factor, the two-phase multiplier, and the heat loss.

The Fanning friction factor is determined from one of three equations which are correlated with the Reynolds number and the relative

roughness of the pipe as follows (Welty, Wicks and Wilson, (28) and Sommerfeld (29)):

for laminar flow ( $Re < 2100$ )

$$f = \frac{16}{Re} \quad (26)$$

for turbulent flow

$$\left( \frac{D/e}{Re \sqrt{f}} > .01 \right)$$

$$\frac{1}{\sqrt{f}} = 4.0 \log_{10} \left( \frac{D}{e} \right) + 2.28 \text{ (Nikuradze), (27)}$$

and for transition flow

$$\frac{1}{\sqrt{f}} = 4.0 \log_{10} \left( \frac{D}{e} \right) + 2.28 - 4.0 \log_{10} \left( 4.67 \frac{D/e}{Re \sqrt{f}} + 1.0 \right) \text{ (Colebrook)} \quad (28)$$

The Reynolds number used in this study was

$$Re = \frac{D \cdot \Gamma}{6.7197 \cdot 10^{-4} \mu_m}$$

where the viscosity,  $\mu$ , is determined from one of three equations depending on the value of the volumetric concentration of the vapor,  $\beta$  (21).

For  $5\% < \beta < 95\%$ , the viscosity,  $\mu_m$ , was chosen by an average of steam and water viscosities weighted with respect to quality as follows:

$$\mu_m = X \mu_g + (1 - X) \mu_w \quad (29)$$

For  $\beta < 5\%$ , the mixture is assumed to be an emulsion of gas bubbles whose viscosity is assumed to be

$$\mu_m = \mu_w (1 + \beta) \quad (30)$$

For  $\beta > 95\%$ , the mixture is assumed to be a mist whose viscosity is assumed to be

$$\mu_m = \mu_g (1 + \beta) \quad (31)$$

The two-phase multiplier,  $\theta_f$ , was determined by using Thom's (30) update of the Martinelli-Nelson (27) correlation. The curve fit of the tabulated values given by Wallis (21) is as follows:

$$\theta_f = .108547 \cdot 10^3 X - .93493 \cdot 10^{-3} P + 2.10933 X^5 - .307153 \cdot 10^{-2} X^4 \cdot P + 1.5943 \quad (32)$$

Heat flow from the wellbore was assumed to take place at a steady state rate from the wellbore to the formation and at an unsteady state rate within the formation. The heat loss from the wellbore was given by:

$$\frac{dq_e}{dz} = -2\pi r_{c1} U (T' = T_{ho}) / 3600 \quad (11)$$

The overall heat transfer coefficient is composed of the resistance of the casing and the resistance of the cement, where the film coefficient at the inside casing wall has been neglected Willhite (32).

The heat loss from the wellbore into the formation at the cement formation interface has been given by Ramey (33) as

$$\frac{dq_e}{dz} = \frac{-2\pi r_{c1} (T_{ho} - T_e)}{3600 F_i(t)} \quad (34)$$

where  $F(t)$  is the transient heat conduction function.

Now Equations (24) and (25) along with the boundary conditions describe the flow within the wellbore.

The reservoir model gives as its solution the pressure and water saturation at the wellbore. The wellbore quality is given by

$$X = \frac{1 - S_w}{S_w \left[ \frac{v_g}{v_w} - 1 + 1 \right]} \quad (35)$$

Hence, using the reservoir pressure and liquid phase saturation given by the reservoir

model, the reservoir quality can be determined by Equation (35). The reservoir pressure and the quality calculated from Equation (35) are then used as boundary conditions for the wellbore model.

#### SOLUTION METHOD

The reservoir model and the wellbore model both involve nonlinear equations, which were solved numerically, employing a finite difference scheme and a fourth order Runge-Kutta method, respectively.

Basically the solution procedure involves solving the two partial differential equations of the reservoir model simultaneously for a given production rate. The solution is then obtained in terms of pressure (or temperature) and liquid phase saturation which are used to calculate the quality of steam at the wellbore. The calculated quality and the pressure used to calculate it serve as boundary conditions for the simultaneous solution of the differential equations of the wellbore model. The wellbore model then gives as its solution the wellhead quality and pressure.

#### Finite Difference Representation

The partial differential equation corresponding to the mass balance Equation (7), written for two-dimensional rectilinear coordinates, after substitution of Equation (14), is discretized, using centered difference approximation to represent spatial derivatives, and a backward difference for the time derivative, obtaining:

$$\begin{aligned} TM_{wx, i + \frac{1}{2}, j}^{n+1} & \left( P_{i+1, j}^{n+1} - P_{i, j}^{n+1} \right) - \\ & TM_{wx, i - \frac{1}{2}, j}^{n+1} \left( P_{i, j}^{n+1} - P_{i-1, j}^{n+1} \right) + \\ & TM_{gx, i + \frac{1}{2}, j}^{n+1} \left( P_{i+1, j}^{n+1} - P_{i, j}^{n+1} \right) - \\ & TM_{gx, i - \frac{1}{2}, j}^{n+1} \left( P_{i, j}^{n+1} - P_{i-1, j}^{n+1} \right) + \\ & TM_{wy, i, j + \frac{1}{2}}^{n+1} \left( P_{i, j+1}^{n+1} - P_{i, j}^{n+1} \right) - \\ & TM_{wy, i, j - \frac{1}{2}}^{n+1} \left( P_{i, j}^{n+1} - P_{i, j-1}^{n+1} \right) \end{aligned}$$

$$TM_{wy, i, j - \frac{1}{2}}^{n+1} \left( P_{i, j}^{n+1} - P_{i, j - 1}^{n+1} \right) +$$

$$TM_{wy, i, j - \frac{1}{2}}^{n+1} + TM_{gy, i, j + \frac{1}{2}}^{n+1}$$

$$\left( P_{i, j + 1}^{n+1} - P_{i, j}^{n+1} \right) - TM_{gy, i, j + \frac{1}{2}}^{n+1} -$$

$$TM_{gy, i, j - \frac{1}{2}}^{n+1} \left( P_{i, j}^{n+1} - P_{i, j - 1}^{n+1} \right) +$$

$$TM_{gy, i, j - \frac{1}{2}}^{n+1}$$

$$\frac{q_{T, i, j}^{n+1}}{\Delta x \Delta y \Delta x} = \frac{1}{\Delta t} \left\{ [\phi \rho_w S_w]_{i, j}^{n+1} - [\phi \rho_w S_w]_{i, j}^n + \right. \\ \left. [\phi \rho_g (1 - S_w)]_{i, j}^{n+1} - [\phi \rho_g (1 - S_w)]_{i, j}^n \right\} \quad (36)$$

If saturation dependent terms are assumed to be highly nonlinear, then only those terms that are functions of saturation need to be taken at the (n + 1) time level. Hence the following temporal evaluation is performed.

$$TM_{wx}^{n+1} = M_{wx}^n k_{rw}^{n+1} \quad TM_{gx}^{n+1} = M_{gx}^n k_{rg}^{n+1}$$

$$TM_{wy}^{n+1} = \frac{\Delta y g}{144 g_c} \rho_w^n k_{rw}^{n+1} M_{wy}^n$$

$$TM_{wy}^{n+1} = M_{wy}^n k_{rw}^{n+1} \quad TM_{gy}^{n+1} = M_{gy}^n k_{rg}^{n+1}$$

$$TM_{gy}^{n+1} = \frac{\Delta y g}{144 g_c} \rho_g^n k_{rg}^{n+1} M_{gy}^n$$

where

$$M_{wx}^n = \frac{6.328 k_x}{\Delta x^2} \left( \frac{\rho_w}{\mu_w} \right)^n \quad M_{gx}^n = \frac{6.328 k_x}{\Delta x^2} \left( \frac{\rho_g}{\mu_g} \right)^n$$

$$M_{wy}^n = \frac{6.328 k_y}{\Delta y^2} \left( \frac{\rho_w}{\mu_w} \right)^n \quad M_{gy}^n = \frac{6.328 k_y}{\Delta y^2} \left( \frac{\rho_g}{\mu_g} \right)^n$$

In regards to spatial evaluation, the interblock transmissibility values are required at positions between grid points. Since the independent variables are only known at the grid points themselves, a suitable average of adjacent grid point values has to be devised. A linear average of adjacent grid points in the direction of the difference was used for the pressure dependent terms. For the saturation dependent terms, a weighted average of adjacent grid points was used based upon fluid potentials. Both of these averages have been implemented with success in other models reported in the literature: Letkeman and Ridings (34), MacDonald and Coats (35), and Diaz and Farouq Ali (36). The secondary parameter, permeability, was evaluated by means of a harmonic average of adjacent grid point values, which has been shown by the author (Toronyi and Farouq Ali, 37) to be correct from geometric and deterministic considerations.

Hence, an interblock transmissibility is exemplified by the following:

$$TM_{wx, i + \frac{1}{2}, j}^{n+1} = M_{wx, i + \frac{1}{2}, j}^n k_{rw, i + \frac{1}{2}, j}^{n+1}$$

where

$$M_{wx, i + \frac{1}{2}, j}^n = \frac{6.328}{\Delta x^2} \cdot \left[ \frac{2 k_{x, i, j} k_{x, i + 1, j}}{k_{x, i, j} + k_{x, i + 1, j}} \right]$$

$$\frac{1}{2} \left[ \left( \frac{\rho_w}{\mu_w} \right)_{i + 1, j}^n + \left( \frac{\rho_w}{\mu_w} \right)_{i, j}^n \right]$$

and

$$k_{rw}^{n+1} = (1 - w_{xf}) k_{rw}^{n+1} + w_{xf} k_{rw}^{n+1}$$

such that,

$$w_{xf} = 1 \quad \text{if} \quad \phi_{w_{i,j}}^n < \phi_{w_{i+1,j}}^n$$

$$w_{xf} = 0 \quad \text{if} \quad \phi_{w_{i,j}}^n \geq \phi_{w_{i+1,j}}^n$$

where

$$\phi_{w_{i,j}}^n = P_{i,j}^n - \frac{y^* g}{144 g_c} \rho_{w_{i,j}}^n$$

$y^*$  = distance from a datum level

The position of the well coincides with a grid point. A constant mass flow rate is assumed for the well. Hence for the partial differential equation corresponding to the mass balance, the mass sink is defined as follows:

$$\text{for } i = K, j = L \quad q_{T_{i,j}}^{n+1} = \omega / 8.64 \cdot 10^4$$

$$\text{for } i \neq K, j \neq L \quad q_{T_{i,j}}^{n+1} = 0$$

where  $(x_K, y_L)$  corresponds to the location of the wellbore.

The partial differential equation corresponding to the energy balance, Equation (11), written in two-dimensional rectilinear coordinates, after substitution of Equation (12) is as follows:

$$\frac{\partial}{\partial x} \left[ \kappa_x \frac{\partial T}{\partial P} \frac{\partial P}{\partial x} \right] + \frac{\partial}{\partial y} \left[ \kappa_y \frac{\partial T}{\partial P} \frac{\partial P}{\partial y} \right] +$$

$$\frac{\partial}{\partial x} \left[ \frac{k_{rw} k_x \rho_w h}{\mu_w} \frac{\partial P}{\partial x} \right] +$$

$$\frac{\partial}{\partial y} \left[ \frac{k_{rw} k_y \rho_w h}{\mu_w} \left( \frac{\partial P}{\partial y} - \frac{\rho_w g}{144 g_c} \right) \right] +$$

$$\frac{\partial}{\partial x} \left[ \frac{k_{rg} k_x \rho_g h}{\mu_g} \frac{\partial P}{\partial x} \right] +$$

$$\frac{\partial}{\partial y} \left[ \frac{k_{rg} k_y \rho_g h}{\mu_g} \left( \frac{\partial P}{\partial y} - \frac{\rho_g g}{144 g_c} \right) \right] - Q_h$$

$$= \frac{\partial}{\partial t} \left[ \phi (S_w \rho_w h_w) + \phi (1 - S_w) \rho_g h_g + (1 - \phi) \rho_r h_r \right] \quad (37)$$

where again the y-direction is assumed to be coincident with the vertical direction.

Similarly to the mass balance, a centered difference approximation is used to represent the spatial derivatives and a backward difference is used for the time derivative. This results in:

$$v_{x_{i+\frac{1}{2},j}}^n \left( P_{i+1,j}^{n+1} - P_{i,j}^{n+1} \right) -$$

$$v_{x_{i-\frac{1}{2},j}}^n \left( P_{i,j}^{n+1} - P_{i-1,j}^{n+1} \right)$$

$$+ v_{y_{i,j+\frac{1}{2}}}^n \left( P_{i,j+1}^{n+1} - P_{i,j}^{n+1} \right) -$$

$$v_{y_{i,j-\frac{1}{2}}}^n \left( P_{i,j}^{n+1} - P_{i,j-1}^{n+1} \right)$$

$$+ TE_{wx_{i+\frac{1}{2},j}}^{n+1} \left( P_{i+1,j}^{n+1} - P_{i,j}^{n+1} \right) -$$

$$TE_{wx_{i-\frac{1}{2},j}}^{n+1} \left( P_{i,j}^{n+1} - P_{i-1,j}^{n+1} \right)$$

$$+ TE_{gx_{i+\frac{1}{2},j}}^{n+1} \left( P_{i+1,j}^{n+1} - P_{i,j}^{n+1} \right) -$$

$$TE_{gx_{i-\frac{1}{2},j}}^{n+1} \left( P_{i,j}^{n+1} - P_{i-1,j}^{n+1} \right)$$



$$+ TE_{wy, j + \frac{1}{2}}^{n+1} \left( P_{i, j+1}^{n+1} - P_{i, j}^{n+1} \right) -$$

$$TE_{wy, j + \frac{1}{2}}^{n+1} - TE_{wy, j - \frac{1}{2}}^{n+1}$$

$$\left( P_{i, j}^{n+1} - P_{i, j-1}^{n+1} \right) + TE_{wy, j - \frac{1}{2}}^{n+1}$$

$$+ TE_{gy, j + \frac{1}{2}}^{n+1} \left( P_{i, j+1}^{n+1} - P_{i, j}^{n+1} \right) -$$

$$TE_{gy, j + \frac{1}{2}}^{n+1} - TE_{gy, j - \frac{1}{2}}^{n+1}$$

$$\left( P_{i, j}^{n+1} - P_{i, j-1}^{n+1} \right) + TE_{gy, j - \frac{1}{2}}^{n+1}$$

$$\frac{q_h^{n+1}}{\Delta x \Delta y \lambda} = \frac{1}{\Delta t}$$

$$\left[ (\phi S_w \rho_w h_w)_{i, j}^{n+1} - (\phi S_w \rho_w h_w)_{i, j}^n \right] + \frac{1}{\Delta t}$$

$$\left[ [\phi(1 - S_w) \rho_g h_g]_{i, j}^{n+1} - [\phi(1 - S_w) \rho_g h_g]_{i, j}^n \right]$$

$$+ \frac{1}{\Delta t} \left[ [(1 - \phi) \rho_r h_r]_{i, j}^{n+1} - [(1 - \phi) \rho_r h_r]_{i, j}^n \right]$$

(38)

where

$$V_x = 24 \kappa_x \frac{\partial T}{\partial P}$$

$$V_y = 24 \kappa_y \frac{\partial T}{\partial P}$$

$$TE_{wx} = h_w TM_{wx}$$

$$TE_{wy} = h_w TM_{wy}$$

$$TE'_{wy} = h_w TM'_{wy}$$

$$TE_{gx} = h_g TM_{gx}$$

$$TE_{gy} = h_g TM_{gy}$$

$$TE'_{gy} = h_g TM'_{gy}$$

Again assuming that saturation dependent terms are highly nonlinear, then only those terms that are functions of saturation need to be taken at the (n + 1) time level. Hence the following temporal evaluation is performed:

$$V_x^n = \frac{24 \kappa_x}{\Delta x^2} \frac{\partial T}{\partial P} \Big|_x^n$$

$$V_y^n = \frac{24 \kappa_y}{\Delta y^2} \frac{\partial T}{\partial P} \Big|_y^n$$

$$TE_{wx}^{n+1} = O_{wx}^n k_{rw}^{n+1}$$

$$TE_{wy}^{n+1} = O_{wy}^n k_{rw}^{n+1}$$

$$TE_{wy}^{n+1} = \frac{\Delta y g}{144 g_c} (\rho_w h_w)^n k_{rw}^{n+1} M_{wy}^n$$

$$TE_{gx}^{n+1} = O_{gx}^n k_{rg}^{n+1}$$

$$TE_{gy}^{n+1} = O_{gy}^n k_{rg}^{n+1}$$

$$TE_{gy}^{n+1} = \frac{\Delta y g}{144 g_c} (\rho_g h_g)^n k_{rg}^{n+1} M_{gy}^n$$

where

$$O_{wx}^n = \frac{6.328 \kappa_x}{\Delta x^2} \left( \frac{\rho_w h_w}{\mu_w} \right)^n$$

$$O_{gx}^n = \frac{6.328 \kappa_x}{\Delta x^2} \left( \frac{\rho_g h_g}{\mu_g} \right)^n$$

$$O_{wy}^n = \frac{6.328 \kappa_y}{\Delta y^2} \left( \frac{\rho_w h_w}{\mu_w} \right)^n$$

$$O_{gy}^n = \frac{6.328 \kappa_y}{\Delta y^2} \left( \frac{\rho_g h_g}{\mu_g} \right)^n$$

In regards to spatial evaluation, the interblock, thermal transconductivity values are formed by using a linear average of adjacent grid point values in the direction of the difference for the pressure dependent terms and by employing a harmonic average of adjacent grid point values for the thermal conductivity. Hence an interblock, thermal transconductivity is exemplified by the following:

$$V_{x_{i+\frac{1}{2},j}}^n = \frac{24}{\Delta x^2} \left[ \frac{2 \kappa_{x_{i,j}} \kappa_{x_{i+1,j}}}{\kappa_{x_{i,j}} + \kappa_{x_{i+1,j}}} \right] \cdot \frac{1}{2} \left[ \left. \frac{\partial T}{\partial P} \right|_{i+1,j}^n + \left. \frac{\partial T}{\partial P} \right|_{i,j}^n \right]$$

The interblock, thermal transmissibilities are formed similar to the interblock mass transmissibilities, i.e., a linear average of pressure dependent terms, a harmonic average of permeability, and a weighted average with respect to fluid potentials for the saturation dependent terms. Hence an interblock, thermal transmissibility is exemplified by the following:

$$TE_{gy_{i,j-\frac{1}{2}}}^{n+1} = O_{gy_{i,j-\frac{1}{2}}}^n \cdot k_{rg_{i,j-\frac{1}{2}}}^{n+1}$$

where

$$O_{gy_{i,j-\frac{1}{2}}}^n = \frac{6.328}{\Delta y^2} \left[ \frac{2 k_{y_{i,j}} k_{y_{i,j-1}}}{k_{y_{i,j}} + k_{y_{i,j-1}}} \right]$$

$$\frac{1}{2} \left[ \left( \frac{\rho_g h_g}{\mu_g} \right)_{i,j}^n + \left( \frac{\rho_g h_g}{\mu_g} \right)_{i,j-1}^n \right]$$

and

$$k_{rg_{i,j-\frac{1}{2}}}^{n+1} = (1 - s_{yb}) k_{rg_{i,j}}^{n+1} + s_{yb} k_{rg_{i,j-1}}^{n+1}$$

such that

$$s_{yb} = 1 \text{ if } \phi_{g_{i,j}}^n < \phi_{g_{i,j-1}}^n$$

$$s_{yb} = 0 \text{ if } \phi_{g_{i,j}}^n \geq \phi_{g_{i,j-1}}^n$$

where

$$\phi_{g_{i,j}}^n = P_{i,j}^n - \frac{y^* g}{144 g_c} \rho_{g_{i,j}}^n$$

$y^*$  - distance below a datum level

The heat sink term is given by

$$q_h = h_w q_T + (h_g - h_w) q_g \quad (39)$$

The steam production rate is determined by the fractional flow of the steam phase within the block containing the wellbore as follows:

$$q_g = \sigma_g q_T \quad (40)$$

where

$$\sigma_g = \frac{k_{rg}}{k_{rg} + \lambda k_{rw}} \text{ and } \lambda = \frac{\mu_g \rho_w}{\mu_w \rho_g}$$

Substituting Equation (40) into Equation (39) and differencing results in:

$$q_{h_{i,j}}^{n+1} = \left[ h_w^n + \frac{(h_g^n - h_w^n) k_{rg}^{n+1}}{k_{rg}^{n+1} + \lambda^n k_{rw}^{n+1}} \right] q_{T_{i,j}}^{n+1} \quad (41)$$

All terms in Equation (36) can be placed on one side of the equation and be defined to be the mass residual  $R_{m_{1,j}}$ ; similarly, all

terms in Equation (38) can be placed on one side of the equation and be defined as the energy residual  $R_{E_{1,j}}$ .

The no-flow boundary conditions are represented by zero fluid transmissibilities on the bounding surfaces, and zero flow velocities on the same surfaces, for mass and heat, respectively.

Initially, a pressure and saturation distribution is specified throughout the reser-

such that gravitational equilibrium is maintained.

Newtonian Formulation

Since Equations (36) and (38) in residual form are defined at every grid point, a system of 2·I·J nonlinear algebraic equations needs to be solved for each time step. Since each grid point is coupled to at most four adjacent grid points, the equations have at most five unknown grid point values for each independent variable, or ten unknowns per equation. These remarks can be summarized by representing the system of equations vectorially as follows:

$$R(z) = 0 \tag{42}$$

where

$$\hat{R} = (R_{m_1, 1}, \dots, R_{m_1, J}, \dots, R_{m_{I-1}, 1}, \dots, R_{m_I, J}, \dots, R_{E_1, 1}, \dots, R_{E_1, J}, \dots, R_{E_{I-1}, 1}, \dots, R_{E_I, J})$$

and

$$\hat{z} = \begin{pmatrix} P_{i, j-1}^{n+1}, P_{i-1, j}^{n+1}, P_{i, j}^{n+1}, P_{i+1, j}^{n+1}, \\ P_{i, j+1}^{n+1}, S_{w_{i, j-1}}^{n+1}, S_{w_{i-1, j}}^{n+1}, S_{w_{i, j}}^{n+1}, \\ S_{w_{i+1, j}}^{n+1}, S_{w_{i+1, j+1}}^{n+1} \end{pmatrix}$$

Such a system of nonlinear equations can be solved by means of a Newton-Raphson technique (Remson, Hornberger, and Molz (38)). The Newton-Raphson method applied to a set of nonlinear equations involves approximating the equation by a truncated Taylor's series expansion about an assumed solution to the set of equations. The result is a set of linear equations which can then be solved by matrix techniques. The method is repeated until the solution of the linearized equations agrees with the assumed solution within a certain tolerance. The Newton-Raphson method applied to Equation (42) results in:

$$\left[ \delta \hat{z}^{(K+1)} \cdot \hat{\nabla}_z \right] \hat{R}(\hat{z}^{(K)}) = -\hat{R}(\hat{z}^{(K)}) \tag{43}$$

where

$$\delta \hat{z}^{(K+1)} = \hat{z}^{(K+1)} - \hat{z}^{(K)} \quad K = 1, 2, \dots$$

$$\hat{\nabla}_z = \begin{pmatrix} \frac{\partial}{\partial P_{i, j-1}^{n+1}}, & \frac{\partial}{\partial P_{i-1, j}^{n+1}}, & \dots & \frac{\partial}{\partial S_{w_{i, j+1}}^{n+1}} \end{pmatrix}$$

The method of solution proceeds by the following inductive argument. A trial solution,  $z^{(0)}$ , is assumed, which for the reservoir model is the initial condition. The vector function,  $R(z^{(0)})$  and the dyadic,  $\hat{\nabla}_z R(z^{(0)})$ , are then calculated. Note that the determinant of the dyadic is the Jacobian of  $R(z)$ . The variables  $\delta z^{(1)}$  are then solved for in Equation (43). If

$$|\delta z^{(1)}| < \epsilon$$

where  $\epsilon$  is sufficiently small, then the trial solution,  $z^{(0)}$ , is assumed the true solution and the method is completed. If

$$|\delta z^{(1)}| > \epsilon$$

then a new guess is made by using the following relation:

$$z^{(1)} = z^{(0)} + \delta z^{(1)}$$

and the process is repeated. The process is terminated when

$$|\delta z^{(K+1)}| < \epsilon$$

and the solution is accepted as

$$z^{(K+1)} = z^{(K)}$$

A direct method was employed for the solution of the linear equations at each iteration.

Mathematical Checks

Mathematical checks were used in stability studies and the debugging of the reservoir model. Since the reservoir model can be viewed as a distributed parameter system, its reduction to a lumped parameter form gives a means for analyzing the stability of the model. The lumped parameter form of Equation (7) and (9)

can be obtained by integrating out all spatial variation and is as follows:

$$\frac{d}{dt} \left[ \langle \phi \rho_w S_w \rangle + \langle \phi \rho_g S_g \rangle \right] = -Q \quad (44)$$

$$\frac{d}{dt} \left[ \langle \phi \rho_w h_w S_w \rangle + \langle \phi \rho_g h_g S_g \rangle + \langle (1 - \phi) \rho_r h_r \rangle \right] = -Q_h \quad (45)$$

In terms of systems theory,  $Q$  and  $Q_h$  are the forcing functions for these equations (Porter (39)), and hence the manner in which the system responds is related to the nature of the forcing function. Thus, the effect of discretization of both time and space upon the system is influenced by the forcing function. These combined effects are measured by means of a dimensionless throughput defined as follows:

$$N_{TP} = \frac{q_T \Delta t}{m_p}$$

where

$m_p$  = total mass per cell containing the well

$\Delta t$  = time step size

$q_T$  = total mass production rate

A similar measure of stability has been developed by Todd, O'Dell, and Hirasaki, (40). A number of numerical stability studies were performed on the reservoir model; it was found that the maximum stable  $N_{TP}$  ranged from about 1.0 to 33, for the various initial conditions and areal and cross-sectional models.

The lumped parameter model can be reduced further, resulting in dimensionless ratios that serve as measures for the accuracy of the model. By integrating out the temporal variation in Equations (44) and (45), the following relations are formed:

$$N_m = 1 \quad (46)$$

$$N_E = 1 \quad (47)$$

where

$$N_m = \frac{\int_{t_0}^{t_1} Q dt}{\Delta_t [\langle \phi \rho_w S_w \rangle + \langle \phi \rho_g S_g \rangle]}$$

$$N_E = \frac{\int_{t_0}^{t_1} Q_h dt}{\Delta_t [\langle \phi \rho_w h_w S_w \rangle + \langle \phi \rho_g h_g S_g \rangle + \langle (1 - \phi) \rho_r h_r \rangle]}$$

and the operator  $\Delta_y$  is defined as  $\Delta_t X = X_{t_1} - X_{t_0}$

for time levels  $t_1$  and  $t_0$ . If the solution to the finite difference representation is to be correct, it must satisfy Equations (46) and (47).

Wellbore Model

The wellbore model is represented by a system of mathematical equations in terms of two independent variables, pressure and quality. A solution is sought for this system in terms of the spatial parameter,  $Z$ . In particular, a solution is sought for the wellhead,  $Z = Z_M$ . Hence, the simultaneous solution of the two differential Equations (24) and (25), which relate the independent variables with space, suffices to solve the system. These equations can be placed in matrix form as follows:

$$\begin{pmatrix} K_1 & K_3 \\ K_2 & K_4 \end{pmatrix} \begin{pmatrix} dP/dZ \\ dX/dZ \end{pmatrix} = \begin{pmatrix} L_1 \\ L_2 \end{pmatrix} \quad (48)$$

where

$$K_1 = \frac{\partial h_m}{\partial P} + \frac{\Gamma^2 v_m}{J_c g_c} \frac{\partial v_m}{\partial P}$$

$$K_2 = 144 v_m + \frac{\Gamma^2 v_m}{g_c} \frac{\partial v_m}{\partial P}$$

$$K_3 = \frac{\partial h_m}{\partial X} + \frac{\Gamma^2 v_m}{g_c J_c} \frac{\partial v_m}{\partial X}$$

$$K_4 = \frac{\Gamma^2 v_m}{g_c} \frac{\partial v_m}{\partial X}$$

$$L_1 = \frac{1}{\omega} \frac{dq_e}{dZ} - \frac{g}{g_c J_c}$$

$$L_2 = -2 \frac{\theta_f f v_m^2 \Gamma^2}{g_c^D} - \frac{g}{g_c}$$

Equation (48) can be rearranged into the following form:

$$\begin{pmatrix} dP/dZ \\ dX/dZ \end{pmatrix} = \begin{pmatrix} K_1 & K_3 \\ K_2 & K_4 \end{pmatrix}^{-1} \begin{pmatrix} L_1 \\ L_2 \end{pmatrix} = \begin{pmatrix} H_1 \\ H_2 \end{pmatrix} \quad (49)$$

Having obtained the differential equations in this form, the Runge-Kutta method can be applied. The step size,  $Z$ , is chosen so that the positions of the wellhead and the borrow of the hole are coincident with the grid points. From the reservoir model and Equation (35), the bottomhole pressure and quality can be obtained, which in this case are the boundary conditions for the set of differential equations given in Equation (49).

The computer flow chart for the entire reservoir-wellbore simulation model is shown in Figures 3 and 4.

### DISCUSSION OF RESULTS

In order to gain insight into the problem of production from a two-phase geothermal reservoir, simulations were performed for various values of porosity, permeability, and initial pressure and saturation distributions. In particular, for the areal formulation five different levels of initial liquid phase saturation were used: 1.0, 0.80, 0.60, 0.40, and 0.20. For the cross-sectional formulation five different levels of initial liquid phase saturation were also used: 0.50, 0.40, 0.30, 0.20, and 0.10. In both formulations two different levels of initial pressure, 650 and 450 psia, two levels of porosity, 0.05 and 0.35, and two levels of permeability, 1.0 and 0.10 darcies, were employed.

Results of these simulations will be discussed in detail in another paper. A few examples of the results obtained, and the main conclusions derived will be stated here.

For the simulation runs, a 6 x 6 grid system was employed for the reservoir model. In order to better determine the effects of the secondary parameters, the reservoir was assumed to be homogeneous and isotropic. The rock density and the coefficient of rock compressibility were assumed constant at the values of 160 lbm/ft<sup>3</sup> and  $5 \cdot 10^{-6}$  psi<sup>-1</sup> respectively. All computer runs were conducted using double precision arithmetic on an IBM 370/168. The convergence tolerance,  $\epsilon$ , employed was  $10^{-9}$ . The typical range of the mass residual was  $10^{-12}$  to  $10^{-15}$ , and the typical range of the energy residual was  $10^{-9}$  to  $10^{-11}$ . The range in percent error associated with both incremental and cumulative mass balance numbers and energy balance numbers was  $10^{-9}$  to  $10^{-10}$ .

The wellbore model was not varied throughout the simulation runs. Its parameters were held constant and are given in Table 1. Step-size,  $\Delta z$ , smaller than 10 ft. demonstrated solutions which differed by no more than  $10^{-5}$  parts in 1.0 from solutions for  $\Delta z$  equal to 10 ft.

### Stability Analysis

The stability or time discretization effect of the reservoir model was tested in both cross-sectional and areal formulations. The difference in the two forms is that in the areal formulation the gravitational force was neglected. In particular, stability was tested by noting the sensitivity of the model to time step size. As has been mentioned in the previous chapter, the reservoir model is ultimately sensitive to

the nature of the forcing function or in this case to the mass rate of production per unit volume of reservoir. Hence the measure employed here in analyzing the stability of the model was the dimensionless mass throughput  $N_{Tp}$ .

For a particular initial saturation and pressure distribution, computer runs of the reservoir model were made progressively increasing time step size. A series of runs was terminated when the model produced physically unrealistic solutions or convergence could not be attained. The last time step size employed was used to calculate the maximum dimensionless throughput. Basically, the determination of this maximum dimensionless throughput to an accuracy of two decimal places was a trial-and-error procedure.

Table 2 shows results of an areal study with various initial saturation and pressure distributions. It is seen that generally the maximum dimensionless throughput increases with increasing initial pressure, except for an initial saturation level of 1.0. For all levels of initial pressure the initial saturation level of 0.20 attained the largest  $N_{Tp}$ . Similar trends were observed for cross-sectional studies, but the trends were not as consistent, and the values of  $N_{Tp}$  were smaller than those for the areal simulations, possibly because of the added effect of gravity.

The effect of dimensionless throughput as a measure stability was also tested, varying the production rate. Close agreement of throughputs was obtained at low initial saturation levels, but at higher levels disparity appeared. This indicates that thermal effects, e.g. flashing, may dominate the stability of the system at high liquid saturations.

The effects of porosity and permeability on reservoir performance are exemplified for a cross-sectional formulation at an initial pressure of 650 psia. Shown in Figures 4 to 7 are plots of bottomhole pressure versus fraction of mass produced for the four different cases resulting from testing two levels of porosity and permeability. In comparison to the higher porosity level, the lower porosity level produces very little bottomhole pressure decline, which can be seen by comparing Figures 4 and 5 and Figures 6 and 7. This result coincides with the finding of Brigham and Morrow (7), who also found that low porosity produced small pressure decline. The lower permeability level produces a larger pressure decline than the higher level, but this decline is not as drastic as for porosity. This follows from comparing Figures 5 and 7 and Figures 4 and 6.

In comparison to the areal simulations, the addition of a gravitational force in the

cross-sectional formulation hastens the development of a superheated region in the reservoir. The level of initial pressure does not change the shape of the pressure decline curves, but does effect the advent of a superheated region. The higher level of initial pressure develops a superheated region before the lower level. Again in regards to the development of a superheated region, the lower porosity level developed a superheated region before the higher porosity level. Also, the lower permeability level developed a superheated region before the higher permeability level. This appears to agree with the results of Donaldson (5), who found that saturation changes were effected by permeability.

In the cross-sectional formulation, the smaller the initial liquid phase saturation level, the smaller the pressure decline, the shape of which is concave upward as can be seen in Figures 4 through 7. In the areal formulation, initial saturation levels larger than 0.40 demonstrated smaller pressure decline for a given amount of mass produced than the 0.40 level. Their shapes were concave downward.

For initial liquid phase saturations lower than 0.50, bottomhole quality increased as production proceeded, except for the case where both the lower level of porosity and permeability occurred, e.g. Figures 4A and 5A. Larger initial liquid phase saturations tended to decrease the bottomhole quality or increase it very slightly as production proceeded.

In the areal formulation, bottomhole quality demonstrated similar behavior, except for the initial saturation of 0.40.

The initial pressure level does not seem to alter the shape of the bottomhole quality curves.

Figures 8 and 8A present examples of the reservoir liquid phase saturation and pressure distributions, respectively, for a selected set of conditions for the cross-sectional formulation. The node indicated by a "+" is the production block.

In an areal formulation the most significant effect was that of the initial liquid phase saturation level upon the saturation distribution. Permeability and porosity levels did not alter this effect. For initial liquid phase saturation levels of 0.40 and smaller, the lowest liquid phase saturation about the wellbore existed at the wellbore grid point and the superheated region formed around the wellbore grid point. In contrast, for initial liquid phase saturation levels above 0.40, the highest liquid phase saturation existed at the wellbore grid point and the superheated region formed away from the wellbore.

### Wellhead Pressure and Quality

Wellhead pressure and quality were determined for every time step in all simulation runs until negative wellhead pressures were obtained. Negative wellhead pressure was interpreted to mean that the mass flow rate was too large to be physically attained. Figures 9 and 9A depict an example of the wellhead and bottomhole quality variation with production.

Wellhead quality was always found to be greater than bottomhole quality, while wellhead pressure was always less than bottomhole pressure. Neither wellhead pressure nor wellhead quality was always monotonic with respect to mass fraction produced. Further, bottomhole quality and pressure variations were often not reflected in wellhead variations.

The pressure drop, i.e., the difference in bottomhole and wellhead pressures, generally increased in time for initial liquid phase saturation levels less than 0.30 while it generally decreased in time for initial liquid phase saturation levels larger than 0.40. The larger level of initial pressure, 650 psia, for a given level of initial saturation gave a larger pressure drop than the smaller level of initial pressure, 450 psia.

For the initial pressure level of 650 psia, pressure drop ranged from 100 to 250 psia for initial liquid phase saturation levels larger than 0.30 and ranged from 100 to 350 psia for initial liquid phase saturation levels smaller than 0.30. For the initial pressure level of 450 psia, pressure drop ranged from 100 to 200 psia for initial liquid phase saturation levels larger than 0.30 and ranged from 100 to 300 psia for initial saturation levels below 0.30.

The quality rise, i.e., the difference in bottomhole and wellhead quality, for a given level of initial saturation was larger for an initial pressure level of 450 psia than for 650 psia, but only in the order of  $10^{-3}$ . Generally, initial quality rise ranged from 0.010 to 0.062, while final quality rise ranged from 0.014 to 0.123. The quality rise also generally increased with respect to mass fraction produced, but there were cases in which quality rise decreased for initial liquid phase saturation levels larger than 0.40.

### Theories and Implications

From the foregoing discussion of results, theories and implications of the production behavior of two-phase geothermal reservoirs may be deduced.

Three types of production behavior can be enumerated, based on the nature of the bottomhole pressure and steam quality variations.

For reservoirs of initial liquid phase saturations below 0.40, bottomhole quality increases with time and larger slopes of the bottomhole pressure decline curve are attained at the onset of production than later in the producing life of the reservoir. Since the initial vapor phase saturation is larger than the liquid phase saturation, this type may be called a vapor dominated system. For reservoirs of initial liquid phase saturations larger than 0.60, large slopes of the bottomhole pressure decline curve are attained near the end of the producing life of the reservoir and bottomhole quality decreases or increases very little with time. Since the initial liquid phase saturation is larger than the vapor phase saturation, this type may be called a liquid dominated system. Reservoirs of initial liquid phase saturations between 0.40 and 0.60 exhibit no uniform production behavior, so these reservoirs may be considered to be mixed domination systems.

This classification system may be considered as an extension of a classification of hydrothermal convection systems proposed by White (1). White classified geothermal reservoirs as hot water systems if water was the dominant pressure-controlling phase and as vapor dominated systems if steam was the dominant pressure-controlling phase. Hence, by considering the production behavior of two-phase geothermal reservoirs, a refinement of White's classification system can be made in terms of the initial liquid phase saturation.

Tight reservoir rock, as well as rock which has low permeability and porosity, develops a superheated region more quickly during its production life than rock which has a large permeability or porosity. Furthermore, the smaller the porosity of the reservoir rock, the smaller the pressure decline within the reservoir, and hence super-heated steam is generated with little loss in reservoir energy, i.e., reservoir pressure. Since porosity and permeability are known to decrease with depth, the chances of finding and producing these types of reservoirs are improved by drilling deeper into the earth. Also, proposed projects which involve the injection of water into hot rock in order to generate steam have a greater chance of developing superheated steam if the reservoir has small porosity and permeability.

#### Utility of the Model Developed

In the light of the preceding theories and discussion, the model developed herein is useful in engineering the production behavior of two-phase geothermal reservoirs. Due to its distributed parameter form, the model can monitor fluid distributions and, hence, production behavior as no other model to date has done. Also, the reservoir model can handle very large time step sizes and still remain stable,

in view of the implicit simultaneous solution scheme employed.

In particular, the model can predict the formation of superheated regions whose locations aid in the production of dry or higher quality steam. The model is able to take into account vaporization and condensation which can generate varied production and saturation behavior as discussed previously. The model also can utilize the heterogeneous and anisotropic nature of the reservoir rock and their resulting effect upon production. Further, since the incorporation of two-phase multipliers enables the wellbore model to handle any type of flow regime, the simulator is able to monitor wellhead behavior.

#### CONCLUSIONS

The following conclusions and observations are derived on the basis of the present study:

1. Both areal and cross-sectional formulations produced stable solutions under large time step sizes.
2. Production behavior of two-phase geothermal reservoirs was classified into three types in terms of the initial liquid phase saturation. These are a vapor dominated system, i.e., initial liquid phase saturations below 0.40, a liquid dominated system, i.e., initial liquid phase saturations larger than 0.60, and a mixed domination system, i.e., initial liquid phase saturations between 0.40 and 0.60.
3. Superheated regions within the reservoirs formed more quickly for reservoirs of low porosity and permeability.
4. Wellhead quality was always found to be greater than the bottomhole quality, although the maximum quality rise was small.

#### ACKNOWLEDGEMENT

The authors are indebted to Mr. Charles R. Faust, U.S. Geological Survey, for helpful suggestions.

#### REFERENCES

1. White, D.E.: "Characteristics of Geothermal Resources," Geothermal Energy, Paul Kruger and Carel Otte, ed., Stanford University Press, Stanford, California (1973) 69-94.
2. Muffler, L.J.P.: "Geothermal Resources," U.S. Geol. Surv. Prof. Pap. No. 820, D.H. Brobst and W.P. Pratt, ed., United States Government Printing Office, Washington, (1973) 251-261.
3. James, R.C.: "Wairakei and Larderello: Geothermal Power Systems Compared," N.Z.

- J. Sci. (December, 1968) 11, 706-719.
4. White, D.E., Muffler, L.J.P. and Truesdell, A.H.: "Vapor-dominated Hydrothermal Systems compared with Hot-water Systems," Econ. Geol. (January-February, 1971) 66, 75-87.
  5. Donaldson, I.G.: "A Possible Model for Hydrothermal Systems and Methods of Studying Such a Model," paper 2580 presented at 3rd Australasian Conference on Hydraulics and Fluid Mechanics, Sidney, Australia, November 25-29, 1968
  6. Whiting, R.L. and Ramey, H.J., Jr.: "Applications of Material and Energy Balances to Geothermal Steam Production," J. Pet. Tech. (July, 1969) 21, 893-900.
  7. Brigham, W.E. and Morrow, W.B.: "P/Z Behavior for Geothermal Steam Reservoirs," paper SPE 4899 presented at SPE - AIME 44th Annual California Regional Meeting, San Francisco, California, April 4-5, 1974.
  8. Elder, J.W.: "Physical Processes in Geothermal Areas," Terrestrial Heat Flow, W. Lee, ed., American Geophysical Union, Washington (1965), 211-239.
  9. Wooding, R.A.: "Steady State Free Thermal Convection of Liquid in a Saturated Permeable Medium," J. Fluid Mech. (May, 1957) 2, 273-285.
  10. Donaldson, I.G.: "Temperature Gradients in the Upper Layers of the Earth's Crust due to Convective Water Flows," J. Geophys. Res. (August, 1962) 67, 3449-3459.
  11. Donaldson, I.G.: "The Flow of Steam/Water Mixtures through Permeable Beds: A Simple Simulation of a Natural Undisturbed Hydrothermal Region," N.Z. J. Sci. (March, 1968) 11, 3-23.
  12. Donaldson, I.G.: "The Simulation of Geothermal Systems with a Simple Convective Model," Geothermics, Special Issue 2 (1970) 2 part 1, 649-654.
  13. Ramey, H.J., Jr., Kruger, P. and Raghavan, R.: "Explosive Stimulation of Hydrothermal Reservoirs," Geothermal Energy, Paul Kruger and Carel Otte, ed., Stanford University Press, Stanford, California (1973) 231-249.
  14. Cady, G.V.: "Model Studies of Geothermal Fluid Production," Ph.D. Thesis, Stanford University, Stanford, California (November, 1969).
  15. Billhartz, H.L., Jr.: "Fluid Production from Geothermal Steam Reservoirs," M.S. Report, Stanford University, Stanford, California (Spring, 1971).
  16. Grover, G.M., Cotter, T.P. and Erickson, G.F.: "Structure of Very High Conductance," J. App. Phys. (June, 1964) 35, 1990-1991.
  17. Gomaa, E.E. and Somerton, W.H.: "Thermal Behavior of Multifluid-saturated Formations Part II: Effect of Vapor Saturation-Heat Pipe Concept and Apparent Thermal Conductivity," paper SPE 4896-B presented at SPE - AIME 44th Annual California Regional Meeting, San Francisco, California, April 4-5, 1974.
  18. Coats, K. H., George, W.D., Chu, C. and Marcum, B.E.: "Three-dimensional Simulation of Steamflooding," paper SPE 4500 presented at SPE - AIME 48th Annual Fall Meeting, Las Vegas, Nevada, September 30 - October 3, 1973.
  19. Shutler, N.D.: "Numerical, Three-phase Simulation of the Two-dimensional Steam-flood Process," Soc. Pet. Eng. J. (December, 1970) 10, 405-417.
  20. Mercer, J.W., Jr.: "Finite Element Approach to the Modeling of Hydrothermal Systems," Ph.D. Thesis, University of Illinois, Urbana-Champaign, Illinois (1973).
  21. Wallis, G.B.: One-dimensional Two-phase Flow, McGraw-Hill, Inc., New York (1969).
  22. Pacheco, E.F. and Farouq Ali, S.M.: "Wellbore Heat Losses and Pressure Drop in Steam Injection," J. Pet. Tech. (February, 1972) 24, 139-144.
  23. James, R.C.: "Factors Controlling Borehole Performance," Geothermics, Special Issue 2 (1970) 2 part 2, 1502-1515.
  24. Nathenson, M.: "Flashing Flow in Hot Water Geothermal Wells," U.S. Geological Survey Open File Report (1974).
  25. Gould, T.L.: "Vertical Two-phase Steam-Water Flow in Geothermal Wells," presented at the National AIChE Meeting, Tulsa, Oklahoma, March 10-13, 1974.
  26. Rumi, O.: "Some Considerations on the Flow-Rate Pressure Curve of the Steam Wells of Larderello," Geothermics (March, 1972) 1, 13-23.
  27. Martinelli, R.C. and Nelson, D.B.: "Prediction of Pressure Drop during Forced-Circulation Boiling of Water," Trans. ASME (1948) 70, 695-702.
  28. Welty, J.R., Wicks, C.E. and Wilson, R.E.: Fundamentals of Momentum, Heat and Mass Transfer, John Wiley and Sons, Inc., New York (1969).
  29. Sommerfeld, J.T.: "Equation for Fluid Friction Factor," Hydrocarbon Processing (July, 1967) 46, 135-136.
  30. Thom, J.R.S.: "Prediction of Pressure Drop During Forced Circulation Boiling of Water," Intern. J. Heat Mass Transfer, (July, 1964) 1, 709-724.
  31. Corey, A.T.: "The Interrelation between Gas and Oil Relative Permeabilities," Producers Monthly (November, 1954) 19, 38-41.
  32. Willhite, G.P.: "Overall Heat Transfer Coefficients in Steam and Hot Water Injection Wells," J. Pet. Tech. (May, 1967) 19, 607-615.
  33. Ramey, H.J.: "Wellbore Heat Transmission," J. Pet. Tech. (April, 1962) 14, 427-435.
  34. Letkeman, J.P. and Ridings, R.L.: "A Numerical Coning Model," Soc. Pet. Eng. J. (December, 1970) 10, 418-424.



35. MacDonald, R.C. and Coats, K.H.: "Methods for Numerical Simulation of Water and Gas Coning," Soc. Pet. Eng. J. (December, 1970) 10, 425-436.
36. Diaz, J.M., and Farouq Ali, S.M.: "Simulation of Hot Water Stimulation of Heavy Oil Formations, presented at the 44th National Meeting of AICLE, Tulsa, Feb., 1974.
37. Toronyi, R.M. and Farouq Ali, S.M.: "Determining Interblock Transmissibility in Reservoir Simulators," J. Pet. Tech. (January, 1974) 26, 77-78.
38. Remson, I., Hornberger, G.M. and Molz, F.J.: Numerical Methods in Subsurface Hydrology, Wiley-Interscience, New York (1971).
39. Porter, W.A.: Modern Foundations of Systems Engineering, The MacMillan Co. New York (1966).
40. Todd, M.R., O'Dell, P.M. and Hirasaki, G.J.: "Methods for Increased Accuracy in Numerical Reservoir Simulators," Soc. Pet. Eng. J. (December, 1972) 12, 515-530.

#### NOMENCLATURE

- $C_r$  = rock compressibility,  $\text{in}^2/\text{lbf}$
- $D$  = pipe diameter, ft
- $J_c$  = mechanical equivalent of heat, 778 ft-lbf/BTU
- $N_E$  = energy balance number, dimensionless
- $N_m$  = mass balance number, dimensionless
- $N_{TP}$  = dimensionless throughput, dimensionless
- $P$  = pressure,  $\text{lbf}/\text{in}^2$
- $Q$  = mass rate of production per unit volume of reservoir,  $\text{lbf}/\text{ft}^3\text{-day}$
- $Q_h$  = rate of heat loss per unit volume of reservoir,  $\text{BTU}/\text{ft}^3\text{-day}$
- $Re$  = Reynolds number, dimensionless
- $R_E$  = energy residual,  $\text{BTU}/\text{ft}^3\text{-day}$
- $R_m$  = mass residual,  $\text{lbf}/\text{ft}^3\text{-day}$
- $S$  = phase saturation (volume fraction), dimensionless
- $T$  = temperature, °F
- $TE$  = thermal transmissibility,  $\text{in}^2\text{-BTU}/\text{lbf-ft-day}$
- $TM$  = mass transmissibility,  $\text{in}^2\text{-lbf}/\text{lbf-ft-day}$

- $U$  = heat transfer coefficient,  $\text{BTU}/\text{hr-ft}^2\text{-}^\circ\text{F}$
- $W_e$  = rate of work, ft-lbf/sec
- $X$  = quality (mass fraction of steam), dimensionless
- $Z$  = linear wellbore coordinate, ft
- $a$  = pipe area,  $\text{ft}^2$
- $e$  = pipe roughness, dimensionless
- $f$  = Fanning friction factor, dimensionless
- $g$  = acceleration due to gravity,  $\text{ft}/\text{sec}^2$
- $g_c$  = gravitational conversion factor, 32.17  $\text{lbf-ft}/\text{lbf-sec}^2$
- $h$  = specific enthalpy, BTU/lbm
- $k$  = absolute permeability, darcy
- $k_r$  = relative permeability, dimensionless
- $\hat{n}$  = normal vector
- $q$  = heat flux,  $\text{BTU}/\text{ft}^2\text{-hr}$
- $q_e$  = heat transfer rate, BTU/sec
- $q_g$  = mass production rate of vapor,  $\text{lbm}/\text{day}$
- $q_h$  = reservoir heat transfer rate, BTU/day
- $q_T$  = mass production rate of both liquid and vapor,  $\text{lbm}/\text{day}$
- $q_w$  = mass production rate of liquid,  $\text{lbm}/\text{day}$
- $r$  = radius, ft
- $s, w$  = weighting parameters
- $t$  = time, day
- $u$  = velocity of fluid mixture within wellbore, ft/sec
- $v$  = darcy (reservoir) velocity, ft/day
- $x, y$  = rectangular reservoir coordinates, ft
- $\Gamma$  = mass flux,  $\text{lbf}/\text{sec-ft}^2$
- $\phi$  = fluid potential,  $\text{lbf}/\text{in}^2$
- $\alpha$  = thermal diffusivity,  $\text{ft}^2/\text{day}$
- $\beta$  = volumetric fraction of vapor within wellbore, dimensionless

$\gamma = \frac{\rho g}{144g_c}, \text{ lbf/ft-in}^2$   
 $\eta = \text{mass fraction, dimensionless}$   
 $\theta_f = \text{two-phase multiplier, dimensionless}$   
 $\kappa = \text{thermal conductivity, BTU/ft-hr-}^\circ\text{F}$   
 $\lambda = \text{viscosity ratio, dimensionless}$   
 $\mu = \text{viscosity, centipoise}$   
 $\nu = \text{specific volume, ft}^3/\text{lbm}$   
 $\xi = \text{vertical coordinate, ft}$   
 $\rho = \text{density, lbm/ft}^3$   
 $\tau = \text{wall shear stress, lbf/ft}^2$   
 $\phi = \text{effective rock porosity, dimensionless}$   
 $\chi = \text{reservoir thickness, ft}$   
 $\omega = \text{mass flow rate, lbm/sec}$

Subscripts

$c_1 = \text{inner casing}$   
 $f = \text{forward}$   
 $g = \text{vapor}$   
 $h = \text{heat}$   
 $ho = \text{hole}$

$I = \text{number of nodes in x-coordinate direction of reservoir grid system}$   
 $J = \text{number of nodes in y-coordinate direction of reservoir grid system}$   
 $K, L = \text{wellbore location indices}$   
 $m = \text{mixture}$   
 $M = \text{number of nodes in wellbore grid system}$   
 $n = \text{time position index}$   
 $o = \text{base or reference point}$   
 $p = \text{pressure}$   
 $r = \text{rock}$   
 $s = \text{vapor}$   
 $T = \text{total}$   
 $w = \text{liquid}$   
 $x, y = \text{reservoir coordinate directions}$

Superscripts

$\langle \rangle = \text{average}$   
 $o = \text{initial}$   
 $- = \text{matrix}$   
 $\wedge = \text{vector}$

TABLE 1 - WELLBORE MODEL PARAMETERS EMPLOYED IN SIMULATION RUNS

$\alpha$	=	0.96	ft <sup>2</sup> /day
$\kappa_{cem}$	=	0.51	BTU/hr-ft-°F
$\kappa_{cas}$	=	25.0	BTU/hr-ft-°F
$\kappa_e$	=	1.0	BTU/hr-ft-°F
$r_{c_o}$	=	0.2916	ft
$r_{c_i}$	=	0.26525	ft
$r_{ho}$	=	0.4073	ft
$e$	=	$0.15 \cdot 10^{-3}$	dimensionless
well depth	=	$14.0 \cdot 10^2$	ft
$\Delta Z$	=	10.0	ft
$\omega$	=	555.56	lbm/sec ( $2 \cdot 10^5$ lbm/hr)

TABLE 2 - RESULTS OF A STABILITY STUDY UNDER A. AREAL FORMULATION

Initial Liq. Sat. $S_w^o$	Initial Pressure $P^o$ (psia)	Max. Dimensionless Throughput	
		Max	$N_{TP}$
0.20	250		24.81
0.40	250		6.85
0.60	250		7.30
0.80	250		7.30
1.00	250		6.80
0.20	450		33.06
0.40	450		16.17
0.60	450		19.36
0.80	450		9.89
1.00	450		5.30
0.20	650		33.47
0.40	650		27.81
0.60	650		6.70
0.80	650		11.72
1.00	650		3.53

where

Cell Size:  $\chi = 1000$  ft  
 $\Delta_x = 100$  ft  
 $\Delta_y = 10$  ft

Production Rate:  $q_T = 4.8 \cdot 10^6$  lbm/day

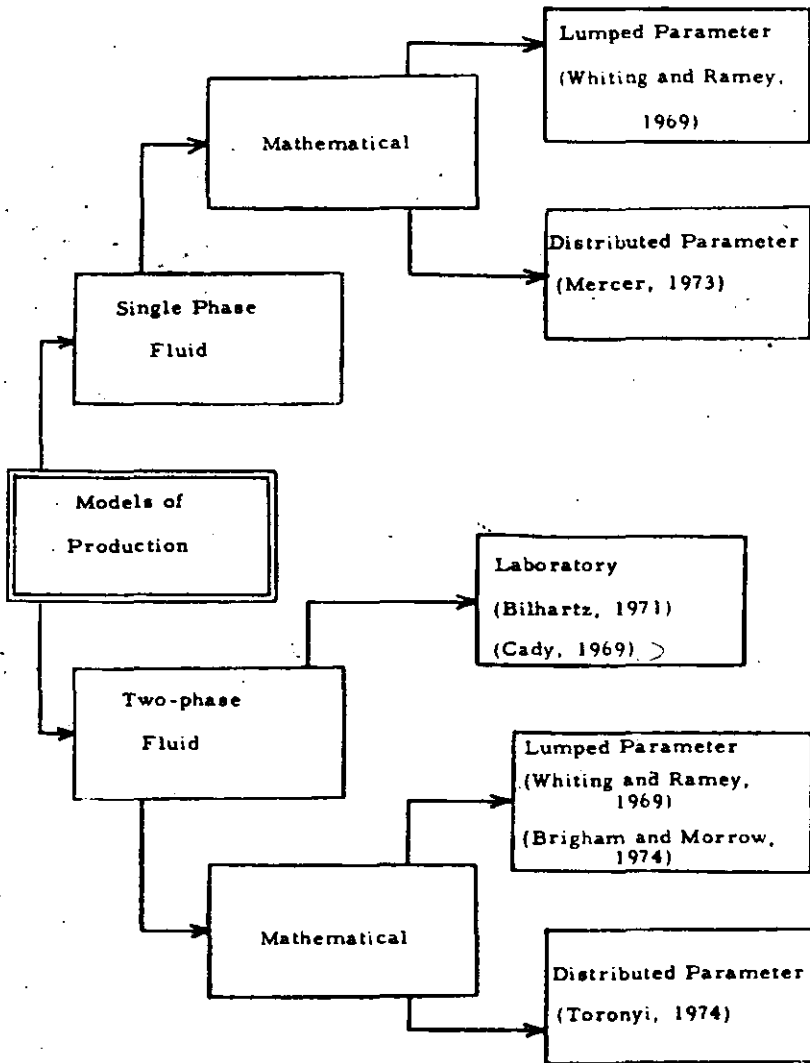


Fig. 1 - Diagrammatic representation of models relating to geothermal systems.

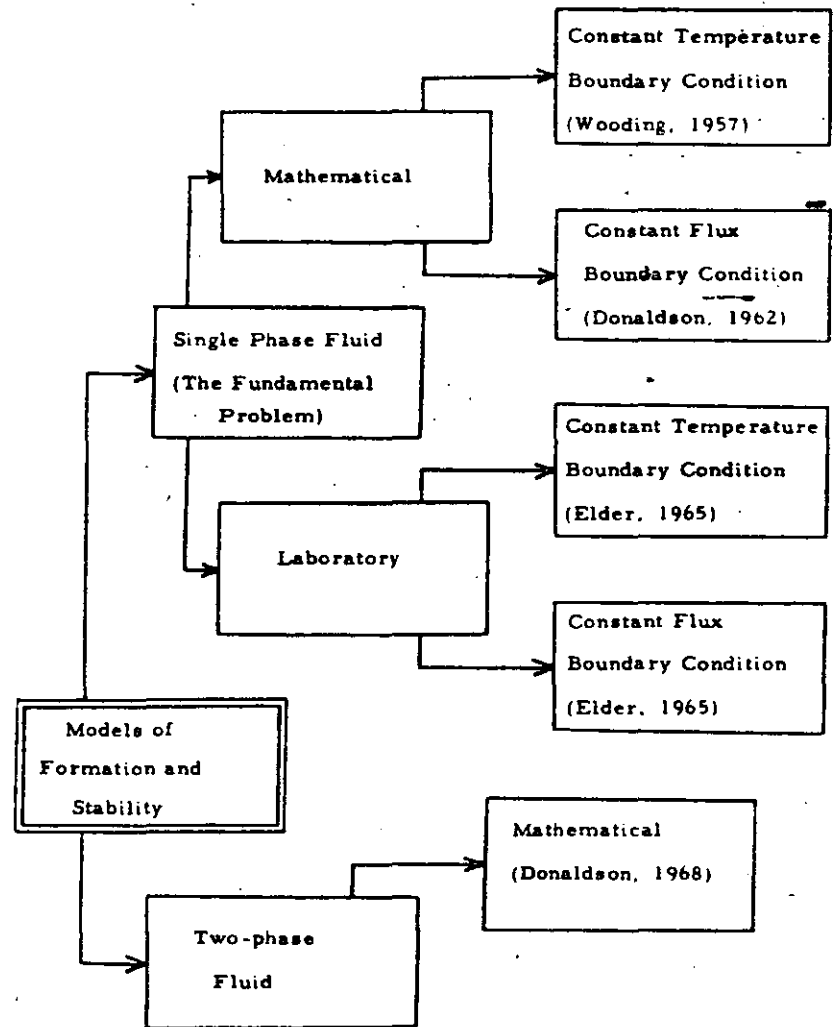


Fig. 1 - (Con't.)

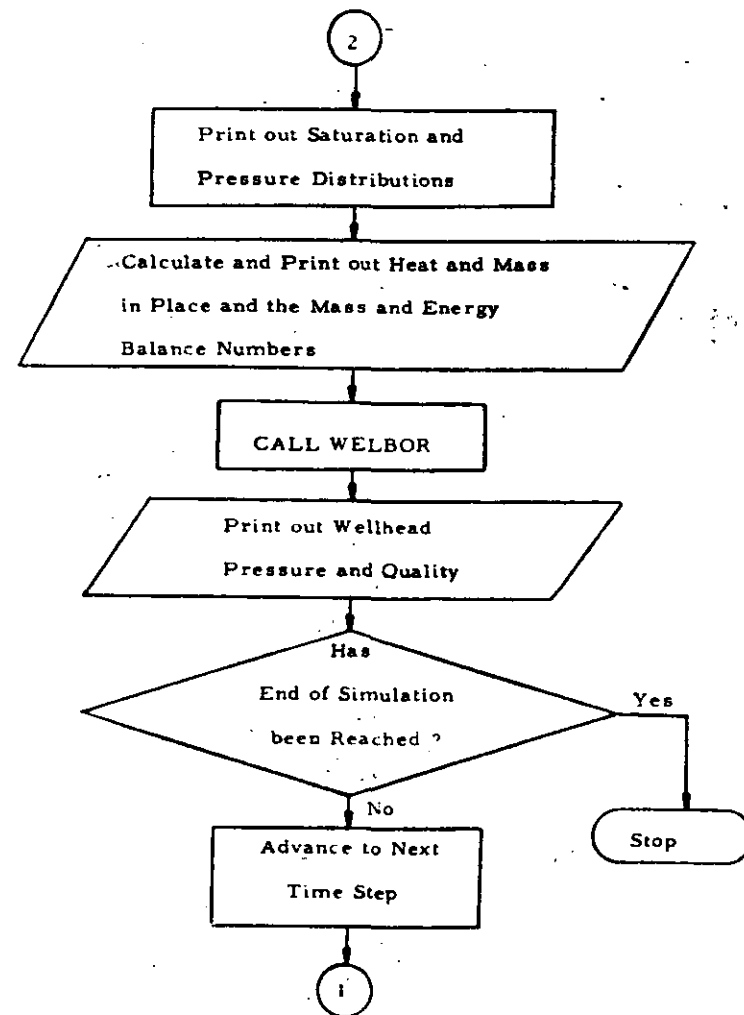
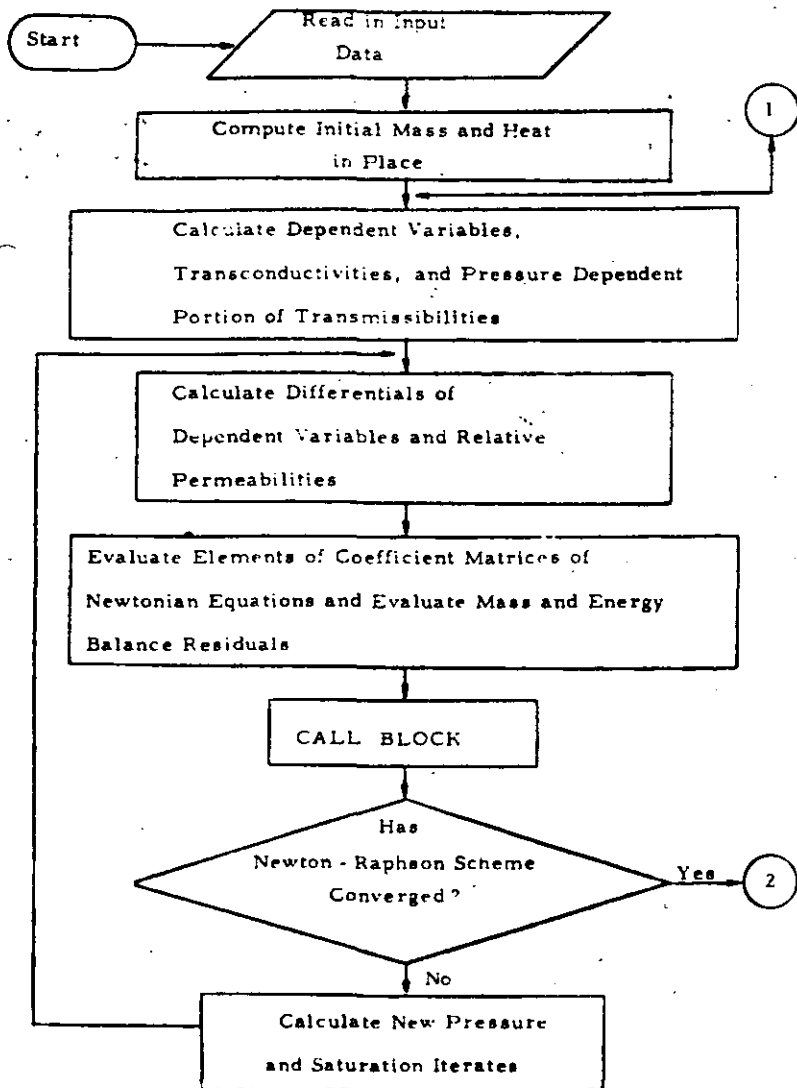


Fig. 7 - (Cont.)

Fig. 6 - Flow chart for the main program of the computational procedure.

24

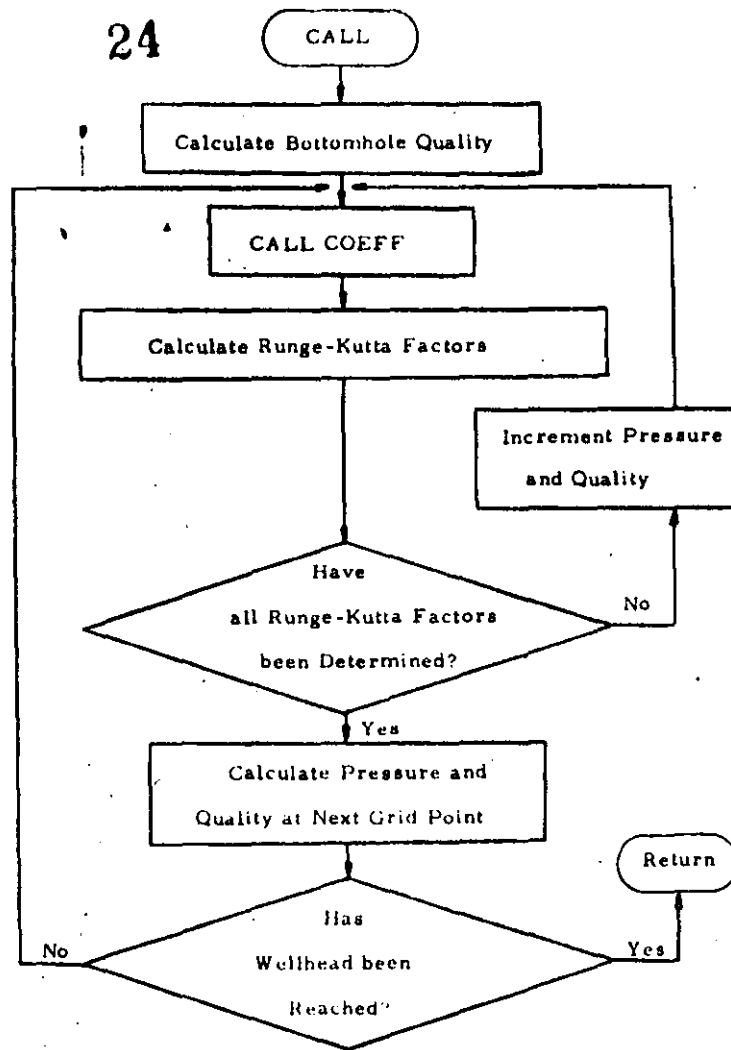


Fig. 3 - Flow chart for subroutine WELNOK of the computational procedure.

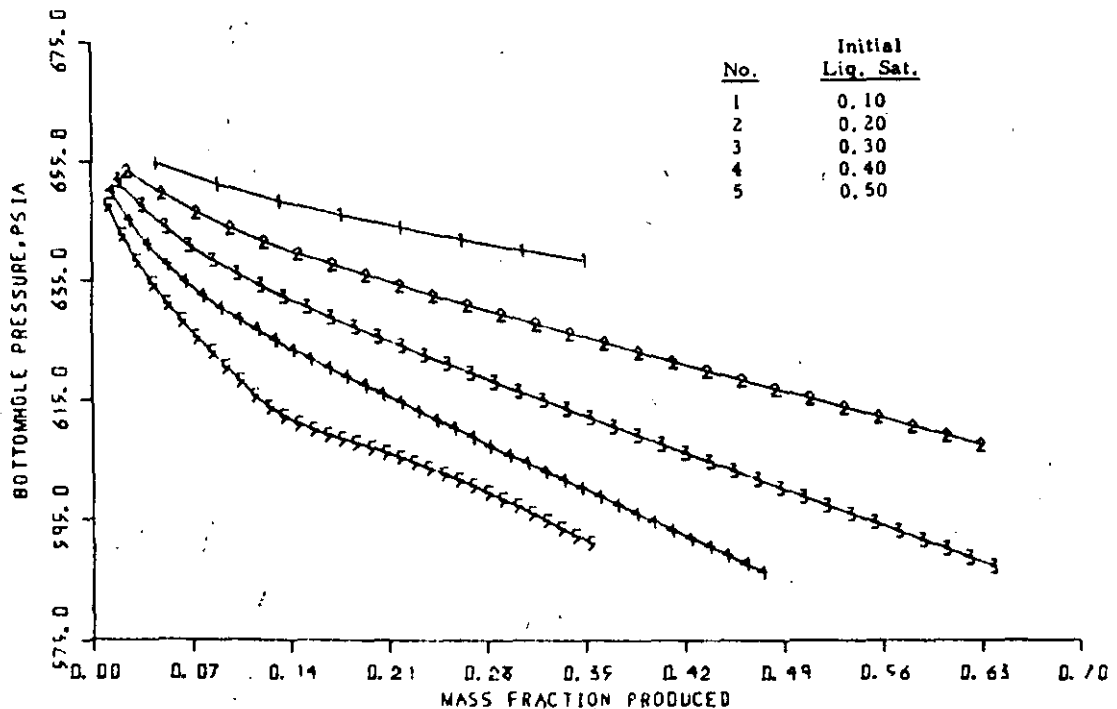


Fig. 4 - Bottomhole pressure v. mass fraction produced for a cross-sectional formulation of a reservoir having permeability = 1.0 darcies, porosity = 0.05, and initial pressure = 650 psia.

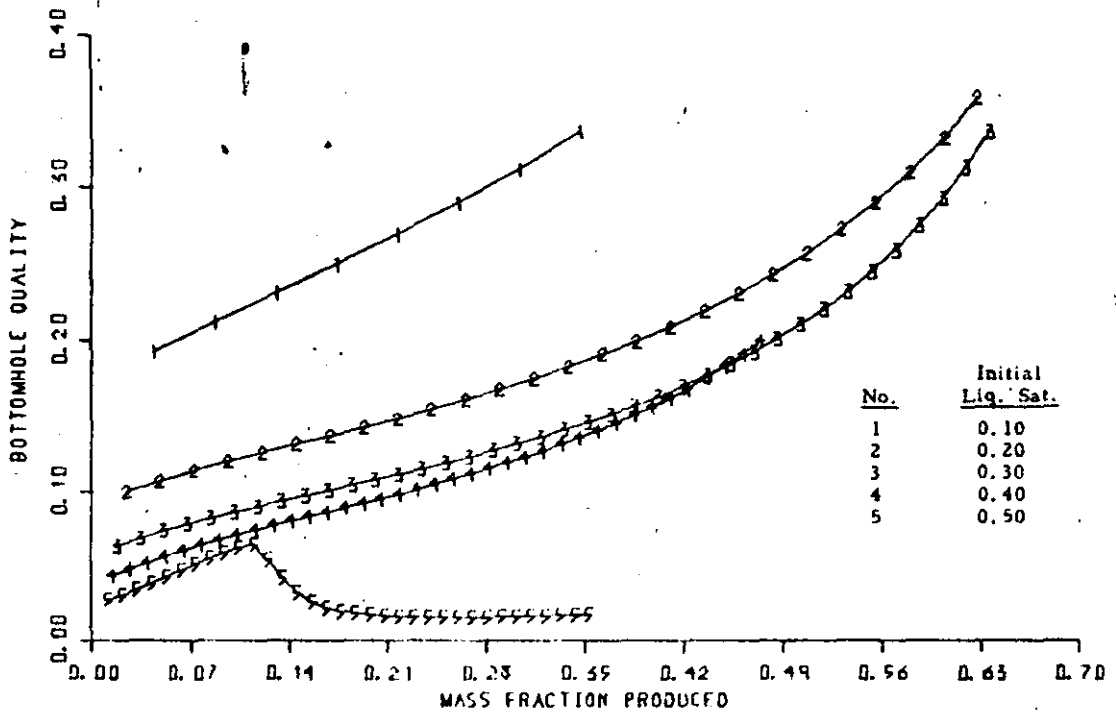


Fig. 4A - Bottomhole quality vs mass fraction produced for a cross-sectional formulation of a reservoir having permeability = 1.0 darcies, porosity = 0.05, and initial pressure = 650 psia.

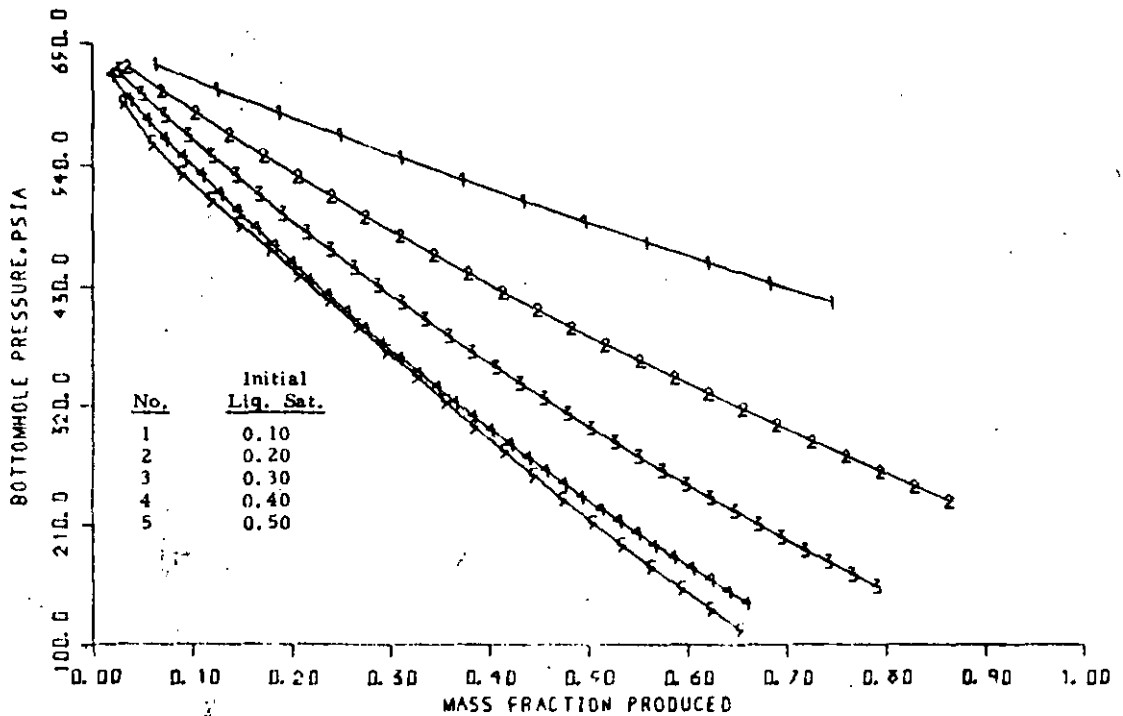


Fig. 5 - Bottomhole pressure vs mass fraction produced for a cross-sectional formulation of a reservoir having permeability = 1.0 darcies, porosity = 0.35, and initial pressure = 650 psia.

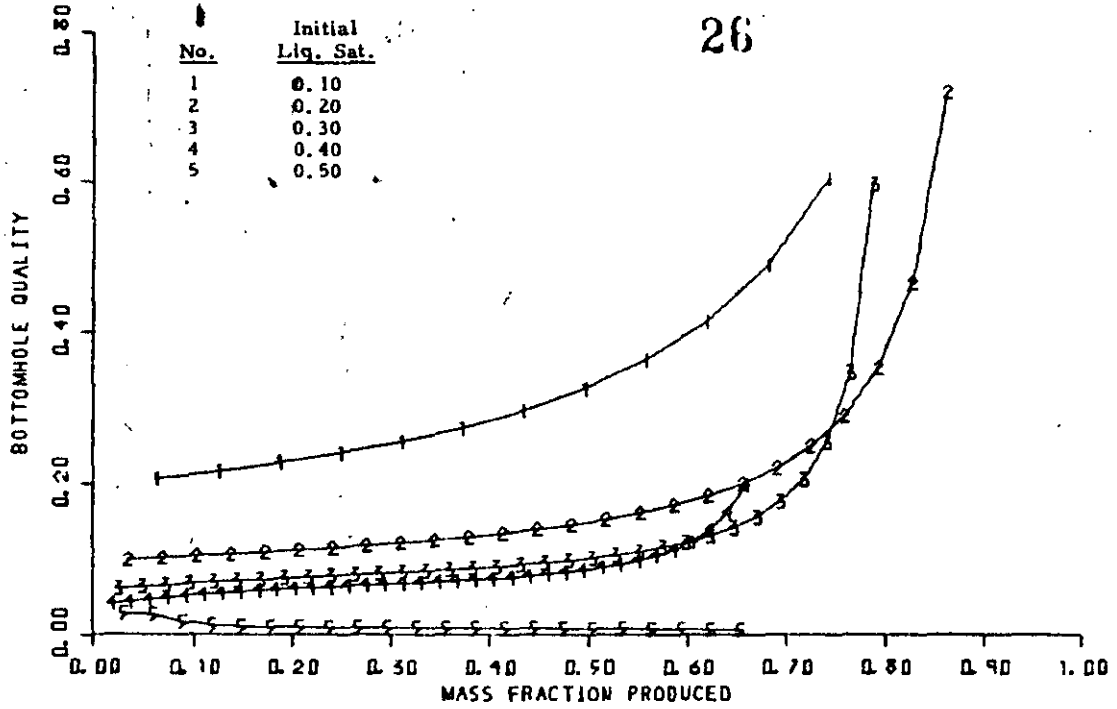


Fig. 5A - Bottomhole quality vs mass fraction produced for a cross-sectional formulation of a reservoir having permeability = 1.0 darcies, porosity = 0.35, and initial pressure = 650 psia.

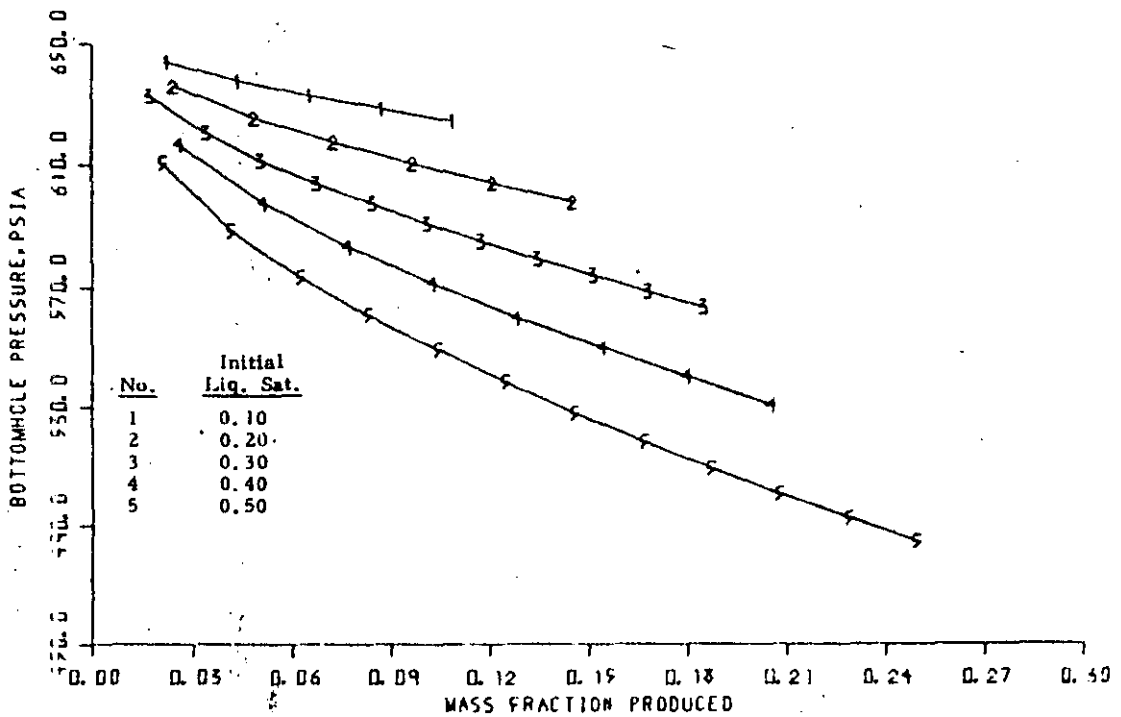


Fig. 6 - Bottomhole pressure vs mass fraction produced for a cross-sectional formulation of a reservoir having permeability = 0.10 darcies, porosity = 0.05, and initial pressure = 650 psia.



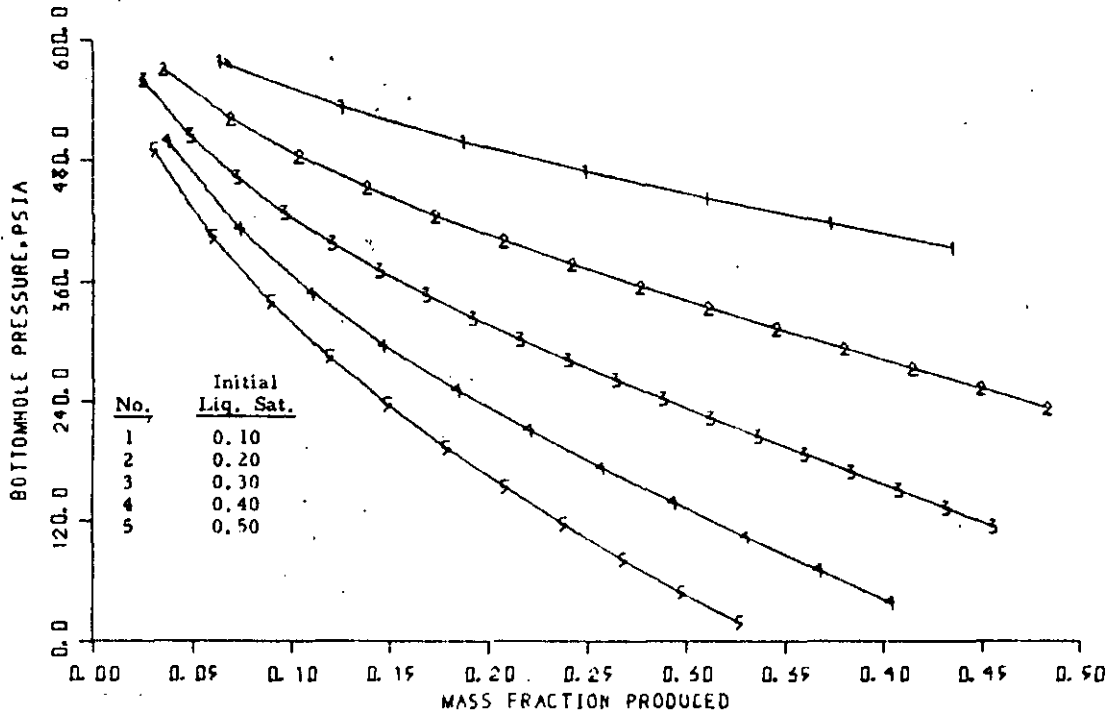


Fig. 7 - Bottomhole pressure vs mass fraction produced for a cross-sectional formulation of a reservoir having permeability = 0.10 darcies, porosity = 0.35, and initial pressure = 650 psia.

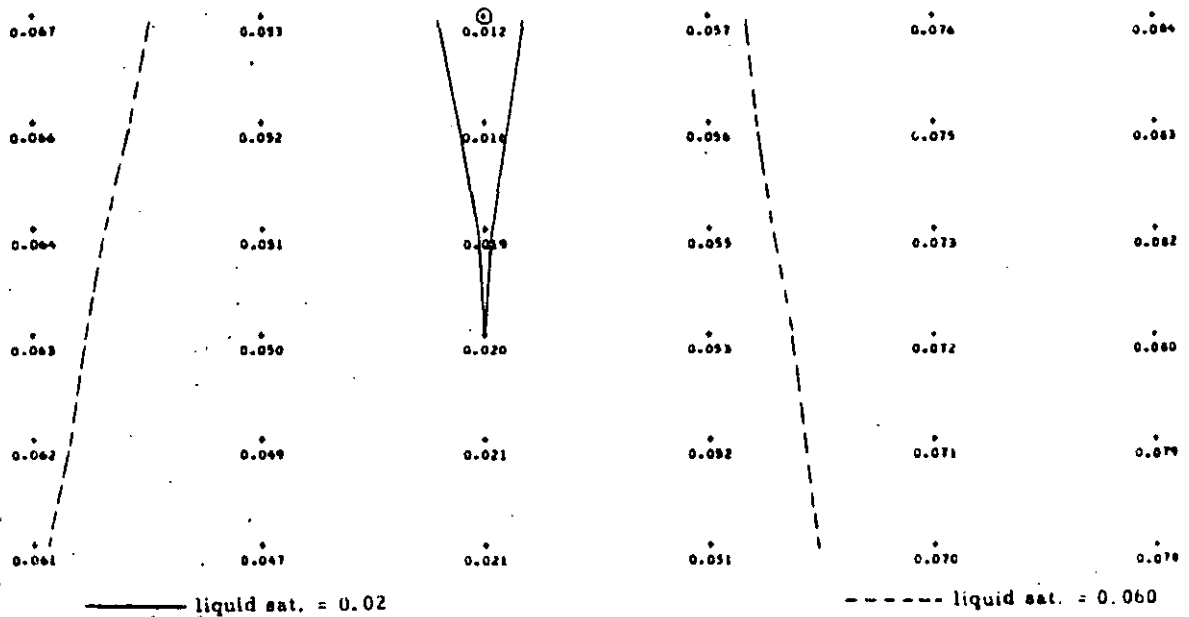


Fig. 8 - Liquid phase saturation distribution where mass fraction produced = 0.37 for a cross-sectional formulation of a reservoir having permeability = 0.10 darcies, porosity = 0.35, initial pressure = 650 psia, and initial liquid phase saturation = 0.10.

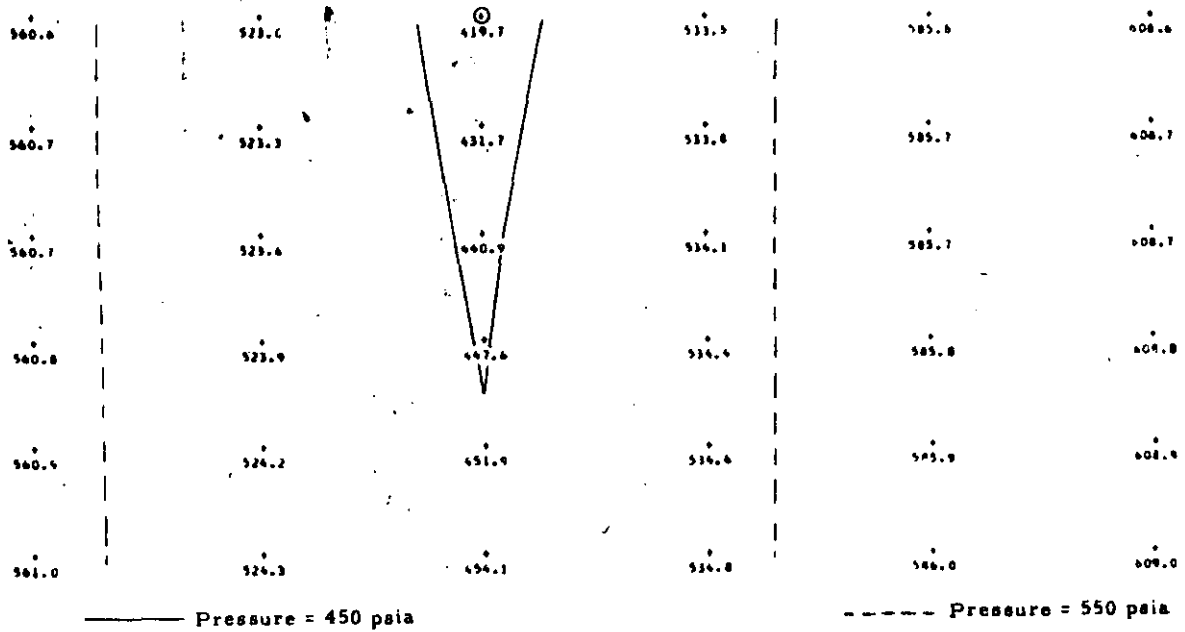


Fig. 3A - Pressure distribution where mass fraction produced = 0.37 for a cross-sectional formulation of a reservoir having permeability = 0.10 darcies, porosity = 0.35, initial pressure = 650 psia, and initial liquid phase saturation = 0.10.

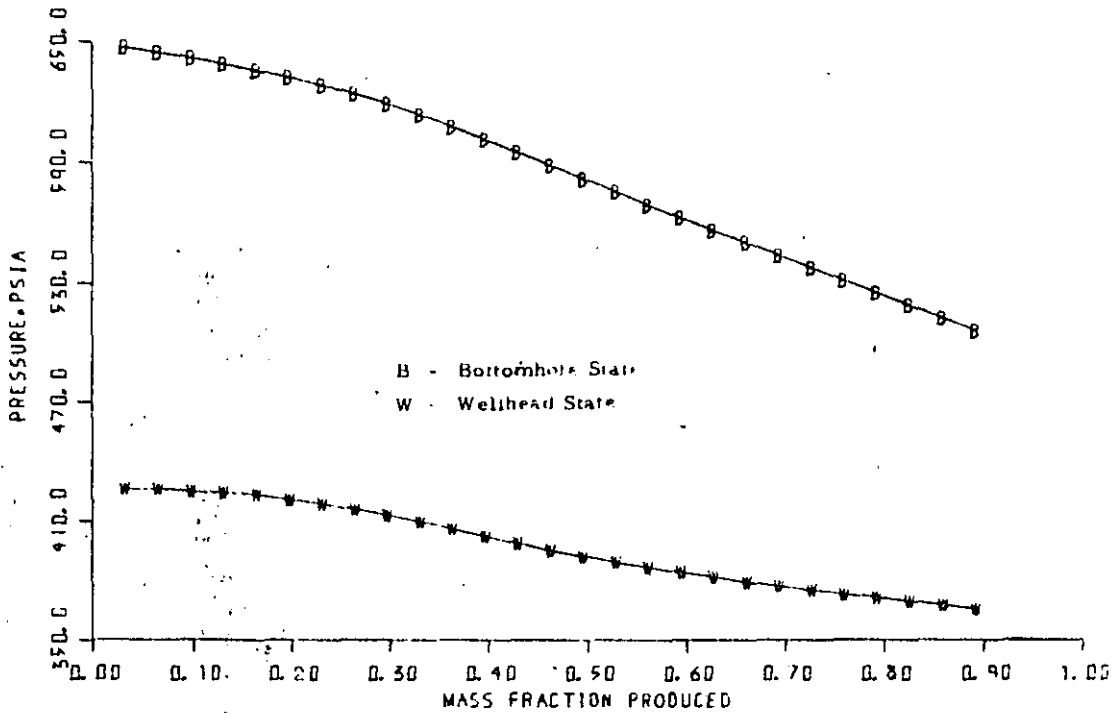


Fig. 3 - Pressure vs. mass fraction produced for an areal formulation of a reservoir having permeability = 1.0 darcies, porosity = 0.05, initial pressure = 650 psia, and initial liquid phase saturation = 0.10.

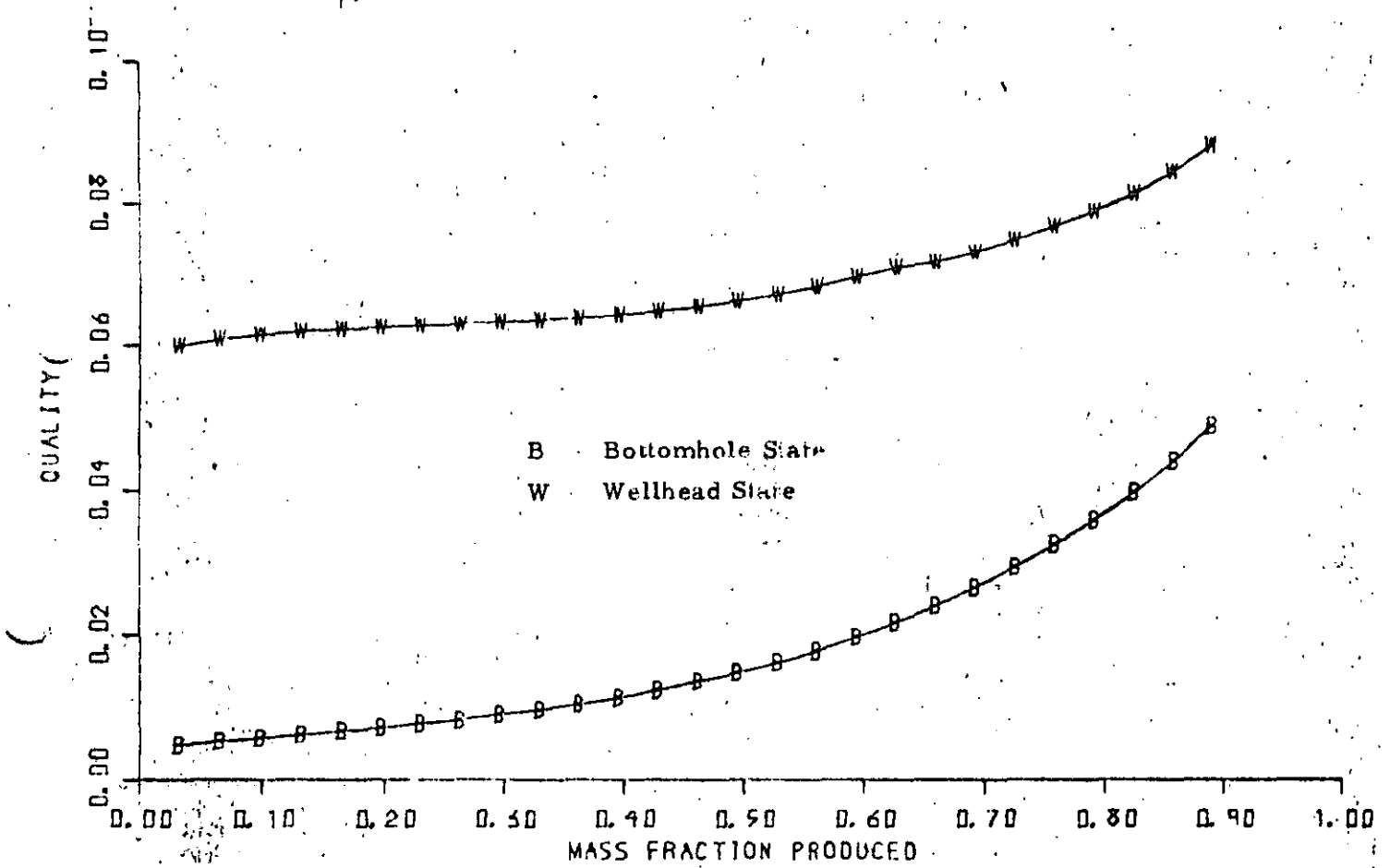


Fig. 9A - Quality vs mass fraction produced for an areal formulation of a reservoir having permeability = 1.0 darcies, porosity = 0.05, initial pressure = 650 psia, and initial liquid phase saturation = 0.80.

SPE 7479

# PRESSURE TRANSIENT ANALYSIS FOR TWO-PHASE (LIQUID WATER/STEAM) GEOTHERMAL RESERVOIRS

by S. K. Garg, Systems, Science and Software

Copyright 1978, American Institute of Mining, Metallurgical, and Petroleum Engineers, Inc.

This paper was presented at the 53rd Annual Fall Technical Conference and Exhibition of the Society of Petroleum Engineers of AIME, held in Houston, Texas, Oct. 1-3, 1978. The material is subject to correction by the author. Permission to copy is restricted to an abstract of not more than 300 words. Write: 6200 N. Central Expy., Dallas, Texas 75206.

### ABSTRACT

A new diffusivity equation for two-phase (liquid water/steam) flow in geothermal reservoirs is derived. The geothermal reservoir may either be initially two-phase or may evolve into a two-phase system during production. Solutions of the diffusivity equation for a continuous line source are presented; the solutions imply that the plot of bottomhole pressure versus  $\log_{10}t$  ( $t$  = time) should be a straight line. The slope of the straight line is inversely proportional to the total kinematic mobility (defined in the text). Comparison of the theory with a limited number of computer simulated drawdown histories shows excellent agreement.

### INTRODUCTION

In petroleum engineering and groundwater hydrology, well tests are routinely conducted to diagnose the well's condition and to estimate formation properties. Analysis of well test data may be made to yield quantitative information regarding (1) formation permeability, storativity and porosity, (2) the presence of barriers and leaky boundaries, (3) the condition of the well (i.e., damaged or stimulated), (4) the presence of major fractures close to the well, and (5) the mean formation pressure. Well testing procedures (and the quality of information obtained) depend on the age of the well. During temporary completion, testing involves producing the reservoir using a temporary plugging system (e.g., Drill Stem Testing); and the estimates obtained for the formation parameters are not very accurate. After completion, testing is usually performed in the hydraulic mode. In hydraulic testing, one or more wells are produced at controlled rates and changes in pressure within the producing well itself or nearby observation wells (interference tests) are monitored.

A major concern of well testing is the interpretation of pressure transient data. Much of the existing literature (see Matthews and Russell<sup>1</sup> and Ramey<sup>2</sup> for reviews) deals with isothermal single-phase (water/oil) and isothermal two-phase (oil with gas in solution, free gas) systems. There is, in general, a lack of a

methodology for the analysis of nonisothermal reservoir systems, either single or two-phase (liquid water/steam). Geothermal reservoirs commonly involve nonisothermal two-phase (water/steam) flow during well testing. In this paper, we present a theoretical framework for analyzing multiphase pressure transient data in geothermal systems.

### TWO-PHASE (LIQUID WATER/STEAM) FLOW IN GEOTHERMAL SYSTEMS

We consider a fully penetrating well located in an infinite reservoir of thickness  $H$ . We will neglect any variations in either formation or fluid properties in the vertical direction (this is a common assumption in pressure transient analysis). The geothermal system may either be two-phase prior to production, or may evolve into a two-phase system as a result of fluid production. In the latter case, a boiling front will propagate outwards from the wellbore. The boiling front may be treated as a constant pressure boundary ( $p$  = saturation pressure corresponding to the local reservoir temperature).

For the sake of simplicity, let us consider a reservoir which is initially two-phase everywhere. Furthermore, it is convenient to assume that the pressure (and hence temperature) is uniform throughout the system. In radial geometry, the pressure response is governed by the following diffusivity equation (see Appendix for a derivation of equation (1)):

$$\frac{\partial p}{\partial t} - \frac{(k/v)_T}{\phi \rho C_T} \left[ \frac{1}{r} \frac{\partial p}{\partial r} + \frac{\partial^2 p}{\partial r^2} \right] = 0 \quad \dots \quad (1)$$

We are interested in solutions of equation (1) for the case of flow into a centrally located well at a constant mass rate of production  $M$ . Mathematically, we have at  $r = r_w$

$$r \frac{\partial p}{\partial r} \Big|_{r=r_w} = - \frac{M}{2\pi H (k/v)_T} \quad \dots \quad (2)$$

For the sake of mathematical convenience, the boundary condition at  $r=r_w$  is replaced by the "line source"

approximation, i.e.,

$$\lim_{r \rightarrow 0} r \frac{\partial p}{\partial r} = - \frac{M}{2\pi H} (k/v)_T \dots \dots \dots 31 \quad (3)$$

The "line source" boundary condition yields identical results (from a practical viewpoint) with those obtained with the original condition.<sup>1,3</sup> We also require that initially (t=0) the reservoir is at a uniform pressure  $p_1$ , and that at  $r=\infty$  (for all t) we have

$$\lim_{r \rightarrow \infty} p(r,t) = p_1 \dots \dots \dots (4)$$

The solution for equation (1) subject to the boundary conditions (3) and (4) can be written as follows<sup>4</sup>

$$p(r,t) = p_1 + \frac{M}{4\pi H (k/v)_T} E_1 \left\{ - \frac{r^2 \phi \rho C_T}{4t (k/v)_T} \right\} \dots \dots \dots (5)$$

Equation (5) implies that the pressure at the well-bottom  $p_w(t)$  is

$$p_w(t) = p_1 + \frac{M}{4\pi H (k/v)_T} E_1 \left[ - \frac{r_w^2 \phi \rho C_T}{4t (k/v)_T} \right] \dots \dots \dots (6)$$

For  $[4t (k/v)_T / \phi r_w^2 \rho C_T] > 100$ , equation (6) yields the approximate solution:

$$p_w(t) = p_1 - \frac{1.15 M}{2\pi H (k/v)_T} \left\{ \log_{10} \left[ \frac{t (k/v)_T}{\phi r_w^2 \rho C_T} \right] + 0.351 \right\} \dots \dots \dots (7)$$

Equation (7) implies that a plot of  $p_w$  versus  $\log_{10} t$  should be a straight line. Let  $m$  be the slope of this straight line; then we have

$$(k/v)_T = \frac{1.15 M}{2\pi H m} \dots \dots \dots (8)$$

Substituting from equation (8) into equation (7), we obtain for compressibility  $C_T$

$$\frac{1}{C_T} = \frac{\phi r_w^2 \rho}{t (k/v)_T} \text{Antilog}_{10} \left[ \frac{p_1 - p_w(t)}{m} - 0.351 \right] \dots \dots \dots (9)$$

**PROPAGATING FLASH-FRONT**

Theoretical considerations for the case when a flash front propagates into an initially single-phase reservoir are much more complex than those outlined above for the purely two-phase case. In this instance, the reservoir is two-phase for  $r < R$  ( $R = R(t)$  denotes the location of the flash-front) and is single phase for  $r > R$ . The flow behavior in these two regimes is governed by

$$\frac{\partial p_j}{\partial t} - \left[ \frac{(k/v)_T}{\phi \rho C_T} \right]_j \frac{1}{r} \frac{\partial}{\partial r} \left[ r \frac{\partial p_j}{\partial r} \right] = 0 \dots \dots \dots (10)$$

where  $j=1$  and 2 denote the two-phase and single-phase regions, respectively. The definitions for the various quantities in equation (10) for the two-phase region ( $j=1$ ) have already been given. In the single-phase region ( $j=2$ ), we have:

$$[(k/v)_T]_2 = k \rho_L / \mu_L$$

$$\rho_2 = \rho_L$$

$$(C_T)_2 = ((1-\phi)/\phi) C_m + C_f$$

Note that with the above definitions, equation (10) (in the single-phase region) reduces to the usual diffusivity equation for the isothermal flow of a liquid of small and constant compressibility.

We will assume that the reservoir is initially at a uniform pressure  $p_1$  and temperature  $T_1$ . We will, furthermore, require the fluid flow to be isothermal in the single-phase region ( $r > R$ ); in practice, this implies no severe restriction as temperature changes in single-phase flow are usually very small. The boundary conditions at the wellbore and at infinity are:

$$\lim_{r \rightarrow 0} r \frac{\partial p_1}{\partial r} = - \frac{M}{2\pi H [(k/v)_T]_1} \dots \dots \dots (11a)$$

$$\lim_{r \rightarrow \infty} p_2(r,t) = p_1 \dots \dots \dots (11b)$$

In addition to the boundary conditions (11), we need to satisfy continuity conditions on mass flow and pressure at the flash-front ( $r=R$ ). Mathematically, we have at  $r=R$ :

$$[(k/v)_T \frac{\partial p}{\partial r}]_1 = [(k/v)_T \frac{\partial p}{\partial r}]_2 \dots \dots \dots (12a)$$

$$p_1 = p_2 = p_s(T_1) \dots \dots \dots (12b)$$

To develop a solution for equations (10) subject to the boundary conditions (11) and (12), we note that these equations are similar to the equations for melting and freezing with cylindrical symmetry presented by Carslaw and Jaeger.<sup>4</sup> The solution for the present case can, therefore, be obtained by following the general approach of Carslaw and Jaeger. We have thus:

$$0 < r < R: p = p_s + \frac{M}{4\pi H [(k/v)_T]_1} \left[ E_1 \left( - \frac{r^2 \left[ \frac{\phi \rho C_T}{(k/v)_T} \right]_1}{4t} \right) - E_1(-\lambda^2) \right] \dots \dots \dots (13a)$$

$$r > R: p = p_1 + \frac{p_s - p_1}{E_1(-\lambda^2 [(k/v)_T / \phi \rho C_T]_1 / [(k/v)_T / \phi \rho C_T]_2)} \times E_1 \left( - \frac{r^2 \left[ \frac{\phi \rho C_T}{(k/v)_T} \right]_2}{4t} \right) \dots \dots \dots (13b)$$

SPE 7479

where

$$R = 2\lambda \left[ \left\{ \frac{(k/v)_T}{\phi \rho C_T} \right\}_1 t \right]^{1/2} \dots \dots \dots (13c)$$

and  $\lambda$  is the root of

$$\begin{aligned} & \left[ \frac{(k/v)_T}{\phi \rho C_T} \right]_2 \frac{p_s - p_i}{Ei(-\lambda^2 \left\{ \frac{(k/v)_T}{\phi \rho C_T} \right\}_1 / \left\{ \frac{(k/v)_T}{\phi \rho C_T} \right\}_2)} \\ & \times \exp \left( -\lambda^2 \left\{ \frac{(k/v)_T}{\phi \rho C_T} \right\}_1 / \left\{ \frac{(k/v)_T}{\phi \rho C_T} \right\}_2 \right) \\ & = \frac{M}{4\pi H} \exp(-\lambda^2) \dots \dots \dots (13d) \end{aligned}$$

Equation (13a) yields the following expression for well-bottom pressure  $p_w(t)$

$$p_w(t) = p_s + \frac{M}{4\pi H \left[ \frac{(k/v)_T}{\phi \rho C_T} \right]_1} \left[ Ei \left( -\frac{r_w^2}{4t} \left[ \frac{\phi \rho C_T}{(k/v)_T} \right]_1 \right) - Ei(-\lambda^2) \right] \dots \dots \dots (14)$$

For  $4t \left[ \frac{(k/v)_T}{\phi \rho C_T} \right]_1 / r_w^2 > 100$ , equation (14) can be approximated as follows:

$$\begin{aligned} p_w(t) = p_s - \frac{M Ei(-\lambda^2)}{4\pi H \left[ \frac{(k/v)_T}{\phi \rho C_T} \right]_1} \\ - \frac{1.15 M}{2\pi H \left[ \frac{(k/v)_T}{\phi \rho C_T} \right]_1} \left\{ \log_{10} \left[ t \frac{\left[ \frac{(k/v)_T}{\phi \rho C_T} \right]_1}{r_w^2} \right] \right. \\ \left. + 0.351 \right\} \dots \dots \dots (15) \end{aligned}$$

Equation (15), like equation (7), implies that a plot of  $p_w$  versus  $\log_{10} t$  should be a straight line and that  $\left[ \frac{(k/v)_T}{\phi \rho C_T} \right]_1$  is given by equation (8).

NUMERICAL RESULTS

In order to test the validity of the preceding theory, the Systems, Science and Software (S<sup>3</sup>) reservoir simulator MUSHRM<sup>5</sup> was exercised in one-dimensional radial configuration to generate a series of drawdown histories. All of the cases described below were simulated using a 50 zone ( $\Delta r_1 = \Delta r_2 = \dots = \Delta r_{11} = 1m$  (3.281 feet);  $\Delta r_{12} = 1.2 \Delta r_{11}$ ,  $\Delta r_{13} = 1.2 \Delta r_{12}$ , ...,  $\Delta r_{50} = 1.2 \Delta r_{49}$ ) radial grid.

The reservoir rock is assumed to be a sandstone with the following properties (unless otherwise indicated):

- $\rho_R = 2.65 \cdot 10^3 \text{ kg/m}^3$  (165.4 lbm/ft<sup>3</sup>)
- $\phi = 0.2$

- $C_m = 0 \text{ MPa}^{-1}$  (0 psi<sup>-1</sup>)
- $K_R = 5.25 \text{ W/m.K}$  (3.03 Btu/h.ft<sup>2</sup>.°F/ft)
- $C_R = 1 \text{ kJ/kg.K}$  (0.239 Btu/lbm °F)
- $k = 0.1 \mu\text{m}^2$  ( $\sim 0.1$  darcy)
- $S_{gr} = 0.3$
- $S_{gr} = 0.05$ .

Relative permeabilities  $R_L$  and  $R_G$  are represented by the Corey equations and the mixture (rock-liquid-vapor) thermal conductivity is approximated by Budiansky's formula.<sup>5</sup> The mass withdrawal rate is assumed to be 0.14 kg/s.m (0.094 lbm/s.ft.).

In the numerical examples discussed here, the effect of mass withdrawal is represented by a volumetric sink term in the well-block (radial extent  $r = 0$  to  $r = \Delta r_1$ ). For purposes of comparison with the analytical results presented earlier, it is necessary to define an equivalent radius  $r_w$  at which the calculated well-block pressure is equal to the actual flowing pressure due to a continuous line source/sink.

In the numerical simulation of reservoir behavior, it is often necessary to employ well-blocks (i.e., a grid block containing a well) with dimensions much larger than the wellbore radius. Naturally, the pressure calculated for the well-block will be, in general, different from the actual flowing bottomhole pressure. Van Poolen, et al.<sup>6</sup> stated that the calculated pressure for a well-block should be the average pressure in the portion of the reservoir represented by the block. Assuming steady-state single-phase flow in the well-block (but not in the reservoir as a whole), this implies that the calculated well-block pressure should be equal to the actual flowing pressure at a radius  $r_w$ .

$$\ln \frac{r_w}{r_0} = \frac{R^2 \ln(R/r_0)}{R^2 - r_0^2} - \frac{1}{2} \dots \dots \dots (16a)$$

where  $r_0$  is the actual well radius and  $R$  is the radius of the grid block. For  $R \gg r_0$ , equation (16a) simplifies to

$$\begin{aligned} r_w &= R \exp(-1/2) \dots \dots \dots (16b) \\ &\sim 0.6065 R \end{aligned}$$

Equations (16a) and (16b), strictly speaking, hold only for a well located in the center of a radial grid block. For rectangular grid blocks (with dimensions  $\Delta x, \Delta y$ ), equation (16b) is usually replaced by the following expression

$$\frac{r_w}{\sqrt{\Delta x \Delta y}} = \frac{0.6065}{\sqrt{\pi}} \dots \dots \dots (17)$$

Assuming  $\Delta x = \Delta y$ , equation (17) yields

$$\frac{r_w}{\Delta x} = 0.342.$$

33

Peaceman<sup>7</sup> examined the grid pressures obtained in the numerical solution of steady incompressible single-phase flow into a single well located in the center of a square grid block ( $\Delta x = \Delta y$ ) and concluded that the well-block pressure should be equal to the actual flowing pressure at a radius of  $0.2 \Delta x$  (and not at the radius given by equation (17)).

In an attempt to evaluate the significance of Peaceman's results for numerical simulation, Garg, et al.<sup>8</sup> analyzed the numerical solution of steady incompressible single-phase flow into a single well located in both radial and rectangular grid blocks. It is found that the equivalent radius depends, among other things, on the shape of the grid block (radial or rectangular) and the type of mesh (uniform or stretch) employed. Thus, for example, use of uniform radial mesh yields  $r_w/R \approx 0.5615$  in the limit  $N \rightarrow \infty$ , where  $N$  denotes the number of grid blocks.

Garg, et al.<sup>8</sup> also compared the numerical solution for transient, slightly compressible (water) single-phase flow into a single well with the line-source solution for the diffusivity equation (see, e.g., Matthews and Russell<sup>1</sup>). It was concluded that the equivalent radius (i.e., the radius at which the actual flowing pressure is equal to the calculated well-block pressure) is approximated by  $0.56 R$ . In this work, we will, therefore, assume that  $r_w$  in transient single-phase flow (and also approximately in transient two-phase flow) is given by  $0.56 R$ .

Figures 1-5 show five examples for the case when the reservoir initially boiling everywhere, was produced at a constant rate. As can be seen, the drawdown data closely fit a straight line; furthermore, the values of  $(k/v)_T$  computed from the slope of the straight line are in excellent agreement with the actual values in the well-blocks (see Tables 1-5 for the actual values). Note that the actual values (Tables 1-5) vary over a range; this variation is the result of slow changes (except at very early times not considered in drawing the straight line) in steam saturation in the computational well-block as a result of continued production. Figure 3 (drawdown history c) and Table 3 present an especially interesting case; in this case the liquid, initially immobile, becomes mobile for  $t > \sim 2 \cdot 10^5$ s due to condensation in the well-block. The condensation is caused by a drop in pressure (and hence temperature); in drawing the straight line the pressure data for  $t > \sim 2 \cdot 10^5$ s was ignored. If the computation had been carried for times sufficiently greater than  $t > 2 \cdot 10^5$ s, one would see another straight line segment (with a different slope).

Table 6 compares the compressibility  $C_T$  values inferred from the slope of the straight line and equation (9) with the actual values. The agreement is quite good for Cases b, c and d. In Cases a and e, the inferred values are quite a bit larger than the actual values; this disagreement is not really surprising in view of the extremely large changes in  $(k/v)_T$  at very early times (see Tables 1 and 5). Large values of  $(k/v)_T$  at very early times lead to relatively small pressure drops compared to those implied by the straight line. Stated somewhat differently, at early times, equation (7) with constant  $(k/v)_T$  cannot be used to calculate the well-block pressure in Cases a and e.

Figures 6 and 7 show two additional drawdown histories generated by MUSHRM. In these examples, the reservoir was initially single-phase (liquid) everywhere. In the case shown in Figure 6, a flash-front starts propagating outward from the wellbore at  $t \sim 0$ ; it takes, however a finite time for conditions to stabilize in the two-phase region. For  $t > 5 \cdot 10^5$ s the data lie on a straight line; and the kinematic mobility calculated from the slope of this straight line agrees quite well with the actual range of values. Figure 7 presents a more interesting case; in this instance the liquid water does not start flashing at the instant the production starts. Thus, we have a short time of single-phase flow followed by a propagating flash-front. The two-phase part of the drawdown curve has a relatively long flat part; this part of the curve is associated with boiling only in the computational well-block. Since the flow behavior in the two-phase region is primarily governed by the location of the flash-front, it follows that a failure to adequately resolve the location of the flash-front in numerical simulations (as it happens when the two-phase flow is restricted to one or two computational zones) would lead to physically meaningless results. In other words, the flat part of the curve in Figure 7 is a purely numerical phenomenon and has no physical significance. A straight line is again seen to fit the late-time data once again the computed value of  $(k/v)_T$  is in good agreement with the actual range of values. We have also examined the numerical solutions (Figures 6 and 7) for flash-front velocities; the flash-front position, as a function of time is given by (within numerical precision)  $R(t) = A t^{1/2}$  where  $A$  is constant. The latter observation is in agreement with equation (13c).

#### CONCLUDING REMARKS

The analytical solutions for two-phase flow discussed in the preceding sections provide a potentially powerful tool for the analysis of pressure transient data from multiphase geothermal systems. Determination of the total kinematic mobility only requires the measurement of mass flow rate  $M$  and the bottomhole pressures  $p_w$ . The mass flow rate  $M$  can be measured at the well-head provided there is no loss of the produced fluid to the non-producing formations as the fluid travels through the wellbore to the well-head. Practical techniques exist for measuring the needed variables. It should be noted that the present analysis does not require separate measurements for liquid and vapor phase mass flow rates. Such data, if available, may be combined with the analysis of the preceding sections to yield additional information regarding relative permeabilities, etc.

#### NOMENCLATURE

- $C_f$  = isothermal liquid compressibility
- $C_m$  = formation compressibility
- $C_R$  = heat capacity of the rock matrix
- $C_T$  = total compressibility, equation (A.12b)
- $h$  = enthalpy of liquid/vapor mixture

$$= (1-Q) h_l + Q h_g$$

$$h_l(h_g) = \text{liquid (vapor) enthalpy}$$

$$h_{gl} = \text{heat of vaporization} = h_g - h_l$$

$h_R$  = enthalpy of rock matrix  
 $H$  = formation thickness  
 $k$  = absolute permeability  
 $K_R$  = thermal conductivity of the rock grain  
 $m$  = slope of  $p_w$  versus  $\log_{10} t$  straight line  
 $M$  = mass production rate  
 $p$  = pressure  
 $p_i$  = initial reservoir pressure  
 $p_s(T_i)$  = saturation pressure at  $T = T_i$   
 $p_w$  = well-bottom pressure  
 $Q$  = steam quality =  $S \rho_g / \rho$   
 $r$  = radius  
 $r_w$  = wellbore radius  
 $R(t)$  = instantaneous position of the flash-front  
 $R_L(R_g)$  = relative liquid (vapor) permeability  
 $S$  = vapor volume fraction  
 $S_{lr}(S_{gr})$  = residual liquid (vapor) saturation  
 $t$  = time  
 $(k/v)_g$  = kinematic mobility for the vapor =  
 $k R_g \rho_g / \mu_g$   
 $(k/v)_L$  = kinematic mobility for the liquid =  
 $k R_L \rho_L / \mu_L$   
 $(k/v)_T$  = total kinematic mobility =  
 $(k/v)_L + (k/v)_g$   
 $\mu_L(\mu_g)$  = liquid (vapor) dynamic viscosity  
 $\rho$  = mixture (liquid and vapor) density =  
 $(1-S) \rho_L + S \rho_g$   
 $\rho_L(\rho_g)$  = liquid (vapor) density  
 $\rho_R$  = rock grain density  
 $\phi$  = porosity

#### ACKNOWLEDGMENTS

This work was performed under Systems, Science and Software IR&D research project No. 93102-06. I would like to thank my colleagues Dr. T. R. Blake, Mr. J. W. Pritchett, Dr. M. H. Rice and Dr. T. D. Riney for many helpful discussions.

#### REFERENCES

1. Matthews, C. S. and Russell, D. G.: Pressure Buildup and Flow Tests in Wells, Society of Petroleum Engineers of AIME, Monograph No. 1, Dallas, Texas (1967).

2. Ramey, H. J., Jr.: "Pressure Transient Analysis for Geothermal Wells", Proceedings Second United Nations Symposium on the Development and Use of Geothermal Resources, San Francisco, California, Volume 3 (May 1975), 1749-1757.
3. Mueller, T. D. and Witherspoon, P. A.: "Pressure Interference Effects within Reservoirs and Aquifers", Journal of Petroleum Technology (April 1965), 471-474.
4. Carslaw, H. S. and Jaeger, J. C.: Conduction of Heat in Solids, Oxford University Press, London, 2nd Edition (1959), 294-296.
5. Garg, S. K., Pritchett, J. W., Rice, M. H. and Riney, T. D.: "U.S. Gulf Coast Geopressured Geothermal Reservoir Simulation", Systems, Science and Software, La Jolla, California, Report SSS-R-77-3147 (1977).
6. Van Poolen, H. K., Breitenbach, E. A. and Thurnau, D. H.: "Treatment of Individual Wells and Grids in Reservoir Modeling", Journal of Petroleum Technology (December 1968), 341-346.
7. Peaceman, D. W.: "Interpretation of Well-Block Pressures in Numerical Reservoir Simulation", paper SPE 6893 presented at Society of Petroleum Engineers 52nd Annual Fall Meeting, Denver, Colorado, October 9-12, 1977.
8. Garg, S. K., Pritchett, J. W., Brownell, D. H., Jr. and Riney, T. D.: "U.S. Gulf Coast Geopressured Geothermal Reservoir Simulation - Year 2", Systems Science and Software, La Jolla, California, Report SSS-R-78-3639 (1978).
9. Donaldson, I. G.: "The Flow of Steam Water Mixtures through Permeable Beds: A Simple Simulation of a Natural Undisturbed Hydrothermal Region", New Zealand Journal of Science, Volume 11 (1968), 3-23.
10. Mercer, J. W., Jr., Faust, C. and Pinder, G. F.: "Geothermal Reservoir Simulation", Proceedings NSF/RANN Conference on Research for the Development of Geothermal Energy Resources, Jet Propulsion Laboratory/California Institute of Technology, Pasadena, California (1974), 256-267.
11. Brownell, D. H., Jr., Garg, S. K. and Pritchett, J. W.: "Governing Equations for Geothermal Reservoirs", Water Resources Research, Volume 13 (1977), 929-934.
12. Garg, S. K. and Pritchett, J. W.: "On Pressure-Work, Viscous Dissipation and the Energy Balance Relation for Geothermal Reservoirs", Advances in Water Resources, Volume 1 (1977), 41-47.
13. Moench, A. F. and Atkinson, P. G.: "Transient Pressure Analysis in Geothermal Steam Reservoirs with an Immobile Vaporizing Liquid Phase - Summary Report", Proceedings Third Stanford Workshop on Geothermal Reservoir Engineering, Stanford, California (1977), 64-69.



**APPENDIX: DERIVATION OF DIFFUSIVITY EQUATION FOR TWO-PHASE (LIQUID WATER/STEAM) FLOW IN POROUS MEDIA**

The balance equations for two-phase flow in porous media have previously been discussed by Donaldson,<sup>9</sup> Mercer, et al.,<sup>10</sup> Brownell, et al.<sup>11</sup> and Garg and Pritchett.<sup>12</sup> For the present application, the most general form of the balance laws will not be required. In particular, we will assume that (1) the rock porosity depends only upon the fluid pressure, (2) the rock matrix, the liquid and the vapor are in local thermal equilibrium and that heat conduction is negligible, (3) the liquid and the vapor are in local pressure equilibrium such that the capillary pressure is negligible, and (4) the fluid flow is governed by Darcy's law. The second assumption implies that we need consider only the mixture (rock, liquid, vapor) energy balance.

With these assumptions, the balance equations for mass and energy in radial geometry can be written as follows<sup>12</sup>

Mass (Liquid and Vapor)

$$\frac{\partial}{\partial t} (\phi \rho) - \frac{1}{r} \frac{\partial}{\partial r} r \left[ (k/v)_T \frac{\partial p}{\partial r} \right] = 0 \quad \dots \quad (A.1)$$

Energy (Rock, Liquid and Vapor)

$$\frac{\partial}{\partial t} [(1-\phi)\rho_R h_R + \phi \rho h - \phi p] - \frac{1}{r} \frac{\partial}{\partial r} \left\{ r \left[ (k/v)_L h_L + (k/v)_G h_G \right] \frac{\partial p}{\partial r} \right\} = 0 \quad \dots \quad (A.2)$$

The first term in equation (A.1) can be expanded and rewritten in the following form:

$$\frac{\partial}{\partial t} (\phi \rho) = \rho \frac{\partial \phi}{\partial t} + \phi \left[ \left( \frac{\partial \rho}{\partial p} \right)_h \frac{\partial p}{\partial t} + \left( \frac{\partial \rho}{\partial h} \right)_p \frac{\partial h}{\partial t} \right]$$

On noting that<sup>5</sup>

$$\frac{\partial \phi}{\partial t} = (1-\phi) C_m \frac{\partial p}{\partial t} \quad \dots \quad (A.3)$$

we obtain

$$\frac{\partial (\phi \rho)}{\partial t} = \phi \rho \left\{ \left( \frac{1-\phi}{\phi} \right) C_m \frac{\partial p}{\partial t} + \frac{1}{\rho} \left( \frac{\partial \rho}{\partial p} \right)_h \frac{\partial p}{\partial t} + \frac{1}{\rho} \left( \frac{\partial \rho}{\partial h} \right)_p \frac{\partial h}{\partial t} \right\} \quad \dots \quad (A.4)$$

We will now proceed to express  $\partial h/\partial t$  in terms of  $\partial h/\partial r$ ,  $\partial p/\partial t$  and  $\partial p/\partial r$ .

For geothermal applications, it will suffice to assume that

$$h_R = c_R T \quad \dots \quad (A.5a)$$

where T is the common local temperature of the rock matrix and the pore fluids. Under the steam dome (i.e., two-phase regime), temperature T is a unique function of fluid pressure p.

$$T = T(p) \quad \dots \quad (A.5b)$$

Combining equations (A.5a) and (A.5b) and differentiating w.r.t. t, we have

$$\frac{\partial h_R}{\partial t} = c_R \frac{dT}{dp} \frac{\partial p}{\partial t} \quad \dots \quad (A.6)$$

Substituting for  $\partial/\partial t$  ( $\phi \rho$ ) from equation (A.1), for  $\partial \phi/\partial t$  from equation (A.3), and for  $\partial h_R/\partial t$  from equation (A.6) into equation (A.2), we obtain:

$$\left\{ -(1-\phi) C_m \rho_R h_R + (1-\phi) \rho_R c_R \frac{dT}{dp} - \phi - (1-\phi) C_m p \right\} \times \frac{\partial p}{\partial t} + \phi \rho \frac{\partial h}{\partial t} = \left[ (k/v)_L h_L + (k/v)_G h_G - (k/v)_T h \right] \frac{1}{r} \frac{\partial}{\partial r} \left( r \frac{\partial p}{\partial r} \right) + \frac{\partial p}{\partial r} \left\{ \frac{\partial}{\partial r} \left[ (k/v)_L h_L + (k/v)_G h_G - (k/v)_T h \right] + (k/v)_T \frac{\partial h}{\partial r} \right\} \quad \dots \quad (A.7)$$

We next note that in practical geothermal applications, the last two terms in the brackets on the left hand side of equation (A.7) ( $\phi$  and  $(1-\phi) C_m p$ ) are liable to be negligible compared to the first two terms. Also, we have

$$\begin{aligned} h_L - h &= -Q h_{gL} \\ h_G - h &= (1-Q) h_{gL} \end{aligned} \quad \dots \quad (A.8)$$

Substitution of equation (A.8) in equation (A.7) yields:

$$\begin{aligned} \phi \rho \frac{\partial h}{\partial t} &= (1-\phi) \rho_R h_R \left[ C_m - \frac{1}{T} \frac{dT}{dp} \right] \frac{\partial p}{\partial t} \\ &+ h_{gL} (k/v)_T \left[ \frac{(k/v)_G}{(k/v)_T} - Q \right] \frac{1}{r} \frac{\partial}{\partial r} \left( r \frac{\partial p}{\partial r} \right) \\ &+ \frac{\partial p}{\partial r} \left\{ \frac{\partial}{\partial r} \left[ h_{gL} (k/v)_T \left( \frac{(k/v)_G}{(k/v)_T} - Q \right) \right] + (k/v)_T \frac{\partial h}{\partial r} \right\} \quad \dots \quad (A.9) \end{aligned}$$

Combining equations (A.1), (A.4) and (A.9) we obtain:

$$\begin{aligned} & \phi \rho \left\{ \frac{1-\phi}{\phi} \right\} C_m + \frac{1}{\rho} \left( \frac{\partial \rho}{\partial p} \right)_h + \frac{1}{\rho^2} \left( \frac{\partial \rho}{\partial h} \right)_p \left( \frac{1-\phi}{\phi} \right) \rho_R h_R \left\{ C_m \right. \\ & \left. - \frac{1}{T} \frac{dT}{dp} \right\} \left\{ \frac{\partial p}{\partial t} - (k/v)_T \left[ 1 \right. \right. \\ & \left. \left. - \frac{1}{\rho} \left( \frac{\partial \rho}{\partial h} \right)_p h_{g\ell} \left\{ \frac{(k/v)_g}{(k/v)_T} - Q \right\} \right] \frac{1}{r} \frac{\partial}{\partial r} \left( r \frac{\partial p}{\partial r} \right) \right. \\ & \left. + \frac{\partial p}{\partial r} \left\{ - \frac{\partial}{\partial r} (k/v)_T + \frac{1}{\rho} \left( \frac{\partial \rho}{\partial h} \right)_p (k/v)_T \frac{\partial h}{\partial r} \right. \right. \\ & \left. \left. + \frac{1}{\rho} \left( \frac{\partial \rho}{\partial h} \right)_p \frac{\partial}{\partial r} \left[ h_{g\ell} (k/v)_T \left( \frac{(k/v)_g}{(k/v)_T} - Q \right) \right] \right\} \right\} = 0 \quad \dots \dots \dots (A.10) \end{aligned}$$

An examination of the numerical solution for equations (A.1) and (A.2) with a constant rate of mass production (e.g., Cases 1-5 discussed elsewhere in this paper) reveals the following important points:

1. The total kinematic mobility  $(k/v)_T$  increases with increasing distance  $r$  from the wellbore.
2. In the vicinity of the wellbore, we have

$$\begin{aligned} & \left\{ (k/v)_T \left[ 1 - \frac{1}{\rho} \left( \frac{\partial \rho}{\partial h} \right)_p h_{g\ell} \left\{ \frac{(k/v)_g}{(k/v)_T} - Q \right\} \right] \frac{1}{r} \frac{\partial}{\partial r} \left( r \frac{\partial p}{\partial r} \right) \right\} \\ & \gg \left\{ \frac{\partial p}{\partial r} \left\{ - \frac{\partial}{\partial r} (k/v)_T + \frac{1}{\rho} \left( \frac{\partial \rho}{\partial h} \right)_p (k/v)_T \frac{\partial h}{\partial r} \right. \right. \right. \\ & \left. \left. + \frac{1}{\rho} \left( \frac{\partial \rho}{\partial h} \right)_p \frac{\partial}{\partial r} \left[ h_{g\ell} (k/v)_T \left( \frac{(k/v)_g}{(k/v)_T} - Q \right) \right] \right\} \right\} \quad \dots \dots \dots (A.11) \end{aligned}$$

This strong inequality does not, however, hold for radial distances greater than a few borehole radii.

3. Both the radial terms in equations (A.10) are maximum (in an absolute sense) near the wellbore, and fall off rapidly with increasing radial distance  $r$ .
4. The radial terms in equation (A.10) are of opposite signs.

We now replace equation (A.10) by the following diffusivity equation:

$$\phi \rho C_T \frac{\partial p}{\partial t} - (k/v)_T \frac{1}{r} \frac{\partial}{\partial r} \left( r \frac{\partial p}{\partial r} \right) = 0 \quad \dots \dots (A.12a)$$

where

$$\begin{aligned} C_T = & \left\{ \frac{1-\phi}{\phi} \right\} C_m + \frac{1}{\rho} \left( \frac{\partial \rho}{\partial p} \right)_h + \frac{1-\phi}{\phi} \frac{1}{\rho^2} \left( \frac{\partial \rho}{\partial h} \right)_p \rho_R h_R \left\{ C_m \right. \\ & \left. - \frac{1}{T} \frac{dT}{dp} \right\} \left\{ 1 - \frac{1}{\rho} \left( \frac{\partial \rho}{\partial h} \right)_p h_{g\ell} \left[ \frac{(k/v)_g}{(k/v)_T} - Q \right] \right\} \quad (A.12b) \end{aligned}$$

Note that  $(k/v)_T$  in equation (A.12a) represents the value of the total kinematic mobility in the vicinity of the borehole. The approximations involved in deriving equation (A.12a) (i.e., (1) neglecting the second radial term in equation (A.10) and (2) replacing  $(k/v)_T$  by its value near the wellbore) are strictly speaking valid only in the immediate neighborhood of the borehole. Even though equation (A.12a) is not expected to apply at large radii, its use should not cause large errors in the computed response since pressures change only very slowly at large radial distances from the borehole.

The diffusivity equation (A.12a) forms the basis for our analysis of two-phase flow in geothermal systems. Unlike in single-phase isothermal flow, the total compressibility  $C_T$  in two-phase flow (c.f., equation (A.12b)) has no simple interpretation; consequently its determination from well-tests, in the absence of data regarding rock thermomechanical properties and detailed knowledge regarding the thermodynamic state of the produced fluid, may have only limited practical utility.

We shall now briefly consider a geothermal steam reservoir with an immobile vaporizing liquid phase in the pores. In this case, we have

$$(k/v)_\ell = 0, \quad (k/v)_T = (k/v)_g = k_g \rho_g / \mu_g \quad (A.13)$$

where  $k_g = kR_g$ . Substituting from equation (A.13) into equation (A.12) and rearranging terms, we obtain:

$$\frac{\partial p}{\partial t} - \frac{k_g}{\phi \mu_g C_T} \frac{1}{r} \frac{\partial}{\partial r} \left( r \frac{\partial p}{\partial r} \right) = 0 \quad \dots \dots (A.14)$$

where

$$C_T = \frac{\rho C_T}{\rho_g} \quad \dots \dots \dots (A.15a)$$

$$\begin{aligned} C_T = & \left\{ \frac{1-\phi}{\phi} \right\} C_m + \frac{1}{\rho} \left( \frac{\partial \rho}{\partial p} \right)_h + \frac{1-\phi}{\phi} \frac{1}{\rho^2} \left( \frac{\partial \rho}{\partial h} \right)_p \rho_R h_R \left\{ C_m \right. \\ & \left. - \frac{1}{T} \frac{dT}{dp} \right\} \left\{ 1 - \frac{1}{\rho} \left( \frac{\partial \rho}{\partial h} \right)_p h_{g\ell} (1-Q) \right\} \quad (A.15b) \end{aligned}$$

We note that equation (A.14) is identical (albeit with a different definition for the total compressibility) to the diffusivity equation for isothermal single-phase reservoir systems; this fact provides the fundamental justification for the application of classical single-

phase procedures to determine the steam-phase permeability of a geothermal steam reservoir with an immobile vaporizing liquid phase (see, e.g., Moench and Atkinson<sup>13</sup>).

TABLE 1  
ACTUAL  $(k/v)_i$  ( $i = l, g, T$ ) AND VAPOR SATURATION (S) VALUES  
IN THE WELL-BLOCK FOR SIMULATED DRAWDOWN HISTORY (a)

Time s	Vapor Saturation (S)	$10^8 (k/v)_l$ s	$10^8 (k/v)_g$ s	$10^8 (k/v)_T$ s
0	0.050	79.85	0	79.85
0.576 $10^4$	0.163	37.26	0.22	37.48
0.1296 $10^5$	0.169	35.43	0.26	35.69
0.3456 $10^5$	0.175	34.00	0.29	34.29
0.7056 $10^5$	0.178	33.12	0.31	33.43
0.14256 $10^6$	0.181	32.36	0.33	32.69
0.35856 $10^6$	0.185	31.52	0.36	31.88
0.71856 $10^6$	0.187	30.96	0.37	31.33
0.100656 $10^7$	0.188	30.69	0.38	31.07

TABLE 2  
ACTUAL  $(k/v)_i$  ( $i = l, g, T$ ) AND VAPOR SATURATION (S) VALUES  
IN THE WELL-BLOCK FOR SIMULATED DRAWDOWN HISTORY (b)

Time s	Vapor Saturation (S)	$10^8 (k/v)_l$ s	$10^8 (k/v)_g$ s	$10^8 (k/v)_T$ s
0	0.350	6.71	3.48	10.19
0.504 $10^4$	0.400	3.59	4.90	8.49
0.1224 $10^5$	0.402	3.49	4.90	8.39
0.3384 $10^5$	0.404	3.41	4.88	8.29
0.6984 $10^5$	0.404	3.39	4.84	8.23
0.14184 $10^6$	0.405	3.37	4.79	8.16
0.35784 $10^6$	0.405	3.34	4.74	8.08
0.71784 $10^6$	0.406	3.30	4.71	8.01
0.100584 $10^7$	0.406	3.29	4.69	7.98

TABLE 3

ACTUAL  $(k/v)_i$  ( $i = \ell, g, T$ ) AND VAPOR SATURATION (S) VALUES  
IN THE WELL-BLOCK FOR SIMULATED DRAWDOWN HISTORY (c)

Time s	Vapor Saturation (S)	$10^8 (k/v)_\ell$ s	$10^8 (k/v)_g$ s	$10^8 (k/v)_T$ s
0	0.702	0	23.02	23.02
0.432 $10^4$	0.731	0	22.26	22.26
0.1152 $10^5$	0.734	0	22.13	22.13
0.3312 $10^5$	0.734	0	21.99	21.99
0.6912 $10^5$	0.729	0	21.89	21.89
0.14112 $10^6$	0.714	0	21.80	21.80
0.35712 $10^6$	0.662*	0*	19.12*	19.12*
0.71712 $10^6$	0.624	0.02	16.58	16.60
0.100512 $10^7$	0.623	0.02	16.53	16.55

\* Liquid slightly mobile.

TABLE 4

ACTUAL  $(k/v)_i$  ( $i = \ell, g, T$ ) AND VAPOR SATURATION (S) VALUES  
IN THE WELL-BLOCK FOR SIMULATED DRAWDOWN HISTORY (d)

Time s	Vapor Saturation (S)	$10^8 (k/v)_\ell$ s	$10^8 (k/v)_g$ s	$10^8 (k/v)_T$ s
0	0.160	35.38	0.10	35.48
0.720 $10^4$	0.298	10.84	0.96	11.80
0.144 $10^5$	0.301	10.47	0.97	11.44
0.360 $10^5$	0.305	10.02	0.99	11.01
0.720 $10^5$	0.308	9.68	1.01	10.69
0.144 $10^6$	0.309	9.58	1.00	10.58
0.360 $10^6$	0.312	9.27	1.00	10.27
0.720 $10^6$	0.314	9.00	1.01	10.01
0.1008 $10^7$	0.315	8.87	1.01	9.88

TABLE 5  
ACTUAL  $(k/v)_i$  ( $i = e, g, T$ ) AND VAPOR SATURATION (S) VALUES  
IN THE WELL-BLOCK FOR SIMULATED DRAWDOWN HISTORY (e)

Time s	Vapor Saturation (S)	$10^8 (k/v)_e$ s	$10^8 (k/v)_g$ s	$10^8 (k/v)_T$ s
0	0.050	74.49	0	74.49
0.720 $10^4$	0.236	19.21	0.45	19.66
0.144 $10^5$	0.241	18.50	0.47	18.97
0.360 $10^5$	0.246	17.62	0.50	18.12
0.720 $10^5$	0.250	16.94	0.53	17.47
0.144 $10^6$	0.254	16.42	0.54	16.96
0.360 $10^6$	0.256	16.01	0.56	16.57
0.720 $10^6$	0.259	15.56	0.57	16.13
0.1008 $10^7$	0.261	15.35	0.58	15.93

TABLE 6  
COMPARISON OF ACTUAL ( $C_{Tact}$ ) AND INFERRED ( $C_{Tinf}$ ) COMPRESSIBILITIES

Drawdown Case	Time s	$C_{Tact}$ MPa <sup>-1</sup> ( $10^{-2}$ psi <sup>-1</sup> )	$C_{Tinf}$ MPa <sup>-1</sup> ( $10^{-2}$ psi <sup>-1</sup> )	$C_{Tinf}/C_{Tact}$
a	0.14256 $10^6$	1.80 (1.24)	6.83 (4.70)	3.79
b	0.14184 $10^6$	0.286 (0.197)	0.305 (0.211)	1.07
c	0.6912 $10^5$	0.309 (0.213)	0.399 (0.275)	1.29
d	0.144 $10^6$	1.99 (1.37)	2.91 (2.00)	1.46
e	0.144 $10^6$	3.75 (2.59)	8.79 (6.06)	2.34

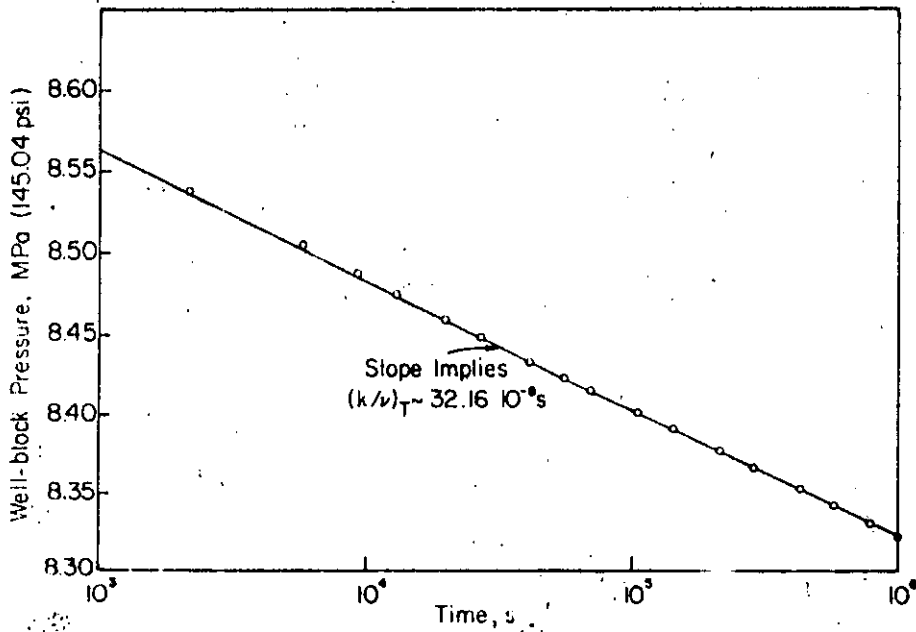


FIG. 1 - SIMULATED DRAWDOWN HISTORY (A). RESERVOIR IS INITIALLY TWO-PHASE EVERYWHERE ( $p=8,5991$  MPa  $\sim$  1247.2 psi,  $S=0.05$ ). SEE TABLE 1 FOR ACTUAL  $(k/v)_T$  VALUES.

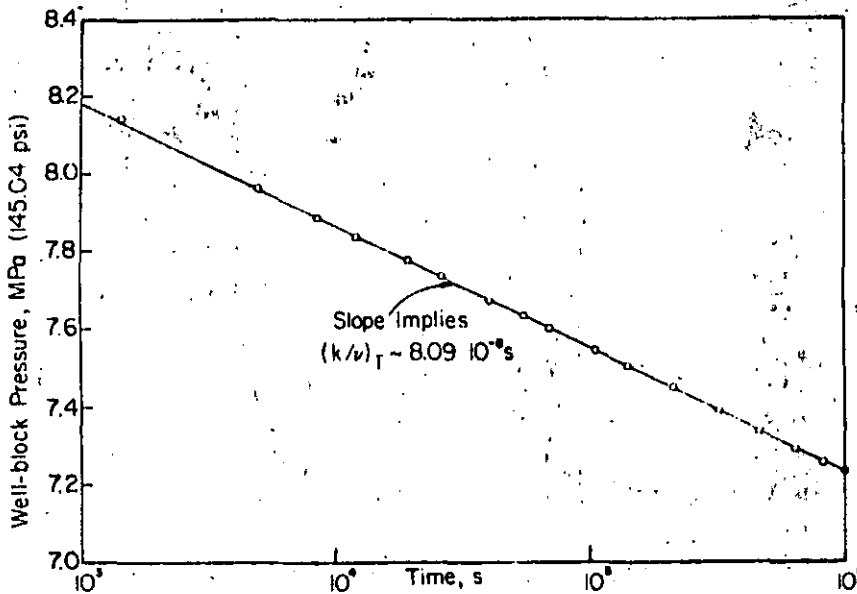


FIG. 2 - SIMULATED DRAWDOWN HISTORY (b). RESERVOIR IS INITIALLY TWO-PHASE EVERYWHERE ( $p=8.5991$  MPa  $\sim$  1247.2 PSI,  $S=0.35$ ). SEE TABLE 2 FOR ACTUAL  $(k/v)_T$  VALUES.

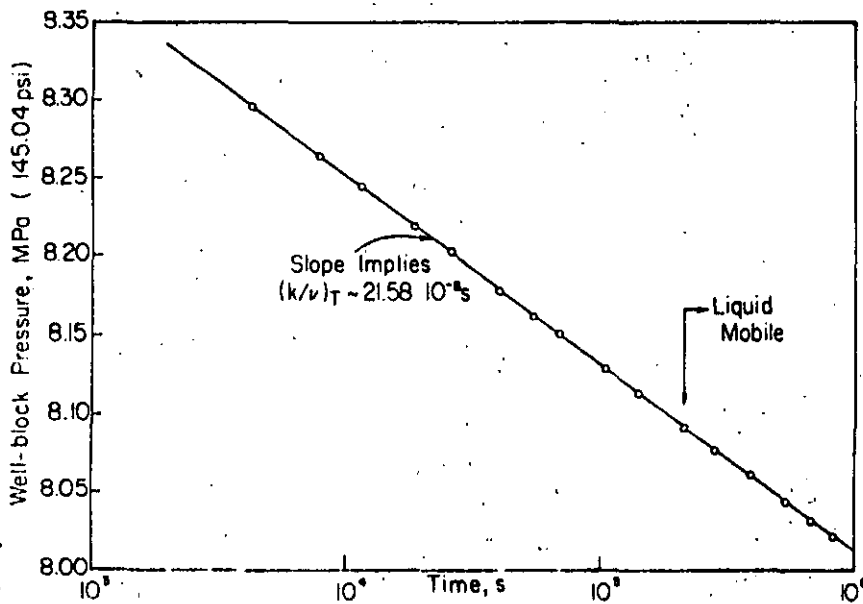


FIG. 3 - SIMULATED DRAWDOWN HISTORY (c). RESERVOIR IS INITIALLY TWO-PHASE EVERYWHERE ( $p=8.5991$  MPa  $\sim$  1247.2 PSI,  $S=0.7015$ ). SEE TABLE 3 FOR ACTUAL  $(k/v)_T$  VALUES.

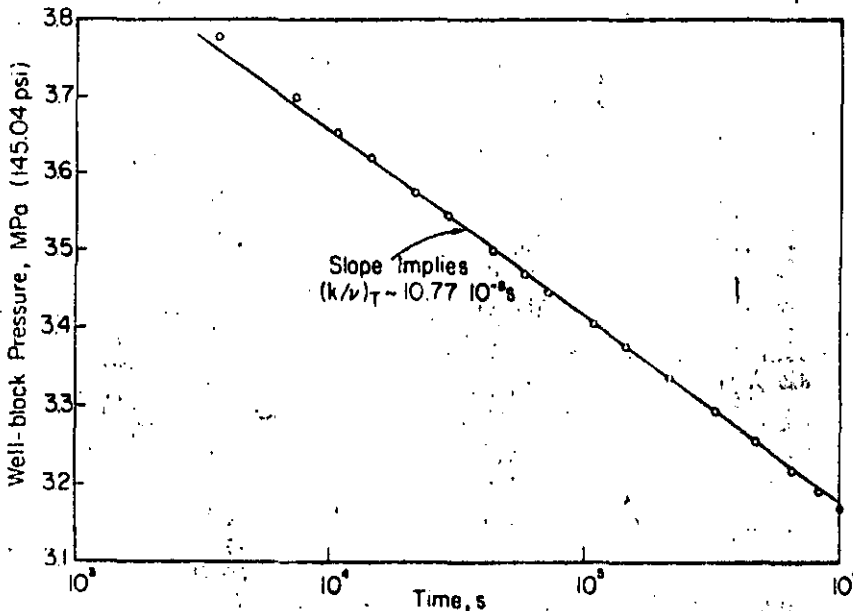


FIG. 4 - SIMULATED DRAWDOWN HISTORY (d). RESERVOIR IS INITIALLY TWO-PHASE EVERYWHERE ( $p=3.9808$  MPa  $\sim$  577.4 PSI,  $S=0.1604$ ). SEE TABLE 4 FOR ACTUAL  $(k/v)_T$  VALUES.

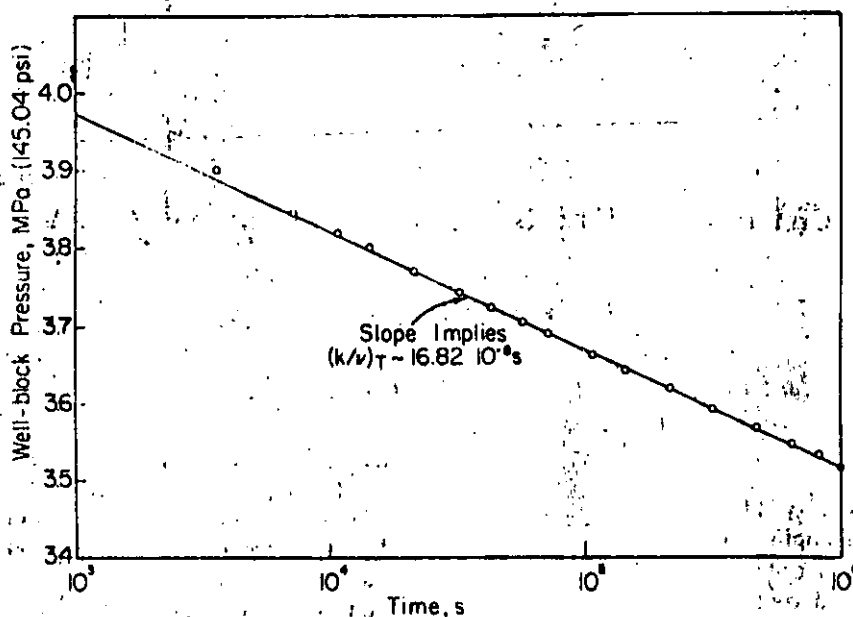


FIG. 5 - SIMULATED DRAWDOWN HISTORY (E). RESERVOIR IS INITIALLY TWO-PHASE EVERYWHERE ( $p=3.9808 \text{ MPa} \sim 577.4 \text{ psi}$ ,  $S=0.0.05$ ). SEE TABLE 5 FOR ACTUAL  $(k/v)_T$  VALUES.

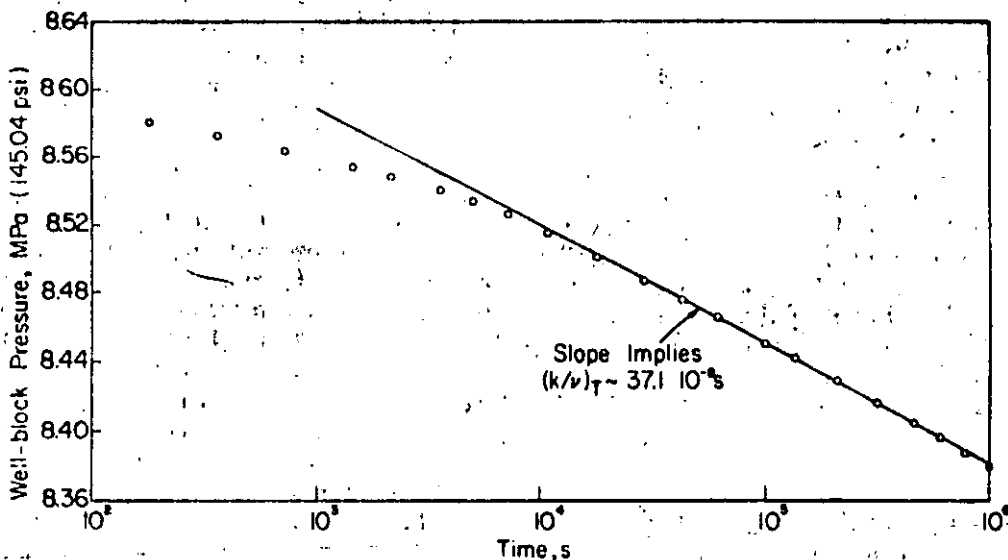


FIG. 6 - SIMULATED DRAWDOWN HISTORY (F). RESERVOIR IS INITIALLY SINGLE-PHASE (LIQUID) EVERYWHERE ( $p=8.62 \text{ MPa} \sim 1250.2 \text{ psi}$ ,  $T=573.15\text{K}=572^\circ\text{F}$ ), ACTUAL RANGE OF  $(k/v)_T$  VALUES FOR POINTS LYING ON THE STRAIGHT LINE IS  $(36.1-42.3) \cdot 10^{-8} \text{ s}$ .

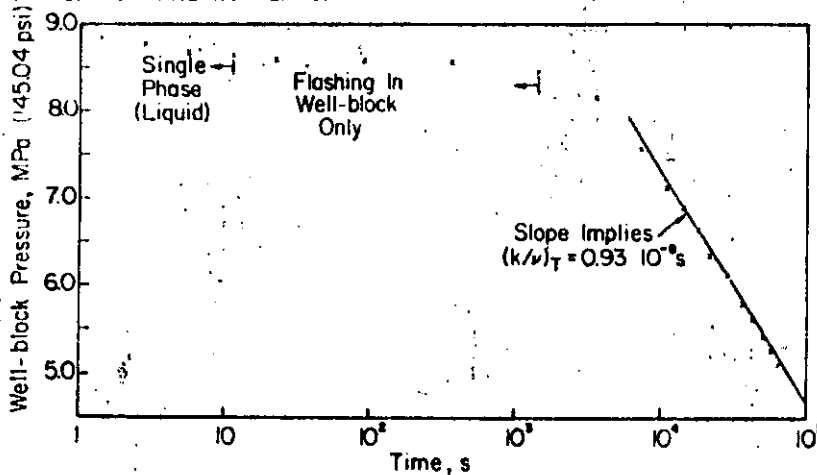


FIG. 7 - SIMULATED DRAWDOWN HISTORY (G). RESERVOIR IS INITIALLY SINGLE-PHASE EVERYWHERE ( $p=9.000 \text{ MPa} \sim 1305.3 \text{ psi}$ ,  $T = 573.15\text{K}=572^\circ\text{F}$ ), ABSOLUTE PERMEABILITY  $K$  FOR THIS CASE IS  $0.01 \mu\text{m}^2 (\sim 0.01 \text{ Darcy})$  AND THE ACTUAL RANGE OF  $(k/v)_T$  VALUES FOR POINTS LYING ON THE STRAIGHT LINE IS  $(0.93-1.15) \cdot 10^{-8} \text{ s}$ .

# Mathematical Modeling of Geothermal Systems

CHARLES R. FAUST\*

JAMES W. MERCER

*U.S. Geological Survey, National Center, Reston, Virginia 22092, USA*

## ABSTRACT

Simulation of geothermal systems yields estimates of recoverable energy, helps determine optimum management techniques, and aids in refining descriptions of reservoir geometry, boundary conditions, and rock properties. To develop an appropriate mathematical model, the continuity equations for mass, momentum, and energy in porous media are reduced to two nonlinear, partial differential equations in which the dependent variables are fluid pressure and enthalpy. These equations include the effects of phase changes and are applicable to both hot-water and vapor-dominated geothermal systems. The equations are solved by a numerical method that combines a Galerkin-finite element approximation in space and finite-difference approximation in time. This method yields results which compare favorably with an analytical solution for the one-dimensional steady vertical flow of hot water in a porous medium. Simulations of more realistic hypothetical problems involving transient, two-phase, two-dimensional (horizontal) flow suggest that this approach is promising for the modeling of natural geothermal systems.

## INTRODUCTION

Most geothermal reservoirs are complex hydrothermal systems controlled by single and multiphase fluid flow, thermodynamics, and the influx of mass and energy. Such systems have many characteristics in common with petroleum reservoirs and ground-water systems. Consequently, some of the engineering methods used in these related fields are applicable to geothermal reservoir engineering.

One of the most promising techniques that has been widely utilized in hydrogeology and petroleum reservoir engineering is mathematical modeling. For the purpose of this discussion we define a geothermal model as: (1) a set of equations which describe the physical processes active in a geothermal reservoir, and (2) the numerical solution of these equations for a given set of reservoir properties, subject to boundary and initial conditions. Since these equations and boundary conditions are generally complicated, the numerical approach is designed for solution on a digital computer.

The application of such geothermal models should play an important role in many aspects of geothermal reservoir engineering. For the preliminary evaluation of potential

reservoirs they provide estimates of reserves and future productivity. At the production stage these models are particularly useful for determining the optimal location, spacing, and production rates of wells. As additional performance data become available during operation, the data base of the model can be increased and predictions of future productivity and reserves refined.

The purpose of this paper is to outline the basis of the geothermal model that we have developed and to consider some hypothetical examples in order to demonstrate its applicability to multiphase fluid flow and energy transport in porous media.

## MATHEMATICAL MODEL

The development of our mathematical model for geothermal systems consists of two parts: (1) the formulation of the continuity equations of mass, momentum and energy for each phase, and (2) the reduction of this system of equations to two nonlinear partial differential equations. The derivation of these equations is given by Mercer, Faust, and Pinder (1974); only the final equations and constitutive assumptions are presented in this paper.

The final equations which serve as the basis of our numerical model are posed in terms of the unknown dependent variables, fluid pressure and enthalpy. They are given by:

$$\begin{aligned} & \nabla \cdot \left\{ \frac{\bar{k} k_{r,p_1}}{\mu_1} (\nabla p - \rho_1 \bar{g}) \right\} \\ & + \nabla \cdot \left\{ \frac{\bar{k} k_{r,p_w}}{\mu_w} (\nabla p - \rho_w \bar{g}) \right\} + q_1 + q_w \quad (1) \\ & = \left\{ \rho \frac{d\phi}{dp} + \phi \left( \frac{\partial \rho}{\partial p} \right)_h \right\} \frac{\partial p}{\partial t} + \phi \left( \frac{\partial \rho}{\partial h} \right)_p \frac{\partial h}{\partial t} \end{aligned}$$

and

$$\begin{aligned} & \nabla \cdot \left\{ \frac{\bar{k} k_{r,p,h_1}}{\mu_1} (\nabla p - \rho_1 \bar{g}) \right\} \\ & + \nabla \cdot \left\{ \frac{\bar{k} k_{r,p,h_w}}{\mu_w} (\nabla p - \rho_w \bar{g}) \right\} \quad (2) \\ & + \nabla \cdot \left\{ \bar{K}_h \left[ \left( \frac{\partial T}{\partial p} \right)_h \nabla p + \left( \frac{\partial T}{\partial h} \right)_p \nabla h \right] \right\} + q_w h_w - q_1 h_1 \end{aligned}$$

\*Also of the Department of Geosciences, Pennsylvania State University, University Park, Pennsylvania 16802. (PhD) candidate, Geology.





$$\left\{ (\rho h + \dot{\rho}, h_r) \frac{d\phi}{dp} + \phi h \left( \frac{\partial \rho}{\partial p} \right)_h \right. \\ \left. + (1 - \phi) \rho_r C_r \left( \frac{\partial T}{\partial p} \right)_h \right\} \frac{\partial p}{\partial t} + \left\{ \phi h \left( \frac{\partial \rho}{\partial h} \right)_p \right. \\ \left. + (1 - \phi) \rho_r C_r \left( \frac{\partial T}{\partial h} \right)_p + \phi \rho \right\} \frac{\partial h}{\partial t}$$

43

where,

- $\bar{k}$  = local intrinsic permeability tensor, [ $L^2$ ]
- $k_{rs}(k_{rw})$  = relative permeability for steam (water), dimensionless
- $\rho_s(\rho_w)$  = average steam (water) density, [ $ML^{-3}$ ]
- $\mu_s(\mu_w)$  = dynamic viscosity, [ $ML^{-1}t^{-1}$ ]
- $p$  = pressure, [ $ML^{-1}t^{-2}$ ]
- $\bar{g}$  = gravitational acceleration, [ $Lt^{-2}$ ]
- $q_s(q_w)$  = mass source term, [ $ML^{-3}t^{-1}$ ]
- $\phi$  = porosity, dimensionless
- $h_s(h_w)$  = enthalpy of saturated steam (water), [ $L^2t^{-2}$ ]
- $\bar{K}_m$  = thermal dispersion tensor for the medium, [ $MLt^{-3}T^{-1}$ ]
- $T$  = temperature, [ $T$ ]
- $\rho_r$  = average rock-grain density, [ $ML^{-3}$ ]
- $h_r$  = rock enthalpy, [ $L^2t^{-2}$ ]
- $C_r$  = rock specific heat, [ $L^2t^{-2}T^{-1}$ ].

Average fluid density,  $\rho$ , is defined by:

$$\rho = S_s \rho_s + S_w \rho_w, \quad (3)$$

where  $S$  = saturation, dimensionless, and  $S_w + S_s = 1.0$ . Finally, the total enthalpy of the mixture,  $h$ , is defined by:

$$h = \frac{S_s \rho_s h_s + S_w \rho_w h_w}{\rho} \quad (4)$$

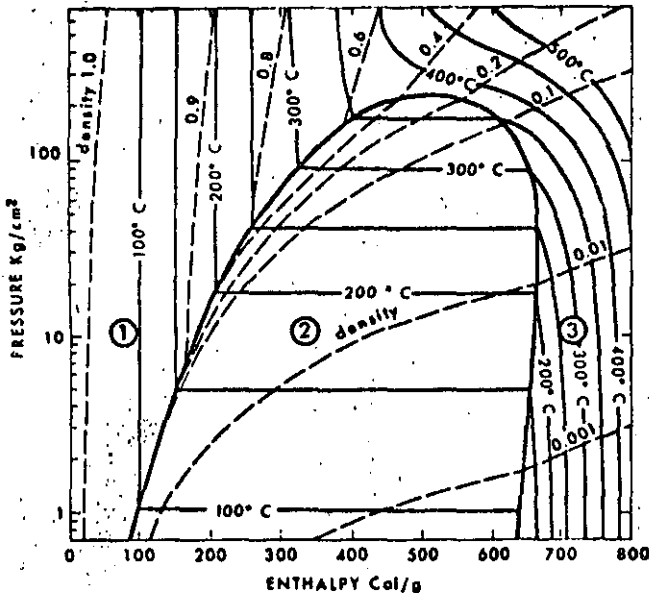


Figure 1. Pressure-enthalpy diagram (equation of state) for pure water and vapor showing three thermodynamic regions below the critical point (apex of parabola): (1) compressed water, (2) two-phase steam-water, and (3) superheated steam (after White, Muffler, and Truesdell, 1971).

The pressure-enthalpy approach is one of several possible approaches. For hot-water geothermal systems (region 1 in Fig. 1), pressure and temperature may be used as unknowns (Mercer, 1973). Toronyi (1974) formulated a two-phase model in terms of fluid pressure and water saturation (this approach is restricted to the saturated vapor-pressure curve; region 2 in Fig. 1). Brownell, Garg, and Pritchett (1975) and T. J. Lasseter (oral commun., 1974) have suggested a method valid in all three regions of Figure 1 which uses fluid density and internal energy as the unknown variables. Fluid pressure and enthalpy have been chosen as unknowns in this study because they define the thermodynamic state of the system (valid in all three regions of Fig. 1), and they are commonly obtained in field situations.

In developing Equations (1) and (2) the following assumptions were made: (1) the reservoir is treated as a porous medium; (2) capillary pressure is negligible—that is, the local pressures in the water and steam phases are equal; and (3) local thermal equilibrium exists among all three phases—rock, steam, and water. As can be seen from Figure 1, consideration of the thermodynamic equation of state for water allows total density, saturated steam density, saturated water density, saturated steam enthalpy, saturated water enthalpy, water saturation, and temperature to be expressed as functions of fluid pressure and enthalpy. For this study, these relationships are expressed as regression equations using data from Meyer et al. (1968). The regression equations were obtained using an enthalpy range of  $2.09 \times 10^9$  to  $3.175 \times 10^{10}$  ergs/gm, a pressure range of  $1.0 \times 10^6$  to  $1.75 \times 10^8$  dynes/cm<sup>2</sup>, and a temperature range of 50 to 350°C. Additional relationships needed to express other parameters in Equations (1) and (2) include (Mercer, Faust, and Pinder, 1974): (1) Porosity as a function of pressure alone; (2) average rock-grain density treated as constant; (3) rock enthalpy considered as a function of temperature; (4) viscosities considered as functions of temperature; (5) relative permeability treated as a function of saturation; and (6) thermal dispersion treated as a property of the medium. (For this paper thermal dispersion and permeability are considered constants.)

Implicit in the above development is the assumption that the geothermal fluid may be treated as a pure aqueous system. For geothermal fields with high salinity this assumption is not valid. Unfortunately, to properly account for transport of chemical species, chemical data such as kinetic reaction rates are required which, in general, are not available. Furthermore, the additional partial differential equations which must be included in such a formulation would produce a model which might be uneconomical to use.

A possible method of avoiding these difficulties for the higher salinity, hot-water systems does exist. For this approach the thermodynamic equation of state for pure water would be modified to account for a mean dissolved-solids concentration of the particular geothermal reservoir. This approximation would account for the thermodynamics of the fluid, but would not account for fluid-solid interactions. Using a mean concentration and the corresponding modified equation of state would require no significant changes in the mathematical model presented in this paper.

### NUMERICAL MODEL

The numerical model used to solve Equations (1) and (2) combines a Galerkin-finite element approximation for

the spatial solution with a finite-difference approximation in time. This method is well documented (Zienkiewicz, 1971) and details of this approach applied to equations similar to (1) and (2) are given in Mercer (1973). Only a brief summary of the method is presented here.

The partial differential Equations (1) and (2) are transformed to approximate integral equations using the Galerkin criterion. The integral equations are solved simultaneously using the finite-element method. In this approach the dependent variables,  $p$  and  $h$ , are approximated using piecewise polynomials, and the problem reduces to determining the coefficients of the polynomials.

To apply the finite-element method, the region of interest is divided into subdomains called "finite elements," which are connected at "nodal points." Although the model is designed for higher-order elements, linear elements are employed for the one-dimensional problems discussed in this paper, and linear quadrilateral elements are used for the two-dimensional problem. Linear polynomials are therefore utilized, and enthalpy is determined at the node points.

For transient (time-dependent) problems, it is a common practice to approximate the time derivative by finite-differences techniques. For the examples presented in this paper we use a backward-difference approximation. The solution proceeds through time using the pressure and enthalpy values at the preceding time-step as initial conditions for the current time-step.

The Galerkin-finite element method offers several advantages. Since the shapes of the finite elements can be arbitrary, this approach yields good approximations of external and internal boundaries. For linear problems involving sharp fronts the finite-element method has been shown to yield better solutions (less numerical dispersion) than finite-difference methods (Price, Cavendish and Varga, 1968). It is also possible to represent coefficients of the partial differential equations which vary in space (for example, permeability and density) as piecewise functions over each element (Pinder, Frind, and Papadopoulos, 1973). The selection of the Galerkin-finite element approach for our geothermal model was based upon these considerations.

**APPLICATIONS**

**One-Dimensional, Steady-State, Vertical Flow**

An analytical solution for the steady-state, one-dimensional vertical flow of water and heat in a porous medium is available (Bredehoeft and Papadopoulos, 1965; Donaldson, 1968). Since this problem involves compressed water, in the above references the equations are formulated in terms of pressure and temperature. The boundary conditions are: at the top of the system (depth,  $z = 0$ ), temperature is  $T_1$  and pressure is  $p_1$ ; at the base ( $z = h$ ), temperature is  $T_2$  and a mass flow rate per unit area is specified as  $Q$ . Assuming constant permeability,  $k$ , thermal conductivity,  $K_m$ , and heat capacity of water,  $C_w$ , the analytical solution for temperature is:

$$T = T_1 + (T_2 - T_1) \left\{ \begin{array}{l} 1 - \exp\left(-\frac{C_w Q z}{K_m}\right) \\ \exp\left(-\frac{C_w Q h}{K_m}\right) \end{array} \right\} \quad (5)$$

Other data used in this problem include: a thickness of 3.0 km;  $T_1 = 116^\circ\text{C}$ ;  $T_2 = 224^\circ\text{C}$ ;  $p_1 = 3.0 \times 10^7$  dynes/cm<sup>2</sup>;  $C_w = 3.2 \times 10^7$  ergs/gm $\cdot^\circ\text{C}$ ; and  $K_m = 3.2 \times 10^5$  ergs/cm $\cdot\text{sec}\cdot^\circ\text{C}$ . The mass flow rate per unit area,  $Q$ , varies from  $3.0 \times 10^{-6}$  to  $3.0 \times 10^{-7}$  gm/sec $\cdot\text{cm}^2$ . Since our model is designed to treat transient problems, an arbitrary set of initial conditions was used and the problem was simulated through time until a steady-state solution was obtained.

Donaldson (1968) defines a fraction,  $C_w Q/K_m$ , which indicates the relative importance of convection in comparison with conduction. For a given reservoir thickness, this ratio increases as convection becomes more dominant. Figure 2 shows results calculated using the vertical, one-dimensional form of the pressure-enthalpy model compared with the results of the analytical solution for several values of the ratio  $C_w Q/K_m$ . As may be seen in Figure 2 the comparison is very good, with the maximum error being only  $0.4^\circ\text{C}$ .

On the basis of this example, the geothermal model presented in this paper appears to be valid for hot-water geothermal systems (subject to the assumptions used in the model and the example). This example does not verify this approach for the more complicated vapor-dominated systems. To test our model for two-phase flow problems we have compared our results with other available numerical results. A report on this aspect of the study is in preparation. In the remainder of this paper we shall discuss several hypothetical two-phase flow examples, concentrating on the problem of conversion from a hot-water reservoir to a two-phase reservoir.

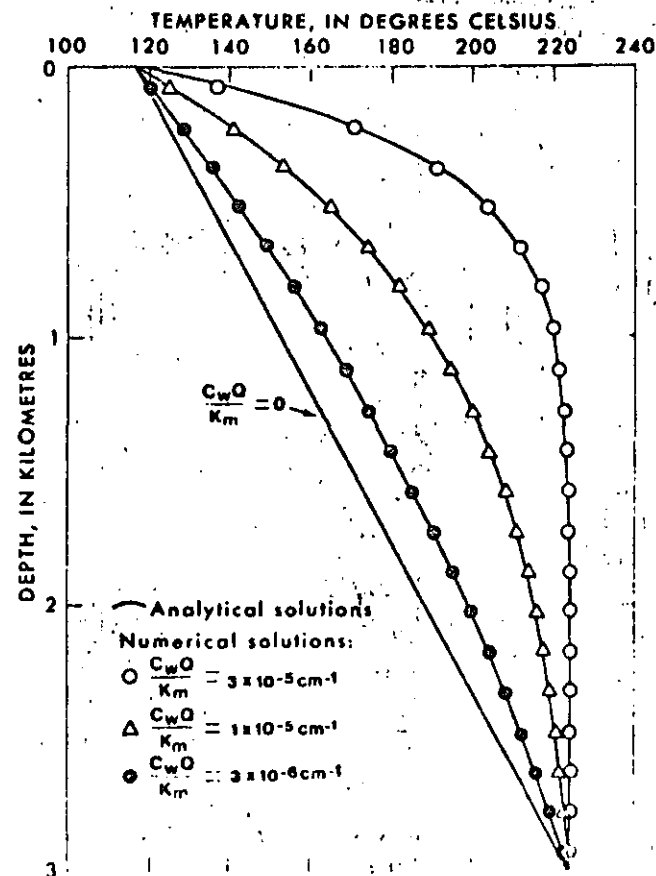


Figure 2. Computed temperatures with depth for the one-dimensional, vertical flow of compressed water.

44

## Multiphase Horizontal Flow

45

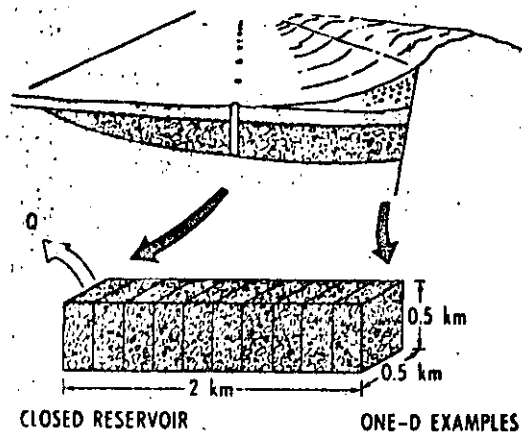
Two one-dimensional examples are presented to demonstrate some characteristics of multiphase horizontal flow in geothermal systems. Figure 3 is a geologic section of a hypothetical geothermal reservoir for which the flow system can be approximated by a one-dimensional model. The reservoir is assumed to be closed to the flow of both energy and mass at the boundaries. This assumption is unrealistic in that some mass leakage does occur in most geothermal reservoirs and conductive heat leakage is always present. Although our model is designed to account for these more realistic boundary conditions, for the purpose of the following examples these simple boundary conditions are sufficient. Additionally, to allow one-dimensional treatment, it is assumed that the reservoir is elongate and contains a line of wells centrally located within the reservoir and parallel to the elongation.

In this one-dimensional problem we consider a vertical slice 0.5 km thick and perpendicular to the elongation. Furthermore, on the basis of symmetry about the line of wells, it is only necessary to examine flow in half the vertical slice. This system is represented by 10 elements (each 0.2 km long) with a sink in the first element (on the left).

Equations (1) and (2) are reduced to their one-dimensional form without the gravity terms (since flow is horizontal). The reservoir property data and initial conditions are given in Figure 3. Additional property data for the reservoir are:  $K_m = 3.2 \times 10^3$  ergs/cm $\cdot$ sec $\cdot$ °C,  $\rho_r = 2.5$  gm/cm $^3$ ,  $C_r = 1.01 \times 10^7$  ergs/gm $\cdot$ °C, and porosity is considered constant. Additionally, water and steam viscosity equations are given by Meyer et al. (1968), modified for cgs system:

$$\mu_w = 10^{-6} \{241.4 \times 10^{[247.8/(T+133.13)]}\} \quad (6)$$

$$\mu_s = 10^{-6} (0.407 T + 80.4) \quad (7)$$

#1) PERMEABILITY =  $10^{-10}$  CM $^2$ 

POROSITY = 0.1

INITIAL CONDITIONS:

PRESSURE =  $0.438 \times 10^8$  dynes/cm $^2$ ENTHALPY =  $1.02 \times 10^{10}$  ergs/cm $^2$ 

TEMPERATURE = 238°C

WATER SAT. = 1.0

#2) PERMEABILITY =

 $(1.0 \times 10^{-14} - 2.5 \times 10^{-9})$  cm $^2$ 

POROSITY = 0.1

INITIAL CONDITIONS:

PRESSURE =  $0.312 \times 10^8$  dynes/cm $^2$ ENTHALPY =  $1.02 \times 10^{10}$  ergs/cm $^2$ 

TEMPERATURE = 238°C

WATER SAT. = 0.25

$$Q = 2.0 \times 10^4 \text{ g/sec}$$

Figure 3. Idealized geological section of a hypothetical geothermal reservoir for one-dimensional, horizontal analysis.

The relative permeabilities for steam and water are essentially unknown, and are assumed to be a variation of those given by Corey (1954) for a drainage displacement process, that is, vaporization dominates condensation:

$$k_{rw} = \frac{(S_w - S_{wi})^4}{(1 - S_{wi})^4} \quad (8)$$

$$k_{rs} = \left[ 1 - \frac{(S_w - S_{wi})^2}{(S_{wm} - S_{wi})^2} \right]^2 \left[ \frac{(S_w - S_{wi})^2}{(S_{wi} - 1)^2} \right] \quad (9)$$

where  $S_{wi} = 0.05$  and  $S_{wm} = 0.95$ . Finally, in the two-phase region, the heat sink term is a function of the mobilities of each phase. That is, the amount of heat lost to the well is defined as,

$$q_h = q_s h_s + q_w h_w \quad (10)$$

and total mass lost to the well as,

$$q_m = q_s + q_w \quad (11)$$

The steam production rate is determined by the fractional flow of the steam phase as follows:

$$q_s = \sigma_s q_m \quad (12)$$

where

$$\sigma_s = k_{rs} / \left( k_{rs} + \frac{\mu_s \rho_w}{\mu_w \rho_s} k_{rw} \right)$$

Since  $h_s$ ,  $h_w$ , and  $q_m$  are known,  $q_s$  is calculated using (12),  $q_w$  is calculated using (11), and  $q_h$  is calculated using (10).

**Example 1.** This example was designed to demonstrate the behavior of an initially hot-water geothermal reservoir which develops a two-phase zone under the influence of production. Two graphs are given in Figure 4. In the upper one, pressure values at various times are plotted against distance from the center of the reservoir (left boundary of the model). The specified times represent the duration of exploitation. In this example the pressure drops rapidly in the early stages of production and at the end of one month the first element has become two-phase. When this occurs the pressure continues to drop rapidly in the rest of the reservoir, but changes only slightly in the element containing the sink. This is expected since once an element becomes two-phase the pressure is maintained by the formation of steam. After three years of exploitation the pressures in the entire reservoir have lowered to a point just slightly above the value where it would become two-phase. At this stage mass extraction results in reduced water saturations in elements near the sink, and pressures drop very slowly.

Water saturations for each element at the end of five years of exploitation are shown in the lower graph of Figure 4. It may be seen that a substantial portion of the reservoir is still single-phase (indicated by the shaded area). This may be an artifact resulting from the numerical method. It is also noticed that a slight oscillation in the saturation distribution occurs. The oscillation is not physically significant, but is due to the numerical approximation.

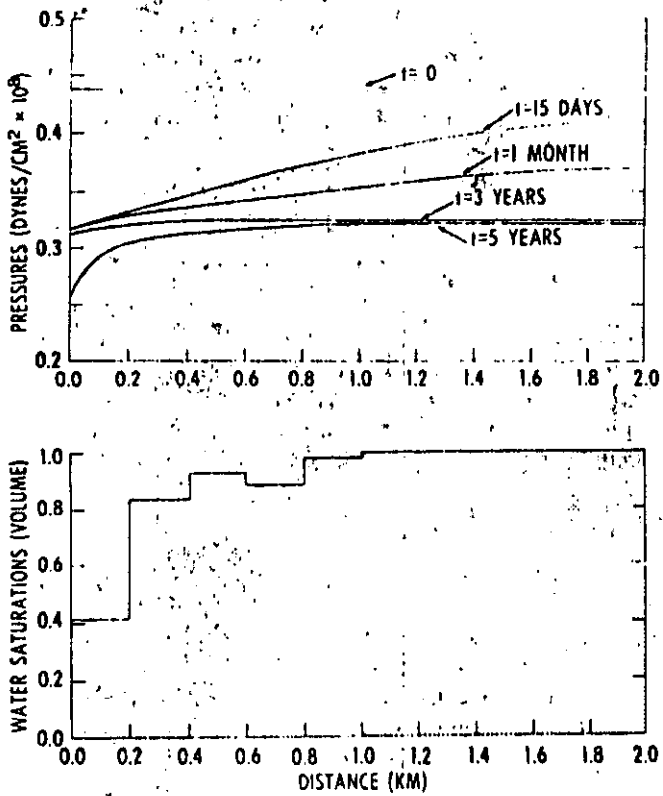


Figure 4. - Top: computed pressure versus distance for various times. Bottom: computed water saturation versus distance after five years of exploitation (shaded area indicates water saturation of 1.0).

For problems such as this example where both single- and two-phase regions exist, it is necessary to take special precautions in order to reduce mass and energy balance errors. Discontinuities in the derivatives of the thermodynamic properties occur at the boundary between these regions. These derivatives appear as coefficients in the partial differential equations and are a major source of mass and energy balance errors. For problems involving both regions, it was not possible to represent these coefficients as functions over each element. Instead, the coefficients were treated as constants over each element and were calculated on the basis of the average element pressure and enthalpy values.

Mass and energy balance errors also occur when an element changes from single- to two-phase. These errors are reduced by checking (at the end of each time step) to determine if an element has become two-phase. If such a change has occurred, the exact time (during the time step) at which the phase change took place is linearly interpolated by using the saturation pressure and the pressures and times at the beginning and end of the time step. To calculate the saturation pressure, this method takes advantage of the fact that during a time step, pressure decreases at a nearly constant enthalpy in the compressed-water region. Once the time at which the phase change occurred is calculated, it is used to compute a new time increment. The program then returns to the previous time step, and using the new time increment, recomputes pressure and enthalpies treating the "phase change" element as being in the compressed-water region. For subsequent time steps, the "phase change" element is assumed to be two-phase. This procedure

is repeated each time an element becomes two-phase, and if several elements change during the same time step, the element which converted first is used to compute the new time increment.

**Example 2.** The permeability of a geothermal reservoir strongly affects the productivity of wells, that is in low-permeability zones wells go "dry" rapidly. In order to examine the effect of reservoir permeability, a series of one-dimensional problems was solved using a range of permeabilities typical of geothermal reservoir rocks (see Figure 3). For this example a reservoir with an initial water saturation of 25% was specified.

In Figure 5, water saturation distributions are shown for a range of permeabilities from  $2.5 \times 10^{-11}$  to  $2.5 \times 10^{-9}$  cm<sup>2</sup>. As anticipated, the reservoirs with lower permeabilities present sharp saturation fronts. The significance of the permeability effect is also demonstrated by Figure 6. In this figure the permeability of the system is plotted against the production time required to reduce the water saturation to 2.0% in the first element (the element including the sink). For reservoirs with low permeability the volume of the sink element dominates the time required to reach 2.0% water saturation, that is, mass is being removed from the sink element instead of from the entire reservoir. Whereas in

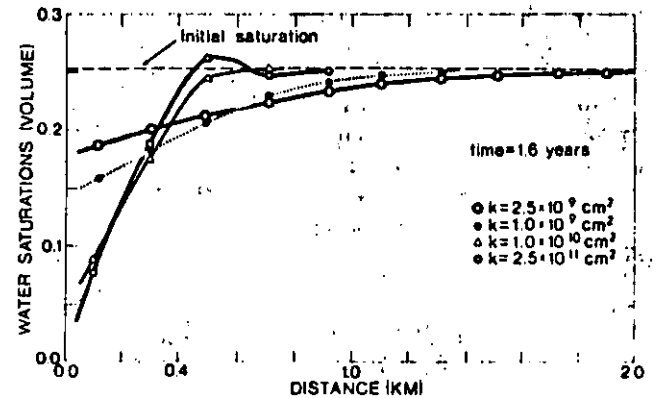


Figure 5. Computed water saturation versus distance for various permeabilities.

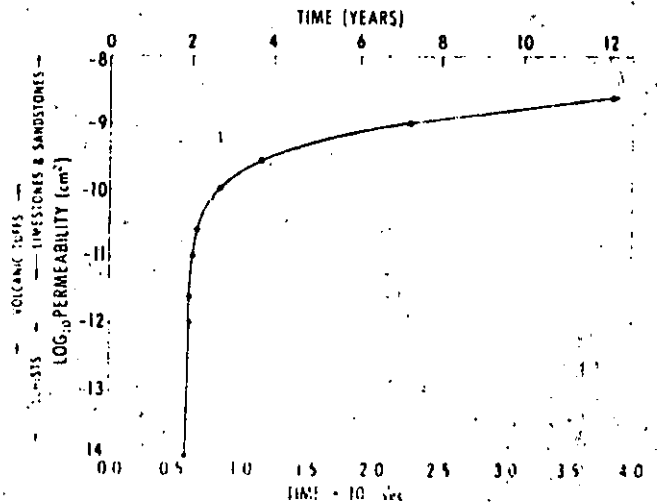


Figure 6. Permeability versus exploitation time to reach a water saturation of 0.02 in the sink element.

47

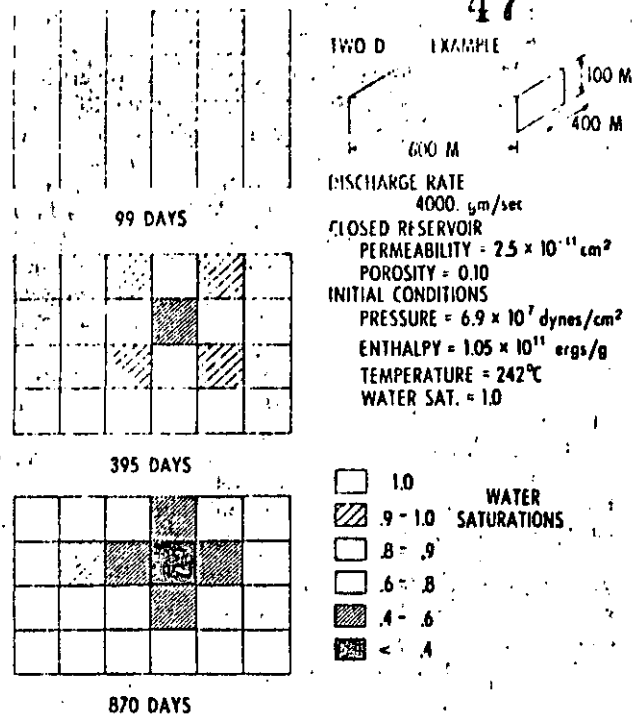


Figure 7. Two-dimensional, two-phase geothermal reservoir analysis showing water saturation distribution for various times.

reservoirs with relatively high permeabilities, fluid is allowed to flow to the sink element and maintain the water saturation longer.

**Two-Dimensional Horizontal Flow**

As an example of two-phase, horizontal flow in two dimensions, a small hypothetical geothermal reservoir is considered. The dimensions, initial conditions and certain properties of the reservoir are specified in Figure 7. Other reservoir properties are:  $K_m = 3.2 \times 10^5$  ergs/cm $\cdot$ sec $\cdot$ °C,  $\rho_f = 2.5$  gm/cm $^3$  and  $C_p = 1.01 \times 10^7$  ergs/gm $\cdot$ °C. Viscosities and relative permeabilities are given by the formulas presented for the earlier examples, and porosity is assumed to vary according to:

$$\phi = \phi_i(x, y) [1 + \beta(p - p_i)] \tag{13}$$

where  $\phi_i$  indicates an initial value and  $\beta$  is the vertical compressibility. For this problem  $\beta = 7.25 \times 10^{-11}$  cm $^2$ /dyn $^2$ . The boundary conditions are no-flow.

The two-dimensional (horizontal) form of Equations (1) and (2) are solved using an element configuration which consists of 35 nodes and 24 elements which are 0.1 km square. The reservoir is initially a hot-water system, but develops a two-phase zone in the vicinity of the sink (the element in the fourth column and third row). The three diagrams in Figure 7 show how the two-phase front changes with time. Figure 8 shows the pressure and temperature distribution after 870 days of exploitation (this corresponds with the final saturation distribution in Fig. 7). Note that the pressures and temperatures in the compressed-water region are essentially the same everywhere, and are slightly above the values that would cause conversion to a steam-water mixture. Since the boundary conditions are no-flow, continued exploitation would result in decreased pressures

and eventually the entire reservoir would become two-phase.

At the end of 870 days approximately 0.15 mass fraction was produced resulting in  $4.6 \times 10^{21}$  ergs of heat removed. Using a fully implicit time step, the overall mass and energy balances had less than 1.0% error.

**CONCLUSIONS**

In this paper we have outlined the important characteristics of a model that has been developed for geothermal reservoir simulation. The mathematical model consists of two nonlinear partial differential equations with fluid pressure and enthalpy as the dependent variables. The complex form of the partial differential equations requires numerical solution, and for this purpose a Galerkin-finite element method has been utilized. This model is valid for compressed water, two-phase mixtures and superheated steam; thus, it permits the simulation of both hot-water and vapor-dominated hy-

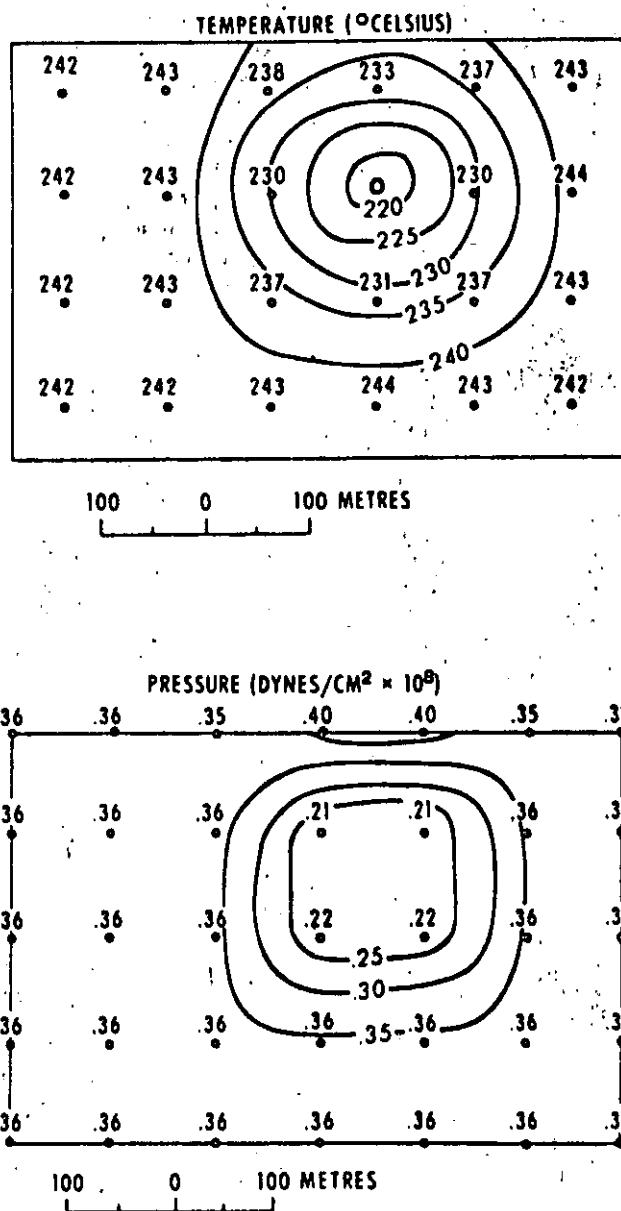


Figure 8. Top: temperature distribution for the two-dimensional example after 870 days of exploitation. Bottom: pressure distribution for the two-dimensional example after 870 days of exploitation.

drothermal systems, as well as the conversion from a hot-water system to a two-phase system.

Several examples have been discussed in order to demonstrate the nature of heat transport and multiphase fluid flow in porous media. For the compressed-water region, the model was verified using an analytical solution for one-dimensional, vertical, steady-state flow. For the two-phase region, the model was verified qualitatively, since results are in accord with observed and expected behavior of geothermal systems.

In the formulation of the mathematical model, several simplifying assumptions were made (for example, negligible capillary pressure and local thermal equilibrium). For some geothermal reservoirs these assumptions are reasonable approximations. For other reservoirs where the assumptions are not valid, the proposed model could serve as a point of departure for a more sophisticated model.

It is evident that the modeling of geothermal systems is a difficult task and that several challenging problems have yet to be adequately considered. Among these are: multiphase flow and heat transport in fractured media, multiphase flow and heat transport in saline systems, three-dimensional simulation of geothermal reservoirs, coupled well-bore and reservoir models, and management models of geothermal reservoirs. In addition, experience with the model described in this paper indicates that further research is needed to determine the most suitable numerical techniques for application to geothermal reservoir engineering.

#### REFERENCES CITED

- Bredenhoeft, J. D., and Papadopoulos, I. S., 1965, Rates of vertical groundwater movement estimated from the earth's thermal profile: *Water Resources Research*, v. 1, no. 2, p. 325.
- Brownell, D. H., Jr., Garg, S. K., and Pritchett, J. W., 1975, Computer simulation of geothermal reservoirs: Ventura, California, 45th Annual California Regional Meeting of the Soc. Petroleum Engineers, paper SPE5381.
- Corey, A. T., 1954, The interrelation between gas and oil relative permeabilities: *Producers Monthly*, v. 19, p. 38.
- Donaldson, I. G., 1968, The flow of steam water mixtures through permeable beds: a simple simulation of a natural undisturbed hydrothermal region: *New Zealand Jour. Sci.*, v. 11, no. 1, p. 3.
- Mercer, J. W., 1973, Finite element approach to the modeling of hydrothermal systems [Ph.D. Thesis]: Urbana-Champaign, University of Illinois.
- Mercer, J. W., Faust, C., and Pinder, G. F., 1974, Geothermal reservoir simulation: *Proceedings of National Science Foundation Conference on Research for the Development of Geothermal Energy Resources*, Pasadena, California, p. 256.
- Meyer, C. A., McClintock, R. B., Silvestri, G. J., and Spencer, R. C., 1968, 1967 ASME steam tables: New York, American Soc. Mechanical Engineers, 328 p.
- Pinder, G. F., Frind, E. O., and Papadopoulos, S. S., 1973, Functional coefficients in the analysis of ground water flow: *Water Resources Research*, v. 9, no. 1, p. 222.
- Price, H. S., Cavendish, J. C., and Varga, R. S., 1968, Numerical methods of higher-order accuracy for diffusion-convection equations: *Soc. Petroleum Engineers Jour.*, v. 8, no. 3, p. 293.
- Toronyi, R. M., 1974, Two-phase, two-dimensional simulation of a geothermal reservoir and the wellbore system [Ph.D. Thesis]: University Park, Pennsylvania State Univ.
- White, D. E., Muffler, L. P. J., and Truesdell, A. H., 1971, Vapor-dominated hydrothermal systems compared with hot-water systems: *Economic Geology*, v. 66, p. 75.
- Zienkiewicz, O. C., 1971, *The finite element method in engineering science*: London, McGraw-Hill, 521 p.

SIMULATION OF HEAT TRANSPORT IN FRACTURED,  
SINGLE-PHASE GEOTHERMAL RESERVOIRS

William G. Gray, Kevin O'Neill and George F. Pinder  
Water Resources Program  
Department of Civil Engineering  
Princeton University  
Princeton, N. J. 08540

Although many geothermal reservoirs depend upon fracture permeability to obtain adequate mass flows, relatively little research effort has been directed toward fractured reservoir simulation. This paper outlines the mathematical apparatus necessary to develop a numerical simulator for a fractured, single-phase geothermal reservoir. It is assumed that the fracturing is extensive and well-distributed (though not necessarily uniform) so that it is reasonable to consider a superficial discharge through the fractures as well as the pores. While mass and heat transport are of course coupled in a system of this kind, we have subdivided the ensuing discussion into mass flow and heat flow for clarity of presentation.

Mass Flow Equation

Analytical solutions for the pressure distributions in porous blocks of various shapes and sizes show that the pressure in the interior of a typical block reaches 95% of the value of an initial "step" input imposed on the block surface in a time which is very short relative to the length of time typically required for overall, macroscopic system changes. In addition, recent modeling analyses and examination of pertinent field data by Closmann (1975) support the point of view that for most purposes one may consider both pore and fracture flow fields to be characterized by a single pressure variable. A net flow of mass may exist between one flow regime and the other, but this will be such as to maintain the near equality of pressure. Application of accepted space-averaging techniques (Gray and Lee, 1976) to a point mass balance equation provides the following mass conservation equation:

$$\frac{\partial}{\partial t} (\rho_w \epsilon_w) = \nabla \cdot [\rho_w \mathbf{v}_w] + S_m = \nabla \cdot [\rho_f \mathbf{v}_f + \rho_p \mathbf{v}_p] + S_m \quad (1)$$



where  $\rho_w$  is the averaged density of all (pore plus fracture) water,  
 $\rho_f$  is the density of fracture water,  
 $\rho_p$  is the density of pore water,  
 $\epsilon_w$  is the void fraction occupied by all water,  
 $v_f$  is the superficial discharge through the fracture (vector),  
 $v_p$  is the superficial discharge through the pores (vector), and  
 $S_m$  is the mass source or sink strength, that is, mass entering or leaving per unit time per unit volume of total medium.

The lefthand side of (1) may be expanded as

$$\begin{aligned} \frac{\partial}{\partial t} (\rho_w \epsilon_w) &= \rho_w \frac{\partial \epsilon_w}{\partial t} + \epsilon_w \frac{\partial \rho_w}{\partial t} \\ &= \rho_w \alpha_p \frac{\partial p}{\partial t} + \rho_w \alpha_T \frac{\partial T_w}{\partial t} + \epsilon_w \rho_w \beta_p \frac{\partial p}{\partial t} + \epsilon_w \rho_w \beta_T \frac{\partial T_w}{\partial t} \end{aligned} \quad (2)$$

where  $\epsilon_f$  is the void fraction of the fractures,  
 $\epsilon_p$  is the void fraction of the pores,  
 $p$  is the incremental fluid pressure,  
 $T_f$  is the local average fluid temperature in the fractures,  
 $T_{pm}$  is the local average temperature of the porous medium, and  
 $T_w$  is the locally averaged temperature of all water defined as

$$T_w = \epsilon_f T_f + \epsilon_p T_{pm} \quad (3)$$

The parameters  $\alpha_p$ ,  $\alpha_T$ ,  $\beta_p$  and  $\beta_T$  are empirical coefficients defined through the relations:

$$\frac{\partial \epsilon_w}{\partial t} = \alpha_p \frac{\partial p}{\partial t} + \alpha_T \frac{\partial T_w}{\partial t} \quad (4a)$$

$$\frac{\partial \rho_w}{\partial t} = \rho_w \beta_p \frac{\partial p}{\partial t} + \rho_w \beta_T \frac{\partial T_w}{\partial t} \quad (4b)$$

Superficial fracture and pore discharges may be expressed in terms of incremental pressure gradients, as

$$\mathbf{v}_f = - \left( \frac{\mathbf{k}_f}{\mu} \right) \cdot \nabla p \quad (5a)$$

$$\mathbf{v}_p = - \left( \frac{\mathbf{k}_p}{\mu} \right) \cdot \nabla p \quad (5b)$$

where  $\mu$  is the fluid viscosity,

$\mathbf{k}_f$  is the fracture permeability (tensor), and

$\mathbf{k}_p$  is the pore permeability (tensor)

Under certain conditions  $\mathbf{k}_f$  may be considered to be a function of  $v_f$ .

Substitution of equations (2) through (5) into (1) yields the following expression for the conservation of all fluid mass:

$$\begin{aligned} & \rho_w (\alpha_p + \epsilon_w \beta_p) \frac{\partial p}{\partial t} + \rho_w (\alpha_T + \epsilon_w \beta_T) \frac{\partial T_w}{\partial t} \\ & = \nabla \cdot \left[ \left( \frac{\rho \mathbf{k}}{\mu} \right)_f + \left( \frac{\rho \mathbf{k}}{\mu} \right)_p \right] \cdot \nabla p + S_m \end{aligned} \quad (6)$$

In addition to the explicit coupling of this equation to the temperature equations through the second term on the lefthand side, temperature dependence also enters implicitly through the changing value of  $\mu$ .

### Heat Flow

The governing equations for heat flow are provided by space averaging of conservation of energy equations written in terms of temperature. For the fracture system, this results in

$$\begin{aligned} & \rho_f c c_f \frac{\partial T_f}{\partial t} + \rho_f c v_f \cdot \nabla T_f - \nabla \cdot \mathbf{D}_f \cdot \nabla T_f \\ & = h(T_{pm} - T_f) + c S_{m,f} (T_{B,f} - T_f) \end{aligned} \quad (7a)$$

and for the porous medium

$$\begin{aligned}
 (\rho c c)_{pm} \frac{\partial T_{pm}}{\partial t} + \rho_p c_v \cdot \nabla T_{pm} - \nabla \cdot \underline{D}_{pm} \cdot \nabla T_{pm} \\
 = h(T_{s,f} - T_{pm}) + c_s S_{m,p} (T_{s,pm} - T_{pm})
 \end{aligned}
 \tag{7b}$$

where  $(\rho c c)_{pm} \equiv \rho_p c_p c_p + \rho_s c_s c_s$ ,

- $\rho_s$  is the rock density,
- $c_s$  is the specific heat of the rock,
- $c_p$  is the volume fraction of the rock,
- $c$  is the specific heat of water,
- $\underline{D}_f$  is the tensor coefficient of dispersion for the fractures,
- $\underline{D}_{pm}$  is the tensor coefficient of dispersion for the porous medium,
- $h$  is a porous medium-fracture heat transfer coefficient relating the time rate of heat transport between those regimes, per volume of the medium, to the temperature difference between the two.  $T_{s,f}$  and  $T_{s,pm}$  are source or sink temperatures of fracture and pore fluids, respectively. (For withdrawal, the sink temperature is the reservoir fluid temperature and the last terms in 7 vanish).
- $S_{m,f}$  is the fracture mass source or sink strength,
- $S_{m,p}$  is the pore mass source or sink strength, and
- $S_m = S_{m,f} + S_{m,p}$  and the ratio of the two components can be determined using the permeabilities of the two systems.

The superficial velocities in (7) must, of course, be computed using the pressure field through equations (5) and (6). Equations (5), (6), and (7) provide five equations in the five dependent variables  $T_{pm}$ ,  $T_f$ ,  $p$ ,  $v_f$  and  $v_p$ . These equations have been solved successfully for a variety of hypothetical problems for which analytical solutions exist. The numerical simulator uses isoparametric Hermitean finite elements (Van Genuchten, et al, 1977) to solve in three space dimensions, and a time-centered difference scheme to solve in time.

Figures 1 and 2 show results for an additional fully coupled, one-dimensional, transient test case, subject to the following conditions:

at  $x = 0$ 

$$T_{pm} = T_f = 40^\circ\text{C}$$

t &gt; 0

$$p = 0$$

at  $x = 100\text{cm}$ 

$$T_{pm} = T_f = 0$$

$$p = -1.0 \times 10^5 \text{ dyne/cm}^2$$

$$\frac{1}{\mu} = 5.38 \times 10^2 + (T-150) \times 3.8 - (T-150)^3 \times 2.6 \times 10^{-5} \text{ cm}\cdot\text{sec/g for } 0 < T < 300^\circ\text{C}$$

(Mercer et al, 1975)

$$\epsilon_f = 0.02, \quad \epsilon_p = 0.2, \quad \alpha_p = 1.0 \times 10^{-10} \text{ cm}^2/\text{dyne}, \quad \alpha_T = 0$$

$$\frac{k_f}{\epsilon_f} = 10^{-7} \text{ cm}^2, \quad \frac{k_{pm}}{\epsilon_p} = 3.0 \times 10^{-8} \text{ cm}^2, \quad \beta_p = 5.0 \times 10^{-11} \text{ cm}^2/\text{dyne}$$

$$\beta_T = 5.0 \times 10^{-4}/^\circ\text{C}$$

$$\rho_s = 2.5\text{g/cm}^3, \quad c_s = 0.2\text{cal/g}\cdot^\circ\text{C}, \quad D_f = 5.0 \times 10^{-4} \text{ cal/}^\circ\text{C}\cdot\text{cm}\cdot\text{sec},$$

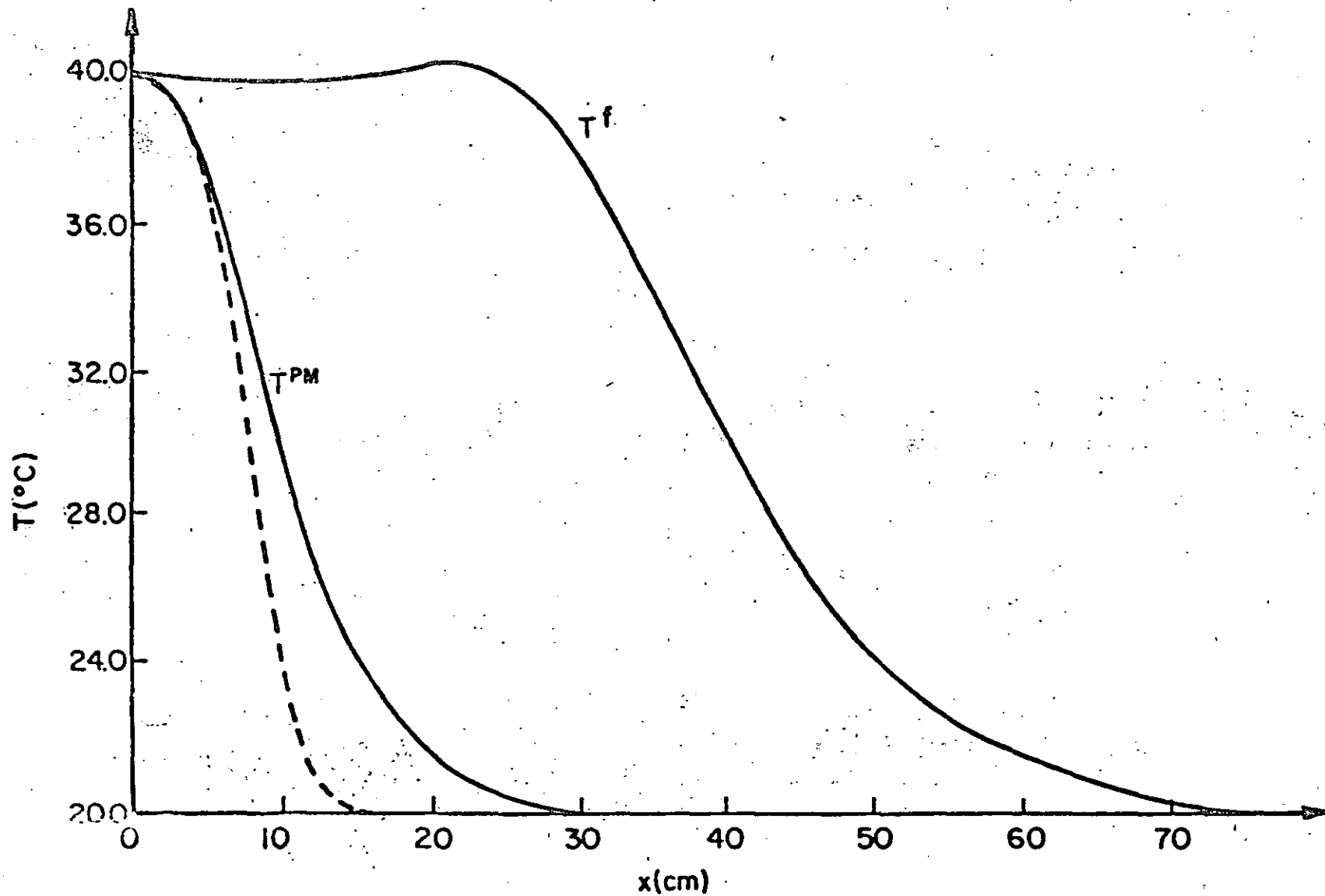
$$D_{pm} = 3.0 \times 10^{-3} \text{ cal/}^\circ\text{C}\cdot\text{cm}\cdot\text{sec}.$$

The initial temperature distribution for both fractures and porous medium is displayed on each figure. As expected, a non-zero value of  $h$  retards translation of the fracture temperature front, increases translation of the porous medium front, and increases dispersion of both. As the fronts progress, the pressure gradient (not shown) decreases from the initial, essentially isothermal value, due primarily to the decrease in fluid viscosity with rising temperature.

### References

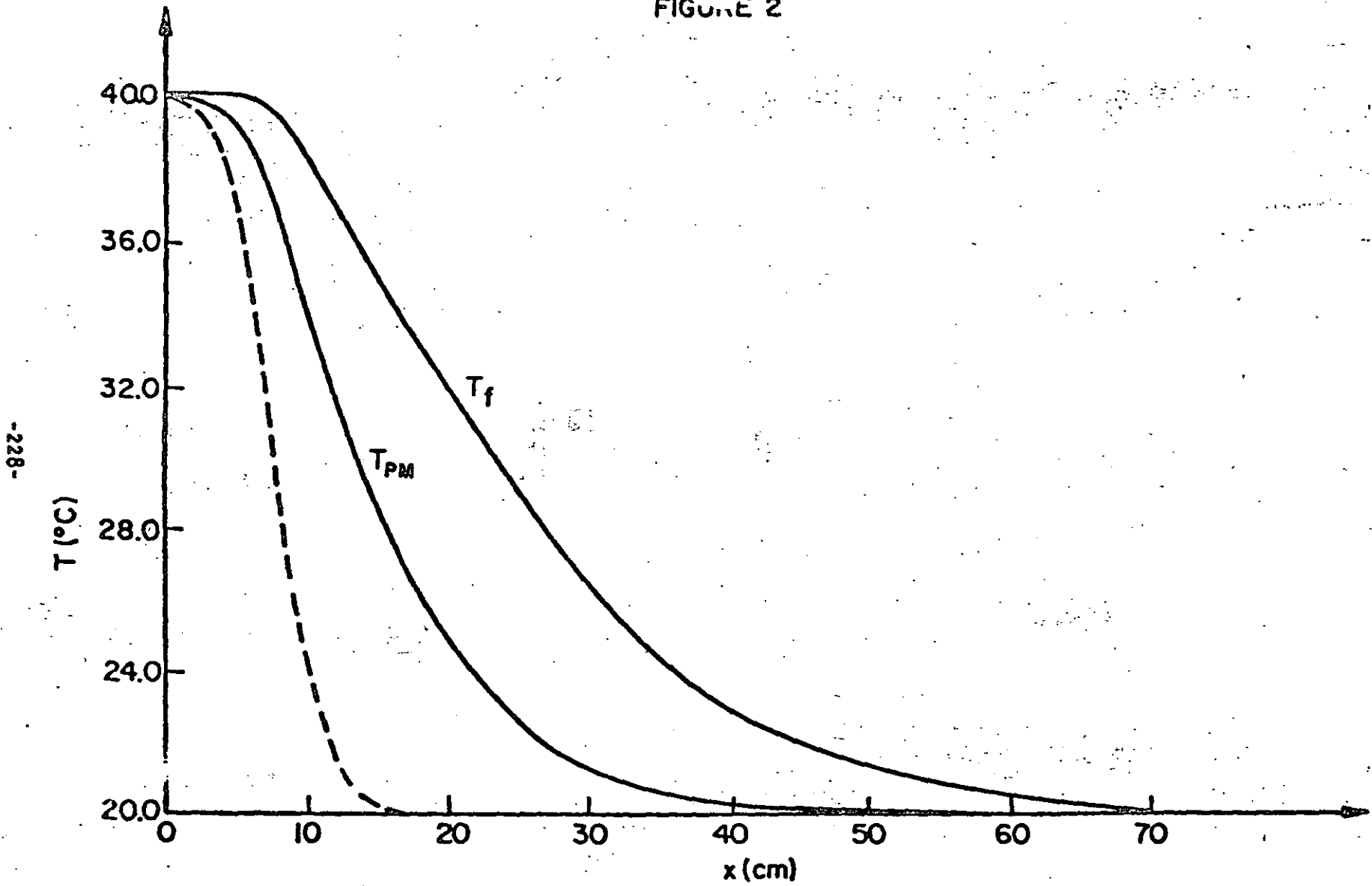
- Closmann, P. J., "An Aquifer Model for Fissured Reservoirs," Society of Petroleum Engineers Journal, October 1975, 385-398.
- Gay, W. G., and P. C. Y. Lee, "On the Theorems for Local Volume Averaging of Multiphase Systems," International Journal of Multiphase Flow, In press 1976.
- Mercer, W. M., G. F. Pinder, and I. G. Donaldson, "A Galerkin Finite Element Analysis of the Hydrothermal System at Wairakei, New Zealand," Journal of Geophysical Research, June 1975, 2608-2621.
- Van Genuchten, M. T., G. F. Pinder, and E. O. Frind, "Simulation of Two-dimensional Contaminant Transport with Isoparametric Hermitean Finite Elements," Water Resources Research, In press 1976.

-227-



$h=0$   
 $t=3.0 \times 10^3 \text{ sec}$   
DASHED LINE SHOWS INITIAL TEMPERATURE  
FIGURE I

FIGURE 2



$$h = 2.0 \times 10^{-5} \text{ CAL/cm}^2 \text{ sec } ^\circ\text{C}$$

$$t = 5.25 \times 10^3 \text{ sec}$$

DASHED LINE SHOWS INITIAL TEMPERATURE

SPE 6892

GEOHERMAL RESERVOIR MODELLING

by

K. H. Coats  
 INTERCOMP Resource Development  
 and Engineering, Inc.

© Copyright 1977, American Institute of Mining, Metallurgical, and Petroleum Engineers, Inc.

This paper was presented at the 52nd Annual Fall Technical Conference and Exhibition of the Society of Petroleum Engineers of AIME held in Denver, Colorado, Oct. 9-12, 1977. The material is subject to correction by the author. Permission to copy is restricted to an abstract of not more than 300 words. Write 6200 N. Central Exp., Dallas, Texas 75206.

ABSTRACT

This paper describes and partially evaluates an implicit, three-dimensional geothermal reservoir simulation model. The evaluation emphasizes stability or time-step tolerance of the implicit finite-difference formulation. In several illustrative multi-phase flow problems, the model stably accommodated time steps corresponding to grid block saturation changes of 80-100% and grid block throughput ratios the order of  $10^8$ . This compares to our experience of limits of 3 to 10% saturation change and roughly 20,000 throughput ratio with semi-implicit oil and geothermal reservoir models.

The illustrative applications shed some light on practical aspects of geothermal reservoir behavior. Applications include single- and two-phase single-well behavior, fractured-matrix reservoir performance and well test interpretation, and extraction of energy from fractured hot dry rock. Model stability allows inclusion of formation fractures and wellbores as grid blocks.

An analytical derivation is presented for a well deliverability reduction factor which can be used in simulations using large grid blocks. The factor accounts for reduced deliverability due to hot water flashing and steam expansion accompanying pressure decline near the well.

References and illustrations at end of paper.

INTRODUCTION

This paper describes a numerical model for simulating geothermal well or reservoir performance. The model is considerably more general than any described in the literature to date. It treats transient, three-dimensional, single- or two-phase fluid flow in normal heterogeneous or fractured-matrix formations. Both conductive and convective heat flow are accounted for and fluid states in the reservoir can range from undersaturated liquid to two-phase steam-water mixtures to superheated steam. Aquifer water influx and heat source/sink terms necessary in simulating free convection cells are included in the model formulation.

The primary purpose of the work described here was evaluation of the capability of an implicit model formulation. Our experience with semi-implicit simulation of petroleum and geothermal reservoirs has shown time step restrictions related to conditional stability. In multiphase flow problems, the maximum tolerable time step size generally corresponds to a maximum of 3 to 10 percent saturation change in any grid block in one time step. In some steamflood and geothermal simulations, we have found this to result in very small time steps and correspondingly high computing costs. This work was performed with the hope that the implicit model formulation would give unconditional stability with no time step restriction other than that imposed by time truncation error.

Calculated results are presented for a variety of geothermal well and reservoir illustrative problems. Emphasis in connection with these results is placed on the stability or time step tolerance of the model. However, the applications are also intended to shed some light on practical aspects of geothermal reservoir behavior.

Following description of the implicit model formulation, the paper presents applications including single-well deliverability under two-phase flow conditions, depletion of a fractured-matrix formation with boiling, drawdown test interpretation in single-phase, fractured-matrix formations, and heat extraction from artificially fractured hot dry rock. An analytical expression is derived to represent the effective transient productivity index of a well which experiences hot water flashing due to pressure drawdown from an exterior radius where steam saturation may be zero or small.

We have applied the model extensively in simulation of natural convection cells with zero porosity (hard rock) grid block definition above and below the formation. This definition eliminates the erroneous imposition of constant temperature boundaries at the top and bottom of the convection cell common in many reported studies of natural convection. Another application simulated development over geologic time of a superheated (Geyser's type) reservoir from an early time of magma or heat source intrusion beneath an initial normal gradient cold water aquifer. These natural convection type applications are omitted here due to the significant length of the paper. Some of this convection work is reported in a recent paper [1].

MODEL DESCRIPTION

The model consists of two equations expressing conservation of mass of H<sub>2</sub>O and conservation of energy. These equations account for three-dimensional, single- or two-phase fluid flow, convective and conductive heat flow in the reservoir and conductive heat transfer between the reservoir and overlying and underlying strata. The phase configuration at any time can vary spatially through the formation from single-phase undersaturated water to two-phase steam-water mixture to single-phase superheated steam.

The equations represent water influx from an aquifer extending beyond the reservoir grid using the Carter-Tracy [2] or simpler approximations. Heat source and sink terms in the equations are useful in imposing temperature and/or heat flux boundary conditions in simulation of natural convection. The model equations do not account for the presence of inert gases or for varying concentration and precipitation of dissolved salts.

The model applies to reservoir grids including one-dimensional, two-dimensional radial-z, x-z or x-y and three-dimensional, either x-y-z Cartesian or r-θ-z cylindrical. In the r-z and r-θ-z case, the wellbore of a well at r = 0 can be included in the grid, resulting in enhanced stability and accuracy as discussed below. The r-z grid can be used in simulating a sector of a fractured-matrix reservoir with the horizontal and vertical fractures represented by grid blocks. The grid can include blocks of zero porosity representing hard rock, with no pressure calculated, and blocks of 100% porosity representing either fractures or wellbores.

The mass balance on H<sub>2</sub>O combines in a single equation the steam-phase and liquid water-phase mass balance equations. This combination was proposed in our early steam-flood work [3] to eliminate difficulties in handling the mass transfer term. The energy balance is the First Law of Thermodynamics applied to each grid block. The grid block is an open system with fixed boundaries. With potential and kinetic energy terms ignored, the energy balance states that (enthalpy flow rate in) - (enthalpy flow rate out) = rate of gain of internal energy in the grid block. For some reason, considerable confusion exists in the literature regarding this energy balance. Enthalpy is U + pv where U is internal energy. Many modelling papers ignore the pv term, in which case the energy balance erroneously becomes (net flow rate of internal energy into the grid block = rate of gain of internal energy in the block). A recent paper [4] uses an erroneous energy balance stating (net flow rate of enthalpy into the grid block = rate of gain of enthalpy in the block).

The two model equations are\*

$$\Delta(T_w(\Delta p_w - \gamma_w \Delta z) + T_g(\Delta p_g - \gamma_g \Delta z)) - q = \frac{V}{\Delta t} \delta(\phi \rho_w S_w + \phi \rho_g S_g) \quad (1a)$$

$$\Delta(T_w H_w (\Delta p_w - \gamma_w \Delta z) + T_g H_g (\Delta p_g - \gamma_g \Delta z)) + \Delta(T_c \Delta T) - q_{HL} - q_H = \frac{V}{\Delta t} \delta(\phi \rho_w S_w U_w + \phi \rho_g S_g U_g) + (1-\phi)(\rho C_p)_R T \quad (1b)$$

For a given grid block (i, j, k), all terms in these equations are single-valued functions of (T, S<sub>g</sub>, p)<sub>i, j, k</sub> and (T, S<sub>g</sub>, p) in the six neighboring grid blocks (i+1, j, k), (i, j+1, k), (i, j, k+1). Thus, transposing the right-hand sides, we can write Equations (1) simply as

\*See Nomenclature for definition of terms.



$$F_1(\underline{x}) = 0 \quad (2)$$

$$F_2(\underline{x}) = 0$$

where  $\underline{x}$  represents the vector of the above listed 21 unknowns.

Following the totally implicit procedure described by Blair and Weinaug [5], we apply the Newton-Raphson iterative method to (2) as

$$F_1(\underline{x}) \approx F_1(\underline{x}^l) + \sum_{i=1}^{21} (\partial F_1 / \partial x_i)^l \delta x_i = 0 \quad (3)$$

$$F_2(\underline{x}) \approx F_2(\underline{x}^l) + \sum_{i=1}^{21} (\partial F_2 / \partial x_i)^l \delta x_i = 0$$

where we temporarily use  $x_i$  to denote the 21 unknowns and superscript  $l$  denotes latest iterate value. The operator  $\delta$  in Equations (1) denotes change over time step while  $\delta$  in Equations (3) denotes change over the coming iteration. The approximation  $\delta x_i \approx x_{i,n+1} - x_i^l$  becomes increasingly exact as we near convergence.

The partial derivatives in Equations (3) are all evaluated at latest iterate values of  $x_i$ . The functions  $F_1, F_2$  involve three different types of terms: right-hand sides (accumulation terms), sink/source terms and interblock flow terms. Differentiation of accumulation terms is straightforward. The heat loss term and its derivative is evaluated as described in Reference [3]. The well injection/production terms and their derivatives are evaluated as described in some detail below. The interblock flow terms are evaluated as follows: Relative permeabilities and enthalpies are evaluated at upstream grid block conditions, interblock  $\rho/\mu$  and  $\gamma$  values are evaluated as arithmetic averages of their values in the two grid blocks. Water phase pressure  $p_w$  is expressed as  $p - P_c$  where  $p$  is gas pressure and capillary pressure  $P_c$  is a single-valued function of  $S_g$ .

For all  $N_x N_y N_z$  grid blocks taken together, Equations (3) are  $2N_x N_y N_z$  equations in  $3N_x N_y N_z$  unknowns,  $(\delta T, \delta S_g, \delta p)$  for each grid block. Only two of these three unknowns in each block are independent. If the block contains undersaturated water or superheated steam,  $\delta S_g = 0$  and  $\delta T, \delta p$  are the block's two unknowns. If the block is saturated, two-phase, then temperature  $T = T_s(p)$  and  $\delta T$  is  $(dT/dp)_s \delta p$  where subscript  $s$  denotes the saturated condition.

Equations (3) can be written for each grid block in the form

$$\Delta(T_{11} \Delta P_1) + \Delta(T_{12} \Delta P_2) + R_1 = C_{11} P_1 + C_{12} P_2 \quad (4)$$

$$\Delta(T_{21} \Delta P_1) + \Delta(T_{22} \Delta P_2) + R_2 = C_{21} P_1 + C_{22} P_2$$

where  $P_1$  is either  $\delta T$  or  $\delta S_g$  and  $P_2$  is  $\delta p$ . The terms  $R_1, R_2$  are  $F_1(\underline{x}^l), F_2(\underline{x}^l)$ , respectively, in Equations (3). The  $\Delta(T \Delta P)$  type terms are not true Laplacians but rather are, as illustrated by the x-direction component

$$\Delta_x (T_x \Delta P) = T_{xi}^+ P_{i+1} + T_{xi}^0 P_i + T_{xi}^- P_{i-1}$$

where the center term  $T_{xi}^0$  can be combined with the appropriate  $C_{ij}$  in Equation (4) and need not be stored. More simply, Equation (4) can be written

$$\Delta(T \Delta P) + \underline{R} = \underline{C} \underline{P} \quad (5)$$

where  $T$  and  $C$  are the  $2 \times 2$  matrices  $T_{ij}$ ,  $C_{ij}$  and  $\underline{R}$  and  $\underline{P}$  are column vectors. We use reduced band width direct solution [6] to solve Equation (5) for  $P_1, P_2$  and obtain new iterate values as  $p^{l+1} = p^l + \delta p$ . Convergence is defined by

$$\begin{aligned} \text{Max} |\delta p_{ijk}| &\leq \epsilon_p \\ \text{Max} |\delta T_{ijk}| &\leq \epsilon_T \\ \text{Max} |\delta S_{gijk}| &\leq \epsilon_S \end{aligned} \quad (6)$$

where MAX denotes maximum over all grid blocks. We generally use tolerances of .1 psia, 1°F, 1% saturation and have not found sensitivity of results to tighter tolerances.

#### PVT TREATMENT

At saturated conditions,  $U_w, U_g, c_w, \rho_g$  are evaluated as single-valued functions of temperature from the Steam Tables [7].  $U_w$  is assumed a single-valued function of temperature for undersaturated water. Density of undersaturated water is calculated as

$$\rho_w = \rho_{ws}(T) [1 + c_w(T)(p - p_s(T))] \quad (7)$$

where subscript  $s$  denotes saturation condition. The "compressibility"  $c_w(T)$  is derived as follows. The Steam Tables [7] include a tabulation of  $(v - v_s)$  for undersaturated water as a function of temperature and pressure, where  $v$  is specific volume, cubic feet per pound. The tabular values are fit well by the expression

$$v - v_s = s(T)(p - p_g(T))$$

where  $s(T)$  is dependent only upon temperature as:

T, °F	s(T) x 10 <sup>5</sup>
< 200	.0054
300	.0072
400	.0109
500	.0205
600	.065
660	.355

This equation can be written

$$\frac{1}{\rho_w} = \frac{1}{\rho_{ws}(T)} - \frac{s(T)\rho_{ws}(T)}{\rho_{ws}(T)}(p - p_g(T))$$

Since  $s(T)\rho_{ws}(T)(p - p_g(T))$  is small in comparison to 1 (except at temperatures approaching 700°F), this equation can be written as Equation (7) where  $c_w(T)$  is  $s(T)\rho_{ws}(T)$ .

For superheated steam, internal energy  $U_g$  and density  $\rho_g$  are approximated by

$$U_g = U_{gs}(p) + C_{p\text{steam}}(T - T_g(p)) \quad (8)$$

$$\rho_g = \rho_{gs}(p) \frac{T_g(p) + 460}{T + 460} \quad (9)$$

where specific heat  $C_{p\text{steam}}$  is constant.

Equation (9) is accurate in proportion to the constancy of steam z-factor from  $p$ ,  $T_g(p)$  to  $p$ ,  $T$ . Water and steam phase viscosities are evaluated as single-valued functions of temperature equal to their respective saturated values. Enthalpies are

$$H_w = U_w + 144/778.2 p/\rho_w \quad (10)$$

$$H_g = U_g + 144/778.2 p/\rho_g$$

The model uses steam phase pressure as the pressure variable in all PVT relationships.

Porosity is calculated from

$$\phi = \phi_0(1 + c_r(p - p_0)) \quad (11)$$

where  $\phi_0$  is porosity at pressure  $p_0$  and  $c_r$  is constant. Reservoir thermal conductivity may vary with spatial position, but is treated as independent of pressure, temperature and saturation. Formation rock heat capacity may vary with position but is independent of temperature. Overburden thermal conductivity and heat capacity are constants.

### IMPLICIT AND SEMI-IMPLICIT ALLOCATIONS

#### OF WELL RATE AMONG LAYERS

Numerical simulation of most reservoir processes encounters the problem of representing production rates from wells located in grid blocks of large areal dimensions. The reservoir grid system consists of  $NZ$  vertical layers with the layers numbered from top to bottom as  $k = 1, k = 2, \dots, k = NZ$ . A producing well located in areal block  $(i, j)$  is perforated or open to flow in layers  $k = k_1, k_1 + 1, \dots, k_2$ . For example,  $NZ$  might be 8 and a well open in layers 3-7, ( $k_1 = 3, k_2 = 7$ ). The wellbore radius is denoted by  $r_w$ . The grid blocks penetrated by the well are of dimensions  $\Delta x, \Delta y, \Delta z_k$  where  $\Delta x$  and  $\Delta y$  are the areal dimensions. Assuming (a)  $\Delta x = \Delta y$ , (b) the well is located areally near the center of the grid block, (c) steady- or semi-steady-state radial flow in each grid block  $\Delta x, \Delta y, \Delta z_k$  open to the well, (d) no vertical crossflow between open layers, we can derive from Darcy's law for single-phase flow of a unit mobility fluid ( $k_r/\mu = 1$ )

$$Q_k = \frac{2\pi(k\Delta z)_k}{\ln(r_e/r_w) + S}(p_k - p_{wbk}) = PI_k(p_k - p_{wbk}) \quad (12)$$

where:

- $Q_k$  = rate of radial flow of a unit mobility fluid in layer  $k$  from grid block to the wellbore, cubic feet/day,
- $k_k$  = absolute permeability of layer  $k$ , md x 0.00633,
- $\Delta z_k$  = layer thickness, feet,
- $S$  = skin factor,
- $r_e$  =  $\sqrt{\Delta x \cdot \Delta y / \pi}$  = equivalent radius feet,
- $p_k$  = pressure in grid block  $i, j, k$  at  $r = r_e$ , psia,
- $p_{wbk}$  = flowing wellbore pressure opposite layer  $k$ , psia.

In practice, for the case where  $r_c \gg r_w$ , we assume  $p_k$  equal to the average grid block pressure calculated in the simulator and, for more rigor, replace  $S$  by  $S - 1/2$  or  $S - 3/4$  for steady- or semi-steady-state flow.  $PI_k$  denotes the coefficient in Equation (12), a layer productivity index in units of cubic feet/day-psi. All pressures  $p_k$ ,  $p_{wbk}$  refer to points vertically centered in the thickness  $\Delta z_k$ .

In the geothermal reservoir case treated here,  $\bar{q}$  denotes the well target or desired production rate, and  $\bar{p}_{wb}$  denotes the minimum flowing wellbore pressure in layer  $k_t$ . If no tubing is in the well, then  $k_t$  would normally be specified as  $k_1$ , the uppermost open layer. If tubing is in the perforated casing, then a minimum (bottomhole tubing) wellbore pressure may be specified at any layer,  $k_1 \leq k_t \leq k_2$ .

$p_{wb}$  denotes the actual flowing wellbore pressure at the center of layer  $k = k_t$  and  $q$  denotes the actual total well production rate, lbs  $H_2O$  per day. The flowing wellbore pressure in layer  $k$  is denoted by

$$p_{wbk} = p_{wb} + \Delta p_{wbk} \quad (13)$$

From Equations (12) and (13) the production rates of water phase, gas (steam) phase, total  $H_2O$  and enthalpy from layer  $k$  are

$$\begin{aligned} q_{wk} &= \alpha_{wk} (p_k - p_{wb} - \Delta p_{wbk}) \\ q_{gk} &= \alpha_{gk} (p_k - p_{wb} - \Delta p_{wbk}) \end{aligned} \quad (14)$$

$$q_k = q_{wk} + q_{gk} = \alpha_k (p_k - p_{wb} - \Delta p_{wbk})$$

$$q_{hk} = q_{wk} H_{wk} + q_{gk} H_{gk}$$

where

$$\alpha_{wk} = PI_k (k_{rw} n_w / \mu_w)_k$$

$$\alpha_{gk} = PI_k (k_{rg} n_g / \mu_g)_k$$

$$\alpha_k = \alpha_{wk} + \alpha_{gk}$$

and  $n_w$ ,  $n_g$  are phase densities in units of lbs  $H_2O$  per cubic foot.

As discussed above, the interblock flow rates and heat loss and conduction terms are all treated implicitly in the simulator described herein. If, in addition, the well sink or source terms are implicit, then the entire simulator is implicit. The logic and coding necessary for implicit well treatment is rather simple for the case of a well completed in a single layer of the reservoir grid. Implicit treatment can be extremely difficult for a producing well completed in several layers.

In this section we describe an implicit treatment for multilayer well completion and present several semi-implicit simplifications. Note that  $\alpha_k$  in Equations (14) is a function of pressure, temperature and, due to relative permeabilities, saturation  $S$ . Enthalpies  $H_w$ ,  $H_g$  are functions of pressure and temperature. Total well production rate  $q$  is the sum of  $q_k$  over layers  $k_1 - k_2$  or

$$q = \sum \alpha_k (p_k - \Delta p_{wbk}) - p_{wb} \sum \alpha_k \quad (15)$$

where the summation term  $\sum$  denotes summation from  $k_1$  to  $k_2$ . Rearranging Equation (15) gives

$$p_{wb} = (\sum \alpha_k (p_k - \Delta p_{wbk}) - \bar{q}) / \sum \alpha_k \quad (16)$$

as the flowing bottomhole wellbore pressure at center of layer  $k_t$  necessary to produce the well target rate  $\bar{q}$  lbs  $H_2O$  per day. The well is on deliverability if  $p_{wb}$  from Equation (16) is less than the specified minimum value  $\bar{p}_{wb}$ . In any event, the production rates of water, steam and  $H_2O$  are given by Equations (14a) - (14c) with  $p_{wb}$  equal to the larger of  $\bar{p}_{wb}$  and the value given by Equation (16).

Implicit well treatment requires that water phase production rate given by Equation (14a) be expressed as

$$\begin{aligned} q_{wk} &= q_{wk} + \sum \frac{\partial q_{wk}}{\partial T_m} \delta T_m + \sum \frac{\partial q_{wk}}{\partial S_{gm}} \delta S_{gm} \\ &+ \sum \frac{\partial q_{wk}}{\partial p_m} \delta p_m + \frac{\partial q_{wk}}{\partial p_{wb}} \delta p_{wb} \end{aligned} \quad (17)$$

where summation here is over  $m$  from  $k_1$  to  $k_2$ , superscript  $i$  denotes evaluation at latest iterate values of all variables, all partial derivatives are evaluated at latest iterate conditions,  $\delta T_m$ ,  $\delta S_{gm}$ ,  $\delta p_m$  are changes in layer  $m$  over the coming iteration and  $q_{wk}$  is an approximation to the end-of-time step (implicit) value  $q_{wk,n+1}$ . The gas

phase production rate  $q_{qk}$  in Equation (14b) is represented in an analogous fashion. If the producing cell is two-phase ( $0 < S_g < 1$ ), then  $\delta T_m = (dT/dp)_s \delta p_m$  where  $(dT/dp)_s$  is the slope of saturated temperature vs. saturated pressure at the latest iterate pressure value. If the producing cell is single-phase ( $S_g = 0$  or  $S_g = 1$ ), then  $\delta S_g = 0$ . Thus only two of the three unknowns  $\delta T_m$ ,  $\delta S_{gm}$ ,  $\delta p_m$  are independent in any case.

The implicit expressions for  $q_{wk}$ ,  $q_{gk}$ ,  $q_{hk}$  of type shown in Equation (17) introduce one additional unknown  $\delta p_{wb}$  for each well. The additional required equation corresponding to this unknown is the constraint equation stating that the summation over  $k$   $\sum (q_{wk} + q_{gk})$  equals target well rate  $\bar{q}$  lbs H<sub>2</sub>O/day:

$$\sum_{k=k_1}^{k_2} \left[ \left( \frac{\partial q_{wk}}{\partial T_m} + \frac{\partial q_{gk}}{\partial T_m} \right) \delta T_m + \left( \frac{\partial q_{wk}}{\partial S_{gm}} + \frac{\partial q_{gk}}{\partial S_{gm}} \right) \delta S_{gm} + \left( \frac{\partial q_{wk}}{\partial p_m} + \frac{\partial q_{gk}}{\partial p_m} \right) \delta p_m + \left( \frac{\partial q_{wk}}{\partial p_{wb}} + \frac{\partial q_{gk}}{\partial p_{wb}} \right) \delta p_{wb} \right] = 0 \quad (18)$$

This Equation (18) guarantees that  $\sum (q_{wk} + q_{gk}) = \bar{q}$  because  $q_{wk}^l$ ,  $q_{gk}^l$  are calculated using latest iterate values in Equations (14) and  $p_{wb}^l$  from Equation (16). That is,  $\sum (q_{wk}^l + q_{gk}^l) = \bar{q}$ . If the well is on deliverability (i.e.  $p_{wb}^l$  from Equation (16) is  $\leq \bar{p}_{wb}$ ), then  $\delta p_{wb} = 0$  and Equation (18) is not required.

The implicit well treatment consisting of Equations (17) (and similar equations for  $q_{gk}$ ,  $q_{hk}$ ) and (18) is extremely difficult to implement due to the derivatives involved. The derivatives  $\partial q_{wk}/\partial p_m$ ,  $\partial q_{gk}/\partial S_{gm}$ , etc., where  $k \neq m$  arise from the wellbore pressure gradient term  $\Delta p_{wbk}$  which is  $p_{wbk} - p_{wb}$ . This term must be obtained by calculating the horizontal flow rates of water and steam phases from each open layer into the well, cumulating these flow rates upward from layers  $k > k_c$ , downward from layers  $k < k_c$ , performing an energy balance in each wellbore layer by flashing the total flowing stream to obtain quality, and then calculating density (psi/ft) in each wellbore layer by volumetrically averaging steam and water densities. At a given iteration, this calculation is laborious and iterative in itself.

61

A significant simplification results if we evaluate the term  $\Delta p_{wbk}$  in Equations (14) at time level  $n$ . This, of course, results in a semi-implicit well treatment and can result in a time step restriction or conditional stability. Using  $\Delta p_{wbk,n}$  in Equations (14) and employing an implicit approach to the remaining terms, we have

$$q_{wk} = q_{wk}^l + \frac{\partial q_{wk}}{\partial T_k} \delta T_k + \frac{\partial q_{wk}}{\partial S_{gk}} \delta S_{gk} + \frac{\partial q_{wk}}{\partial p_k} \delta p_k + \frac{\partial q_{wk}}{\partial p_{wb}} \delta p_{wb} \quad (19)$$

and similar equations for  $q_{gk}$ ,  $q_{hk}$ , where  $q_{wk}^l$  and all partial derivatives are evaluated at latest iterate conditions (except for  $\Delta p_{wbk,n}$ ). The impact of taking  $\Delta p_{wbk}$  at time level  $n$  is that all derivatives of type  $\partial Y_k/\partial X_m$  are zero unless  $m = k$ . Again, the constraint Equation (18) applies (with  $\partial Y_k/\partial X_m = 0$  if  $m \neq k$ ) if the well is not on deliverability ( $p_{wb}^l > \bar{p}_{wb}$ ) and Equation (18) is inactive with  $\delta p_{wb} = 0$  if the well is on deliverability ( $p_{wb}^l = \bar{p}_{wb}$ ).

A further simplification, for the case where the well is not on deliverability, is

$$q_{wk} = q_{wk}^l + q_{wk}^l \left( \frac{\partial f_{wk}}{\partial T_k} \delta T_k + \frac{\partial f_{wk}}{\partial p_k} \delta p_k + \frac{\partial f_{wk}}{\partial S_{gk}} \delta S_{gk} \right) + \frac{\partial q_{wk}}{\partial p_k} \delta p_k + \frac{\partial q_{wk}}{\partial p_{wb}} \delta p_{wb} \quad (20)$$

where  $\partial q_{wk}/\partial p_k$  is simply  $q_{wk}^l$  and  $f_{wk}$  is mass fractional flow of water phase from layer  $k$ ,

$$f_{wk} = q_{wk} / (q_{wk} + q_{gk}) \quad (21)$$

This simplification automatically holds constant over the coming iteration the  $q_{wk}^l$  lbs H<sub>2</sub>O/day from each layer, as well as the sum  $\sum (q_{wk}^l + q_{gk}^l) = \bar{q}$ . This constancy of  $q_{wk}^l$  eliminates the need for terms involving  $\delta S_{gk}$ ,  $\delta T_k$  in the constraint Equation (18) and the constraint equation becomes simply

62

$$\Sigma \left( \frac{\partial q_{wk}}{\partial p_k} + \frac{\partial q_{gk}}{\partial p_k} \right) \delta p_k + \Sigma \left( \frac{\partial q_{wk}}{\partial p_{wb}} + \frac{\partial q_{gk}}{\partial p_{wb}} \right) \delta p_{wb} = 0 \quad (22)$$

or

$$\Sigma (\alpha_{wk} + \alpha_{gk}) \delta p_k = [\Sigma (\alpha_{wk} + \alpha_{gk})] \delta p_{wb} \quad (23)$$

Thus the constraint equation involves only pressures and if a single-variable pressure equation is solved in a simulator, then Equation (23) is compatible in that no saturation unknowns appear. We used this latter type of constraint equation four years ago in a black oil coning simulation and found that addition of the  $\delta p_{wb}$  unknown considerably improved stability and increased time step size.

If the well is on deliverability, no constraint equation or additional variable  $p_{wb}$  is involved and the simplification of evaluating  $\delta p_{wbk}$  at time level  $n$  is generally satisfactory in geothermal simulations. The incorporation of terms of type  $\partial y_k / \partial x_m$  where  $m \neq k$  in expressions for  $q_{wk}$ ,  $q_{gk}$ ,  $q_{Hk}$  or incorporation of the constraint equation is often difficult from a coding point of view. The difficulty is minimized if z-line SOR or vertical-plane block SOR or direct solution is used, but even in these cases the storage and/or computing time requirements for many-well problems can rise appreciably. If the well is on deliverability, then the first simplification of  $\Delta p_{wbk,n}$  requires only  $\partial y_k / \partial x_k$  derivatives and no constraint equation applies. Therefore, we use this simplification for the deliverability case.

If the well is not on deliverability, we use a simplification even more explicit than those described above. We express

$$q_{wk} = q_{wk}^e + q_k^e \left( \frac{\partial f_{wk}}{\partial T_k} \delta T_k + \frac{\partial f_{wk}}{\partial S_{gk}} \delta S_{gk} + \frac{\partial f_{wk}}{\partial p_k} \delta p_k \right) \quad (24a)$$

$$q_{gk} = q_{gk}^e + q_k^e \left( \frac{\partial f_{gk}}{\partial T_k} \delta T_k + \frac{\partial f_{gk}}{\partial S_{gk}} \delta S_{gk} + \frac{\partial f_{gk}}{\partial p_k} \delta p_k \right) \quad (24b)$$

$$q_{Hk} = \left( q_{wk}^e \left( \frac{\partial H_{wk}}{\partial T_k} \delta T_k + \frac{\partial H_{wk}}{\partial p_k} \delta p_k \right) + q_{gk}^e \left( \frac{\partial H_{gk}}{\partial T_k} \delta T_k + \frac{\partial H_{gk}}{\partial p_k} \delta p_k \right) + H_{wk}^e \delta q_{wk} + H_{gk}^e \delta q_{gk} \right) \quad (24c)$$

where  $q_{wk}^e$  and  $q_{gk}^e$  are computed from Equations (14) using  $\Delta p_{wbk,n}$  and  $p_{wb,n}$  from Equation (16). Thus,  $\Sigma (q_{wk}^e + q_{gk}^e) = \bar{q}$ . The derivatives  $\partial f_{wk} / \partial T_k$ , etc., are evaluated at latest iterate conditions. This simplification runs the risk of pressure instability since no  $\partial q_{wk} / \partial p_k = \alpha_{wk}$ , etc., terms are used. This instability increases as well productivity index PI increases and as rate  $q$  decreases. In two-dimensional areal calculations, no such instability exists since there is no pressure allocation among layers. In many three-dimensional and two-dimensional cross-sectional problems, the PI is sufficiently low that the instability is not significant. In many radial-z single-well problems, the instability is severe and we return to implicit procedures.

In radial-z single-well problems, we achieve implicit well treatment by simply incorporating the wellbore in the reservoir grid system. The result of this inclusion is an even more rigorous well treatment than the implicit treatment described in Equations (17) - (18). For inclusion of the wellbore results in transient mass and energy balances applied within the wellbore. Also, reverse flow in any layers from wellbore to the formation is automatically modelled, whereas this injection in a producing well is very difficult to account for if the wellbore is not modeled by inclusion in the grid. An apparent disadvantage of wellbore modelling is the very small volume grid blocks giving rise to very large throughput ratios (defined below) for reasonable time step sizes. Our hope at the outset of this work was that the implicit treatment throughout the wellbore and reservoir would eliminate instabilities regardless of very high throughput ratios.

The multiphase flow vertically within or laterally from the column of wellbore grid blocks cannot be modeled by the usual multiphase Darcy flow expressions. The large gas-liquid density difference and high effective vertical "permeability" of the wellbore results in domination by gravity forces even at very high producing rates. This gravity dominance gives low calculated steam saturations in the wellbore resulting in a liquid pressure gradient and high back pressure on the lower formation. At normal rates of geothermal wells, the Reynolds number is so high that assumption of fully developed turbulent flow in the wellbore is usually a good one and assumption of no-slip two-phase flow is an even better one. This no-slip condition is equivalent to volumetric fractional flow equalling saturation.

We programmed this no-slip flow in lieu of usual Darcy flow logic for the wellbore. Alternatively, we could use the Darcy flow logic but calculate wellbore pseudo relative permeabilities which result in volumetric fractional flow  $f_g = S_g$ . This approach would

require two sets of pseudo relative permeabilities since gravity enters for vertical but not for lateral flow. The vertical wellbore effective permeability used in calculations described below was sufficiently large to hold viscous pressure drops over 500 feet of wellbore to less than 3 psi.

This inclusion of the wellbore in the grid system allows radial-z or r- $\theta$ -z simulation of the entire wellbore and overburden from the formation to the surface (well-head). A problem arises here in altering the no-slip wellbore two-phase flow calculation so that agreement is obtained with two-phase vertical pipe flow correlations. Apart from this problem, the model allows simulation of transient wellbore flow conditions and wellbore heat loss, in addition to the transient multiphase heat and fluid flow in the reservoir. Vertical grid definition in this case would extend from ground surface down to and through the permeable formation.

#### EFFECT OF STEAM FLASHING ON WELL DELIVERABILITY

A problem in use of Equations (14) arises even in an areal simulation where  $NZ = 1$ ,  $k = 1$  and  $\Delta p_{wbk} = 0$ . The mobilities and specific volumes in Equations (14) are generally evaluated at average (exterior) grid block conditions. If flashing of steam occurs between  $r_e$  and  $r_w$ , then Equations (14) can give considerable error since they do not account for the increasing volumetric flow rate (at constant mass flow rate) toward the well due to water flashing and steam expansion accompanying pressure decline.

Deliverability of a single layer can be corrected to account for water flashing and steam expansion by inserting a fraction  $f$ , equal to or less than 1, as

$$q = f(\alpha_w + \alpha_g)(p - p_{wb}) \quad (25)$$

where, as before,  $\alpha_w$  and  $\alpha_g$  are evaluated at known block average (exterior) conditions. The factor  $f$  is a calculable function of  $p_{wb}$ ,  $p$  and  $S_{ge}$  where  $S_{ge}$  is gas saturation at  $r = r_e$ , which in turn is generally very close to average grid block saturation. Equation (25) presumes that the average grid block condition is saturated. The Appendix describes the calculation of  $f$  and gives a revision of Equation (25) for the case where the saturation point lies between  $r_w$  and  $r_e$ . The calculation of  $f$  ignores capillary pressure and assumes steady-state radial flow from pressure  $p$  at  $r_e$  to pressure  $p_{wb}$  at  $r_w$ .

63

In addition to  $p_{wb}$ ,  $p$  and  $S_{ge}$ ,  $f$  is also dependent upon the relative permeability curves. Therefore, a completely general representation of  $f$  is not possible. Figure 1 gives  $f$  as a function of  $p_{wb}$ ,  $p (= p_e)$  and  $S_{ge}$  for relative permeability curves

$$k_{rw} = [(S_w - S_{wc}) / (1 - S_{wc})]^{n_w} \quad (26a)$$

$$k_{rg} = k_{rgcw} [(S_g - S_{gc}) / (1 - S_{wc} - S_{gc})]^{n_g} \quad (26b)$$

with  $S_{wc} = .2$ ,  $S_{gc} = 0$ ,  $n_w = n_g = 2$  and  $k_{rgcw} = .5$ .

Figure 1 shows that the deliverability reduction factor is 1 for minimal drawdowns ( $p_e - p_{wb}$ ), decreases with increasing drawdown and, for a given drawdown, it increases with increasing grid block steam saturation,  $S_{ge}$ . The factor can reach values of .25 or lower for low  $S_{ge}$ , high drawdown and/or low reservoir pressure  $p_e$ . This means that deliverabilities calculated using Equation (14) can be erroneously high by a factor of four or more.

#### Comparison of Numerical Model and Analytical Deliverabilities

A radial test problem was used to compare the simulator's calculated deliverability with that of Equation (25). This problem was also used as a preliminary test of simulator stability and time-truncation error. Reservoir and fluid property data for this problem are given in Table 1. A 9x1 radial grid was employed with the well producing on deliverability against a wellbore pressure of 160 psia.

In the past, we have performed radial gridding by specifying  $r_w$ ,  $r_e$  and an arbitrary first block "center" radius  $r_1$ . Geometric block center spacing gives  $r_i = \alpha r_{i-1}$  where  $i$  is r-direction grid block index. Thus,  $r_N = \alpha^{N-1} r_1$  and  $r_{N+1} = \alpha^N r_1$  where  $N$  is the number of radial reservoir grid blocks. Demanding that  $r_e$  be the log mean radius between  $r_N$  and  $r_{N+1}$  gives the equation

$$\frac{\alpha^{N-1} (\alpha - 1) r_1}{\ln \alpha} = r_e \quad (27)$$

64

which is solved for  $\alpha$  by the Newton-Raphson technique. Generally  $r_1$  values of at least 3 feet or more have been used to avoid excessively small grid blocks adjoining the wellbore.

In this work we retain the geometric spacing  $r_i = \alpha r_{i-1}$  but eliminate the arbitrary specification of  $r_1$ . Rather we invoke an imaginary radius  $r_0$  within the wellbore in addition to radius  $r_{N+1}$  outside  $r_e$  and require  $r_w$  be the log mean radius of  $r_0$  and  $r_1$  and  $r_e$  be the log mean of  $r_N$  and  $r_{N+1}$ . This gives

$$\frac{(\alpha - 1)r_0}{\ln \alpha} = r_w \quad (28a)$$

$$\frac{\alpha^N (\alpha - 1)r_0}{\ln \alpha} = r_e \quad (28b)$$

and division of Equation (28b) by Equation (28a) gives a direct solution for  $\alpha$  as

$$\alpha = (r_e/r_w)^{1/N} \quad (29)$$

Grid block boundary radii used to calculate block pore volumes are calculated as log mean values of adjacent block center radii. Table 1 gives the resulting block center and boundary radii for the case of nine radial increments. The pore volume of the first grid block is 22.27 RB corresponding to 500 feet of formation thickness.

The simulator was run in one-dimensional radial mode using constant 250-day time steps to 16,000 days. Zero capillary pressure was used and the well was on deliverability against the 160 psia flowing bottomhole pressure. The solid curve in Figure 2 shows the calculated flow rates, expressed per foot of formation thickness, vs. average formation steam saturation. This saturation is close to the exterior grid block 9 saturation, but was calculated as a volume weighted average of all blocks. Figure 2 shows an initial deliverability decline followed by a temporary increase. This behavior was unaffected by time step size, closure tolerances, number of radial blocks and inclusion or exclusion of heat conduction and heat loss in the calculation.

The dotted lines in Figure 2 show deliverability from the steady-state Equation (25) for  $P_{wb} = 160$ ,  $p = p_e = 251$ . The agreement between model production rate and Equation (25) is good considering that

(a) the model used a closed exterior boundary, (b) the model is in a transient decline exhibiting semi-steady-state neither in pressure nor saturation, (c) Equation (25) assumes steady-state with an open exterior boundary. Further, the deliverability factor  $f$  varies from .3428 at  $S_{ge} = 0$  to .78 at  $S_{ge} = .5$  and the discrepancy between the two curves is much less than the error which would occur using Equation (25) with  $f = 1$ .

The one-dimensional radial test problem was run to a large time to reach steady-state with an exterior-block well injecting 400°F water at a bottomhole pressure of 251.08 psia at  $r = r_e$ . Following several time steps to 100 days to allow pressure in grid block 9 to fall below 251 psia (to activate the injection well), two 60,000-day time steps (these steps required 7 and 2 iterations) were taken. The steady-state flow rate calculated was 130,000 lbs H<sub>2</sub>O/hour. Equation (37) gives for  $p_{wb} = 160$ ,  $p_e = 251$  and  $S_{ge} = 0$  (corresponding to injection of saturated 100% liquid water),

$$q_{H_2O} = \frac{2\pi k \Delta z I}{r_e \ln \frac{r_e}{r_w}} = \frac{2\pi (100) (500) (.00633)}{\ln \frac{2000}{.25}} \cdot \frac{12,728 \text{ lbs}}{24 \text{ hr}} = 117,349 \text{ lbs/hr}$$

The discrepancy between 130,000 and 117,349 lbs/hour is believed due to the model's upstream weighting of mobilities as opposed to the integration of mobility in Equation (37). In any event, since  $f = .3428$  for  $p_e = 251$ ,  $p_{wb} = 160$  and  $S_{ge} = 0$ , the discrepancy of about 13,000 lbs/hour is small in comparison with the error in using Equation (25) with no correcting  $f$  factor. Equations (14) used for an areal grid block of 2,000 feet equivalent exterior radius would give a deliverability of 343,000 lbs/hour. Use of the  $f$  factor and Equation (25) would give a calculated deliverability of 117,349 lbs/hour.

#### THROUGHPUT RATIO

Evaluation of any term in the interblock flow rates explicitly (at time level  $n$ ) with respect to any of the dependent variables ( $p$ ,  $T$ ,  $S_g$ ) in general will result in a conditional stability. This conditional stability takes the form of an expression giving a maximum time step. Use of a time step size exceeding this maximum will result in divergence of the calculations. The expression for maximum time step generally involves, at least in part, a throughput ratio defined in some manner.

One of the most severe instabilities in multiphase flow simulation is that arising from explicit evaluation of saturation-dependent relative permeabilities in the interblock transmissibilities. The throughput ratio that arises in analysis of this instability is

$$R_{Ti} = \frac{q_i \Delta t}{V_p S_i} \quad (30)$$

where  $i$  denotes phase (e.g., water, gas or oil),  $q_i$  is volumetric phase flow rate through the grid block,  $S_i$  is grid block saturation of phase  $i$  and  $V_p$  is grid block pore volume. Thus  $R_{Ti}$  is the ratio of total volume of phase  $i$  passing through the grid block in one time step divided by the volume of phase  $i$  in the block.

Actually, this ratio appears with a multiplier equal to fractional flow derivative, but we are not concerned here with detailed derivations or presentations of stability analysis results. As a practical matter, we have rated the stability of a multiphase flow formulation or model by the cruder ratio

$$R_T = \frac{q_v \Delta t}{V_p} \quad (31)$$

where  $q_v$  is total (all phases) volumetric flow rate through the grid block.

In the geothermal case we can express the above ratio in terms of total mass flow rate of  $H_2O$  and quality  $X$  of the flowing stream. Many of the results discussed below involve a well producing on deliverability at a flowing bottomhole pressure of 160 psia. Using corresponding water and steam densities of 55 and .355 lbs/cu.ft., respectively, we can express  $R_T$  as

$$R_T = 4.27(2.8X + .018)q\Delta t/V_p \quad (32)$$

where  $q$  is total mass flow rate in lbs  $H_2O$ /hour,  $\Delta t$  is time step in days and  $V_p$  is reservoir barrels (RB).

Our previous experience with a variety of semi-implicit isothermal and thermal simulators, producing under multiphase flow conditions, has indicated instability or time step restriction at throughput ratios in the range of 1,000 to 20,000. We will return to Equation (32) in connection with results discussed below.

### TIME TRUNCATION ERROR AND STABILITY FOR ONE-DIMENSIONAL RADIAL PROBLEM

Time truncation error and model stability were examined in the one-dimensional radial case by repeating the 16,000-day run described above with time steps of 500, 1,000, 2,000, 4,000, 8,000 and 16,000 days. Table 2 shows the effect of time step size on calculated recovery, producing quality and rate at 4,000, 8,000 and 16,000 days. The time truncation error is quite acceptable for time steps up to 1,000 days.

All these runs converged each time step with two to three iterations per step except for the first step when steam saturation increased from zero to about .45 at the well and 0 - .39 at the 9th block. The first time step required 20-23 iterations, the 23 iterations corresponding to the 16,000-day time step run. The largest throughput ratio occurred for the 16,000-day time step which, from Equation (32), is

$$\begin{aligned} R_T &= 4.27(2.8(.0835) + \\ &.018)(67,900)(16,000)/22.27 \\ &= 52.45 \times 10^6 \end{aligned}$$

This ratio is more than three orders of magnitude larger than the 20,000 ratios of our previous experience mentioned earlier. However, one-dimensional problems are generally poor tests or indicators of true model competence and ratios from two-dimensional results presented below will be given more emphasis.

### TWO-DIMENSIONAL SINGLE-WELL PROBLEM RESULTS

We simulated the radial flow problem described in Table 1 using a two-dimensional 10 x 5 radial-z grid. The five layers were each 100 feet thick. The 10 radial grid blocks included the wellbore. Table 1 gives the grid block center radii, boundary radii and pore volumes calculated using Equation (29). Note that the first reservoir grid block has a center radius of only .40 feet and a pore volume of only 4.45 RB. The pore volume of each wellbore grid block is 3.5 PB so that the throughput ratio, Equation (32), becomes

$$R_T = 1.22(2.8Q + .018)q\Delta t \quad (33)$$



Rock capillary pressure was assumed negligible in this problem and a pseudo straight-line capillary pressure curve [8, 9] corresponding to layer thickness of 100 feet was employed. Use of saturated steam-water densities at 400°F gives a density difference of .369 psi/foot which translates, for 100-foot layer thickness, to a pseudo capillary pressure equalling 18.45 psi at  $S_w = S_{wc} = .2$  and -18.45 at  $S_w = 1.0$ .

A number of 10,000-day model runs were performed for different well completion intervals. We assumed a tubing/casing configuration so that an additional variable was the layer in which the tubing bottom or withdrawal point was located. For example, with all layers 1-5 perforated, the tubing bottom could be placed in any one of the layers. A packer was assumed placed at top of formation.

A well target rate of 300,000 lbs/hour was specified for all runs with a minimum flowing wellbore pressure at tubing bottom of 160 psia. For all runs, time step was specified as 500 days. Table 3 summarizes model results at 10,000 days. The listed mass fraction produced, producing bottomhole quality, producing rate and produced Btu/lb all apply at the 10,000-day point in time. Average Btu/lb produced is cumulative energy produced over 10,000 days divided by cumulative mass produced. Energy produced is enthalpy, defined as  $U + pv$  at producing cell conditions. Internal energy  $U$  is relative to a zero value for  $U$  of saturated water at 60°F.

Table 3 shows that the location of a single-layer (100 feet) completion is very important. Comparing runs 1-3 shows that cumulative mass fraction recovered at 10,000 days varies from 11.7% to 47.4% as a 100-foot producing interval is lowered from the top 100 feet to the bottom 100 feet of the 500-foot formation.

Runs 4-11 in Table 3 indicate that the perforated or open interval location is important while the location of the tubing bottom or withdrawal point within a given open interval is relatively unimportant. For example, Runs 4 and 5 show about equal recovery values for their top 300 feet open interval regardless of whether the tubing withdrew from the top 100 feet or bottom 100 feet of the interval. Runs 6-7 show the same result for a bottom 300-foot open interval regardless of the tubing position within the open interval. The best recoveries occur for a completely penetrated or open formation -- Runs 9-11 -- and performance is nearly independent of whether the tubing is set at top or bottom of the formation.

In Runs 1-5 the well was on deliverability in the first 500-day time step. Runs 6-7 and 9-11 produced the target 300,000 lbs/hour rate for 1,500 days and Run 8 produced the target rate for 500 days.

Taken together, Runs 1-11 indicate that a partial completion interval effectively drains the portion of the reservoir formation opposite and above the interval, but inefficiently drains the formation below it.

Spatial truncation errors in the results of Table 3 are very small as indicated by several runs we made using a 10 x 10 grid with ten 50-foot thick layers. Time truncation error was examined by repeating Run No. 10 using time steps of 250, 1,000, 2,000 and 5,000 days. Figure 3 shows producing rate and bottomhole producing quality vs. time calculated using the various time steps. The results with  $\Delta t = 250$  and  $\Delta t = 500$  days are virtually identical. The error with  $\Delta t = 1,000$  days is significant but not large while  $\Delta t = 2,000$  days causes an error bordering on acceptability. The surprising feature of these results is the small time truncation error for steps of 1,000 days or less in light of the large changes in saturation which occur in a single step.

The saturation changes stably computed in a single step are illustrated in Table 4 which shows saturations and pressures at the end of the first 2,000-day time step (all layers open, tubing at layer 3). Maximum saturation change was .9989 in grid block ( $i=1, k=1$ ) and maximum pressure change was -441.4 psi in grid block ( $i=1, k=5$ ). Initial pressures ranged from 469 to 618 psia from formation top to bottom, some 200 to 350 psi above saturation pressure corresponding to 400°F. That is, the model in this single step proceeded from a highly undersaturated, 100% liquid configuration to that shown in Table 4. Note, also, from Figure 3 that time truncation error for this first time step is virtually negligible. The reader should recall in viewing Table 4 that the first column of cells is the wellbore.

The calculated producing rate for this first 2,000-day step was 286,400 lbs/hour and bottomhole quality was .05794. Using Equation (33), the throughput ratio for withdrawal cell ( $i=1, k=3$ ) was

$$R_T = 1.22(286,400)(2.8(.05794) + .018)(2,000) = 126 \times 10^6$$

This throughput ratio was achieved with the producing cell steam saturation changing from 0 to .8993. That is, it is not a throughput ratio corresponding to stabilized conditions

with small changes per time step. This ratio is three to four orders of magnitude larger than the 20,000 ratios we have previously achieved with semi-implicit models under high rate-of-change conditions.

Table 5 shows the number of required iterations per time step for each step for the three runs using  $\Delta t = 500, 1,000$  and  $2,000$  days. The numbers in parentheses in Table 5 are the maximum grid block saturation changes over the grid during each time step.

Table 6 shows calculated pressures and saturations after the first 500-day time step of Run No. 8. Producing rate and quality were 300,000 lbs/hour and .04, respectively, so that the throughput ratio from Equation (33) was

$$R_T = 1.22(300,000)(2.8(.04) + .018)(500) = 23.8 \times 10^6$$

This ratio was achieved with a high steam saturation change in the producing cell from 0 to .8481. Required iterations for this first step were 30. The iterations declined to 24 when initial pressure at formation top was reduced to 270 rather than 450 psia. The throughput ratio at 10,000 days for this run was  $11.5 \times 10^6$  corresponding to a producing rate and quality of 53,100 lbs/hour and .1208, respectively.

Run 12 in Table 3 is identical to Run 10, except that permeability is 500 md rather than 100 md. The higher permeability resulted in a greater recovery of .7459 compared to .5656 at 10,000 days and gave a considerably higher producing quality of .7058 at 10,000 days. Run 12 produced the target 300,000 lbs/hour rate until 5,000 days. Figure 4 shows the effect of permeability on producing rate and quality vs. mass fraction produced. Producing quality in Figure 4 is calculated at a separator condition of 100 psia. The curves of average reservoir pressure (volumetrically weighted average of all grid blocks) vs. mass fraction produced are not plotted, but are identical for the two runs. Figure 4 shows that produced stream quality at the fixed separator condition is nearly a single-valued function of mass fraction produced and independent of permeability level.

Figure 5 shows average reservoir pressure vs. mass fraction produced calculated for 10,000-day runs using  $k = 100$  and  $500$  md and  $\phi = .05$  and  $.35$ . The figure indicates that permeability level has a negligible effect on average pressure vs. mass fraction produced. The large porosity results in a very slightly lower average reservoir pressure. The small effect is due to the lower

rock heat capacity (i.e. less rock) in a higher porosity formation. This small effect of porosity on pressure decline is in contradiction to results reported elsewhere [4].

The average computer time per run for Runs 1-11 was 16 CDC 6600 CPU seconds. For the  $10 \times 5$  grid and 20 steps per run this translates to .016 seconds per grid block-time step. This figure compares to a rough value of .01 seconds\* per grid block-time step for our semi-implicit models.

### SIMULATION OF A FRACTURED-MATRIX RESERVOIR

Many geothermal reservoirs are known or believed to be fractured-matrix systems. Conventional simulation is often used where extensive fractures are known to exist. Such simulation employs an assumption that flow in the matrix-fissure system can be adequately modeled by assuming an unfractured matrix formation with a high effective permeability reflecting the fracture system conductivity.

Here we examine the difference in simulated performances of a fractured reservoir sector modelled first as an unfractured formation, and second as a matrix-fissure system. While nature seldom provides near-uniformity in spacing of fractures, we must employ some semblance of uniform spacing to perform any calculations. We consider a fractured system consisting on the average of  $40 \times 40 \times 40$  feet matrix blocks separated by a three-dimensional orthogonal planar system of vertical and horizontal fractures.

To reduce the dimensionality of the matrix calculation, we treat the matrix cubes as cylinders of equivalent radius 22.5676 feet ( $\pi r^2 = 40 \times 40$ ) and height of 40 feet. We have used this cylindrical approximation for several years in black oil fractured matrix simulation; it is partially justified since the physically real irregularity of fracture spacing and angles undoubtedly yields a variety of matrix block shapes deviating considerably from rectangular parallelepipeds.

Use of a fracture volume equal to 1% of combined fracture plus matrix volume leads to a fracture width of .029 feet. This figure assumes equal widths of horizontal and vertical fractures. From Muskat [10], fracture permeability for width  $w$  in cm, is

\*This number can vary considerably. For "easy" multiphase flow problems (we omit definitions of "easy" for brevity), we have achieved times as low as .0018 seconds per block-step.

$$k = 10^8 w^2 / 12 = 6.5 \times 10^6 \text{ Darcies}$$

(34)

for the .029 feet width. In simulating flow in fracture grid blocks, it is only necessary to use fracture permeabilities large enough to render viscous forces negligible in comparison with gravitational forces. In previous black oil fractured matrix reservoir work and in this work, we have found results insensitive to use of fracture permeabilities higher than 10 to 20 Darcies.

For the purpose of computations described here, the fracture system conductivity is assumed sufficiently large that the reservoir behavior is dominated by vertical transients in pressure, temperature and saturation. The fracture conductivity is assumed sufficient to maintain negligible areal gradients of these quantities. For example, by this assumption any steam-water contact in the fractures will be nearly horizontal over a wide areal expanse.

The withdrawal rate used for computations was based on a well spacing of about 300 acres with rates of 300,000 lbs H<sub>2</sub>O/hour per well. This translates to a rate of about 40 lbs/hour for a 1,240-foot vertical column section of the reservoir with areal dimensions 40x40 feet. The vertical gridding consisted of six matrix blocks each subdivided vertically into 10-foot grid blocks and one last deep 1,000-foot matrix grid block. Calculations were terminated before steam-water contacts reached the deep block so that its lack of gridding is immaterial.

In the matrix-fissure simulation, the vertical and horizontal fractures were included in the grid system. Vertically, then, six additional grid blocks each .029 feet thick separated the six matrix blocks and the total number of vertical blocks was 6 x 4 + 1 or 31. We obtained nearly identical results using three and two grid blocks radially for the matrix-fissure system. Results given here are for the case of two radial grid blocks. The first radial block was matrix with an inner boundary radius of 0, an outer boundary radius of 22.5676 feet and a "center" radius equal to the volume mean value of 15.96 feet. The second radial grid block was vertical fracture with inner radius of 22.5676 feet and outer radius of 22.5676 + .029/2 feet. Figure 6 illustrates this radial-z grid for the fissure-matrix simulation. Fluid was withdrawn from the bottom 1,000-foot thick vertical fracture block.

Matrix permeability and porosity were 1 md and 0.2, respectively. Grid block pore volumes for the matrix-fissure system illustrated in Figure 6 were

68 Pore Volume,  
Res. Bbls.

Grid Block	Pore Volume, Res. Bbls.
10-foot matrix	569.9
.029-foot horizontal fracture radial block #1	8.26
.029 x .0145-foot fracture intersection block	.0106
10-foot vertical fracture	3.66

Initial reservoir pressure was 270 psia at top of formation and temperature was 400°F. Overburden heat loss (gain) had a small effect and was ignored. Heat conduction in the matrix was modeled using a thermal conductivity of 38 Btu/ft-day-°F. Matrix rock heat capacity was 35 Btu/cu.ft. rock-°F. Relative permeabilities of Equations (26) and a linear rock capillary pressure curve of  $P_c = 0$  at  $S_w = 1$ ,  $P_c = 10$  psi at  $S_w = 0$  were used for matrix and zero capillary pressure and linear  $k_r = S$  curves were used for the fractures.

The 2 x 31 (radial-z) matrix-fissure simulation was run to 1,500 days for a rate of 40 lbs/hour and to 4,200 days for a rate of 10 lbs/hour. Two runs were made for the 40 lbs/hour rate, the first with a constant 30-day time step, the second with a constant 60-day time step.

Figure 7 shows calculated water saturation vs. depth from top of formation at 1,500 days for the 40 lbs/hour production rate. The solid lines correspond to the 30-day time step while the circles and dashed line show results for the 60-day step. The vertical tic marks indicate water saturations in the first radial horizontal fracture blocks.

This figure shows the poor recovery of water from the matrix blocks due to the capillary discontinuities imposed by the horizontal fractures. Each matrix block above the (vertical fracture) steam-water contact transiently drains toward an equilibrium final saturation vs. depth distribution determined by the rock capillary pressure curve and the zero  $P_c$  condition at each matrix block bottom imposed by the horizontal fracture. The significant transient effect is indicated by the decrease in water recovery with matrix block depth. This is due, of course, to the longer times of drainage experienced by higher located matrix blocks.

The horizontal fracture blocks opposite the 100% steam saturated vertical fracture grid blocks rapidly rise toward 100% steam saturation. Above the steam-water contact, the water draining from the bottom of a matrix block enters the horizontal fracture block and then preferentially flows vertically down into the top of the next lower matrix block rather than laterally into the vertical fracture. This preference is very close to 100%. These latter results are shown by model printouts of water and steam interblock flow rate magnitudes and directions at selected times.

Table 7 summarizes average iterations per time step, average saturation change (maximum over grid) per time step and computing times for the three fractured-matrix simulation runs. The negligible time truncation error for 30- and 60-day time steps shown in Figure 7 is somewhat surprising in light of the average saturation change rising from .38 for the 30-day step to .66 for the 60-day step. The .66 figure is actually conservative since 27 vertical fracture grid blocks were swept from 0 to 100% steam saturation in only 25 steps in Run 2. No time steps were repeated due to divergence in any of these runs in spite of nearly 100% saturation changes in one step for the .01 RB pore volume fracture-intersection grid blocks. Both Runs 1 and 2 experienced a number of time steps of 90-100% saturation change. Run No. 1 computing time corresponds to a time per block-step of about .01 seconds.

Figure 8 compares the effect of producing rate on matrix-fissure simulation results. The calculated saturations for Run 1 at 40 lbs/hour and Run 3 at 10 lbs/hour are compared at times of equal cumulative production. The steam-water contact for the higher rate is 40% (140 feet vs. 101 feet) deeper due to the shorter time available for transient water drainage from the matrix blocks above the contact.

Conventional simulation results were generated by running the model in one-dimensional vertical mode using 24 10-foot blocks and one 1,000-foot block. The dashed line in Figure 9 shows resulting calculated water saturation vs. depth at 1,500 days for an "effective" permeability of 50 md and a producing rate of 40 lbs/hour. Gravity forces dominate and the conventional results show a sharp transition zone from a drained ( $S_w = S_{wc} = .2$ ) upper region to the 100% water zone. The transition zone is considerably higher than the matrix-fissure simulation results viewing either the matrix or the vertical fracture steam-water contact.

We can achieve somewhat greater realism in the conventional simulation by utilizing the fact that the capillary discontinuities each 40 feet impose a maximum final recovery of water (by flow alone) which can be predetermined using the rock capillary pressure curve, the 40-foot matrix block height and the .369 psi/foot water-steam density (gradient) difference. Following Reference [8] we integrate the  $S_w - P_c$  relation over the 40 feet using the fact that  $P_c = 0$  at matrix block bottom and find that final minimum average matrix block water saturation is .417. Using this value for  $S_{wc}$  in the relative permeability equations, the conventional simulation gives the water saturation profile indicated by the larger dashed line in Figure 9.

Further adjustments in various data might be made to narrow the difference between matrix-fissure and conventional simulation results. Considering the basic difference in mechanisms for the conventional and more correct matrix-fissure calculations, we hold little hope for forcing accuracy from a conventional simulation. In particular, the above described rate effect (Figure 8) is shown by the more rigorous matrix-fissure simulation, but not by conventional simulation (unless the permeability used is very low).

A full three-dimensional simulation of a fractured-matrix reservoir will require tying in this vertical two-dimensional R-Z matrix-fissure calculation to a two-dimensional areal calculation where the areal blocks communicate through the fracture system and the interblock flows reflect the different "sector" or areal block steam-water contacts. This task will involve a significant effort in logic and coding and will in many cases require diskings on fixed memory machines. The two-dimensional R-Z matrix-fissure calculation described here is adequate only if the areal gradients within the reservoir are assumed small due to high fracture conductivity.

#### Interpretation of Pressure Drawdown Tests

The major differences between conventional and matrix-fissure simulation results just described arose because of the two-phase flow in a system having capillary discontinuities. Here we illustrate difficulties which can arise in using conventional simulation to interpret pressure drawdown tests in fractured-matrix, hot water systems with single-phase water flow.

Simulation of a well test in a system having a three-dimensional network of orthogonal fracture planes would require a full three-dimensional Cartesian grid. To simplify for the purpose of illustration, we consider a system of 44-foot matrix layers separated by horizontal fractures. A 10x5 radial-z grid was used to model a horizontal disk of matrix beneath a horizontal fracture. The disk dimensions were exterior radius  $r_e = 10,000$  feet and thickness = 22 feet. The five layer thicknesses were  $w/2, 2, 4, 8, 8$  feet where  $w$  is horizontal fracture thickness. This disk is a symmetrical element for the case where the well penetrates the entire formation thickness.

The radial spacing was calculated using Equation (29) with the wellbore included in the grid. Wellbore radius was .25 and the 10 block "center" radii were .25, .43, 1.38, 4.48, 14.55, . . . , 5,242.37 feet. Pore volumes of the wellbore cells varied from .00014 to .2798 RB in layers 1-5 for a small fracture width  $w = .245$  mm.

Matrix and fracture layer porosities were .2 and 1.0, respectively. Initial temperature was uniformly 350°F and initial pressure was 2800 psia at top of formation. The illustrative pressure drawdown test consisted of producing 10,000 lbs/hour from a well open in all five layers for ten days. Fracture conductivity and matrix permeability were varied in five simulation runs as tabulated in Figure 10. The fracture permeabilities were related to fracture width by the relationship  $k = 10^8 w^2/12$  where  $k$  is in Darcies and  $w$  in cm. The homogeneous (no fracture) case, Run 4, has a permeability of 90.9 md, which gives a total md-ft product for the 22-foot thickness equal to that of the fracture cases.

Figure 10 shows calculated pressure drawdown (initial pressure-flowing wellbore pressure) vs. time on a semi-log plot for five cases. The homogeneous case (Run 4) gives a straight-line and use of the well-known relationship, slope =  $Q_w/4\pi kh$ , gives  $k = 90.9$  md, in agreement with the value used. Arbitrary use of the average slope from .1 to 1 days with the relation slope =  $Q_w/4\pi kh$  gives  $k = 247, 188$  and  $157$  md for Runs 1-3, respectively. These permeabilities bear little resemblance to either fracture or matrix permeabilities.

The semi-log plots of pressure drawdown vs. time actually are not linear for the fracture cases, but are rather concave upward. This results from the fact that the reservoir transient is primarily a crossflow (vertical) bleeding of fluid into the fracture rather than the radial transient of a homogeneous unfractured formation. The degree of upward curvature of the drawdown curve increases as matrix permeability increases.

The cases of small fracture width, Runs 1-3, exhibit a rapid initial drawdown of 60-80 psia in the first few minutes of flow. The calculated effect of a fivefold larger fracture width is one of reducing this early drawdown to 2-3 psi. However, for times after the first few minutes, the larger fracture gives a calculated, concave upward drawdown curve of shape virtually identical to that for the smaller fracture. This is illustrated by the curves for Runs 1 and 5 in Figure 10.

Figure 11 shows calculated drawdowns for a tenfold larger horizontal fracture spacing of 440 feet. The simulations used a 10 x 8 grid with the eight layer thicknesses equal to .0004, 2, 4, 8, 16, 32, 64 and 94 feet (a total thickness of 220 feet). The  $kw$  product for the total fracture width of .0008 feet (.245 mm) is 4 Darcy-feet. A drawdown test flow rate of 100,000 lbs/hour was specified. The curve for this Run 6 in Figure 11 shows a linearity of drawdown vs.  $\ln(t)$  past 10 days to about 30 days. The upward concave curve shape from 100 to 1,000 days is due to establishment of semi-steady-state conditions throughout the reservoir.

The curve labeled Run 7 in Figure 11 was calculated for a 220-foot homogeneous reservoir with  $k = 9.09$  md corresponding to an equivalent total md-feet product of 2,000. The slopes of the curves for Runs 6 and 7 on Figure 11 give formation permeabilities of 18 md and 9.09 md, respectively. If the 10-day test portion of the Run 6 curve were analyzed by conventional radial flow theory, then a permeability of 18 md and a skin factor of 9.65 would be determined. The circles of Run 8 in Figure 11 show the simulator results for a homogeneous reservoir with this permeability and skin factor. Figure 11 shows that calculated drawdowns for the fractured formation (Run 6) and for an 18 md, homogeneous formation with skin (Run 8) agree well through 1,000 days.

These results of Figure 11 indicate that for the particular fracture spacing and width of 440 feet and .245 mm, respectively, conventional radial flow analysis would (a) yield erroneous permeability and skin but (b) give accurate long-term deliverability predictions. This conclusion does not hold for the previously discussed results of Figure 10 corresponding to the smaller fracture spacing of 44 feet. For this spacing, the short-term drawdown test can fail to yield any linearity from which conventional analysis can determine effective permeability and skin.

Several additional complexities that may exist in practice need mentioning in connection with the results just discussed. A naturally fractured formation will generally have vertical as well as horizontal fractures. Accounting for a three-dimensional network of fracture planes with the model

71

## HEAT EXTRACTION FROM HOT DRY ROCK

described herein would require a three-dimensional simulation. If fracture spacing were the order of 100 feet or less, a very large number of grid blocks would be required. A better modelling approach in this case would be a dual porosity formulation where interblock flow is assumed to occur only in the fracture system. The matrix would be accounted for by zero-dimensional, one-dimensional spherical or two-dimensional cylindrical subcalculations tied into the fracture porosity in each grid block. The heat-loss calculation described in Reference [3] is an example of this type of formulation.

The model described here may apply well to an artificially fractured formation since in this case the vertical fractures will intersect the well. An  $r-\theta-z$  grid representing a symmetrical element in this case may accurately model well performance with a reasonably low number of grid blocks.

An upward concave deviation from linearity in a drawdown test curve may result from factors other than formation fractures. Geothermal reservoirs with brines of high salinity may precipitate salt with pressure drawdown near the well. This can cause a skin factor increasing with time and the mentioned deviation from linearity. It is well-known that faults or other flow barriers near a well can cause upward curvature. Short-term drawdown tests on wells which partially penetrate thick formations, especially where the ratio of vertical to horizontal permeability is small, can result in deviation from linearity. Regardless of penetration, a formation consisting of alternating tight and permeable streaks of large permeability contrast can yield deviation from linearity through the same vertical, crossflow type of transient treated above in the horizontally fractured formation calculations. Quoting from Reference [11], which treated simulation of single-phase gas flow, ". . . The reservoir picture finally employed with success stemmed from the hypothesis that the well communicated with a number of thin permeable stringers . . . fed by severely limited crossflow from large sand volumes. . . . In that work, for such reservoirs, the calculated and observed drawdown/buildup curves failed to yield the linearity of conventional analysis.

Finally, the fractured formation, drawdown test illustrative calculations and interpretations presented here are not unique to geothermal reservoirs, but apply to any formation subject to single-phase flow of a low compressibility fluid -- oil, water or high pressure gas.

We consider a vertical fracture in a hot dry rock initially at 530°F. A 5x5x5 three-dimensional grid describes a rectangular parallelepiped with  $\Delta x = \Delta z = 80$  feet and  $\Delta y = .01, 30, 120, 160, 320$ . These dimensions resulted from combining blocks in a comparison run which used  $y$ -direction increments of .01, 10, 20, 40, 80, 160 and 320 feet. The overall dimensions are a 400x400-foot vertical crack of .02-foot width with 630 feet of rock either side of it. The 630 feet of rock in the  $y$ -direction is sufficiently large that the system acts as infinite for the 3,000 days of simulation. Different grids were used to determine the acceptably low spatial truncation error of the 5x5x5 grid.

Since the system is symmetrical about the vertical midplane of the crack, this 5x5x5 grid represents half the system. Crack width is of no consequence except in its relation to the  $kw$  product where  $k$  is fracture permeability and  $w$  is fracture total width. In the grid plane  $j = 1$  (the crack) an  $x-z$  thermal conductivity of 3.8 Btu/ft-day-°F was used, porosity was 1.0 and permeability was varied over a number of runs from 10 Darcies to 800,000 Darcies. In the planes,  $j = 2-5$  (hard rock) thermal conductivity was 38 Btu/ft-day-°F, rock specific heat was 35 Btu/cu.ft.rock-°F and porosity and permeability were zero.

100°F cold water injection rate was specified as 25,000 lbs/hour into the bottom left corner of the crack (cell  $i=1, j=1, k=5$ ). A withdrawal well at the upper right corner of the crack (cell  $i=5, j=1, k=1$ ) maintained pressure at 800 psia due to a large specified productivity index. This withdrawal well produced on deliverability against the 800 psia pressure. The 25,000 lbs/hour injection rate corresponds to actual injection well rate of 50,000 lbs/hour since the grid represents a symmetrical half of the total system.

Figure 12 shows calculated energy recovery and producing well bottomhole temperature vs. time. Energy recovery is defined as cumulative enthalpy produced divided by the sensible heat above 100°F initially contained in a portion of the rock. The portion used is the first 310 feet since the last 320 feet experienced essentially no recovery (temperature decline) at 3,000 days. The initial energy in place on these bases is  $6.944 \times 10^{11}$  Btu. Enthalpy of produced water is  $U + pv$  where internal energy  $U$  is zero at 100°F.

72

Figure 12 shows a rapid decline of produced water temperature from 500°F to less than 300°F in the first few days followed by a very flat decline from 170°F to 137°F from 1,000 to 3,000 days. Fractional energy recovery is 0.1663 at 3,000 days, equivalent to  $1.155 \times 10^{11}$  Btu or an average of 64 Btu/lb water produced (enthalpy relative to zero U at 100°F). The average temperature corresponding to this average enthalpy is about 162°F.

The fracture width  $w$  controls system conductivity or throughput. The corresponding parameter or group of importance is the  $kw$  Darcy-feet product, which is proportional to  $w^3$  since fracture permeability is proportional to  $w^2$ . We used permeabilities up to 800,000 Darcies with the .02-foot model dimension for the fracture. This 16,000 Darcy-foot  $kw$  product corresponds to a fracture width of 4 mm using the fracture permeability equation  $k = 10^8 w^2 / 12$  ( $w$  in cm). Fracture width, i.e. the  $kw$  product, had no effect on the calculated recovery and temperature shown in Figure 12.

Model runs were made with the injection well located higher, 200 feet from top of formation in cell  $i=1, j=1, k=3$ . The change of injection location had no effect on calculated recovery and producing temperature.

Figure 12 also shows calculated recovery and temperature for a larger fracture of dimension 800x800 feet. Again, the above described  $kw$  product and injection well location variations had no effect on the calculated recovery and producing temperature. The larger fracture resulted in a considerably higher bottomhole producing temperature vs. time and a lower fractional energy recovery. Calculated absolute energy recovery at 3,000 days was higher for the larger fracture --  $3.53 \times 10^{11}$  Btu vs.  $1.155 \times 10^{11}$  Btu for the 400x400 foot fracture. Thus, a fourfold increase in fracture area caused a threefold increase in energy recovery. Average enthalpy of produced water was 196 Btu/lb corresponding to an average temperature of produced water of 292°F.

The runs were performed using automatic time step control due to the rapid initial transients. With a first time step of .1 days, a subsequent minimum  $\Delta t$  of .2 days, control by 150°F maximum grid block temperature change per time step and a maximum time step of 500 days, the model took 13 time steps to 3,000 days for the 100,000 Darcy permeability. Computer time for this run was 46 CDC 6600 CPU seconds. Twenty of these seconds were required for the first two time steps.

Calculated results for permeabilities less than 100,000 Darcies exhibited no circulatory "free" convection type cells in the vertical fracture plane. Table 8 shows an example of these results at 3,000 days for the case of a 400x400 foot fracture, and 100,000 Darcies fracture permeability which corresponds to a 2 mm fracture width. The table shows calculated pressures in the fracture plane, temperatures in all planes and interblock flow rates (positive to the right and vertically downward). Water flow is uniformly to the right and upwards away from the injection in grid cell  $i=1, j=1, k=5$ . Temperature uniformly increases to the right and upward (in the directions of water flow) except in the top row.

Results for the 800,000 Darcy permeability differed markedly from those just described. Table 9 shows pressure, temperature and flow rate distributions at 75 days for the 800x800 foot fracture with 800,000 Darcies.  $y$ -direction spacing was altered in this run to .01, 10, 30, 50, 180 feet. The flow rates in Table 9 show extremely strong "free" convection cells in the 5x5 grid of the vertical fracture plane. Water is in fact flowing downward into the injecting cell  $i=1, j=1, k=5$ . The flow distribution is complex and the temperature change from left to right alternates in sign in alternate rows corresponding to alternation in direction of horizontal flow rate.

Table 10 shows pressure, temperature and flow rate distributions for this 800,000 Darcy case at 3,000 days. While the flow rates are much more uniform with flow uniformly upward, the free convection still exists with some horizontal flow from right to left. Deviations from a pattern of uniform temperature increase to the right and upward are small but exist and are complex. This 800,000 Darcy run was much more difficult than the runs for 100,000 or fewer Darcies. The number of time steps increased to 21 and computer time increased to 144 CDC 6600 CPU seconds, largely due to divergence and repeat of one of the time steps.

These fractured hot rock simulations did not employ any enhanced heat conduction to the fracture due to thermal cracking induced by temperature decrease. A functional relationship between thermal conductivity and temperature or temperature change can be included in the model. Such a relationship and associated parameters might be deduced from laboratory or field experimental data.

### SUMMARY

An implicit, three-dimensional geothermal model is described and partially evaluated in respect to stability or time step tolerance. The model is only partly implicit in certain applications where various terms associated with allocation of well rates among open layers are treated explicitly.

The implicit model stably accommodated time steps corresponding to 80-100% saturation change in a grid block and throughput ratios the order of  $10^8$  in several illustrative multiphase flow problems. This compares with our experience of limits of 3-10% saturation change and throughput ratio of roughly 20,000 with semi-implicit geothermal and oil reservoir models. The implicit model stability allowed inclusion of fractures and wellbores as small-volume grid blocks in several multiphase flow test problems.

An analytical derivation is presented for a well deliverability reduction factor which can be used in simulations using large grid blocks. The factor accounts for increased pressure drop near the well due to hot water flashing and steam expansion.

The model was used to simulate two-phase depletion of a fractured matrix reservoir with horizontal and vertical fractures included as grid blocks. The results were poorly matched by conventional simulation which treats the reservoir as an unfractured formation with high effective permeability.

Simulation of a single-phase flow, pressure drawdown test in a tight formation with horizontal fractures showed upward concave curvature of the pressure drawdown vs.  $\ln(t)$  plot. The degree of calculated curvature and attendant interpretation difficulty increased with decreasing matrix permeability level and decreasing horizontal fracture spacing.

The final illustrative application treated heat extraction from a fractured, hot dry rock system. For a given cold water injection rate, the calculated energy recovery and production well water temperature vs. time were not affected by fracture permeability-width product or injection well location. The fracture conductance was varied from 2 to 16,000 Darcy-ft, while injection well location was varied only from the bottom corner to the mid-depth of the fracture plane. A fourfold increase in fracture area from 400x400 to 800x800 square feet resulted in a threefold increase in calculated energy recovery at 3,000 days for the same cold water injection rate.

73

A limited investigation of time truncation error indicates that acceptably low levels can occur in spite of average maximum (over grid) saturation changes per time step as high as 60%.

### NOMENCLATURE

A	cross-sectional area normal to flow, $\text{ft}^2$
c	compressibility, 1/psi
C <sub>p</sub>	specific heat, Btu/lb-°F
( $\rho C_p$ ) <sub>R</sub>	rock specific heat, Btu/cu.ft rock-°F
f <sub>w</sub>	water phase volumetric fractional flow
f <sub>g</sub>	gas phase volumetric fractional flow
f	well deliverability factor, fraction
H	enthalpy, U + pv, Btu/lb
k	absolute permeability, md
k <sub>r</sub>	relative permeability, fraction
k <sub>rgcw</sub>	relative permeability to gas at irreducible water saturation S <sub>wc</sub>
K	thermal conductivity, Btu/ft-day-°F
N <sub>x</sub> , N <sub>y</sub> , N <sub>z</sub>	numbers of grid blocks in reservoir grid system, in x, y, z directions, respectively
$\bar{q}$	desired or target production rate, lbs H <sub>2</sub> O/day
q	production rate, lbs H <sub>2</sub> O/day
q <sub>H</sub>	enthalpy production rate, Btu/day
q <sub>HL</sub>	heat loss rate, Btu/day
p <sub>s</sub> (T)	water vapor pressure
p	gas phase pressure, psia
p <sub>wb</sub>	wellbore flowing pressure, psia
p <sub>c</sub>	capillary pressure, p <sub>g</sub> - p <sub>w</sub> , psi
R <sub>T</sub>	throughput ratio, Equation (31)
r	radius, feet



Figure 12 shows a rapid decline of produced water temperature from 500°F to less than 300°F in the first few days followed by a very flat decline from 170°F to 137°F from 1,000 to 3,000 days. Fractional energy recovery is 0.1661 at 3,000 days, equivalent to  $1.155 \times 10^{11}$  Btu or an average of 64 Btu/lb water produced (enthalpy relative to zero U at 100°F). The average temperature corresponding to this average enthalpy is about 162°F.

The fracture width  $w$  controls system conductivity or throughput. The corresponding parameter or group of importance is the  $kw$  Darcy-feet product, which is proportional to  $w^3$  since fracture permeability is proportional to  $w^2$ . We used permeabilities up to 800,000 Darcies with the .02-foot model dimension for the fracture. This 16,000 Darcy-foot  $kw$  product corresponds to a fracture width of 4 mm using the fracture permeability equation  $k = 10^8 w^2 / 12$  ( $w$  in cm). Fracture width, i.e. the  $kw$  product, had no effect on the calculated recovery and temperature shown in Figure 12.

Model runs were made with the injection well located higher, 200 feet from top of formation in cell  $i=1, j=1, k=3$ . The change of injection location had no effect on calculated recovery and producing temperature.

Figure 12 also shows calculated recovery and temperature for a larger fracture of dimension 800x800 feet. Again, the above described  $kw$  product and injection well location variations had no effect on the calculated recovery and producing temperature. The larger fracture resulted in a considerably higher bottomhole producing temperature vs. time and a lower fractional energy recovery. Calculated absolute energy recovery at 3,000 days was higher for the larger fracture --  $3.53 \times 10^{11}$  Btu vs.  $1.155 \times 10^{11}$  Btu for the 400x400 foot fracture. Thus, a fourfold increase in fracture area caused a threefold increase in energy recovery. Average enthalpy of produced water was 196 Btu/lb corresponding to an average temperature of produced water of 292°F.

The runs were performed using automatic time step control due to the rapid initial transients. With a first time step of .1 days, a subsequent minimum  $\Delta t$  of .2 days, control by 150°F maximum grid block temperature change per time step and a maximum time step of 500 days, the model took 13 time steps to 3,000 days for the 100,000 Darcy permeability. Computer time for this run was 46 CDC 6600 CPU seconds. Twenty of these seconds were required for the first two time steps.

74

Calculated results for permeabilities less than 100,000 Darcies exhibited no circulatory "free" convection type cells in the vertical fracture plane. Table 8 shows an example of these results at 3,000 days for the case of a 400x400 foot fracture, and 100,000 Darcies fracture permeability which corresponds to a 2 mm fracture width. The table shows calculated pressures in the fracture plane, temperatures in all planes and interblock flow rates (positive to the right and vertically downward). Water flow is uniformly to the right and upwards away from the injection in grid cell  $i=1, j=1, k=5$ . Temperature uniformly increases to the right and upward (in the directions of water flow) except in the top row.

Results for the 800,000 Darcy permeability differed markedly from those just described. Table 9 shows pressure, temperature and flow rate distributions at 75 days for the 800x800 foot fracture with 800,000 Darcies.  $y$ -direction spacing was altered in this run to .01, 10, 30, 50, 180 feet. The flow rates in Table 9 show extremely strong "free" convection cells in the 5x5 grid of the vertical fracture plane. Water is in fact flowing downward into the injecting cell  $i=1, j=1, k=5$ . The flow distribution is complex and the temperature change from left to right alternates in sign in alternate rows corresponding to alternation in direction of horizontal flow rate.

Table 10 shows pressure, temperature and flow rate distributions for this 800,000 Darcy case at 3,000 days. While the flow rates are much more uniform with flow uniformly upward, the free convection still exists with some horizontal flow from right to left. Deviations from a pattern of uniform temperature increase to the right and upward are small but exist and are complex. This 800,000 Darcy run was much more difficult than the runs for 100,000 or fewer Darcies. The number of time steps increased to 21 and computer time increased to 144 CDC 6600 CPU seconds, largely due to divergence and repeat of one of the time steps.

These fractured hot rock simulations did not employ any enhanced heat conduction to the fracture due to thermal cracking induced by temperature decrease. A functional relationship between thermal conductivity and temperature or temperature change can be included in the model. Such a relationship and associated parameters might be deduced from laboratory or field experimental data.

SUMMARY

An implicit, three-dimensional geothermal model is described and partially evaluated in respect to stability or time step tolerance. The model is only partly implicit in certain applications where various terms associated with allocation of well rates among open layers are treated explicitly.

The implicit model stably accommodated time steps corresponding to 80-100% saturation change in a grid block and throughput ratios the order of  $10^8$  in several illustrative multiphase flow problems. This compares with our experience of limits of 3-10% saturation change and throughput ratio of roughly 20,000 with semi-implicit geothermal and oil reservoir models. The implicit model stability allowed inclusion of fractures and wellbores as small-volume grid blocks in several multiphase flow test problems.

An analytical derivation is presented for a well deliverability reduction factor which can be used in simulations using large grid blocks. The factor accounts for increased pressure drop near the well due to hot water flashing and steam expansion.

The model was used to simulate two-phase depletion of a fractured matrix reservoir with horizontal and vertical fractures included as grid blocks. The results were poorly matched by conventional simulation which treats the reservoir as an unfractured formation with high effective permeability.

Simulation of a single-phase flow, pressure drawdown test in a tight formation with horizontal fractures showed upward concave curvature of the pressure drawdown vs.  $\ln(t)$  plot. The degree of calculated curvature and attendant interpretation difficulty increased with decreasing matrix permeability level and decreasing horizontal fracture spacing.

The final illustrative application treated heat extraction from a fractured, hot dry rock system. For a given cold water injection rate, the calculated energy recovery and production well water temperature vs. time were not affected by fracture permeability-width product or injection well location. The fracture conductance was varied from 2 to 16,000 Darcy-ft, while injection well location was varied only from the bottom corner to the mid-depth of the fracture plane. A fourfold increase in fracture area from 400x400 to 800x800 square feet resulted in a threefold increase in calculated energy recovery at 3,000 days for the same cold water injection rate.

75

A limited investigation of time truncation error indicates that acceptably low levels can occur in spite of average maximum (over grid) saturation changes per time step as high as 60%.

NOMENCLATURE

A	cross-sectional area normal to flow, $\text{ft}^2$
c	compressibility, 1/psi
Cp	specific heat, Btu/lb-°F
$(\rho C_p)_R$	rock specific heat, Btu/cu.ft rock-°F
$f_w$	water phase volumetric fractional flow
$f_g$	gas phase volumetric fractional flow
f	well deliverability factor, fraction
H	enthalpy, $U + pv$ , Btu/lb
k	absolute permeability, md
$k_r$	relative permeability, fraction
$k_{rgcw}$	relative permeability to gas at irreducible water saturation $S_{wc}$
K	thermal conductivity, Btu/ft-day-°F
$N_x, N_y, N_z$	numbers of grid blocks in reservoir grid system, in x, y, z directions, respectively
$\bar{q}$	desired or target production rate, lbs $\text{H}_2\text{O}/\text{day}$
q	production rate, lbs $\text{H}_2\text{O}/\text{day}$
$q_H$	enthalpy production rate, Btu/day
$q_{HL}$	heat loss rate, Btu/day
$p_s(T)$	water vapor pressure
p	gas phase pressure, psia
$p_{wb}$	wellbore flowing pressure, psia
$p_c$	capillary pressure, $p_g - p_w$ , psi
$R_T$	throughput ratio, Equation (31)
r	radius, feet

76

$r_e$  exterior radius  
 $r_w$  wellbore radius  
 $NB$  Reservoir Barrels  
 $S$  skin factor  
 $S_w$  water phase saturation, fraction  
 $S_g$  gas phase saturation, fraction  
 $S_{ge}$  gas saturation at  $r = r_e$   
 $S_{wc}$  irreducible water saturation  
 $S_{gc}$  critical gas saturation  
 $t$  time, days  
 $\Delta t$  time step,  $t_{n+1} - t_n$ , days  
 $T$  temperature, °F  
 water saturation temperature,  $T_s(p)$ , °F  
 $U$  internal energy, Btu/lb  
 $V_p$  grid block pore volume,  $V\phi$   
 $V$  grid block bulk volume,  $\Delta x\Delta y\Delta z$ , cubic feet  
 $v$  specific volume, cu.ft/lb  
 $w$  fraction width  
 $X$  quality, mass fraction steam  
 $x, y, z$  Cartesian coordinates, feet,  $z$  measured positively vertically downward  
 $\Delta x, \Delta y, \Delta z$  grid block dimensions, feet

$T_c$  reservoir heat conduction transmissibility  $KA/l$ , where  $l =$  distance between grid block centers, Btu/day-°F  
 $T_g$  gas phase transmissibility,  $(kA/l)(k_{rg}\rho_g/\mu_g) \times .00633$ , lbs gas phase/day-psi  
 $T_w$  water phase transmissibility,  $(kA/l)(k_{rw}\rho_w/\mu_w) \times .00633$ , lbs water phase/day-psi  
 $\Delta(TAP) = \Delta_x(T_x \Delta P) + \Delta_y(T_y \Delta P) + \Delta_z(T_z \Delta P)$ , defined as indicated above Equation (5)  
 $\mu$  viscosity, cp

SUBSCRIPTS

$e$  exterior  
 $g$  gas (steam) phase  
 $i, j, k$  grid block indices,  $x_i, y_j, z_k$   
 $k$  grid layer number or index  
 $l$  (superscript) iteration number  
 $n$  time level,  $t_n$   
 $s$  saturation condition  
 $x, y, z$  denotes  $x, y$  or  $z$  direction, respectively  
 $w$  water phase  
 $wb$  wellbore

REFERENCES

1. Coats, K. H., and Ramesh, A. B., "Numerical Modeling of Thermal Reservoir Behavior", Preprint presented at the 28th Annual Technical Meeting of the Petroleum Society of C.I.M., Edmonton, Alberta, May 27-June 6, 1977.
2. Carter, R. D., and Tracy, G. W., "An Improved Method for Calculating Water Influx", Trans. AIME (1960), 219, 415-417.
3. Coats, K. H., George, W. D., Chu, Chieh, and Marcum, B. E., "Three-Dimensional Simulation of Steamflooding", Trans. AIME (1974), 257, 573.

CREEK

$\bar{\delta}$  time difference operator,  
 $\bar{\delta}X = X_{n+1} - X_n$   
 $\delta$  iteration difference operator,  
 $\delta X = X^{l+1} - X^l$   
 $\phi$  porosity, fraction  
 $\rho$  density, lbs/cu.ft  
 $\gamma$  specific weight or gradient, psi/ft ( $\gamma_w = \rho_w/144$ )  
 $\lambda$  mobility,  $k_r/\mu$

4. Toronyi, R. M., and Ali, S. M. Farouq, "Two-Phase, Two-Dimensional Simulation of a Geothermal Reservoir"; Soc. Pet. Eng. J. (June, 1977), 171-183.
5. Blair, P. M., and Weinaug, C. F., "Solution of Two-Phase Flow Problems Using Implicit Difference Equations", Trans. AIME (1969), 246, 417.
6. Price, H. S., and Coats, K. H., "Direct Method in Reservoir Simulation", Trans. AIME (1974), 257, 295.
7. Steam Tables, Keenan, J. H., and Keyes, F. G., Hill, P. G., and Moore, J. G., John Wiley & Sons, 1969.
8. Coats, K. H., Nielsen, R. L., Terhune, M. H., and Weber, A. G., "Simulation of Three-Dimensional Two-Phase Flow in Oil and Gas Reservoirs", Soc. Pet. Eng. J. (December, 1967), 377-388.
9. Coats, K. H., Dempsey, J. R., and Henderson, J. H., "The Use of Vertical Equilibrium in Two-Dimensional Simulation of Three-Dimensional Reservoir Performance", Trans. AIME (1971), 251, 63-71.
10. Flow of Homogeneous Fluids, Muskat, M., J. W. Edwards, Ann Arbor, Michigan, 1946.
11. Coats, K. H., Dempsey, J. R., Ancell, K. L., and Gibbs, D. E., "Analysis and Prediction of Gas Well Performance", SPE 3474 presented at 46th Annual Meeting of SPE, New Orleans, Louisiana, October 3-6, 1971.

#### APPENDIX

##### CALCULATION OF DELIVERABILITY FACTOR $f$

We consider two-phase, steady-state steam-water flow from some exterior radius  $R$  to wellbore radius  $r_w$ . The point  $R$  is assumed to be saturated, and pressure is  $P$  at  $R$  and  $p_{wb}$  at  $r_w$ .

Darcy's law gives liquid water phase flow rate at any radius as

$$q_w = q(1 - X) = -2\pi k \Delta z \lambda_w \rho_w r dp/dr \quad (35)$$

where  $X$  is flowing steam quality,  $q$  is total flow rate, lbs  $H_2O/day$ ,  $k \Delta z$  is md-ft product  $\times .00633$ ,  $\lambda_w$  is  $k_{rw}/\mu_w$  and  $\rho_w$  is water density in lbs/cu.ft. Integration using the fact that  $q$  is constant gives

$$q = \frac{2\pi k \Delta z}{\ln \frac{R}{r_w}} \int_{p_{wb}}^P \frac{\lambda_w \rho_w}{1-X} dp \quad (36)$$

or

$$q = \frac{2\pi k \Delta z}{\ln \frac{R}{r_w}} I(P, p_{wb}, S_g) \quad (37)$$

where the integral  $I$  is a function only of the integration limits  $p_{wb}$ ,  $P$  and of steam saturation  $S_g$  at  $R$  because, as we will now show, the integrand  $\lambda_w \rho_w / (1-X)$  is a single-valued calculable function of pressure  $p$ .

Flowing quality  $X$  is related to fractional flow by

$$X = 1 / (1 + f_w \rho_w / ((1 - f_w) \rho_g)) \quad (38)$$

and enthalpy per lb of flowing stream is

$$H = XH_g + (1 - X)H_w \quad (39)$$

At steady-state, flowing stream enthalpy is constant and from (39),

$$X = (H - H_w) / (H_g - H_w) = X(p), \quad (40)$$

where the dependence upon pressure alone follows from the fact that  $H$  is constant and saturated water and steam enthalpies are single-valued functions of pressure. From Equation (38),

$$f_w = 1 / [1 + X \rho_w / ((1 - X) \rho_g)] = f_w(p) \quad (41)$$

where the dependence upon pressure alone follows from the fact that saturated water and steam densities are single-valued functions of pressure.

If  $p$  and  $S_g$  at  $R$  are given, then enthalpy  $H$  can be calculated from Equations (38) and (39). Given  $H$ , we can calculate the values of  $X(p)$  and  $f_w(p)$  at any pressure from Equations (40) and (41). Thus, the integral in Equation (36) can be numerically integrated for any given values of  $P$ ,  $p_{wb}$  and  $S_g$ .

We now consider a grid block of large dimensions,  $\Delta x \Delta y$ , with equivalent exterior radius  $r_e$  determined by  $\pi r_e^2 = \Delta x \Delta y$ . Assuming steady-state single-phase water flow from an undersaturated condition at  $r_e$  to saturation point R, Darcy's law gives

$$q = \frac{2\pi k \Delta z}{r_e \ln \frac{R}{r_e}} (\lambda_{we} \rho_{we} + \lambda_{ge} \rho_{ge}) (p_e - P) \quad (42)$$

where P is pressure at saturation point radius R and  $\lambda_{ge}$  is zero if  $R < r_e$ . Equation (37) describes flow from saturation point R to  $r_w$  and can be written

$$q = \frac{2\pi k \Delta z}{\ln \frac{R}{r_w}} \frac{I(\lambda_{we} \rho_{we} + \lambda_{ge} \rho_{ge})}{(\lambda_{we} \rho_{we} + \lambda_{ge} \rho_{ge}) (P - p_{wb})} (P - p_{wb}) \quad (43)$$

Solving for  $p_e - P$  from (42) and  $P - p_{wb}$  from (43) and adding the results gives

$$q = \frac{2\pi k \Delta z (\lambda_{we} \rho_{we} + \lambda_{ge} \rho_{ge})}{\ln \frac{r_e}{R} + \frac{1}{f} \ln \frac{R}{r_w}} (p_e - p_{wb}) \quad (44)$$

where

$$f = \frac{I(P, p_{wb}, S_{ge})}{(\lambda_{we} \rho_{we} + \lambda_{ge} \rho_{ge}) (P - p_{wb})} \quad (45)$$

In Equations (44), (45), if the exterior radius  $r_e$  is undersaturated,  $\lambda_{ge} = 0$  and R must be calculated by trial and error if  $p_e$  and  $p_{wb}$  are given. P is, of course, equal to saturation pressure corresponding to temperature at  $r_e$ . If q is given, then R can be calculated directly from (42).

If the exterior radius  $r_e$  is saturated, then  $R = r_e$ ,  $P = p_e$  and Equation (44) becomes

$$q = \frac{2\pi k \Delta z}{r_e \ln \frac{r_e}{r_w}} f (\lambda_{we} \rho_{we} + \lambda_{ge} \rho_{ge}) (p_e - p_w) \quad (46)$$

where f is given by (45) with  $P = p_e$ .

We have used an analysis similar to that given here to calculate reduced deliverability of oil wells due to release and expansion of solution gas accompanying pressure decline near the well.

TABLE 1

SINGLE-WELL RADIAL FLOW TEST PROBLEM

79

Formation Thickness	=	500 ft
Permeability	=	100 md
Porosity	=	0.2
Wellbore Radius	=	0.25 ft
Exterior Radius	=	2,000 ft
Initial Pressure at Formation Top	=	450 psia
Initial Temperature	=	400°F
Initial Saturation $S_w$	=	1.0
Capillary Pressure	=	0
$k_{rw}$ , $k_{rg}$ from Equations (26)		
Res. and Overburden K	=	38 Btu/ft-D-°F
Res. and Overburden $C_p$	=	35 Btu/cu.ft Rock-°F
Rock Compressibility	=	$4 \times 10^{-6}$ 1/psi
Minimum Wellbore Pressure	=	160 psia

BLOCK	WELLBORE NOT INCLUDED IN GRID		WELLBORE INCLUDED IN GRID		BLOCK PORE VOLUME RES. BBLs*
	CENTER	INNER BOUNDARY	CENTER	INNER BOUNDARY	
1	.4	.25	.25	0	3.50
2	1.07	.68	.40	.25	4.45
3	2.91	1.84	1.07	.68	$3.28 \times 10$
4	7.91	5.00	2.91	1.84	$2.42 \times 10^2$
5	21.46	13.57	7.91	5.00	$1.78 \times 10^3$
6	58.25	36.84	21.46	13.57	$1.31 \times 10^4$
7	158.10	100.00	58.25	36.84	$9.67 \times 10^4$
8	429.16	271.44	158.10	100.00	$7.13 \times 10^5$
9	1164.92	736.81	429.16	271.44	$5.25 \times 10^6$
10	-	-	1164.92	736.81	$3.87 \times 10^7$

\*THESE PORE VOLUMES ARE FOR BLOCKS IN ONE 100-FOOT LAYER.

TABLE 2

EFFECT OF TIME STEP SIZE ON ONE-DIMENSIONAL RADIAL FLOW RESULTS

TIME, DAYS	TIME STEP SIZE, DAYS						
	4000	250	500	1000	2000	4000	
MASS FRACTION PRODUCED		.1670	.1669	.1669	.1665	.1642	
BOTTOMHOLE QUALITY		.0559	.0566	.0576	.0583	.0576	
RATE, 1000's LBS/HR		115.3	113.8	111.9	111.6	115.4	
TIME, DAYS	250	500	1000	2000	4000	8000	
MASS FRACTION PRODUCED	.3150	.3133	.3102	.3048	.2950	.2756	
BOTTOMHOLE QUALITY	.0674	.0671	.0668	.0667	.0665	.0638	
RATE, 1000's LBS/HR	90.5	90.9	91.2	91.3	92	96.9	
TIME, DAYS	250	500	1000	2000	4000	8000	16000
MASS FRACTION PRODUCED	.4959	.4935	.4889	.4803	.4644	.4357	.3865
BOTTOMHOLE QUALITY	.1442	.1420	.1380	.1310	.1197	.1039	.0835
RATE, 1000's LBS/HR	43.5	44	45	46.9	50.2	56.3	67.9



**TABLE 5**  
**NUMBER OF ITERATIONS PER TIME STEP**  
**ALL LAYERS OPEN; TUNING IN LAYER 3**

<u>Δt, DAYS</u>		
<u>500</u>	<u>1000*</u>	<u>2000</u>
25 (.9164)	29 (.9891)	41 (.9989)
7 (.5446)	4 (.2000)	22 (.4297)
8 (.7186)	14 (.6517)	6 (.4101)
8 (.2142)	9 (.3229)	5 (.1813)
10 (.2012)	5 (.2239)	5 (.2205)
6 (.1571)	6 (.2273)	
5 (.1064)	4 (.1826)	
5 (.1329)	5 (.0948)	
9 (.1211)	4 (.1334)	
3 (.1200)	4 (.1176)	
4 (.1040)	2 (.0973)	
5 (.0645)		
6 (.0481)		
4 (.0589)		
4 (.0681)		
3 (.0672)		
3 (.0624)		
2 (.0591)		
2 (.0551)		
2 (.0529)		

\*THE SECOND TIME STEP AUTOMATICALLY CUT TO 100 DAYS DUE TO DIVERGENCE; THE 11TH STEP WAS 900 DAYS; ALL OTHER STEPS WERE 1,000 DAYS.

**TABLE 6**  
**CALCULATED RESULTS AFTER FIRST 500-DAY TIME STEP**  
**TWO-DIMENSIONAL RADIAL-Z RESULTS; LAYERS 2-4 OPEN; TUNING AT LAYER 3**

<u>PRESSURE AT GRID BLOCK CENTER (psia)</u>										
	<u>1</u>	<u>2</u>	<u>3</u>	<u>4</u>	<u>5</u>	<u>6</u>	<u>7</u>	<u>8</u>	<u>9</u>	<u>10</u>
1		248.1	248.1	248.1	248.2	248.3	248.5	248.8	249.2	249.9
2	172.2	183.5	206.4	224.6	238.2	247.0	250.5	257.9	267.9	275.7
3	177.6	196.1	227.3	245.5	251.8	266.4	280.9	294.1	304.8	312.8
4	184.7	209.5	242.5	254.4	276.1	297.4	316.7	331.2	341.9	350.0
5		360.8	360.8	360.8	360.9	361.4	363.4	369.6	379.1	387.2

<u>TEMPERATURE, DEGREES FAHRENHEIT</u>										
1		398.8822	398.8827	398.8855	398.8981	398.9423	399.0276	399.1301	399.3082	399.5553
2	366.8782	372.9753	383.0746	389.9853	395.1166	398.4603	399.7671	399.8496	399.8979	399.9522
3	369.8058	379.2011	390.9933	397.9063	399.9886	399.9776	399.9721	399.9694	399.9802	399.9904
4	373.6334	384.2601	396.7470	400.2618	400.2153	400.1472	400.0841	400.0282	399.9943	399.9954
5		400.0292	400.0296	400.0304	400.0311	400.0312	400.0275	400.0141	399.9995	399.9978

<u>STEAM SATURATION</u>										
1		.5693	.5692	.5692	.5686	.5654	.5489	.4935	.3755	.2414
2	.8640	.4688	.3697	.3098	.2471	.1669	.0444	0.0000	0.0000	0.0000
3	.8481	.4225	.2978	.1772	0.0000	0.0000	0.0000	0.0000	0.0000	0.0000
4	.8249	.3840	.2147	0.0000	0.0000	0.0000	0.0000	0.0000	0.0000	0.0000
5		0.0000	0.0000	0.0000	0.0000	0.0000	0.0000	0.0000	0.0000	0.0000

**TABLE 7**  
**SUMMARY OF FRACTURED MATRIX RUN CHARACTERISTICS**

<u>RUN NO.</u>	<u>PRODUCTION RATE, LBS/HR</u>	<u>TIME STEP, DAYS</u>	<u>TOTAL TIME, DAYS</u>	<u>AVERAGE NUMBER OF ITERATIONS PER STEP</u>	<u>AVERAGE MAXIMUM SATURATION CHANGE/STEP</u>	<u>TOTAL RUN TIME, CDC 6600 CPU SECONDS</u>
1	40	30	1500	5.1	0.38	12.3
2	40	60	1500	8.5	0.66	26.5
3	10	120	4200	4.4	0.31	20.7

8  
0  
2  
4  
1

0  
12  
10  
10  
10



TABLE 8.

HOT DRY ROCK RESULTS AT 1,000 DAYS  
400 x 400 FEET, 100,000 Darcy FRACTURE

<u>PRESSURE, PSIA</u>					
J = 1					
	1	2	3	4	5
1	801.8	801.7	801.6	801.4	801.0
2	836.1	836.0	835.9	835.7	835.6
3	870.6	870.4	870.3	870.1	870.0
4	905.2	905.0	904.8	904.6	904.5
5	940.2	939.6	939.2	939.0	938.8

<u>TEMPERATURE, °F</u>					
J = 1					
	1	2	3	4	5
1	138.4375	139.1442	139.1278	137.9985	137.4555
2	120.3707	123.2967	126.2684	129.1460	134.0118
3	110.5972	114.3772	118.9110	124.1954	132.1117
4	104.7869	108.3930	113.2686	119.6754	129.3627
5	101.5197	104.4184	108.9581	115.5032	126.0568

J = 2					
	1	2	3	4	5
1	192.0262	192.6029	192.6152	191.7483	191.3081
2	176.3268	178.7883	181.4228	184.0100	187.8308
3	166.5993	169.9373	174.1229	178.9975	185.4905
4	160.7664	164.0263	168.6004	174.5594	182.6227
5	157.5881	160.3054	164.6232	170.7594	179.5778

J = 3					
	1	2	3	4	5
1	429.3812	429.4605	429.4268	429.2234	429.0697
2	425.2453	425.7926	426.4512	427.0833	427.7481
3	421.5898	422.5007	423.7477	425.1202	426.4752
4	419.1658	420.1519	421.6267	423.4105	425.2228
5	417.9100	418.8160	420.2795	422.1785	424.2129

J = 4					
	1	2	3	4	5
1	494.8779	494.8820	494.8786	494.8643	494.8519
2	494.5635	494.6016	494.6501	494.6957	494.7357
3	494.2421	494.3122	494.4119	494.5182	494.6096
4	494.0161	494.0965	494.2197	494.3629	494.4906
5	493.8991	493.9765	494.1023	494.2578	494.4033

J = 5					
	1	2	3	4	5
1	499.9092	499.9092	499.9092	499.9090	499.9088
2	499.9036	499.9042	499.9051	499.9059	499.9065
3	499.8974	499.8986	499.9005	499.9024	499.9039
4	499.8928	499.8943	499.8966	499.8993	499.9014
5	499.8905	499.8919	499.8944	499.8973	499.8998

X-DIRECTION FLOW RATE, LBS/HR

J = 1					
	1	2	3	4	5
1	0.0000	2016.3670	4220.8752	7060.5410	12124.8302
2	0.0000	1894.5775	3315.5218	4256.6210	4316.0297
3	0.0000	2721.4537	3732.2798	3633.6808	2548.8300
4	0.0000	5329.2430	5442.0878	4342.7514	2582.6891
5	0.0000	13038.3583	8289.2342	5706.4035	3427.6178

Z-DIRECTION FLOW RATE, LBS/HR

J = 1					
	1	2	3	4	5
1	0.0000	0.0000	0.0000	0.0000	0.0000
2	-2016.3674	-2204.5087	-2839.6660	-5064.2894	-12875.1657
3	-3910.9451	-3625.4529	-3780.7657	-5123.6984	-8559.1363
4	-6632.3988	-4636.2794	-3682.1667	-4038.8478	-6010.3065
5	-11961.6419	-4749.1240	-2582.8306	-2278.7858	-3427.6175

TABLE 9  
HOT DRY ROCK RESULTS AT 75 DAYS  
800 x 800 FEET, 800,000 DARCY FRACTURE

PRESSURE, PSIA

J = 1

	1	2	3	4	5
1	800.3	800.3	800.3	800.3	800.2
2	856.7	856.8	856.8	856.8	856.9
3	914.9	914.9	914.8	914.8	914.8
4	975.2	975.3	975.3	975.4	975.4
5	1039.3	1039.2	1039.1	1039.1	1039.0

TEMPERATURE, °F

J = 1

	1	2	3	4	5
1	468.3370	471.2289	474.2237	477.2610	479.9644
2	462.7538	457.2984	452.0257	446.7013	441.5233
3	399.0010	407.6237	416.3509	425.0627	433.5945
4	375.0946	361.0486	347.2332	333.3667	318.6657
5	189.6355	220.9219	247.4867	271.6548	295.6675

J = 2

1	483.8634	485.4144	486.9969	488.4728	489.6844
2	480.5561	477.4840	474.5136	471.6448	469.0360
3	444.7546	449.7848	454.8366	459.6667	464.3795
4	427.2917	419.0025	410.6463	402.3857	394.1028
5	318.5235	336.7667	352.4652	366.8352	380.9695

J = 3

1	498.8198	498.9383	499.0600	499.1664	499.2459
2	498.5441	498.2961	498.0542	497.8271	497.6309
3	495.6178	496.0338	496.4561	496.8485	497.2234
4	493.9525	493.2536	492.5389	491.8334	491.1513
5	484.7310	486.2680	487.6116	488.8412	490.0439

J = 4

1	499.9913	499.9922	499.9931	499.9939	499.9944
2	499.9891	499.9871	499.9852	499.9835	499.9820
3	499.9660	499.9693	499.9726	499.9757	499.9786
4	499.9520	499.9464	499.9407	499.9350	499.9296
5	499.8779	299.8902	499.9011	499.9110	499.9207

J = 5

1	500.0000	500.0000	500.0000	500.0000	500.0000
2	500.0000	500.0000	500.0000	500.0000	500.0000
3	499.9999	500.0000	500.0000	500.0000	500.0000
4	499.9999	499.9999	499.9999	499.9999	499.9999
5	499.9998	499.9998	499.9998	499.9999	499.9999

X-DIRECTION FLOW RATE, LBS/HR

J = 1

	1	2	3	4	5
1	0.0000	20882.9777	23901.9082	24797.3057	24949.6943
2	0.0000	-23698.1287	-27798.6156	-28338.0482	-26240.1155
3	0.0000	25170.5939	29614.1274	29702.3133	26689.1928
4	0.0000	-28661.3533	-32354.1902	-32389.5505	-28477.6646
5	0.0000	31305.4018	31635.7540	31226.4479	28076.8419

Z-DIRECTION FLOW RATE, LBS/HR

J = 1

	1	2	3	4	5
1	0.0000	0.0000	0.0000	0.0000	0.0000
2	-20883.0478	-3018.9908	-895.4625	-152.4403	-47.8279
3	2015.0301	1081.4271	-356.1100	-2250.4732	-26288.0461
4	-22355.7438	-3362.2535	-444.4305	762.5207	401.0460
5	6305.5481	330.4875	-409.1554	-3149.4712	-28076.7050

HOT DRY ROCK RESULTS AT 3,000 DAYS  
800 x 800 FEET, 800,000 DARCY FRACTURE

PRESSURE, PSIA

J = 1

	1	2	3	4	5
1	800.5	800.5	800.5	800.5	800.4
2	866.5	866.5	866.5	866.5	866.5
3	933.3	933.4	933.4	933.4	933.4
4	1000.9	1000.9	1000.9	1001.0	1001.0
5	1069.4	1069.3	1069.2	1069.1	1069.1

TEMPERATURE, °F

J = 1

	1	2	3	4	5
1	249.9689	248.0220	246.8849	245.8461	244.6164
2	216.5695	218.9366	219.5740	219.3443	218.4954
3	194.9029	190.9242	188.9332	188.3424	188.9908
4	153.6767	160.1790	163.8029	164.3298	161.8779
5	106.4226	113.7653	122.3591	132.9277	147.4336

J = 2

1	265.8360	263.9998	262.9122	261.9491	260.8865
2	233.9842	236.1508	236.7515	236.5108	235.6197
3	212.3962	208.7877	206.9809	206.5027	207.2386
4	172.9634	178.9138	182.1814	182.5563	180.1299
5	126.2235	133.4061	141.8190	152.1030	165.9797

J = 3

1	324.7246	323.3435	322.4850	321.8252	321.3318
2	299.2753	300.7499	301.1835	300.8914	299.8991
3	279.0948	276.7346	275.5776	275.4845	276.4692
4	246.9943	251.0076	253.0511	252.9464	250.6793
5	204.0660	210.4347	217.8984	226.8161	238.1241

J = 4

1	451.0672	450.7327	450.5302	450.4661	450.5618
2	443.0764	443.3598	443.3921	443.1553	442.6485
3	434.2412	433.8323	433.7200	433.9624	434.5498
4	423.0384	423.8462	424.1298	423.7657	422.7861
5	404.4443	407.1044	410.1953	413.6774	417.5579

J = 5

1	497.0347	497.0183	497.0098	497.0131	497.0286
2	496.5171	496.5274	496.5235	496.5012	496.4625
3	496.8260	495.8133	495.8179	495.8454	495.8922
4	495.0225	495.0594	495.0655	495.0298	494.9592
5	493.5814	493.7861	494.0234	494.2813	494.5475

X-DIRECTION FLOW RATE, LBS/HR

J = 1

	1	2	3	4	5
1	0.0000	3823.3153	8511.9081	13606.8777	19054.8352
2	0.0000	2706.8557	2765.7626	2153.8488	1207.0627
3	0.0000	-3422.8521	-3693.5112	-2396.7712	-729.3971
4	0.0000	214.0614	-935.5022	-3068.0366	-4893.8505
5	0.0000	21678.6244	18351.3309	14704.0595	10361.3012

Z-DIRECTION FLOW RATE, LBS/HR

J = 1

	1	2	3	4	5
1	0.0000	0.0000	0.0000	0.0000	0.0000
2	-3823.8456	-4688.5961	-5094.9711	-5447.9598	-5945.1321
3	-6530.4336	-4748.0656	-4483.0575	-4501.1982	-4738.0462
4	-3107.2900	-4477.0181	-5779.8014	-6168.5727	-5467.4493
5	-3321.3739	-3327.2930	-3647.2701	-4342.7575	-10361.3018

**FIGURE 1**  
**DELIVERABILITY FACTOR  $f$  VS.  $P_w$  FOR RELATIVE PERMEABILITY**  
**CURVES OF EQN (26)**

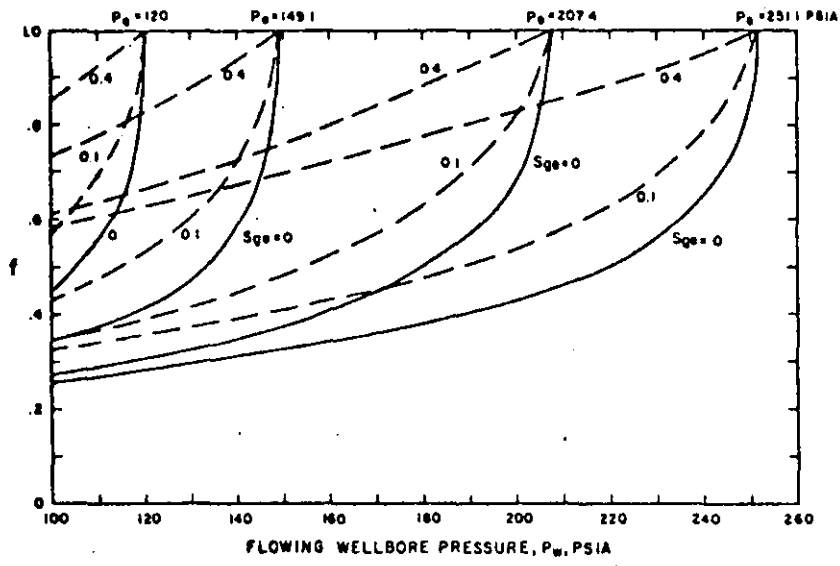


**FIGURE 2**  
**PRODUCTION RATE VS.  $S_{ge}$  FOR RADIAL**  
**WATER-STEAM FLOW**

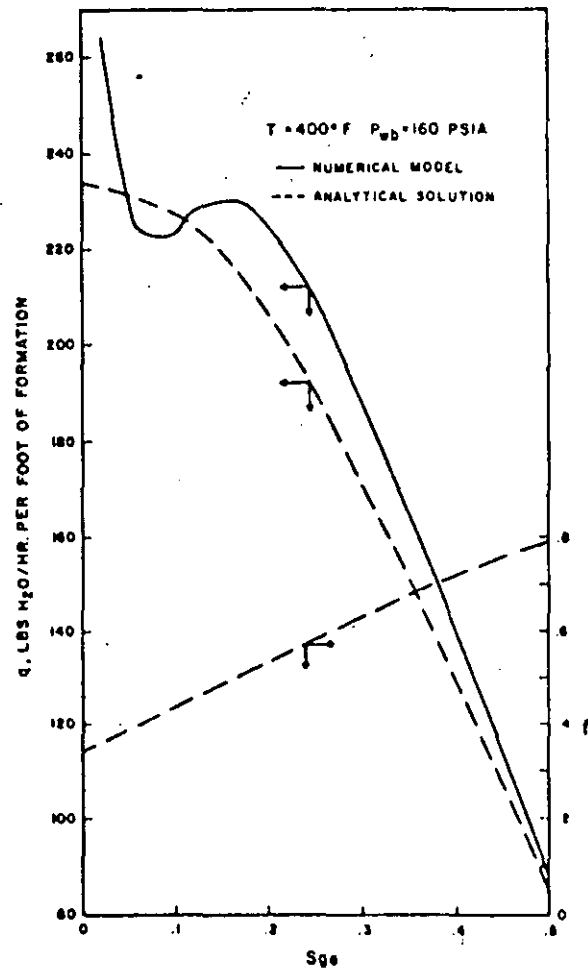


FIGURE 3  
TIME TRUNCATION ERROR

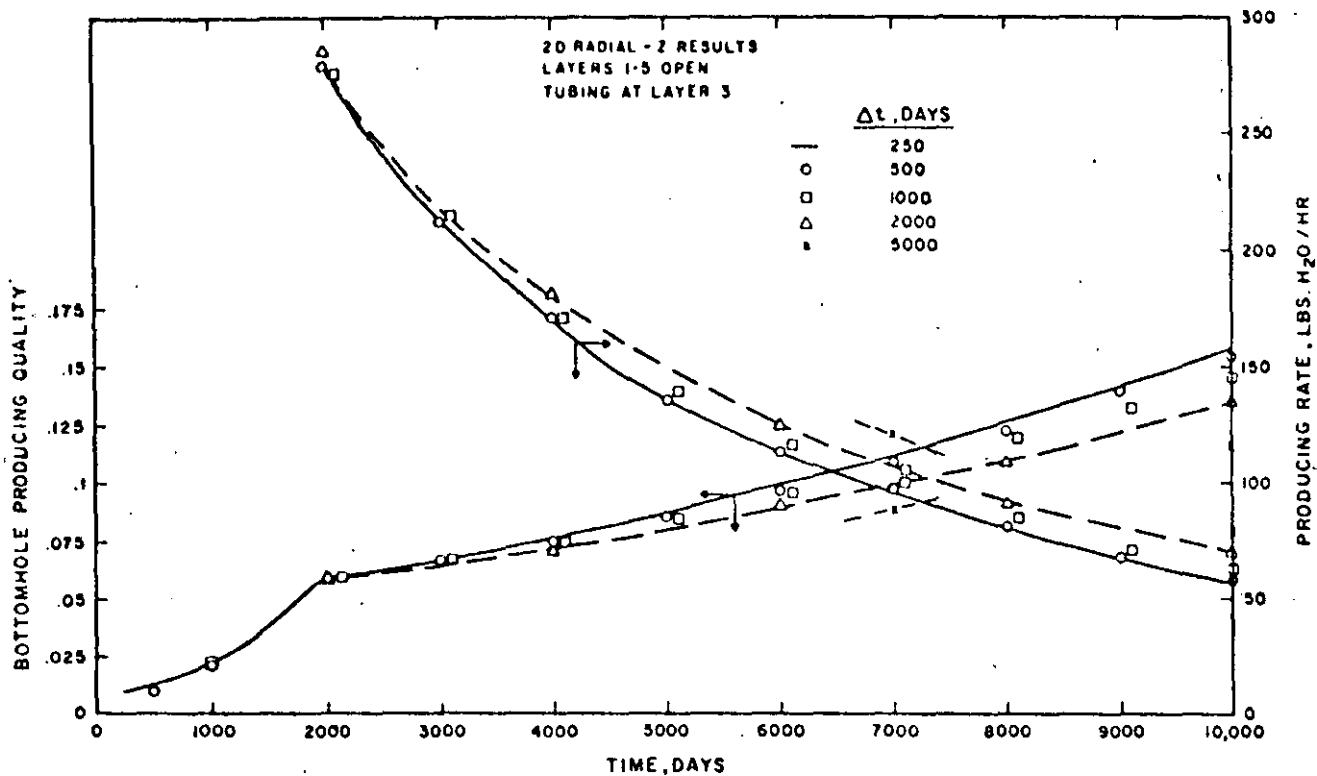


FIGURE 4  
EFFECT OF PERMEABILITY ON PRODUCTION RATE AND QUALITY

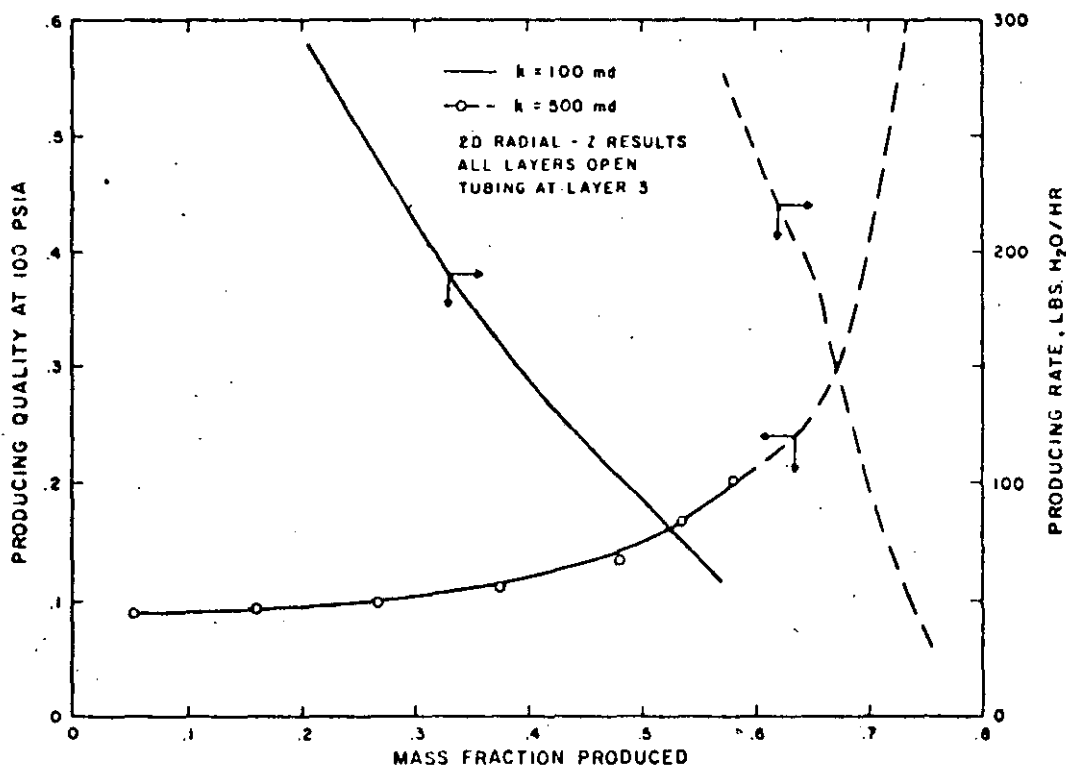


FIGURE 5  
EFFECT OF PERMEABILITY AND POROSITY ON  
AVERAGE RESERVOIR PRESSURE DECLINE

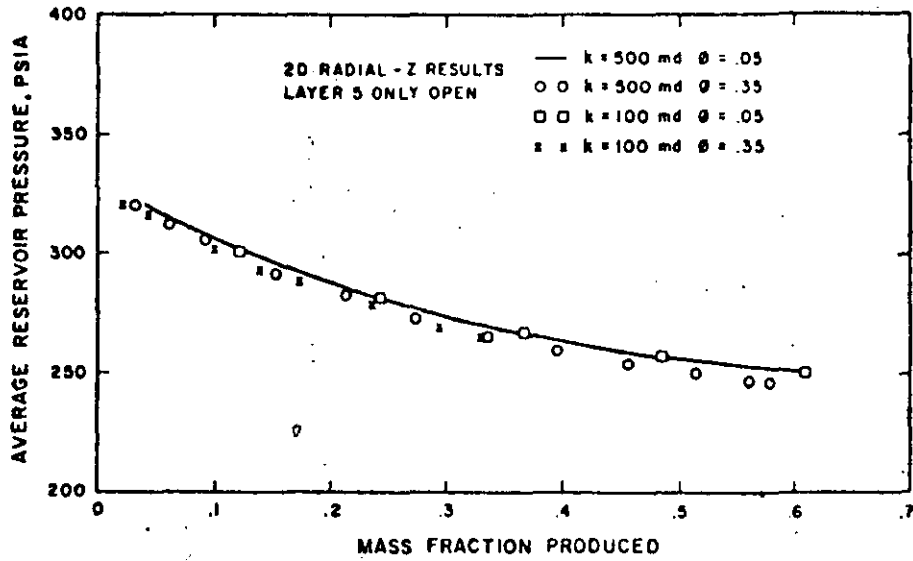


FIGURE 6  
RADIAL-Z GRID FOR MATRIX-FISSURE SYSTEM

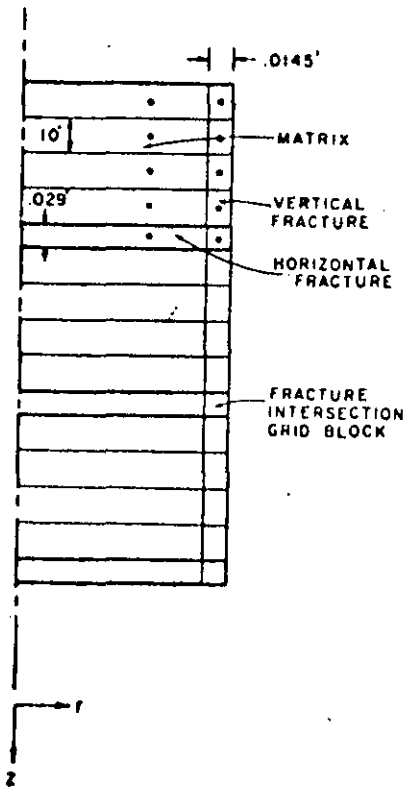


FIGURE 7

MATRIX-FISSURE SIMULATION RESULTS  
AT 1500 DAYS

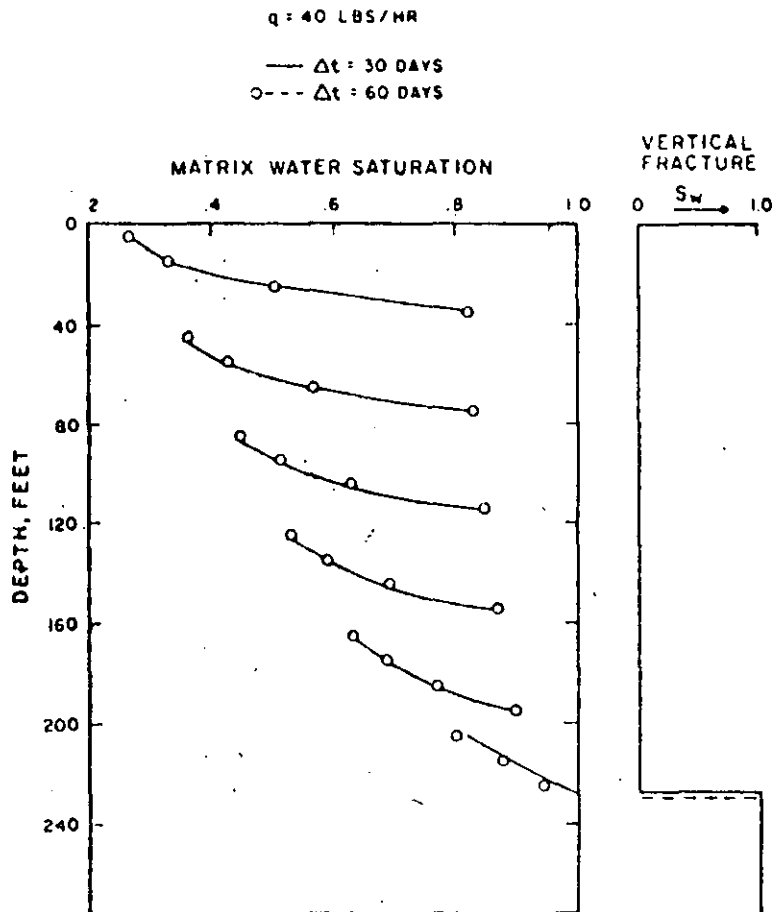
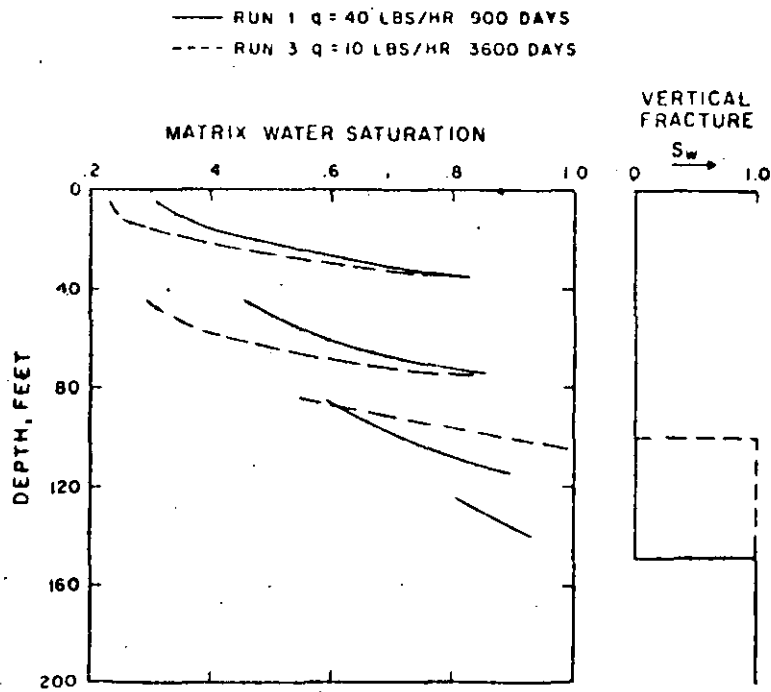
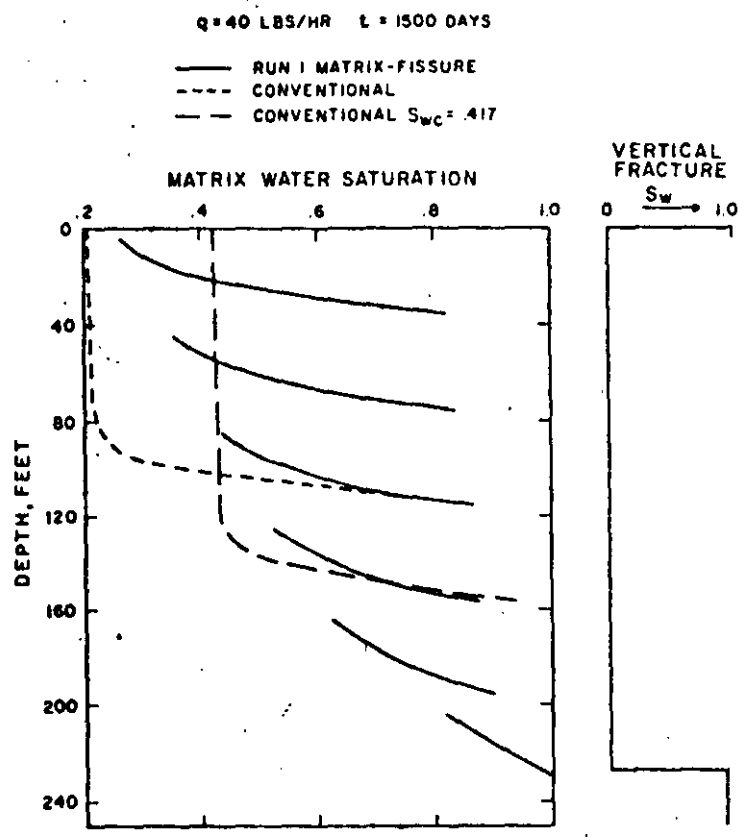


FIGURE 8

EFFECT OF PRODUCTION RATE ON  
MATRIX-FISSURE SIMULATION RESULTS



**FIGURE 9**  
COMPARISON OF MATRIX-FISSURE AND  
CONVENTIONAL SIMULATION RESULTS



**FIGURE 10**  
CALCULATED PRESSURE DRAWDOWN,  $\Delta p$  VS. TIME

HORIZONTAL FRACTURE SPACING = 44 FT.  
RATE = 10,000 LBS/HR

RUN	FRACTURE k <sub>w</sub> , DARCY-FT.	w, MM	MATRIX PERMEABILITY, MD
1	4	.245	.0001
2	4	.245	.001
3	4	.245	.01
4	HOMOGENEOUS, k = 90.9 MD		
5	546.4	1.26	.0001

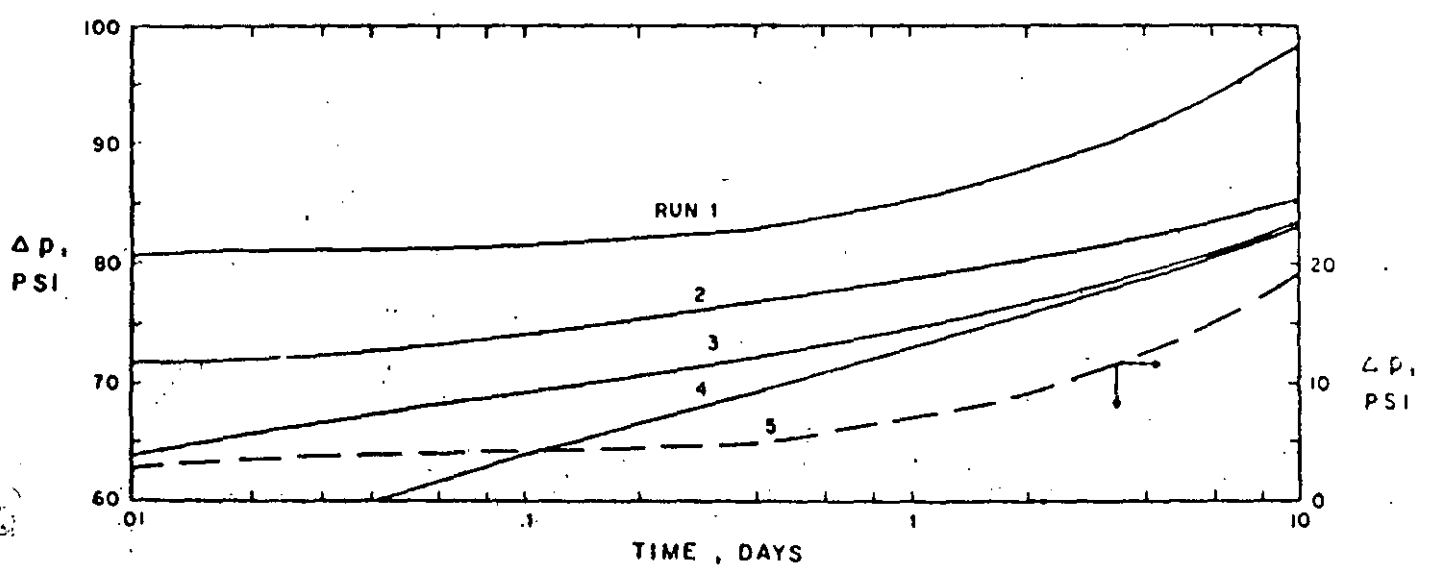




FIGURE 11  
 CALCULATED PRESSURE DRAWDOWN,  $\Delta p$  VS. TIME  
 HORIZONTAL FRACTURE SPACING = 440 FT.  
 RATE = 100,000 LBS/MR

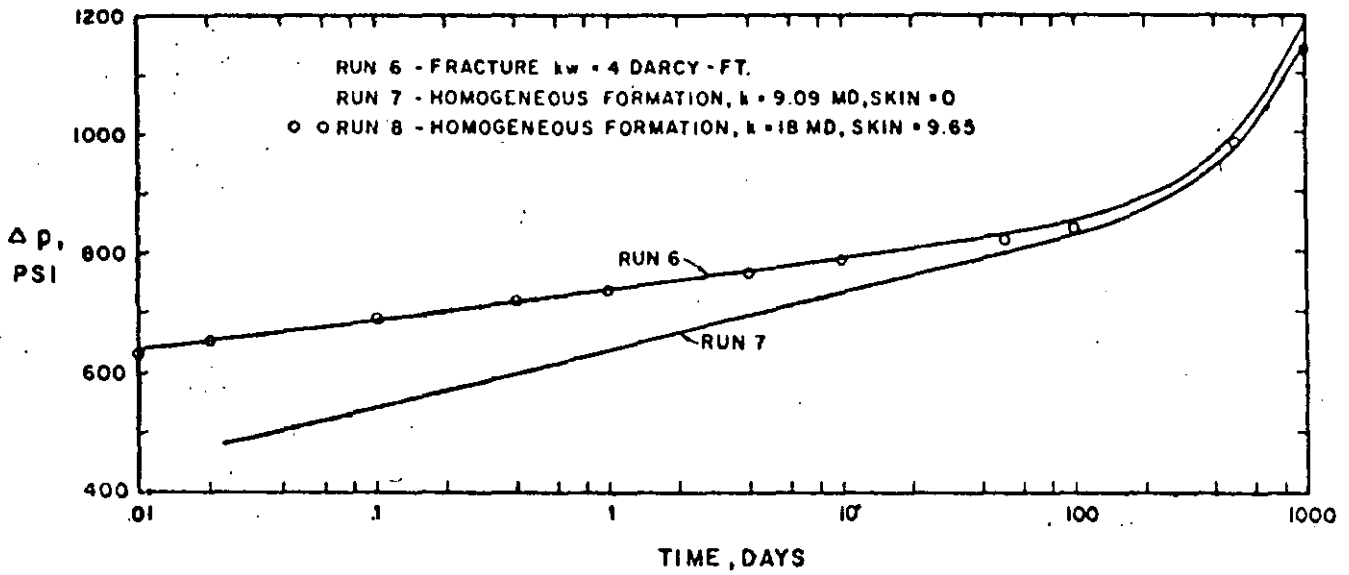
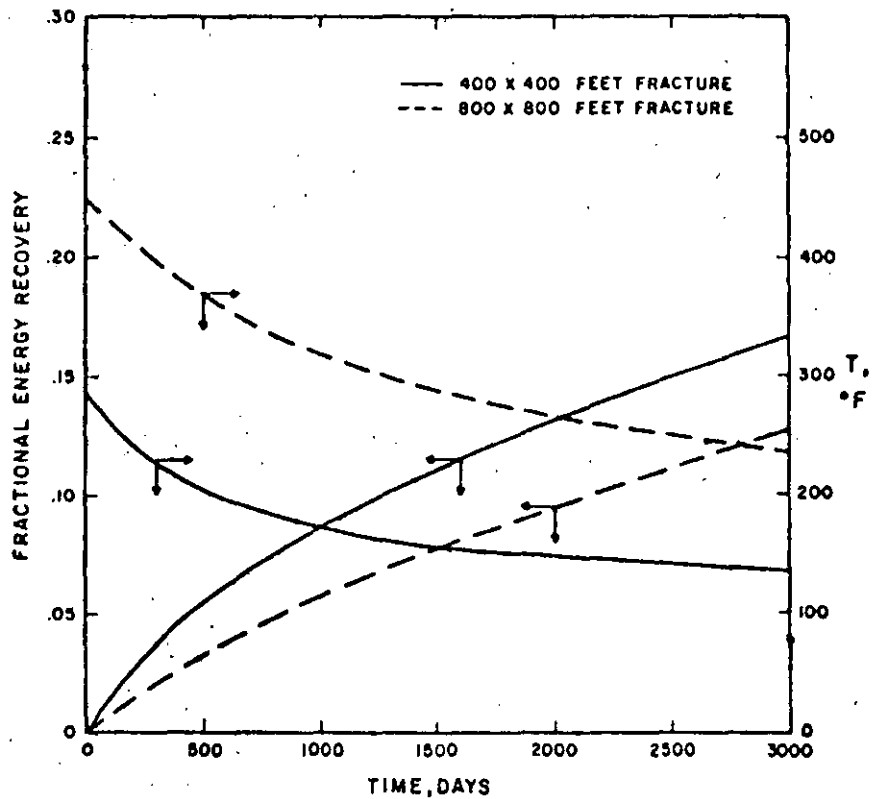


FIGURE 12  
 CALCULATED ENERGY RECOVERY AND PRODUCED WATER TEMPERATURE VS. TIME FOR HOT DRY ROCK SYSTEM





## INTRODUCTION

Utilization of geothermal energy is currently limited to a small number of naturally occurring geothermal steam and hot water reservoirs. The growing interest in this new source of energy has also stimulated attempts to develop a method of extracting thermal energy from the numerous regions of the earth's crust containing deposits of hot dry rock, which may constitute a resource at least ten times as large as that permeated by groundwater. The basis of this concept is to develop an adequate fracture surface to be used for heat transfer purposes. Because of the low thermal conductivity of rock, a very large heat-transfer area must be provided, otherwise meaningful amounts of energy cannot be extracted at practical rates.

One proposal (American Oil Shale Corporation, et al., 1971) describes a method for recovering heat through a closed loop cycle of surface water, from dry geothermal sites previously fractured by a suitable array of sequentially fired, fully contained nuclear explosives. Results from a preliminary analysis forecast operation of a 200 megawatt power plant for 30 years (Burnham and Stewart, 1973). Soviet workers have also been considering the use of in-situ explosions to create a highly fractured rock system so that circulating water could extract geothermal heat (Diadkin, et al., 1973).

Another technique, developed by Robinson, et al. (1971), of the Los Alamos Scientific Laboratory requires drilling two parallel deep boreholes, the second of which is directed so as to intersect a vertically oriented crack produced by hydraulic fracturing in the first hole. Water circulating down one well, through the crack, and up the other well would carry off heat from the hot rock to the surface. A supporting theoretical analysis was presented by Harlow and Pracht (1972), which indicates that many tens of

megawatts of thermal power could be supplied for several decades, provided that the initial fracture zone could be extended through the effects of thermal stress cracking in the adjacent hot rocks. A field experiment, conducted in a test well drilled to a depth of 780 m at one edge of a volcanic caldera in the Jemez Mountains of Northern New Mexico, has shown that granite could indeed be fractured hydraulically and was impermeable enough in this region to hold water tightly (Hammond, 1973). The propagation of the fracture from thermal stress effects, however, has not yet been demonstrated.

A third concept that could greatly increase the economic life of hot rock geothermal systems is that proposed by Raleigh et al. (1974). Observing that in many regions the stresses in subsurface rock are reasonably constant over large areas, they suggest that geothermal wells be drilled at an angle, in a direction perpendicular to the expected orientation of fractures, and that a series of parallel, vertical cracks be created from a single well. The horizontal distance between cracks can be controlled and might be of the order of a few tens of meters (Figure 1).

It is the purpose of this paper to present the results of a mathematical analysis of this third method.

#### MATHEMATICAL MODEL

The following discussion will be based on a linear model involving an infinite series of parallel, equidistant, vertical fractures of uniform thickness, separated by blocks of homogeneous and isotropic, impermeable rock, the width of the individual fracture being assumed to be negligible when compared to the spacing between the fractures.

Owing to the spatial periodicity of the temperature field, it is possible to replace the infinite system by a finite one, consisting of a single vertical

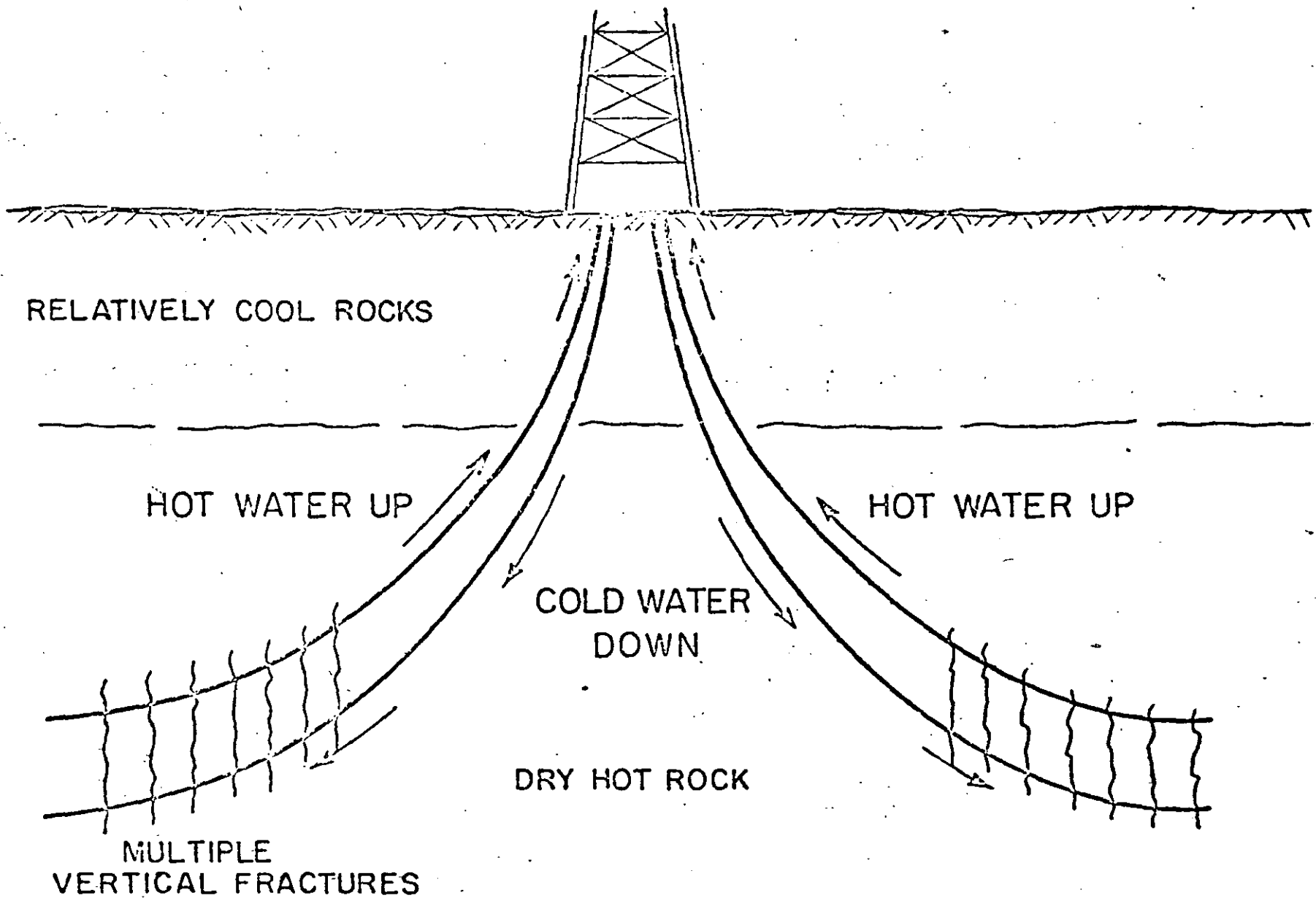


Fig. 1. Schematic diagram of heat extraction from multiple fractures in hot dry rock.

fracture of thickness  $2b$ , between two matrix blocks with an adiabatic outer boundary at a distance from the mid-plane of the fracture equal to half the fracture spacing. As illustrated in Figure 2, a rectilinear coordinate system is placed such that the  $x=0$  plane coincides with the mid-plane of the fracture. Water is injected at  $z=0$ , and is flowing upward in the fracture.

The following simplifying assumptions are made:

(1) The product of the density and heat capacity for both the water and the formation, and the formation thermal conductivity are constant. The linear volumetric and mass flow rate of the water is constant in the fracture.

(2) The water temperature,  $T_W(z,t)$ , is uniform in any cross section of the fracture, and equal, for all  $z$ , to the formation temperature at  $x=b$ .

(3) There is no heat transfer by radiation within the fracture, nor by conduction in the vertical direction within the fracture or the formation.

All heat transport is by horizontal conduction in the rock, and forced convection along the  $z$  axis within the fracture.

(4) Initially, both the water in the fracture and the formation are at the same temperature, given by the initial rock temperature at the point of injection,  $T_{RO}$ , minus the product of distance  $z$  above injection point, and geothermal gradient  $\omega$ , assumed constant. At time  $t=0$ , water is injected at constant injection temperature  $T_{WO}$ . No heat flux is assumed across the boundary at  $x=x_E$ .

The differential equation governing the water temperature,  $T_W(z,t)$ , is obtained by writing a heat balance on an element of fracture volume,  $(2b \cdot dz \cdot 1)$ , between the elevations  $z$  and  $z+dz$  above the injection point. Because of the symmetry with respect to the fracture mid-plane, this can be written as:

$$b\rho_W c_W \left[ \frac{\partial T_W(z,t)}{\partial t} + v \frac{\partial T_W(z,t)}{\partial z} \right] = K_R \left. \frac{\partial T_R(x,z,t)}{\partial x} \right|_{x=b} \quad (1)$$

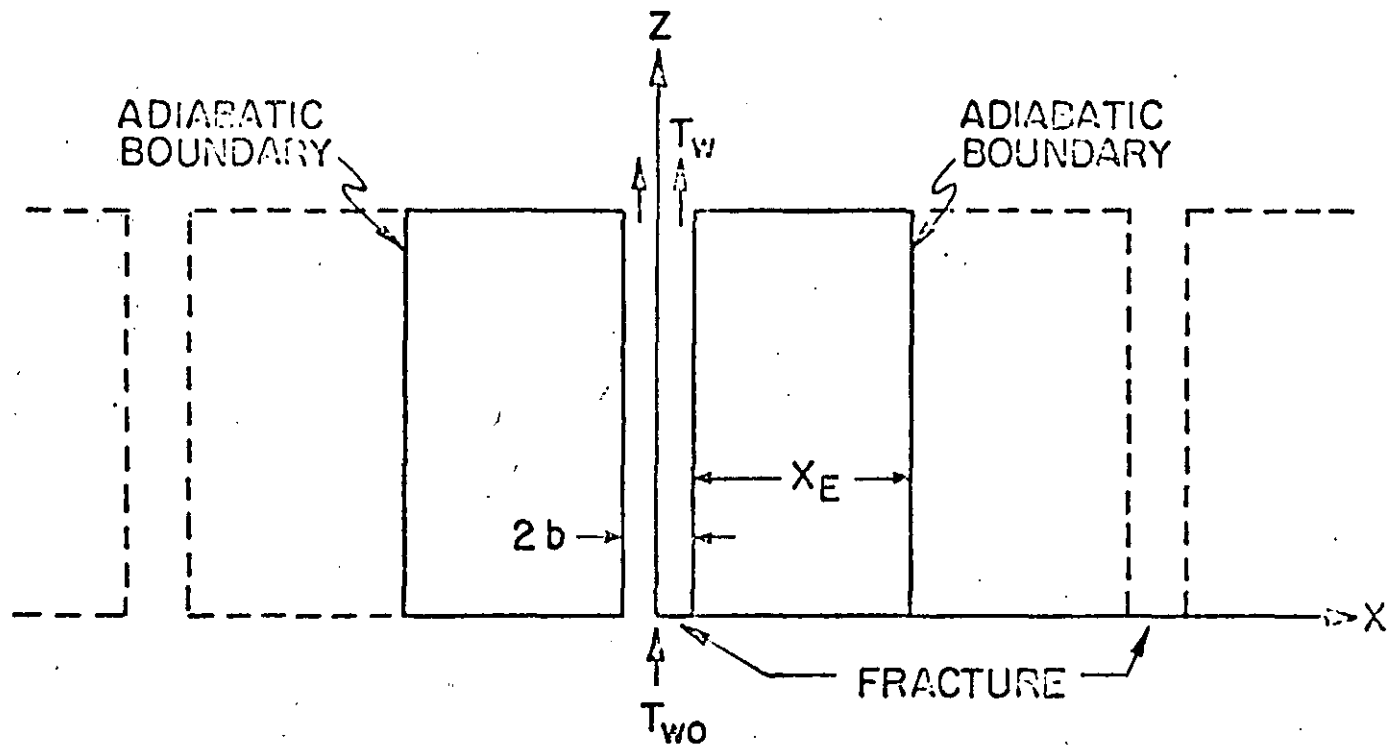


Fig. 2. Mathematical model for fractured hot dry rock.

where  $v$  is the water velocity,  $\rho_W$  and  $c_W$  the water density and specific heat, and  $K_R$  is the rock thermal conductivity.  $T_R(x, z, t)$  is the rock temperature, which is governed by the heat conduction equation:

$$\frac{\partial^2 T_R(x, z, t)}{\partial x^2} = \frac{\rho_R c_R}{K_R} \frac{\partial T_R(x, z, t)}{\partial t} \quad (2)$$

The temperatures must also satisfy the following initial and boundary conditions:

$$T_R(x, z, t) = T_W(z, t) = T_{RO} - \omega z, \quad t < \frac{z}{v} \quad (3)$$

$$T_R(x, 0, t) = T_W(0, t) = \begin{cases} T_{RO} & \text{if } t < 0 \\ T_{WO} & \text{if } t \geq 0 \end{cases} \quad (4)$$

$$T_W(z, t) = T_R(b, z, t) \text{ for all } z \text{ and } t \quad (5)$$

$$\left. \frac{\partial T_R(x, z, t)}{\partial x} \right|_{x=x_E} = 0 \quad (6)$$

The simultaneous solution of Eqs. 1 and 2, subject to conditions 3 through 6, is derived in Appendix A. The result for the outlet water temperature, at a distance  $z$  from the injection point, can be expressed in a general form as a function,  $T_{WD}(S, X_{ED}, t'_D)$  of dimensionless parameters, such that:

$$T_{WD} = \frac{T_{RO} - T_W(z, t)}{T_{RO} - T_{WO}} \quad (7)$$

$$\beta = \frac{\omega z}{T_{RO} - T_{WO}} \quad (8)$$

$$X_{ED} = \frac{\rho_W c_W}{K_R} \left(\frac{0}{z}\right) x_E \quad (9)$$

$$t'_D = \frac{(\rho_W c_W)^2}{K_R \rho_R c_R} \left(\frac{0}{z}\right)^2 t \quad (10)$$



where  $Q$  is the volumetric flow rate per fracture per unit thickness of the system in the y direction, and  $t' = t - \frac{z}{v}$ .  $\frac{z}{v}$  is the time lag between the departure of the water from the injection point and the arrival at point  $z$ . Because this time lag is very small in comparison with the lengths of time involved in our problem,  $t'$  is practically identical to  $t$ .

The dimensionless parameter  $\beta$  was found to have little effect on the time variation of the outlet water dimensionless temperature, except at small  $t'_D$  values, even in the case of a high geothermal gradient. The geothermal gradient can thus safely be neglected,  $T_{RO}$  being now taken as the average rock temperature over the zone of interest. The results for this case are shown in Figure 3, where  $T_{WD}$  is plotted as a function of  $t'_D$ , for various values of the dimensionless half-fracture spacing  $X_{ED}$ .

The ratio of the amount of heat extracted by the water flowing through the fracture to the initial total heat available in the rock was also computed and is shown in Figure 4.

Although the model presented in this paper is strictly valid only for an infinite number of fractures, it can also be used as a good approximation when the number of fractures is finite, but large enough, which should be the case in most practical applications.

#### EXAMPLE OF CALCULATION

When designing a geothermal power plant that uses this concept, a number of parameters are imposed and others have to be adjusted. In the system under consideration, the rock and water properties are given, and the total volumetric flow rate, minimum usable outlet temperature, and useful reservoir life are fixed by technical and economical considerations. What has to be chosen is the number of fractures, the dimensions of the individual fracture, and the

DIMENSIONLESS WATER OUTLET TEMPERATURE,

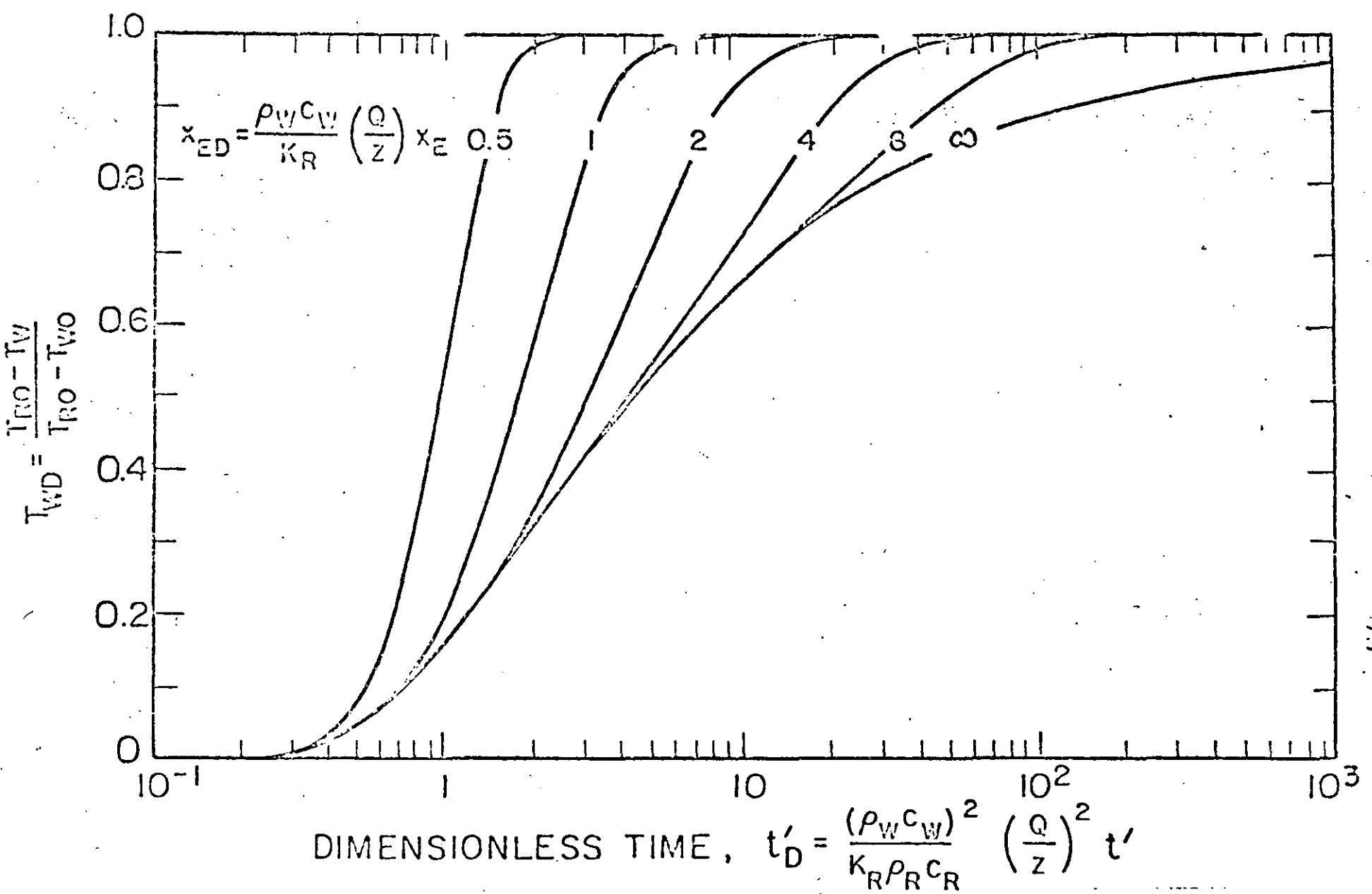


Fig. 3. Dimensionless water outlet temperature versus dimensionless time showing effect of fracture spacing.

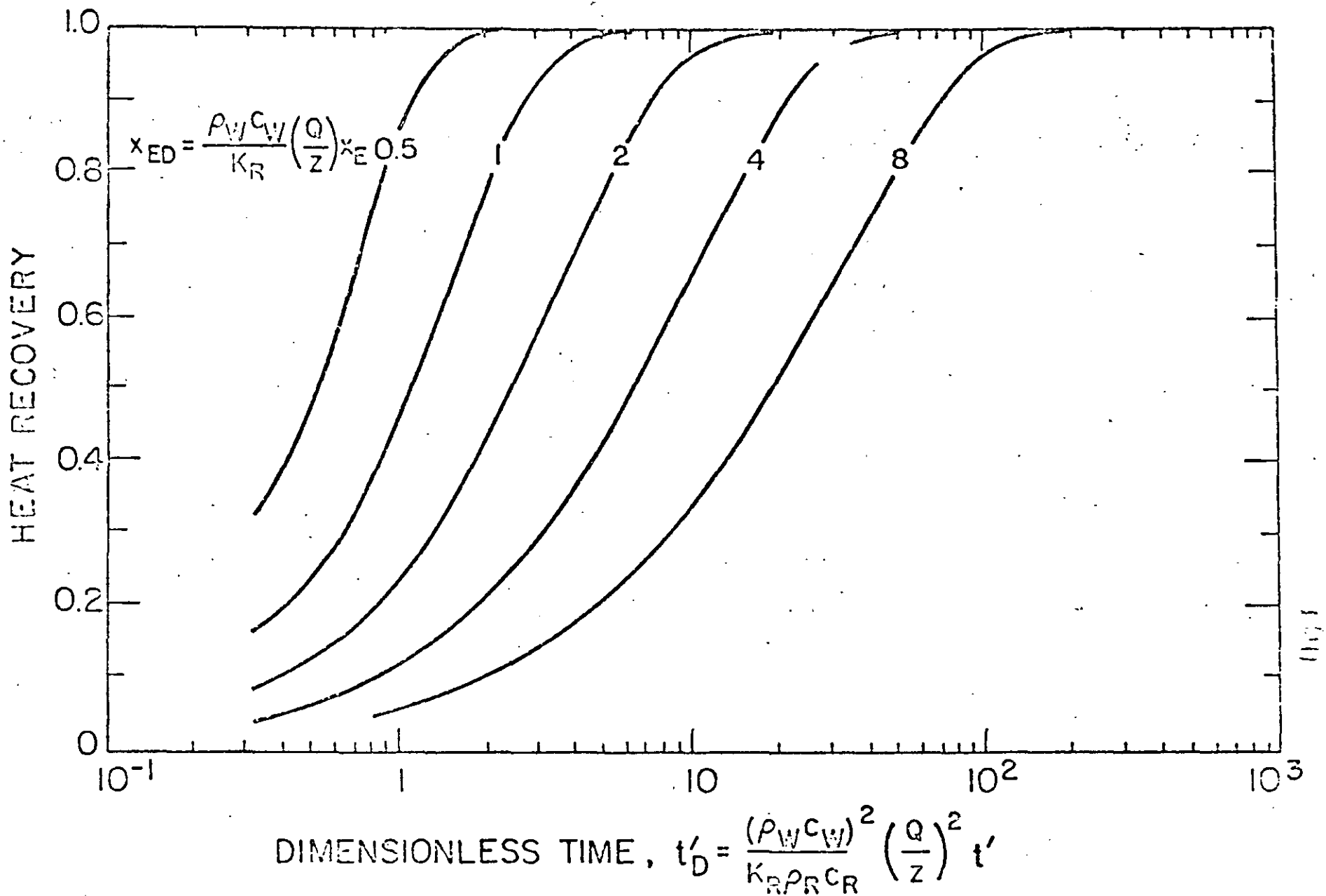


Fig. 4. Fractional heat recovery versus dimensionless time.

spacing between the fractures. These can be determined from Figure 3. An example of this type of calculation is described below.

In order to allow comparison with the system proposed by the Los Alamos group, the data given by Harlow and Pracht (1972) were used in the computations. They assumed a single fracture with a height of 1 km and a length (y direction) of 1 km and used a volumetric flow rate of  $1.45 \times 10^5 \text{ cm}^3/\text{sec}$ . They adopted a rock temperature of  $300^\circ\text{C}$  and an inlet water temperature of  $65^\circ\text{C}$ . Their remaining material properties were:  $K_R = 6.2 \times 10^{-3} \text{ cal/cm sec } ^\circ\text{C}$ ,  $\rho_R = 2.65 \text{ g/cm}^3$ ,  $c_R = 0.25 \text{ cal/g } ^\circ\text{C}$ ,  $\rho_W = 1.0 \text{ g/cm}^3$ , and  $c_W = 1.0 \text{ cal/g } ^\circ\text{C}$ . Resulting temperatures are shown in Figure 5. With a single fracture, the water outlet temperature drops very quickly after only a few years. This should be the case in Harlow and Pracht's model if thermal fracture propagation turns out to be negligible. On the other hand, if ten fractures are used, the water outlet temperature will drop at a much lower rate, depending on the fracture spacing.

The number of fractures in this example was determined by the requirement of a  $297^\circ\text{C}$  water outlet temperature ( $T_{WD} = 0.013$ ) after 20 years. It can be seen from Figure 3 that this temperature corresponds to  $t'_D = 0.325$  and  $X_{ED} > 0.5$ , which, for  $t' = 20$  years, yields  $Q = 0.145 \text{ cm}^3/\text{sec}$ . Since this number by definition, is also equal to the total volumetric flow rate ( $1.45 \times 10^5 \text{ cm}^3/\text{sec}$ ) divided by the number of fractures,  $N$ , and by the fracture length (1 km), the number of fractures follows immediately. The result is  $N = 10$ .

The spacing between the fractures is determined by the value of the dimensionless spacing parameter  $X_{ED}$ , which for this example would be  $> 0.5$ . It is obvious from Figure 3 that temperature will drop at a faster rate for smaller  $X_{ED}$ . On the other hand, one can see from Figure 4 that the fraction of energy recovered from the rock will be higher. For example, if one were to increase the time period to 100 years ( $t'_D = 1.6$ ), it can be seen from

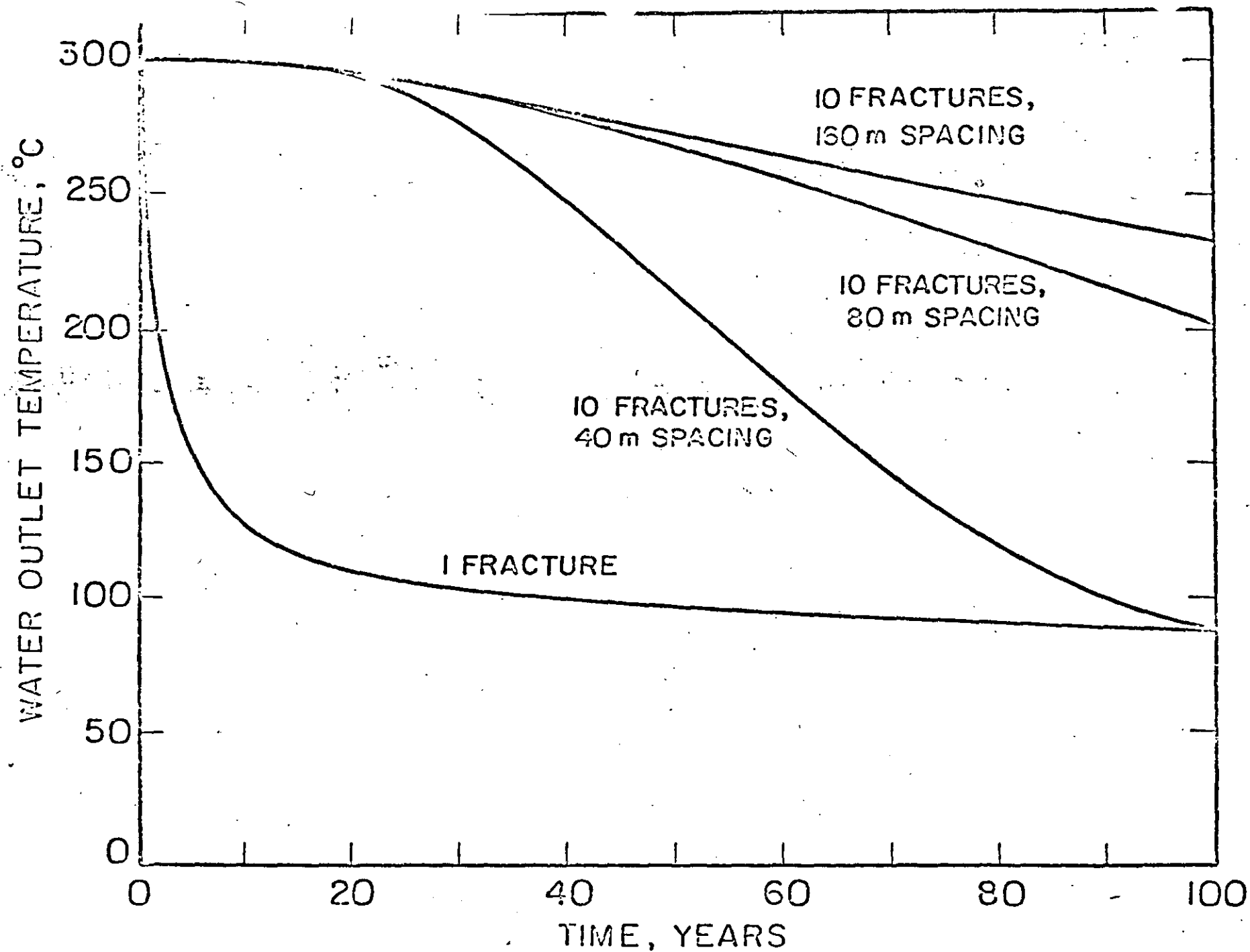


Fig. 5. Water outlet temperature versus time for  $1 \text{ km}^2$  fractures with  $T_{R0} = 300^\circ\text{C}$  and  $T_{W0} = 40^\circ\text{C}$ .

Figures 3 and 4 that there is no advantage in taking  $X_{ED}$  greater than 2 (which corresponds to a fracture spacing of 160 m) because a lower heat recovery would result and the drilling costs would be increased with no improvement in the outlet temperatures.

Obviously, the best choice for the fracture spacing is that which would yield the highest electrical power output for the longest period of time. The formulas for computing the electrical power output are given in Appendix B. The results are shown in Figure 6. It can be seen that electrical power output is highest for 10 fractures with a 160 m spacing, and this spacing is capable of producing many times the power output of a single fracture. If 20 fractures were used instead of ten, the maximum output of about 30 MW could be maintained for a century.

#### CONCLUSION

Although much simplified, the mathematical model used in this study shows that the multi-fracture concept could greatly increase the economic utilization of hot dry rock geothermal systems. If fracture propagation occurs through the effects of thermal stress cracking, as expected by some authors, geothermal energy extraction will even be greater than that reported in the present study.

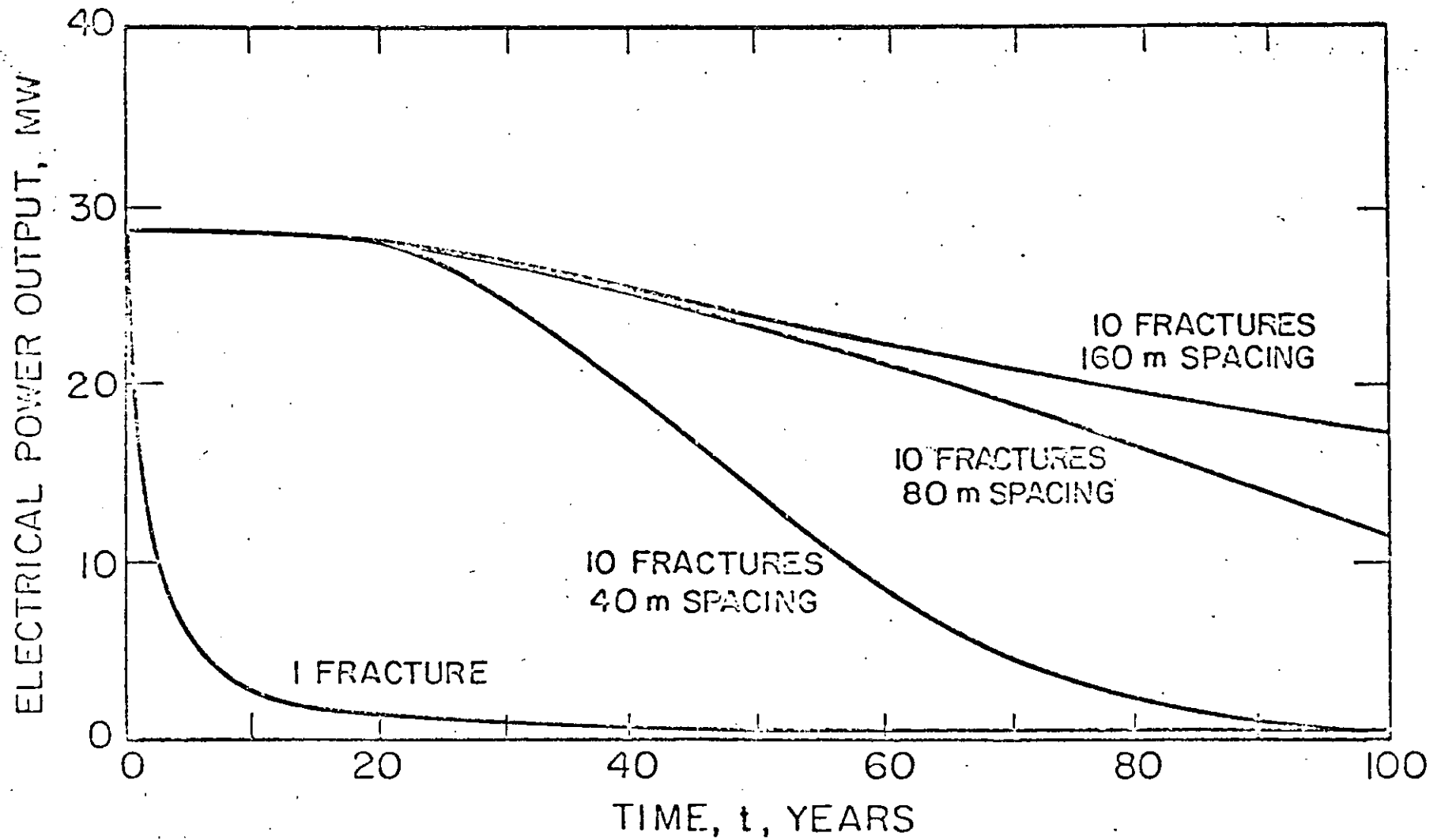


Fig. 6. Electrical power output from  $1 \text{ km}^2$  fractures at 50% Carnot efficiency.

## APPENDIX A. DERIVATION OF WATER OUTLET TEMPERATURE

Special cases of the mathematical problem considered in the present paper have been studied by previous authors. Bodvarsson (1969) solved the problem of constant flow with sinusoidal temperature through laminated solid, and solutions for  $x_E = \infty$  were published by Lauwerier (1955) and Carslaw and Jaeger (1959).

An exact analytical solution for finite  $x_E$  was recently presented by Romm (1972). In the present paper, the problem is solved in a slightly different way, and the results for infinite and finite  $x_E$  values are presented on the same graph in terms of suitable dimensionless quantities.

A solution is obtained as follows: we first substitute  $t'$  in place of  $t$  into Eqs. 1 to 4:

$$\rho_W c_W b v \frac{\partial T_W(z, t')}{\partial z} = K_R \frac{\partial T_R(x, z, t')}{\partial x} \Big|_{x=b} \quad (A-1)$$

$$\frac{\partial^2 T_R(x, z, t')}{\partial x^2} = \frac{\rho_R c_R}{K_R} \frac{\partial T_R(x, z, t')}{\partial t'} \quad (A-2)$$

$$\lim_{t' \rightarrow 0} T_R(x, z, t') = \lim_{t' \rightarrow 0} T_W(z, t') = T_{RO} - \omega z \quad (A-3)$$

$$\lim_{z \rightarrow 0} T_W(z, t') = T_{WO}, \quad t' > 0 \quad (A-4)$$

We then introduce the following dimensionless quantities:

$$\alpha = \frac{2K_R H}{\rho_W c_W Q b} \quad (A-5)$$

where  $H$  is an arbitrary length, and  $Q$  is the volumetric flow rate per fracture, per unit length of the system in the  $y$  direction;

$$\beta^* = \frac{\omega H}{T_{RO} - T_{WO}} \quad (A-6)$$



$$x_D = x/b \quad (A-7)$$

$$z_D = z/H \quad (A-8)$$

$$t_D^* = \frac{(\rho_W c_W)^2}{4K_R \rho_R c_R} \left(\frac{Q}{H}\right)^2 t' \quad (A-9)$$

$$T_{RD}(x_D, z_D, t_D^*) = \frac{T_{RO} - T_R(x, z, t')}{T_{RO} - T_{WO}} \quad (A-10)$$

Eqs. A-1 to A-4, and 5 and 6 thus become:

$$\frac{1}{\alpha} \frac{\partial T_{WD}(x_D, t_D^*)}{\partial z_D} = \frac{\partial T_{RD}(x_D, z_D, t_D^*)}{\partial x_D} \Big|_{x_D=1} \quad (A-11)$$

$$\frac{\partial^2 T_{RD}(x_D, z_D, t_D^*)}{\partial x_D^2} = \frac{1}{\alpha^2} \frac{\partial T_{RD}(x_D, z_D, t_D^*)}{\partial t_D^*} \quad (A-12)$$

$$\lim_{t_D^* \rightarrow 0} T_{RD}(x_D, z_D, t_D^*) = \lim_{t_D^* \rightarrow 0} T_{WD}(z_D, t_D^*) = \beta^* z_D \quad (A-13)$$

$$T_{WD}(z_D, t_D^*) = T_{RD}(1, z_D, t_D^*) \quad (A-14)$$

$$\lim_{z_D \rightarrow 0} T_{WD}(z_D, t_D^*) = 1, \quad t_D^* > 0 \quad (A-15)$$

$$\frac{\partial T_{RD}(x_D, z_D, t_D^*)}{\partial x_D} \Big|_{x_D=x_{ED}} = 0 \quad (A-16)$$

Applying the Laplace transform with respect to  $t_D^*$  and solving for the water outlet temperature yields:

$$\begin{aligned} \overline{T_{WD}}(z_D, s) = & \frac{1}{s} \left[ 1 + \left( \frac{\beta^*}{\sqrt{s} \tanh \frac{x_{ED}^{-1}}{\alpha} \sqrt{s}} \right) \exp(-z_D \sqrt{s} \tanh \frac{x_{ED}^{-1}}{\alpha} \sqrt{s}) \sqrt{s} \right] \\ & + \frac{\beta^* z_D}{s} - \frac{\beta^*}{s^{3/2} \tanh \frac{x_{ED}^{-1}}{\alpha} \sqrt{s}} \end{aligned} \quad (A-17)$$

where  $\bar{T}_{WD}(z_D, s)$  is the Laplace transform of the dimensionless water outlet temperature.

Eq. A-17 is most difficult to invert analytically, except in the case of a single fracture ( $x_E = \infty$ ), where inversion of Eq. A-17 shows that  $T_{WD}$  can be expressed as a function of  $\beta$  (Eq. 8) and  $t_D'$  (Eq. 10) only:

$$T_{WD}(t_D') = 1 - 2\beta(t_D'/\pi)^{1/2} [1 - \exp(-1/4t_D')] - (1-\beta)\text{erf}(1/2\sqrt{t_D'}) \quad (\text{A-18})$$

$T_{WD}$  has been plotted versus  $t_D'$  in Figure A-1, for various  $\beta$  values. The curves are very similar, except at early  $t_D'$  values. This indicates that the geothermal gradient can be safely neglected as a first approximation, if  $T_{RO}$  is taken as the average temperature along the fracture height. Setting  $\beta=0$  into Eq. A-17 and neglecting 1 in front of  $x_{ED}$  yields:

$$\bar{T}_{WD}(z_D, s) = \frac{1}{s} \exp(-z_D \sqrt{s} \tanh \frac{\rho_W c_W Q x_E}{2K_R H} \sqrt{s}) \quad (\text{A-19})$$

Eq. A-19 was inverted by means of a numerical method (Papoulis, 1957) and the result expressed as a function of  $x_{ED}$  (Eq. 9) and  $t_D'$  (Eq. 10) is plotted in Figure 3.

#### APPENDIX B. ELECTRICAL POWER OUTPUT

The total amount of heat in the hot rock per unit length of the system in the y direction, which could be recovered by cooling from  $T_{RO}$  to  $T_{WO}$  is:

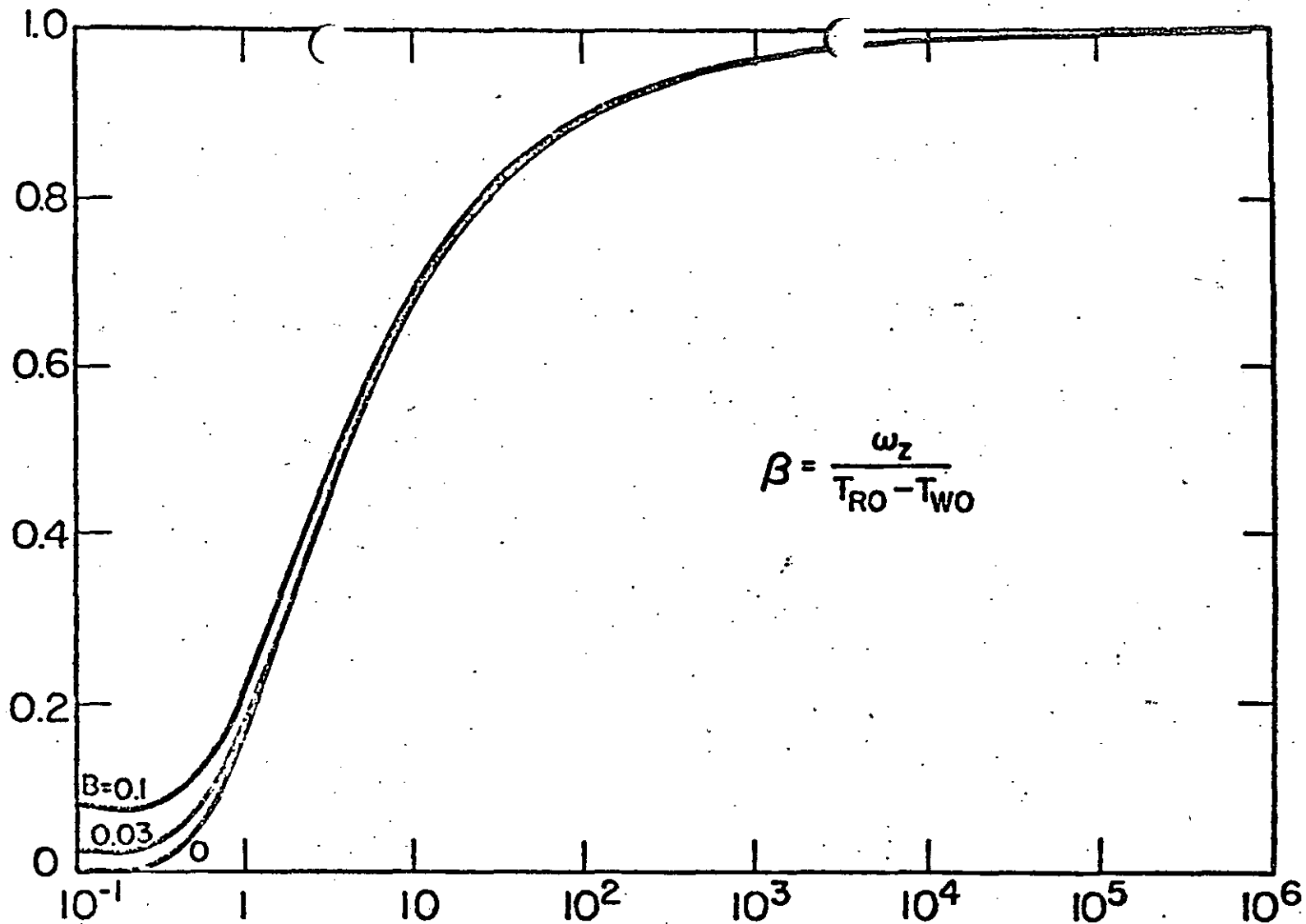
$$H_R = 2\rho_R c_R z x_E (T_{RO} - T_{WO}) \quad (\text{B-1})$$

The heat extraction rate or thermal power output by the water between  $T_W$  and  $T_{WO}$  is:

$$\rho_W c_W Q (T_W - T_{WO}) \text{ or } \rho_W c_W Q (T_{RO} - T_{WO}) \left(1 - \frac{T_{RO} - T_W}{T_{RO} - T_{WO}}\right)$$

DIMENSIONLESS WATER OUTLET TEMPERATURE,

$$T_{WD} = \frac{T_{RO} - T_W}{T_{RO} - T_{WO}}$$



$$\beta = \frac{\omega_z}{T_{RO} - T_{WO}}$$

$$\text{DIMENSIONLESS TIME, } t'_D = \frac{(\rho_W c_W)^2}{K_R \rho_R c_R} \left(\frac{Q}{z}\right)^2 t'$$

Fig. A1. Dimensionless water outlet temperature versus dimensionless time for a single fracture ( $X_{ED} = \infty$ ) showing effect of geothermal gradient.

Use of this water in a power plant working between  $T_W$  and  $T_{WO}$  at 50% of the Carnot efficiency would yield an electric power output equal to:

$$h_W = 0.50 \rho_W c_W Q \frac{(T_W - T_{WO})^2}{T_W + 273} \quad (B-2)$$

The cumulative heat extraction by water over a period  $t'$  is given by:

$$H_W = \int_0^{t'} \rho_W c_W Q (T_{RO} - T_{WO}) \left(1 - \frac{T_{RO} - T_W}{T_{RO} - T_{WO}}\right) dt' \quad (B-3)$$

The ratio of the amount of heat extracted by the water to the initial heat content in the rock is thus equal to:

$$\frac{H_W}{H_R} = \int_0^{t'} \frac{\rho_W c_W Q}{2\rho_R c_R z x_E} \left(1 - \frac{T_{RO} - T_W}{T_{RO} - T_{WO}}\right) dt'$$

or

$$\frac{H_W}{H_R} = \frac{1}{2x_{ED}} \int_0^{t_D'} [1 - T_{WD}(t_D')] dt_D' \quad (B-4)$$

- American Oil Shale Corporation - U. S. Atomic Energy Commission, "A Feasibility Study of a Geothermal Power Plant" PNE-1550, 1971.
- Bodvarsson, G. "On the Temperature of Water Flowing through Fractures", J. Geo. Res., v. 74, no. 8, p. 1987, April 5, 1969.
- Burnham, J. B. and Stewart, D. H. "Recovery of Geothermal Energy from Hot, Dry Rock with Nuclear Explosives", Geothermal Energy, ed. by Kruger and Otte, Stanford University Press, Stanford, California, p. 223, 1973.
- Carslaw, H. S. and Jaeger, J. C. Conduction of Heat in Solids, 2nd ed. Oxford at the Clarendon Press, p. 396, 1959.
- Diadkin, Yu. D., Pariiskii, Yu. M., Vainblat, A. B., and Romanov, B. A., "Issledovanie i razrabotka ratsional'nykh sistem izvlecheniya i ispol'zovaniya tepla, akkumulirovannogo glubinnymi sloyami zemnoi kory v raionakh Krainego Severa i Severo-Vostoka SSSR", (Investigation and development of rational systems of extraction and utilization of heat accumulated in deep layers of the earth in the extreme north and northeast regions of the USSR) Izuchenie i Ispol'zovanie Glubinnogo Tepla Zemli, Izdatel'stvo Nauka, Moscow, p. 43, 1973.
- Hammond, A. L. "Dry Geothermal Wells: Promising Experimental Results", Science, vol. 182, p. 43, October 5, 1973.
- Harlow, F. H. and Pracht, W. E. "A Theoretical Study of Geothermal Energy Extraction", J. Geo. Res., v. 77, no. 35, p. 7038, December, 1972.
- Lauwerier, H. A. "The Transport of Heat in an Oil Layer Caused by the Injection of Hot Fluid", Appl. Sci. Res., Sec. A, v. 5, p. 145, 1955.
- Papoulis, A. "A New Method of Inversion of the Laplace Transform", Quart. Appl. Math., v. 14, pp. 405-414, 1957.
- Robinson, E. S., Potter, R. M., McInteer, B. B., Rowley, J. C., Armstrong, D. E., Mills, R. L. and Smith, M. C. "A Preliminary Study of the Nuclear Subterranean" Rep. LA-4547, Los Alamos Scientific Lab., 1971.
- Romm, E. S. "Ob Odnom Sluchae Teploperenosa v Treshchinovatoi Gornoj Porode" (On one case of heat transfer in fractured rock) Problemy Razrabotki Mestorozhdenii Poleznykh Iskopaemykh Severa, Leningrad Mining Institute, pp. 92-96, 1972.
- Raleigh, C. B., Witherspoon, P. A., Gringarten, A. C., and Ohnishi, Y., "Multiple Hydraulic Fracturing for the Recovery of Geothermal Energy," EOS Trans. AGU, v. 55, no. 4, p. 4026, 1974.

THIS IS A PREPRINT - SUBJECT TO CORRECTION

# Analysis of Internal Steam Drive in Geothermal Reservoirs

J. C. Martin, Chevron Oil Field Research Company, Member SPE-AIME

© Copyright 1975

American Institute of Mining, Metallurgical, and Petroleum Engineers, Inc.

This paper was prepared for the 45th Annual California Regional Meeting of the Society of Petroleum Engineers of AIME, to be held in Ventura, Calif., April 2-4, 1975. Permission to copy is granted to an abstract of not more than 300 words. Illustrations may not be copied. The abstract should contain conspicuous acknowledgment of where and by whom the paper is presented. Reproduction elsewhere after publication in the JOURNAL OF PETROLEUM TECHNOLOGY or the SOCIETY OF PETROLEUM ENGINEERS JOURNAL is usually granted upon request to the Editor of the appropriate journal provided agreement to give proper credit is made.

Discussion of this paper is invited. Three copies of any discussion should be sent to the Society of Petroleum Engineers office. Such discussion may be presented at the above meeting and, if approved, the paper, may be considered for publication in one of the two SPE magazines.

## ABSTRACT

Reservoir analysis methods are applied to simple closed geothermal reservoirs that produce by internal steam drive. Relations are presented between the reservoir temperature, pressure, and fluid saturations, with the assumption that the fluids are produced according to their respective relative permeabilities. Calculated performance curves are given for various types of reservoirs. Results indicate that hot-water reservoirs can have complicated behavior, including changing from production of hot water to dry steam.

## INTRODUCTION

Exploitation of geothermal energy has accelerated in recent years. Increased understanding is being gained of the fundamental heat and mass transfer involved in geothermal energy production. Techniques used by petroleum production researchers are particularly well suited to the study of these fundamentals, and to the application of reservoir engineering principles in general.

Appendix, and illustrations are included.

Some geothermal reservoirs are similar to oil and gas reservoirs. The reservoir is a porous media, through which the fluids flow according to Darcy's law. Furthermore, some geothermal reservoirs have the equivalent of cap rocks.

The analogy between oil and gas reservoirs is the basis for the fundamental assumption of this paper: fluid flow in a geothermal reservoir can be treated as the flow through a porous medium, and Darcy's law and relative permeabilities are applicable.

There are many analogies between petroleum and geothermal reservoir engineering. For example, a number of the drives which supply reservoir energy are similar. The edge water drive in a petroleum reservoir is analogous to influx from cooler aquifers in geothermal reservoirs. Solution gas drive in petroleum reservoirs is analogous to two-phase internal steam drive in geothermal reservoirs. Compaction drive can occur in both. Waterflooding an oil reservoir is analogous to water cycling in a hot-water geothermal reservoir.

112

Methods of analysis similar to those used in petroleum reservoir engineering can be used for geothermal reservoirs as illustrated by the development of the material and heat balances in Reference 1. The present paper presents an analysis of internal steam drive, using methods analogous to those used for solution gas drive in Reference 2. The analysis presented herein is based on the following assumptions: the temperature, pressure, and fluid saturation gradients are small; the steam and hot water are produced according to their respective mobilities as determined by relative permeabilities and viscosities; and the effects of capillary pressure and gravity can be neglected. Some gravitational effects however, are treated qualitatively in the discussion. Throughout the analysis and discussion the produced steam and hot water are calculated neglecting the pressure and temperature drops near the wells and in the wellbores. The effects of these additional changes must be introduced to obtain steam and hot water production rates at the wellhead.

## DISCUSSION

### Temperature-Pressure Behavior

As pointed out in Reference 1, initial temperature and pressure in a geothermal reservoir determine its reservoir type. The solid line in Figure 1 presents the boiling curve for pure water. (Curves for actual geothermal brines will be modified by the dissolved salts<sup>3</sup>.) Points to the right of the curve and below the critical temperature represent hot water reservoirs. Points to the left of the curve and also points above the critical temperature represent single-phase or steam reservoirs.

The mathematical analysis is presented in the Appendix. Ordinary differential equations are derived for the fluid saturations and reservoir pressure (for two-phase flow) and for the pressure and temperature (for single-phase flow). Equations 13 and 16 of the Appendix were solved numerically for the temperature-pressure behavior of closed geothermal reservoirs containing fresh water and having the relative permeability curves presented in Figure 2. Other values used in the calculations are: 162 lbs/ft<sup>3</sup>

rock grain density, 0.20 Btu/°F-lb specific heat of rock, 40 Btu/ft-day thermal conductivity, and 1.0 Darcy permeability. Results of these calculations for a porosity of .25 are presented by the dashed lines in Figure 1.

As production causes the reservoir pressure to decline, the temperature follows the dashed line that passes through initial temperature and pressure. Several such lines are presented in Figure 1. For example, from initial conditions corresponding to Point A in Figure 1, the temperature will move to the left along line 1 as the pressure declines. This case (reservoir A) corresponds to a single-phase (essentially steam) reservoir with initial temperature and pressure above the critical values. No hot water is formed during pressure depletion, since line 1 does not intersect the boiling curve. The reservoir temperature remains high after the pressure is depleted. Thus, additional energy could be extracted by water injection, beginning at any point along line 1.

The initial conditions correspond to Point B (reservoir B) in Figure 1 represent a dry-steam reservoir in which no hot water is formed during pressure depletion and much heat would remain unproduced if the pressure were depleted. The temperature would move along line 3 as the pressure declines.

Point C (reservoir C) in Figure 1 corresponds to an initial hot water reservoir with pressure above the boiling curve. Unless a strong rock drive exists, initially the pressure declines rapidly with production, since only liquid expansion and rock compaction supply the driving energy. The reservoir performs essentially isothermally along line 4 until the boiling curve is reached. Then steam begins to be generated within the reservoir and a steam phase begins to build up within the rock pores. This supplies a gas drive similar to a solution gas drive in a petroleum reservoir. As production continues, the temperature and pressure decline along the boiling curve. The steam saturation increases with production and when it reaches its equilibrium saturation the reservoir begins to produce steam along with hot water.

The produced steam-hot water ratio continues to increase until the water saturation is reduced to its maximum immobile saturation. Then only saturated steam is produced. Water saturation continues to decline until all the water has been boiled away. The temperature then departs from the boiling curve and its decline essentially stops. The produced steam becomes increasingly superheated, as indicated by line 4 in Figure 1.

Point D (reservoir D) in Figure 1 corresponds to a relatively low-temperature hot water reservoir. Except for those cases with strong rock drives, rapid pressure decline with production should occur, since only liquid expansion and rock drive supply the driving energy above the boiling curve. Two-phase internal steam drive does not begin until the reservoir pressure has declined to a small fraction of its initial value. There is sufficient water in the pores that some water will remain even if the pressure reaches atmospheric. Most of the steam produced through pressure depletion of this type of reservoir will be at low pressures. These low pressures result in low efficiencies if used in steam turbines to produce power. For this reason power production from such reservoirs is perhaps best accomplished by cycling hot water through the reservoirs and using a binary cycle power plant (Reference 4).

#### Fluid and Heat Production Performance

Figures 3 and 4 present the variations of the reservoir pressure and temperature with the percent of initial fluid mass produced. Reservoirs A and B perform essentially by isothermal steam expansion; reservoirs C and D involve two-phase internal steam drive. Almost all of the initial fluid is produced from reservoirs A, B and C and much of it is produced from reservoir D. Reservoirs A and B experience little temperature drop during production and in reservoir C the temperature declines from 650 to 530°F. Thus, in these cases much heat remains in the reservoir rock at the end of pressure depletion.

Figure 5 presents the pressure versus steam saturation for reservoirs C and D. The increasing negative slope of the reservoir C curve with steam

saturation reflects the increasing produced steam-hot water ratios as the steam saturation increases with pressure depletion.

Figure 6 presents the variation of pressure with the amount of heat produced which is over and above the amount of heat that would be in the reservoir if it contained only saturated steam at atmospheric pressure and 212°F. Results for reservoirs A and B indicate that relatively small amounts of the total heat are produced during pressure depletion. Figure 7 presents the pressure versus heat recovered in the form of steam and in the form of hot water for reservoirs C and D. These results indicate that more heat is produced in the form of steam than hot water. This reflects the higher heat content and the lower viscosity of the steam as compared to the hot water. Figure 8 presents the pressure versus heat produced for six hot water reservoirs with three different porosities. The increase in heat recovered with porosity for the higher initial pressure cases results from the larger volume of initial water present relative to the reservoir rock volume.

#### Gravity Segregation

The results presented to this point are based on the assumption that the fluids are uniformly distributed throughout the reservoir. In reality gravity segregation of the steam and hot water will begin as soon as the steam phase becomes mobile. Reservoir performance and gravity segregation studies of oil and gas in oil reservoirs indicate that in many cases segregation occurs rapidly (References 5, 6 and 7). Similar segregation of the steam and hot water should occur in geothermal reservoirs.

The results for uniformly distributed fluids are useful in visualizing the behavior of reservoirs in which rapid gravity segregation takes place and in which heat conduction, natural convection, and capillarity, can be neglected to a first approximation. Steam accumulation at the top of a reservoir resulting from gravity segregation can greatly reduce the amount of water available there to generate steam. Similarly the drainage of hot water to the lower portion of the reservoir increases the amount of water



available there for steam generation. Under gravity segregation reservoir C should perform the same as given in Figures 1 and 3 through 8 until the steam saturation reaches its equilibrium value. Then the steam phase becomes mobile and gravity segregation begins. Steam saturation will increase rapidly near the top of the reservoir. If the wells are completed high in the reservoir or significant steam coning occurs, the produced steam-hot water ratio will increase rapidly. The hot water saturation will decrease rapidly until the water in the region is exhausted. Thus this region will depart from the boiling curve at considerably higher temperatures and pressures than for reservoir C. Points low in the reservoir will have high water saturations longer than if the fluid were to remain uniformly distributed, and these points will remain on the boiling curve to lower temperatures and pressures.

If the wells are completed low in the reservoir and significant steam coning does not take place, the produced steam-hot water ratio will remain low until the steam zone has expanded sufficiently to cause production from the steam zone. Points in the steam zone will depart from the boiling curve at higher pressures and temperatures than in the uniform saturation case and the lower portion of the reservoir will remain on the boiling curve to lower pressures and temperatures.

Thus the relative amounts of steam and hot water produced will depend upon, among other things, the amount of gravity segregation, the relative permeability curves, the structural position of the completion intervals, and the amount of steam and water coning. For many conditions the amount of water initially present is so limited that much usable heat should remain in the reservoir after the water is exhausted. This heat may be distributed in a highly nonuniform manner, with generally higher temperatures in the upper portion of the reservoir. In most cases the produced steam contains much more heat than an equal mass of produced water. Thus for many conditions more total heat can be produced by completing the wells high in the reservoir, to enhance steam production and suppress water production. This should result in more of the dissolved salts being left in the reservoir. This would be an

additional advantage provided problems associated with salt deposition are not too severe.

#### CONCLUSIONS

1. Reservoir analysis methods can be applied to those geothermal reservoirs that involve the flow of steam or hot water through porous media.
2. Hot-water reservoirs can have complicated producing characteristics including changing from hot water to steam as they are produced.
3. Under certain conditions only a relatively small amount of the heat initially contained in a geothermal reservoir will be produced during pressure depletion. Much of this heat may be contained in the produced steam even though initially the reservoir contains only hot water.
4. For many conditions where gravity segregation of the steam and hot water occur during depletion, more of the total heat can be produced by completing wells high in the reservoir to enhance steam production and suppress water production.

#### REFERENCES

1. Whiting, R. L. and Ramey, H. J.: "Application of Material and Energy Balances to Geothermal Steam Production", J. Pet. Tech. (July 1969) pp. 893-900.
2. Martin, J. C.: "Simplified Equations of Flow in Gas Drive Reservoirs and the Theoretical Foundation of Multiphase Pressure Buildup Analyses", Trans AIME (1959) vol. 216, pp. 309-311.
3. Hass, J. L.: "The Effect of Salinity on the Maximum Thermal Gradient of a Hydrothermal System at Hydrostatic Pressure", Econ. Geology, Vol. 66 (1971) pp. 940-946.
4. Kruger, P. and Otte, Carel: Geothermal Energy, Stanford Univ. Press, Stanford, Calif. (1973).
5. Spivak, A.: "Gravity Segregation in Two-Phase Displacement Processes", SPEJ (Dec. 1974) Vol. 14, No. 6, pp. 619-632.

6. Martin, J. C.: "Reservoir Analysis for Pressure Maintenance Operations Based on Complete Segregation of Mobile Fluids", Trans. AIME (1958) Vol. 213, pp. 220-227.

7. Martin, J. C.: "Some Mathematical Aspects of Two-Phase Flow with Applications to Flooding and Gravity Segregation Problems", Prod. Monthly (April 1958), pp. 22-35.

### APPENDIX

The mathematical relations for both two-phase (boiling) and single phase flow are derived in this appendix.

#### Two Phase Relations

The basic equations for conditions along the boiling curve are:

Darcy's law for hot water:

$$u_w = - \frac{k k_{rw}}{\mu_w} \nabla p \quad (1)$$

Darcy's law for steam:

$$u_s = - \frac{k k_{rs}}{\mu_s} \nabla p \quad (2)$$

The equation of continuity for mass:

$$\nabla \cdot (\rho_w u_w + \rho_s u_s) = - \frac{\partial}{\partial t} [\phi (\rho_w S_w + \rho_s S_s)] \quad (3)$$

The equation of continuity for heat:

$$\nabla \cdot (\rho_w h_w u_w + \rho_s h_s u_s - k_h \nabla T) = - \frac{\partial}{\partial t} \left\{ \phi [\rho_w h_w S_w + \rho_s h_s S_s + \left(\frac{1-\phi}{\phi}\right) \rho_r C_r T] \right\} \quad (4)$$

saturation:

$$S_w + S_s = 1 \quad (5)$$

Substituting equations 1 and 2 into 3 yields:

$$\nabla \cdot \lambda_f \nabla p = \frac{\partial M_f}{\partial t} \quad (6)$$

$$\nabla \cdot \lambda_h \nabla p = \frac{\partial M_h}{\partial t} \quad (7)$$

where

$$\lambda_f = \frac{\rho_w k k_{rw}}{\mu_w} + \frac{\rho_s k k_{rs}}{\mu_s}$$

$$\lambda_h = \frac{\rho_w h_w k k_{rw}}{\mu_w} + \frac{\rho_s h_s k k_{rs}}{\mu_s} + k_h \psi'$$

$$M_f = \phi (\rho_w S_w + \rho_s S_s)$$

$$M_h = \phi [\rho_w h_w S_w + \rho_s h_s S_s + \left(\frac{1-\phi}{\phi}\right) \rho_r C_r \psi]$$

$$T = \psi(p) \quad (8)$$

and

$$\psi' = \frac{d\psi}{dp}$$

The symbol  $\lambda_f$  denotes the mobility of the fluids in terms of mass;  $\lambda_h$ , the mobility of the heat;  $M_f$ , the mass of fluid per unit volume of reservoir rock; and  $M_h$ , the total heat per unit volume of rock.

Equations 5 and 6 can be written as

$$\begin{aligned} & \frac{\partial \lambda_f}{\partial p} \nabla p \cdot \nabla p + \frac{\partial \lambda_f}{\partial T} \nabla T \cdot \nabla p \\ & + \frac{\partial \lambda_f}{\partial S_w} \nabla S_w \cdot \nabla p + \frac{\partial \lambda_f}{\partial S_s} \nabla S_s \cdot \nabla p \\ & + \lambda_f \nabla^2 p = \frac{\partial M_f}{\partial t} \quad (9) \end{aligned}$$

$$\begin{aligned} & \frac{\partial \lambda_h}{\partial p} \nabla p \cdot \nabla p + \frac{\partial \lambda_h}{\partial T} \nabla T \cdot \nabla p \\ & + \frac{\partial \lambda_h}{\partial S_w} \nabla S_w \cdot \nabla p + \frac{\partial \lambda_h}{\partial S_s} \nabla S_s \cdot \nabla p \\ & + \lambda_h \nabla^2 p = \frac{\partial M_h}{\partial t} \quad (10) \end{aligned}$$

In those cases where the saturation gradient, temperature gradient, and pressure gradients are small, the vector products  $\nabla p \cdot \nabla p$ ,  $\nabla T \cdot \nabla p$ ,  $\nabla S_w \cdot \nabla p$  and  $\nabla S_s \cdot \nabla p$  are small compared to the magnitudes of  $\nabla^2 p$ ,  $\frac{\partial M_f}{\partial t}$ , and  $\frac{\partial M_h}{\partial t}$ , and the terms containing the vector products can be neglected to a first approximation.

Equations 9 and 10 reduce to:

$$\nabla^2 p = \frac{1}{\lambda_f} \frac{\partial M_f}{\partial t} \quad (11)$$

$$\nabla^2 p = \frac{1}{\lambda_h} \frac{\partial M_h}{\partial t} \quad (12)$$

Equations 11 and 12 require that the variations of  $P$ ,  $S_w$ ,  $S_s$ , and  $T$  are small with distance. Fortunately the variations of these quantities with time need not be small.

The elimination of  $\nabla^2 p$  from Equations 11 and 12 yield (replacing  $T$  by  $\psi(p)$  and  $S_s$  by  $1-S_w$ ):

$$\frac{\partial M_f}{\partial p} \frac{\partial p}{\partial t} + \frac{\partial M_f}{\partial S_w} \frac{\partial S_w}{\partial t} = \frac{\lambda_f}{\lambda_h} \left( \frac{\partial M_h}{\partial p} \frac{\partial p}{\partial t} + \frac{\partial M_h}{\partial S_w} \frac{\partial S_w}{\partial t} \right)$$

This equation reduces to the following ordinary differential equation:

$$\frac{dS_w}{dp} = \frac{\lambda_h \frac{\partial M_f}{\partial p} - \lambda_f \frac{\partial M_h}{\partial p}}{\lambda_f \frac{\partial M_h}{\partial S_w} - \lambda_h \frac{\partial M_f}{\partial S_w}} \quad (13)$$

Equation 13 can be integrated numerically to obtain  $S_w$  as a function of  $P$ . This relation is similar to the Muskat solution gas relation which relates oil or gas saturation to reservoir pressure.

The relation between  $S_w$  and  $P$  obtained from Equation 13 can be used to eliminate  $S_w$  from  $\lambda_f$ ,  $\lambda_h$ ,  $M_f$ , and  $M_h$ . This allows Equations 11 and 12 to be expressed in terms of pressure, thereby obtaining a partial differential equation for pressure that can be used in the analysis of transient well pressure data which involve two-phase flow in the reservoir.

### Single Phase Flow

116

The temperature and pressure are not related to the boiling curve for single-phase flow. Equation 11, however, is valid and the equivalent of Equation 12 is:

$$\nabla^2 p + \frac{k_h}{\rho h \lambda} \nabla^2 T = \frac{1}{\rho h \lambda} \frac{\partial M_h}{\partial t} \quad (14)$$

where  $h$  is the enthalpy,  $\lambda$  is the mobility, and  $M_h$  is the single phase equivalent of  $M_h$ .

In the case of two phase flow it was possible to obtain an ordinary differential equation for the water saturation versus pressure without neglecting the effects of heat conduction, because temperature and pressure are related by the boiling curve. Unfortunately, this is not the case for single phase flow; however, if we neglect the effects of heat conduction, Equation 14 reduces to:

$$\nabla^2 p = \frac{1}{\rho h \lambda} \frac{\partial M_h}{\partial t} \quad (15)$$

Eliminating  $\nabla^2 p$  from Equations 11 and 15 leads to the following differential equation for  $P$  and  $T$ :

$$\frac{dT}{dp} = \frac{\frac{\partial M_h}{\partial p} - h \frac{\partial M_f}{\partial p}}{h \frac{\partial M_f}{\partial T} - \frac{\partial M_h}{\partial T}} \quad (16)$$

This equation was used to calculate  $T$  versus  $P$  for single phase flow. As expected, numerical results reveal small values of  $\frac{dT}{dp}$  indicating essentially isothermal behavior.

### Additional Relations

Solutions of Equations 13 and 16 yield the temperature and fluid saturations as functions of reservoir pressure. Heat and mass balances can be used to obtain the fluid and heat productions as functions of pressure. These relations are:

$$Q_f = 1 - \frac{M_f}{M_{fi}}$$

where  $Q_f$  is the fraction of the original fluid mass that has been produced and the subscript 1 refers to initial conditions.

$$Q_h = \frac{M_{h1} - M_h}{M_{h1} - M_{ha}}$$

where  $Q_h$  is the fraction of the original heat that has been produced which is above the heat contained in the reservoir at atmospheric pressure and 212°F containing only saturated steam. The subscript a refers to these conditions.

Expressions for the relative amounts of heat produced in the steam and in the hot water can be obtained by integration. These relations are:

$$Q_{hw} = \left( \frac{1}{M_{h1} - M_h} \right) \int_{p_1}^p \left( \frac{\rho_w h_w k_{rw}}{\lambda_h \mu_w} \right) \frac{dM_h}{dp} dp$$

$$Q_{hs} = \left( \frac{1}{M_{h1} - M_h} \right) \int_{p_1}^p \left( \frac{\rho_s h_s k_{rs}}{\lambda_h \mu_s} \right) \frac{dM_h}{dp} dp$$

where  $Q_{hw}$  and  $Q_{hs}$  are the fractions of the produced heat contained in the hot water production and in the steam production respectively.

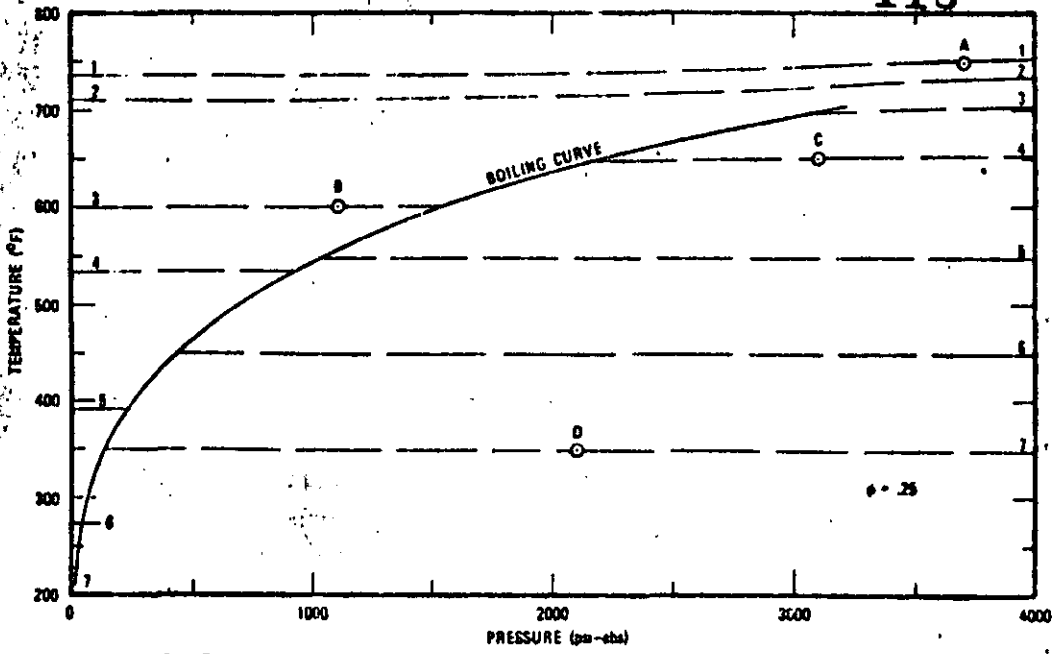


Fig. 1 - Temperature vs pressure for geothermal reservoirs containing fresh water, a porosity of .25, and with other data given in text.

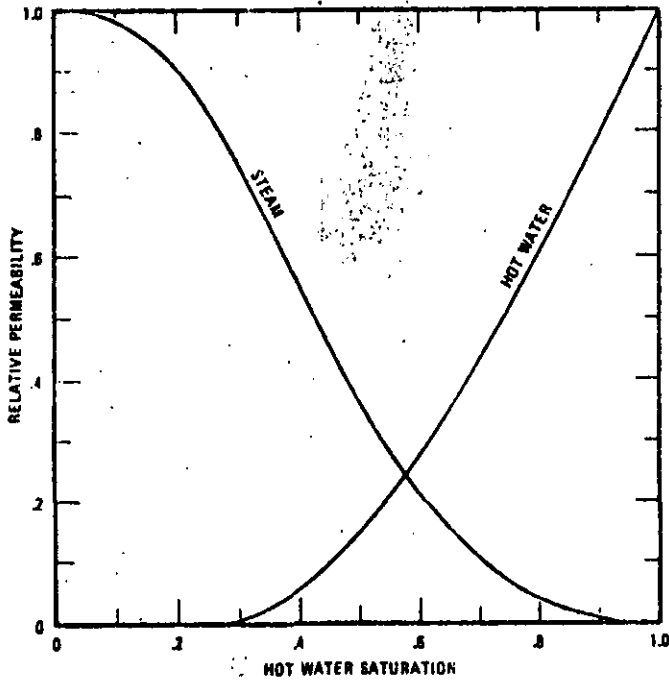


Fig. 2 - Steam and hot water relative permeability curves used in the calculations.

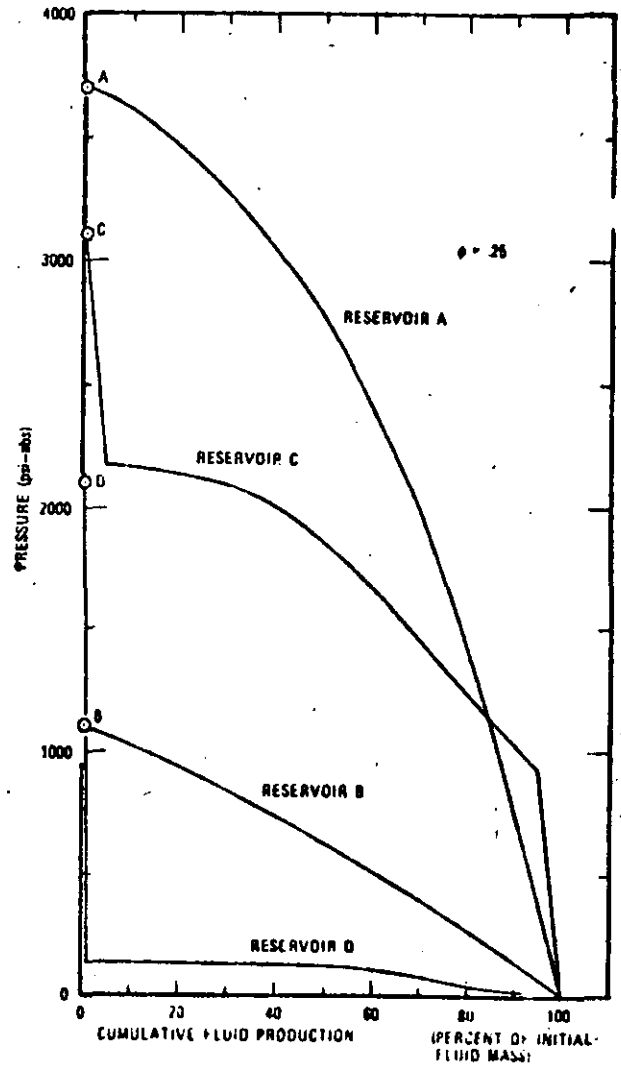


Fig. 3 - Pressure vs cumulative fluid production for reservoirs A, B, C, and D.

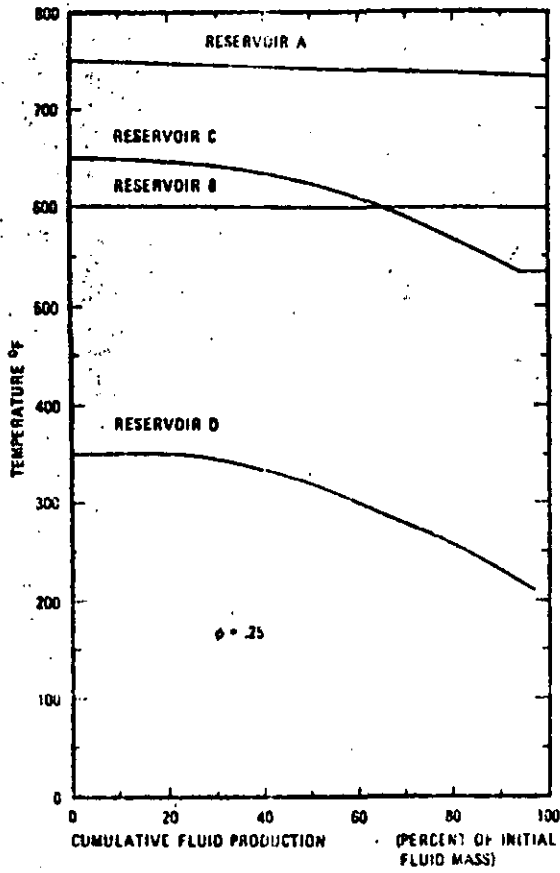


Fig. 1 - Temperature vs. cumulative fluid production for reservoirs, A, B, C, and D.

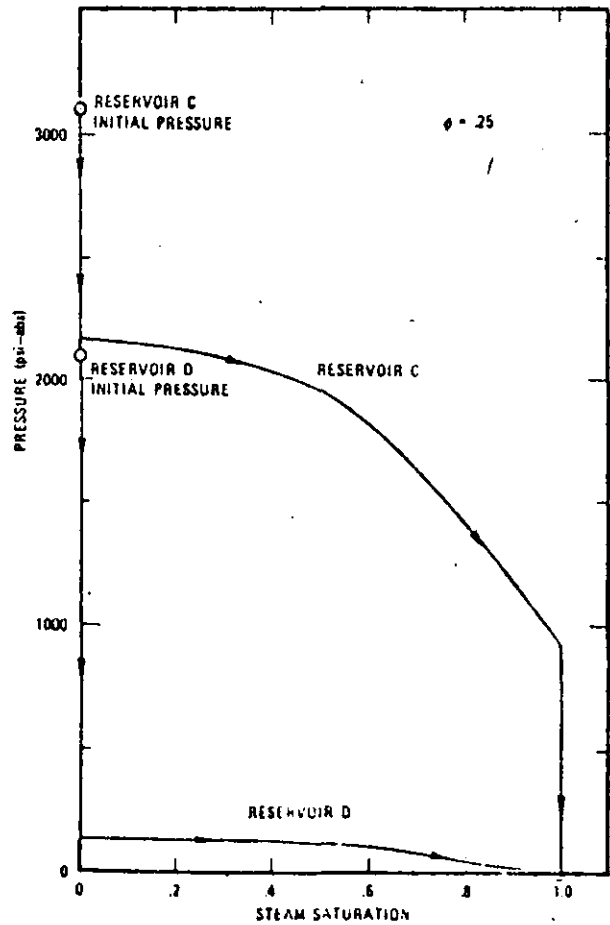


Fig. 2 - Pressure vs. steam saturation for reservoirs, C and D.

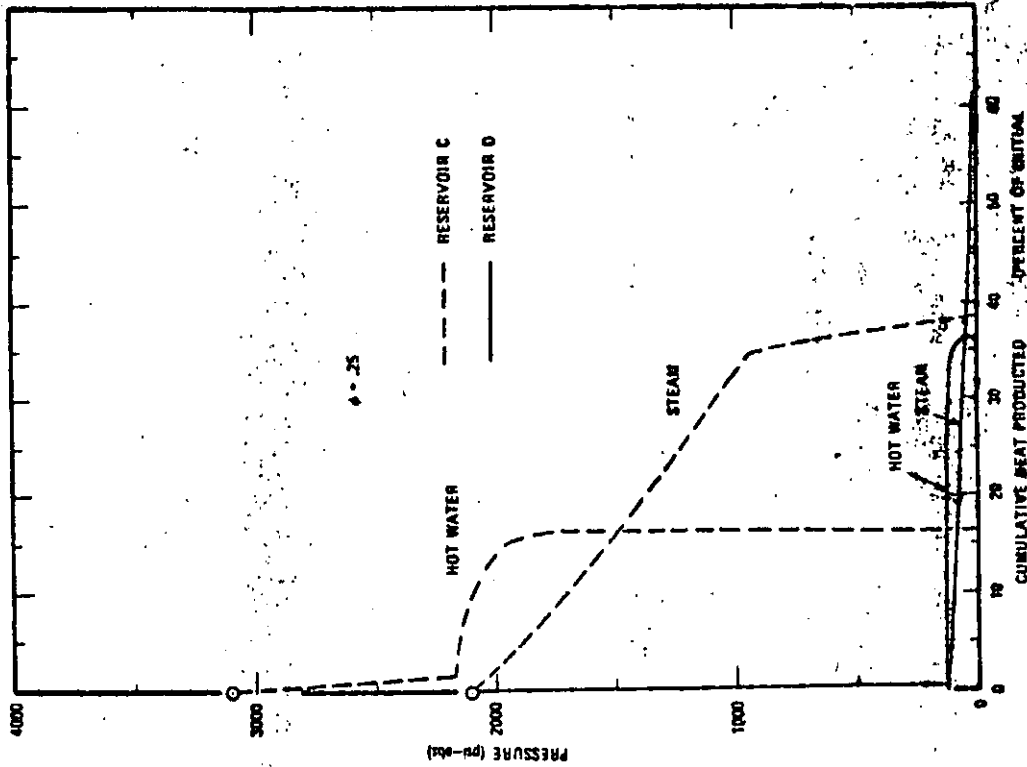


FIG. 2 - Pressure vs cumulative heat produced as steam and as hot water for reservoirs C and D.

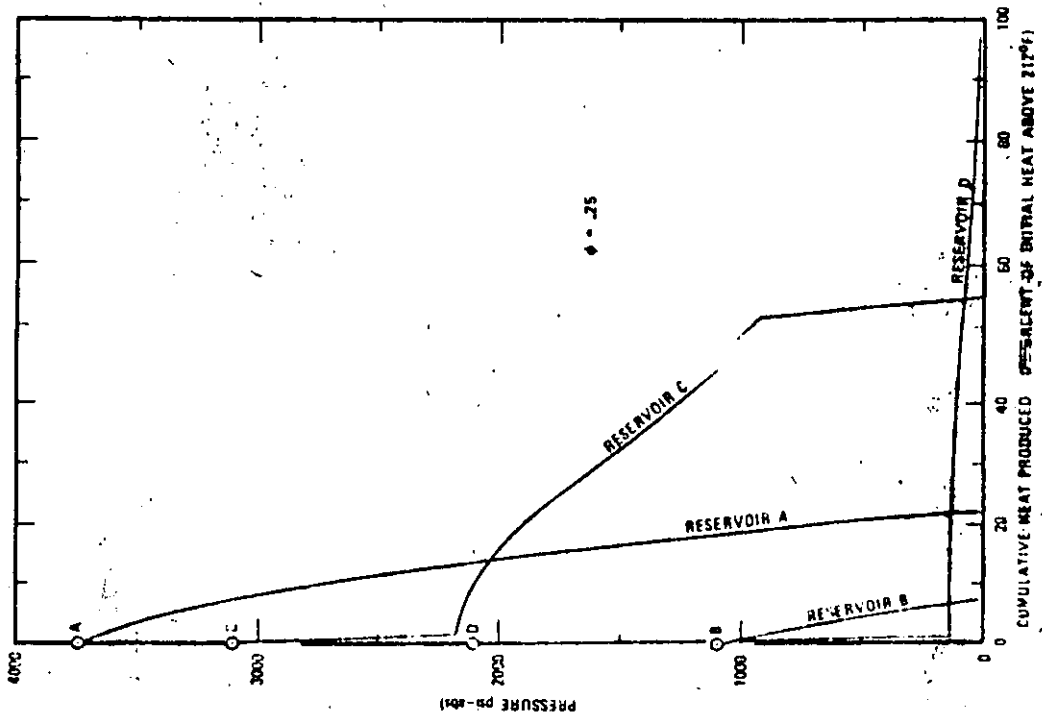


FIG. 3 - Pressure vs cumulative heat produced for reservoirs A, B, C, and D.

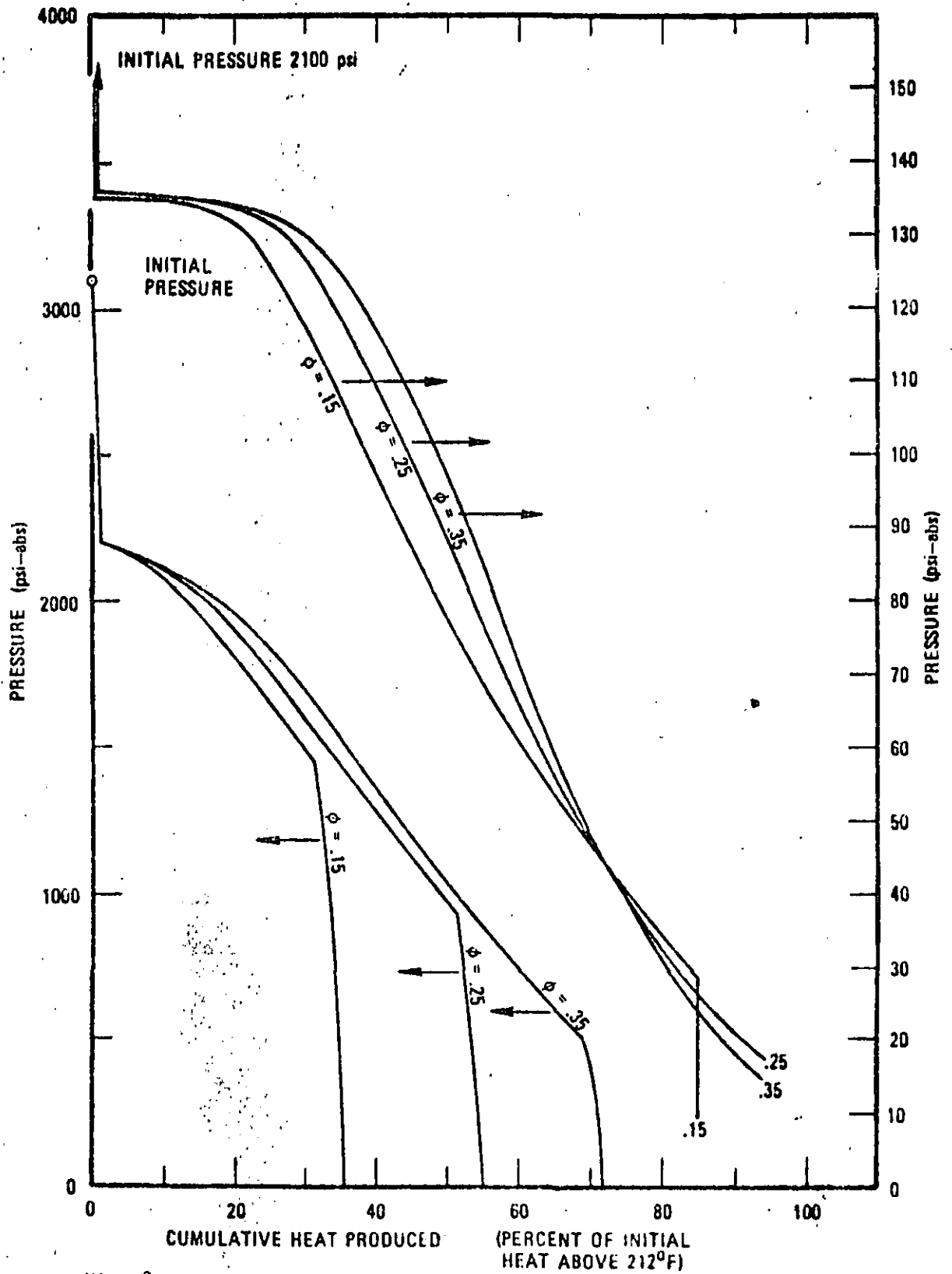


Fig. 9 - Pressure vs cumulative heat produced for three different porosities and two different initial conditions (3100 psi, 350 °F and 2100 psi, 350°F).



## MODELING GEOTHERMAL SYSTEMS

by

P. A. Witherspoon,<sup>1</sup> S. P. Neuman,<sup>1</sup> M. L. Sorey<sup>2</sup>  
and M. J. Lippmann<sup>3</sup>

## ABSTRACT

Geothermal systems are receiving more and more attention as an alternative source of energy and, consequently, there is growing interest in attempting to understand their nature and behavior. One approach to this problem is to attempt to deduce the physical behavior of such systems using a mathematical model. This paper presents the governing equations for energy and mass transfer in porous media that must be solved in using such models. Fundamental concepts that have been developed for factors that affect the development of free and forced convection in geothermal systems under natural conditions are reviewed. The results of modeling geothermal systems during exploitation using lumped-parameter and distributed-parameter models are also presented.

---

<sup>1</sup> Lawrence Berkeley Laboratory and Department of Civil Engineering, University of California, Berkeley.

<sup>2</sup> U. S. Geological Survey, Menlo Park, California.

<sup>3</sup> Department of Civil Engineering, University of California, Berkeley.

## 123

INTRODUCTION

Geothermal systems are receiving more and more attention as an alternative source of energy and, consequently, there is growing interest in attempting to understand their nature and behavior. One approach to this problem is to attempt to deduce the physical behavior of such systems using a mathematical model. Such a model consists of a set of equations that describe the processes occurring within the system and the solution to these equations subject to conditions that prevail at a particular site.

The model approach has two important applications: (1) the geothermal system under natural conditions before being disturbed by man, and (2) the geothermal system during exploitation. Natural geothermal systems have been investigated by a great many workers. The main thrust of such studies has been to understand how geothermal systems can form and persist within the earth's crust.

The mathematical model can also be applied to the problem of evaluating the behavior of a geothermal system during exploitation. One of the most critical problems in developing such systems as a viable source of energy is that of determining that a particular reservoir once discovered is capable of producing significant quantities of energy over meaningful periods of time. The model is one of several tools that can be used to analyze this problem. During the early stages, the model may be crude, but its application in parametric analysis of the field data can provide valuable limits as to what can be expected. As more data become available, the model can be refined and such engineering questions as well spacing, optimum rates of fluid withdrawal and effects of reinjection can be studied.

In this review, we shall restrict our attention to hydrothermal systems, i.e., to geothermal systems involving water. We shall pay particular attention

to hydrothermal-convection systems, in which most of the heat is transferred in circulating fluids rather than by heat conduction. Two broad types of hydrothermal systems are recognized: (1) hot-water, and (2) vapor-dominated (White 1973).

In the hot-water type, water is the continuous phase throughout the system and thus provides the pressure control. Continuity of the liquid phase is evident from reservoir pressures that are near hydrostatic and the presence of soluble salts that are not found to any significant degree in low-pressure steam. In the vapor-dominated type, steam is the continuous, pressure-controlling phase, although there is general agreement that liquid water must also be present (Facca and Tonani, 1964, Elder, 1965; Craig, 1966; James, 1968; Marinelli, 1969; Sestini, 1970; White et al., 1971).

An intriguing question arises concerning the initial conditions of vapor-dominated systems. At depths below 350 m, they all tend to have temperatures near  $240^{\circ}\text{C}$  and pressures near  $35 \text{ kg/cm}^2$ , which usually means well below hydrostatic (White, 1973). This uniformity in the initial conditions is believed to be strongly influenced by the maximum enthalpy of saturated steam (James, 1968; Sestini, 1970; White et al., 1971).

The material and thermodynamic properties of the different components of geothermal systems are an important consideration in any attempt to develop realistic models of such systems. Fig. 1 presents a pressure-enthalpy diagram for pure water at pressures up to  $700 \text{ kg/cm}^2$  and temperatures up to  $500^{\circ}\text{C}$ . Dissolved salts are, of course, common in geothermal waters and studies on the effect of salinity on heat capacity (Nevens and Pool, 1964; Likke and Bromley, 1973), density (Haas, 1970), viscosity (Matthews and Russell, 1967, Fig. G4), and maximum thermal gradient (Haas, 1971) of brines are available. Helgeson (1968) has investigated the thermodynamic characteristics of the Salton Sea geothermal system where the highest concentrations, approaching 300,000 ppm, have been found.

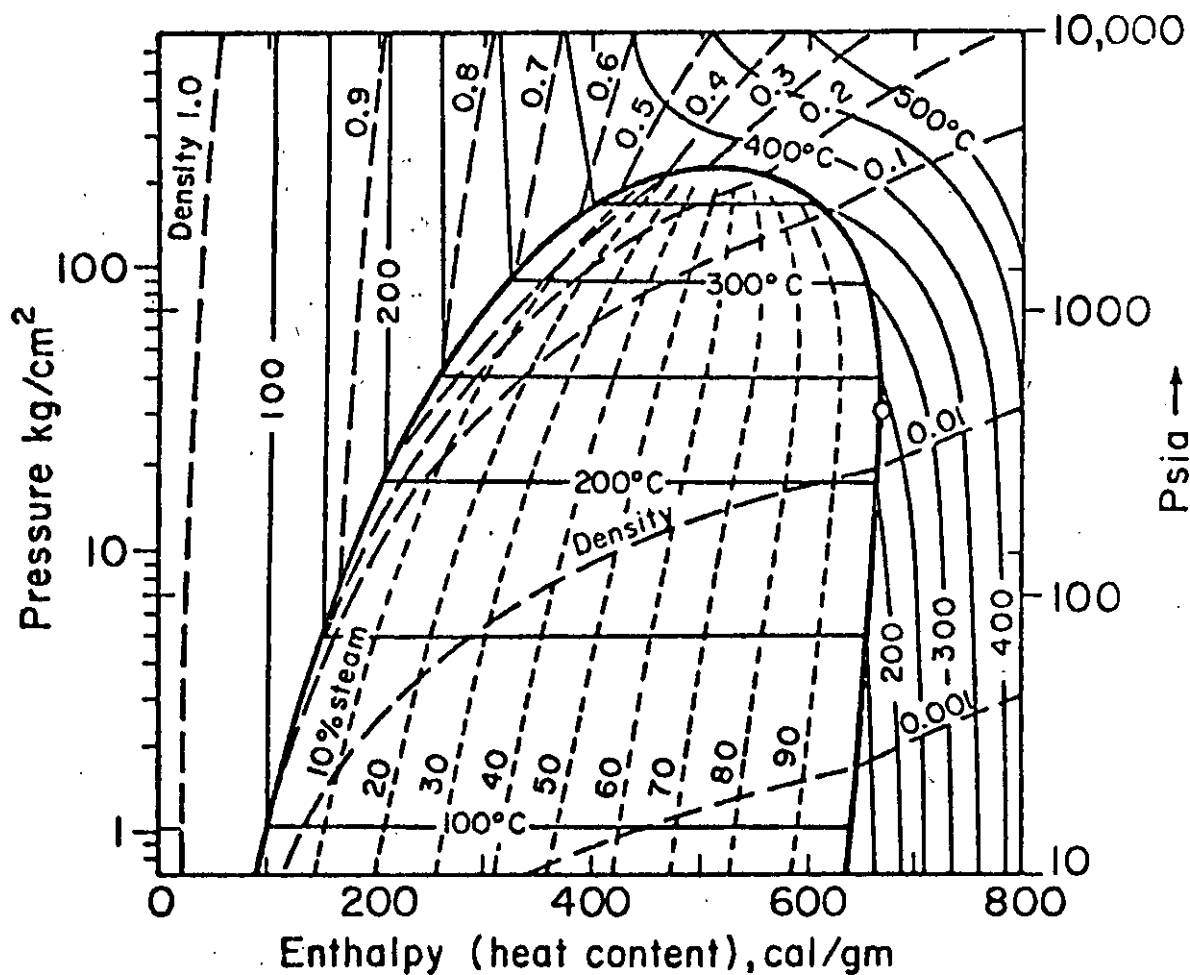


Fig. 1. Pressure-enthalpy diagram for pure water and vapor, showing contours of equal temperature, density and mass proportions of steam to water. Open circle indicates maximum enthalpy of saturated steam, 670 cal/gm at 236°C and 31.8 kg/cm<sup>2</sup> (after White et al., 1971).

The thermal properties of rocks are very important since the dominant fraction of the total energy in a geothermal system is in the solid matrix. Comprehensive tables of these properties for dry rocks have recently been compiled by Kappelmeyer and Haenel (1974). Thermal conductivities for most dry rocks range from 4 to 10 mcal/cm sec °C; specific heats are approximately 0.2 cal/g °C; and thermal diffusivities range from 5 to 15 cm<sup>2</sup>/sec. Kappelmeyer and Haenel also include the effects on these thermal properties of temperature and pressure.

The thermal conductivity of fluid-saturated rocks is dependent on the conductivities of the dry rock and the saturating fluid as well as the physical properties of the rock. Anand et al. (1973) and Somerton et al. (1974) have shown how thermal conductivities increase with brine saturation and become more sensitive to temperature change. They discuss correlations for predicting thermal conductivity from other rock properties.

The hydraulic properties of the rocks are also important since they control the fluid movement. The absolute values of permeability and porosity for rocks vary considerably and must be measured or estimated for any given system. A few workers have studied the thermal effects and report that the absolute permeability tends to decrease, sometimes significantly, with increasing temperature (Greenberg et al., 1968; Sanyal et al., 1972; Casse, 1974). There are also important effects of temperature on relative permeability (Edmonson, 1965; Davidson, 1969; Poston et al., 1970; Weinbrandt et al., 1972; Lo and Mungan, 1973; Ramey et al., 1974). In studying the effects of pressure, a number of workers (Knutson and Bohor, 1963; Brace et al., 1968; Vairogs et al., 1971) have suggested that permeability depends only on effective stress; that is, permeability is dependent only on the difference between hydrostatic confining pressure and internal pore pressure. However, Zoback and Byerlee (1975), have recently shown that pore pressure has a significantly larger effect on permeability under isothermal conditions than does confining pressure.

In this review of the problems involved in modeling geothermal reservoirs, we shall first present the governing equations for energy and mass transfer in porous media. Then we shall consider some of the fundamental concepts that have been developed for factors that affect the development of free and forced convection in geothermal systems under natural conditions. Lastly, we shall review the results of several efforts that have been made to model geothermal systems during exploitation.

### GOVERNING EQUATIONS

Let us consider a porous medium completely saturated with a single-component homogeneous fluid which can be either in a liquid or gaseous state. The liquid and gas phases are assumed to be separated locally by a distinct interface due to capillarity. Since mass may be transferred from one phase to another across the interface by vaporization or condensation, it is convenient to write a single mass balance equation for both phases

$$\frac{\partial}{\partial \tau} (\phi S^L \rho^L + \phi S^G \rho^G) = - \frac{\partial}{\partial x_1} (\rho^L v_1^L + \rho^G v_1^G) \quad (1)$$

Rate of mass accumulation                      Convective mass flux

All mathematical symbols appearing in the text are macroscopic quantities defined over a representative elementary volume of the porous medium. For a definition of these symbols the reader is referred to the Nomenclature.

It is generally believed that capillary pressure between the phases is small relative to absolute pressure, and as each phase may flow independently, we shall assume Darcy's law in the form

$$v_1^L = - \frac{k_{1j} k_r^L}{\mu^L} \left( \frac{\partial p}{\partial x_j} - \rho^L g_j \right) \quad (2)$$

$$v_1^G = - \frac{k_{1j} k_r^G}{\mu^G} \left( \frac{\partial p}{\partial x_j} - \rho^G g_j \right) \quad (3)$$

The relative permeabilities  $k_r^L$  and  $k_r^G$  are functions of fluid saturation and, as mentioned earlier, they may also be functions of temperature. Recent studies (Coats et al., 1974) indicate the latter effect is important and should be taken into account.

An energy balance equation must also be considered, and one way to derive such an equation in terms of macroscopic quantities is to follow an averaging procedure (see Appendix). Equation A21 is a general form of the macroscopic energy balance for the case where irreversible viscous dissipation of mechanical energy and transfer of kinetic energy between fluid and rock are neglected. An attempt to derive a set of more general equations considering mechanical interaction between rock and fluid has been reported recently by Brownell et al. (1975). It is customary to assume that not only is the capillary pressure zero, but also that the solid, liquid, and gas are locally in thermal equilibrium. In this case (A21) reduces to (A22) which can be written more conveniently without the angular brackets as

$$\frac{\partial}{\partial t} \left[ \phi S^L \rho^L e^L + \phi S^G \rho^G e^G + (1-\phi) \rho^S e^S \right] = \frac{\partial}{\partial x_j} \left( \kappa_{ij}^{eff} \frac{\partial T}{\partial x_j} \right) \quad (4)$$

Rate of internal energy accumulation
Conductive and dispersive internal energy flux

$$- \frac{\partial}{\partial x_j} \left( \rho^L e^L v_j^L + \rho^G e^G v_j^G \right) - p \frac{\partial}{\partial x_j} \left( v_j^L + v_j^G \right)$$

Convective internal energy flux
Rate of reversible mechanical energy (work) conversion to internal energy

Our mathematical analysis indicates that

$$\kappa_{ij}^{eff} = \phi S^L \kappa_{ij}^L + \phi S^G \kappa_{ij}^G + (1-\phi) \kappa^S \delta_{ij} \quad (5)$$

Laboratory experiments show that  $\kappa_{ij}^{eff}$  is not always given by (5) (Combarous and Bories, 1973, Fig. 6), thus implying that the assumption of local thermal equilibrium may not always hold. Moreover, as mentioned earlier, thermal conductivity may also be a function of temperature.

Equation 4 can be reformulated in terms of enthalpy by writing  $h = p/\rho$

instead of  $e$  and, as shown in (A25), one then has

$$\begin{aligned} \frac{\partial}{\partial t} \left[ \phi S^L \rho^L h^L + \phi S^G \rho^G h^G + (1-\phi) \rho^S h^S \right] &= \frac{\partial}{\partial x_1} \left( \kappa_{1j}^{\text{eff}} \frac{\partial T}{\partial x_j} \right) \\ - \frac{\partial}{\partial x_1} \left( \rho^L h^L v_1^L + \rho^G h^G v_1^G \right) + \frac{\partial(\phi p)}{\partial t} + \left( v_1^L + v_1^G \right) \frac{\partial p}{\partial x_1} & \quad (6) \end{aligned}$$

This is identical with an expression reported earlier by Mercer et al. (1974) except that we have omitted source terms.

In the particular case where only one fluid phase is present, the energy equation can be conveniently expressed in terms of temperature and, as shown in (A31), one obtains for a liquid saturated medium

$$\begin{aligned} \left[ \phi \rho^L c_v^L + (1-\phi) \rho^S c_v^S \right] \frac{\partial T}{\partial t} &= \frac{\partial}{\partial x_1} \left( \kappa_{1j}^{\text{eff}} \frac{\partial T}{\partial x_j} \right) \\ - \rho^L v_1^L c_v^L \frac{\partial T}{\partial x_1} - T \left( \frac{\partial p}{\partial T} \right)_v \frac{\partial v_1^L}{\partial x_1} & \quad (7) \end{aligned}$$

A similar expression holds for a medium saturated with gas.

The above equations must be supplemented by equations of state relating the thermodynamic variables  $e$ ,  $h$ ,  $\rho$ ,  $\mu$ ,  $S$ ,  $p$ ,  $T$ . Here it is customary to assume that all phases are in equilibrium and that thermodynamic relationships between macroscopic quantities remain the same as those between the equivalent point quantities. In particular, the macroscopic saturations  $S^L$  and  $S^G$  are assumed to be uniquely determined by the pressure and total energy or enthalpy of the fluid (both phases combined). In other words, whenever two phases occur simultaneously at a point in the system, their  $p$ - $T$  relationship is uniquely determined by conditions at the vapor pressure.

Although capillary pressure is neglected in the governing equations, it may still have an important effect on thermodynamic properties. Ramey et al. (1973) explain that the vapor-pressure curve in the presence of uneven capillary surfaces may be lower than that quoted in steam tables. Calhoun et al. (1949) showed that in consolidated sandstones the vapor-pressure curve at  $36^\circ\text{C}$  is significantly



affected by a decreasing liquid saturation. However, Cady (1969) and Bilhartz (1971) were unable to confirm this effect on unconsolidated sands with temperatures between 121°C and 240°C. The effect of capillary pressure therefore remains unclear.

Some geothermal systems such as those in Imperial Valley (California) involve waters of high salinity which cannot be treated as a homogeneous fluid because salt concentrations are not uniform. In this case the mass as well as energy balance equations (see Appendix) may have to be modified to include a term for dispersive mass flux and an additional equation for mass balance of the solute. Another complication may arise due to coupling between thermal and chemical gradients which modifies the form of Fourier's law of heat conduction (Dufour effect) and Fick's first law of diffusion (Soret effect). The presence of salts may also cause a slight lowering of the vapor-pressure curve (Haas, 1971; Ramey et al., 1973) and this effect becomes progressively more important as boiling proceeds, due to the increasing salt concentration (White, 1973). Very little is known about the behavior of these so-called thermohaline systems, but a few theoretical analyses have appeared (Nield, 1968, 1974; Rubin, 1973, 1975 a,b,c). The discussion that follows will be concerned solely with homogeneous fluids.

#### GEOHERMAL SYSTEMS UNDER NATURAL CONDITIONS

##### Fundamental Characteristics of Free Convection

Mathematical modeling related to geothermal systems has long centered on problems of convective heat transfer in a homogeneous porous layer heated from below. Pioneering work on this subject has been performed independently by Horton and Rogers (1945), Lapwood (1948), and Goguel (1953). Their efforts were directed primarily toward developing criteria for the onset of convection currents in a horizontal and laterally infinite layer. These analyses followed the pattern of earlier work by Rayleigh (1916), Jeffreys (1930), and others who showed that in a static layer of viscous fluid the critical temperature gradient (i.e., the

gradient at which cellular or Bénard convection is formed) depends on thermal conductivity, thermal coefficient of expansion, kinematic viscosity, thickness of the layer, and the boundary conditions. When fluid cannot enter or leave the system, the resulting flow pattern is referred to as "natural" or "free" convection. When fluid flow is entirely due to hydraulic forces acting at the boundaries, the result is known as "forced" convection, whereas "mixed" convection includes a combination of both phenomena. Early work on the subject was restricted to free convection.

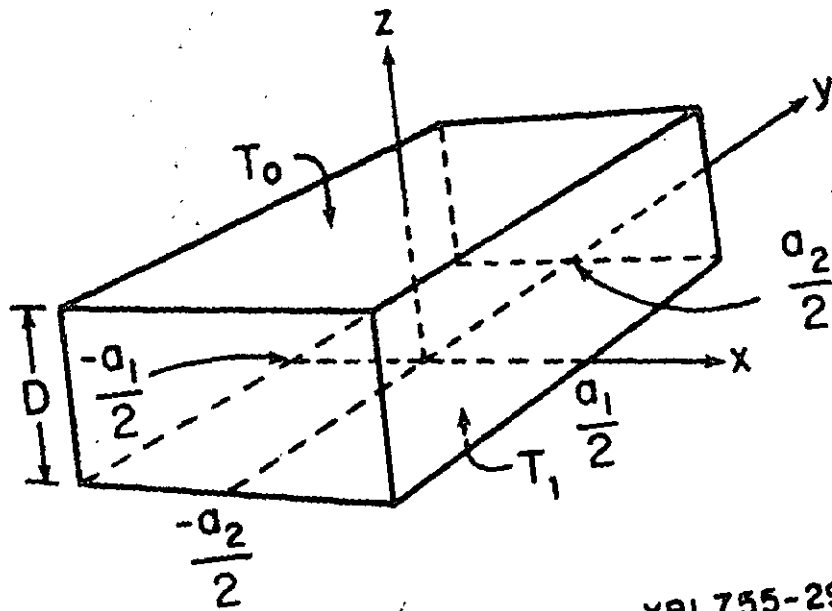
In reviewing the mathematical approach to free convection in porous media, we find it instructive to follow a recent development by Beck (1972). Consider a rectangular box of porous material resting on a horizontal surface and saturated by a homogeneous liquid (see Fig. 2). The vertical sides are thermally insulated (i.e., adiabatic), and the lower ( $z = 0$ ) and upper ( $z = D$ ) surfaces are isothermal. Temperature  $T_1$  at the bottom is greater than  $T_0$  at the top, and all boundaries are impermeable to fluid.

In most analytical studies of thermal convection, it is customary to invoke the Boussinesq approximation that spatial as well as temporal variations in fluid density can be neglected except for buoyancy effects (i.e., everywhere except in the gravity term in the equation of motion). In addition, all coefficients in the governing equations are assumed to be constant scalars. Under these conditions the mass balance equation 1 reduces to

$$\frac{\partial v_1}{\partial x_1} = 0 \quad (8)$$

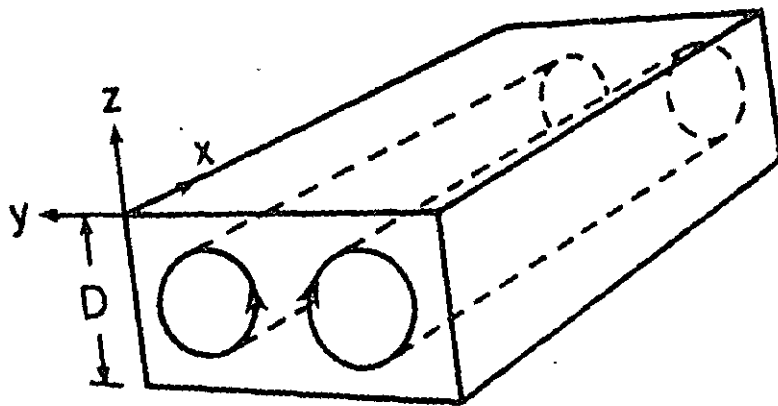
In writing Darcy's law, it is customary to replace  $\rho$  by  $\rho_0 [1 - \beta(T - T_0)]$  in the gravity term and add a term including the time derivative of velocity (compare with Eq. 2),

$$\frac{1}{\phi} \frac{\partial v_1}{\partial t} + \frac{\mu}{k\rho_0} v_1 = [1 - \beta(T - T_0)] g_1 - \frac{1}{\rho_0} \frac{\partial p}{\partial x_1} \quad (9)$$



XBL755-2915

Fig. 2. Rectangular box of porous media saturated with a homogeneous liquid.



XBL755-2916

Fig. 3. Two convective rolls in rectangular box heated from below.

$$\theta = 0 \quad \text{at} \quad Z = 0, 1 \quad (28)$$

$$\frac{\partial \theta}{\partial X_1} n_1 = 0 \quad \text{at} \quad X = \pm \frac{1}{2} D_1; \quad Y = \pm \frac{1}{2} D_2 \quad (29)$$

The dynamic stability of this system can be investigated by a linear method or by an energy approach. In the linear approach the disturbances are assumed to be small enough for second-order terms to be neglected. The conditions for marginal stability (i.e., stability just at the onset of convection) can thus be determined from the above equations after reducing (25) and (26) to

$$- Ra^{\frac{1}{2}} \theta \delta_{13} + v_i = - \frac{\partial p_D}{\partial X_1} \quad (30)$$

$$Ra^{\frac{1}{2}} v_i \delta_{13} = - \frac{\partial^2 \theta}{\partial X_1^2} \quad (31)$$

According to the linear theory, the critical Rayleigh number,  $Ra_c^{\text{linear}}$ , is the smallest eigenvalue of the resulting problem. However, this theory indicates only a necessary condition for stability, and the true critical Rayleigh number may therefore be smaller,  $Ra_c^{\text{true}} \leq Ra_c^{\text{linear}}$ .

The energy method was first applied to porous media by Westbrook (1969) and was later extended by Wankat and Schowalter (1970) and Beck (1972). Stability is established relative to arbitrary disturbances subject only to the equation of continuity and corresponding boundary conditions. Since stability actually depends on a more restricted class of disturbances satisfying (24) - (29), the critical Rayleigh number obtained may be too conservative and we therefore have  $Ra_c^{\text{energy}} \leq Ra_c^{\text{true}}$ . However, in the particular case considered here, both methods lead to the same eigenvalue problem and therefore  $Ra_c^{\text{linear}} = Ra_c^{\text{energy}}$ .

Beck showed that the eigenvalue problem has separable eigenfunctions, the velocity components of which are

$$\begin{aligned}
 v_1 &= \sin \left[ \left( \frac{1}{2} m \pi \right) (1 + 2X/D_1) \right] \cos \left[ \left( \frac{1}{2} n \pi \right) (1 + 2Y/D_2) \right] U(Z) \\
 v_2 &= \cos \left[ \left( \frac{1}{2} m \pi \right) (1 + 2X/D_1) \right] \sin \left[ \left( \frac{1}{2} n \pi \right) (1 + 2Y/D_2) \right] V(Z) \\
 v_3 &= \cos \left[ \left( \frac{1}{2} m \pi \right) (1 + 2X/D_1) \right] \cos \left[ \left( \frac{1}{2} n \pi \right) (1 + 2Y/D_2) \right] \sin(\ell \pi Z)
 \end{aligned} \tag{32}$$

$$m, n = 0, 1, 2, \dots; \quad \ell = 1, 2, \dots$$

where  $U(Z)$  and  $V(Z)$  are functions of  $Z$  only. The corresponding critical Rayleigh numbers are

$$Ra_c = \pi^2 \min_{\ell, m, n} (b + \ell^2/b)^2 = \pi^2 \min_{m, n} (b + b^{-1})^2 \tag{33}$$

$$\text{where } b = \left[ \left( \frac{m^2}{D_1^2} \right) + \left( \frac{n^2}{D_2^2} \right) \right]^{1/2} \text{ and } \ell = 1.$$

Equation 33 shows that the critical Rayleigh number depends entirely on aspect ratios  $D_1$  and  $D_2$ . The minimum possible value of  $Ra_c$  is  $4\pi^2$  corresponding to  $b = 1$ . Lapwood (1948) obtained  $Ra_c = 4\pi^2$  for the case of a laterally infinite layer, thus indicating that vertical walls tend to stabilize the system. However,  $Ra_c$  remains nearly equal to  $4\pi^2$  unless  $D_1$  or  $D_2$  are less than about 0.8, as may happen in a narrow and tall box.

Geometry becomes more important when one considers the mode of convection. It is evident from (32) that when  $m = 0$ , the horizontal velocity  $v_1$  vanishes, which gives rise to  $n$  convective cells known as "rolls" (see Fig. 3). Since  $Ra_c$  corresponds to  $\ell = 1$ ,  $v_3$  in (32) is identically zero only at  $Z = 0$  and  $Z = 1$ , and thus the vertical extent of each roll is equal to the height of the box. A typical temperature profile in a plane perpendicular to the axis of such a roll is shown in Fig. 4. Rolls are invariably preferred over three-dimensional cells whenever the height  $D$  is not the smallest dimension. When rolls do form, they are usually parallel to the shorter side, although the overriding rule is for the number of rolls and the direction of their axes to be such that each roll has the closest approximation to a square cross-section as possible. Three-dimensional cells are preferred when  $a_1$ ,  $a_2$ , and  $D$  are nearly the same size (i.e., a cube)

Energy balance is usually expressed by a simplified version of equation 7, and Beck writes, using our notation

$$(\rho c_v)^{\text{eff}} \frac{\partial T}{\partial t} = -\rho_o c_v v_1 \frac{\partial T}{\partial x_1} + \kappa^{\text{eff}} \frac{\partial^2 T}{\partial x_1^2} \quad (10)$$

where  $(\rho c_v)^{\text{eff}} = \phi \rho_o c_v + (1-\phi) \rho^S c_v^S$ .

Initially, the system is assumed to be in static equilibrium so that the pressure is hydrostatic. Thus,

$$v_1^o = (0, 0, 0) \text{ and } T^o = T_1 + (T_o - T_1) \frac{z}{D} \quad (11)$$

Under these conditions, there are no convective currents and the system is said to be "statically stable." Let a small volume of fluid suddenly be brought from elevation  $z = 0$  to a higher elevation  $z > 0$ , thus superimposing a disturbance  $(v_1', T', p')$  upon the "basic state"  $(v_1^o, T^o, p^o)$ . We now want to determine whether or not the system is "dynamically stable," i.e., whether this disturbance will die out or build up to the level of a discernible convective current. Equations 8 - 11 as well as the boundary conditions must be satisfied by the disturbed state as well as by the basic state. Thus, by writing these equations first in terms of  $(v_1^o + v_1', T^o + T', p^o + p')$  and then in terms of  $(v_1^o, T^o, p^o)$ , we can subtract the second set from the first to obtain

$$\frac{\partial v_1'}{\partial x_1} = 0 \quad (12)$$

$$\frac{1}{\phi} \frac{\partial v_1'}{\partial t} + \frac{\mu}{k\rho_o} v_1' = -\beta T' \varepsilon_1 - \frac{1}{\rho_o} \frac{\partial p'}{\partial x_1} \quad (13)$$

$$(\rho c_v)^{\text{eff}} \frac{\partial T'}{\partial t} = -\rho_o c_v v_1' \frac{\partial (T^o + T')}{\partial x_1} + \kappa^{\text{eff}} \frac{\partial^2 T'}{\partial x_1^2} \quad (14)$$

subject to the boundary conditions

$$v_1' n_1 = 0 \text{ at } x = \pm \frac{1}{2} a_1; y = \pm \frac{1}{2} a_2; z = 0, D \quad (15)$$

$$T' = 0 \text{ at } z = 0, D \quad (16)$$

$$\frac{\partial T'}{\partial x_i} n_i = 0 \text{ at } x = \pm \frac{1}{2} a_1; y = \pm \frac{1}{2} a_2 \quad (17)$$

where  $n_i$  is the unit outward normal to the boundaries of the box.

To reduce these equations to a dimensionless form it is helpful to use the following dimensionless groups:

$$\text{Thermal diffusivity: } \alpha = \kappa^{\text{eff}} / (\rho_o c_v) \quad (18)$$

$$\text{Rayleigh number: } Ra = k \rho_o g \beta (T_1 - T_o) D / (\mu \alpha) \quad (19)$$

$$\text{Prandtl number: } Pr = k \alpha \rho_o / (\mu D^2 \phi) \quad (20)$$

$$\text{Heat capacity ratio: } H = (\rho c_v)^{\text{eff}} / (\rho_o c_v) \quad (21)$$

$$\text{Aspect ratios: } D_1 = a_1 / D; D_2 = a_2 / D. \quad (22)$$

The Rayleigh number relates buoyancy to viscous retardation, whereas the Prandtl number relates thermal diffusivity to viscous retardation. If we also define a set of dimensionless variables

$$\left. \begin{aligned} v_i &= D v_i' / (\alpha Ra^{1/2}) & \theta &= T' / (T_1 - T_o) & p_D &= k p' / (\mu \alpha Ra^{1/2}) \\ \tau &= t \alpha / D^2 & X &= x / D & Y &= y / D & Z &= z / D \end{aligned} \right\} \quad (23)$$

we can rewrite (12) - (17) as

$$\frac{\partial v_i}{\partial X_i} = 0 \quad (24)$$

$$Pr \frac{\partial v_i}{\partial \tau} + v_i = \underbrace{Ra^{1/2} \theta \delta_{i3}}_{\text{zero for } i = 1, 2} - \frac{\partial p_D}{\partial X_i} \quad (25)$$

$$H \frac{\partial \theta}{\partial \tau} = - Ra^{1/2} v_i \frac{\partial \theta}{\partial X_i} + \underbrace{Ra^{1/2} v_i \delta_{i3}}_{\text{zero for } i = 1, 2} + \frac{\partial^2 \theta}{\partial X_i^2} \quad (26)$$

$$v_i n_i = 0 \text{ at } X = \pm \frac{1}{2} D_1; Y = \pm \frac{1}{2} D_2; Z = 0, 1 \quad (27)$$

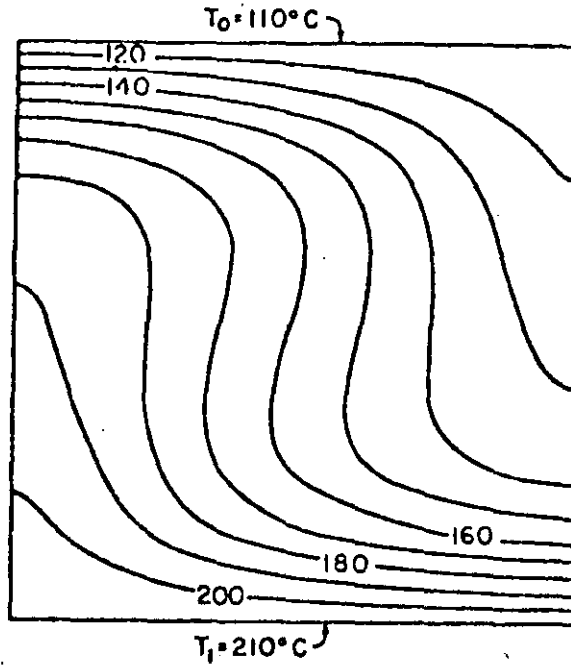


Fig. 4. Typical temperature distribution in plane perpendicular to axis of single convective roll with  $Ra = 100$  (after Sorey, 1975).

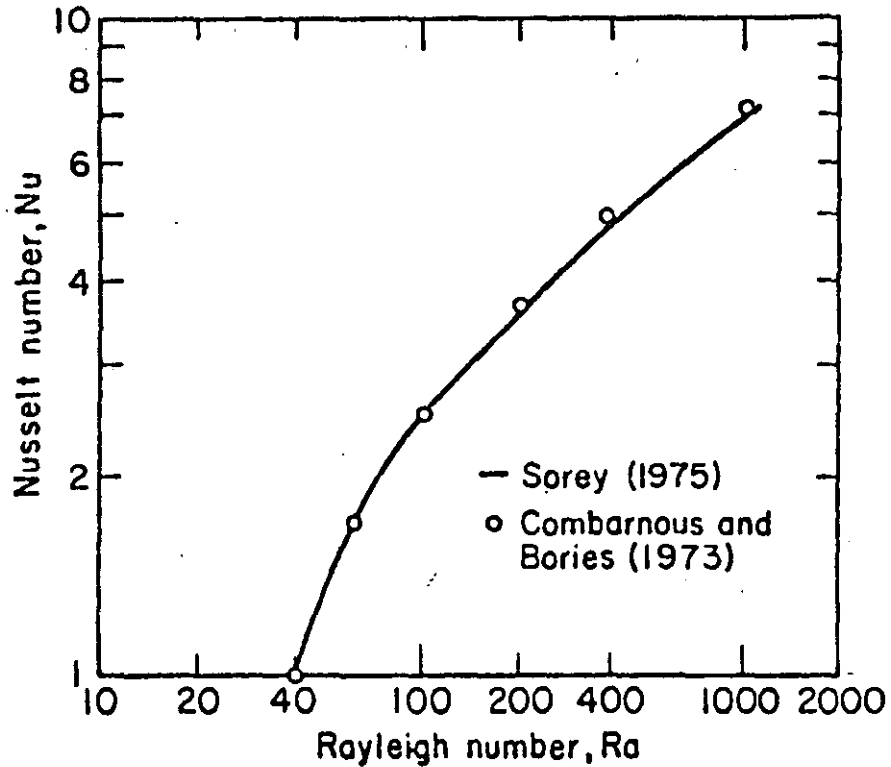


Fig. 5. Maximum Nusselt number versus Rayleigh number for cellular convection in a laterally infinite layer (after Sorey, 1975).



or when the height is less than both lateral dimensions. For a cube, the motion resembles a toroid with vertical axis through the center of the box. For further details regarding these conclusions, the reader is referred to Beck (1972).

It is important to recognize that all of these results have been obtained from an analysis of marginal stability and are therefore limited to Rayleigh numbers in the immediate neighborhood of  $Ra_c$ . In order to obtain results for higher Rayleigh numbers one must either perform experiments or solve the governing equations by an appropriate analytical or numerical technique. A large number of such studies concerned with both steady and nonsteady state situations have been reported in the literature and we shall try to summarize briefly some of the most important aspects of this work.

One effect of convective motion is to increase the rate of vertical heat transfer through the system. This is measured by the Nusselt number,  $Nu$ , which is defined as the ratio of total heat flow in the presence of convection to that by conduction only. For Rayleigh numbers less than the critical value,  $Nu = 1$ ; otherwise  $Nu \geq 1$ . Fig. 4 shows the steady state temperature distribution corresponding to a roll at  $Ra = 100$  for which  $Nu = 2.6$ .

According to the criterion of Platzman (1965), a system will tend to establish a mode of convection which maximizes the rate of heat transfer. At Rayleigh numbers near  $Ra_c$ , this means that cells with nearly square cross sections are preferred. However, at large Rayleigh numbers, Combarous and Bories (1973) and Horne and O'Sullivan (1974) show that the preferred cell width depends on  $Ra$ , with aspect ratios of 0.5, .33, and .25 corresponding to Rayleigh numbers of 280, 400 and 700, for layers with no restraining side walls. Similar effects of reduced cell width with increased  $Ra$  are observed for box models with restraining side walls. Combarous and Bories (1973), Holst and Aziz (1972b), and Sorey (1975) found that Nusselt numbers are nearly the same for two- and three-dimensional motions in stable

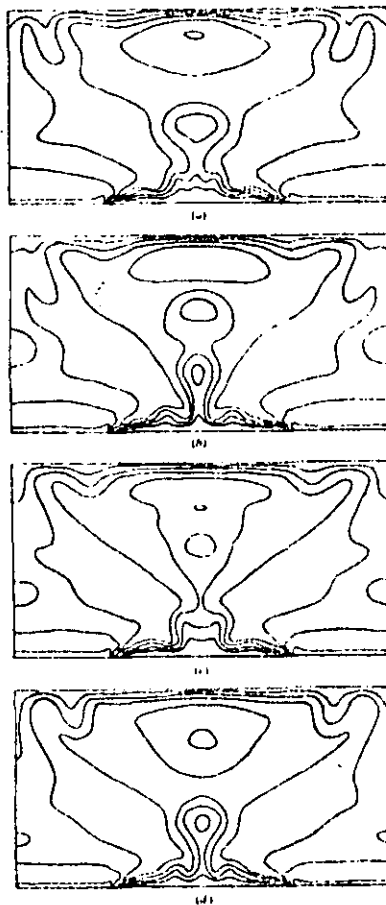
convection states. The relationship between  $Ra$  and the maximum Nusselt number for a laterally infinite layer is plotted in Fig. 5.

Sorey (1975) further indicates that the cellular pattern and Nusselt number at steady state may depend on the initial conditions in the box. Using uniform initial temperature and pressure distributions in a square (two-dimensional problem) with  $Ra = 100$  led to development of two cells with  $Nu = 2.2$ . With a non-uniform temperature distribution, the result was a single cell with  $Nu = 2.6$ . Horne and O'Sullivan (1974) report from numerical as well as laboratory experiments that for a uniform initial temperature distribution, heating the lower boundary slowly instead of instantaneously results in unicellular rather than multicellular motion. In other words, the mode of convection is not necessarily unique but may depend on the past history of the system. A hysteresis effect has also been noted by Elder (1967) and Karra (1968).

As  $Ra$  increases to 280, the system tends to develop a more favorable mode of convection and, as a result, the fluid may start fluctuating. These fluctuations will be irregular when the boundary conditions are uniform, but may develop into stable oscillations when the boundaries are heated in a nonuniform fashion. Horne and O'Sullivan (1974) report isotherms during a single oscillation when half of the bottom boundary has an elevated uniform temperature as shown in Fig. 6. A rough calculation for the Wairakei geothermal region indicates that, if the depth is 5 km, the oscillations would have a time constant on the order of 1000 years, and it would therefore be practically impossible to detect them.

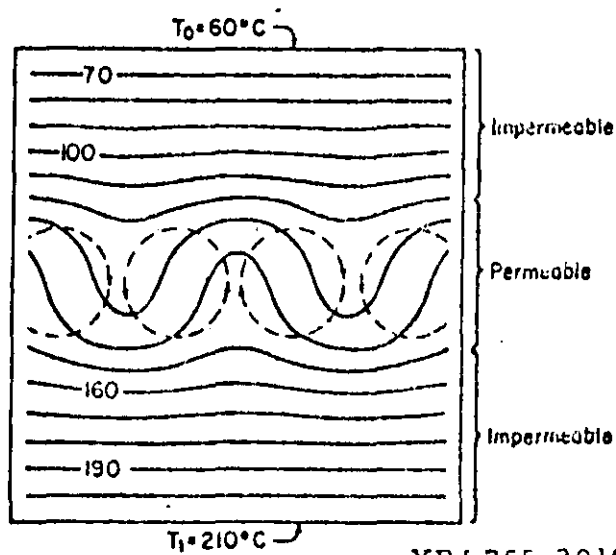
#### Free Convection Models

Numerous authors have attempted to extend the analysis of free convection to more realistic systems. There are, however, several complicating factors. The concept of a critical Rayleigh number may not apply in geothermal reservoirs where horizontal temperature variations undoubtedly exist along bounding surfaces. Free convection is then set up for any value of  $Ra > 0$ , although its effect on the



XBL 75.1 119

Fig. 6. Isotherm plots at equal intervals of time during a single stable oscillation with  $Ra = 750$  (after Horne and O'Sullivan, 1974).



XBL755-2919

Fig. 7. Distortion of isotherms due to convection in central permeable layer (after Sorey, 1975).

thermal and hydrologic regimes should be negligible unless  $Ra$  is large. Donaldson (1968b) estimates that in geothermal areas  $Ra$  is in the range of 500-5000.

Caltagirone et al. (1971) suggest the concept of a local Rayleigh number which varies spatially within the reservoir to account for the fluctuating convective motions observed.

Combarrous and Bories (1973) evaluated the effects of assuming thermal equilibrium between solid and fluid phases (Eqs. 4-7) for systems with Rayleigh numbers well above theoretical critical values. Comparisons of experimental and numerical results for the relationship between  $Ra$  and  $Nu$  numbers using various combinations of porous media and fluid types indicate that the assumption of thermal equilibrium between solid and fluid phases is adequate for  $Ra$  at least as high as 2000.

Holst and Aziz (1972a) and Sorey (1975) investigated effects of temperature and pressure-dependent parameters on heat transfer in convecting systems. For water, the dominant influence is the viscosity variation such that as the temperature difference across the permeable layer  $T_1 - T_0$  increases, the effective Rayleigh number increases over the value calculated from equation 19 using parameters computed at  $T = T_0$ . The Nusselt number would be correspondingly greater and the critical Rayleigh number, lower than for the constant parameter case. Alternatively, if parameters are evaluated at  $T = (T_1 + T_0)/2$ , values of  $Ra_c$  and the  $Ra$  versus  $Nu$  relationship still vary with  $T_1 - T_0$  due to the nonlinearity in the temperature dependence of  $c_v$ ,  $\rho$ , and  $\mu$  (Sorey, 1975). In contrast, realistic variations in fluid density with pressure were found to have negligible effects on the cellular convection problem.

Studies have also been made on the effect of various uniform boundary conditions at the surfaces of the homogeneous region on  $Ra_c$ . Lapwood (1948) investigated a laterally infinite layer in which the lower boundary is impermeable and the upper boundary is maintained at constant pressure and found that  $Ra_c = 27.1$ . Lapwood also found that when the upper boundary is a perfectly conducting free

surface, then  $Ra_c = 4\pi^2$ ; but when it becomes an imperfect conductor, then  $27.1 \leq Ra_c \leq 4\pi^2$ . A table of  $Ra_c$  values for a variety of uniform boundary conditions is given by Nield (1968) and in all cases,  $Ra_c \leq 4\pi^2$ .

Donaldson (1962) analyzed free convection in a two-layer system in which a permeable layer was underlain by an impermeable but thermally conductive layer of equal thickness. This removes the assumption of an isothermal surface at the bottom of the convecting layer. Sorey (1975) extended the analysis to a three-layer system with impermeable zones above and below the reservoir and found, in agreement with Donaldson's results, that vertical heat transfer rates in the multilayer systems were significantly less than in the single-layer system for the same values of  $Ra$ . The critical Rayleigh number was also less for the multilayer systems. Fig. 7 shows how temperatures within the impermeable layers are distorted by convection in the central layer.

Some work has also been done on the problem of an inclined system bounded by isothermal surfaces (Combarous and Bories, 1973; Kaneko et al., 1974). Combarous and Bories show that, since the temperature gradient and gravity are no longer colinear, the fluid is constantly moving regardless of the Rayleigh number. In a layer of infinite lateral extent, the tendency at low Rayleigh numbers is to develop unicellular convection parallel to the slope. If this is considered the stable state, instabilities develop at critical Rayleigh numbers which depend on the angle of inclination. When this angle is less than  $15^\circ$ ,  $Ra_c \approx 40$  and the mode of convection is similar to that observed in a horizontal layer. Above this lower limit,  $Ra_c$  increases rapidly with the angle of inclination and convective movements take the form of adjacent coils climbing upslope. Fluctuating conditions develop at higher and higher Rayleigh numbers ( $Ra \geq 240 - 280$  for horizontal layer) as the angle of inclination increases. The case of the inclined box is more complex (Holst and Aziz, 1972a; Kaneko et al., 1974).

Wooding (1963) and McNabb(1965) have studied the effect of localized heat sources on the formation of vertical jet flows. McNabb developed a boundary layer theory for convective flow over a finite circular "hot plate" at the bottom of a semi-infinite porous medium. He estimated the amount of heat convected from the hot plate as a function of its temperature and suggested that a similar approach could be used to evaluate the rate of cooling of a magma chamber beneath a water saturated porous formation.

Cheng and Lau (1974) have investigated steady state free convection in a vertical cross section of an unconfined aquifer in which the position of the water table is not known a priori. The aquifer is assumed to rest on an impermeable horizontal heat source of variable temperature and is bounded on its sides by vertical isothermal surfaces of constant hydraulic head, representing contact with the ocean on a volcanic island. Dispersion and gravity effects due to variations in salt content between fresh water and sea water (mixing occurs by virtue of the vertical boundary conditions) are implicitly neglected. By solving a linearized version of the governing equations, the authors show that pressure in the aquifer remains nearly hydrostatic. Temperature is greatly affected by the size of the heat source but its location is less important. There is a noticeable upwelling of the water table directly above the heat source, which depends primarily on vertical temperature gradients and nature of the heat source.

Much additional literature on various theoretical and experimental aspects of free convection in homogeneous media is available. Holst (1970) has published an extensive review of the literature and the state of the art has been summarized more recently by Combarous and Bories (1973). For subsequent developments, the reader should consult the works of Fernandez (1972), Holst and Aziz (1972 a,b), Masuoka (1972), Palm et al. (1972), Sun et al. (1972), Gupta and Joseph (1973), Cheng and Lau (1974), Combarous and Bories (1974), Horne and O'Sullivan (1974), Kaneko et al. (1974), Straus (1974), Yen (1974), Weber (1975 a,b), and Sorey (1975).

### Pipe Models

An alternative concept for convection in geothermal areas is the pipe system in which the fluid no longer flows through a homogeneous layer but is channeled through zones of relatively high permeability. Such zones may be caused by fissures or fractures which are known to control local phenomena such as springs, fumaroles, and geysers. As discussed by Einarsson (1942), Bodvarsson (1961), and Donaldson (1970), the occurrence and distribution of thermal areas in Iceland and New Zealand could be controlled by variations in permeability as well as by spatial distribution of the heat source.

Einarsson (1942) and Bodvarsson (1961) discuss the thermal areas of Iceland in terms of pipe systems involving deep circulation of water (2 to 3 km) and discharge in hot springs. Elder (1966) analyzed hydrothermal systems in Iceland and New Zealand using lumped parameter and multi-dimensional models to quantify the general features of heat and mass transfer. White (1957, 1961) used pipe systems to explain the chemical composition of waters associated with volcanic and hydrothermal systems.

Donaldson (1968b, 1970) suggests the model in Fig. 8 for a hot-water geothermal system. The model consists of cold reservoirs recharged from the surface, a vertical column through which hot water flows, and a permeable horizontal channel connecting the two. The surrounding medium is assumed impermeable, and heat supplied at the lower boundary maintains the density imbalance and resulting convective motion. Though the model is oversimplified, Donaldson's analysis allows for throughflow from recharge to discharge areas and secondary (circulatory) convection in the upflow column. Gross characteristics of hydrothermal systems are simulated by adjusting temperatures at the base of the model, dimensions and permeability of the vertical column, and resistance to flow in the remainder of the pipe system.

Mathematical description of the model involves the single phase, steady state equivalents of (1) and (7) which are solved by numerical relaxation for the boundary conditions shown in Fig. 8. Uniform thermal properties are assumed throughout

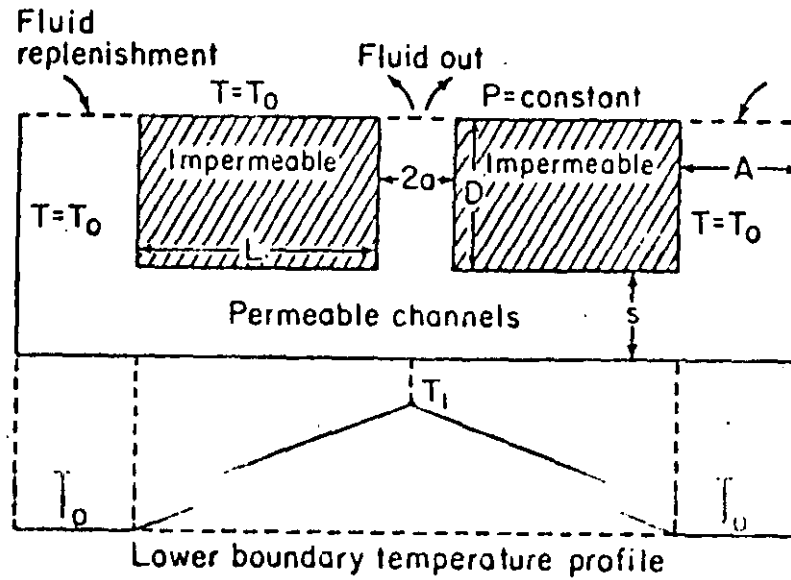


Fig. 8. Pipe model for hot-water geothermal system (after Donaldson, 1968b).

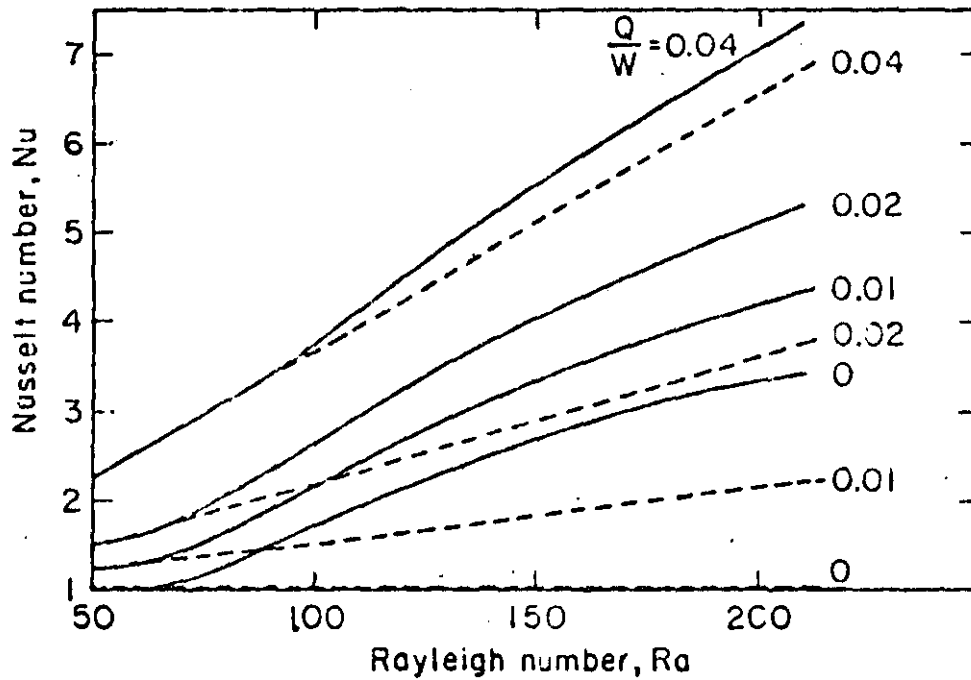


Fig. 9. Nusselt number versus Rayleigh number for combined through and circulatory flows in vertical column with  $2a/D = 0.5$ . Solid lines show combined effect, dashed lines show throughflow effect only (after Donaldson, 1970).



and constant values for  $k$  and  $\mu$  are used in each of the permeable channels. In the absence of secondary convection in the upflow column, the mean mass flow rate is given by

$$Q = \frac{\rho_o k \beta g (T_m - T_o)}{(\mu/\rho) b} \quad (34)$$

where  $T_m$  = mean temperature in the column and  $b = 1 + aL/sD + A/D$ . It is not clear from Donaldson's analysis whether  $\mu/\rho$  is determined at  $T_o$  or  $T_m$ . Fig. 9 illustrates the relationship between  $Ra$  and  $Nu$  with throughflow and secondary convection for a column aspect ratio  $2a/D = 0.5$ . Here  $W = \rho_o k \beta g (T_1 - T_o)/(\mu/\rho)$  is a measure of the maximum possible throughflow from buoyancy unbalance alone. Hence,  $Q/W = [(T_m - T_o)/(T_1 - T_o)] (1/b)$ . It is seen from Fig. 9 that the heat transferred by circulatory flow decreases markedly as the throughflow increases. Fig. 10 illustrates how throughflow in a column with  $2a/D = 0.2$  and  $Q/W = 0.05$  tends to sweep the circulatory motion up the channel.

Sorey (1975) modeled heat and liquid mass transfer in hot spring systems using the two-dimensional models shown in Fig. 11. Transient and steady state conditions were simulated numerically to determine conductive heat losses from the vertical conduit and its effect on temperature  $T_{sp}$  of water discharging at the spring. The lower boundary was formed by the top of a reservoir with water at temperature  $T_b$ , and the upper boundary was the land surface at temperature  $T_g$ . The relationships between dimensionless temperature drop,  $1 - \theta_{sp}$ , and the dimensionless mass flow rates for the circular conduit,  $m_c$ , and the fault plane conduit,  $m_p$ , are plotted in Fig. 12.

Expressions for the total conductive heat loss are  $[2\pi \kappa^{eff} D (T_b - T_g) m_c (1 - \theta_{sp})]$  for the cylinder and  $[2 \kappa^{eff} D (T_b - T_g) m_p (1 - \theta_{sp}) L/a]$  for the plane. The plane model applies where fluid rises in a fault zone whose lateral extent is considerably greater than the discharge area of the hot springs. Comparing the two models for the same total massflow, the fault plane model has greater

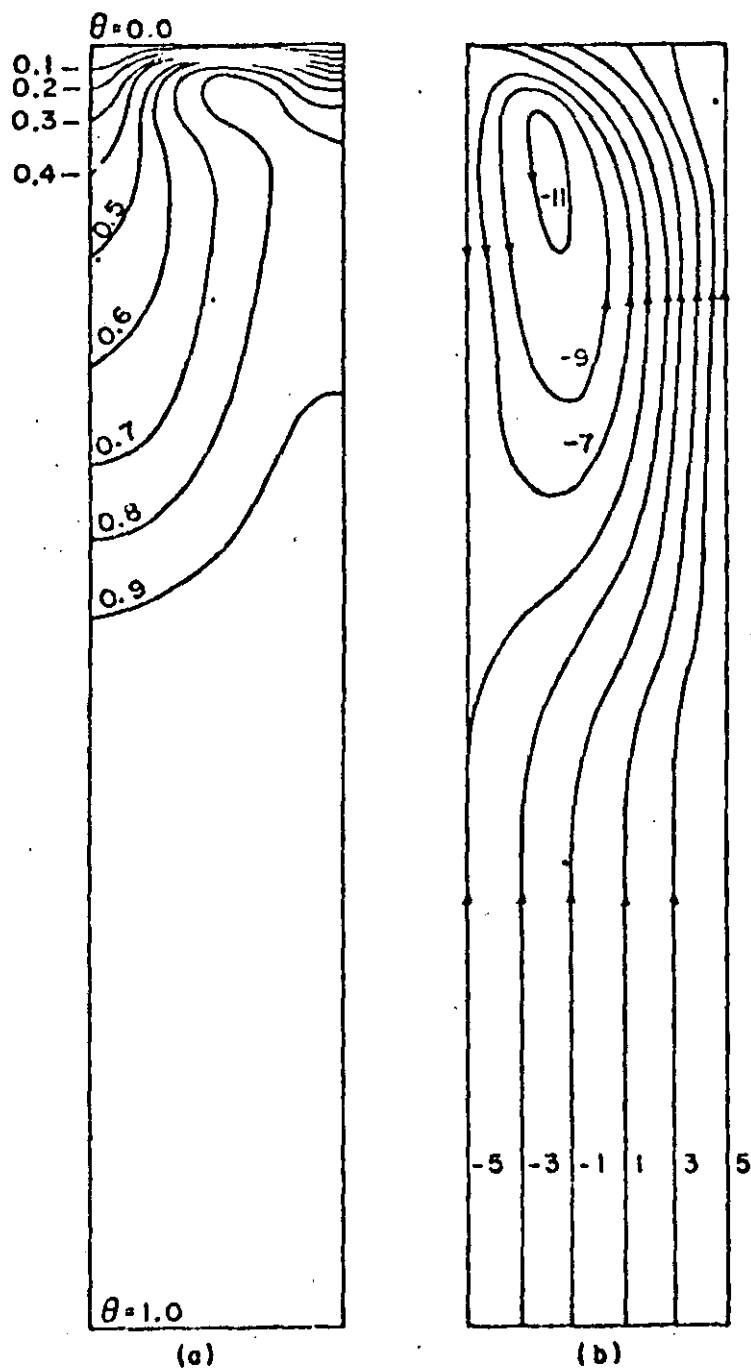


Fig. 10. Effect of throughflow on circulatory convection with  $Ra = 420$ ,  $2a/D = 0.2$ ,  $Q/W = 0.05$ ; (a) isotherms normalized such that  $0 \leq \theta \leq 1.0$ , (b) streamlines in arbitrary units (after Donaldson, 1970).

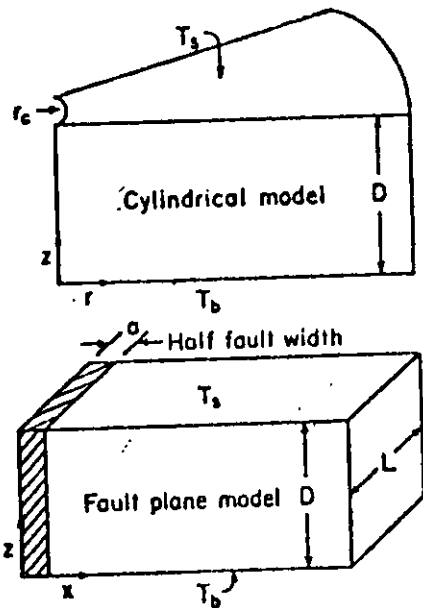


Fig. 11. Two-dimensional models for hot spring systems (after Sorey, 1975).

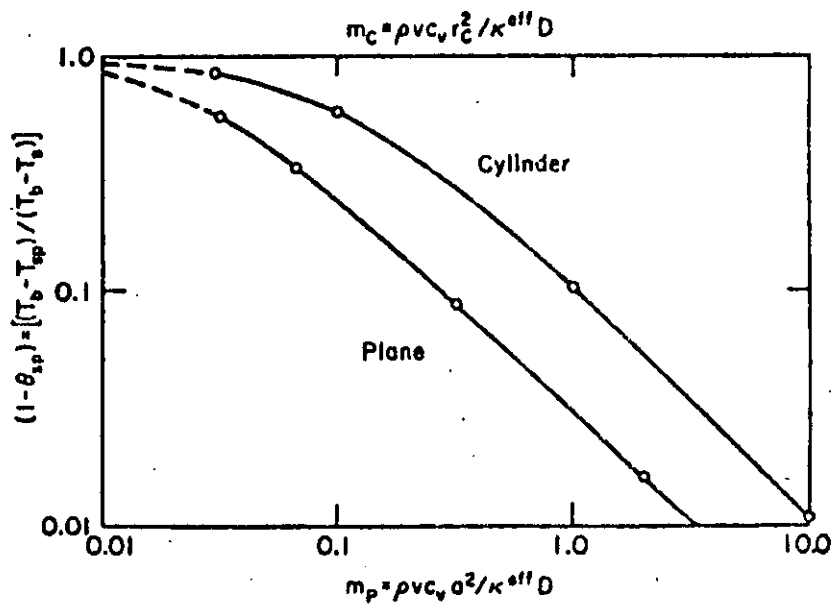


Fig. 12. Dimensionless temperature drop,  $1-\theta_{sp}$ , versus dimensionless mass flow rates for circular conduit,  $m_c$ , and fault plane conduit,  $m_p$ , in hot spring systems (after Sorey, 1975).

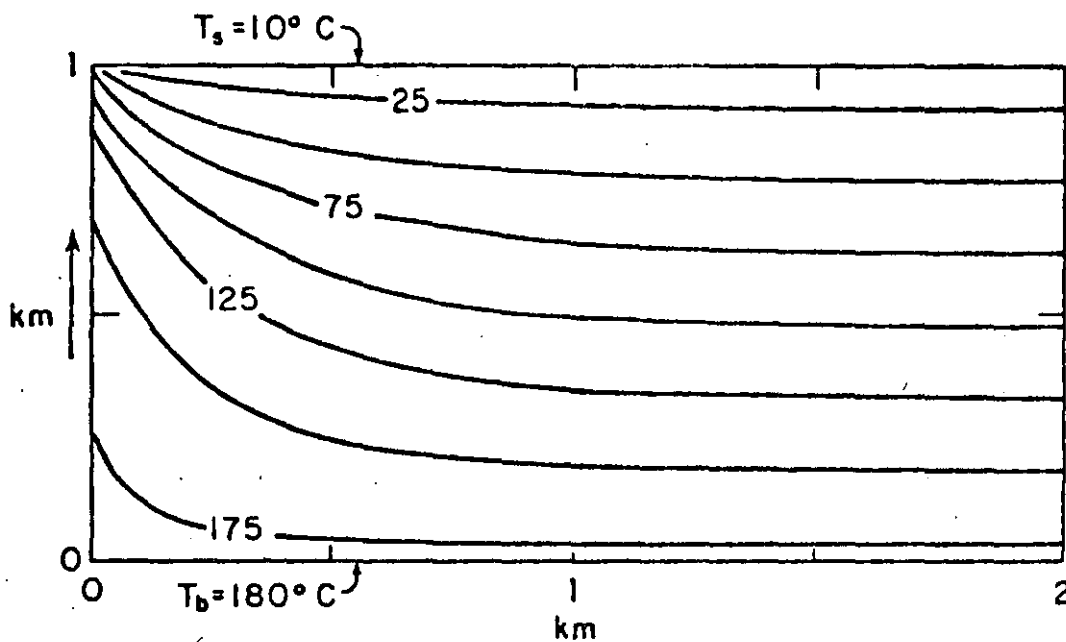
heat loss and more temperature drop than the cylindrical conduit model.

The steady-state temperature distribution in a fault plane model with a spring discharge of 100 lpm is shown in Fig. 13. Distortion of the temperatures due to convective motion in the conduit is confined to a zone of about 1 km on either side of the fault. At the land surface, the conductive heat flux near the spring is approximately 50 heat flow units ( $50 \mu\text{cal/sec cm}^2$ ) and decreases to about 3.4 heat flow units as distance exceeds 1 km. These results were obtained using  $\kappa^{\text{eff}} = 2 \times 10^{-3} \text{ cal/cm sec } ^\circ\text{C}$  and  $c_v = 1 \text{ cal/gm } ^\circ\text{C}$ .

Analysis of the transient behavior of these systems (Sorey, 1975) shows that periods of 30,000 years or more are required for the conductive thermal regime to reach equilibrium following the geologic development of the spring system. Somewhat shorter time periods are required if convective motions in the rock surrounding the spring conduit are considered. Simulations under these conditions are described by Sorey (1975).

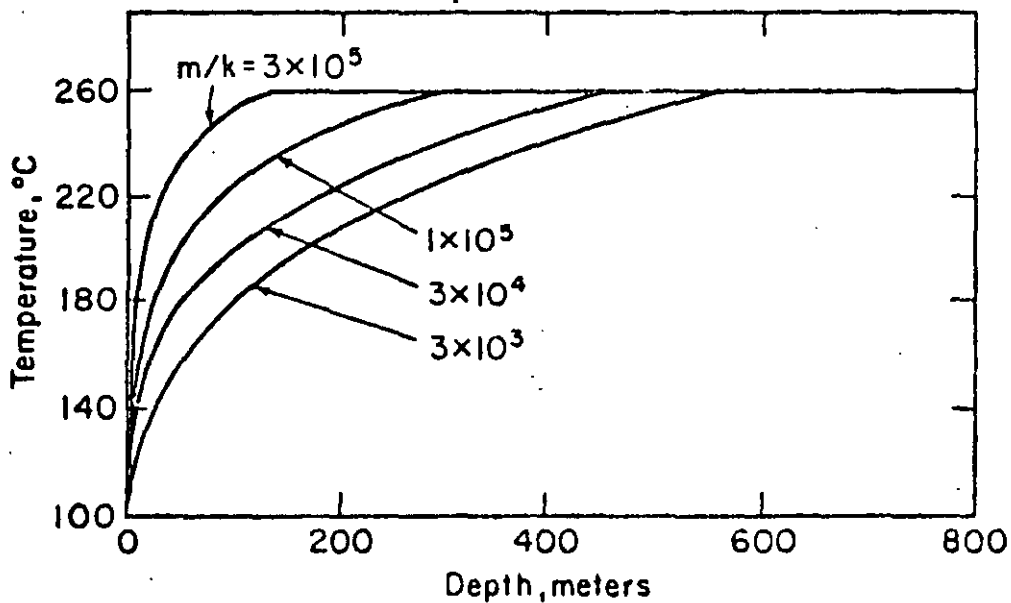
Analysis of pipe models has been extended by Elder (1966) and Donaldson (1968a, 1970) to include boiling in the upflow channel. Elder has developed relationships between mass flow rate, fluid enthalpy, resistance to flow, and the energy supplied by a heat source for channeled circulation caused by buoyancy differences between recharge and discharge areas. He concludes that for systems with large energy input or large resistance, the discharge (mass flow) is not sufficient to transport the energy unless the fluid moves in the form of steam. With low energy inputs or small resistance, the circulating fluid should remain a liquid except for a shallow zone which may contain steam. This approach has been applied to the Tuscany thermal areas near Lardarello, Italy, and the Taupo systems in New Zealand.

Donaldson's (1968a) work involves steady flow of a boiling liquid in a vertical channel. The remainder of the circulation system including the heat source is considered only as controlling temperature, pressure, and mass flux at the bottom of the discharge channel. Lateral heat conduction is neglected so that the



XBL755-2924

Fig. 13. Distortion of steady-state isotherms in vertical fault plane model with discharge = 100 lpm,  $a = 10 \text{ m}$ ,  $L = 1 \text{ km}$ , and  $Ra = 0$  (after Sorey, 1975).



XBL755-2925

Fig. 14. Temperature versus depth in a boiling system as a function of  $m/k$  (after Donaldson, 1968a).

equations are one-dimensional. For the case of uniform permeability and small mass flow rate, only liquid flow is considered. Comparison of the resultant pressure-depth relations with saturation pressure curves indicates that boiling will not occur for systems with  $c_v m/\kappa^{\text{eff}} \leq 7 \times 10^{-5} \text{ cm}^{-1}$ , where  $m$  is mass flux per unit area. When this critical value is exceeded, boiling must occur in the upper section of the channel.

Two-phase flow in this upper region is described by the one-dimensional, steady state forms of equations 1 - 3 and 6 without the pressure terms. At the interface between the two-phase and liquid-saturated regions, the boundary conditions are constant mass flux and constant temperature equal to that at the channel base. Thus, the lower region is treated as isothermal, and in the upper region, temperature and pressure are related by the vapor pressure curve for water. The equations are solved analytically to yield temperature and pressure, water fraction, and water and steam flow rates as functions of depth. The controlling parameter in these relationships is  $m/k$  as seen in Fig. 14. Thus, the onset of boiling is indicated by the value of  $c_v m/\kappa^{\text{eff}}$ , whereas when two-phase conditions exist, the controlling parameter is  $m/k$ . Effects of vertical heat conduction are significant only if  $\kappa^{\text{eff}}/k$  is greater than  $3 \times 10^8 \text{ cal/cm}^3 \text{ sec } ^\circ\text{C}$ . Donaldson concludes that once boiling commences, it must extend some 200 - 500 meters downward and hence this two-phase region must be considered in studying geothermal systems. Two-phase conditions in columns with variations in vertical permeability have also been discussed by Donaldson (1968a, 1970).

### GEOTHERMAL SYSTEMS DURING EXPLOITATION

#### Lumped-Parameter Models

The concept of a lumped-parameter model provides one of the simplest means for describing behavior of a geothermal system during exploitation. The basic idea is to view the entire system as a perfect mixing cell for both mass and energy so that spatial variations in concentration can be neglected. Instead of

considering the internal distribution of mass and energy, attention is restricted to the total amounts generated within the system as well as that crossing the boundaries. Since time is the only independent variable, the system can be characterized mathematically by a set of ordinary differential equations or an equivalent set of algebraic expressions representing total mass and energy balance.

The first and best known lumped-parameter model of a producing geothermal reservoir was developed by Whiting and Ramey (1969). Their system has a bulk volume  $V$  and contains vapor, water, and rock. Figure 15 is a schematic diagram of the system from which a simple mass balance yields

$$M_c - M_o = M_e - M_p - M_l \quad (35)$$

where  $M_c$  = current mass of water (vapor + liquid) in place,  $M_o$  = initial mass of water in place,  $M_e$  = influx of liquid (no vapor is assumed to enter the system),  $M_p$  = mass of water (vapor + liquid) produced, and  $M_l$  = mass of water (vapor + liquid) lost by leakage. Water may flow in from an adjacent aquifer or leak out of the system via steam vents, springs, wild wells, etc. The water influx,  $M_e$ , is represented by a linear combination of terms each of which is the product of a theoretical time-dependent response function characterizing a certain aquifer flow geometry (hemispherical, linear, or radial) and pressure. These calculations further assume that the liquid inflow is isothermal with constant enthalpy,  $h_e$ .

In the energy balance calculation the system is assumed to be in complete thermodynamic equilibrium. According to the first law of thermodynamics one then has

$$\begin{aligned}
 & M_c e_c - M_o e_o + V (1-\phi)(\rho c_v)^{eff} (T_c - T_o) \\
 & \text{Internal energy change in fluid} \quad \text{Internal energy change in solid rock} \\
 & = -Q \quad + M_e h_e - M_p h_p - M_l h_l \quad (36) \\
 & \text{Net conductive heat influx} \quad \text{Net convective enthalpy influx}
 \end{aligned}$$

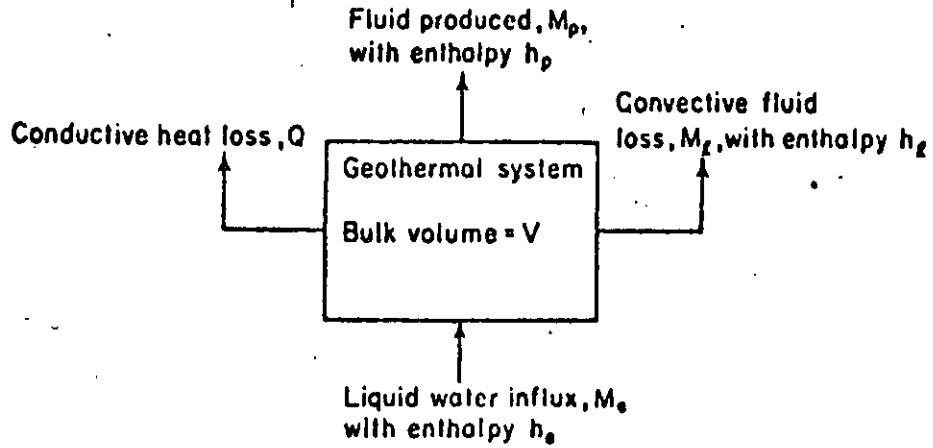


Fig. 15. Schematic diagram of lumped-parameter model for geothermal systems (after Whiting and Ramey, 1969).

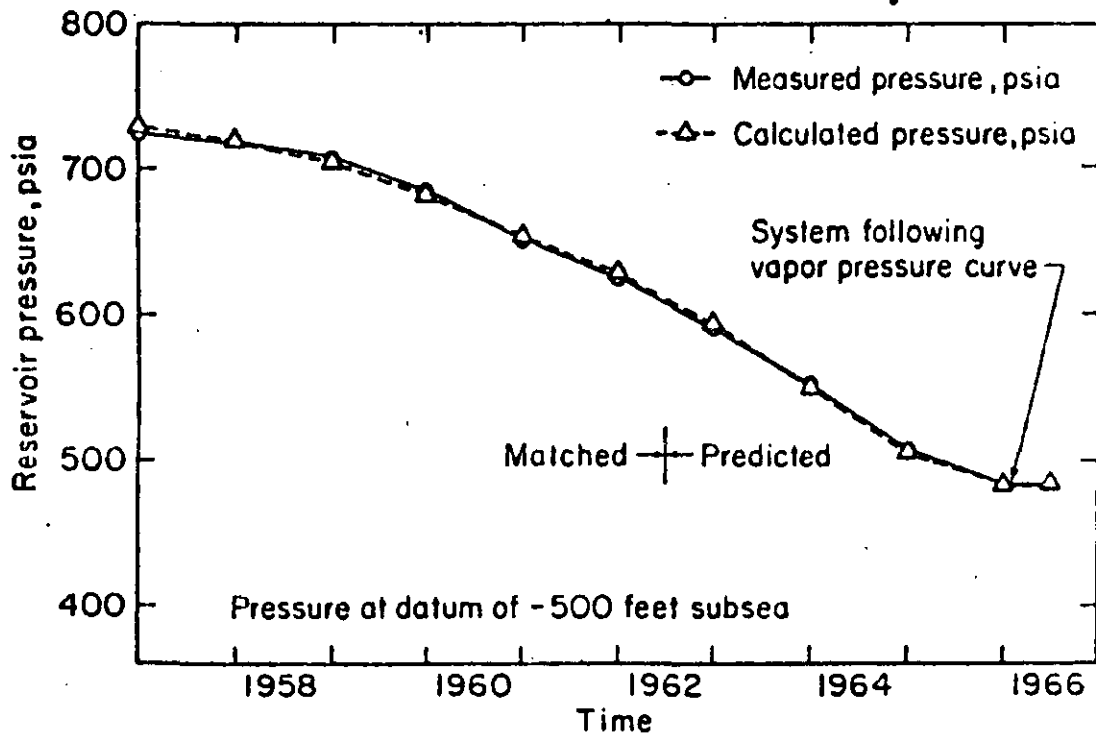


Fig. 16. Comparison of calculated with measured pressures for Wairakei geothermal system (after Whiting and Ramey, 1969).



The volume  $V$  can be expressed as

$$V\phi = M_o [S_o^G v_o^G + (1-S_o^G) v_o^L] = M_c [S_c^G v_c^G + (1-S_c^G) v_c^L] \quad (37)$$

where  $S^G$  is vapor (gas) saturation and  $v^G$  and  $v^L$  are specific volumes of vapor and liquid, respectively. The phase diagram for water (see Fig. 1) indicates that in the particular case where the system contains only compressed liquid, the thermodynamic path of decreasing pressure due to production will be essentially isothermal and isoenthalpic. Equations 35-37 then lead to a mass-volumetric balance similar to that employed for petroleum production above the bubble-point,

$$M_o (v^L - v_o^L) + M_e v^L - (M_p + M_l) v^L = 0 \quad (38)$$

Additional working hypotheses made by Whiting and Ramey are that  $Q$  is negligibly small relative to other terms in (36) and that  $h_p = h_l$  (i.e., the enthalpy of produced and lost fluid is the same).

The compressed liquid version of this lumped-parameter model was applied by Whiting and Ramey to the Wairakei geothermal system in New Zealand. The initial temperature and enthalpy were estimated from field data, and a least-square fit to the production history from 1956 to 1961 was used to determine the initial water in place and the initial pressure. The model was then used to predict performance through 1965 and agreement with measured data was excellent (see Fig. 16). Prediction of future performance from 1966 to the year 2000 took into account two-phase conditions and indicated that pressure and temperature would decrease very little during this period. Recent field data from Wairakei have shown this prediction to be incorrect. The model was also used by Cady (1969) to simulate a laboratory setup but had to be applied separately to the two-phase and dry steam regions that developed.

Brigham and Morrow (1974) have adapted the lumped-parameter approach to vapor-dominated systems (i.e., systems with a significant dry steam region) by considering three different distributions of vapor and liquid. In each case

the system is assumed to be completely closed (i.e., the boundaries are impermeable and adiabatic) and energy is derived only from the rock mass itself.

Their first model concerns a single-phase system completely saturated with vapor. They assume that since the heat capacity of solid rock is much greater than that of steam, the system is essentially isothermal. Thus, there is no need for an energy equation and one can use a mass balance approach similar to that commonly employed in natural gas reservoirs. This approach leads to a linear relationship between  $p/Z$  and cumulative production  $\Delta M^G$  according to the equation of state for a real gas,

$$\frac{p_1}{Z_1} = \frac{p_o}{Z_o} \frac{M_1^G}{M_o^G} = \frac{p_o}{Z_o} \left( \frac{M_o^G - \Delta M^G}{M_o^G} \right) \quad (39)$$

where  $Z$  is compressibility factor,  $M^G$  is mass of steam in place, and the subscripts indicate different values of time. The intercept of this line on the abscissa is equal to the original fluid in place,  $M_o^G$ .

In the second model the vapor phase is separated from an underlying layer of liquid by a horizontal interface at which boiling takes place. Since the vapor phase is again assumed to be isothermal, its treatment is similar to that in the previous model. The liquid phase changes its volume continuously and the corresponding lumped system is therefore defined as the pore space filled with liquid at the beginning of each pressure decrement. For this system the mass balance is simply

$$\Delta M^G = - \Delta M^L \quad (40)$$

whereas the energy balance for the fluid is expressed as

$$\begin{aligned} M_1^L e_1^L + M_1^G \bar{e}^G - M_o^L e_o^L &= M_1^S c_p^S (T_o - T_1) \\ \text{Internal energy change} & \quad \text{Heat transferred from rock to liquid} \\ + \left( M_o^S - M_1^S \right) c_p^R \left( T_o - \frac{T_o + T_1}{2} \right) &- \left( M_o^L - M_1^L - M_1^G \right) \bar{h}^G \\ \text{Heat transferred from rock to steam} & \quad \text{Enthalpy of vapor leaving system} \end{aligned} \quad (41)$$

where  $M^S$  is mass of rock in contact with liquid,  $\bar{h}^G$  is average enthalpy of vapor leaving system and  $\bar{e}^G$  is average internal energy of vapor (both calculated at the average temperature  $(T_o + T_1)/2$ ) and the subscripts o and l indicate the beginning and end of a depletion step, respectively. Brigham and Morrow further simplified this equation by reformulating it in terms of enthalpy and neglecting the resulting pressure terms and obtained

$$M_1^L h_1^L - M_o^L h_o^L = M_1^S c_p^S (T_o - T_1) + (M_o^S - M_1^S) c_p^S \left( \frac{T_o - T_1}{2} \right) - (M_o^L - M_1^L) \bar{h}^G \quad (42)$$

Given a rate of production, the resulting system of nonlinear equations can be solved in an iterative manner.

The third model considers a vapor phase overlying a layer of liquid except that now boiling occurs throughout the entire thickness of this layer and its depth remains fixed in time. The resulting energy equation is essentially similar to that of Whiting and Ramey (1969) with the exception that only steam is allowed to leave the system.

Application of these models to various hypothetical reservoirs has shown that in estimating available reserves by extrapolation of early p/Z behavior, the results will tend to be optimistic when porosity is low, but pessimistic when porosity is high. The constant liquid level model was found to predict higher recovery for a given pressure depletion than the falling liquid level model. The presence of even a small amount of liquid in the lower part of a geothermal system was shown to be extremely important because it can account for a large fraction of the total fluid mass and can significantly affect the results of a p/Z analysis. Finally, Brigham and Morrow conclude that "the steam portion of a reservoir will always remain isothermal whether or not there is boiling water below the steam. Thus pressure, temperature, and enthalpy measurements will not be completely diagnostic for determining the original state of the reservoir

fluid system. Because the steam remains essentially isothermal, it gradually increases in enthalpy and becomes superheated as the pressure declines."

An interesting lumped-parameter model based on the assumption that the liquid and gas phases are uniformly distributed throughout the system has been proposed recently by Martin (1975). The system is assumed to be completely closed and each phase is produced at a rate which is related to its relative permeability. His approach is based on a simplified form of equations 1-3 and 6. If we neglect the gravity term in Darcy's law and substitute (2) and (3) into (1), we can write for an isotropic medium

$$\frac{\partial}{\partial x_1} \left( \lambda^f \frac{\partial p}{\partial x_1} \right) = \frac{\partial M^f}{\partial t} \quad (43)$$

where

$$\lambda^f = k \left( \frac{\rho^L k_r^L}{\mu^L} + \frac{\rho^G k_r^G}{\mu^G} \right)$$

$$M^f = \phi (\rho^L S^L + \rho^G S^G)$$

Neglecting heat dispersion and the pressure terms in (6) we obtain by the same procedure

$$\frac{\partial}{\partial x_1} \left( \lambda^h \frac{\partial p}{\partial x_1} \right) = \frac{\partial M^h}{\partial t} \quad (44)$$

where

$$\lambda^h = \frac{\rho^L h^L k_r^L}{\mu^L} + \frac{\rho^G h^G k_r^G}{\mu^G} + \kappa^{eff} \frac{dT}{dp}$$

$$M^h = \phi S^L \rho^L h^L + \phi S^G \rho^G h^G + (1-\phi) \rho^S c_v^S T$$

since T and p are uniquely related by the boiling curve. The notion of a lumped-parameter model implies that gradients of pressure, temperature, and saturation are small. Expanding (43) and (44) and neglecting the products of these gradients leads to

$$\frac{1}{\lambda^f} \frac{\partial M^f}{\partial t} = \frac{\partial^2 p}{\partial x_1^2} = \frac{1}{\lambda^h} \frac{\partial M^h}{\partial t} \quad (45)$$

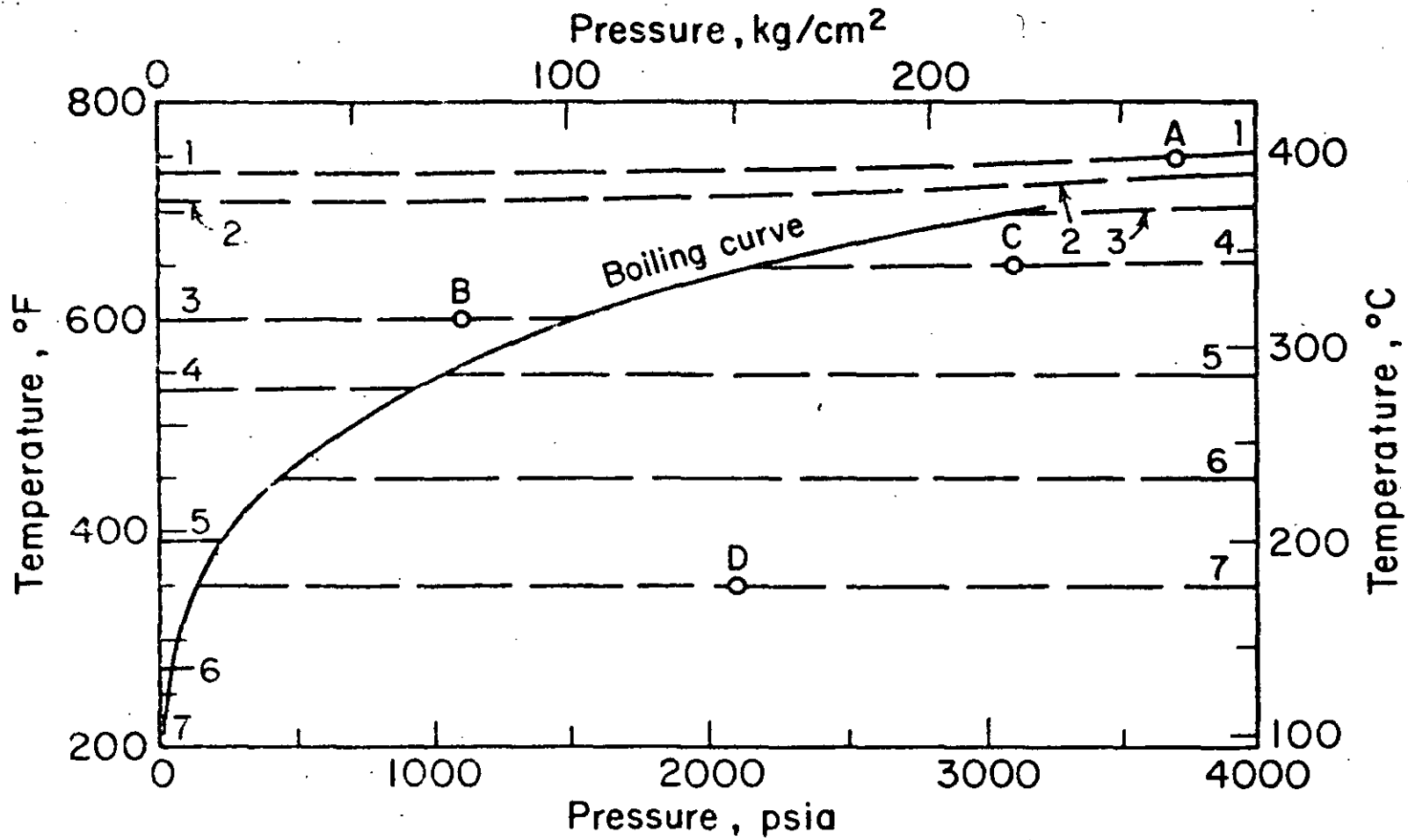
Expanding the time derivatives with respect to  $p$  and  $S$  yields the nonlinear ordinary differential equation

$$\frac{dS^L}{dp} = \frac{\lambda^h \frac{\partial M^f}{\partial p} - \lambda^f \frac{\partial M^h}{\partial p}}{\lambda^f \frac{\partial M^h}{\partial S^L} - \lambda^h \frac{\partial M^f}{\partial S^L}} \quad (46)$$

In the case of single-phase flow,  $T$  and  $p$  are not related uniquely to each other, and the above procedure must therefore be modified. If we neglect heat conduction as well as dispersion, we obtain the single-phase equivalent of (45) with  $\lambda^h = h\lambda^f$ . Expanding the time derivatives with respect to  $p$  and  $T$  leads to the following nonlinear ordinary differential equation,

$$\frac{dT}{dp} = \frac{\frac{\partial M^h}{\partial p} - h \frac{\partial M^f}{\partial p}}{h \frac{\partial M^f}{\partial T} - \frac{\partial M^h}{\partial T}} \quad (47)$$

Equations 46 and 47 were used by Martin to calculate numerically the relationships between  $T$ ,  $p$  and  $S$  in a hypothetical system free of gravity effects. Integration of (47) showed that in the case of a single phase,  $dT/dp$  is very small and the exploitation process is essentially isothermal. This is clearly illustrated in Fig. 17 which shows the thermodynamic paths for various initial  $p$ - $T$  conditions in a system with  $\phi = 0.25$ ,  $\rho^S = 162 \text{ lb/ft}^3$  ( $2.6 \text{ gm/cm}^3$ ),  $c_v^S = 0.2 \text{ Btu/lb } ^\circ\text{F}$  ( $0.2 \text{ cal/gm } ^\circ\text{C}$ ),  $\kappa^{\text{eff}} = 40 \text{ Btu/ft day } ^\circ\text{F}$  ( $0.0069 \text{ cal/cm sec } ^\circ\text{C}$ ),  $k = 1 \text{ darcy}$  ( $9.87 \times 10^{-9} \text{ cm}^2$ ), and typical  $k_r$  values. For example, from initial conditions corresponding to point A, the temperature will drop slightly along line 1 as pressure declines. This corresponds to a single phase (essentially steam) reservoir with temperature and pressure above the critical point. However, if the system is initially saturated with liquid water at point C, production causes an isothermal decrease in pressure until the boiling curve is reached. At this stage  $p$  and  $T$  begin to follow the boiling curve with a gradual increase in steam saturation. Production of



XBL755-2928

Fig. 17. Pressure-temperature diagram for pure water and vapor showing various thermodynamic paths for depleting a geothermal system (after Martin, 1975).

steam, however, starts only when  $S^G$  reaches its so-called equilibrium value at which the vapor phase becomes mobile (below this value  $k_r^G = 0$ ). The ratio between produced steam and liquid water continues to increase until  $S^L$  is reduced to a stage where the liquid becomes immobile and production is restricted to saturated steam. When all the water has been boiled away and  $S^L = 0$ , the temperature departs from the boiling curve and superheated steam is produced under essentially isothermal conditions.

From his study Martin further concluded that "under certain conditions only a relatively small amount of the heat initially contained in a geothermal reservoir will be produced during pressure depletion. Much of this heat may be contained in the produced steam even though initially the reservoir contains only hot water." This is due to the higher heat content and lower viscosity of steam as compared with liquid water. A similar reasoning also led Martin to conclude that "for many conditions where gravity segregation of the steam and hot water occurs during depletion, more of the total heat can be produced by completing wells high in the reservoir to enhance steam production and suppress water production." When gravity effects are important, system C should follow the path shown in Fig. 17 until the steam phase becomes mobile and gravity segregation begins. Since  $S^G$  increases rapidly in the upper portion of the system, departure from the boiling curve will occur at considerably higher  $p$  and  $T$  values than is shown in the figure. In the lower portion of the system  $S^L$  decreases slowly and therefore departure from the boiling curve will occur at lower  $p$  and  $T$  values than in Fig. 17.

#### Distributed-Parameter Models

A model in which the properties of the rock and/or the fluid (e.g., saturation, viscosity, pressure, etc.) are allowed to vary in space will be called a distributed-parameter model. By taking into account spatial variations of these properties the resulting problem may become too complex to be treated analytically.

An alternative approach is to replace the governing partial differential equations by an equivalent set of algebraic equations and then solve the problem numerically with the aid of a computer. The purpose of the following discussion is to acquaint the reader with some of the results obtained to date by numerical simulation of relatively complex geothermal systems.

A considerable degree of sophistication in the numerical simulation of immiscible, multiphase and multicomponent fluid flow problems under nonisothermal conditions has been achieved in recent years by petroleum engineers. A brief review of this work has been included in a recent paper by Coats et al. (1974). Most of this effort, however, was not concerned with geothermal systems but was directed toward the problem of oil recovery by steamflooding, hot waterflooding, steam stimulation, and other thermal processes which are of immediate concern to the petroleum industry. For example, Spillette and Nielsen (1968) have studied the response of an oil reservoir to hot water injection by assuming that the hydrocarbons and the water will appear only as a liquid phase. Their model consists of a vertical cross-section including a horizontal layer of sand enclosed between two impermeable shale strata. Energy is transported by conduction and convection in the sand layer and by conduction in the shale layers. Fluid densities and viscosities are taken to be temperature dependent and capillary pressure between the two fluid components is taken into account. The equations governing mass transport are solved by an alternating direction implicit (ADI) iterative finite difference procedure whereas the energy equation is solved by the method of characteristics. One of the conclusions of this study was that fluid segregation due to gravity has a significant effect on the system considered.

Another two-dimensional vertical model consisting of a sand layer sandwiched between two impermeable strata has been developed more recently by Weinstein et al. (1974). In this model fluid flow is allowed to take place only in one horizontal direction whereas energy may be transferred by conduction both



horizontally and vertically through the entire system. However, the hydrocarbons and water can coexist both in the liquid and vapor states, so that one must now deal with three distinct phases: oil, water, and gas. The gas phase is a mixture of steam and hydrocarbon vapor. Interphase mass transfer within each component is allowed to account for processes such as water vaporization, steam condensation, hydrocarbon distillation, solvent extraction, and solution-gas drive. The energy equation is expressed in terms of enthalpy, rock compressibility is taken into account, but capillary pressure effects are neglected. A finite difference approach is employed with an implicit pressure-explicit saturation formulation of the mass balance equation, which is solved simultaneously with the energy equation. The authors also discuss various improved numerical techniques for invoking phase constraints and calculating mass transfer terms.

A three-dimensional finite difference model describing nonisothermal, three-phase flow of oil, liquid water, and steam has been described by Coats et al. (1974) for the purpose of simulating oil recovery by steam and hot water injection. In this model fluid densities are taken to be linear functions of temperature and pressure, and the effect of pressure on porosity is also taken into account. The mass and energy balance equations are solved simultaneously by a direct method. A comparison of calculated results with experimental data indicated that the simulation process is sensitive to temperature effects on relative permeability. The authors concluded that such data, especially the temperature dependence of water relative permeabilities, must be taken into account.

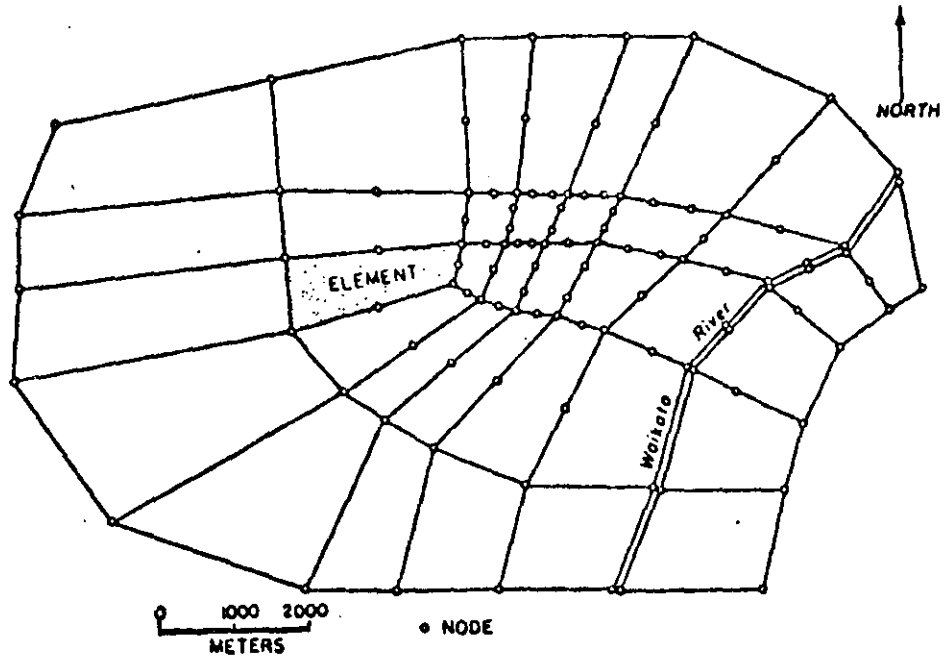
The first application of a distributed-parameter model to a geothermal system was made by Mercer (1973) and Mercer and Pinder (1974). A comprehensive account of this work has been described more recently by Mercer et al. (1975). The model consists of a single-phase, two-dimensional areal (horizontal) representation of the hot-water Waiora aquifer in the Wairakei hydrothermal system of New Zealand. The mass and energy balance (Eq. 7 without the pressure term)

are solved in the horizontal plane of the aquifer by the Galerkin finite element approach, using isoparametric elements as shown in Fig. 18. Since the governing equations are averaged over the thickness of the aquifer, cellular convection does not play a role in the resulting model.

However, vertical flow of fluid as well as energy is allowed to take place between the Waiora formation and the overlying Wairakei breccia aquifer through the intervening Huka Falls shale (see Fig. 19). The rate of this vertical leakage is taken to be proportional to the differences in head and temperature between the two aquifers, the values of  $p$  and  $T$  in the upper aquifer being kept constant. Inflows of heat from the underlying ignimbrites into the Waiora aquifer are treated as unknown source terms to be determined by model calibration. The lateral boundaries of the Waiora aquifer are assumed to be impermeable and isothermal. Viscosity is allowed to vary with temperature whereas fluid density is calculated as a linear function of temperature and pressure. The model is also capable of treating the heat dispersion term in its proper tensorial form.

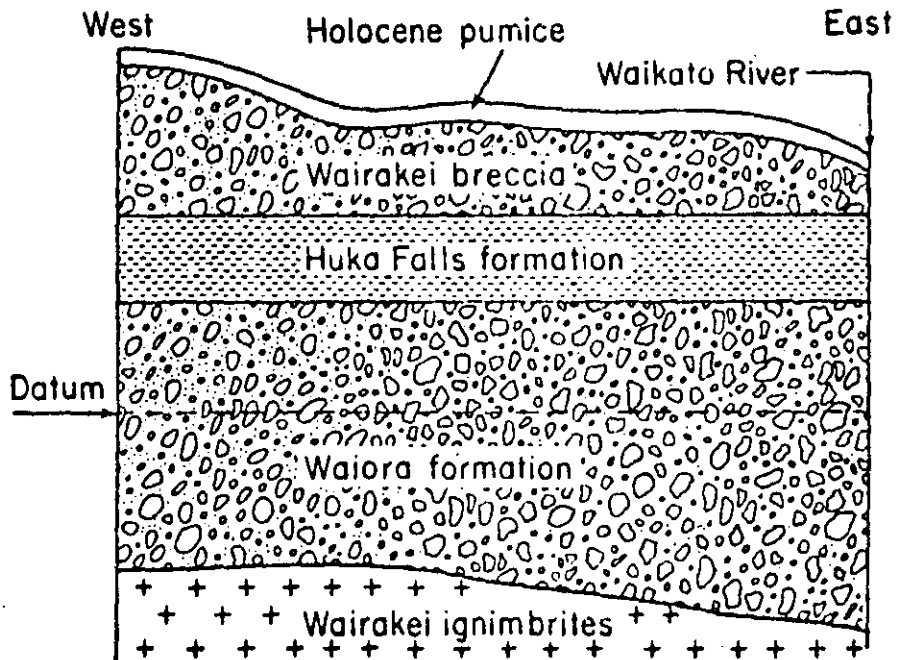
The first step in applying the model to Wairakei was to adjust the parameters so as to reproduce the steady state conditions existing in 1955, prior to exploitation. The parameters that were adjusted at this stage included element configuration, heat sources at the bottom of the aquifer, dispersion coefficients, and permeabilities. A sensitivity analysis was performed indicating that dispersion had little influence on the results, whereas the permeability of the Huka Falls formation had an important effect on the temperature distribution in the thermal reservoir.

The second step was to simulate the response of the geothermal field to withdrawal of hot water from a series of wells during the period between 1955 and 1962, using time steps of 30 days. The parameters of the model were again adjusted so as to bring about a fit between calculated and observed data. The results showed only a slight change in the configuration of the isotherms during



XBL755-2912

Fig. 18. Network of isoparametric elements used in distributed-parameter model of Wairakei geothermal system (after Mercer et al., 1975).



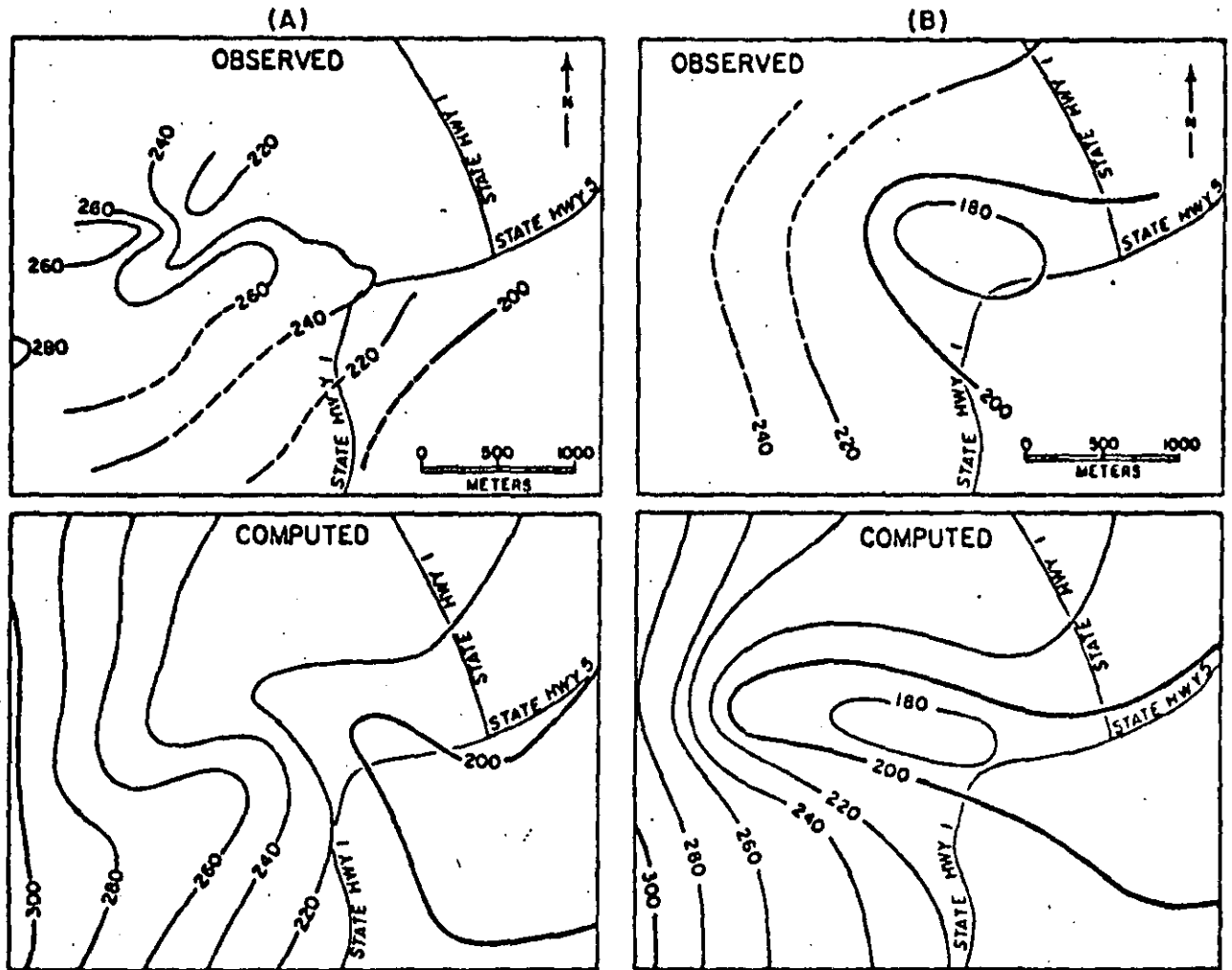
XBL755-2929

Fig. 19. Generalized geologic cross-section of Wairakei geothermal system. Datum plane 152.4 m above sea level (after Mercer et al., 1975).

the period investigated. Fig. 20 is a comparison of computed and observed potentiometric surfaces in the Waiora aquifer for 1958 and 1962. The single-phase model failed to reproduce historical data after the calibration period of 1955-1962 due to a considerable quantity of steam that had formed in the Waiora aquifer as a result of exploitation. Faust and Mercer (1975) are now developing a two-phase model to handle such problems.

A two-dimensional model of transient single-component, two-phase flow in a geothermal system has been developed by Toronyi (1974). The model is based on Equations 1-3 and 6 (without the last two terms involving pressure) and utilizes a block-centered rectangular finite difference grid capable of simulating flow in either a horizontal or vertical plane. The resulting equations are expressed in an implicit backward difference form and are solved simultaneously by a line iterative quasi-linearization (Newton-Raphson) scheme. Anisotropy is taken into account with the restriction that principal permeabilities and heat conductivities must remain parallel to the coordinates. Thermal conductivity is calculated according to (5) but dispersion is not taken into account. The fluids are assumed to have temperatures and pressures that are always on the vapor pressure curve implying that liquid and vapor co-exist at every point in the system. Consequently  $p$  and  $S$  are the two dependent variables for which a solution is sought simultaneously.

The external boundaries are impermeable and adiabatic with the understanding that forced convection due to production is much greater than conduction across these boundaries. The distributed-parameter model is coupled to a one-dimensional steady state model of a producing well in which the fluid is assumed to form a homogeneous two-phase mixture. The well is treated as a point source in the finite difference model which, in turn, provides boundary values of  $p$  and  $S$  for the steady state wellbore model. The wellbore model is represented mathematically by first order ordinary differential equations which are solved by the Runge-Kutta method.



KBL 753-2811

Fig. 20. Comparison of computed with observed potentiometric surfaces in Waiora hot-water aquifer for (A) 1958 and (B) 1962. Values in meters from datum 152.4 m above sea level (after Mercer et al., 1975).

Toronyi applied his model only to a homogeneous and isotropic geothermal system by using a 6 x 6 rectangular finite difference grid. His purpose was to investigate the effects of porosity, permeability, and various uniform initial  $p$  and  $S$  distributions on the production of geothermal fluid in a horizontal and vertical plane. On the basis of these studies, Toronyi classified the behavior of two-phase geothermal systems into three types in terms of initial liquid saturation: (1) vapor dominated, with initial  $S^L < 40\%$ ; (2) liquid dominated, with initial  $S^L > 60\%$ , and (3) mixed or intermediate, with initial  $S^L$  within the range 40 - 60%. Condensation and vaporization were found to be very important phenomena that could create exceedingly high liquid saturations near a wellbore and disrupt gravitational equilibrium by causing more liquid to occur at the top of the system than at the bottom. Toronyi also found that superheated regions form faster in rocks having relatively low porosity and permeability values. The quality of the produced fluid (in terms of percent steam) was always found to be greater at the wellhead than at the bottom, although the maximum change in quality was small.

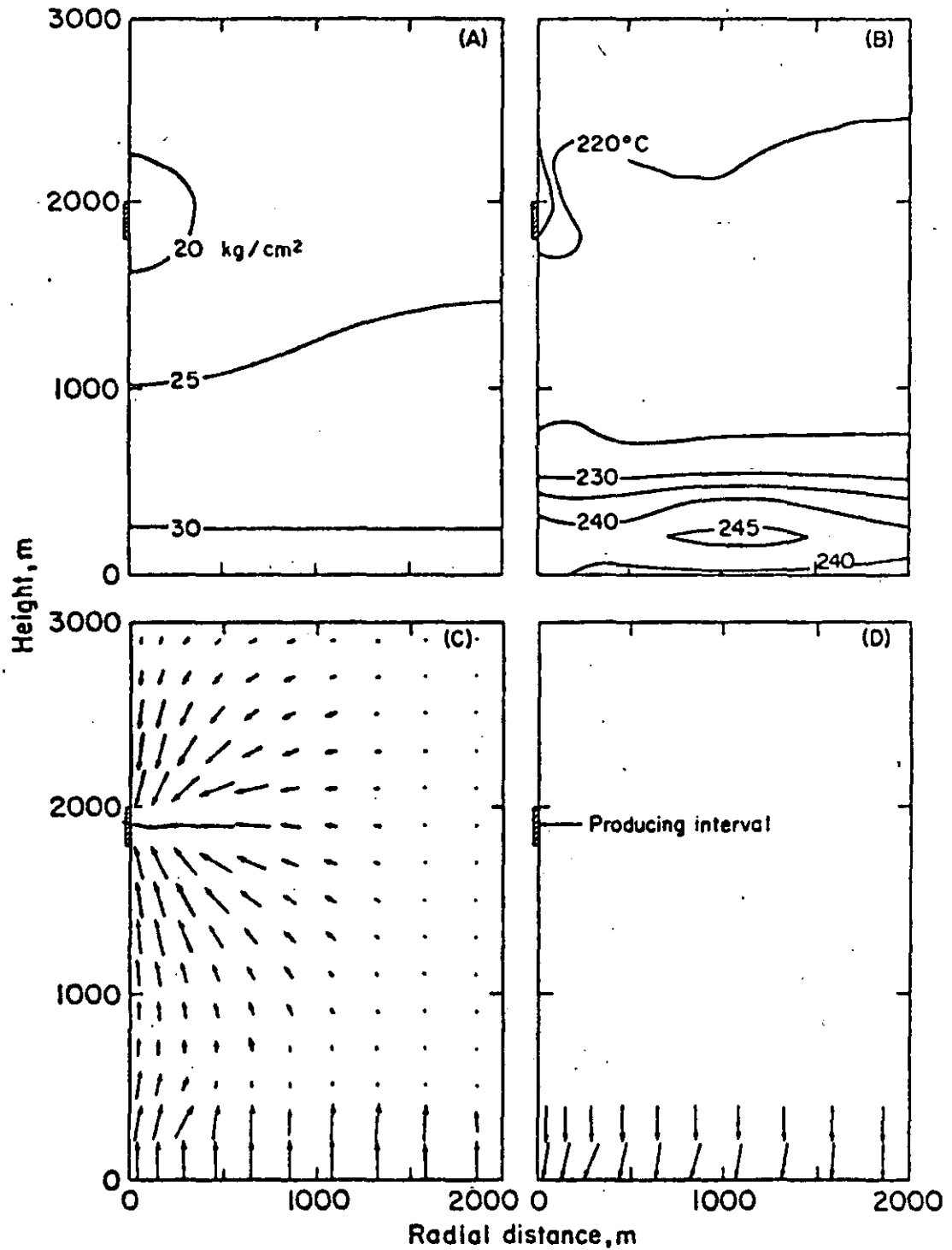
A two-phase, multi-dimensional model for geothermal systems has recently been developed by Lasseter et al. (1975) based on an extension of an earlier investigation of single-phase flow under nonisothermal conditions (Lasseter and Witherspoon, 1974). This model utilizes Equations 1 through 4. In the numerical process, Equations 1 through 3 are combined into a flow equation which is then solved in conjunction with the energy equation (Eq. 4). These two equations expressed in an integrated finite difference form (Narasimhan and Witherspoon, 1975) are solved for the two dependent variables, density and energy of the fluids, as a function of time and position within the system. Advantage can be taken of the fact that the time constants for the energy equation are typically several orders of magnitude larger than the time constants of the flow equation, which permits one to decouple the governing equations and still handle the

non-linearities satisfactorily. Thus, while it is necessary to take relatively small time steps to accurately solve the flow equation, the energy field time steps can be much larger.

Some preliminary results for a model of a vapor-dominated geothermal system are shown in Fig. 21. A vertical cross-section of a cylindrical system with a height of 3000 m and a radius of 2000 m was set up using 150 elements. The vapor column had an average initial temperature and pressure of 250°C and 40 kg/cm<sup>2</sup> throughout, and an attempt was also made to simulate a 200 m bottom layer that was essentially liquid saturated. The lower boundary of the boiling water layer was maintained at 250°C while the other boundaries were arbitrarily made impermeable to both heat and fluid. Typical values for thermal and flow properties of the materials were assumed. Relative permeability data were temperature independent.

Figure 21 shows reproductions of computer plots after about 1500 days at a steam withdrawal rate from the producing interval of  $3 \times 10^7$  kg/day (1380 t/h). As a result of this high rate of production, the pressure in the vapor column dropped to about 25 kg/cm<sup>2</sup> (Fig. 21A) and the temperature decreased to about 225°C (Fig. 21B). Figure 21C is a vector plot of the vapor flux showing how vigorous boiling at the bottom of the system is producing substantial steam. Figure 21D is a vector plot of the liquid flux and shows how water is separating from the steam at the base of the system. These preliminary results serve to illustrate the power of this numerical approach in analyzing such complex systems.

Gringarten and Sauty (1975) have developed an analytical model for nonsteady temperature behavior of production wells during reinjection of heat-depleted water into a horizontal aquifer with uniform regional flow. The aquifer is of infinite lateral extent and is confined between two impermeable semi-infinite layers. Initially, the system has a uniform temperature,  $T_0$ . At time  $t = 0$ , a well starts producing water at rate  $Q$  and injection of relatively cold water starts in a second well in the same aquifer at the same rate. The temperature



EEL 755-2930

Fig. 21. Distributed-parameter model of vapor-dominated geothermal system showing reservoir conditions after 1500 days of production: (A) pressure field, (B) temperature field, (C) vapor flux, (D) liquid flux.



of the injected water is set equal to  $T_1$  and maintained constant thereafter. Such a pair of wells is known as a "doublet."

The authors assume that steady state fluid flow is established much faster than thermal equilibrium and that temperature transfer occurs only by forced horizontal convection in the aquifer and vertical conduction in the confining beds. Assuming further that the waters at temperatures  $T_0$  and  $T_1$  do not mix (piston displacement), they have arrived at a simple closed form mathematical relationship between temperature, certain dimensionless parameters, and the stream function characterizing water flow. Gringarten and Sauty used their solution to calculate the optimum spacing of isolated doublets to be drilled for space heating purposes in the 1800 m deep Dogger aquifer around Paris, under the requirement that the cold front does not reach the producing well in less than 30 years when  $Q = 100 \text{ m}^3/\text{h}$ . By introducing a safety factor into their calculations, the optimum spacing was found to be about 900 m for an aquifer 50 m thick.

#### NOMENCLATURE

<u>Symbol</u>	<u>Description</u>	<u>Dimensions</u>
$a, a_1, a_2$	width	L
$c_p$	specific heat at constant pressure	$L^2 t^{-2} T^{-1}$
$c_v$	specific heat at constant volume	$L^2 t^{-2} T^{-1}$
D	depth	L
$D_1, D_2$	aspect ratio	-
$D_{ij}$	mechanical heat dispersion tensor	$MLt^{-3} T^{-1}$
e	specific internal energy	$L^2 t^{-2}$
f	fluid property	arbitrary
g	acceleration due to gravity	$Lt^{-2}$
$g_i$	gravity vector (0, 0, -g)	$Lt^{-2}$

## 169

<u>Symbol</u>	<u>Description</u>	<u>Dimensions</u>
$h$	specific enthalpy	$L^2 t^{-2}$
$H$	heat capacity ratio	-
$k$	intrinsic permeability	$L^2$
$k_{ij}$	intrinsic permeability tensor	$L^2$
$k_r$	relative permeability	-
$L$	length	$L$
$m$	specific mass flux	$ML^{-2} t^{-1}$
$M$	mass	$M$
$n_i$	outward unit normal vector on $\Gamma$	-
$Nu$	Nusselt number	-
$p$	pressure	$ML^{-1} t^{-2}$
$p_D$	dimensionless pressure	-
$Pr$	Prandtl number	-
$q_i$	specific conductive heat flux vector	$Mt^{-3}$
$Q$	heat flux	$ML^2 t^{-3}$
$r$	radius	$L$
$R$	representative elementary volume	$L^3$
$Ra$	Rayleigh number	-
$Ra_c$	critical Rayleigh number	-
$S$	fluid saturation	-
$t$	time	$t$
$T$	temperature	$T$
$v$	specific volume	$L^3 M^{-1}$
$v_i$	darcy velocity vector	$LT^{-1}$
$V$	volume	$L^3$
$w_i$	velocity vector of solid fluid interface	$Lt^{-1}$

<u>Symbol</u>	<u>Description</u>	<u>Dimensions</u>
$x_i$	vector of space coordinates (x,y,z) z being the vertical	L
Z	compressibility factor for real gas	-
$\alpha$	thermal diffusivity	$L^2 t^{-1}$
$\beta$	coefficient of volumetric thermal expansion	$T^{-1}$
$\Gamma^{LS}$	liquid-solid interface in R	$L^2$
$\Gamma^{LG}$	liquid-gas interface in R	$L^2$
$\Gamma^{GS}$	gas-solid interface in R	$L^2$
$\delta_{ij}$	kroncker delta (1 if $i = j$ and 0 if $i \neq j$ )	-
$\theta$	dimensionless temperature °	-
$\kappa$	thermal conductivity	$MLt^{-3}T^{-1}$
$\kappa_{ij}$	thermal dispersion tensor	$MLt^{-3}T^{-1}$
$\mu$	viscosity	$ML^{-1}t^{-1}$
$v_i$	dimensionless velocity vector	-
$\rho$	density	$ML^{-3}$
$\tau$	dimensionless time	-
$\phi$	porosity	-
$\langle \rangle$	average over R	arbitrary
$\langle \rangle^*$	average over pore space of R	arbitrary
$\langle \rangle^{L,G,S}$	average over liquid, gas, or solid phases in R	arbitrary

Subscripts

o reference quantity

Superscripts

eff effective quantity for fluid-filled rock

G gas phase

<u>Symbol</u>	<u>Description</u>	<u>Dimensions</u>
L	liquid phase	
S	solid phase	
o	deviation from average over R	

#### ACKNOWLEDGMENTS

We would like to acknowledge the support for this work provided by the U. S. Atomic Energy Commission, the U. S. Geological Survey, and the University of California.

### APPENDIX

The purpose of this appendix is to derive a macroscopic form of the energy balance equation for a two-phase, single component fluid in a porous medium. This is accomplished by averaging the microscopic equations over a representative elementary volume (Bear, 1972, p. 19) of the medium. The particular method of averaging that is used here has been applied by Lee et al. (1975) to the energy equation and, in this context, was brought to our attention by Gray and Pinder (1974, personal communication). We recognize that the macroscopic energy equation can be derived directly from macroscopic balance considerations, without resorting to an averaging process. However, the formal averaging procedure is helpful in gaining insight into the numerous assumptions that one must make in order to arrive at a manageable macroscopic expression. Such assumptions are implicitly inherent in every macroscopic equation and, by facing them explicitly, one should be able to appreciate some of the limitations of the differential equations used to describe geothermal systems.

#### Mathematical Preliminaries

Let  $R$  be a representative elementary volume of the porous medium and let  $\phi$  be the porosity of  $R$ . Whitaker (1969) demonstrated that the averaging procedure used below will lead to meaningful results if the characteristic length of  $R$  is much greater than the characteristic length of the pores, and is much smaller than the characteristic length of the entire porous medium. An obvious requirement is that  $R$  be large enough to provide a fair representation of all the statistical properties of the pore space. Our analysis is restricted to homogeneous porous media which means that the porosity,  $\phi$ , as well as all other statistical properties of the pore space, must remain unchanged as one focuses his attention on different elementary representative volumes in the medium. Furthermore, the size and shape of  $R$  must be constant and its orientation must remain unchanged.

Let  $f^L(x_1)$  be some property of the liquid (e.g., density, temperature, etc.) which, by definition, is zero in the gas phase and in the solids. Then the "liquid phase average" of  $f^L$  is defined as

$$\langle f^L \rangle^L = \frac{1}{\phi S^L R} \int_R f^L dR \quad (A1)$$

Similarly, the "pore volume average" of  $f^L$  is defined as

$$\langle f^L \rangle^* = \frac{1}{\phi R} \int_R f^L dR \quad (A2)$$

and the "bulk volume average" as

$$\langle f^L \rangle = \frac{1}{R} \int_R f^L dR \quad (A3)$$

From (A1) - (A3) it is evident that

$$\langle f^L \rangle = \phi \langle f^L \rangle^* = \phi S^L \langle f^L \rangle^L \quad (A4)$$

These averages can be viewed as point macroscopic quantities associated with the centroid of  $R$ . Thus, there is an average associated with each point in  $R$  (each such point being the centroid of another  $R$ ), and it therefore makes sense to talk about the average value of these averages over  $R$ . Whitaker (1969) showed that

$$\langle \langle f^L \rangle \rangle = \langle f^L \rangle \quad (A5)$$

i.e., the average of the average is equal to the average (note that this is by no means self evident).

At any point in the liquid phase within  $R$ ,  $f^L$  can be expressed as

$$f^L = \langle f^L \rangle^L + \overset{\circ}{f}^L \quad (A6)$$

where  $\overset{\circ}{f}^L$  is simply the deviation from the phase average of  $f^L$ . From (A5) and (A6) it follows that

$$\langle \overset{\circ}{f}^L \rangle \equiv 0 \quad (A7)$$

Note that just like  $f^L$ , the function of  $\overset{\circ}{f}^L$  is taken to be zero everywhere outside the liquid phase.

According to the general transport theorem (c.f. Whitaker, 1968) one has

$$\left\langle \frac{\partial f^L}{\partial t} \right\rangle = \frac{\partial \langle f^L \rangle}{\partial t} - \frac{1}{R} \int_{\Gamma^{LS}, \Gamma^{LG}} f^L w_i n_i d\Gamma \quad (A8)$$

where  $n_i$  is a unit normal pointing out of the liquid phase. Another useful relationship known as the "averaging theorem" (Whitaker, 1969; Slattery, 1972, pp. 192-196) states that

$$\left\langle \frac{\partial f^L}{\partial x_i} \right\rangle = \frac{\partial \langle f^L \rangle}{\partial x_i} + \frac{1}{R} \int_{\Gamma^{LS}, \Gamma^{LG}} f^L n_i d\Gamma \quad (A9)$$

Similar relationships will hold for properties of the solid phase,  $f^S$ , and the gas phase,  $f^G$ .

#### Derivation of Energy Equation for Two-Phase Fluid

In the following analysis, the pore space is assumed to be saturated by a single-component fluid which can be either in a liquid or gaseous state. The liquid and gas phases are assumed to be separated by a distinct interface,  $\Gamma^{LG}$ , across which there may be a finite change in pressure. If one neglects viscous dissipation, then the energy equation at a point within the liquid can be written (c.f., Currie, 1974, p. 17) as

$$\frac{\partial}{\partial t} (\rho^L e^L) = - \frac{\partial}{\partial x_i} (\rho^L e^L v_i^L) - \rho^L \frac{\partial v_i^L}{\partial x_i} - \frac{\partial q_i^L}{\partial x_i} \quad (A10)$$

Taking the average of (A10) over a representative elementary volume,  $R$ , and using (A8) and (A9), the result (after rearrangement) is

$$\begin{aligned}
\frac{\partial}{\partial t} \langle \rho^L e^L \rangle &= - \frac{\partial}{\partial x_1} \langle \rho^L e^L v_1^L \rangle - \frac{1}{R} \int_{\Gamma^{LG}} \rho^L e^L (v_1^L - w_1) n_1 d\Gamma \\
&- \phi S^L \langle p^L \rangle \frac{\partial \langle v_1^L \rangle}{\partial x_1} - S^L \langle p^L \rangle \frac{1}{R} \int_{\Gamma^{LG}} v_1^L n_1 d\Gamma \\
&- \frac{\partial \langle q_1^L \rangle}{\partial x_1} - \frac{1}{R} \int_{\Gamma^{LS}, \Gamma^{LG}} q_1^L n_1 d\Gamma
\end{aligned} \tag{A11}$$

Equation A11 is based on the assumption that fluid velocity normal to a solid-fluid interface is zero (i.e., there is no transfer of kinetic energy between the fluid and the solid). Furthermore, in order to replace the term  $p^L (\partial v_1^L / \partial x_1)$  in (A10) by its macroscopic equivalent in (A11), it is necessary to assume that  $p^L$  and  $\partial v_1^L / \partial x_1$  are uncorrelated so that the average of their product is zero. A possible physical justification for this is to say that local variations in fluid velocity within a pore are controlled primarily by viscous stresses and can therefore be assumed to be independent of pressure.

The energy equation for the gas phase at a point within R has the same form as (A11). When this equation is averaged over R, the result is

$$\begin{aligned}
\frac{\partial}{\partial t} \langle \rho^G e^G \rangle &= - \frac{\partial}{\partial x_1} \langle \rho^G e^G v_1^G \rangle + \frac{1}{R} \int_{\Gamma^{LG}} \rho^G e^G (v_1^G - w_1) n_1 d\Gamma \\
&- \phi S^G \langle p^G \rangle \frac{\partial \langle v_1^G \rangle}{\partial x_1} + S^G \langle p^G \rangle \frac{1}{R} \int_{\Gamma^{LG}} v_1^G n_1 d\Gamma \\
&- \frac{\partial \langle q_1^G \rangle}{\partial x_1} - \frac{1}{R} \int_{\Gamma^{GS}} q_1^G n_1 d\Gamma + \frac{1}{R} \int_{\Gamma^{LG}} q_1^G n_1 d\Gamma
\end{aligned} \tag{A12}$$

Here  $n_1$  points into the gas along  $\Gamma^{LG}$  and into the solid along  $\Gamma^{GS}$ .

The energy equation at a point within the solid is simply



$$\frac{\partial}{\partial t} (\rho^S e^S) = - \frac{\partial q_1^S}{\partial x_1} \quad (A13)$$

Integrating over R gives

$$\rho^S \frac{\partial \langle e^S \rangle}{\partial t} = - \frac{\partial \langle q_1^S \rangle}{\partial x_1} + \frac{1}{R} \int_{\Gamma^{LS}, \Gamma^{GS}} q_1^S n_1 d\Gamma \quad (A14)$$

where  $n_1$  points into the solid.

From the requirement of energy continuity at a liquid-gas interface, it can be shown that

$$\int_{\Gamma^{LG}} [q_1^L + \rho^L e^L (v_1^L - w_1)] n_1 d\Gamma = \int_{\Gamma^{LG}} [q_1^G + \rho^G e^G (v_1^G - w_1)] n_1 d\Gamma \quad (A15)$$

A similar condition must also hold for the conductive energy flux  $q_1 n_1$  at any solid-fluid interface. Thus, by adding (A11), (A12), and (A14) and using (A4) we obtain

$$\begin{aligned} & \frac{\partial}{\partial t} [\phi S^L \langle \rho^L e^L \rangle + \phi S^G \langle \rho^G e^G \rangle + (1 - \phi) \rho^S \langle e^S \rangle] \\ &= - \frac{\partial}{\partial x_1} [\phi S^L \langle \rho^L e^L v_1^L \rangle + \phi S^G \langle \rho^G e^G v_1^G \rangle] \\ &- \frac{\partial}{\partial x_1} [\phi S^L \langle q_1^L \rangle + \phi S^G \langle q_1^G \rangle + (1 - \phi) \langle q_1^S \rangle] \\ &- \phi S^L \langle p^L \rangle \frac{\partial \langle v_1^L \rangle}{\partial x_1} - \phi S^G \langle p^G \rangle \frac{\partial \langle v_1^G \rangle}{\partial x_1} \\ &- S^L \langle p^L \rangle \frac{1}{R} \int_{\Gamma^{LG}} v_1^L n_1 d\Gamma + S^G \langle p^G \rangle \frac{1}{R} \int_{\Gamma^{LG}} v_1^G n_1 d\Gamma \end{aligned} \quad (A16)$$

We now introduce another assumption that thermodynamic relationships between average (macroscopic) quantities remain exactly the same as those between the equivalent point (microscopic) quantities. This assumption is implicit in all macroscopic equations that we have encountered in the literature. Its implication is that  $\rho$  and  $e$  are uncorrelated and one can thus replace  $\langle \rho^L e^L \rangle$  by  $\langle \rho^L \rangle \langle e^L \rangle$  and  $\langle \rho^G e^G \rangle$  by  $\langle \rho^G \rangle \langle e^G \rangle$ . Since mass dispersion is not considered in the

present analysis,  $\rho$  and  $\dot{v}_1$  are also uncorrelated and we can therefore write

$$\begin{aligned} \phi S^L \langle \rho^L e^L v_1^L \rangle^L &= \phi S^L (\langle \rho^L \rangle^L \langle e^L \rangle^L \langle v_1^L \rangle^L + \langle \rho^L e^L v_1^L \rangle^L) \\ &= \langle \rho^L \rangle^L \langle e^L \rangle^L \langle v_1^L \rangle^L + \phi S^L \langle \rho^L e^L v_1^L \rangle^L \end{aligned} \quad (A17)$$

where the second term represents mechanical dispersion of energy. Following the current trend in the literature (c.f., Bear, 1972; Gray, 1975) we assume that dispersion is mathematically equivalent to a diffusion process, so that one can write

$$\langle \rho^L e^L v_1^L \rangle^L = - D_{1j}^L \frac{\partial \langle T^L \rangle^L}{\partial x_j} \quad (A18)$$

where  $D_{1j}^L$  is known as the mechanical (or convective) dispersion tensor. The conductive flux,  $q_1^L$ , is expressed by Fourier's law using a scalar thermal conductivity,

$$q_1^L = - \kappa^L \frac{\partial T^L}{\partial x_1} \quad (A19)$$

the average of which is given by (A9) as

$$\langle q_1^L \rangle = - \kappa^L \frac{\partial \langle T^L \rangle}{\partial x_1} - \frac{\kappa^L}{R} \int_{\Gamma^{LG}, \Gamma^{LS}} T^L n_1 d\Gamma \quad (A20)$$

In order to eliminate the surface integral from (A20) we assume that the orientation vector  $n_1$  is symmetrically distributed about a zero average value (this is true if the orientations of  $\Gamma^{LG}$  and  $\Gamma^{LS}$  are random). Then, since temperature is independent of interface orientation (i.e., random temperatures may exist at various points along  $\Gamma$  having a given orientation)  $T^L$  and  $n_1$  are uncorrelated and the surface integral in (A20) can be neglected. In a similar manner, it may appear reasonable to assume that  $v_1^L n_1$  is symmetrically distributed about a zero average value along  $\Gamma^{LG}$  so that the first surface integral in (A16) vanishes. Similar considerations hold for the gas phase. If we further assume that  $\phi$ ,  $S^L$ , and  $S^G$  remain practically constant for any averaging volume whose centroid is

inside R, then (A16) can finally be reduced to

$$\begin{aligned}
 & \frac{\partial}{\partial t} [\phi^L \langle \rho^L \rangle^L \langle e^L \rangle^L + \phi^G \langle \rho^G \rangle^G \langle e^G \rangle^G + (1 - \phi) \rho^S \langle e^S \rangle^S] \\
 &= - \frac{\partial}{\partial x_1} (\langle \rho^L \rangle^L \langle e^L \rangle^L \langle v_1^L \rangle + \langle \rho^G \rangle^G \langle e^G \rangle^G \langle v_1^G \rangle) \\
 &+ \frac{\partial}{\partial x_1} \left[ \phi^L \kappa_{1j}^L \frac{\partial \langle T^L \rangle^L}{\partial x_j} + \phi^G \kappa_{1j}^G \frac{\partial \langle T^G \rangle^G}{\partial x_j} + (1 - \phi) \kappa^S \frac{\partial \langle T^S \rangle^S}{\partial x_1} \right] \\
 &- \langle p^L \rangle^L \frac{\partial \langle v_1^L \rangle}{\partial x_1} - \langle p^G \rangle^G \frac{\partial \langle v_1^G \rangle}{\partial x_1}
 \end{aligned} \tag{A21}$$

where  $\kappa_{1j} = \kappa_{1j}^{\delta} + D_{1j}$  is the combined conductive and mechanical dispersion tensor.

In the literature it is customary to assume that all phases are in thermal equilibrium and that capillary pressure differences between the fluid phases are negligible. In this case (A21) reduces to

$$\begin{aligned}
 & \frac{\partial}{\partial t} [\phi^L \langle \rho^L \rangle^L \langle e^L \rangle^L + \phi^G \langle \rho^G \rangle^G \langle e^G \rangle^G + (1 - \phi) \rho^S \langle e^S \rangle^S] \\
 &= - \frac{\partial}{\partial x_1} (\langle \rho^L \rangle^L \langle e^L \rangle^L \langle v_1^L \rangle + \langle \rho^G \rangle^G \langle e^G \rangle^G \langle v_1^G \rangle) \\
 &+ \frac{\partial}{\partial x_1} \left( \kappa_{1j}^{\text{eff}} \frac{\partial \langle T \rangle^*}{\partial x_j} \right) - \langle p \rangle^* \frac{\partial}{\partial x_1} (\langle v_1^L \rangle + \langle v_1^G \rangle)
 \end{aligned} \tag{A22}$$

where

$$\kappa_{1j}^{\text{eff}} = \phi^L \kappa_{1j}^L + \phi^G \kappa_{1j}^G + (1 - \phi) \kappa^S \delta_{1j}$$

This shows that the assumption of thermal equilibrium implies viewing the solid, liquid, and gas as three anisotropic conductors arranged parallel to the direction of heat flow.

Recalling our assumption that thermodynamic relationships between average fluid properties are the same as between the equivalent point properties, we can define the average (macroscopic) enthalpy of the liquid as

$$\langle h^L \rangle^L = \langle e^L \rangle^L + \frac{\langle p^L \rangle^L}{\langle \rho^L \rangle^L} \tag{A24}$$

Similar definitions will hold for the gas and the solid. If we now replace each  $\langle e \rangle$  in (A22) by  $\langle h \rangle - \langle p \rangle / \langle \rho \rangle$ , we obtain a macroscopic energy equation in terms of enthalpy.

$$\begin{aligned} & \frac{\partial}{\partial t} [\phi S^L \langle \rho^L \rangle^L \langle h^L \rangle^L + \phi S^G \langle \rho^G \rangle^G \langle h^G \rangle^G + (1 - \phi) \rho^S \langle h^S \rangle^S] \\ & = - \frac{\partial}{\partial x_i} (\langle \rho^L \rangle^L \langle h^L \rangle^L \langle v_i^L \rangle + \langle \rho^G \rangle^G \langle h^G \rangle^G \langle v_i^G \rangle) \\ & + \frac{\partial}{\partial x_i} \left( \kappa_{ij}^{\text{eff}} \frac{\partial \langle T \rangle^*}{\partial x_j} \right) + \frac{\partial (\phi \langle p \rangle^*)}{\partial t} + (\langle v_i^L \rangle + \langle v_i^G \rangle) \frac{\partial \langle p \rangle^*}{\partial x_i} \end{aligned} \quad (\text{A25})$$

### Temperature Equation for a Single Phase

In the particular case where the pores are completely saturated by a single fluid phase (say liquid), one can use the equation of mass continuity to rewrite (A21) in the form

$$\begin{aligned} & \phi \langle \rho^L \rangle^* \frac{\partial \langle e^L \rangle^*}{\partial t} + (1 - \phi) \rho^S \frac{\partial \langle e^S \rangle^S}{\partial t} = - \langle \rho^L \rangle^* \langle v_i^L \rangle \frac{\partial \langle e^L \rangle^*}{\partial x_i} \\ & + \frac{\partial}{\partial x_i} \left[ \phi \kappa_{ij}^L \frac{\partial \langle T^L \rangle^*}{\partial x_j} + (1 - \phi) \kappa^S \frac{\partial \langle T^S \rangle^S}{\partial x_i} \right] - \langle p^L \rangle^* \frac{\partial \langle v_i^L \rangle^L}{\partial x_i} \end{aligned} \quad (\text{A26})$$

Assuming that the thermodynamic relationships

$$\frac{\partial e}{\partial \bullet} = \left( \frac{\partial e}{\partial v} \right)_T \frac{\partial v}{\partial \bullet} + c_v \frac{\partial T}{\partial \bullet} \quad (\text{A27})$$

$$p = T \left( \frac{\partial p}{\partial T} \right)_v - \left( \frac{\partial e}{\partial v} \right)_T \quad (\text{A28})$$

hold for the average quantities appearing in (A26), this latter equation can be rewritten as

$$\begin{aligned}
& \left( \frac{\partial e^L}{\partial v} \right)_T \left[ \phi \langle \rho^L \rangle^* \frac{\partial (\langle \rho^L \rangle^*)^{-1}}{\partial t} + \langle \rho^L \rangle^* \langle v_i^L \rangle \frac{\partial (\langle \rho^L \rangle^*)^{-1}}{\partial x_i} - \frac{\partial \langle v_i^L \rangle}{\partial x_i} \right] \\
& + \phi \langle \rho^L \rangle^* c_v^L \frac{\partial \langle T^L \rangle^*}{\partial t} + (1 - \phi) \rho^S c_v^S \frac{\partial \langle T^S \rangle^S}{\partial t} \\
& = - \langle \rho^L \rangle^* \langle v_i^L \rangle c_v^L \frac{\partial \langle T^L \rangle^*}{\partial x_i} + \frac{\partial}{\partial x_i} \left[ \phi \kappa_{ij}^L \frac{\partial \langle T^L \rangle^*}{\partial x_j} + (1 - \phi) \kappa^S \frac{\partial \langle T^S \rangle^S}{\partial x_i} \right] \\
& - \langle T^L \rangle^* \left( \frac{\partial p}{\partial T} \right)_v \frac{\partial \langle v_i^L \rangle}{\partial x_i} \tag{A29}
\end{aligned}$$

The first term in brackets can be reformulated as

$$- \frac{1}{\langle \rho^L \rangle^*} \left[ \phi \frac{\partial \langle \rho^L \rangle^*}{\partial t} + \frac{\partial}{\partial x_i} (\langle \rho^L \rangle^* \langle v_i^L \rangle) \right]$$

which vanishes by virtue of mass continuity. Thus, the energy equation for the liquid phase can be expressed entirely in terms of temperature,

$$\begin{aligned}
& \phi \langle \rho^L \rangle^* c_v^L \frac{\partial \langle T^L \rangle^*}{\partial t} + (1 - \phi) \rho^S c_v^S \frac{\partial \langle T^S \rangle^S}{\partial t} = - \langle \rho^L \rangle^* \langle v_i^L \rangle c_v^L \frac{\partial \langle T^L \rangle^*}{\partial x_i} \\
& + \frac{\partial}{\partial x_i} \left[ \phi \kappa_{ij}^L \frac{\partial \langle T^L \rangle^*}{\partial x_j} + (1 - \phi) \kappa^S \frac{\partial \langle T^S \rangle^S}{\partial x_i} \right] - \langle T^L \rangle^* \left( \frac{\partial p}{\partial T} \right)_v \frac{\partial \langle v_i^L \rangle}{\partial x_i} \tag{A30}
\end{aligned}$$

If the solid and the liquid are assumed to be in thermal equilibrium, (A30) reduces to

$$\begin{aligned}
& \left[ \phi \langle \rho^L \rangle^* c_v^L + (1 - \phi) \rho^S c_v^S \right] \frac{\partial \langle T \rangle^*}{\partial t} = - \langle \rho^L \rangle^* \langle v_i^L \rangle c_v^L \frac{\partial \langle T \rangle^*}{\partial x_i} \\
& + \frac{\partial}{\partial x_i} \left( \kappa_{ij}^{\text{eff}} \frac{\partial \langle T \rangle^*}{\partial x_j} \right) - \langle T \rangle^* \left( \frac{\partial p}{\partial T} \right)_v \frac{\partial \langle v_i^L \rangle}{\partial x_i} \tag{A31}
\end{aligned}$$

where  $\kappa_{ij}^{\text{eff}} = \phi \kappa_{ij}^L + (1 - \phi) \kappa^S \delta_{ij}$ .

Equations A30 and A31 are also applicable when the pores are completely saturated by the gas phase, provided that the superscript L is replaced by G.

REFERENCES

- Anand, J., W. H. Somerton and E. Goma, 1973, Predicting thermal conductivities of formations from other known properties, Soc. Petrol. Engr. Jour., v. 13, no. 5, pp. 267-273.
- Bear, J., 1972, Dynamics of Fluids in Porous Media, Am. Elsevier, New York.
- Beck, J. L., 1972, Convection in a box of porous material saturated with fluid, Phys. of Fluids, v. 15, no. 8, pp. 1377-1383.
- Billhartz, H. L., Jr., 1971, Fluid Production from Geothermal Steam Reservoirs, M. S. thesis, Stanford Univ., Calif.
- Bodvarsson, G., 1961, Physical characteristics of natural heat resources in Iceland, paper G.6, U. N. Conf. on New Sources of Energy, Rome, August 21-31.
- Brace, W. F., J. B. Walsh and W. T. Francos, 1968, Permeability of granite under high pressure, Jour. Geophys. Research, v. 73, no. 6, pp. 2225-2236.
- Brigham, W. E. and W. B. Morrow, 1974, P/Z behavior for geothermal steam reservoirs, paper SPE 4899, 44th Annual Calif. Regional Meeting SPE-AIME, San Francisco, April 4-5.
- Brownell, D. H., Jr., S. K. Garg and J. W. Pritchett, 1975, Computer simulation of geothermal reservoirs, paper SPE 5381, 45th Annual Calif. Regional Meeting SPE-AIME, Ventura, Calif. April 2-4.
- Cady, G. V., 1969, Model Studies of Geothermal Fluid Production, Ph.D. dissertation, Stanford Univ., Calif.
- Calhoun, J. C., M. Lewis, Jr. and R. C. Newman, 1949, Experiments on the capillary properties of porous solids, Trans. AIME, v. 186, pp. 189-196.
- Caltagirone, J. P., M. Cloupeau and M. Combarous, 1971, Convection naturelle fluctuante dans une couche poreuse horizontale, Comptes Rendus, Acad. Sci., Paris, B273, pp. 833-836.
- Casse, F. J., 1974, The Effect of Temperature and Confining Pressure on Fluid Flow Properties of Consolidated Rocks, Stanford Geothermal Program, Rep. SGP-TR3, Stanford Univ., Calif.
- Cheng, P. and K. H. Lau, 1974, Steady state free convection in an unconfined geothermal reservoir, Jour. Geophys. Res., v. 79, no. 29, pp. 4425-4431.
- Coats, K. H., W. D. George, C. Chu and B. E. Marcum, 1974, Three-dimensional simulation of steamflooding, Soc. Petrol. Engr. Jour., v. 15, no. 6, pp. 573-592.
- Combarous, M. A. and S. A. Bories, 1973, Thermal Convection in Saturated Porous Media, Report prepared for Advances in Hydroscience, Institut Francais du Pétrole and Institute de Mecanique des Fluides de Toulouse.

- Combarrous, M. and S. Bories, 1974, Modelisation de la convection naturelle au sein d'une couche poreuse horizontale a l'aide d'un coefficient de transfert solide-fluide, Int. Jour. Heat Mass Transfer, v. 17, pp. 505-515.
- Craig, H., 1966, Superheated steam and mineral-water interactions in geothermal areas, Trans. Am. Geophys. Union, v. 47, pp. 204-205 (abstract).
- Currie, I. G., 1974, Fundamental Mechanics of Fluids, McGraw-Hill, New York.
- Davidson, L. B., 1969, The effect of temperature on the permeability ratio of different fluid pairs in two-phase systems, Jour. Petrol. Tech., Aug. 1969, pp. 1037-1046.
- Donaldson, I. G., 1962, Temperature gradients in the upper layers of the earth's crust due to convective water flows, Jour. Geophys. Res., v. 67, no. 9, pp. 3449-3459.
- Donaldson, I. G., 1968a, The flow of steam water mixtures through permeable beds: A simple simulation of a natural undisturbed hydrothermal region, New Zealand Jour. Sci., v. 11, pp. 3-23.
- Donaldson, I. G., 1968b, A possible model for hydrothermal systems and methods of studying such a model, paper 2580, Third Australian Conf. on Hydraulics and Fluid Mechanics, Nov. 25-29.
- Donaldson, I. G., 1970, The simulation of geothermal systems with a simple convective model, Geothermics, Special issue 2, v. 2, part 1, pp. 649-654.
- Edmonson, J. A., 1965, Effect of temperature on waterflooding, Jour. Canadian Petrol. Tech., v. 4, no. 4, pp. 236-242.
- Einarsson, T., 1942, Ueber das Wesen der heissen Quellen Islands, Rit. Vísind. Ísl., v. 26, 91 p.
- Elder, J. W., 1965, Physical processes in geothermal areas in Terrestrial Heat Flow, W. H. K. Lee, ed., Am. Geophys. Union Mon., ser. 8, pp. 211-239.
- Elder, J. W., 1966, Heat and mass transfer in the earth: Hydrothermal systems, New Zealand D.S.I.R. Bull. 169, 115 p.
- Elder, J. W., 1967, Transient convection in a porous medium, Jour. Fluid Mech., v. 27, part 3, pp. 609-623.
- Facca, G. and F. Tonani, 1964, Theory and technology of a geothermal field, Bull. Volcanol., v. 27, part 1, pp. 143-189,
- Faust, C. F. and J. W. Mercer, 1975, Mathematical modeling of geothermal systems, paper to be presented at Second United Nations Symposium on the Development and Use of Geothermal Resources, San Francisco, May 20-29.

- Fernandez, R. T., 1972, Natural Convection from Cylinders Buried in Porous Media, Ph.D. dissertation, Univ. of Calif., Berkeley.
- Goguel, J., 1953, Le regime thermique de l'eau souterraine, Annales des Mines, v. 10, pp. 3-32.
- Gray, W. G., 1975, A derivation of the equations for multi-phase transport, paper submitted to Chem. Engr. Sci.
- Greenberg, D. B., R. S. Cresap and T. A. Malone, 1968, Intrinsic permeability of hydrological porous mediums: Variation with temperature, Water Resour. Res., v. 4, no. 4, pp. 791-800.
- Gringarten, A. C. and J. P. Sauty, 1975, A theoretical study of heat extraction from aquifers with uniform regional flow, paper submitted to Jour. Geophys. Res.
- Gupta, V. P. and D. D. Joseph, 1973, Bounds for heat transport in a porous layer, Jour. Fluid Mech., v. 57, part 3, pp. 491-514.
- Haas, J. L., Jr., 1970, An equation for the density of vapor-saturated NaCl-H<sub>2</sub>O solutions from 75° to 325°C, Am. Jour. Sci., v. 269, pp. 489-493.
- Haas, J. L., Jr., 1971, The effect of salinity on the maximum thermal gradient of a hydrothermal system at hydrostatic pressure, Econ. Geol., v. 66, pp. 940-946.
- Helgeson, H. C., 1968, Geologic and thermodynamic characteristics of the Salton Sea geothermal system, Am. Jour. Sci., v. 266, pp. 129-166.
- Holst, P. H., 1970, A Theoretical and Experimental Investigation of Natural Convection in Porous Media, Ph.D. dissertation, Univ. of Calgary, Alberta, Canada.
- Holst, P. H. and K. Aziz, 1972a, A theoretical and experimental study of natural convection in a confined porous medium, Canadian Jour. Chem. Engr., v. 50, pp. 232-241.
- Holst, P. H. and K. Aziz, 1972b, Transient three-dimensional natural convection in confined porous media, Jour. Heat and Mass Transfer, v. 15, pp. 73-90.
- Horne, R. N. and M. J. O'Sullivan, 1974, Oscillatory convection in a porous medium heated from below, Jour. Fluid Mech., v. 66, part 2, pp. 339-352.
- Horton, C. W. and F. T. Rogers, Jr., 1945, Convection currents in a porous medium, Jour. Appl. Phys., v. 16, no. 6, pp. 367-370.
- James, R., 1968, Wairakei and Lardarello geothermal power systems compared, New Zealand Jour. Sci. and Tech., v. 11, pp. 706-719.
- Jeffreys, H., 1930, The instability of a compressible fluid heated below, Proc. Cambridge Phil. Soc., v. 26, pp. 170-172.



- Kaneko, T., M. F. Mohtadi and K. Aziz, 1974, An experimental study of natural convection in inclined porous media, Int. Jour. Heat Mass Transfer, v. 17, pp. 485-496.
- Kapplermeier, O. and R. Haenel, 1974, Geothermics with Special Reference to Application, Geopublication Associates, Berlin, tables 6.3-6.6, pp. 208-218.
- Karra, P. S., 1968, A numerical Study of Natural Convection in Porous Media, M. S. thesis, Univ. of Calgary, Alberta, Canada.
- Knutson, C. F. and B. F. Bohor, 1963, Reservoir rock behavior under moderate confining pressure in Symposium on Rock Mechanics, Univ. Minnesota, MacMillan, New York, pp. 627-659.
- Lapwood, E. R., 1948, Convection of a fluid in a porous medium, Proc. Cambridge Phil. Soc., v. 44, pp. 508-521.
- Lasseter, T. J. and P. A. Witherspoon, 1974, Underground Storage of Liquefied Natural Gas in Cavities Created by Nuclear Explosives, Geotechnical Engineering Pub. No. 74-1, Univ. Calif., Berkeley.
- Lasseter, T. J., P. A. Witherspoon and M. J. Lippmann, 1975, Multiphase multi-dimensional simulation of geothermal reservoirs, paper submitted to Second United Nations Symposium on the Development and Use of Geothermal Resources, San Francisco, May 20-29.
- Lee, P. C. Y., W. G. Gray and G. F. Pinder, 1975, Thermoenergy transport in porous media, paper in preparation.
- Likke, S. and L. A. Bromley, 1973, Heat capacities of aqueous NaCl, KCl, MgCl<sub>2</sub>, MgSO<sub>4</sub>, and Na<sub>2</sub>SO<sub>4</sub> solutions between 80° and 200°C, Jour. Chem. Engr. Data, v. 18, no. 2, pp. 189-195.
- Lo, H. Y. and N. Mungan, 1973, Effect of temperature on water-oil relative permeabilities in oil-wet and water-wet systems, paper SPE 4505, 48th Annual Meeting SPE-AIME, Las Vegas, Nev., Sept. 30-Oct. 3.
- Marinelli, G., 1969, Some geological data on the geothermal areas of Tuscany, Bull. Volcanol., v. 33, no. 1, pp. 319-334.
- Martin, J. C., 1975, Analysis of internal steam drive in geothermal reservoirs, paper SPE 5382, 45th Annual Calif. Regional Meeting SPE-AIME, Ventura, Calif., April 2-4.
- Masouka, T., 1972, Heat transfer by free convection in a porous layer heated from below, Heat Transfer-Japan Res., v. 1, no. 1, pp. 39-45.
- Matthews, C. S. and D. G. Russell, 1967, Pressure Buildup and Flow Tests in Wells, Soc. Petr. Engr. AIME Mon., v. 1.
- McNabb, A., 1965, On convection in a porous medium, Proc. Australasian Conf. on Hydraulics and Fluid Mechanics, v. 2, pp. C161-C171.

- Mercer, J. W., Jr., 1973, Finite Element Approach to the Modeling of Hydrothermal Systems, Ph.D. dissertation, Univ. of Illinois, Urbana-Champaign.
- Mercer, J. W., Jr., C. F. Faust and G. F. Pinder, 1974, Geothermal reservoir simulation, Proc. NSF Conference on Research for the Development of Geothermal Energy Resources, Pasadena, Calif., Sept. 23-25, pp. 256-267.
- Mercer, J. W. and G. F. Pinder, 1974, Finite element analysis of hydrothermal systems, in Finite Elements in Fluid Flow, J. T. Oden, et al., eds., Univ. Alabama Huntsville Press, pp. 401-414.
- Mercer, J. W., G. F. Pinder and I. G. Donaldson, 1975, A Galerkin-finite element analysis of the hydrothermal system at Wairakei, New Zealand, Jour. Geophys. Res., in press.
- Narasimhan, T. N. and P. A. Witherspoon, 1975, An integrated finite difference method for analyzing fluid flow in porous media, paper submitted to Water Resour. Res.
- Nevens, T. O. and M. J. Pool, 1964, Determination of Thermodynamic Properties of Brines, Denver Research Inst., Contract Research Report 2151.
- Nield, D. A., 1968, Onset of thermohaline convection in a porous medium, Water Resour. Res., v. 4, no. 3, pp. 553-560.
- Nield, D. A., 1974, Comments on 'Effect of solute dispersion on thermal convection in a porous medium layer' by H. Rubin, Water Resour. Res., v. 10, no. 4, p. 889.
- Palm, E., J. E. Weber and O. Kvernfold, 1972, On steady convection in a porous medium, Jour. Fluid Mech., v. 54, part 1, pp. 153-161.
- Platzman, G. W., 1965, The spectral dynamics of laminar convection, Jour. Fluid Mech., v. 23, part 3, pp. 481-510.
- Poston, S. W., S. C. Ysrael, A. K. M. S. Hossain, E. F. Montgomery, III and H. J. Ramey, Jr., 1970, The effect of temperature on irreducible water saturation and relative permeability of unconsolidated sands, Soc. Petrol. Eng. Jour., v. 10, no. 2, pp. 171-180.
- Ramey, H. J., Jr., W. E. Brigham, H. K. Chen, P. G. Atkinson and N. Arihara, 1974, Thermodynamic and hydrodynamic properties of hydrothermal systems, in The Utilization of Volcano Energy, J. L. Colp and A. S. Furumoto, eds., Proc. of Conference, Hilo, Hawaii, Feb. 4-8.
- Ramey, H. J., Jr., P. Kruger and R. Raghavan, 1973, Explosive stimulation of hydrothermal reservoirs in Geothermal Energy, P. Kruger and C. Otte, eds., Stanford Univ. Press, pp. 231-249.
- Rayleigh, Lord, 1916, On convection currents in a horizontal layer of fluid when the higher temperature is on the underside, Phil. Mag., Ser. 6, v. 32, pp. 529-246.
- Rubin, H., 1973, Effect of solute dispersion on thermal convection in a porous medium layer, Water Resour. Res., v. 9, no. 4, pp. 968-974.

- Rubin, H., 1975a, Effect of solute dispersion on thermal convection in a porous medium layer, 2, Water Resour. Res., v. 11, no. 1, pp. 154-158.
- Rubin, H., 1975b, On the analysis of cellular convection in porous media, Unpublished manuscript.
- Rubin, H., 1975c, Effect of hydrodynamic dispersion on thermohaline convection in a porous medium, Unpublished manuscript.
- Sanyal, S. K., S. S. Marsden and H. J. Ramey, Jr., 1972, The effect of temperature on electrical resistivity of porous media, Soc. Prof. Well Logging Assoc., 13th Annual Logging Symposium, May 1972.
- Sestini, G., 1970, Superheating of geothermal steam, Geothermics, Special issue 2, v. 2, pt. 1, pp. 622-648.
- Slattery, J. C., 1972, Momentum, Energy and Mass Transfer in Continua, McGraw-Hill, New York.
- Somerton, W. H., J. A. Keese and S. L. Chu, 1974, Thermal behavior of unconsolidated oil sands, Soc. Petrol. Engr. Jour., v. 14, no. 5, pp. 513-521.
- Sorey, M. L., 1975, Numerical Modeling of Liquid Geothermal Systems, Ph.D. dissertation, Univ. of Calif., Berkeley (in preparation).
- Spillette, A. G. and R. L. Nielsen, 1968, Two-dimensional method for predicting hot waterflood recovery behavior, Jour. Petrol. Tech., v. 20, no. 6, pp. 627-638.
- Straus, J. M., 1974, Large amplitude convection in porous media, Jour. Fluid Mech., v. 64, part 1, pp. 51-63.
- Sun, Z. S., C. Tien and Y. C. Yen, 1972, Onset of convection in a porous medium containing liquid with a density maximum, paper NC2-11, Fourth Intern. Heat Transfer Conf., Paris-Versailles, v. 4.
- Toronyi, R. M., 1974, Two-Phase, Two-Dimensional Simulation of a Geothermal Reservoir and the Wellbore System, Ph.D. dissertation, Pennsylvania State Univ., University Park.
- Vairogs, J., C. L. Hearn, D. W. Dareing and V. W. Rhoades, 1971, Effect of rock stress on gas production from low-permeability reservoirs, Jour. Petrol. Tech., Sept. 1971, pp. 1161-1167.
- Wankat, P. C. and W. R. Schowalter, 1970, Stability of combined heat and mass transfer in a porous medium, Phys. of Fluids, v. 13, no. 9, pp. 2418-2420.
- Weber, J. E., 1975a, Thermal convection in a tilted porous layer, Int. Jour. Heat Mass Transfer, v. 18, pp. 474-475.
- Weber, J. E., 1975b, The boundary-layer regime for convection in a vertical porous layer, Int. Jour. Heat Mass Transfer, v. 18, pp. 659-573.

- Weinbrandt, R. M., H. J. Ramey, Jr. and F. J. Casse, 1972, The effect of temperature on relative and absolute permeability of sandstones, 47th Annual Meeting SPE-AIME, San Antonio, Texas, Oct. 1972.
- Weinstein, H. G., J. A. Wheeler and E. G. Woods, 1974, Numerical model for steam stimulation, paper SPE 4759, SPE-AIME Improved Oil Recovery Symposium, Tulsa, Oklahoma, April 22-24.
- Westbrook, D. R., 1969, Stability of convective flow in a porous medium, Phys. of Fluids, v. 12, no. 8, pp. 1547-1551.
- Whitaker, S., 1968, Introduction to Fluid Mechanics, Prentice-Hall, Englewood Cliffs, N. J.
- Whitaker, S., 1969, Advances in theory of fluid motion in porous media, Ind. Engr. Chem., v. 61, no. 12, pp. 14-28.
- White, D. E., 1957, Thermal waters of volcanic origin, Bull. Geol. Soc. Am., v. 68, pp. 1637-1658.
- White, D. E., 1961, Preliminary evaluation of geothermal areas, paper G.2, U. N. Conf. on New Sources of Energy, Rome, August 21-31.
- White, D. E., 1973, Characteristics of geothermal resources, in Geothermal Energy, P. Kruger and C. Otte, eds., Stanford Univ. Press, pp. 69-94.
- White, D. E., L. J. P. Muffler and A. H. Truesdell, 1971, Vapor-dominated hydrothermal systems compared with hot-water systems, Econ. Geol., v. 66, pp. 75-97.
- Whiting, R. L. and H. J. Ramey, Jr., 1969, Application of material and energy balances to geothermal steam production, Jour. Petrol. Tech., v. 21, no. 7, pp. 893-900.
- Wooding, R. A., 1963, Convection in a saturated porous medium at large Rayleigh number or Péclet number, Jour. Fluid Mech., v. 15, part 4, pp. 527-544.
- Yen, Y. C., 1974, Effects of density inversion on free convective heat transfer in porous layer heated from below, Int. Jour. Heat Mass Transfer, v. 17, pp. 1349-1356.
- Zoback, M. D. and J. D. Byerlee, 1975, Permeability and effective stress, AAPG Bull., v. 59, no. 1, pp. 154-158.

## STEAM TRANSPORT IN POROUS MEDIA

A. F. Moench  
U. S. Geological Survey  
Water Resources Division  
345 Middlefield Road  
Menlo Park, CA 94025

Numerous investigators have pursued development of large-scale two-phase digital simulation models of vapor-dominated geothermal systems. These represent significant advances in the capability to numerically simulate complex systems. However, the basic physical phenomena which are being modeled are still under investigation. The purpose of this discussion is to present the results of a numerical study in which some of the physical phenomena which may occur in vapor-dominated geothermal reservoirs are examined. These phenomena include: (1) superheating of discharging steam, (2) energy changes due to compressible work, (3) conductive heat transport, and (4) gravitational effects of the steam column. Further details pertaining to this study are available in a report by Moench (1976).

The numerical model used in this study draws upon the concepts of White and others (1971) for a vapor-dominated geothermal system, though of necessity some simplifications have been made. The physical system is idealized as a one-dimensional column of porous or highly fractured rock filled with a mixture of steam and liquid water under high pressure. This reservoir is overlaid by a "cap rock" that has low permeability. At the bottom of the reservoir there is a zone where liquid water saturates the pores. Heat is supplied by a magma chamber at depth and transferred upward through the liquid-saturated zone by conduction and convection. The primary mechanisms for heat transfer through the vapor-dominated zone are vaporization and condensation. Figure 1 illustrates the distributions of temperature and pressure to be expected in this idealized natural system.

The model is designed to determine the time-varying distributions of liquid-water saturation, pressure, and temperature within the vapor-dominated region. These distributions may be due to the withdrawal of steam at either constant pressure or constant discharge. Basic assumptions of the model include the following: (1) liquid water within the vapor zone is stationary, but subject to vaporization, (2) Darcy's law is valid for two fluids, (3) the rock matrix is rigid, (4) local thermal equilibrium occurs between the fluids and rock, (5) negligible viscous dissipation, (6) negligible thermal dispersion, and (7) negligible surface tension effects.

To simulate the vertical flow of steam through variably saturated porous media, two controlling equations are used (see Appendix): a

fluid-flow equation and an energy equation. These equations contain parameters which are dependent upon pressure, temperature, and liquid-water saturation. The energy equation accounts for heat conduction, convection, vaporization, compressible work, and heat storage. These partial differential equations are coupled through the velocity terms, the vaporization terms, the liquid saturation, and the pressure- and temperature-dependent parameters. The equations are solved simultaneously at discrete time intervals by a finite-difference technique.

### Results

Figure 2 shows the pressure, temperature, and liquid-water saturation after  $10^9$  sec (31.6 years) of steam production from the top of a one kilometer column of reservoir rock. This represents the effect of removing about 70% of the mass that was initially available. Steam is produced at a rate which declines with time due to withdrawal at constant pressure. All the liquid water in the top 300 m has been vaporized and steam in this region is superheated.

Temperature distributions "A" and "B" in Figure 2 show the influence of heat conduction and compressible work (as defined by the second term on the righthand side of the energy equation). Distribution "A" shows the temperature profile obtained using the complete energy equation. Distribution "B" shows the temperature profile obtained when the compressible work term is omitted from the calculations. It is clear that compressible work is significant only where superheated steam is present. Both profiles show the temperature increase at the top of the reservoir brought about by conduction from the base of the cap rock at a distance of approximately 50 m. Conduction from the cap rock or other nearby rocks not cooled by the vaporization process may be responsible for the temperature increase of produced steam observed in some wells (Sestini, 1970). The time variation in temperature at the top of the reservoir is shown in Figure 3 for curves "A" and "B". In the early part of the production history, the cooling effect of compressible work counteracts the heating due to conduction from the cap rock.

The effect of eliminating gravity from the calculations upon the pressure and temperature distributions is shown by the dashed lines in Figure 2. Apart from its possible influence upon the vertical distribution of liquid water (not included in this study) the effect of gravity can be safely neglected. The weight of the steam column has little, if any, effect upon reservoir production characteristics.

### References

- Moench, A.F., 1976, Simulation of steam transport in vapor-dominated geothermal reservoirs, U. S. Geol. Survey open-file report 76-607, 43 p.

Sestini, G., 1970, Superheating of geothermal steam, Geothermics Special Issue, v. 2, pt. 1, p. 622-648.

White, D.E., Muffler, L.J.P., and Truesdell, A.H., 1971, Vapor-dominated hydrothermal systems compared with hot-water systems, Econ. Geology, v. 66, p. 75-97.

### APPENDIX

The basic equations used in this study are reproduced here for convenience. Additional details and constitutive relationships are given in the report by Moench (1976).

#### Flow Equation

$$\frac{\partial}{\partial z} \left[ \rho_v \frac{k k_r}{\mu_v} \left( \frac{\partial P}{\partial z} - \rho_v g \right) \right] + q + q' = \phi(1-S) \rho_v \kappa \frac{\partial P}{\partial t} - \phi(1-S) \rho_v \beta \frac{\partial T}{\partial t} - \phi \rho_v \frac{\partial S}{\partial t}$$

where

- $\rho_v$  density of the water vapor
- $\mu_v$  dynamic viscosity of the water vapor
- $k$  intrinsic permeability
- $k_r$  relative permeability to water vapor
- $g$  acceleration of gravity
- $\phi$  porosity
- $S$  liquid-water saturation
- $P$  pressure
- $q$  source or sink of steam through wells (positive if source of steam)
- $q'$  source or sink of steam by vaporization or condensation (positive if source of steam)
- $z$  vertical coordinate (positive downward)
- $t$  time
- $\kappa$  compressibility of water,  $\frac{1}{\rho_v} \left( \frac{\partial \rho_v}{\partial P} \right)_T$
- $\beta$  thermal expansivity of water vapor,  $-\frac{1}{\rho_v} \left( \frac{\partial \rho_v}{\partial T} \right)_P$
- $T$  temperature

## Energy Equation

$$\frac{\partial}{\partial z} \left( K \frac{\partial T}{\partial z} \right) - c_1 v \frac{\partial T}{\partial z} - Lq' + Q = [c_1 + c_2 + c_3] \frac{\partial T}{\partial t} - \phi(1-S) T \beta \frac{DP}{Dt}$$

where

- K effective thermal conductivity  
 v average interstitial velocity  
 $c_1$  heat capacity of vapor,  $\phi(1-S)\rho_v c_{pv}$   
 $c_2$  heat capacity of liquid,  $\phi S \rho_l c_{pl}$   
 $c_3$  heat capacity of solid,  $(1-\phi)\rho_s c_{ps}$   
 $\rho_l$  density of liquid water,  
 $\rho_s$  density of solid rock particles  
 $c_{pv}$  specific heat at constant pressure of vapor  
 $c_{pl}$  specific heat at constant pressure of liquid  
 $c_{ps}$  specific heat at constant pressure of solid  
 L latent heat of vaporization  
 Q energy source or sink by means other than condensation  
 or vaporization (positive if source of heat)  
 $\frac{D}{Dt}$  substantial derivative,  $\frac{\partial}{\partial t} + v \frac{\partial}{\partial z}$

## Liquid-Water Saturation Equation

$$\frac{\partial S}{\partial t} = - \frac{q'}{\phi \rho_l}$$



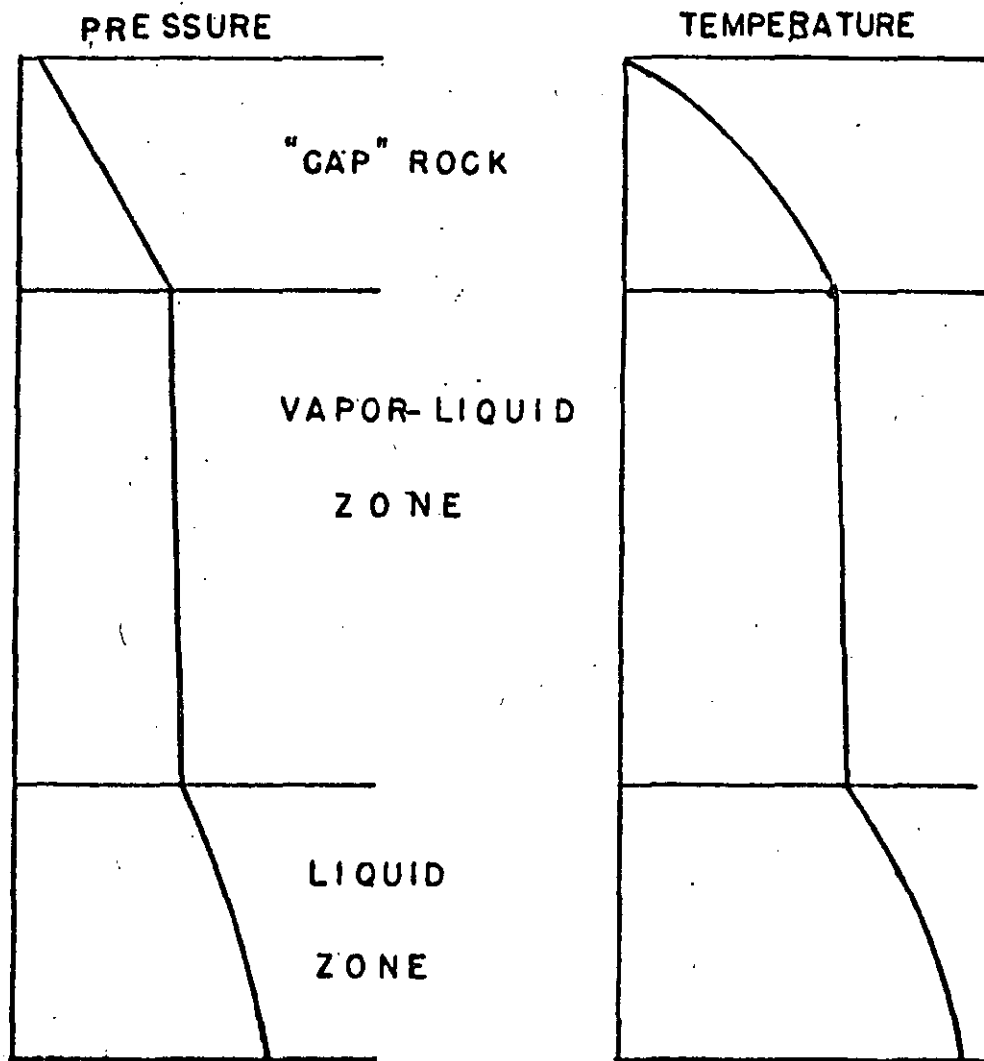
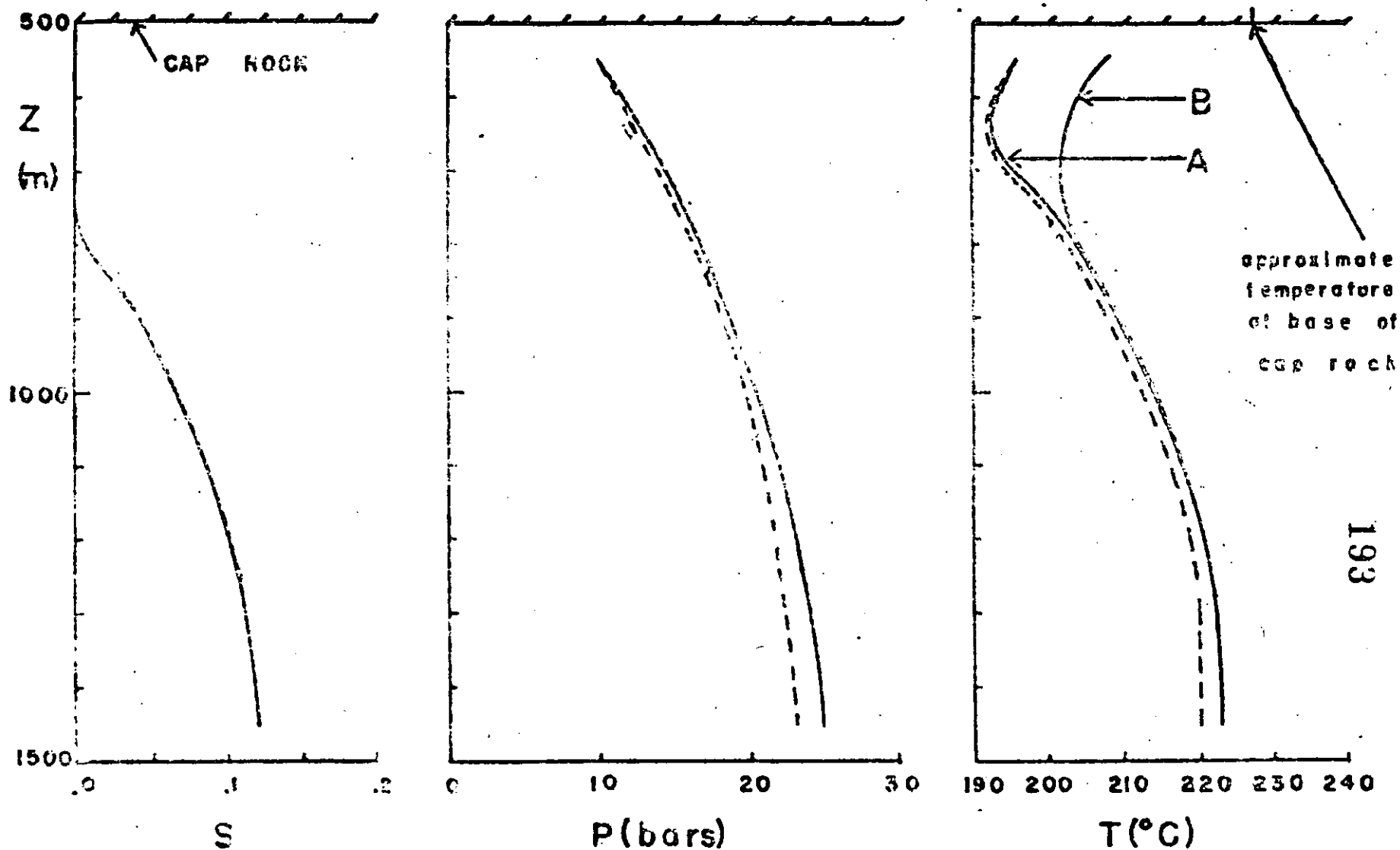


Figure 1. Vertical temperature and pressure distributions in an idealized natural vapor-dominated system.

FIGURE 2. Pressure, temperature and liquid water saturation distributions in a one-kilometer column of reservoir rock which has been producing steam at a pressure of 10 bars for  $10^9$  sec. 500 m of cap rock overlies the reservoir. Dashed lines indicate effect of eliminating gravity.



initial pressure at top = 30 bars  
 initial saturation = 0.2  
 porosity = 0.2  
 permeability = 10 md

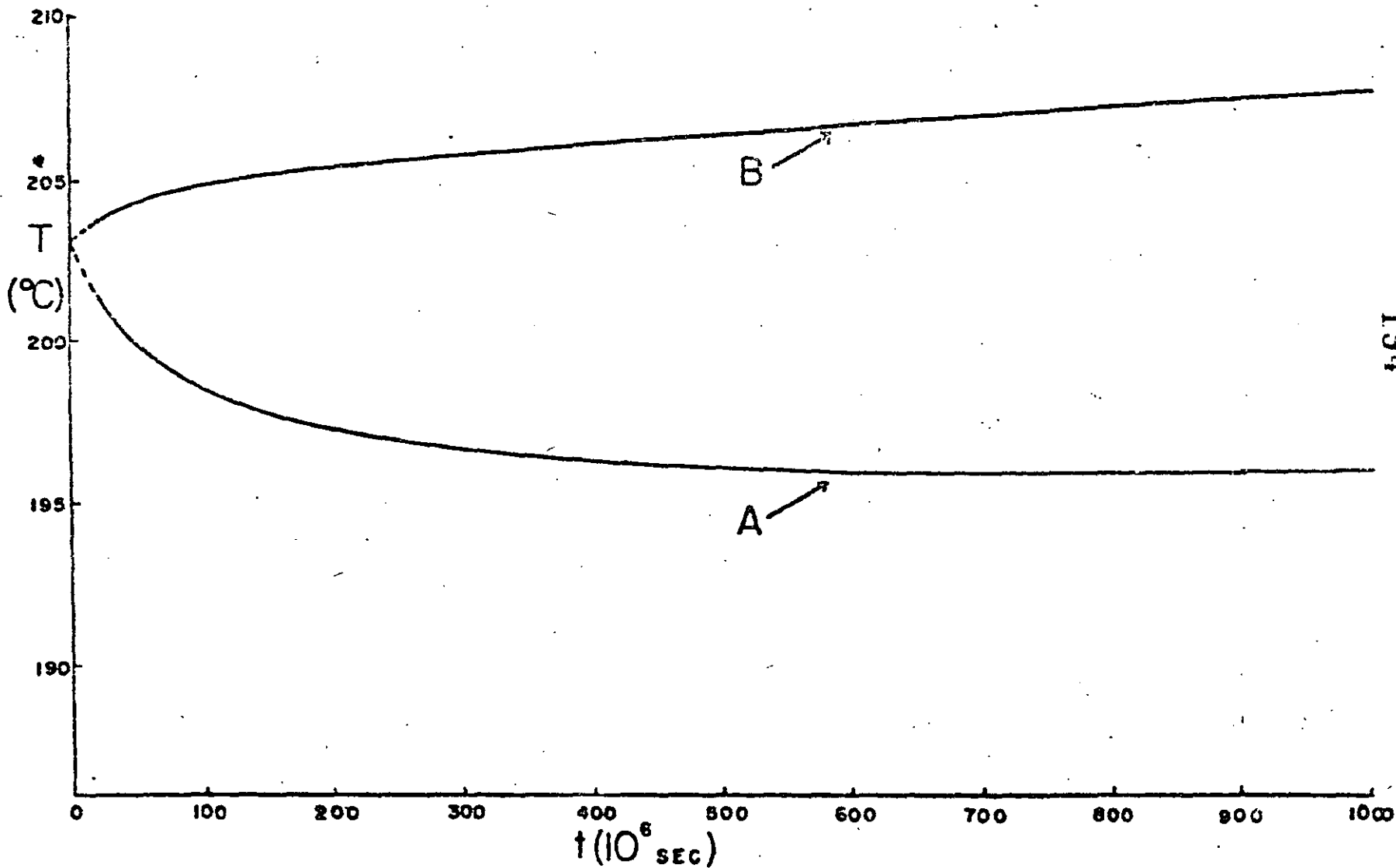


Figure 3. Temperature versus time at top of reservoir for conditions shown in Figure 2.



**DIVISION DE EDUCACION CONTINUA  
FACULTAD DE INGENIERIA U.N.A.M.**

CURSO: "INGENIERIA DE YACIMIENTOS GEOTERMICOS"  
13 DE MARZO AL 18 DE MAYO DE 1984

THERMODYNAMIC AND HYDRODINAMIC PROPERTIES  
OF HYDROTHERMAL SYSTEMS

PROF. DR. HEBER CINCO LEY  
26-30 de marzo

Fortunately there is an extensive body of literature available to help one estimate many of these fluid and rock properties. Much of this information can be found in the petroleum literature, for the petroleum industry has had an interest in the use of underground heat for oil recovery since the early 1900's. In the paper we summarize some of the data that is useful for geothermal systems. A large fraction of these data are extracted from the petroleum literature.

#### STORAGE AND TRANSPORT OF HEAT IN ROCKS

Neglecting heat of phase change and heat of reaction, there are three important thermal properties in any process involving heat transfer: thermal conductivity, heat capacity, and thermal diffusivity. Thermal conductivity is generally shown by the symbol,  $k$ , and units in the c-g-s system are cal/sec-cm-°C. Many of the references, however, are given in British thermal units, Btu/hr-ft-°F. The conversion factor is:

$$1 \frac{\text{Btu}}{\text{hr-ft-}^\circ\text{F}} = \frac{4,134 \times 10^{-3} \text{ cal}}{\text{sec-cm-}^\circ\text{C}} \quad (1)$$

The specific heat generally used is the specific heat at constant pressure, or  $(\partial H/\partial T)_p$ , and the symbol is  $C_p$ . The c-g-s unit, cal/gm-°C, is numerically the same as the British unit, Btu/lb-°F. Thermal diffusivity is a collection of terms,  $k/\rho C_p$ , where  $\rho$  is the density. It is often indicated by the symbol  $\alpha$ . This grouping is the ratio of the ability to transfer heat,  $k$ , to the ability to store heat,  $\rho C_p$ . In the c-g-s system the dimensions are cm<sup>2</sup>/sec, and in the British system ft<sup>2</sup>/hr. Many references use British units. The conversion factor is:

$$1 \frac{\text{ft}^2}{\text{hr}} = \frac{0.258 \text{ cm}^2}{\text{sec}} \quad (2)$$

### Thermal Conductivity

An early evaluation of rock thermal conductivity was made by Birch and Clark.<sup>1,2</sup> They studied a broad range of rock materials including some eighteen igneous rocks, seven sedimentary and metamorphic rocks, and certain single crystals and glasses. With the exception of the anorthosites and the glasses (both man-made and natural) all the materials showed a reduction of thermal conductivity with temperature increase. This behavior is as should be expected. See Figures 1 and 2, from Birch and Clark.<sup>1</sup>

Probably the most important finding by Birch and Clark was that the thermal conductivity of a mixture could be estimated by assuming that the various components of the system were in series. The total thermal resistivity of the system is equal to the volumetric weighted average of resistivity of each component. The total conductivity is thus the harmonic average:

$$\frac{1}{k_{\text{ave}}} = \frac{x_1}{k_1} + \frac{x_2}{k_2} + \dots + \frac{x_n}{k_n} \quad (3)$$

where  $x$  = volumetric fraction of each component.

Birch and Clark's data were mostly for rocks of low porosity. Somerton<sup>3</sup> was an early investigator of the thermal conductivity of fluid-containing rocks. He studied unconsolidated sands, sandstones, silty sandstones, siltstone, shale and limestone. He developed an empirical equation to predict the effect of fluid saturation on the thermal conductivity of porous rocks. It was:

$$\frac{k}{k_1} = \left( \frac{k_2}{k_1} \right)^{c\phi} \quad (4)$$

where  $k$  = thermal conductivity of fluid-saturated rock

$k_1$  = thermal conductivity of rock solids

$k_2$  = thermal conductivity of saturating fluid

$\phi$  = porosity - fraction

$c$  = empirical constant approximately equal to 1.

The empirical constant,  $c$ , was actually found to range from 0.9 to 2.3 with the larger values found at lower porosities. The product,  $c\phi$ , ranged from 0.325 to 0.460.

In 1961 Kunii and Smith<sup>4</sup> measured thermal conductivities of porous rocks saturated with various fluids. They proposed an equation (their Eqn. 3) to relate the fluid saturated conductivity to the conductivity of dry rock. Some of their results are reproduced here as Figures 3 and 4 to show the correspondence of their data to their model. Water may increase conductivity more than two-fold depending on the nature of the porous medium. Their data were run on Boise, Bartlesville, Berea and Rangely sandstones.

Smith and his coworkers<sup>5,6</sup> also studied the effect of fluid flow on the thermal conductivity of porous systems. In general they found that thermal conductivity in the direction of flow was increased as the flow velocity increased.<sup>5</sup> Figure 5 shows this effect with water and brine. They made a correlation of this effect through use of the product of the Reynolds' Number and the Prandtl Number (Fig. 6). Thermal conductivity perpendicular to the direction of flow, however, remained nearly constant--unaffected by flow rate.<sup>6</sup>

Anand, Somerton and Gomaa<sup>7</sup> recently have shown empirical methods of predicting thermal conductivities of fluid saturated rocks when there is little thermal data available. These methods are based on regression analysis equations. The thermal conductivity of dry rock (containing air) was correlated as follows:

$$\lambda_d = 0.3386 \rho^{1.034} - 3.194 \phi + 0.5304 k^{0.100} + 0.0131 F - 0.0311 \quad (5)$$

where  $\lambda_d$  = thermal conductivity of dry rock, Btu/hr-ft-°F  
 $\rho$  = bulk density, gm/cc  
 $\phi$  = fractional porosity  
 $k$  = permeability, millidarcies  
 $F$  = formation electrical resistivity factor

The formation resistivity factor is a common formation evaluation term which can be extracted from electric logs. It is the ratio of the actual resistivity to that if the rock pores were totally filled with formation water. In the absence of data on this parameter, the following empirical relationship can be used:

$$F = 1/\phi^m \quad (6)$$

where  $m$  = cementation factor, often near 2.0 for sandstones.

Where the rock is fluid saturated the thermal conductivity is higher, and Anand, et al., found the following empirical equation was useful:



$$\frac{\lambda_s}{\lambda_d} = 1 + 0.299 \left[ \left( \frac{\lambda_f}{\lambda_a} \right)^{0.330} - 1 \right] + 4.57 \left[ \frac{\phi}{(1-\phi)} \frac{\lambda_f}{\lambda_d} \right]^{0.482m} \left( \frac{\rho_s}{\rho_d} \right)^{-4.30} \quad (7)$$

where  $\lambda_s$  = thermal conductivity of fluid-saturated rock,  
Btu/hr-ft-°F

$\lambda_f$  = thermal conductivity of the saturating fluid

$\lambda_a$  = thermal conductivity of air

$\rho_s$  = bulk density of saturated rock

$\rho_d$  = bulk density of dry rock

Lastly, the effects of temperature were included. Anand, et al., used a modification of Tikhomirov's<sup>8</sup> correlation to show this effect.

Their results were as follows:

$$\lambda_T = \lambda_{68^\circ} - 0.709 \times 10^{-3} (T - 528) (\lambda_{68^\circ} - 0.800) \cdot \left[ \lambda_{68^\circ} \left( T \times 10^{-3} \right)^{0.545} \lambda_{68^\circ} + 0.738 \right] \quad (8)$$

where  $\lambda_T$  = thermal conductivity at temperature, T, Btu/hr-ft-°F

$\lambda_{68^\circ}$  = thermal conductivity at 68°F

T = temperature, °R = °F + 460

A graph of their data compared to this equation is shown in Figure 7. The match appears to be satisfactory. The equation properly predicts that high conductivity materials have lower thermal conductivity at higher temperatures, while low conductivity materials exhibit increasing conductivities with temperature.

Often rocks contain two fluids rather than one. Goma and Somerton<sup>9,10</sup> discuss this effect in two recent papers. If both fluids are liquid, or if neither fluid is boiling or condensing, the thermal conductivity of the system is a simple square root relationship between the thermal conductivity and the fluid content, as follows:

$$\lambda - \lambda_1 = (\lambda_2 - \lambda_1) (S_2)^{1/2} \quad (9)$$

where  $\lambda$  = thermal conductivity of rock containing two fluids  
 $\lambda_1$  = thermal conductivity of rock saturated with fluid 1  
 $\lambda_2$  = thermal conductivity of rock saturated with fluid 2  
 $S_2$  = the fraction of pore space filled with fluid 2

If the fluids are a liquid and vapor in equilibrium with each other, for example water and steam, the thermal conductivity may be far higher than predicted by Eqns. 8 and 9. The combination of heat transfer by boiling and mass flow by capillary pressure effects can cause the effective thermal conductivity to increase 2 to 5 fold. This is called the "heat pipe" effect. The amount of increase depends on the permeability of the rock, the latent heat of vaporization, the vapor saturation and the direction of heat flow with respect to gravity. The empirical equation they found to predict this additional term is as follows:

$$\lambda_{HP} = 0.003 \phi^{0.357} k^{0.424} \frac{LY}{\sqrt{v_l v_v}} (1 + 0.107 \sin \phi) F(S) \quad (10)$$

$$F(S) = \sin \left[ \frac{\pi(1-S_l)}{1-S_{lc}} \right] \sin \left[ \frac{\pi(1-S_v)}{1-S_{vc}} \right] \cdot \left[ 0.74 + 0.61S_v + 1.56S_v^2 + 2.85S_v^3 \right] \quad (11)$$

$$S_{lc} = 0.098 k^{-0.236} \quad (12)$$

$$S_{vc} = 0.060 k^{-0.236} \quad (13)$$

where  $S_l$  and  $S_v$  = the fraction of pore space filled with liquid and vapor, respectively

$\phi$  = porosity, fraction

$k$  = permeability, darcies

$L$  = latent heat of vaporization, Btu/lb

$\gamma$  = vapor pressure-temperature derivative, lb/in<sup>2</sup>-°F

$\nu_l$  and  $\nu_g$  = viscosity of liquid and vapor, ft<sup>2</sup>/day

$\psi$  = angle of heat flow direction, positive upward

$\lambda_{HP}$  = additional thermal conductivity due to heat pipe effect, Btu/hr-ft-°F

By this stage, it should be clear that there is a problem in this study with respect to symbols and units. The symbol  $k$  has been used widely to represent both the thermal conductivity and permeability. Even the Greek symbol  $\lambda$  has been used often in various literatures to represent both heat and fluid conductivities of porous solids. Rather than totally recast equations in a single set of symbols and units, we have elected to preserve the symbols of the original study, where possible, and to define symbols and units where presented. This is done because the purpose of

of studies such as this is usually to guide a reader to further information, rather than to replace it. The pertinent literature is far too voluminous for a single paper to serve a true summary purpose.

We turn now to a review of pertinent information on heat capacity and density.

### Heat Capacity and Density

Somerton's<sup>3</sup> data on heat capacity of rocks shows that most reservoir materials behave similarly. Figure 8 shows some of the results of his work. Martin and Dew<sup>11</sup> point out that these data can be approximated roughly by a linear equation for heat capacity as a function of temperature:

$$c_p = \frac{T + 2000}{10,000} \quad (14)$$

where  $c_p$  = heat capacity of rock, Btu/lb-°F  
 $T$  = temperature, °F

Somerton also found that where rock is made up of minerals with many differing materials, the average heat capacity follows Kopp's Law, which states that the heat capacity is the mass weighted average of the constituents.

In general, rock volume changes only slightly with temperature. Further, many rocks containing large percentages of quartz behave much alike. Figure 9 shows the data of Somerton and Selim<sup>12</sup> for three sandstones and quartz. There is little difference in the results for the four materials.

### Thermal Diffusivity

Because the thermal conductivity of many materials behaves similarly as a function of temperature, and because many materials have similar heat capacity-temperature behavior, it seems logical to expect that thermal diffusivity-temperature relationships will agree for many materials.

The data of Somerton and Boozer<sup>13</sup> show that, indeed, many porous materials do exhibit similar trends in thermal diffusivity as a function of temperature. A notable exception was found with a tuffaceous sandstone, as seen in Figure 10; however, a fairly good approximating line could be drawn through the rest of the data in Figure 10. Thus use of this figure for quick estimation appears reasonable.

### Heats of Phase Change and Reaction

In gas and oil reservoirs, very low heats of phase change and low heats of solution, plus the high heat capacity of the solid phase (rock) due to high mass of rock leads to nearly isothermal behavior for most fluid production thermodynamic paths. Exceptions are: (1) the process of oil recovery by underground combustion<sup>57</sup> and (2) oil recovery by steam injection.<sup>58</sup> The first involves release of large amounts of heat due to oxidation of a part of the oil, and the second releases heat by condensation of the injected steam. Actually several types of spontaneous oil oxidation reactions may occur leading even to ignition.<sup>59</sup> There appears little purpose to cite existing studies of oil oxidation reaction kinetics, other than to warn such information is available should pore space reactions become important in geothermal energy extraction. We turn now to a consideration of the effects of elevated temperatures on the flow characteristics of porous rocks.

TEMPERATURE AND PRESSURE EFFECT ON PERMEABILITY OF POROUS MEDIA

It is well known that the viscous flow of fluids through porous media follows Darcy's Law, which is expressed as:

$$v = -\frac{k}{\mu} \left[ \frac{dp}{ds} - \rho g \frac{dz}{ds} \right] \quad (15)$$

where  $v$  is volume rate of flow across a unit area of the porous medium,  $k$  is permeability of the medium to a fluid at constant temperature,  $\mu$  is viscosity of the fluid,  $p$  is pressure,  $\rho$  is the density of the fluid,  $g$  is the acceleration due to gravity,  $z$  is the vertical coordinate, and  $s$  is the coordinate along the direction of flow.

The permeability of a porous medium to a gas phase usually exceeds the permeability of the same medium to a liquid phase. The difference in these permeabilities is due to the phenomenon known as slip<sup>14</sup>, reactions between liquids and the solid, and relative permeabilities. Slip is related to the mean free path of the gas molecules. Consequently, the permeability of a porous medium to gas should be a function of the temperature, pressure, and the nature of the gas. Klinkenberg<sup>14</sup> developed the relation between the permeability of a porous medium to gas and to a non-reactive liquid, viz:

$$k_g = k_l \left( 1 + \frac{4C\bar{\lambda}}{r} \right) \quad (16)$$

This equation was derived assuming that all the capillaries in the porous medium are of the same diameter, and are oriented at random through the

solid material. In Eqn. 16,  $k_g$  and  $k_l$  are permeabilities respectively to gas and to a single liquid phase completely filling the pores of the medium at constant temperature,  $\bar{\lambda}$  is the mean free path of the gas molecules,  $r$  is the radius of capillaries, and  $c$  is a proportionality constant. Then, the mean free path can be expressed as:

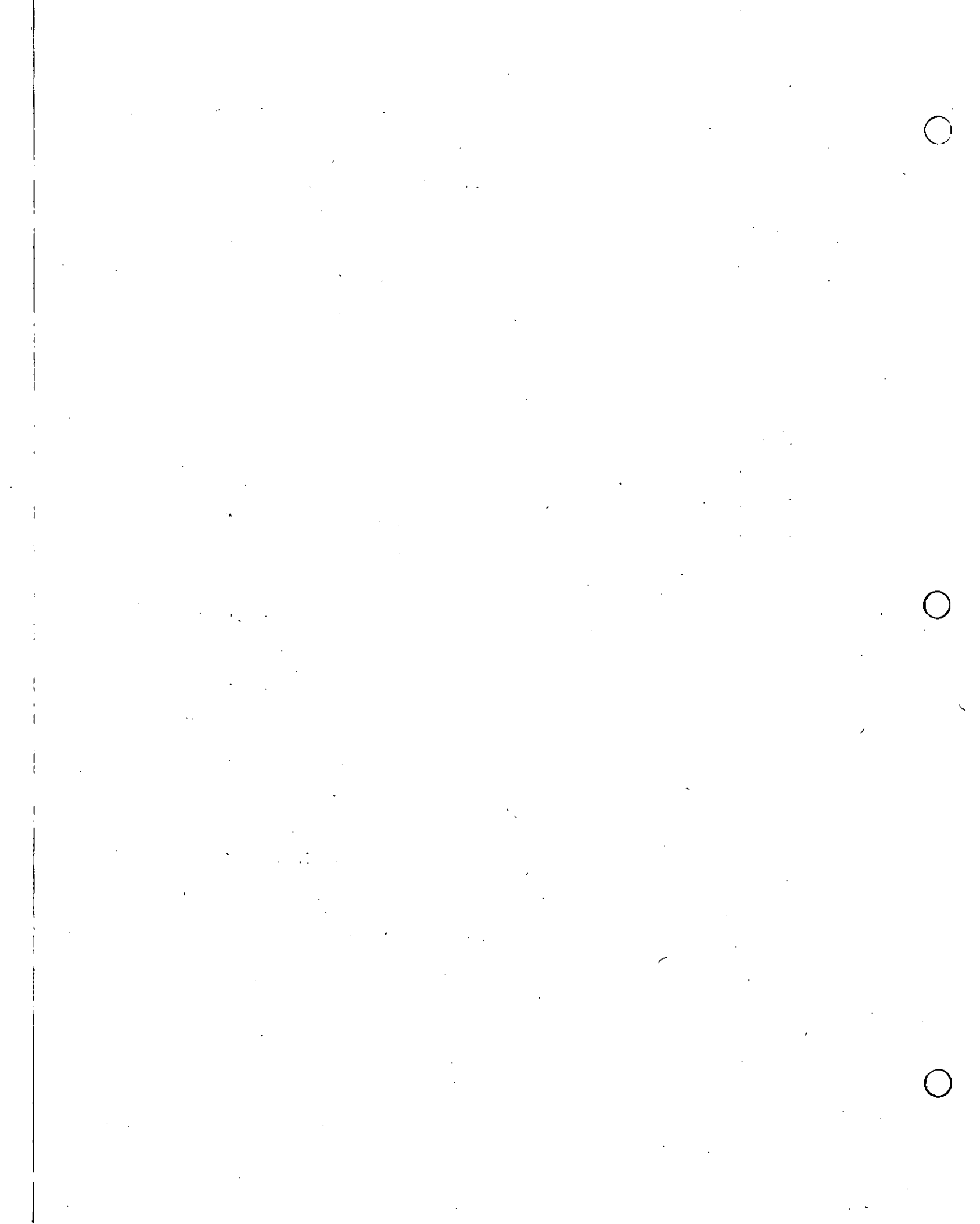
$$\bar{\lambda} = \frac{1}{\sqrt{2\pi} d^2 n} = \frac{RT}{\sqrt{2\pi} p_m N d^2} \quad (17)$$

where  $d$  is collision diameter,  $n$  is concentration of molecules per unit volume,  $N$  is Avogadro's Number,  $p_m$  is mean pressure,  $T$  is temperature, and  $R$  is universal gas constant. Therefore, by combining Eqns. 16 and 17, we obtain:

$$k_g = k_l \left( 1 + \frac{4CRT}{\sqrt{2\pi} r N d^2 p_m} \right) = k_l \left( 1 + \frac{b}{p_m} \right) \quad (18)$$

where  $b$  is called the Klinkenberg factor, which is constant for a given gas and a given porous medium at a constant temperature. As easily seen from Eqn. 18, a graph of  $k_g$  vs.  $1/p_m$  should result in a straight line with an intercept of  $k_l$  and a slope of  $b k_l$  as shown in Figure 11. Slope must become steeper as the temperature increases. Thus, the permeability to a gas is greater at low pressures, and is at a minimum at a maximum pressure of flow.

The permeability defined in Eqn. 15 requires that the porous medium is saturated completely with one homogeneous, single-phase fluid. The permeability thus defined is called the absolute permeability. When the





Contact angles of less than  $90^\circ$ , measured through the water phase, indicate preferentially water-wet conditions, whereas contact angles greater than  $90^\circ$  indicate preferentially oil-wet conditions. The distribution of either the wetting or non-wetting phase within the pore spaces does not depend solely upon the saturation of that phase, but depends also upon the direction of the saturation change. The terms "drainage" and "imbibition" refer to flow resulting in a decrease and increase, respectively, in the wetting phase saturation.

Since the wettability and direction of saturation change influence the fluid distribution, these factors would be expected to affect similarly both the capillary pressure and relative permeability characteristics. The capillary pressure,  $p_c$ , in porous media is defined as the pressure difference existing across the interface separating two immiscible fluids at rest, one of which wets the surfaces of the rock in preference to the other. The water-oil capillary pressure is defined as the pressure in the oil phase minus the pressure in the water phase, or:

$$p_c = p_o - p_w \quad (20)$$

For the gas-liquid case (or steam-water):

$$p_c = p_g - p_l \quad (21)$$

Figure 13 shows the capillary pressure characteristics of a strongly water-wet rock. It is seen in Figure 13 that the pressure in the oil phase (non-wetting) must exceed that in the water phase (wetting) before oil will enter the initially water-saturated rock. This would also be seen in a steam-water system. This entrance pressure is referred to as the threshold pressure

or displacement pressure. The minimum saturation point in Figure 13 gives the irreducible water saturation.

It has long been recognized that the vapor pressure above the curved surface of a liquid is a function of the curvature of the liquid surface. The capillary pressure is also a function of the curvature of the liquid surface. Considering that the liquid and vapor respectively are the wetting and non-wetting phases, the capillary pressure, pertaining to static equilibrium at curved surfaces of vapor-liquid phase separation, may be written as<sup>16</sup>:

$$p_c = p_g - p_{g'} + \frac{RT}{Mv_l} \ln \frac{p_{g'}}{p_g} \quad (22)$$

where  $p_g$  is the pressure in the vapor phase,  $p_{g'}$  is the equilibrium vapor pressure of the liquid above a flat surface,  $M$  is the molecular weight, and  $v_l$  is the specific volume of liquid. Then, the pressure in the liquid phase is:

$$p_l = p_{g'} - \frac{RT}{Mv_l} \ln \frac{p_{g'}}{p_g} \quad (23)$$

As the liquid is the wetting phase,  $p_{g'}$  is greater than  $p_g$ . Then  $p_l$  is smaller than  $p_{g'}$ . Therefore, if liquid pressures and temperatures are measured in the two-phase portion of the porous medium, liquid pressures must be lower than the normal (plane-surface) saturation pressures corresponding to the measured temperatures. Since capillary pressure values are a function of the liquid saturation, the vapor pressure lowering must be a function of the liquid saturation of the porous medium.

### Relative Permeability

Figure 14 shows typical water-oil relative permeability characteristics for a water-wet core.<sup>17</sup> In this figure the permeability to oil at reservoir connate water saturation was used as the base value for relative permeabilities. These data were taken for the case where the water saturation increased while the oil saturation decreased. If the data had been taken for decreasing water saturation, there would be a marked difference. The water (wetting phase) permeability data would be unchanged, but the oil (non-wetting phase) permeabilities would have been higher, especially at the right hand side of the graph. Further, the end points of the curves--the irreducible water saturation and the residual oil saturation--likely would have changed.

Muskat, et al.,<sup>18</sup> presented relative permeability curves for gases and liquids in unconsolidated sands, as given in Figure 15, which shows that for practical purposes the curves for the relative permeabilities  $k_{rg}$  and  $k_{rl}$  are independent of the nature of the unconsolidated sand. This is in marked contrast with most consolidated media, where the relative permeabilities must nearly always be measured, for they vary widely depending on the nature of the fluids and the porous system.

### Temperature Effect on Relative Permeability

The relative permeability is affected by the test environment. The important factors are temperature, pressure, fluids and core condition. Several investigators have reported experimental results of the effect of temperature on relative permeability.

Poston, et al.,<sup>19</sup> using unconsolidated sand, found that the irreducible water saturation increased and the residual oil saturation decreased

with increasing temperature, as shown in Figures 16 and 17. This observation can be seen another way by considering Figure 14. In effect the higher temperature caused both relative permeability curves to shift to the left on the saturation axis. Poston, et al., speculated that if the relative permeability has changed, the capillary pressure should also be temperature sensitive.

Sinnokrot, et al.,<sup>20</sup> studied capillary pressure behavior of three consolidated sandstones and one limestone sample over a temperature range of 75° to 325°F by the restored state method. Their work confirmed the observation of Poston, et al., that the irreducible water saturation increased and apparent residual oil saturation decreased with increase in temperature. They concluded that capillary pressure curves for sandstones were displaced toward higher wetting phase saturations with an increase in temperature level, indicating an increase in water wetness with temperature level increase. Figure 18 shows part of their work.

Weinbrandt, et al.,<sup>21</sup> found results similar to Poston's when increasing from room temperature to 175°F in Boise sandstone. Representative data are shown in Figure 19. They also obtained data on absolute permeability in an increasing temperature level sequence from 75 to 315°F, as shown in Figure 20. The absolute permeability decreased drastically as temperature increased. Afinogenov<sup>22</sup> found similar results up to temperatures of 212°F.

Lo and Mungan<sup>23</sup> also studied relative permeabilities as a function of temperature and found results similar to Weinbrandt, et al. and Poston. They also studied systems of differing wetness characteristics and the results were found to be similar in both oil-wet and water-wet systems.

Poston, et al., pointed out that the changes in rock-fluid characteristics as functions of temperature level were all in a direction suggestive of an increase in water wetness with temperature increase. Contrary to this, Weinbrandt, et al., considered that temperature induced changes were too large to be explained by obvious factors such as change in contact angle interfacial tension, etc. They speculated that most of the above observations concerning temperature sensitivity may have been a result of thermally-induced mechanical stress. Work is continuing to attempt to clarify these results and the reasons for them.

#### Pressure Effect on Pore Volume

Von Gonten and Choudhary<sup>20</sup> investigated experimentally the temperature effect on pore volume compressibility, which is defined as:

$$c_f = -\frac{1}{V_p} \left[ \frac{\partial V_p}{\partial p} \right]_T \quad (24)$$

where  $V_p$  is pore volume and  $p$  is compacting pressure which is equal to overburden pressure minus pore pressure. Figure 21 is a plot of cumulative fractional pore volume change versus compacting pressure for sandstone at 75°F and 400°F. The pore volume compressibility, which is the slope of these curves, becomes smaller at higher pressure.

Somerton and Selim<sup>12</sup> showed the effect of temperature on sandstone volume, as indicated earlier in the paper in Figure 9.

### Pressure Effect on Permeability

Afinogenov<sup>22</sup> presented data on the absolute permeability decrease as affected by external pressure. From his data he introduced an empirical formula to predict this effect:

$$\frac{k_p}{k_o} = \left( 1 + \frac{127 \times 10^{-5}}{p} \right)^{-1} \quad (25)$$

where effective pressure,  $p$ , is defined as:

$$p = p_{con} - 0.85 p_{pore}$$

$p_{con}$  and  $p_{pore}$  are confining pressure and pore pressure respectively in atmospheres. He deduced that this permeability decrease was due to a decrease in the cross-sectional area of the pores and to a more torturous pore space configuration under the effect of pressure.

Zoback and Byerlee<sup>25</sup> measured the permeability of Berea sandstone as a function of both confining pressure and pore pressure. They reported that the permeability decreased with increased confining pressure, and increased as pore pressure was increased. Qualitatively, this agrees with Afinogenov's results. They found also that pore pressure had a significantly larger effect upon permeability than did confining pressure. This does not agree with the results of Afinogenov. They speculated that the matrix through which the fluid flows has a higher compressibility than does the granular framework through which the confining pressure stresses are transmitted.

Many other investigators, such as Fatt and Davis<sup>26</sup>, Wyble<sup>27</sup>, Dobrynin<sup>28</sup>, Gray, et al.<sup>29</sup>, and Wilhelmi and Somerton<sup>30</sup>, have reported the effect of overburden pressure on the permeability of sandstone. Figure 22 is the

experimental results provided by Fatt and Davis. The permeability of sandstone decreased with increase in overburden pressure. Most of the decrease took place over the range of zero to 3000 psi overburden pressure.

#### PHYSICAL STATES OF WATER

The physical states of water of interest in geothermal reservoirs are: compressed liquid, saturated liquid, superheated (also called dry or unsaturated) steam, saturated (or wet) steam, and the dense fluid state.

The term "saturation" may thus have several meanings in geothermal reservoir engineering. "Saturation" can refer to: (1) the volume fraction of pore space occupied by a fluid phase, (2) the thermodynamic state of the fluid phases with reference to some appropriate vapor pressure curve, and (3) the usual sense of solids and gases being dissolved in a liquid phase. Care must be used that the term "saturation" is not misunderstood.

Figure 23 is a graph of the vapor pressure curve of water, showing the position of the critical point at 221.07 bar and 374.1°C (3206.2 psia and 705.4°F). Point A on this figure is in the superheated steam region, point B is at saturation conditions where both liquid and vapor may coexist, and point C is in the compressed liquid region. Points D and E are in the dense fluid region. Figure 24 is an expanded form of Figure 23 showing the initial thermodynamic state of various geothermal fields around the world. Note that the geopressured aquifers found in the Gulf Coast area of the United States, with temperatures of 260°C (500°F) and pres-

tures in excess of 700 bar (10,000 psia), are off the scales of both Figures 23 and 24, and might be considered as dense fluids.

Gibb's Phase Rule teaches that in order to specify the thermodynamic state of a single phase of water, two independent thermodynamic properties (e.g., pressure and temperature) must be specified. But if two phases are present (e.g., saturated steam and water) specification of only one intensive property defines the system. A geothermal aquifer at saturated conditions must follow some appropriate vapor pressure curve as fluid is produced.

It can be shown from thermodynamic analysis that a geothermal system initially containing a single-phase fluid (either compressed liquid or superheated steam) will tend to deplete isothermally. But once two phases form, a system should deplete along some sort of vapor pressure curve appropriate for the fluids in the pore space.

#### Properties of Interest

A thermodynamic equation of state for water expresses the pressure-volume-temperature (PVT) relationships. These describe the specific volume,  $v$ , (or density,  $\rho = 1/v$ ) as a function of pressure and temperature for the various phases. In addition we require the energy related properties, specific enthalpy,  $h$ , and specific entropy,  $s$ , and specific heats,  $c_p$  and  $c_v$ .

The transport properties that are important are viscosity and thermal conductivity. Viscosity is basically an internal resistance of the fluid to flow, due to molecular interaction. Thermal conductivity affects the rate of heat transfer of the rock-fluid system.



Data describing the forementioned properties for impure water is meager, although a fair amount is known about the solubility of numerous substances found in geothermal waters. Ionic equilibrium calculations can be used to estimate which chemicals will remain dissolved, and which ones will precipitate under changing pressure, temperature, and composition conditions. The reader is referred to textbooks on geochemistry (Krauskopf<sup>31</sup>) and ionic equilibrium calculations (Butler<sup>32</sup>) and also to work on the chemistry of geothermal systems by White<sup>33</sup>, Fournier and Truesdell<sup>34</sup>, and Helgeson.<sup>62</sup>

#### Equations of State

Since the early part of this century there has been an international effort to standardize the various thermodynamic and transport properties of pure water. The well-known Keenan and Keyes<sup>35</sup> steam tables were a result of these efforts. The ASME Steam Tables<sup>36</sup> are one of the more recent products of these efforts, and are used as a basis for much of the data in this report. These tables present the results of a series of accurate matching of analytic functions (the 1967 IFC Formulation for Industrial Use) to accepted and standardized experimental data (the 1963 International Skeleton Tables). The results are presented in tabular and graphical form. The analytic functions are also given, and can be programmed for use on a computer. Another recent source of water properties is the Steam Tables by Keenan, et al.<sup>37</sup>

The rest of this review will be devoted to describing the properties mentioned above, both for pure and impure water. Data will be presented in tabular or graphical form, and several simplified analytic forms will be discussed.

Pure Saturated Steam and Water

For conditions below the critical state (221.07 bar, 374.1°C; 3206.2 psia, 705.4°F) the liquid and vapor phases can coexist in equilibrium. When liquid and vapor are in equilibrium they are described as being saturated, and such states lie along the vapor pressure curve (see Figures 23 and 24). This curve is of great interest, and a number of simplified analytic approximations have been presented. A few will be given here. Whiting and Ramey<sup>30</sup> used an integrated form of the Clausius-Clapeyron equation to develop the following approximation by a least mean square curve match over the temperature range 150-315°C (300-600°F):

$$\ln p = \frac{-4667.0754}{(T + 273)} + 12.59833 ; \text{ where } p = \text{bar, } T = \text{°C.} \quad (26-a)$$

Or:

$$\ln p = \frac{-8400.7358}{(T + 460)} + 15.272703 ; \text{ where } p = \text{psia, } T = \text{°F.} \quad (26-b)$$

This match is claimed to have an average difference from the actual data of only 0.048%.

In oil and gas technology, the Cox Chart is a useful empirical technique for representing the vapor pressure curves of hydrocarbon fluids. This is a graph of  $\ln p$  vs.  $1/(T-77.4)$ ,  $T$  in °R, and it is useful because both hydrocarbon and water vapor pressure curves tend to graph as straight lines. Thus, by choosing two points for water at opposite ends of the vapor pressure curve we can determine that the equation of this straight line is of the form:<sup>61</sup>

$$\ln p = \frac{-7001.4928}{(T + 382.2)} + 14.46928 ; \text{ where } p = \text{psia}, T = ^\circ\text{F}. \quad (27)$$

This function is a match over the whole vapor pressure curve, whereas the Whiting and Ramey approximation is for the range 150-315°C. Finally, Farouq Ali<sup>39</sup> observed that a graph of pressure vs. temperature on log-log paper yields a straight line. Hence:

$$T = 115.1 p^{0.225} \quad (T = ^\circ\text{F}, p = \text{psia}) \quad (28-a)$$

or

$$T = 116.7 p^{0.225} - 17.778 \quad (T = ^\circ\text{C}, p = \text{bar}) \quad (28-b)$$

Equation 28 is reported to have a maximum of 1% error over the pressure range 1-200 bar (10-3,000 psia).

The specific volume of saturated steam,  $v_g$ , and water,  $v_f$ , are shown as a function of pressure on Figure 25. The overall specific volume of mixtures of steam and water can be determined at a particular pressure (or temperature) if the quality,  $x$ , of the mixture is known. Quality is defined:

$$x \triangleq \frac{\text{Mass of mixture as steam}}{\text{Total mass of mixture}} \quad (29)$$

The effect of quality on specific volume can be seen on Figure 25, and can be calculated from tables using the relation:

$$\begin{aligned} v_{\text{mix}} &= x v_g + (1 - x) v_f \\ &= v_f + x v_{fg} \end{aligned} \quad (30)$$

where  $v_{mix}$  = mixture specific volume  
 $v_g$  = saturated gas specific volume  
 $v_f$  = saturated liquid specific volume  
 $v_{fg} = v_g - v_f$

The second expression results in more accurate numerical results in hand calculations if steam quality is low.

The enthalpy of saturated steam and water is shown as a function of pressure in Figure 26. Points B and C on this diagram correspond with those on Figure 23. There is a maximum enthalpy of  $2.8 \times 10^6$  Joules/kg (1204.8 Btu/lb<sub>m</sub>) that saturated steam may have under any conditions. This occurs between 31.16 and 31.85 bar (452 and 462 psia).

The overall enthalpy of saturated mixtures can be calculated from the relation:

$$\begin{aligned} h_{mix} &= x h_g + (1 - x) h_f \\ &= h_f + x h_{fg} \end{aligned} \quad (31)$$

where  $h_{mix}$  = mixture specific enthalpy

$h_f$  = saturated liquid specific enthalpy

$h_g$  = saturated gas specific enthalpy

$h_{fg}$  = latent heat of vaporization per unit mass

The specific enthalpy of such mixtures is shown in Figure 26.

The latent heat of vaporization per unit mass,  $h_{fg}$ , is the increase in enthalpy as a fluid vaporizes from saturated liquid to saturated steam at constant pressure or temperature. At atmospheric pressure  $h_{fg}$  is approximately  $2.3 \times 10^6$  Joules/kg (1000 Btu/lb<sub>m</sub>). Farouq Ali<sup>19</sup> (p. 5) has presented the approximation:

$$h_{fg} = 1318 p^{-0.08774} \quad (32)$$

for use in hand calculations. The maximum error is reported to be 1.9%.

The units used in Eqn. 32 are  $p$ , psia;  $h_{fg}$ , Btu/lb<sub>m</sub>.

There appears to be some uncertainty about the viscosity of saturated steam and water. Accepted values are presented in the ASME Steam Tables. Figure 27 shows the viscosity of saturated steam and water vs. temperature. The viscosities of the two phases tend to approach one another as they approach the critical temperature.

Farouq Ali<sup>33</sup> recommends use of the following equation for the viscosity of steam:

$$\mu/100 = 88.02 + 0.32827 T + 0.0002135 T^3 - \rho (1858 - 5.90 T) \quad (33)$$

where  $\mu$  = viscosity of steam, centipoise

$T$  = temperature, °C

$\rho$  = density of steam, gm/cc

The density of steam can be determined from steam tables. For pressures up to 1000 psia, the density of steam can also be determined from the following relation developed by Farouq Ali (p. 22):

$$\rho = 0.0000440189 p^{0.9588} \quad (34)$$

where  $\rho$  = density of steam, gm/cc

$p$  = pressure, psia

The thermal conductivity of water first increases as the temperature increases and reaches a maximum at about 150°C. Thereafter it decreases. This is shown in Figure 28.

### Impure Saturated Water

Chemical content will tend to have the same effect on the properties of saturated water and steam as they will on the unsaturated phases. Hence, with the exception of the vapor pressure curve, discussion of the effect of impurities will be postponed until later sections.

The vapor pressure of water in a geothermal system will not necessarily be that presented in the steam tables. For a fixed pressure, the boiling temperature of water will be elevated by the presence of impurities. This is equivalent to a lowering of vapor pressure. However, the effect is usually rather small. For example, at 4.621 bar (67.013 psia) pure water would boil at 148.89°C (300°F), whereas a 100,000 ppm (parts per million) sodium chloride brine would boil at 150.62°C (303.113°F). This difference would probably not be measurable in a geothermal system. However, significant vapor pressure lowering has been observed with production of 350,000 ppm brines in the Imperial Valley, California.

The vapor pressure data presented in steam tables were measured for flat surface interfaces. If the steam-water interface is a strongly curved surface, as might occur in small pores in porous media, then there could be significant vapor pressure lowering effects (Calhoun, et al.<sup>40</sup>; Edlefsen and Anderson<sup>41</sup>). Cady, Bilhartz, and Ramey<sup>42</sup> have investigated this phenomenon with regard to geothermal aquifers. They did not observe vapor pressure lowering in unconsolidated sandstone cores. However, a recent study by Strobel<sup>56</sup> indicates a potential vapor pressure lowering at very low liquid contents in experiments with a single, consolidated core. Continued experimentation is in progress.

Pure Compressed Liquid Water

The compressed liquid region lies above the vapor pressure curves in the pressure-temperature planes of Figure 23 and Figure 24. Enthalpy and PVT behavior for compressed water is given in various tables<sup>35,37</sup> and in the ASME Steam Tables<sup>36</sup> for pressures up to 1070 bar (15,500 psia).

A technique commonly used in oil reservoir engineering for relating compressed water at some given reservoir condition to its state at surface conditions is via the formation volume factor,  $B_w$ . This is defined as the volume of liquid at reservoir conditions divided by the volume of liquid that would remain if it were brought to some standard surface conditions, commonly 20°C and 1 bar (70°F and 14.67 psia).

$$B_w = \frac{\Delta}{\square} \frac{\text{initial volume of liquid at reservoir conditions}}{\text{volume of liquid remaining at standard conditions}} \quad (35)$$

Figure 29 is a graph of the Formation Volume Factor,  $B_w$ , for pure liquid water as function of pressure and temperature. Note that for constant temperature, as pressure decreases,  $B_w$  increases slowly up to saturation conditions, below which it falls rapidly.

The specific volume-pressure behavior of a compressed liquid under an isothermal expansion or contraction process is often of interest (particularly in unsteady liquid flow through an aquifer). This P-V behavior is usually expressed in terms of the isothermal coefficient of compressibility,  $c_l$ , which is defined:

$$c_l = \frac{\Delta}{\square} - \frac{1}{v} \left( \frac{\partial v}{\partial p} \right)_T \quad (36)$$

$c_p$  can be viewed as the fractional decrease in specific volume caused by an isothermal unit increase in pressure. Although the isothermal compressibility of liquid water is often used in ground water hydrology and oil reservoir engineering, it appears to have been seldom reported for high values of temperature (greater than  $120^{\circ}\text{C}$ ;  $240^{\circ}\text{F}$ ). Table 1 summarizes high temperature results reported by Whiting and Ramey.<sup>38</sup> As can be seen, the isothermal compressibility for water is reasonably constant with pressure, but varies with temperature.

Table 2 presents the enthalpy of compressed pure water over a range of pressures and temperatures. It can be seen that the liquid enthalpy is only weakly dependent on pressure, but strongly dependent on temperature.

The viscosity of pure compressed water is presented in various Steam Tables.<sup>35-37</sup> The viscosity of high pressure liquid is almost constant with pressure, and generally only about 10-15% higher than the corresponding value for saturated liquid at the same temperature. Hence Figure 27, which shows the viscosity of saturated liquid as a function of temperature, can be used as a good estimate of compressed liquid viscosity.

The specific heat,  $c_p$ , of compressed water is also presented in the Steam Tables<sup>35-37</sup> for pressures up to 1035 bar (15000 psia). Values of  $c_p$  range from 4100 to 5000 Joules/Kg.  $^{\circ}\text{C}$  (1.00 to 1.20 Btu/lb<sub>m</sub>  $^{\circ}\text{F}$ ), except at temperatures greater than  $260^{\circ}\text{C}$  ( $500^{\circ}\text{F}$ ). Near the critical point values become very high.

#### Impure Compressed Water

The waters produced from geothermal systems often contain a dissolved chemical content high in chlorides and sulfates. Brines from some areas,



such as the Imperial Valley Salton Sea Geothermal Resource Area, have up to ten times the dissolved solids content of seawater. In addition, geothermal liquids often contain dissolved noncondensable gases.

Amyx, Bass and Whiting<sup>43</sup> (p. 450) state "Literature relative to the effect of composition on the properties (of water) is meager, and is limited to gas solubility data over the temperature range 32-250°F (0-121°C) at pressures ranging from 0-6000 psia (0-415 bar)." These authors summarize the work of numerous workers (Dodson and Standing<sup>44</sup>, Rowe<sup>45</sup>, Beal<sup>46</sup>, Bridgman<sup>47</sup>) on the effect of natural gas solubility on the PVT behavior of water.

Long and Chierici<sup>48</sup> have presented experimental data on the PVT behavior of aqueous solutions of sodium chloride. Their results were measured for temperatures over the range 20-100°C, pressures from 2-500 kg/cm<sup>2</sup>, and salinities from 0-300g/L. They also presented analytic curve matches giving density,  $\rho$ , as a function of salinity, pressure, and temperature over the range of experimental conditions. It is unfortunate that data for higher temperatures were not measured. But results do give a quantitative indication of the effect of chemical composition on the PVT behavior of water.

Amyx, Bass and Whiting<sup>43</sup> (p. 466) present data from Van Wingen<sup>49</sup> on the viscosity of oil field brines at pressures to 7100 psia, and temperatures to 300°F. This data suggests that dissolved solids have only a small effect on the viscosity of saline brines. Stanley and Batten<sup>50</sup> have presented data on the viscosity of sea water compared to pure water from 0-30°C. They observed that for practical purposes, the increase is not significant.

Although important information is available there is a need for PVT data for geothermal waters at conditions characteristic of geothermal reservoirs, showing the effect of chemical composition. In addition, more information is needed about the solubility and PVT characteristics of noncondensable gases dissolved in geothermal waters.

#### Pure Superheated Steam

Superheated steam occurs on the pressure-temperature plane at temperatures above the vapor pressure line, e.g., point A on Figure 23. This state is also called "dry" steam. The ASME Steam Tables<sup>36</sup> (1967, Table 3) present data for the enthalpy and PVT behavior of superheated steam for temperatures up to 815°C (1500°F). Figure 30 is a diagram showing the specific volume of dry steam as a function of pressure and temperature. One convenient means of calculating specific volumes of dry steam is via the real gas law equation of state:

$$Pv_g = \frac{zRT}{M} \quad (37)$$

$$= z\bar{R}T$$

where P = pressure, bar

$v_g$  = specific volume of steam, m<sup>3</sup>/kg

z = gas law deviation (also compressibility) factor

$$R = 0.08288 \frac{\text{bar m}^3}{\text{kg}_{\text{mole}} \text{ } ^\circ\text{K}}$$

M = molecular weight of water, 18 kg/kg<sub>mole</sub>

$$\bar{R} = R/M = 0.004605 \frac{\text{bar m}^3}{\text{kg } ^\circ\text{K}}$$

T = absolute temperature, °K

OR, for English units

32

$$p = \text{psia}$$

$$v_g = \text{ft} / \text{lb}_m$$

$$R = 10.72 \frac{\text{ft psia}}{16 \text{ mole}^\circ\text{R}}$$

$$M = 18 \text{ lb}_m / \text{lb}_{\text{mole}}$$

$$\bar{R} = 0.5956 \frac{\text{ft psia}}{\text{lb}_m \text{ }^\circ\text{R}}$$

$$T = \text{ }^\circ\text{R}$$

The gas law deviation factor,  $z$ , for steam is presented in Figure 31.

Figure 32 presents a pressure-enthalpy diagram for superheated steam. Point A on this diagram corresponds to point A in Figure 23. If a dry steam reservoir were to produce at constant temperature, its state would follow the isotherms on Figure 32. As indicated by the arrow below point A, the produced steam would tend to increase in enthalpy. Whiting and Ramey<sup>38</sup> have suggested that this tendency is a potential means of identifying the initial state of a geothermal fluid reservoir as dry steam.

Values for the viscosity of superheated steam are presented in the ASME Steam Tables<sup>36</sup> (1967, Table 10 and Fig. 7). Table 3 presents values of dry steam viscosity over a range of conditions. Except near the vapor pressure curve, the viscosity of dry steam is essentially independent of pressure, and is also only slightly higher than that of saturated steam at the same temperature.

The specific heat at constant pressure,  $c_p$ , of dry (and saturated) steam is presented in Table 9 of the ASME Steam Tables. Except near the vapor pressure curve and at higher pressures and temperatures, it is approximately  $2100 \text{ J/kg-}^\circ\text{C}$  ( $0.5 \text{ Btu/lb}_m\text{-}^\circ\text{F}$ ).

Mixtures of Dry Steam and Other Noncondensable Gases

Two of the recognized dry steam geothermal reservoirs in the world (the Geysers Field in California, and Larderello in Italy) are known to produce quantities of noncondensable gases along with their steam.

Typically such gases contain carbon dioxide, hydrogen sulfide, ammonia, methane, and ethane. The quantity and proportions produced vary as a function of time, flow rate, and from well to well over the fields.

It is clear that the noncondensable gas content of a dry steam reservoir will effect the thermodynamic and transport properties of the produced fluid. Unfortunately, almost no experimental work seems to have been done on the properties of dry steam and noncondensable gas mixtures. However, generalized correlations have been extensively developed for natural gas mixtures of hydrocarbons. These correlations are based on reduced pressures and temperatures:

$$\text{Reduced Pressure, } P_r \triangleq \frac{\text{actual pressure}}{\text{pseudo critical pressure}} \quad (38)$$

$$\text{Reduced Temperature, } T_r \triangleq \frac{\text{actual temperature}}{\text{pseudo critical temperature}} \quad (39)$$

where the pseudo critical pressure and temperature are the molar average of the component critical values.

Amyx, Bass and Whiting<sup>43</sup> (pp. 260-268) have discussed and summarized correlations available for determining the PVT behavior of mixtures of natural gases with impurities such as nitrogen and carbon dioxide. On the basis of their discussion, the best method for estimating the effect of a noncondensable gas on steam compressibility appears to be through the use of an additive compressibility factor as first defined by Eilerts et al.<sup>51</sup>

$$Z_a = Z_{st} Y_{st} + Z_{ncg} Y_{ncg} \quad (40)$$

where  $Z_a$  = additive compressibility factor

$Z_{st}$  = steam compressibility factor

$Y_{ncg}$  = noncondensable gas compressibility factor

$Z_{st}$  = Mole fraction steam in mixture

$Y_{ncg}$  = mole fraction noncompressible gas in mixture

Amyx, Bass and Whiting<sup>43</sup> (pp. 260-268) present graphs of the compressibility factor,  $z$ , for nitrogen (from Eilerts et al.<sup>51</sup>), carbon dioxide (from Olds et al.<sup>52</sup>), and hydrogen sulfide (from Reamer et al.<sup>53</sup>). For purposes of reservoir calculations, it is expected that the noncondensable gas content of many geothermal steams will have a minimal effect on PVT behavior.

The effect of noncondensable gases on geothermal steam viscosity is also of interest. Again, there appears to be almost no experimental data available, and we must resort to correlations. Amyx, Bass and Whiting<sup>43</sup> (pp. 278-286) present the results of numerous correlations for natural gases. On the basis of their discussion, a rule proposed by Herning and Zipperer<sup>54</sup> for calculating the viscosity of mixtures of gases appears to be the most promising correlating method. In this rule the viscosity of the mixture,  $\mu_m$ , is given by

$$\mu_m = \frac{\sum_{i=1}^n \mu_i Y_i M_i}{\sum_{i=1}^n Y_i M_i} \quad (41)$$

where  $\mu_m$  = viscosity of mixture  
 $\mu_i$  = viscosity of  $i^{\text{th}}$  component  
 $M_i$  = molecular weight of  $i^{\text{th}}$  component  
 $Y_i$  = mole fraction of the  $i^{\text{th}}$  component in mixture  
 $n$  = total number of components in the mixture

Basically this is an averaging calculation weighted by the mass of each component present. The viscosity of various gases over a range of temperatures can be found in standard physical properties reference books (e.g., see Weast<sup>55</sup>, pp. F41-F44). For practical purposes, the non-condensable gas content will not significantly affect the viscosity of most geothermal steams.

#### A Note on Units

In general, equations and numerical values have been expressed in metric units (bar, °C, m, kg), with values for engineering units given in parenthesis (psia, °F, ft, lb<sub>m</sub>). Viscosity is given in centipoise. For convenience of writing this is not true in every case. Units are always specified where equations are presented throughout the paper.

Note the following conversions:

Pressure:	1 psia	= 0.06895 bar
	1 bar	= 1.0197 kg/cm <sup>2</sup>
	1 bar	= 0.9869 atm.
Specific Volume:	1 ft <sup>3</sup> /lb <sub>m</sub>	= 0.062428 m <sup>3</sup> /kg
	1 ft <sup>3</sup> /lb <sub>m</sub>	= 62.43 cc/gm
Enthalpy:	1 Btu/lb <sub>m</sub>	= 2324.4 Joules/kg
Viscosity	1 c.p.	= 6.72x10 <sup>-4</sup> lb <sub>m</sub> ft sec
	1 c.p.	= 2.089x10 <sup>-8</sup> lb <sub>F</sub> sec/ft <sup>2</sup>

Acknowledgment

Preparation of this report was funded by the National Science Foundation as a portion of the study "Stimulation of Geothermal Aquifers," Grant No. GI-34925, principal investigators Drs. Paul Kruger and Henry J. Ramsey, Jr., Stanford University.

TABLE 1

Isothermal Compressibility of Liquid Water, psia<sup>-1</sup>

<u>P, psia</u>	<u>300°F</u>	<u>400°F</u>	<u>500°F</u>
700	$3.793 \times 10^{-6}$	$5.811 \times 10^{-6}$	$7.146 \times 10^{-6}$
800	$3.795 \times 10^{-6}$	$5.815 \times 10^{-6}$	$7.152 \times 10^{-6}$
1000	$3.913 \times 10^{-6}$	$5.821 \times 10^{-6}$	$10.703 \times 10^{-6}$

TABLE 2  
Enthalpy of Compressed Water in Btu/lb  
and Joules/kg [(Btu/lb)/(J/kg)] at Various Pressures and Temperatures

(Data from Ref. 36)

Temperature		Pressure, psia/bar				
°F	°C	100/6.9	500/34.5	1000/69.0	2000/138.	5000/345
70	21	38.33/8.91x10 <sup>4</sup>	39.44/9.17x10 <sup>4</sup>	40.82/9.49x10 <sup>4</sup>	43.58/1.013x10 <sup>5</sup>	51.7/1.202x10 <sup>5</sup>
200	93	168.3/3.91x10 <sup>5</sup>	169.2/3.93x10 <sup>5</sup>	170.3/3.96x10 <sup>5</sup>	172.6/4.01x10 <sup>5</sup>	179.5/4.17x10 <sup>5</sup>
400	204	X	375.4/8.73x10 <sup>5</sup>	376.0/8.74x10 <sup>5</sup>	377.2/8.77x10 <sup>5</sup>	381.2/8.86x10 <sup>5</sup>
600	316	X	X	X	614.5/1.43x10 <sup>6</sup>	604.6/1.40x10 <sup>6</sup>



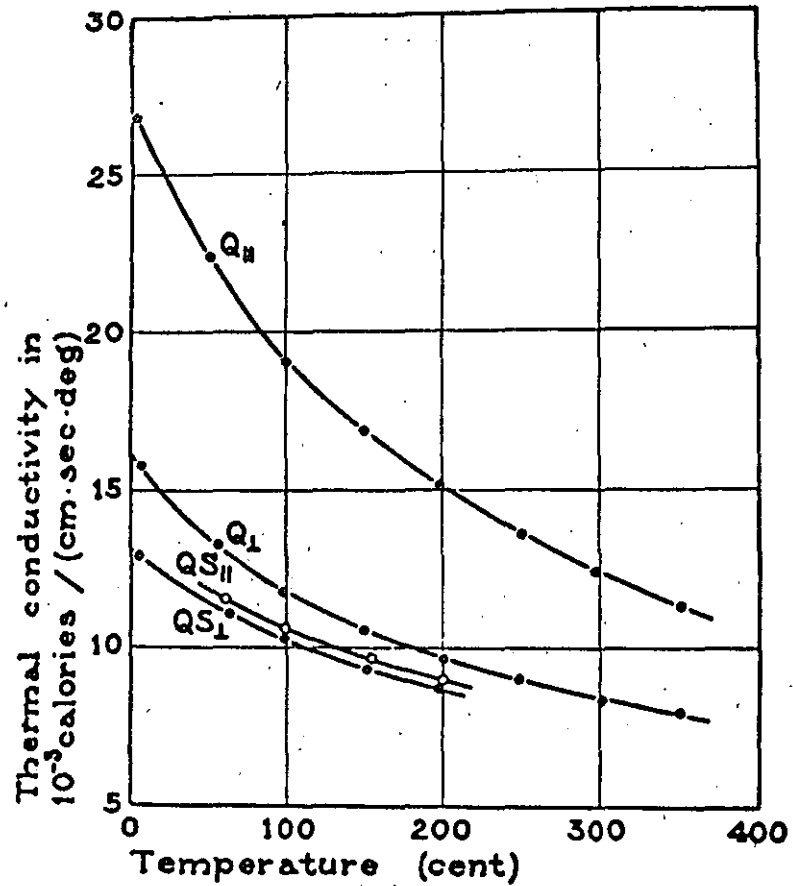
TABLE 3

Viscosity in Centipoise of Superheated Steam at Various Conditions

(Data from Ref. 36)

Temperature		Saturation Conditions			Pressure psia bar						
°F	°C	P, psia	P, bar	.c.p.	1/.06895	5/.345	10/.690	50/3.45	100/6.9	500/34.5	1000/69
200	93	11.5	.79	.01	.012	.012	.012	X	X	X	X
300	149	67	4.62	.014	.014	.014	.014	.014			
400	204	247.3	17.1	.0155	.016	.016	.016	.016			
500	260	681	47.0	.0177	.0186	.0186	.0186	.0186	.0186	.0180	
600	316	1543	106.4	.02	.02	.02	.02	.02	.02	.02	.02

FIGURE 1



Thermal conductivity of quartz and of a quartzitic sandstone.  
 $QS_{\perp}$  Quartzitic sandstone, Penn.,  $\perp$  bed-plane.  
 $QS_{||}$  Quartzitic sandstone, Penn.,  $\parallel$  bed-plane.  
 $Q_{\perp}$  Quartz single crystal  $\perp$  optic axis.  
 $Q_{||}$  Quartz single crystal  $\parallel$  optic axis.

(Ref. 1)

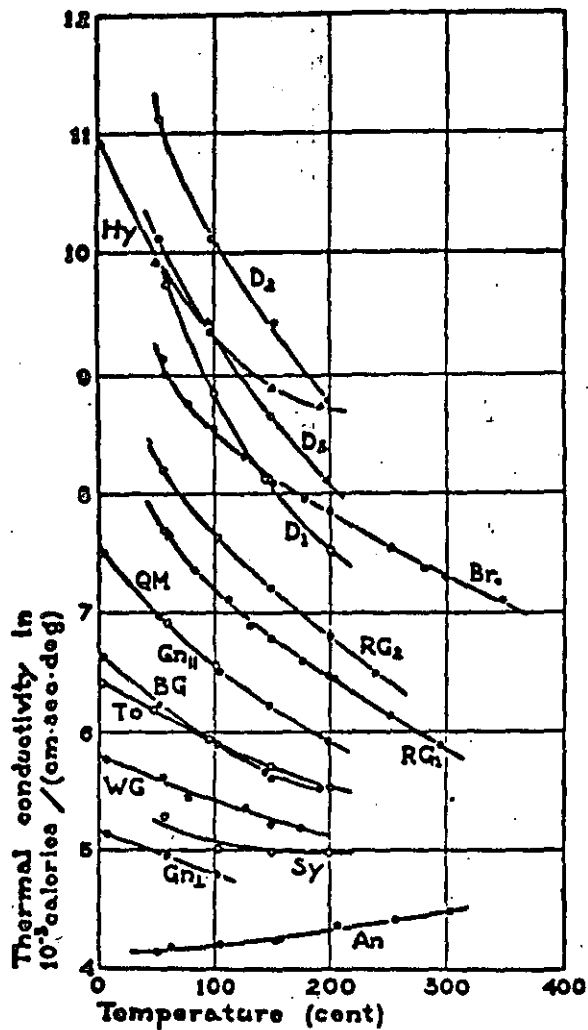


FIGURE 2 Thermal conductivity of holocrystalline rocks. (Ref. 1)

An	Anorthosite, Quebec.	RG <sub>1</sub>	Rockport Granite 1.
G <sub>nl</sub>	Gneiss, Pelham, $\perp$ bed-plane.	RG <sub>2</sub>	Rockport Granite 2.
G <sub>nl</sub>	Gneiss, Pelham, $\parallel$ bed-plane.	Br	Bronzite.
Sy	Syenite, Ontario.	Hy	Hypersthene.
WG	Westerly Granite.	D <sub>1</sub>	Dunite 1.
To	Tonalite, Calif.	D <sub>2</sub>	Dunite 2.
BG	Barre Granite.	D <sub>3</sub>	Dunite 3.
QM	Quartz monzonite, Calif.		

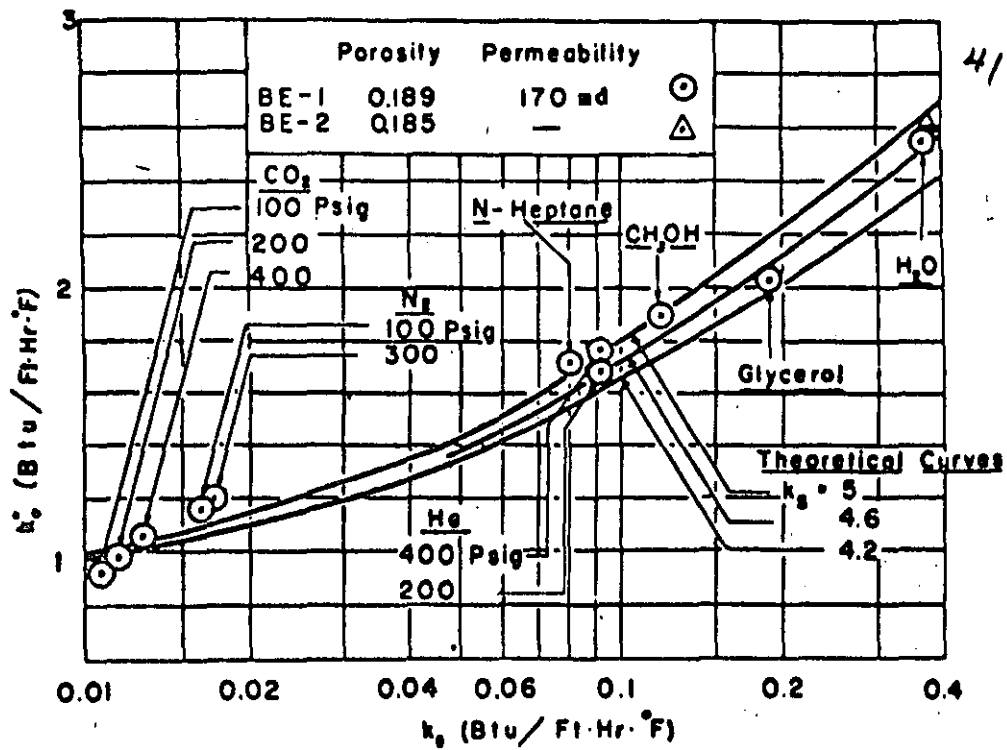


FIGURE 3 — STAGNANT CONDUCTIVITIES VS CONDUCTIVITIES OF FLUIDS, BEREA SANDSTONE. (Ref. 4)

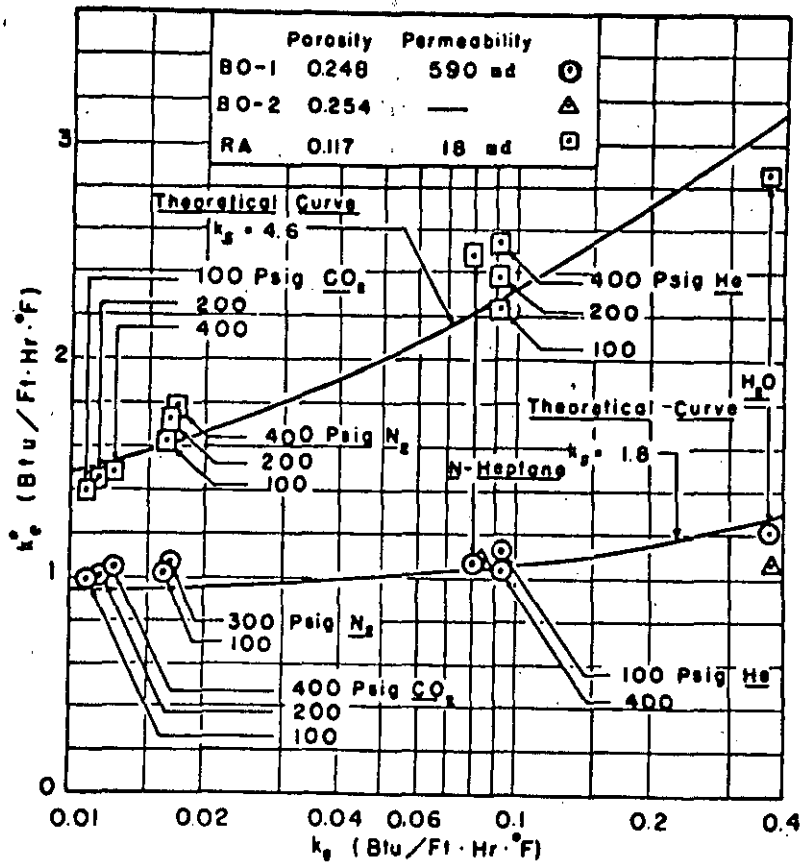


FIGURE 4 — STAGNANT CONDUCTIVITIES VS CONDUCTIVITIES OF FLUIDS, BOISE AND RANGELY SANDSTONES. (Ref. 4)

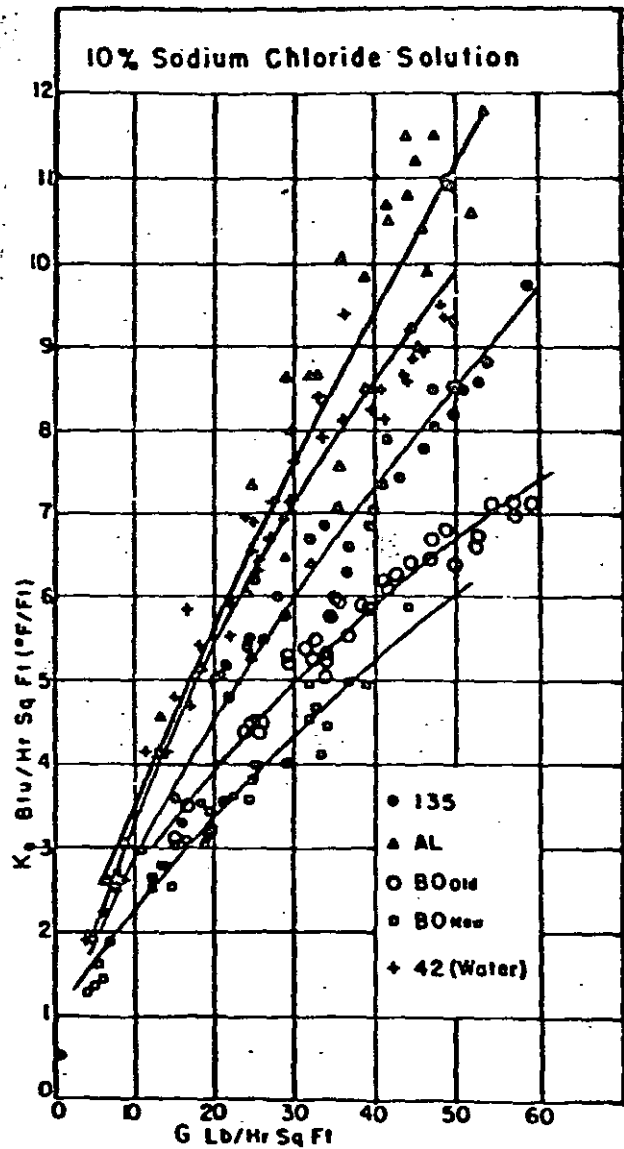


FIGURE 5 — Effective thermal conductivity ( $K_e$ ) as a function of mass flow rate (G). See Ref. 5 for legend. (After Adivarahan, Kunii and Smith, Courtesy Soc. of Petrol. Engrs. of AIME.) (Ref. 5)

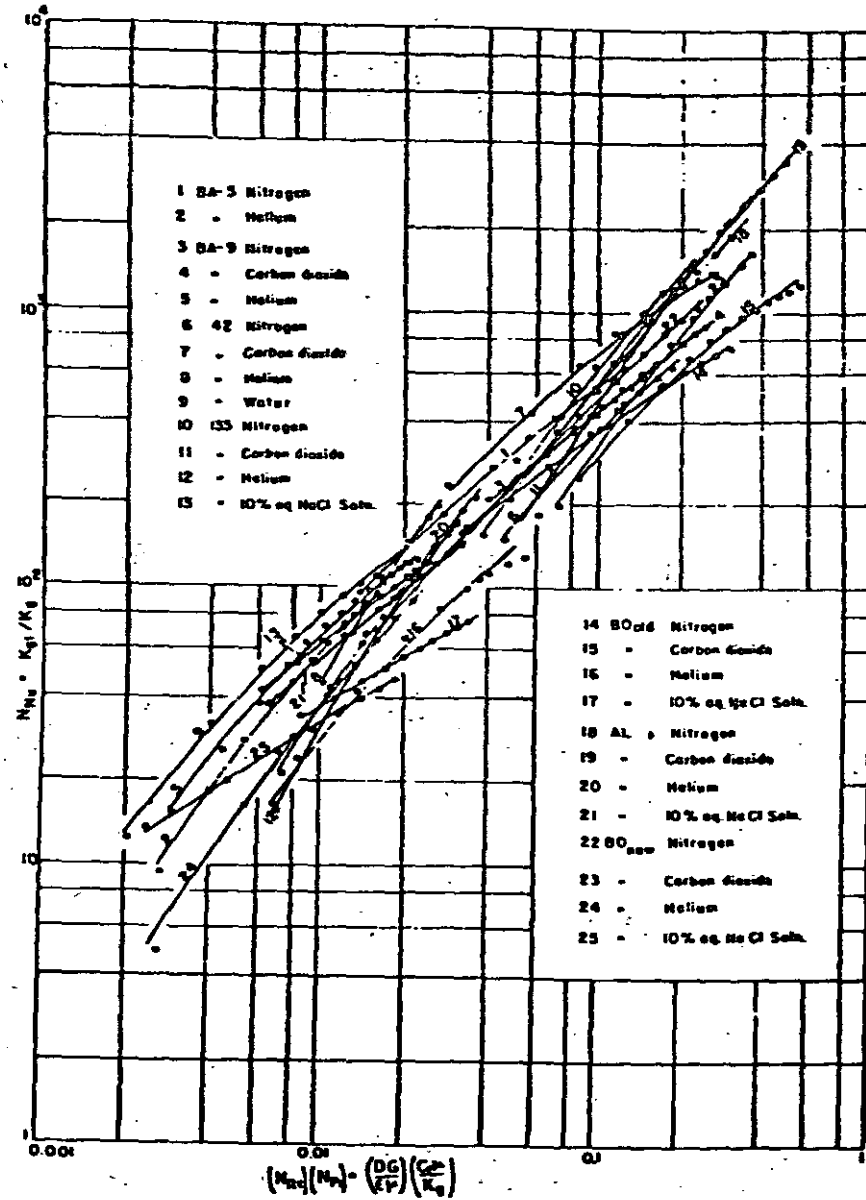


FIGURE 6 — CORRELATION OF  $k_{gt}/k_g$  WITH  $(DG/\epsilon)(C_p \mu / k_g)$ . (Ref. 5)

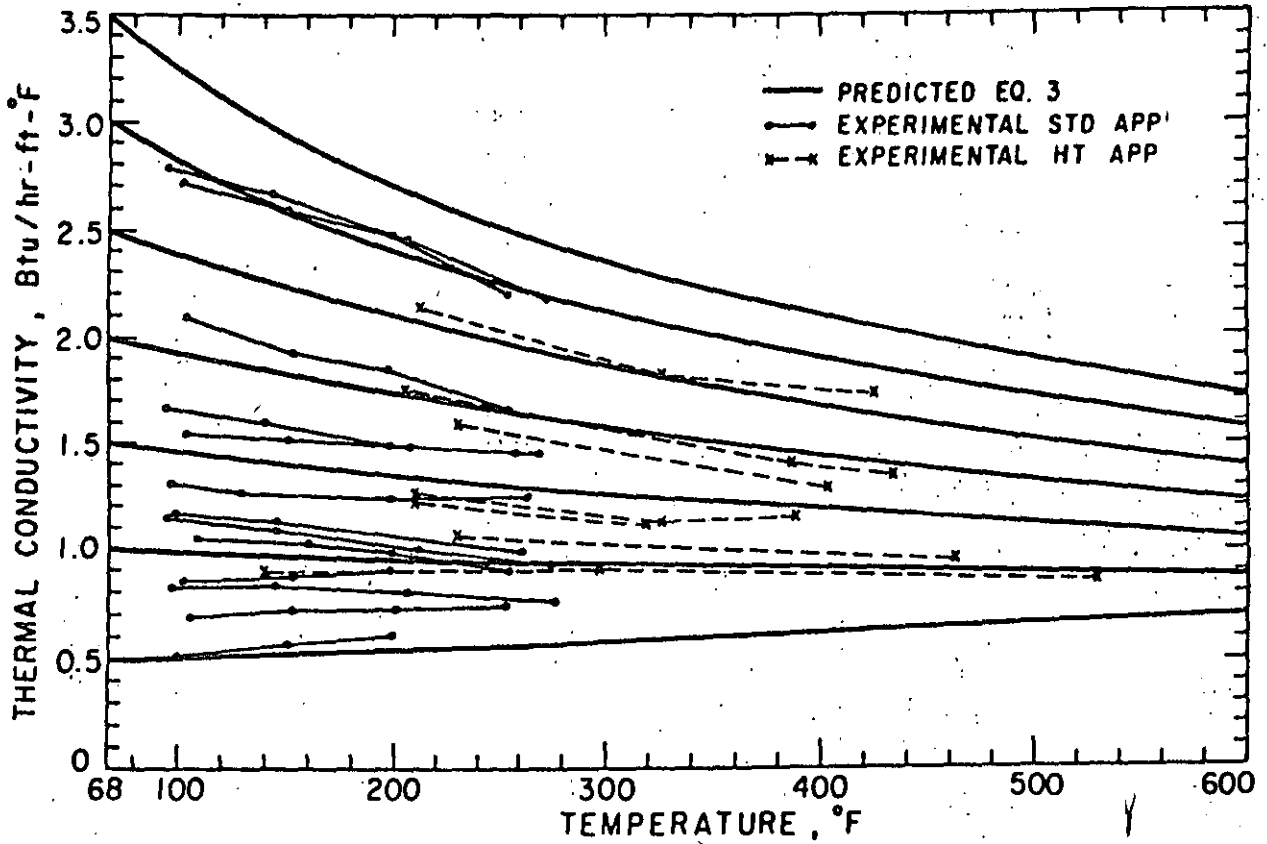


FIGURE 7 Effect of Temperature on Thermal Conductivity of Sandstone. (Ref. 7)

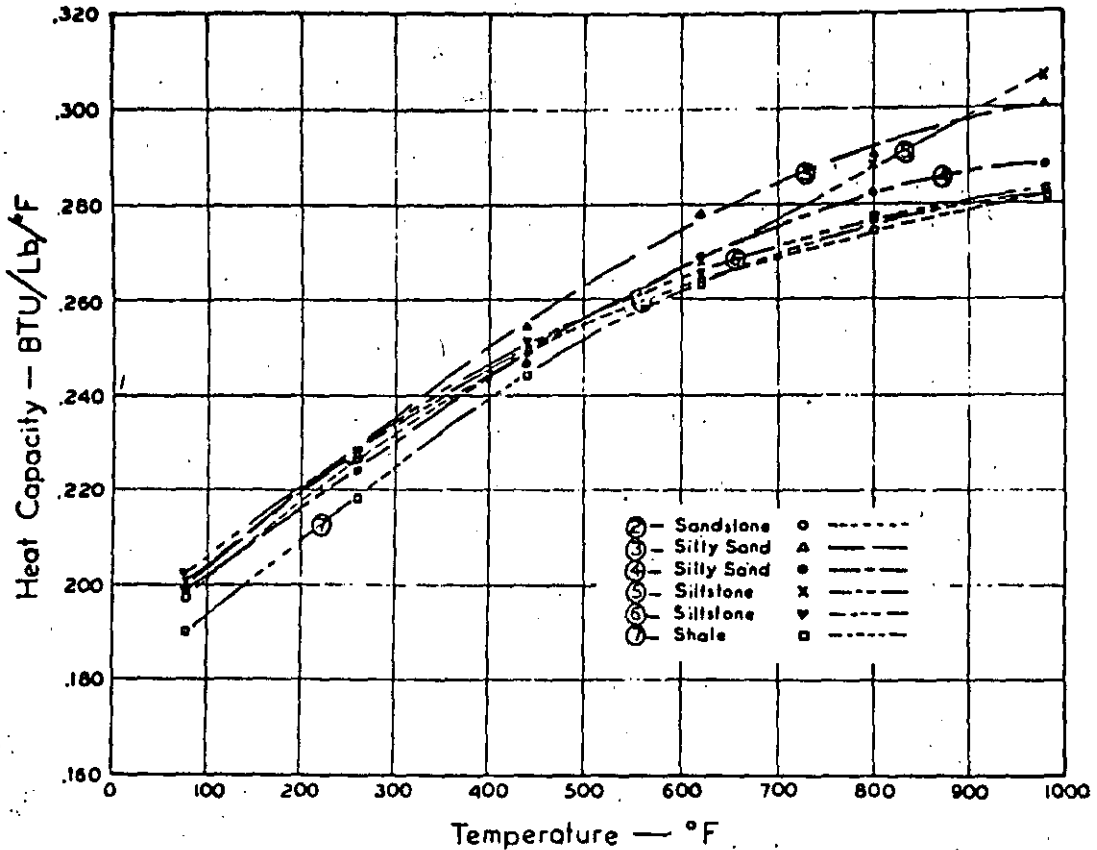


FIGURE 8 —EXPERIMENTAL HEAT CAPACITIES. (Ref. 3)

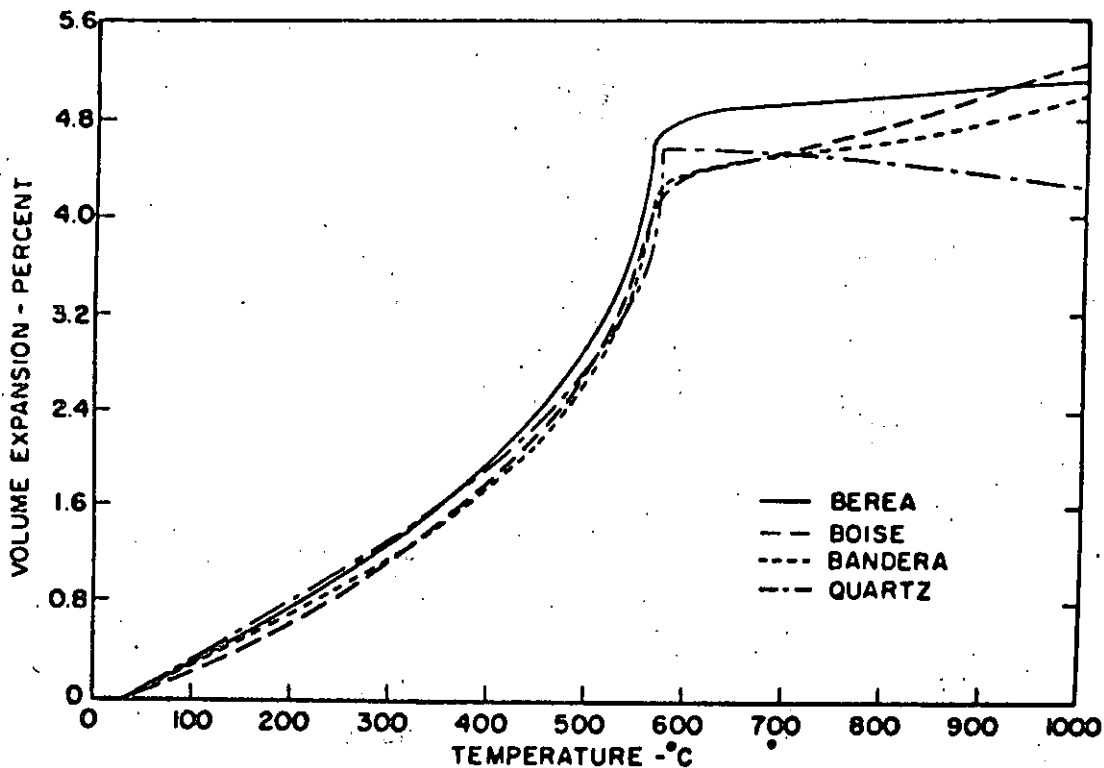


FIGURE 9 - VOLUME EXPANSION OF SANDSTONES.  
(Ref. 12)

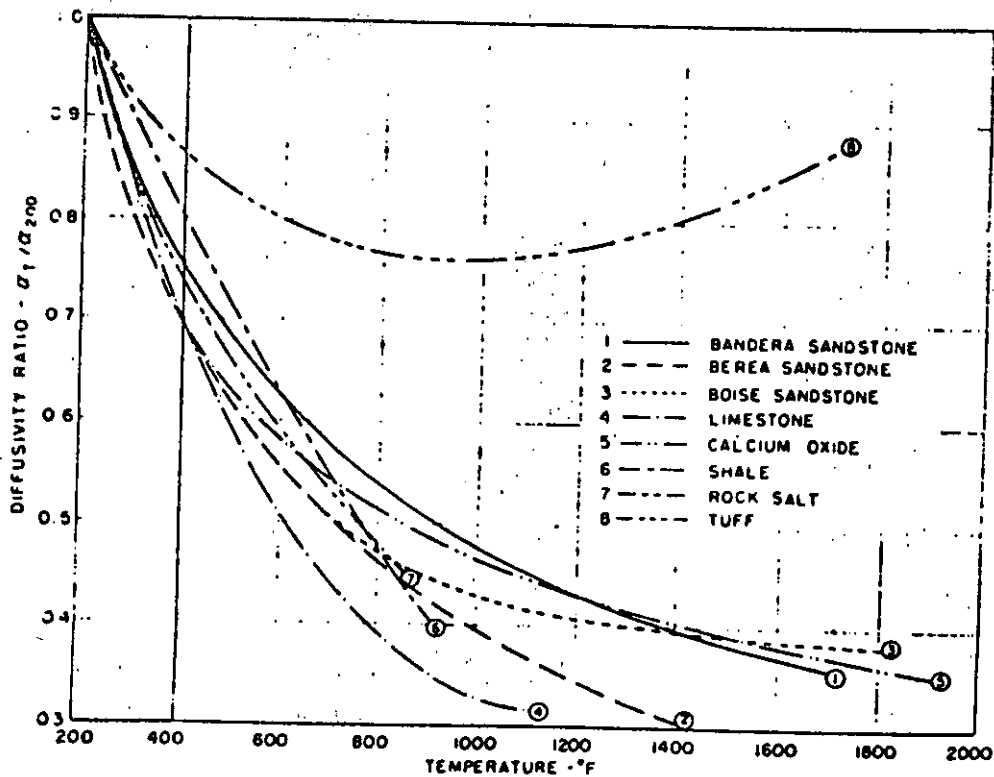


FIGURE 10 - THERMAL DIFFUSIVITY RATIO, INITIAL RUNS.  
(Ref. 13)

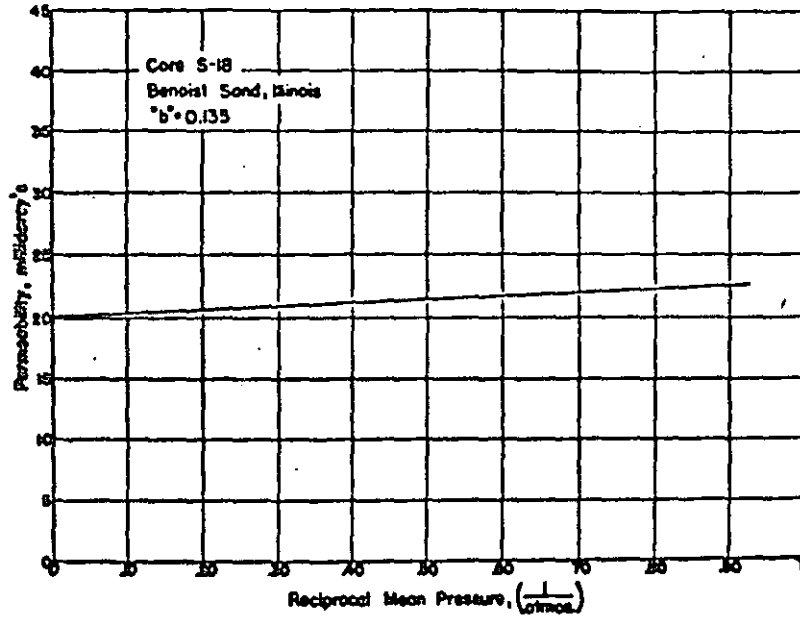


FIG. 5

FIGURE 11 Relationship between the Permeability to Gas and the Mean Pressure at which Gas Flows through a Medium, a Relationship Making Possible the Determination of the Permeability of the Medium to a Non-Reacting Liquid

(from API RP 27, Am. Petr. Inst., Aug. 1956)

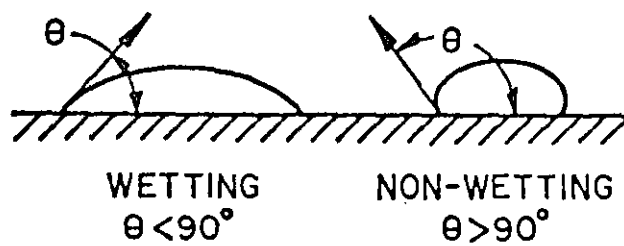
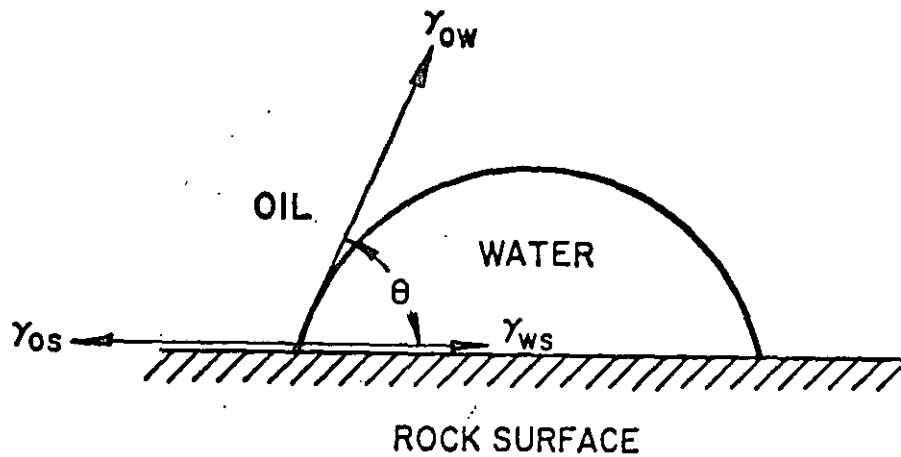


FIGURE 12

Relationship between preferential wetting and contact angle. (Ref. 15)



51

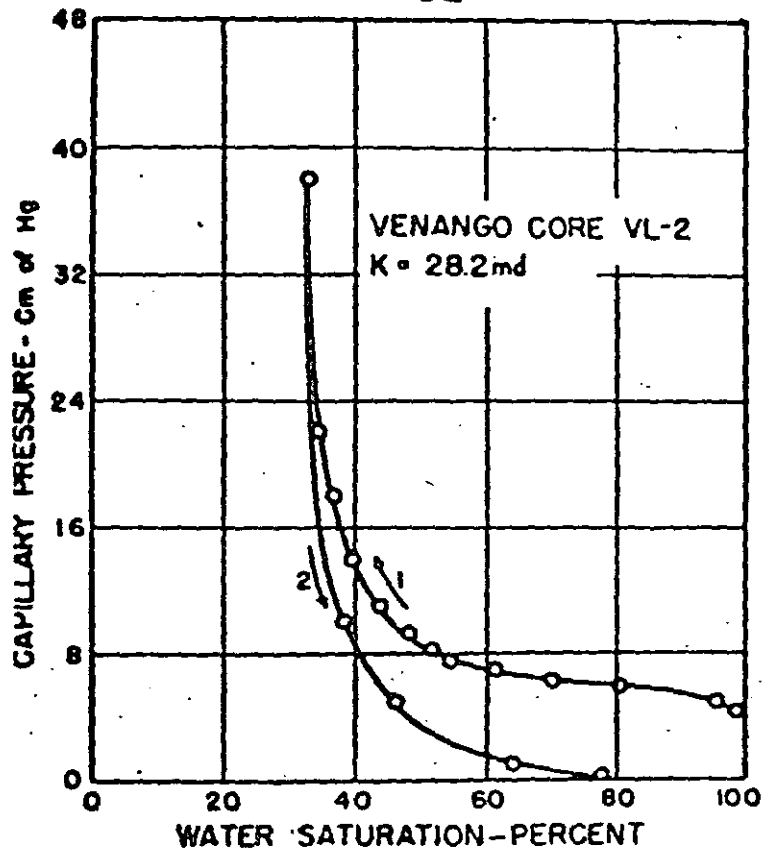


FIGURE 13 —Capillary pressure vs. water saturation.

(Ref. 16)

52

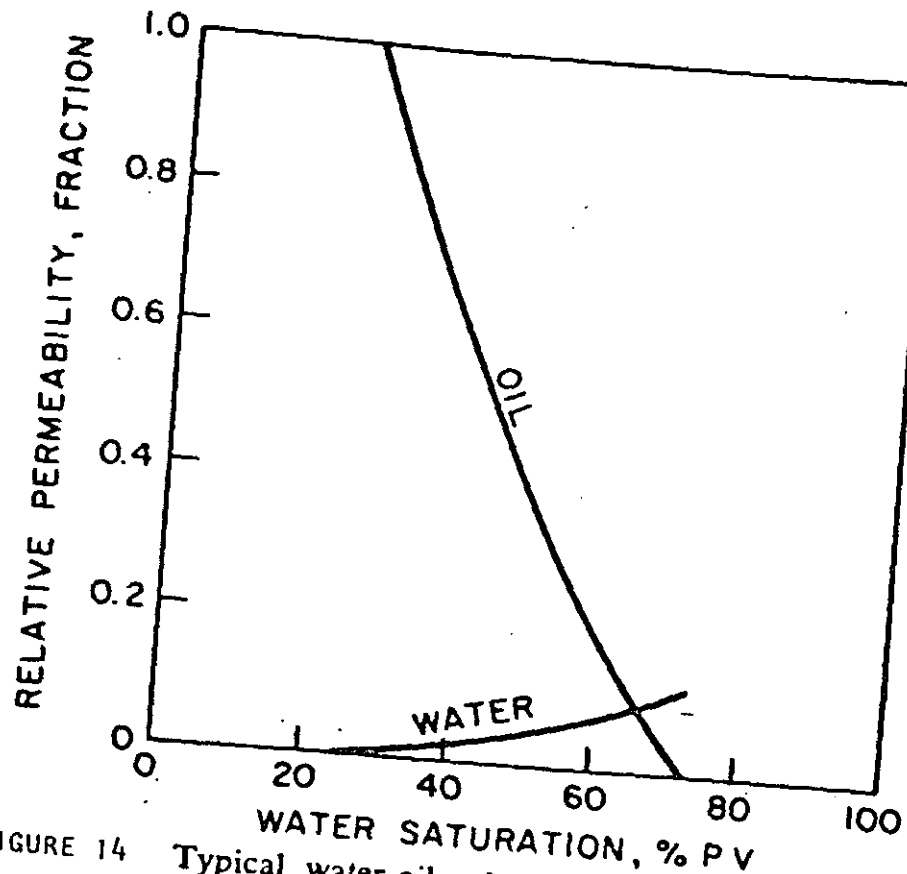


FIGURE 14 Typical water-oil relative permeability characteristics, strongly water-wet rock. (Ref. 17)

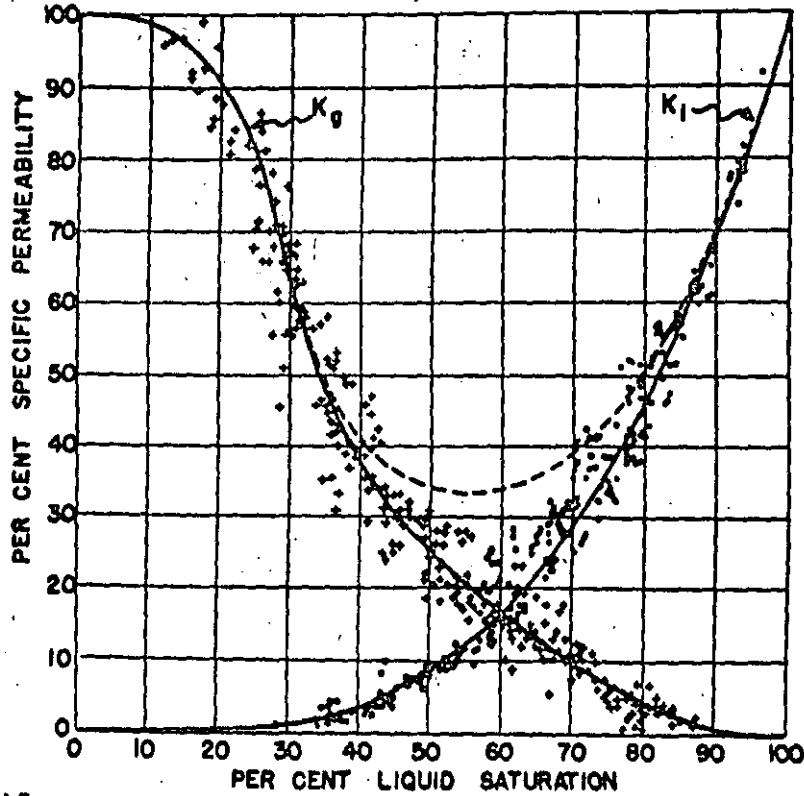


FIGURE 15 -PERMEABILITY-BATURATION DATA FOR FOUR DIFFERENT SANDS, INCLUDING THOSE OF FIGS. 4 AND 5. (Ref. 18)

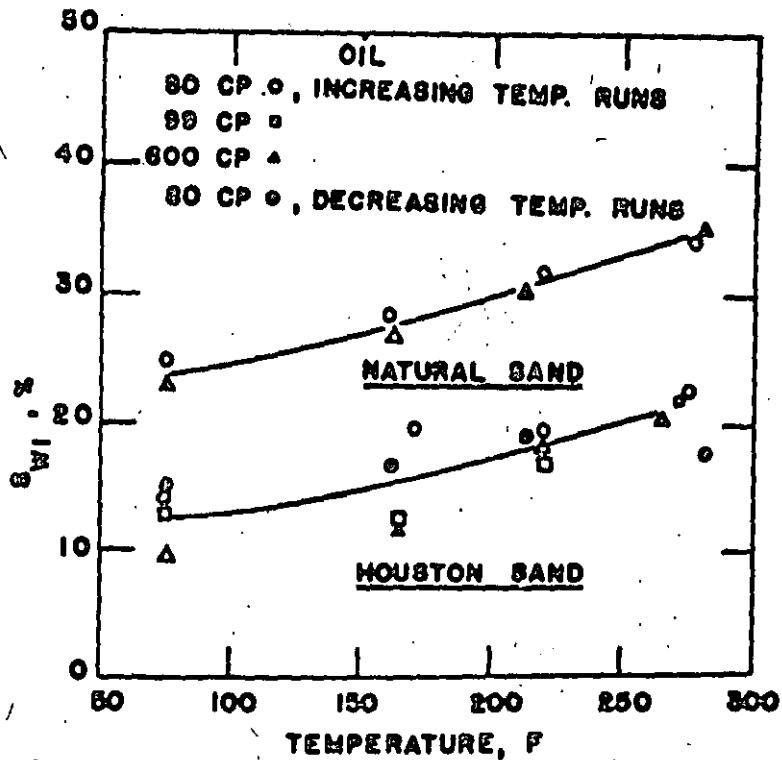


FIGURE 16 IRREDUCIBLE WATER SATURATION VS TEMPERATURE FOR HOUSTON SAND AND NATURAL SAND. (Ref. 19)

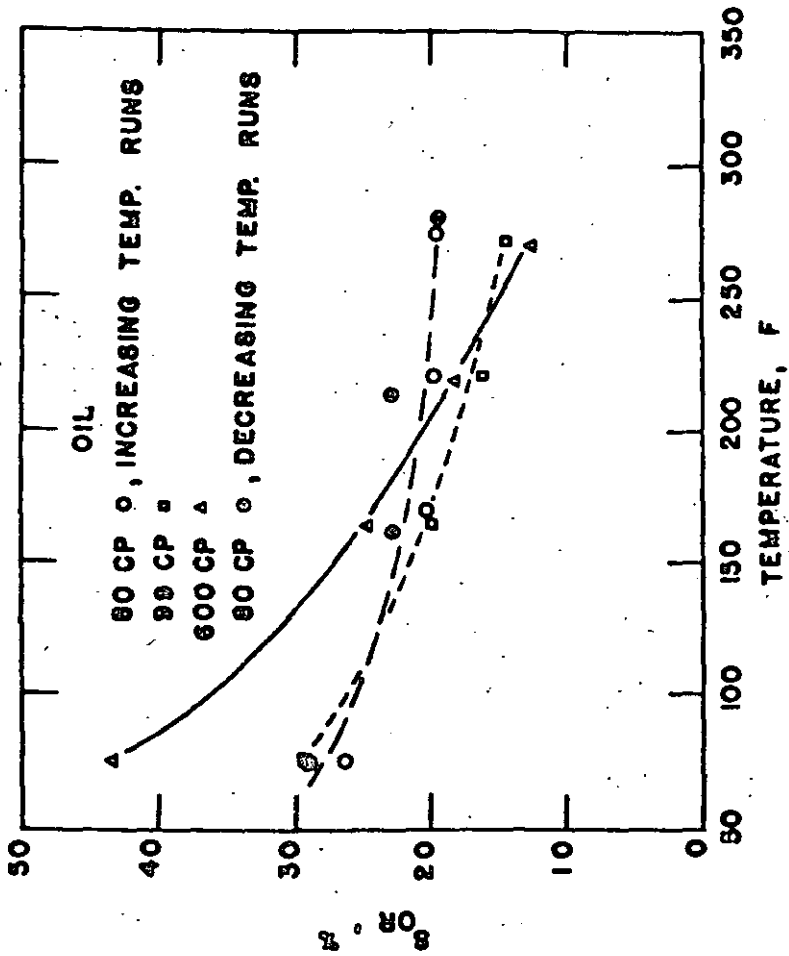


FIGURE 17 RESIDUAL OIL SATURATION VS TEMPERATURE FOR HOUSTON SAND. (Ref. 19)

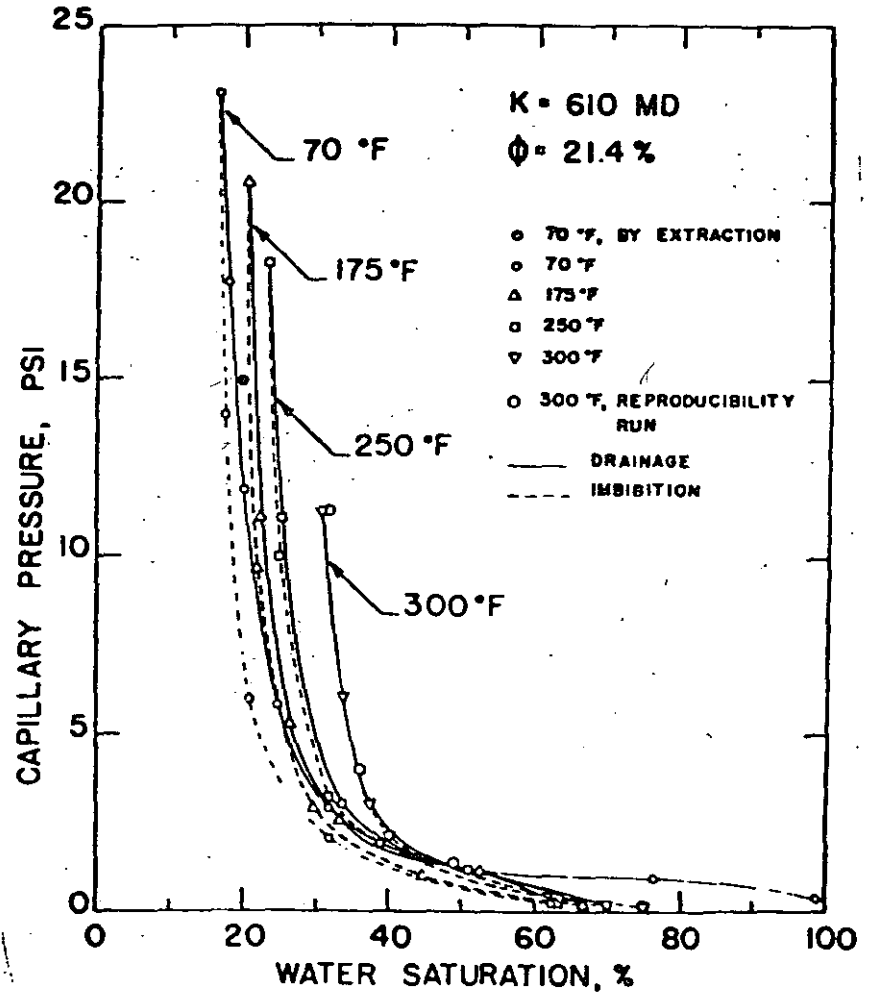


FIGURE 18 Capillary pressure vs water saturation for Berea sandstone core A. (Ref. 20)

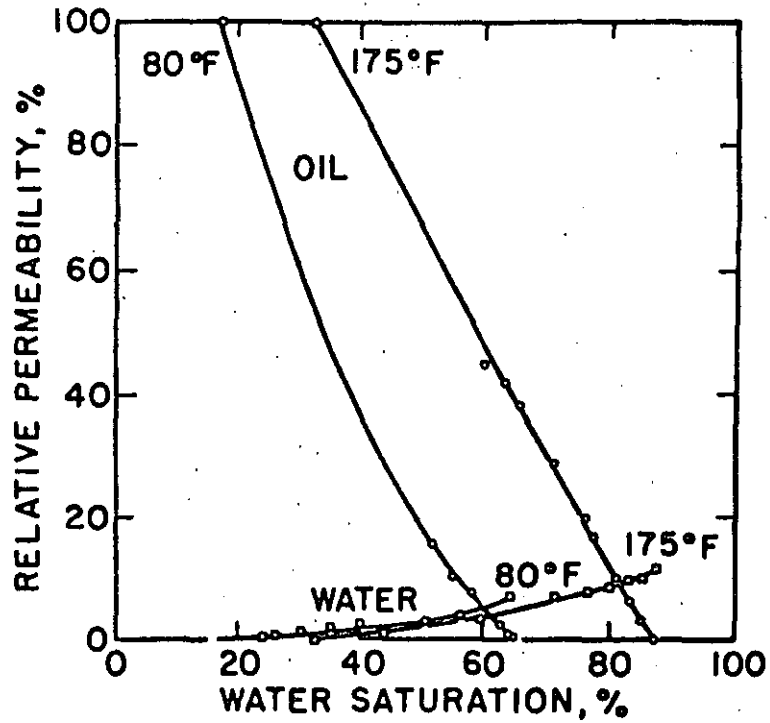


FIGURE 19 Individual relative permeabilities as a function of temperature; Core 4, Boise sandstone. (Ref. 21)

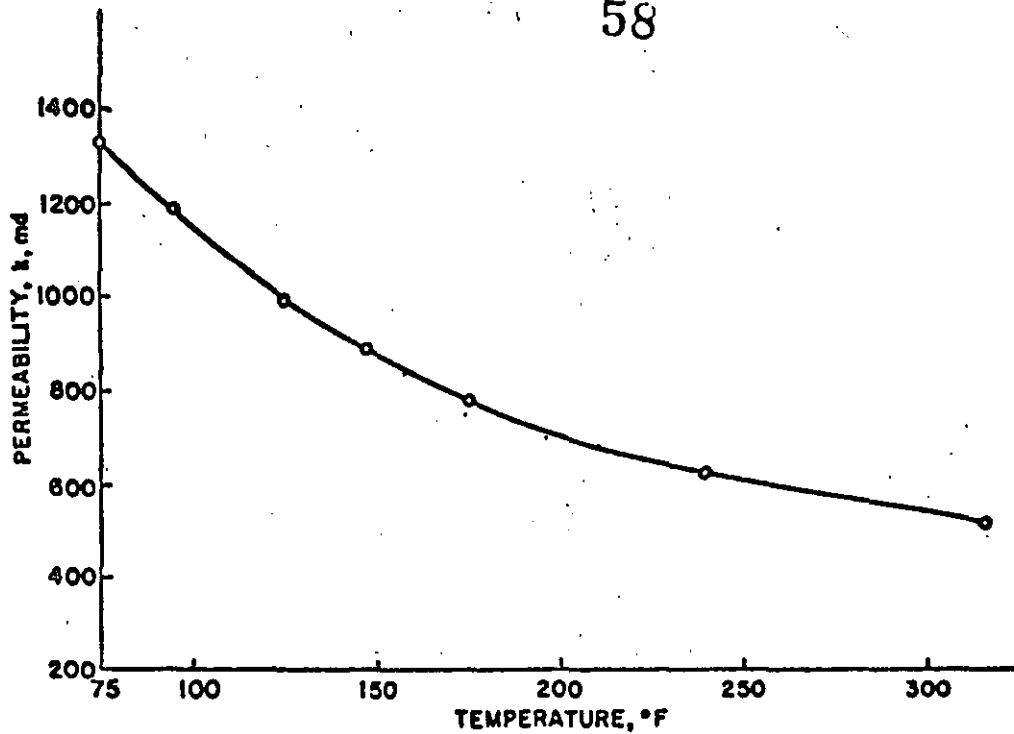


FIGURE 20 EFFECT OF TEMPERATURE ON ABSOLUTE PERMEABILITY OF BOISE SANDSTONE ; CORE NUMBER 7 (Ref. 21)

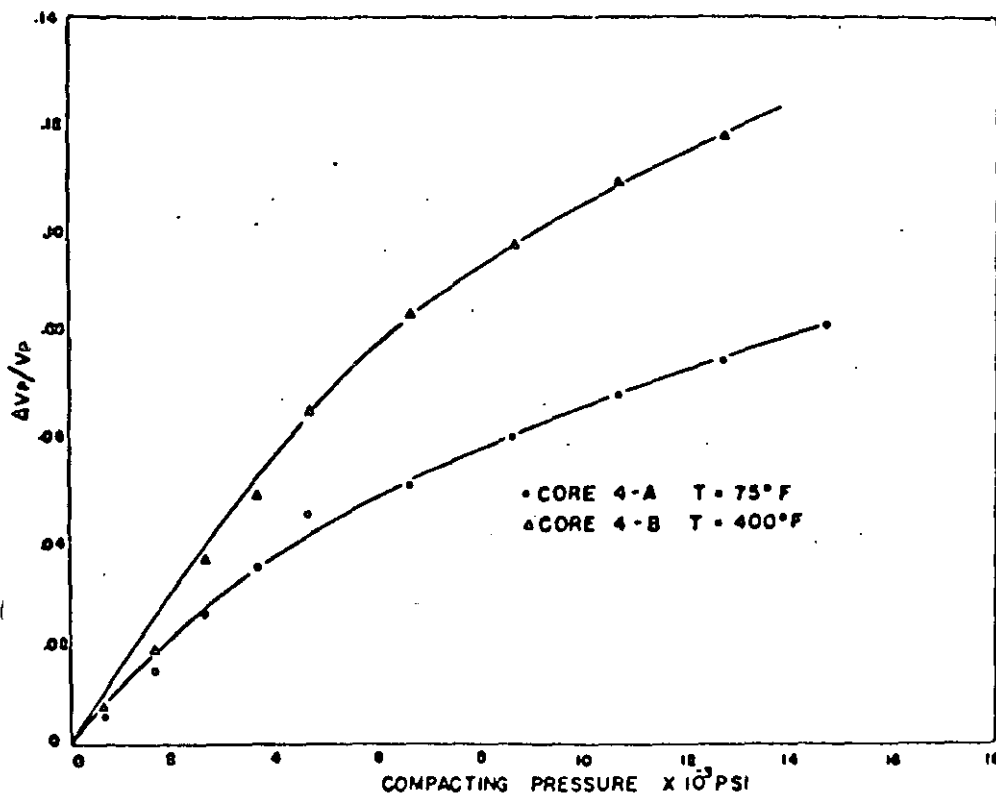


FIGURE 21 - Change in cumulative fractional pore volume with pressure core 4 at 75 and 400°F. (Ref. 24)

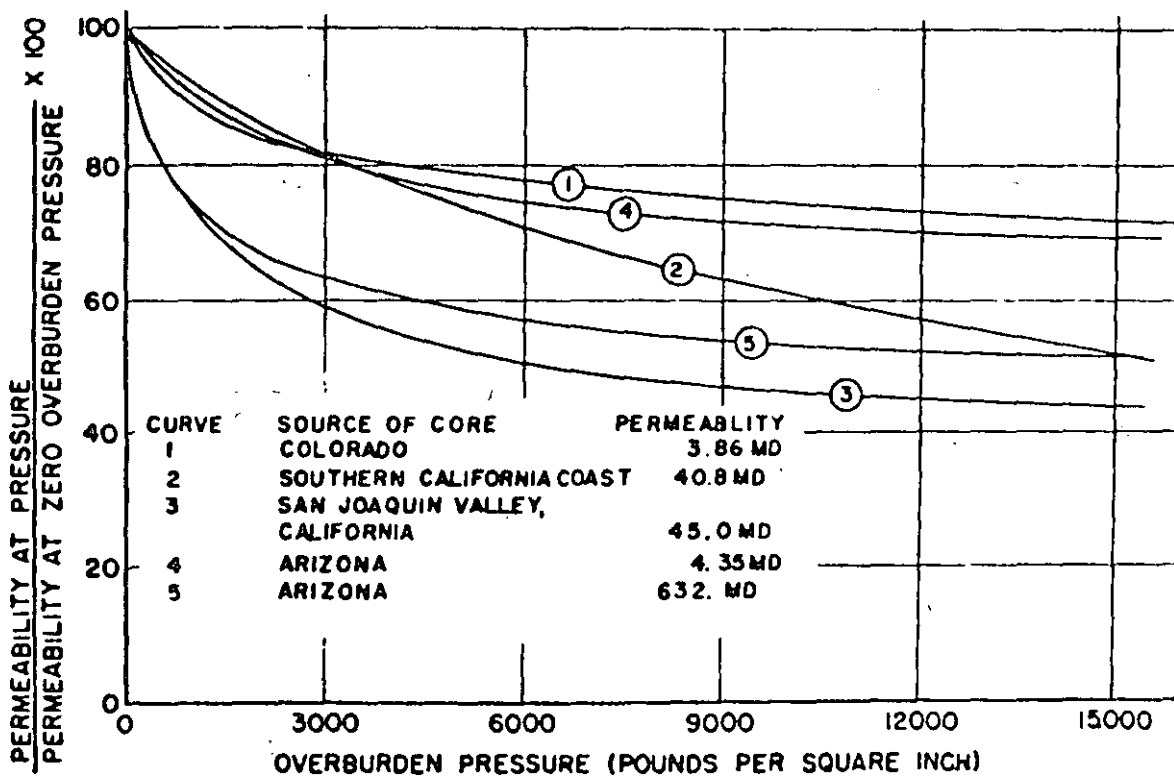


FIGURE 22

CHANGE IN PERMEABILITY WITH OVERBURDEN PRESSURE.

(Ref. 26)

FIGURE 23

PRESSURE-TEMPERATURE DIAGRAM FOR WATER

(Ref. 38)

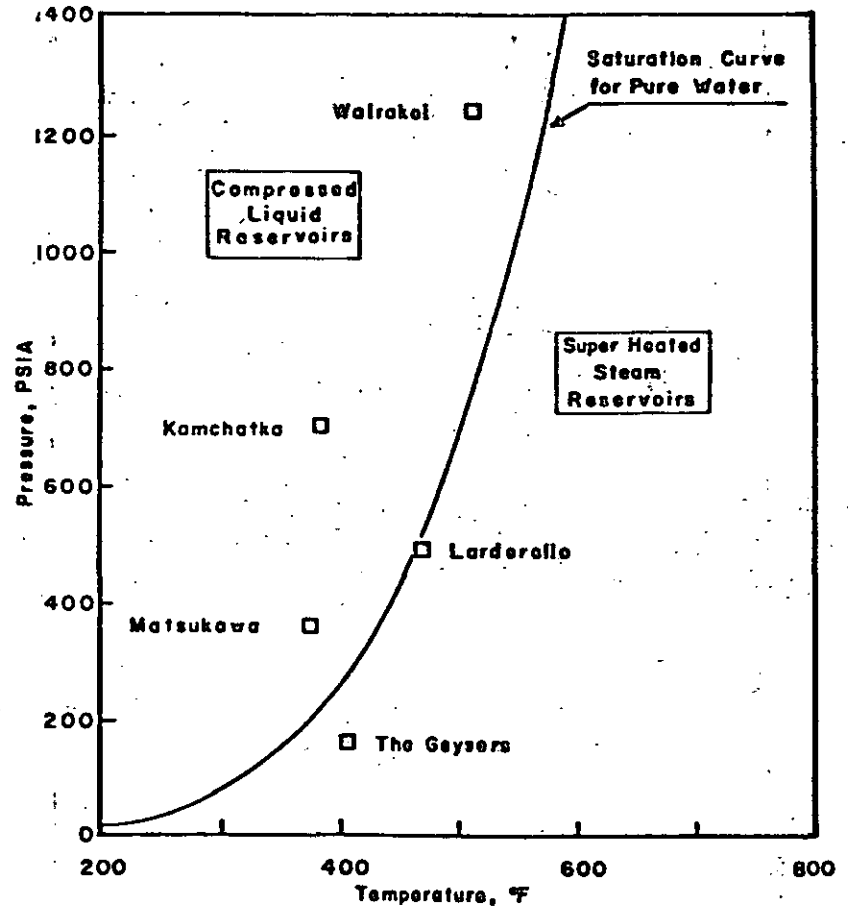
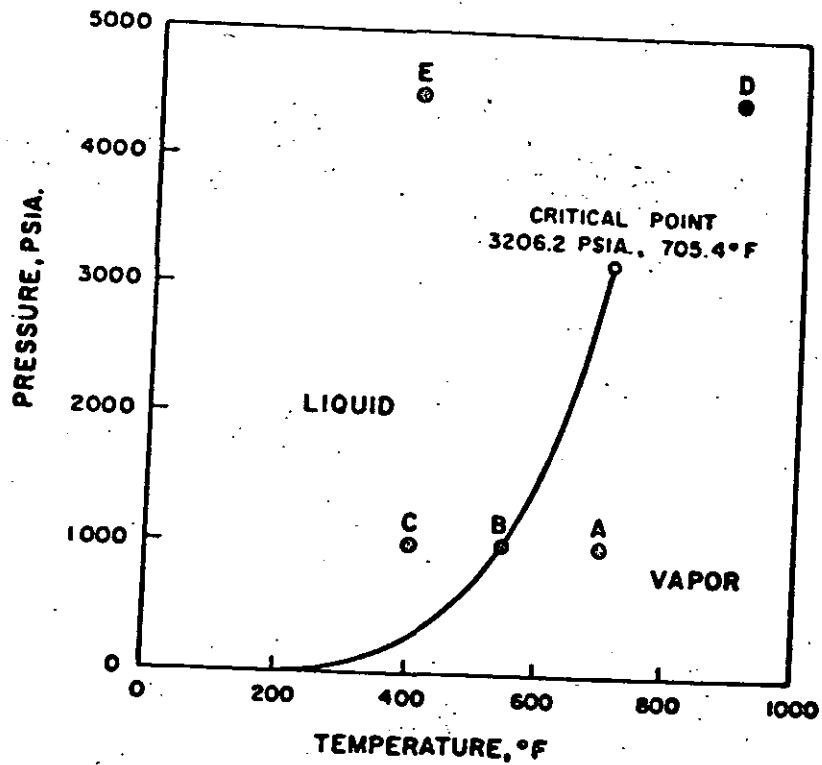


FIGURE 24 Reservoir temperature and pressure data for geothermal reservoirs

(Ref. 60)

FIGURE 25

PRESSURE-SPECIFIC VOLUME CHART FOR WATER

(Ref. 38)

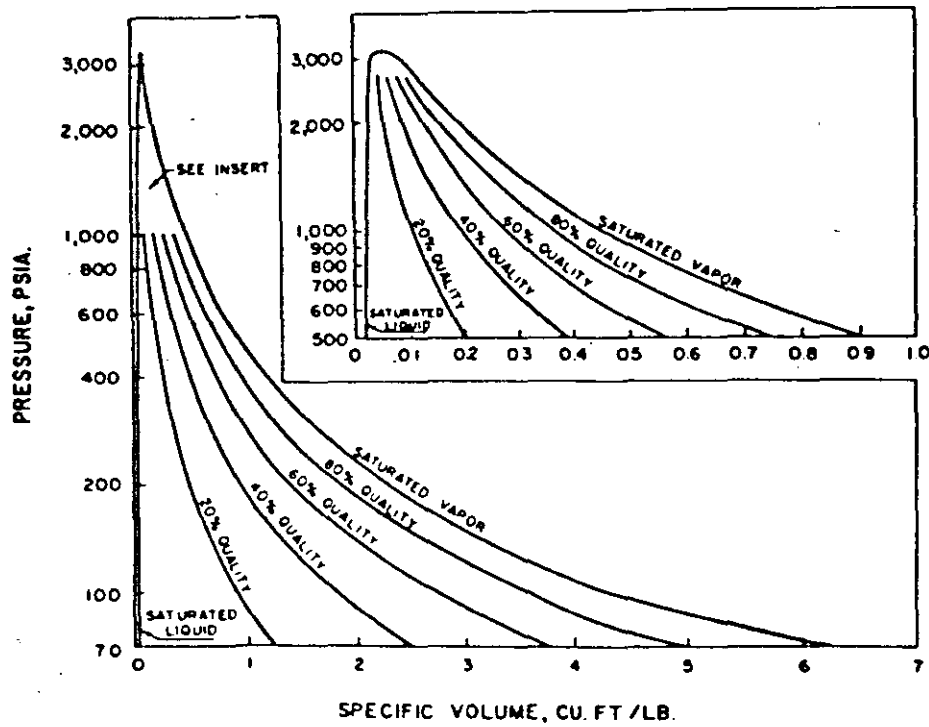


FIGURE 26

PRESSURE-ENTHALPY DIAGRAM FOR WATER

(Ref. 38)

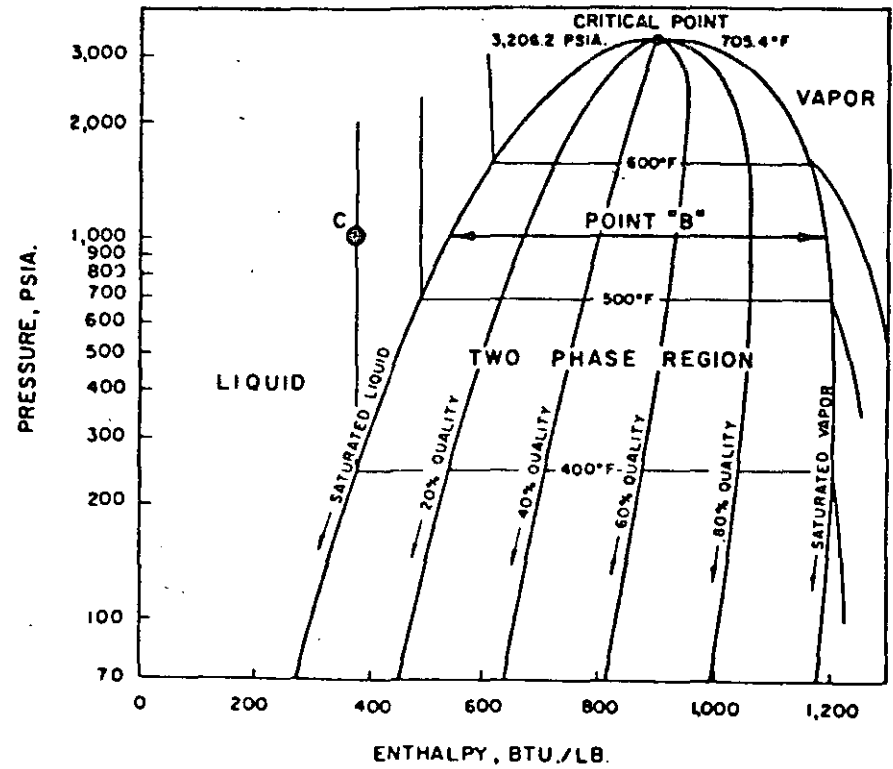


FIGURE 27

Viscosity of Saturated Water and Steam

(modified from Ref. 38)

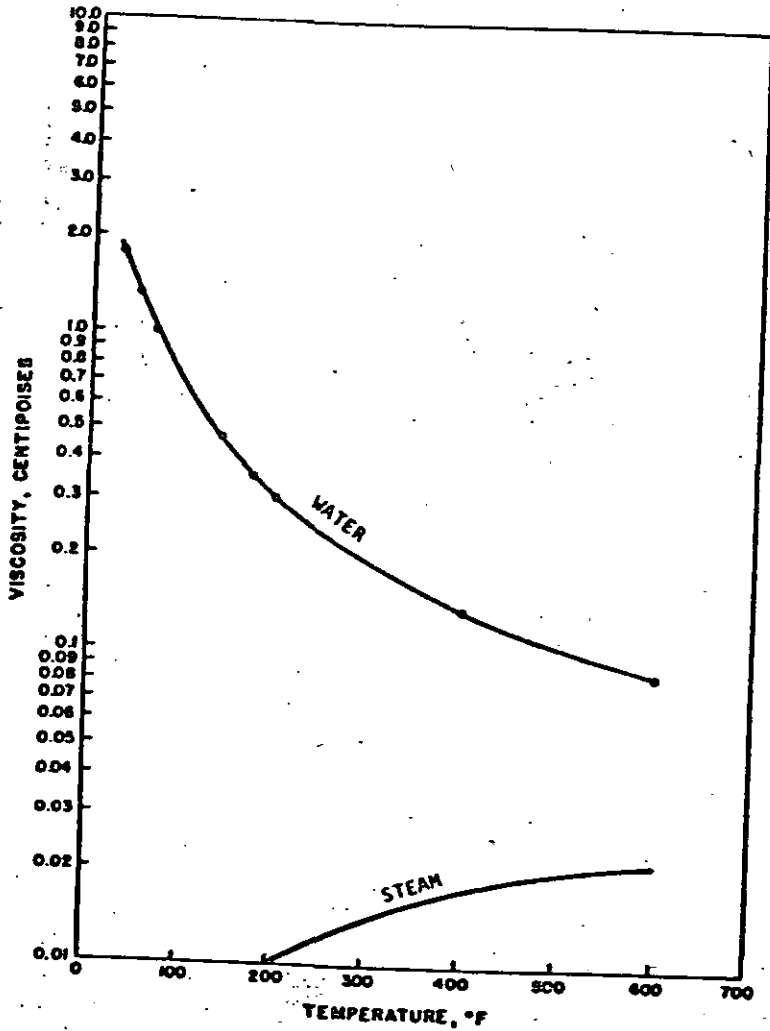


FIGURE 28. THE THERMAL CONDUCTIVITY OF SATURATED LIQUID WATER (Ref. 39)

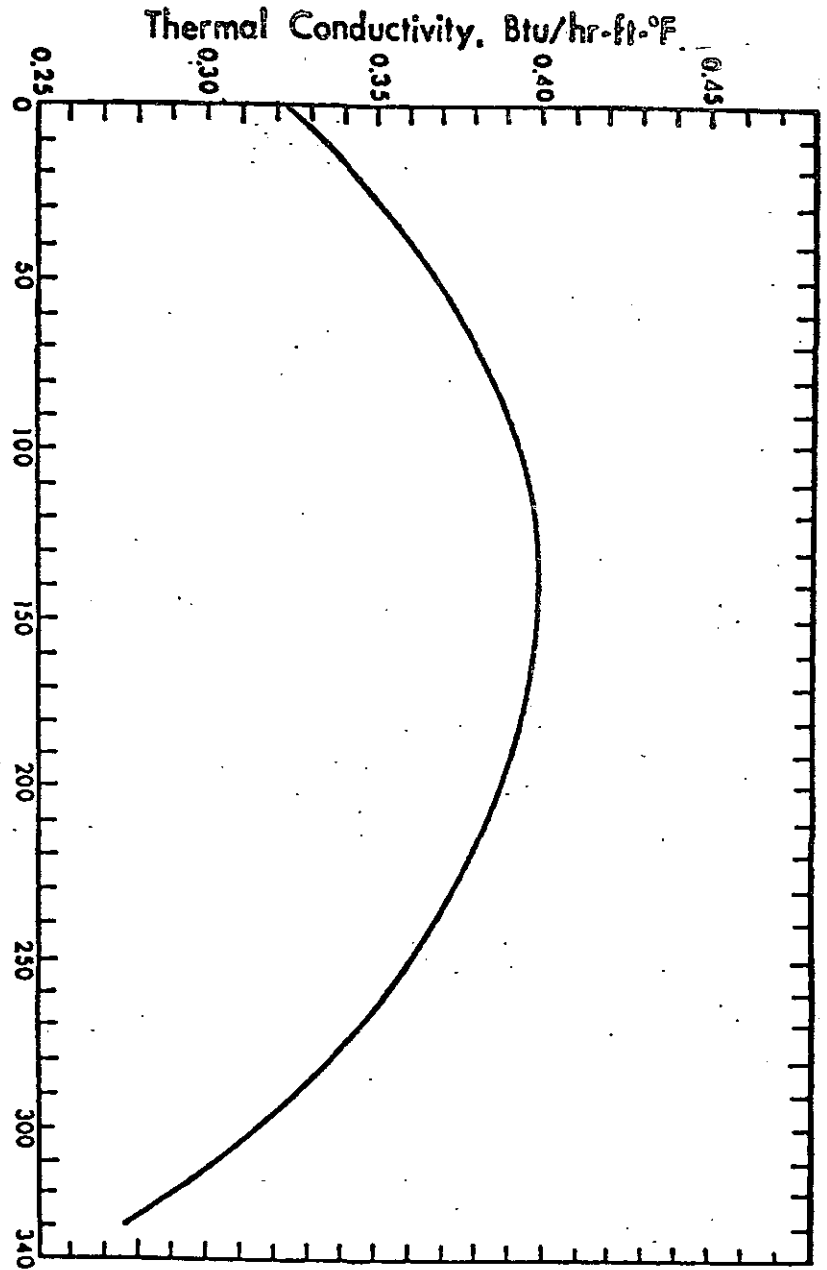




FIGURE 30

PRESSURE-SPECIFIC VOLUME CHART FOR SUPERHEATED STEAM

(Ref. 38)

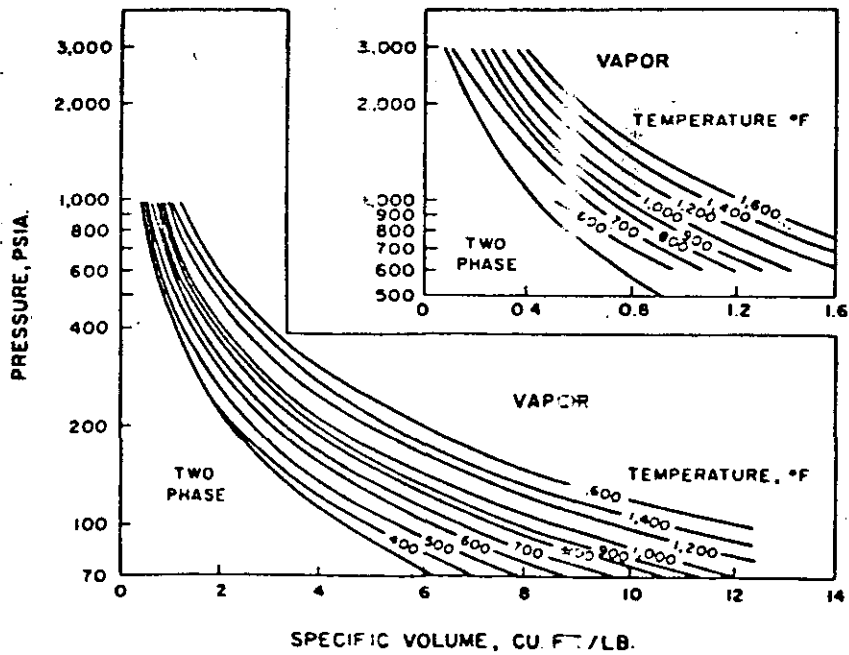


FIGURE 29

FORMATION VOLUME FACTOR FOR PURE LIQUID WATER AS A FUNCTION OF PRESSURE AND TEMPERATURE

(Ref. 38)

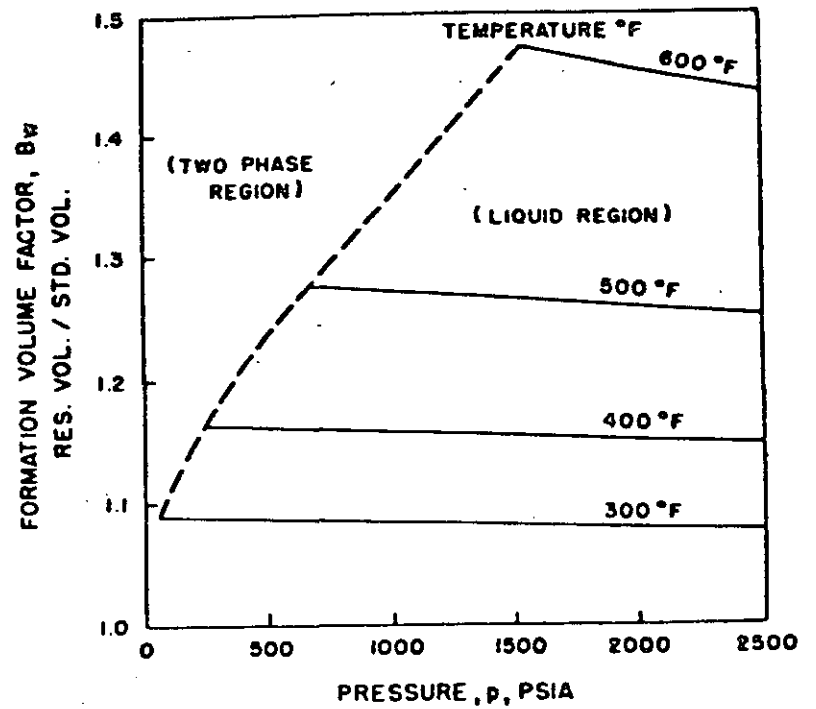


FIGURE 32  
 PRESSURE - ENTHALPY DIAGRAM FOR SUPERHEATED STEAM  
 (Ref. 38)

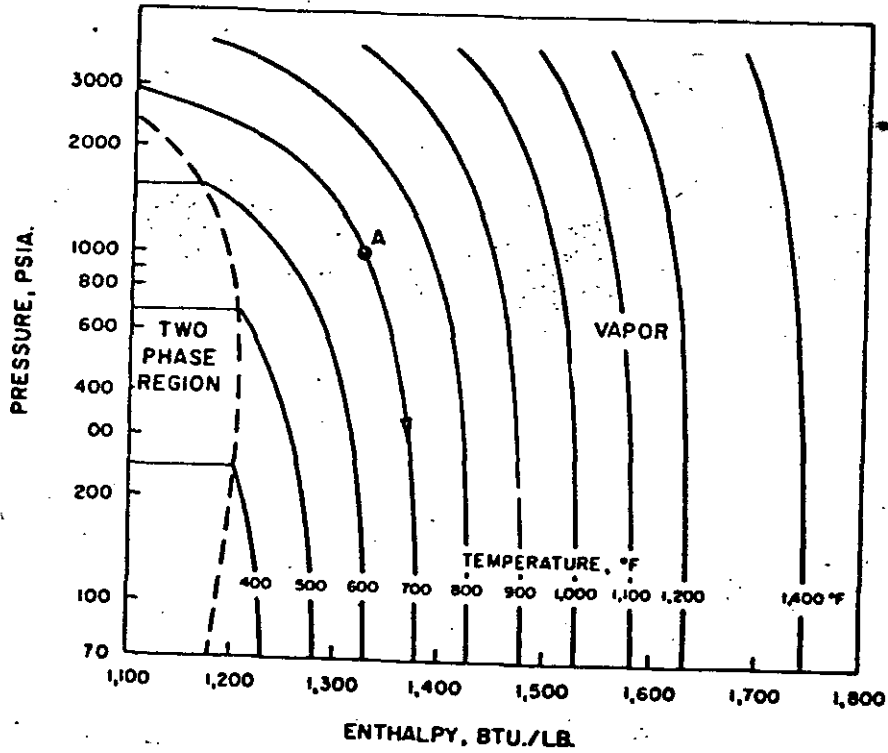
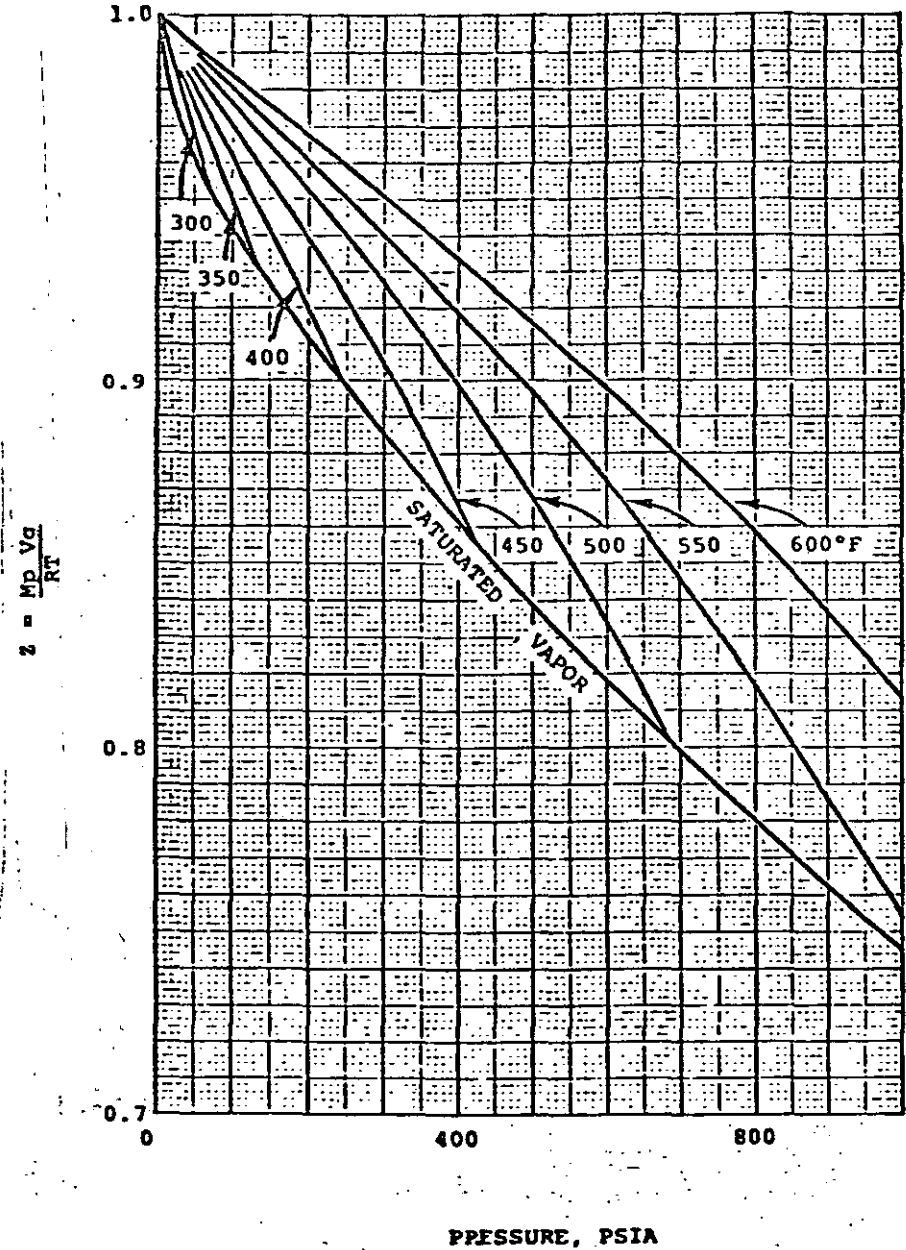


FIGURE 31  
 GAS LAW DEVIATION FACTOR FOR STEAM (Ref. 33)



1. Birch, Francis and Clark, Harry: "The Thermal Conductivity of Rocks and Its Dependence upon Temperature and Composition, Part I", Am. J. Science, 238, No. 8 (Aug. 1940), pp. 529-558.
2. Birch, Francis and Clark, Harry: "The Thermal Conductivity of Rocks and Its Dependence upon Temperature and Composition, Part II", Am. J. Science, 238, No. 9 (Sept. 1940), pp. 613-635.
3. Somerton, Wilbur H.: "Some Thermal Characteristics of Porous Rocks," Trans. AIME, 213 (1958), pp. 375-378.
4. Kunii, D. and Smith, J. M.: "Thermal Conductivities of Porous Rocks Filled with Stagnant Fluid," Soc. Pet. Engr. J. (Mar. 1961), pp. 37-42.
5. Adivarahou, P., Kunii, D. and Smith, J. M.: "Heat Transfer in Porous Rocks Through Which Single-Phase Fluids Are Flowing," Soc. Pet. Engr. J. (Sept. 1962), pp. 290-296.
6. Willhite, G. P., Dranoff, J. S. and Smith, J. M.: "Heat Transfer Perpendicular to Fluid Flow in Porous Rocks," Soc. Pet. Engr. J. (Sept. 1963), pp. 185-188.
7. Anand, J., Somerton, W. H. and Gomaa, E.: "Prediction of Thermal Properties of Formations from Other Known Properties," Paper No. SPE-4171, 43rd California Regional Meeting, SPE of AIME, Bakersfield, Calif., Nov. 8-10, 1972.
8. Tikhomirov, V. M.: "Conductivity of Rocks and Their Relationship with Density, Saturation and Temperature," Neftianoe Khoziaistro (in Russian), 46, No. 4 (1968), p. 36.
9. Gomaa, Ezzat E. and Somerton, W. H.: "Thermal Behavior of Multifluid-Saturated Formations, Part I: Effect of Wettability, Saturation and Grain Structure," Paper No. SPE 4896-A, 44th California Regional Meeting, SPE of AIME, San Francisco, Calif., April 4-5, 1974.
10. Gomaa, Ezzat E. and Somerton, W. H.: "Thermal Behavior of Multifluid-Saturated Formations, Part II: Effect of Vapor Saturation - Heat Pipe Concept and Apparent Thermal Conductivity," Paper No. SPE 4896-B, 44th California Regional Meeting, SPE of AIME, San Francisco, Calif., April 4-5, 1974.
11. Martin, W. L. and Dew, J. N.: "How to Calculate Air Requirements for Forward Combustion," Petroleum Engineer (Dec. 1964 and Feb. 1965).
12. Somerton, W. H. and Selim, M. A.: "Additional Thermal Data for Porous Rocks - Thermal Expansion and Heat of Reaction," Soc. Pet. Engr. J. (Dec. 1961), pp. 249-253.
13. Somerton, W. H. and Boozer, G. D.: "Thermal Characteristics of Porous Rocks at Elevated Temperatures," Trans. AIME, 219 (1960), pp. 418-422.
14. Klinkenberg, L. J.: "The Permeability of Porous Media to Liquids and Gases," Drilling and Production Practice (1941), pp. 200-213.

15. Raza, S. H., Treiber, L. E., and Archer, D. L.: "Wettability of Reservoir Rocks and Its Evaluation," Prod. Monthly (April 1968), 32, No. 4, pp. 2-7.
16. Killins, C. R., Nielsen, R. F. and Calhoun, J. C.: "Capillary Desaturation and Imbibition in Porous Rocks," Prod. Monthly (Dec. 1953) 18, No. 2, pp. 30-39.
17. Craig, F. F., Jr.: The Reservoir Engineering Aspects of Waterflooding, SPE Monograph, Vol. 3.
18. Muskat, M., Wyckoff, R. D., Botset, H. G. and Meres, M. W.: "Flow of Gas-liquid Mixtures through Sands," Trans., AIME (1937), 123, pp. 69-96.
19. Poston, S. W., Ysrael, S., Hossain, A. K. M. S., Montgomery, E. F. IV and Ramey, H. J., Jr.: "The Effect of Temperature on Irreducible Water Saturation and Relative Permeability of Unconsolidated Sands," Soc. Pet. Engr. J. (June 1970), pp. 171-180.
20. Sinnokrot, A. A., Ramey, H. J., Jr. and Marsden, S. S.: "Effect of Temperature Level upon Capillary Pressure Curves," Paper No. SPE 2517, presented at the 44th Annual SPE Fall Meeting, Denver, Colo., Sept. 28-Oct. 1, 1969.
21. Weinbrandt, R. M., Ramey, H. J., Jr. and Cassé, F.: "The Effect of Temperature on Relative Permeability of Consolidated Rocks," Paper No. SPE 4142, presented at the 47th Annual SPE Fall Meeting, San Antonio, Texas, Oct. 8-11, 1972.
22. Afinogenov, Y. A.: "How the Liquid Permeability of Rocks Is Affected by Pressure and Temperature," SNIGGINS (1969), No. 6, pp. 34-42 (translation from Consultants Bureau, 227 W. 17 St., New York, NY 10011).
23. Lo, H. Y. and Mungan, N.: "Effect of Temperature on Water-Oil Relative Permeabilities in Oil-Wet and Water-Wet Systems," Paper No. SPE 4505, presented at the 48th Annual SPE Fall Meeting, Las Vegas, Nevada, Sept. 30-Oct. 3, 1973.
24. Von Gonten, W. D. and Choudhary, B. K.: "The Effect of Pressure and Temperature on Pore Volume Compressibility," Paper No. SPE 2526, presented at the 44th Annual SPE Fall Meeting, Denver, Colorado, Sept. 28-Oct. 1, 1969.
25. Zoback, M. D. and Byerlee, J. D.: "Permeability, Compressibility and Effective Stress," unpublished report (Feb. 1974).
26. Fatt, I. and Davis, D. H.: "Reduction in Permeability with Overburden Pressure," Trans., AIME (1952), 195, 329.
27. Wyble, D. O.: "Effect of Applied Pressure on the Conductivity, Porosity and Permeability of Sandstones," Trans., AIME (1958), 213, pp. 430-432.
28. Dobrynin, V. M.: "Effect of Overburden Pressure on Some Properties of Sandstones," Soc. Pet. Engr. J. (Dec. 1962) 2, No. 4, pp. 360-366.
29. Gray, D. H., Fatt, I. and Bergamini, G.: "The Effect of Stress on Permeability of Sandstone Cores," Soc. Pet. Engr. J. (June 1963), pp. 95-100.

30. Wilhelmi, B. and Somerton, W. H.: "Simultaneous Measurement of Pore and Elastic Properties of Rocks under Triaxial Stress Conditions," Paper No. SPE 1706 (1967).
31. Krauskopf, K. B.: Introduction to Geochemistry, McGraw-Hill, New York, NY, 1967.
32. Butler, J. N.: Solubility and pH Calculations, Addison-Wesley, Palo Alto, CA, 1964.
33. White, E. E.: "Geochemistry Applied to the Discovery, Evaluation and Exploitation of Geothermal Energy Resources," Geothermics, Special Issue 2, Proc. of U. N. Symposium on the Development and Utilization of Geothermal Resources, Pisa, 1970, Vol. 1.
34. Fournier, R. O. and Truesdell, A. H.: "Chemical Indications of Subsurface Temperature Applied to Hot Spring Waters of Yellowstone National Park, Wyoming, U.S.A.," Geothermics, Special Issue 2, Proc. of U. N. Symposium on the Development and Utilization of Geothermal Resources, Pisa, 1970, Vol. 2, Part 1.
35. Keenan, J. H. and Keyes, F. G.: Thermodynamic Properties of Steam, John Wiley and Sons, Inc., New York, NY, 1936.
36. Meyer, C. A., McClintock, R. B., Silvestri, G. J. and Spencer, R. C., Jr.: 1967 ASME Steam Tables, Am. Soc. Mech. Engrs., 2nd ed., New York, NY, 1968.
37. Keenan, J. H.; Keyes, F. G., Hill, P. G. and Moore, J. G.: Steam Tables: Thermodynamic Properties of Water Including Vapor, Liquid and Solid Phases (English Units), John Wiley and Sons, Inc., New York, NY, 1969.
38. Whiting, R. L. and Ramey, H. J., Jr.: "Application of Material and Energy Balances to Geothermal Steam Production," J. Pet. Tech. (July 1969), pp. 893-900.
39. Farouq Ali, S. M.: Oil Recovery by Steam Injection, Producers Pub. Co., Bradford, PA, 1970.
40. Calhoun, J. C., Lewis, M., Jr. and Newman, R. C.: "Experiments on the Capillary Properties of Porous Solids," Trans. AIME, 186 (1949), pp. 189-196.
41. Edlefsen, N. E. and Anderson, A. B. C.: "Thermodynamics of Soil Moisture," Hilgardia, Calif: Agricultural Exp. Station, Univ. of Calif. at Berkeley, 15, No. 2 (Feb. 1943), p. 31.
42. Cady, G. V., Bilhartz, H. L., Jr. and Ramey, H. J., Jr.: "Model Studies of Geothermal Steam Production," Water 1972, AIChE Symposium Series (1973).
43. Amyx, J. W., Bass, D. M., Jr. and Whiting, R. L.: Petroleum Reservoir Engineering, McGraw-Hill, New York, NY, 1960.
44. Dodson, C. R. and Standing, M. B.: "Pressure-Volume-Temperature and Solubility Relations to Natural Gas-Water Mixtures," API Drilling and Production Practice, American Petroleum Institute, 1944.
45. Rowe, W. E.: "Effect of Salinity on Physical Properties of Water," Secondary Recovery of Oil in the United States, American Petroleum Institute, 1950.

Discussion Following Ramey PaperRinehart

Do you think these things would hold for large, fractured mass when you have microscopic fractures with impermeable rock in between?

Ramey

In some cases we already know that they do. There are many oil and gas reservoirs that are in fact large, fractured masses. Generally speaking, the laws of nature seem to work the same there. Now some of the details on these homogeneous porous structures, the relative permeability curve details, would not be identically the same. It has amazed me to find that some of the massive, fractured reservoirs seem to follow simple mechanics.

Okl

The permeability is a function of temperature. When the temperature is increased, the permeability becomes lower; then when the temperature is reduced, the original numerical value for permeability is reached. I mean it is almost reversible.

Ramey

It is reversible. One other thing: the shapes of the curves, whether it's temperature or pressure, are almost the same. In data where permeability ratio is plotted versus effective pressure, you will note that the shape is almost identical with what you get for temperature. In our temperature work we have kept the confining pressure constant, just varying the temperature in the system, and we see this reversible result. In our data it is perhaps not totally reversible; it will move down the line and come back up slightly below its original path. But the difference is not much. Within the experimental accuracy it appears to be reversible. On the other work, on relative permeability, most of it does seem to be temperature level reversible. If you heat a core and measure relative permeability you get one value; if you cool it off and heat it up again you get the same value.

Rinehart

These are all corrected for viscosity?

RameyRinehart

Do you feel that your correction is good?

6000 ✓ Dr. Heber Cinco

# THE APPLICATION OF THE LAPLACE TRANSFORMATION TO FLOW PROBLEMS IN RESERVOIRS.

A. F. VAN EVERDINGEN, SHELL OIL CO., HOUSTON, AND W. HURST, PETROLEUM CONSULTANT, HOUSTON, MEMBERS AIME

## ABSTRACT

For several years the authors have felt the need for a source from which reservoir engineers could obtain fundamental theory and data on the flow of fluids through permeable media in the unsteady state. The data on the unsteady state flow are composed of solutions of the equation

$$\frac{\partial^2 P}{\partial r^2} + \frac{1}{r} \frac{\partial P}{\partial r} = \frac{\partial P}{\partial t}$$

Two sets of solutions of this equation are developed, namely, for "the constant terminal pressure case" and "the constant terminal rate case." In the constant terminal pressure case the pressure at the terminal boundary is lowered by unity at zero time, kept constant thereafter, and the cumulative amount of fluid flowing across the boundary is computed, as a function of the time. In the constant terminal rate case a unit rate of production is made to flow across the terminal boundary (from time zero onward) and the ensuing pressure drop is computed as a function of the time. Considerable effort has been made to compile complete tables from which curves can be constructed for the constant terminal pressure and constant terminal rate cases, both for finite and infinite reservoirs. These curves can be employed to reproduce the effect of any pressure or rate history encountered in practice.

Most of the information is obtained by the help of the Laplace transformations, which proved to be extremely helpful for analyzing the problems encountered in fluid flow. The application of this method simplifies the more tedious mathematical analyses employed in the past. With the help of Laplace transformations some original developments were obtained (and presented) which could not have been easily foreseen by the earlier methods.

## INTRODUCTION

This paper represents a compilation of the work done over the past few years on the flow of fluid in porous media. It concerns itself primarily with the transient conditions prevailing in oil reservoirs during the time they are produced. The study is limited to conditions where the flow of fluid obeys the

diffusivity equation. Multiple-phase fluid flow has not been considered.

A previous publication by Hurst<sup>1</sup> shows that when the pressure history of a reservoir is known, this information can be used to calculate the water influx, an essential term in the material balance equation. An example is offered in the literature by Old<sup>2</sup> in the study of the Jones Sand, Seale, Field, Arkansas. The present paper contains extensive calculated data (from which work curves can be constructed) which data are derived by a more rigorous treatment of the subject matter than available in an earlier publication. The application of this information will enable those concerned with the analysis of the behavior of a reservoir to obtain quantitatively correct expressions for the amount of water that has flowed into the reservoirs, thereby satisfying all the terms that appear in the material balance equation. This work is likewise applicable to the flow of fluid to a well whenever the flow conditions are such that the diffusivity equation is obeyed.

## DIFFUSIVITY EQUATION

The most commonly encountered flow system is radial flow toward the well bore or field. The volume of fluid which flows per unit of time through each unit area of sand is expressed by Darcy's equation as

$$v = \frac{K}{\mu} \frac{\partial P}{\partial r}$$

where K is the permeability,  $\mu$  the viscosity and  $\partial P / \partial r$  the pressure gradient at the radial distance r. A material balance on a concentric element AB, expresses the net fluid traversing the surfaces A and B, which must equal the fluid lost from within the element. Thus, if the density of the fluid is expressed by  $\rho$ , then the weight of fluid per unit time and per unit sand thickness, flowing past Surface A, the surface nearest the well bore, is given as

$$2\pi r \rho \frac{K}{\mu} \frac{\partial P}{\partial r} = \frac{2\pi r K}{\mu} \left( \rho \frac{\partial P}{\partial r} \right)$$

The weight of fluid flowing past Surface B, an infinitesimal distance  $\delta r$ , removed from Surface A, is expressed as

$$\frac{2\pi K}{\mu} \left[ \rho \frac{\partial P}{\partial r} + \frac{\partial \left( \rho \frac{\partial P}{\partial r} \right)}{\partial r} \delta r \right]$$

Manuscript received at office of Petroleum Branch January 14, 1949. Paper presented at the AIME Annual Meeting in San Francisco, February 13-17, 1949. References are given at end of paper.

The difference between these two terms, namely,

$$\frac{2\pi K}{\mu} \frac{\partial}{\partial r} \left( \rho r \frac{\partial P}{\partial r} \right) \delta r,$$

is equal to the weight of fluid lost by the element AB, or

$$- 2\pi f r \frac{\partial \rho}{\partial T} \delta r$$

where  $f$  is the porosity of the formation.

This relation gives the equation of continuity for the radial system, namely,

$$\frac{K}{\mu} \frac{\partial}{\partial r} \left( \rho r \frac{\partial P}{\partial r} \right) = f r \frac{\partial \rho}{\partial T} \quad \dots \quad (II-1)$$

From the physical characteristics of fluids, it is known that density is a function of pressure and that the density of a fluid decreases with decreasing pressure due to the fact that the fluid expands. This trend expressed in exponential form is

$$\rho = \rho_0 e^{-c(P_0 - P)} \quad \dots \quad (II-2)$$

where  $P$  is less than  $P_0$ , and  $c$  the compressibility of the fluid. If we substitute Eq. II-2 in Eq. II-1, the diffusivity equation can be expressed using density as a function of radius and time, or

$$\left( \frac{\partial^2 \rho}{\partial r^2} + \frac{1}{r} \frac{\partial \rho}{\partial r} \right) \frac{K}{\mu c} = \frac{\partial \rho}{\partial T} \quad \dots \quad (II-3)$$

For liquids which are only slightly compressible, Eq. II-2 simplifies to  $\rho \cong \rho_0 [1 - c(P_0 - P)]$  which further modifies Eq. II-3 to give

$$\left( \frac{\partial^2 P}{\partial r^2} + \frac{1}{r} \frac{\partial P}{\partial r} \right) \frac{K}{\mu c} = \frac{\partial P}{\partial T} \quad \dots \quad (II-4)$$

Furthermore, if the radius of the well or field,  $R_w$ , is referred to as a unit radius, then the relation simplifies to

$$\frac{\partial^2 P}{\partial r^2} + \frac{1}{r} \frac{\partial P}{\partial r} = \frac{\partial P}{\partial t} \quad \dots \quad (II-4)$$

where  $t = KT/\mu c R_w^2$  and  $r$  now expresses the distance as a multiple of  $R_w$ , the unit radius. The units appearing in this paper are always used in connection with Darcy's equation, so that the permeability  $K$  must be expressed in darcys, the time  $T$  in seconds, the porosity  $f$  as a fraction, the viscosity  $\mu$  in centipoises, the compressibility  $c$  as volume per volume per atmosphere, and the radius  $R_w$  in centimeters.

LAPLACE TRANSFORMATION

In all publications, the treatment of the diffusivity equation has been essentially the orthodox application of the Fourier-Bessel series. This paper presents a new approach to the solution of problems encountered in the study of flowing fluids, namely, the Laplace transformation, since it was recognized that Laplace transformations offer a useful tool for solving difficult problems in less time than by the use of Fourier-Bessel series. Also, original developments have been obtained which are not easily foreseen by the orthodox methods.

If  $P_{(r)}$  is a pressure at a point in the sand and a function of time, then its Laplace transformation is expressed by the infinite integral

$$\bar{P}_{(r)} = \int_0^\infty e^{-pt} P_{(r)} dt \quad \dots \quad (III-1)$$

where the constant  $p$  in this relationship is referred to as the operator. If we treat the diffusivity equation by the process

implied by Eq. III-1, the partial differential can be transformed to a total differential equation. This is performed by multiplying each term in Eq. II-4 by  $e^{-pt}$  and integrating with respect to time between zero and infinity, as follows:

$$\int_0^\infty e^{-pt} \left( \frac{\partial^2 P}{\partial r^2} + \frac{1}{r} \frac{\partial P}{\partial r} \right) dt = \int_0^\infty e^{-pt} \frac{\partial P}{\partial t} dt \quad (III-2)$$

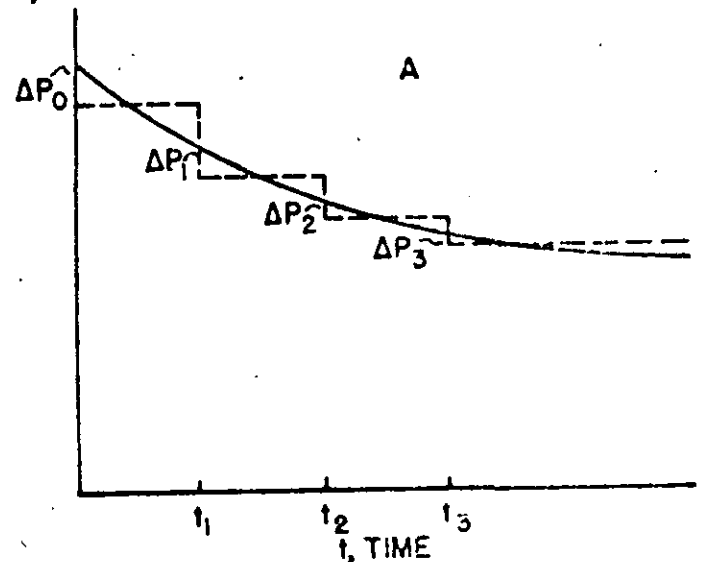
Since  $P$  is a function of radius and time, the integration with respect to time will automatically remove the time function and leave  $P$  a function of radius only. This reduces the left side to a total differential with respect to  $r$ , namely,

$$\int_0^\infty e^{-pt} \frac{\partial^2 P}{\partial r^2} dt = \frac{\partial^2 \int_0^\infty e^{-pt} P dt}{\partial r^2} = \frac{d^2 \bar{P}_{(r)}}{dr^2} \quad \text{etc.}$$

and Eq. III-2 becomes

$$\frac{d^2 \bar{P}_{(r)}}{dr^2} + \frac{1}{r} \frac{d \bar{P}_{(r)}}{dr} = \int_0^\infty e^{-pt} \frac{dP}{dt} dt$$

P, PRESSURE



q(t), RATE

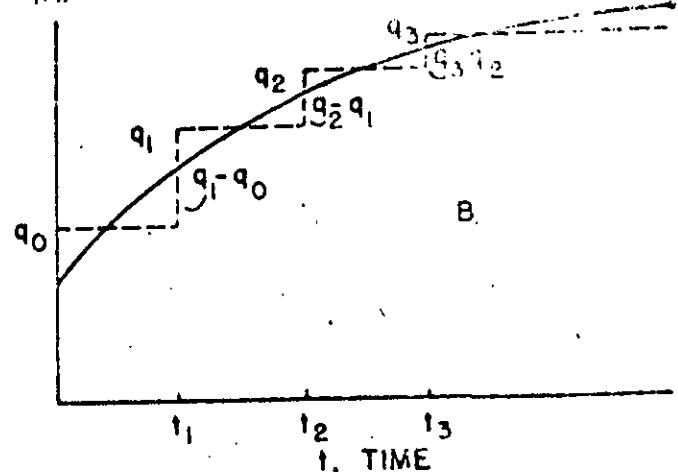


FIG. 1A - SEQUENCE CONSTANT TERMINAL PRESSURES. 1B - SEQUENCE CONSTANT TERMINAL RATES.





VI-2, with respect to  $r$  at  $r = 1$ , gives

$$\left(\frac{\partial \bar{P}}{\partial r}\right)_{r=1} = -B\sqrt{p} K_1(\sqrt{p})$$

and since

$$\left(\frac{\partial \bar{P}}{\partial r}\right)_{r=1} = -\frac{1}{p}$$

the constant  $B = 1/p^{3/2} K_1(\sqrt{p})$ . Therefore, the transform for the pressure drop for the constant rate case in an infinite medium is given by

$$\bar{P}_{(r,s)} = \frac{K_0(r\sqrt{p})}{p^{3/2} K_1(\sqrt{p})} \quad \text{VI-4}$$

To determine the inverse of Eq. VI-4 in order to establish the pressure drop at radius unity, we can resort to the simplification that for small times the operator  $p$  is large. Since

$$K_0(z) = \sqrt{\frac{\pi}{2z}} e^{-z} \quad \text{VI-5}$$

for  $z$  large, W.B.F., p. 202, then

$$\bar{P}_{(r,s)} = \frac{1}{p^{3/2}} \quad \text{VI-6}$$

The inversion for this transform is given in Campbell and Foster, Eq. 516, as

$$P_{(r,t)} = \frac{2}{\sqrt{\pi}} t^{3/2} \quad \text{VI-7}$$

In brief, Eq. VI-7 states that when  $t = KT/f\mu cR_0^2$  is small, which can be caused by the boundary radius for the field,  $R_0$ , being large, the pressure drop for the unit rate of production approximates the condition for linear flow.

To justify this conclusion, the treatment of the linear flow equation, Eq. IV-5, by the Laplace transformation gives

$$\frac{d^2 \bar{P}_{(x,p)}}{dx^2} = p\bar{P}_{(x,p)} \quad \text{VI-8}$$

for which the general solution is the expression

$$\bar{P}_{(x,p)} = Ae^{-x\sqrt{p}} + Be^{x\sqrt{p}} \quad \text{VI-9}$$

By repeating the reasoning already employed in this development, the transform for the pressure drop at  $x = 0$  gives

$$\bar{P}(0\sqrt{p}) = 1/p^{3/2}$$

which is identical with (VI-6) with  $p$  the operator of  $t = KT/f\mu c$ .

The second simplification for the transform (VI-4) is to consider  $p$  small, which is equivalent to considering time,  $t$ , large. The expansions for  $K_0(z)$  and  $K_1(z)$  are given in Carslaw and Jaeger, p. 248.

$$K_0(z) = -I_0(z) \left\{ \log \frac{z}{2} + \gamma \right\} + \left(\frac{z}{2}\right)^2 + \frac{\left(1 + \frac{1}{2}\right) \left(\frac{z}{2}\right)^4}{(2!)^2} + \frac{\left(1 + \frac{1}{2} + \frac{1}{3}\right) \left(\frac{z}{2}\right)^6}{(3!)^2} + \dots \quad \text{VI-10}$$

$$K_1(z) = -(-1)^{n-1} I_n(z) \left\{ \log \frac{z}{2} + \gamma \right\} + \frac{1}{2} (-1)^n \sum_{r=1}^{\infty} \frac{\left(\frac{z}{2}\right)^{2n+r}}{r! (n+r)!} \left[ \sum_{m=1}^n m^{-1} + \sum_{m=1}^{\infty} m^{-1} \right] + \frac{1}{2} \sum_{r=1}^{n-1} \frac{(-1)^r \left(\frac{z}{2}\right)^{2n+r}}{r!} \frac{(n-r-1)!}{r!} \quad \text{VI-11}$$

where  $\gamma$  is Euler's constant 0.57722, and the logarithmic term consists of natural logarithms. When  $z$  is small

$$K_0(z) \cong - \left[ \log \frac{z}{2} + \gamma \right] \quad \text{VI-12}$$

$$K_1(z) \cong 1/z \quad \text{VI-13}$$

Therefore, Eq. VI-4 becomes

$$\bar{P}_{(r,s)} = \frac{-\log p}{2p} + \frac{(\log 2 - \gamma)}{p} \quad \text{VI-14}$$

The inversion for the first term on the right is given by Campbell and Foster, Eq. 892, and the inverse of the second term by

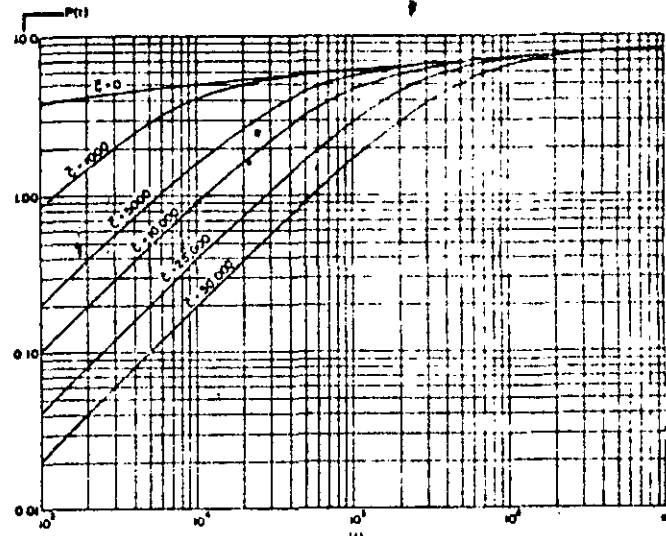


FIG. 8 - CONSTANT RATE OF PRODUCTION IN THE STOCK TANK, ADJUSTING FOR THE UNLOADING OF FLUID IN THE ANNULUS,  $P(t)$  VERSUS  $t$  WHERE  $c = c/2\pi r_0^2$ , AND  $c$  IS THE VOLUME OF FLUID UNLOADED FROM THE ANNULUS, CORRECTED TO RESERVOIR CONDITIONS, PER ATMOSPHERE BOTTOM-HOLE PRESSURE DROP, PER UNIT SAND THICKNESS.

Eq. V-1. Therefore, the pressure drop at the boundary of the field when  $t$  is large is given by

$$P_{(r,t)} = \frac{1}{2} [\log 4t - \gamma] = \frac{1}{2} [\log t + 0.60206] \quad \text{VI-15}$$

The solution given by Eq. VI-15 to the problem of the continuous point source for large time  $t$ . The relationship has been applied to the flow of fluids by Ellis, et al and others, and is particularly applicable to the case of interference between flowing wells.

The point source solution originally developed by Lord Kelvin and discussed in Carslaw can be expressed as

$$P_{(r,t)} = \frac{1}{2} \int_0^{\infty} \frac{e^{-u}}{u} du = \frac{1}{2} \left\{ -Ei \left( -\frac{1}{4t} \right) \right\} \quad \text{VI-16}$$

often referred to as the logarithmic integral or the Ei-function. Its values are given in Tables of Sine, Cosine, and Exponential Integrals, Volumes I and II, Federal Works Agency, W.P.A., City of New York. For large values of the time,  $t$ ,

Eq. VI-16 reduces to  $P_{(r,t)} = \frac{1}{2} [\log 4t - \gamma]$  which is Eq. VI-15, and this relation is accurate for values of  $t > 100$ .



$$P_{(r, t)} - P_{(r, 0)} = \frac{2}{\pi} \int_0^\infty \frac{(e^{-u^2 t} - e^{-u^2 t_0}) [J_0(u) Y_0(ur) - Y_0(u) J_0(ur)] du}{u^2 [J_0^2(u) + Y_0^2(u)]} \quad (VI-26)$$

If we are interested in the cumulative fluid influx at the field radius,  $r = 1$ , then the relationship Eq. IV-3 applies, or

$$Q_{(t)} = \int_0^t \left( \frac{\partial P}{\partial r} \right)_{r=1} dt \quad (IV-3)$$

The determination of the transform of the gradient of the pressure drop at the field's edge follows from Eq. VI-25,

$$\left( \frac{\partial \bar{P}_{(r, p)}}{\partial r} \right)_{r=1} = - \frac{K_1(\sqrt{p})}{p^{3/2} K_0(\sqrt{p})}$$

since  $K_0'(z) = -K_1(z)$ . Since the pressure drop  $P_{(r, t)}$  corresponds to the difference between the initial and actual pressure, the transform of the gradient of the actual pressure at  $r = 1$  is given by

$$\left( \frac{\partial \bar{P}}{\partial r} \right)_{r=1} = \left( \frac{-\partial \bar{P}_{(r, p)}}{\partial r} \right)_{r=1}$$

or

$$\left( \frac{\partial \bar{P}}{\partial r} \right)_{r=1} = \frac{K_1(\sqrt{p})}{p^{3/2} K_0(\sqrt{p})}$$

which corresponds to the integrand of Eq. IV-3. Further, from the definition given by Theorem B, namely, that if  $\bar{P}(p)$  is the transform of  $P_{(r, t)}$ , then the transform of  $\int_0^t P_{(r, t)} dt$  is given by  $\bar{P}(p)/p$  and the Laplace transform for  $Q_{(t)}$  is expressed by

$$\bar{Q}_{(t)} = \frac{K_1(\sqrt{p})}{p^{3/2} K_0(\sqrt{p})} \quad (VI-27)$$

The application of the Mellin's inversion formula to Eq. VI-27 follows the paths shown in Fig. 2, giving

$$Q_{(t)} = \frac{4}{\pi} \int_0^\infty \frac{(1 - e^{-u^2 t}) du}{u^2 [J_0^2(u) + Y_0^2(u)]} \quad (VI-28)$$

With respect to the transform  $\bar{Q}_{(t)}$ , there is the simplification that for time small,  $p$  is large, or Eq. VI-27 reduces to

$$Q_{(t)} = 1/p^{3/2} \quad (VI-29)$$

and the inversion is as before

$$Q_{(t)} = \frac{2}{\sqrt{\pi}} t^{3/2} \quad (VI-30)$$

which is identical to the linear flow case. For all other values of the time, Eq. VI-28 must be solved numerically.

*Relation Between  $\bar{Q}(p)$ , and  $\bar{P}(p)$*

It is evident from the work that has already gone before, that the Laplace transformation and the superimposition theorem offer a basis for interchanging the constant terminal pressure to the constant terminal rate case, and vice versa. In any reservoir study the essential interest is the analyses of the flow either at the well bore or the field boundary. The purpose of this work is to determine the relationship between  $Q(t)$ , the constant terminal pressure case, and  $P(t)$ , the constant terminal rate case, which explicitly refer to the boundary  $r = 1$ . Therefore, if we conceive of the influx of fluid into a

TABLE I — Radial Flow, Constant Terminal Pressure and Constant Terminal Rate Cases for Infinite Reservoirs

$t_D$	$Q_{(t)}$	$P_{(t)}$	$t$	$Q_{(t)}$
1.0(10) <sup>-2</sup>	0.112	0.112	1.5(10) <sup>2</sup>	4.186(10) <sup>2</sup>
5.0 "	0.278	0.278	2.0 "	3.315 "
1.0(10) <sup>-1</sup>	0.404	0.316	2.5 "	6.466 "
1.5 "	0.520	0.376	3.0 "	7.560 "
2.0 "	0.606	0.424	4.0 "	9.757 "
2.5 "	0.689	0.469	5.0 "	11.68 "
3.0 "	0.758	0.503	6.0 "	13.75 "
4.0 "	0.898	0.564	7.0 "	15.99 "
5.0 "	1.020	0.616	8.0 "	18.00 "
6.0 "	1.140	0.659	9.0 "	19.99 "
7.0 "	1.251	0.702	1.0(10) <sup>1</sup>	21.96 "
8.0 "	1.359	0.738	1.5 "	23.146(10) <sup>1</sup>
9.0 "	1.469	0.772	2.0 "	4.079 "
1.0 "	1.570	0.802	2.5 "	4.964 "
1.5 "	2.032	0.927	3.0 "	5.851 "
2.0 "	2.442	1.020	4.0 "	7.634 "
2.5 "	2.838	1.101	5.0 "	9.312 "
3.0 "	3.209	1.169	6.0 "	11.03 "
4.0 "	3.897	1.275	7.0 "	12.69 "
5.0 "	4.541	1.362	8.0 "	14.31 "
6.0 "	5.148	1.436	9.0 "	15.95 "
7.0 "	5.749	1.500	1.0(10) <sup>1</sup>	17.56 "
8.0 "	6.314	1.556	1.5 "	2.538(10) <sup>1</sup>
9.0 "	6.861	1.614	2.0 "	3.308 "
1.0(10) <sup>1</sup>	7.417	1.671	2.5 "	4.066 "
1.5 "	9.965	1.829	3.0 "	4.817 "
2.0 "	1.229(10) <sup>1</sup>	1.960	4.0 "	6.267 "
2.5 "	1.455 "	2.067	5.0 "	7.499 "
3.0 "	1.681 "	2.147	6.0 "	9.113 "
4.0 "	2.088 "	2.252	7.0 "	10.81 "
5.0 "	2.482 "	2.338	8.0 "	11.69 "
6.0 "	2.860 "	2.470	9.0 "	13.26 "
7.0 "	3.228 "	2.580	1.0(10) <sup>1</sup>	14.62 "
8.0 "	3.699 "	2.614	1.5 "	2.120(10) <sup>1</sup>
9.0 "	3.942 "	2.672	2.0 "	2.751 "
1.0(10) <sup>1</sup>	4.301 "	2.723	2.5 "	3.427 "
1.5 "	5.980 "	2.921	3.0 "	4.064 "
2.0 "	7.586 "	3.064	4.0 "	5.313 "
2.5 "	9.120 "	3.173	5.0 "	6.544 "
3.0 "	10.58 "	3.253	6.0 "	7.761 "
4.0 "	13.48 "	3.406	7.0 "	8.963 "
5.0 "	16.24 "	3.516	8.0 "	10.16 "
6.0 "	18.97 "	3.608	9.0 "	11.34 "
7.0 "	21.60 "	3.681	1.0(10) <sup>1</sup>	12.52 "
8.0 "	24.23 "	3.750		
9.0 "	26.77 "	3.809		
1.0(10) <sup>1</sup>	29.31 "	3.860		

TABLE I — Continued

$t_D$	$Q_{(t)}$	$t$	$Q_{(t)}$
1.5(10) <sup>1</sup>	1.828(10) <sup>1</sup>	1.5(10) <sup>1</sup>	1.77(10) <sup>1</sup>
2.0 "	2.398 "	2.0 "	1.55 "
2.5 "	2.961 "	2.5 "	1.37 "
3.0 "	3.517 "	3.0 "	2.29 "
4.0 "	4.610 "	4.0 "	3.62 "
5.0 "	5.689 "	5.0 "	3.73 "
6.0 "	6.758 "	6.0 "	4.47 "
7.0 "	7.818 "	7.0 "	5.19 "
8.0 "	8.868 "	8.0 "	5.53 "
9.0 "	9.911 "	9.0 "	5.54 "
1.0(10) <sup>2</sup>	10.95 "	1.0(10) <sup>2</sup>	5.24 "
1.5 "	1.601(10) <sup>2</sup>	1.5 "	1.04(10) <sup>2</sup>
2.0 "	2.168 "	2.0 "	1.42 "
2.5 "	2.647 "		
3.0 "	3.100 "		
4.0 "	4.071 "		
5.0 "	5.022 "		
6.0 "	5.951 "		
7.0 "	6.925 "		
8.0 "	7.865 "		
9.0 "	8.797 "		
1.0(10) <sup>3</sup>	9.725 "		
1.5 "	1.429(10) <sup>3</sup>		
2.0 "	1.890 "		
2.5 "	2.328 "		
3.0 "	2.771 "		
4.0 "	3.645 "		
5.0 "	4.510 "		
6.0 "	5.368 "		
7.0 "	6.220 "		
8.0 "	7.066 "		
9.0 "	7.909 "		
1.0(10) <sup>4</sup>	8.747 "		
1.5 "	1.268(10) <sup>4</sup>		
2.0 "	1.697 "		
2.5 "	2.103 "		
3.0 "	2.563 "		
4.0 "	3.299 "		
5.0 "	4.057 "		
6.0 "	4.863 "		
7.0 "	5.643 "		
8.0 "	6.414 "		
9.0 "	7.183 "		
1.0(10) <sup>5</sup>	7.948 "		

TABLE II — Constant Terminal Pressure Case  
Radial Flow, Limited Reservoirs

R = 1.5 a <sub>1</sub> = 2.8599 a <sub>2</sub> = 0.2452		R = 2.0 a <sub>1</sub> = 1.3604 a <sub>2</sub> = 4.6168		R = 2.5 a <sub>1</sub> = 0.8563 a <sub>2</sub> = 3.0876		R = 3.0 a <sub>1</sub> = 0.6256 a <sub>2</sub> = 2.3041	
t	Q <sub>(t)</sub>	t	Q <sub>(t)</sub>	t	Q <sub>(t)</sub>	t	Q <sub>(t)</sub>
0.0(10) <sup>-3</sup>	0.276	0.0(10) <sup>-1</sup>	0.278	0.0(10) <sup>-1</sup>	0.408	0.0(10) <sup>-1</sup>	0.765
0.0	0.301	7.5	0.318	1.5	0.800	4.0	0.805
0.0	0.330	1.0(10) <sup>-1</sup>	0.404	2.0	0.809	5.0	1.023
0.0	0.354	1.25	0.458	2.5	0.881	6.0	1.143
0.0	0.373	1.50	0.507	3.0	0.768	7.0	1.258
0.0	0.395	1.75	0.553	3.5	0.829	8.0	1.303
0.0	0.414	2.00	0.597	4.0	0.897	9.0	1.406
0.0	0.431	2.25	0.638	4.5	0.902	1.00	1.543
0.0	0.446	2.50	0.678	5.0	1.024	1.25	1.701
0.0	0.461	2.75	0.715	5.5	1.043	1.50	1.907
0.0	0.474	3.00	0.751	6.0	1.140	1.75	2.184
0.0	0.486	3.25	0.785	6.5	1.195	2.00	2.353
0.0	0.497	3.50	0.817	7.0	1.248	2.25	2.507
0.0	0.507	3.75	0.848	7.5	1.220	2.50	2.646
0.0	0.517	4.00	0.877	8.0	1.348	2.75	2.772
0.0	0.525	4.25	0.905	8.5	1.395	3.00	2.890
0.0	0.533	4.50	0.932	9.0	1.440	3.25	2.990
0.0	0.541	4.75	0.958	9.5	1.484	3.50	3.084
0.0	0.548	5.00	0.983	1.0	1.526	3.75	3.170
0.0	0.554	5.25	1.008	1.1	1.605	4.00	3.247
0.0	0.559	5.50	1.070	1.2	1.679	4.25	3.317
0.0	0.565	5.75	1.108	1.3	1.747	4.50	3.381
0.0	0.571	6.00	1.145	1.4	1.811	4.75	3.439
0.0	0.582	6.25	1.174	1.5	1.870	5.00	3.491
0.0	0.588	6.50	1.203	1.6	1.924	5.25	3.538
0.0	0.594	6.75	1.233	1.7	1.978	5.50	3.581
0.0	0.599	7.00	1.258	1.8	2.022	5.75	3.717
0.0	0.603	7.25	1.330	2.0	2.106	6.00	3.767
0.0	0.606	7.50	1.358	2.2	2.178	6.25	3.809
0.0	0.613	7.75	1.382	2.4	2.241	6.50	3.843
0.0	0.617	8.00	1.402	2.6	2.294	6.75	3.894
0.0	0.621	8.25	1.432	2.8	2.340	7.00	3.928
0.0	0.623	8.50	1.444	3.0	2.380	7.25	3.951
0.0	0.624	8.75	1.453	3.4	2.444	7.50	3.987
0.0		9.00	1.468	3.8	2.491	7.75	3.985
0.0		9.25	1.487	4.2	2.525	8.00	3.993
0.0		9.50	1.495	4.6	2.551	8.25	3.997
0.0		9.75	1.499	5.0	2.570	8.50	3.999
0.0		10.00	1.500	5.5	2.589	8.75	3.999
0.0				6.0	2.619	9.00	4.000
0.0				7.0	2.622	9.25	
0.0				8.0		9.50	
0.0				9.0		9.75	
0.0				10.0	2.624	10.00	

well or field as a constant rate problem, then the actual cumulative fluid produced as a function of the cumulative pressure drop is expressed by the superposition relationship in Eq. IV-14 as

$$Q_{(t)} = 2\pi cR_s^2 \int_0^t \frac{d\Delta P}{dt'} Q_{(t-t')} dt' \quad (IV-14)$$

when  $\Delta P$  is the cumulative pressure drop at the well bore affected by producing the well at constant rate which is established by

$$\Delta P = \frac{q_{(t)} \mu P_{(t)}}{2\pi K} \quad (IV-11)$$

The substitution of Eq. IV-11 in IV-14 gives

$$Q_{(t)} = \frac{q_{(t)} \mu c R_s^2}{K} \int_0^t \frac{d P_{(t')}}{dt'} Q_{(t-t')} dt'$$

Since the rate is constant,  $Q_{(t)} = q_{(t)} \times T$ , and as  $t = KT / \mu c R_s^2$  this relation becomes

$$t = \int_0^t \frac{d P_{(t')}}{dt'} Q_{(t-t')} dt' \quad (VI-31)$$

To express Eq. VI-31 in transformation form, the transform for  $t$  is  $1/p^2$ , Campbell and Foster, Eq. 408.1. The transform for  $P_{(t)}$  at  $r = 1$  is  $\bar{P}_{(t)}$ , and it follows from Theorem A that the transform of  $\frac{dP_{(t)}}{dt}$  is  $p\bar{P}_{(t)}$ , as the cumulative pressure drop  $P_{(t)}$  for constant rate is zero at time zero. Finally from Theorem D, the transform for the integration of the form Eq. VI-31 is equal to the product of the transforms for each of the two terms in the integrand, or

TABLE II — Continued

R = 3.5 a <sub>1</sub> = 0.4851 a <sub>2</sub> = 1.8574		R = 4.0 a <sub>1</sub> = 0.3935 a <sub>2</sub> = 1.5267		R = 4.5 a <sub>1</sub> = 0.3298 a <sub>2</sub> = 1.3051		R = 5.0 a <sub>1</sub> = 0.2823 a <sub>2</sub> = 1.1892		R = 6.0 a <sub>1</sub> = 0.2162 a <sub>2</sub> = 0.9025	
t	Q <sub>(t)</sub>	t	Q <sub>(t)</sub>	t	Q <sub>(t)</sub>	t	Q <sub>(t)</sub>	t	Q <sub>(t)</sub>
1.00	1.571	2.00	2.442	2.5	2.835	3.0	3.195	6.0	5.148
1.20	1.781	2.20	2.598	3.0	3.195	3.5	3.542	6.5	5.440
1.40	1.940	2.40	2.748	3.5	3.537	4.0	3.875	7.0	5.724
1.60	2.111	2.60	2.893	4.0	3.859	4.5	4.193	7.5	6.002
1.80	2.273	2.80	3.034	4.5	4.165	5.0	4.499	8.0	6.273
2.00	2.427	3.00	3.170	5.0	4.454	5.5	4.792	8.5	6.537
2.20	2.574	3.25	3.314	5.5	4.727	6.0	5.074	9.0	6.785
2.40	2.718	3.50	3.453	6.0	4.986	6.5	5.345	9.5	7.047
2.60	2.849	3.75	3.645	6.5	5.231	7.0	5.605	10.0	7.293
2.80	2.978	4.00	3.792	7.0	5.464	7.5	5.854	10.5	7.533
3.00	3.098	4.25	3.932	7.5	5.684	8.0	6.094	11	7.767
3.25	3.212	4.50	4.068	8.0	5.892	8.5	6.325	12	8.220
3.50	3.319	4.75	4.198	8.5	6.089	9.0	6.547	13	8.661
3.75	3.407	5.00	4.323	9.0	6.276	9.5	6.760	14	9.083
4.00	3.488	5.25	4.500	9.5	6.453	10	6.965	15	9.456
4.25	3.562	5.50	4.770	10	6.621	11	7.150	16	9.820
4.50	3.630	5.75	4.982	11	6.930	12	7.706	17	10.19
4.75	3.691	6.00	5.169	12	7.208	13	8.035	18	10.53
5.00	3.747	6.25	5.343	13	7.457	14	8.339	19	10.83
5.25	3.800	6.50	5.504	14	7.680	15	8.620	20	11.16
5.50	3.850	6.75	5.653	15	7.880	16	8.879	22	11.74
5.75	3.897	7.00	5.790	16	8.060	18	9.338	24	12.20
6.00	3.940	7.25	5.917	18	8.365	20	9.731	25	12.50
6.25	3.979	7.50	6.035	20	8.611	22	10.07	31	13.74
6.50	4.016	7.75	6.246	22	8.809	24	10.35	33	14.40
6.75	4.051	8.00	6.423	24	8.968	26	10.59	35	14.93
7.00	4.080	8.25	6.580	26	9.097	28	10.80	51	16.08
7.25	4.107	8.50	6.712	28	9.200	30	10.98	60	16.56
7.50	4.133	8.75	6.825	30	9.283	34	11.26	70	16.91
7.75	4.158	9.00	6.922	34	9.404	38	11.46	80	17.14
8.00	4.181	9.25	7.004	38	9.481	42	11.61	90	17.27
8.25	4.202	9.50	7.076	42	9.532	46	11.71	100	17.38
8.50	4.221	9.75	7.135	46	9.565	50	11.79	110	17.41
8.75	4.238	10.00	7.172	50	9.588	60	11.91	120	17.45
9.00	4.253		7.232	60	9.612	70	11.96	130	17.48
9.25	4.267		7.277	70	9.621	80	11.98	140	17.49
9.50	4.279		7.314	80	9.628	90	11.99	150	17.49
9.75	4.289		7.344	100	9.634	100	12.00	160	17.49
10.00	4.298		7.369	120	9.638	120	12.0	180	17.50
								200	17.50
								220	17.50

TABLE II — Continued

R = 7.0 a <sub>1</sub> = 0.1787 a <sub>2</sub> = 0.7584		R = 8.0 a <sub>1</sub> = 0.1476 a <sub>2</sub> = 0.6438		R = 9.0 a <sub>1</sub> = 0.1264 a <sub>2</sub> = 0.5740		R = 10.0 a <sub>1</sub> = 0.1104 a <sub>2</sub> = 0.4979	
t	Q <sub>(t)</sub>	t	Q <sub>(t)</sub>	t	Q <sub>(t)</sub>	t	Q <sub>(t)</sub>
9.00	6.881	9	6.881	10	7.417	15	9.063
9.50	7.127	10	7.398	15	9.945	20	12.32
10	7.389	11	7.920	20	12.26	23	13.22
11	7.902	12	8.431	22	13.13	24	14.09
12	8.397	13	8.930	24	13.68	26	14.85
13	8.876	14	9.418	26	14.79	28	15.78
14	9.341	15	9.895	28	15.59	30	16.50
15	9.791	16	10.361	30	16.35	32	17.38
16	10.23	17	10.82	32	17.10	34	18.18
17	10.65	18	11.28	34	17.82	36	18.91
18	11.03	19	11.70	36	18.52	38	19.55
19	11.46	20	12.13	38	19.19	40	20.37
20	11.85	22	12.95	40	19.85	42	21.07
22	12.58	24	13.74	42	20.48	44	21.76
24	13.27	26	14.50	44	21.09	46	22.42
26	13.92	28	15.23	46	21.69	48	23.07
28	14.53	30	15.92	48	22.26	50	23.71
30	15.11	34	17.22	50	22.82	52	24.33
35	16.30	38	18.41	52	23.36	54	24.94
40	17.49	40	18.97	54	23.89	56	25.53
45	18.43	45	20.26	56	24.39	58	26.11
50	19.24	50	21.42	58	24.88	60	26.67
60	20.51	55	22.46	60	25.38	65	28.02
70	21.46	60	23.10	65	26.48	70	29.29
80	22.13	70	24.48	70	27.52	75	30.49
90	22.63	80	26.28	75	28.48	80	31.61
100	23.00	90	27.28	80	29.36	85	32.67
120	23.47	100	28.11	85	30.18	90	33.68
140	23.71	120	29.31	90	30.93	95	34.60
160	23.85	140	30.08	95	31.63	100	35.48
180	23.92	160	30.58	100	32.27	120	38.51
200	24.00	180	30.91	120	34.39	140	40.59
		200	31.12	140	35.92	160	42.78
		240	31.43	160	37.01	180	44.21
		280	31.47	180	37.45	200	45.38
		320	31.47	200	38.44	210	46.85
		360	31.49	240	39.17	240	47.94
		400	31.50	280	39.56	320	48.84
		480	31.50	320	39.77	360	49.81
				360	39.88	400	49.14
				400	39.94	440	49.28
				440	39.97	480	49.38
				480	39.98		

$$\frac{1}{p^2} = p \bar{P}_{(p)} \bar{Q}_{(p)} \dots (VI-32)$$

Evidence of this identity can be confirmed by substituting Eqs. VI-4 and VI-27 in Eq. VI-32. In brief, Eq. VI-32 is the relationship between constant terminal pressure and constant terminal rate cases. If the Laplace transformation for one is known, the transform for the other is established. This interchange can only take place in the transformations and the final solution must be by inversion.

Computation of  $P_{(t)}$  and  $Q_{(t)}$

To plot  $P_{(t)}$  and  $Q_{(t)}$  as work-curves, it is necessary to determine numerically the value for the integrals shown in Eqs. VI-24 and VI-23. In treating the infinite integrals for  $P_{(t)}$  and  $Q_{(t)}$ , the only difficult part is in establishing the integrals for small values of  $u$ . For larger values of  $u$  the integrands converge fairly rapidly, and Simpson's rule for numerical integration has proved sufficiently accurate.

To determine the integration for  $Q_{(t)}$  in the region of the origin, Eq. VI-23 can be expressed as

$$Q_{\delta(t)} = \frac{4}{\pi^2} \int_0^{\delta} \frac{(1-e^{-u^2}) du}{u^2 [J_0^2(u) + Y_0^2(u)]} \dots (VI-33)$$

where the value for  $\delta$  is taken such that  $1 - e^{-u^2} \cong u^2$ , which is true for  $u^2$  equal to or less than 0.02, or  $\delta = \sqrt{0.02/t}$  and the simplification for Eq. VI-33 becomes

$$Q_{\delta(t)} = \frac{4t}{\pi^2} \int_0^{\delta} \frac{du}{u [J_0^2(u) + Y_0^2(u)]}$$

For  $u$  less than 0.02,  $J_0(u) = 1$ , and

$$Y_0(u) \cong \frac{2}{\pi} \left\{ \log \frac{u}{2} + \gamma \right\} = \frac{2}{\pi} \left\{ \log u - 0.11593 \right\}$$

As the logarithmic term is most predominant in the denominator for small values of  $u$ , this equation simplifies to

$$Q_{\delta(t)} = t \int_0^{\delta} \frac{du}{u [\log u - 0.11593]^2} = \frac{t}{[0.11593 - \log \delta]} \dots (VI-34)$$

The integration for  $P_{(t)}$  close to the origin is expressed by

$$P_{\delta(t)} = \frac{4}{\pi^2} \int_0^{\delta=0.02} \frac{(1-e^{-u^2}) du}{u^2 [J_0^2(u) + Y_0^2(u)]} \dots (VI-35)$$

For  $u$  equal to or less than 0.02,  $J_0(u) = 1$ , and  $Y_0(u) = 2/\pi u$  so that Eq. VI-35 reduces to

$$P_{\delta(t)} = \int_0^{\delta} \frac{(1-e^{-u^2})}{u} du \dots (VI-36)$$

If we let  $n = u^2$

$$P_{\delta(t)} = \frac{1}{2} \int_0^{\delta t} \frac{(1-e^{-n})}{n} dn \dots (VI-37)$$

Further,

$$\int_0^{\delta t} \frac{(1-e^{-n})}{n} dn = \int_0^1 \frac{(1-e^{-n})}{n} dn - \int_{\delta t}^1 \frac{(1-e^{-n})}{n} dn \dots (VI-38)$$

Since Euler's constant  $\gamma$  is equal to

$$\gamma = \int_1^{\infty} \frac{(1-e^{-n})}{n} dn = \int_0^{\infty} \frac{e^{-n}}{n} dn$$

Substitution of this relation in Eq. VI-38 gives

$$\int_0^{\delta t} \frac{(1-e^{-n})}{n} dn = \gamma + \int_{\delta t}^{\infty} \frac{e^{-n}}{n} dn - \int_{\delta t}^1 \frac{1}{n} dn$$

and since the second term on the right is the Ei-function already discussed in the earlier part of this work, Eq. VI-37 reduces to

$$P_{\delta(t)} = \frac{1}{2} [\gamma - Ei(-\delta t) + \log \delta t] \dots (VI-39)$$

TABLE III -- Constant Terminal Rate Case Radial Flow -- Limited Reservoirs

$R = 1.5$ $\beta_1 = 6.8275$ $\beta_2 = 11.924$		$R = 2.0$ $\beta_1 = 8.1985$ $\beta_2 = 6.3118$		$R = 2.5$ $\beta_1 = 2.1564$ $\beta_2 = 4.2230$		$R = 3.0$ $\beta_1 = 1.6858$ $\beta_2 = 3.1787$		$R = 3.5$ $\beta_1 = 1.3218$ $\beta_2 = 2.5626$		$R = 4$ $\beta_1 = 1.1120$ $\beta_2 = 2.1542$		$R = 4.5$ $\beta_1 = 0.9609$ $\beta_2 = 1.8526$	
$t$	$P_{(t)}$	$t$	$P_{(t)}$	$t$	$P_{(t)}$	$t$	$P_{(t)}$	$t$	$P_{(t)}$	$t$	$P_{(t)}$	$t$	$P_{(t)}$
0.010 <sup>-1</sup>	0.231	2.2(10) <sup>-1</sup>	0.443	4.0(10) <sup>-1</sup>	0.568	5.2(10) <sup>-1</sup>	0.627	1.0	0.802	1.5	0.927	2.0	1.021
0.02	0.288	2.4	0.459	4.2	0.576	5.4	0.636	1.1	0.830	1.6	0.945	2.1	1.030
0.03(10) <sup>-1</sup>	0.322	2.6	0.476	4.4	0.587	5.6	0.645	1.2	0.857	1.7	0.968	2.2	1.036
0.04	0.355	2.8	0.492	4.6	0.598	5.8	0.652	1.3	0.882	1.8	0.988	2.3	1.042
0.05	0.387	3.0	0.507	4.8	0.608	6.0	0.659	1.4	0.906	1.9	1.007	2.4	1.047
0.06	0.420	3.2	0.522	5.0	0.618	7.0	0.703	1.5	0.929	2.0	1.025	2.5	1.052
0.08	0.452	3.4	0.536	5.2	0.628	7.5	0.721	1.6	0.951	2.2	1.049	2.6	1.056
0.10	0.484	3.6	0.551	5.4	0.638	8.0	0.740	1.7	0.973	2.4	1.067	2.7	1.060
0.12	0.516	3.8	0.565	5.6	0.647	8.5	0.758	1.8	0.994	2.6	1.084	2.8	1.064
0.14	0.548	4.0	0.579	5.8	0.657	9.0	0.776	1.9	1.014	2.8	1.101	2.9	1.068
0.16	0.580	4.2	0.593	6.0	0.666	9.5	0.791	2.0	1.034	3.0	1.114	3.0	1.071
0.18	0.612	4.4	0.607	6.5	0.688	1.0	0.800	2.28	1.063	3.5	1.225	3.2	1.077
0.20	0.644	4.6	0.621	7.0	0.710	1.2	0.865	2.50	1.130	4.0	1.371	3.4	1.082
0.22	0.676	4.8	0.634	7.5	0.731	1.4	0.920	2.75	1.176	4.5	1.492	3.6	1.087
0.24	0.708	5.0	0.648	8.0	0.752	1.6	0.973	3.0	1.221	5.0	1.660	3.8	1.092
0.26	0.740	5.2	0.715	8.5	0.772	2.0	1.076	4.0	1.401	5.5	1.777	4.0	1.097
0.28	0.772	5.4	0.782	9.0	0.792	3.0	1.328	5.0	1.579	6.0	1.954	4.5	1.102
0.30	0.804	5.6	0.849	9.5	0.812	4.0	1.578	6.0	1.757	6.5	1.970	5.0	1.107
0.32	0.836	5.8	0.915	1.0	0.832	5.0	1.828			7.0	1.757	5.5	1.112
0.34	0.868	1.0	0.982	2.0	1.215					8.0	1.871	6.0	1.117
0.36	0.900	2.0	1.049	3.0	1.596					9.0	1.984	7.0	1.122
0.38	0.932	3.0	2.318	4.0	1.977					10.0	2.127	8.0	1.127
0.40	0.964	5.0	3.649	5.0	2.358							9.0	1.132
0.42												10.0	1.137
0.44												11.0	1.142
0.46												12.0	1.147
0.48												13.0	1.152
0.50												14.0	1.157
0.52												15.0	1.162
0.54												16.0	1.167
0.56												17.0	1.172
0.58												18.0	1.177
0.60												19.0	1.182
0.62												20.0	1.187

The values for the integrands for Eqs. VI-24 and VI-23 have been calculated from Bessel Tables for or greater than 0.02 as given in W.B.F., pp. 666-697. The calculations have been somewhat simplified by using the square of the modulus of

$|H_0^{(3)}(u)| = |J_0(u) + i Y_0(u)|$  and  $|H_1^{(3)}(u)| = |J_1(u) + i Y_1(u)|$  which are the Bessel functions of the third kind or the Hankel functions.

Table I shows the calculated values for  $Q_{(t)}$  and  $P_{(t)}$  to three significant figures, starting at  $t = 0.01$ , the point where linear flow and radial flow start deviating.  $P_{(t)}$  is calculated only to  $t = 1,000$  since beyond this range the point source solution of Eq. VI-15 applies. The values for  $Q_{(t)}$  are given up to  $t = 10^4$ .

The reader may reproduce these data as he sees fit; Fig. 4 is an illustrative plot for  $Q_{(t)}$ , and Fig. 7 is a semi-logarithmic relationship for  $P_{(t)}$ .

LIMITED RESERVOIRS

As already mentioned, the solutions for limited reservoirs of radial symmetry have been developed by the Fourier-Bessel type of expansion.<sup>4,5,6</sup> Their introduction here is not only to show how the solutions may be arrived at by the Laplace transformation, but also to furnish data for  $P_{(t)}$  and  $Q_{(t)}$  curves when such cases are encountered in practice.

No Fluid Flow Across Exterior Boundary

The first example considered is the constant terminal pressure case for radial flow of limited extent. The boundary conditions are such that at the well bore or field's edge,  $r = 1$ , the cumulative pressure drop is unity, and at some distance removed from this boundary at a point in the reservoir  $r = R$ ,

there exists a restriction such that no fluid can flow past this barrier so that at that point  $\left(\frac{\partial P}{\partial r}\right)_{r=R} = 0$ .

The general solution of Eq. VI-1 still applies, but to fulfill the boundary conditions it is necessary to re-determine values for constants A and B. The transformation of the boundary condition at  $r = 1$  is expressed as

$$\frac{1}{p} = AI_0(\sqrt{p}) + BK_0(\sqrt{p}) \quad \dots \quad (VII-1)$$

and at  $r = R$  the condition is

$$0 = AI_1(\sqrt{p}R) - BK_1(\sqrt{p}R) \quad \dots \quad (VII-2)$$

since it is shown in W.B.F., p. 79, that  $K_0'(z) = -K_1(z)$ , and  $I_0'(z) = I_1(z)$ . The solutions for A and B from these two simultaneous algebraic expressions are

$$A = K_1(\sqrt{p}R) / p [K_1(\sqrt{p}R) I_0(\sqrt{p}) + K_0(\sqrt{p}) I_1(\sqrt{p}R)]$$

and

$$B = I_1(\sqrt{p}R) / p [K_1(\sqrt{p}R) I_0(\sqrt{p}) + K_0(\sqrt{p}) I_1(\sqrt{p}R)]$$

By substituting these constants in Eq. VI-1, the general solution for the transform of the pressure drop is expressed by

$$\bar{P}_{(t,p)} = \frac{[K_1(\sqrt{p}R) I_0(\sqrt{p}r) + I_1(\sqrt{p}R) K_0(\sqrt{p}r)]}{p [K_1(\sqrt{p}R) I_0(\sqrt{p}) + I_1(\sqrt{p}R) K_0(\sqrt{p})]} \quad (VII-3)$$

To find  $Q(t)$  the cumulative fluid produced for unit pressure drop, then the transform for the pressure gradient at  $r = 1$  is obtained as follows:

$$\left(\frac{\partial \bar{P}}{\partial r}\right)_{r=1} = \frac{[I_1(\sqrt{p}R) K_1(\sqrt{p}) - K_1(\sqrt{p}R) I_1(\sqrt{p})]}{p^{3/2} [K_1(\sqrt{p}R) I_0(\sqrt{p}) + I_1(\sqrt{p}R) K_0(\sqrt{p})]}$$

where the negative sign is introduced in order to make  $Q(t)$

TABLE III—Continued

R = 5 $\beta_1 = 0.8472$ $\beta_2 = 1.6112$		R = 6.0 $\beta_1 = 0.6864$ $\beta_2 = 1.2903$		R = 7.0 $\beta_1 = 0.5782$ $\beta_2 = 1.0860$		R = 8.0 $\beta_1 = 0.4999$ $\beta_2 = 0.9352$		R = 9.0 $\beta_1 = 0.4406$ $\beta_2 = 0.8216$		R = 10 $\beta_1 = 0.3940$ $\beta_2 = 0.7333$	
t	P <sub>(t)</sub>	t	P <sub>(t)</sub>	t	P <sub>(t)</sub>	t	P <sub>(t)</sub>	t	P <sub>(t)</sub>	t	P <sub>(t)</sub>
3.0	1.167	4.0	1.275	6.0	1.438	8.0	1.556	10.0	1.651	12.0	1.732
3.1	1.180	4.5	1.322	6.5	1.470	8.5	1.592	10.5	1.673	12.5	1.750
3.2	1.192	5.0	1.364	7.0	1.501	9.0	1.607	11.0	1.693	13.0	1.768
3.3	1.204	5.5	1.404	7.5	1.531	9.5	1.631	11.5	1.713	13.5	1.784
3.4	1.215	6.0	1.441	8.0	1.559	10.0	1.653	12.0	1.732	14.0	1.801
3.5	1.227	6.5	1.477	8.5	1.586	10.5	1.675	12.5	1.751	14.5	1.817
3.6	1.238	7.0	1.511	9.0	1.612	11.0	1.697	13.0	1.769	15.0	1.832
3.7	1.249	7.5	1.544	9.5	1.638	11.5	1.717	13.5	1.786	15.5	1.847
3.8	1.259	8.0	1.576	10.0	1.663	12.0	1.737	14.0	1.803	16.0	1.862
3.9	1.270	8.5	1.607	11.0	1.711	12.5	1.757	14.5	1.819	17.0	1.879
4.0	1.281	9.0	1.636	12.0	1.752	13.0	1.776	15.0	1.835	18.0	1.917
4.2	1.301	9.5	1.668	13.0	1.801	13.5	1.795	15.5	1.851	19.0	1.943
4.4	1.321	10.0	1.698	14.0	1.816	14.0	1.813	16.0	1.867	20.0	1.968
4.6	1.346	11.0	1.757	15.0	1.888	14.5	1.831	17.0	1.897	22.0	2.017
4.8	1.369	12.0	1.815	16.0	1.931	15.0	1.849	18.0	1.926	24.0	2.063
5.0	1.378	13.0	1.873	17.0	1.974	17.0	1.919	19.0	1.955	26.0	2.108
5.5	1.424	14.0	1.931	18.0	2.016	19.0	1.956	20.0	1.983	28.0	2.151
6.0	1.469	15.0	1.988	19.0	2.058	21.0	2.051	22.0	2.037	30.0	2.194
6.6	1.513	16.0	2.045	20.0	2.100	23.0	2.116	24.0	2.090	32.0	2.238
7.0	1.556	17.0	2.103	22.0	2.184	25.0	2.180	26.0	2.142	34.0	2.278
7.5	1.598	18.0	2.160	24.0	2.267	30.0	2.349	28.0	2.163	36.0	2.319
8.0	1.641	19.0	2.217	26.0	2.351	35.0	2.499	30.0	2.214	38.0	2.360
9.0	1.725	20.0	2.274	28.0	2.434	40.0	2.658	31.0	2.345	40.0	2.401
10.0	1.803	25.0	2.560	30.0	2.517	46.0	2.817	38.0	2.416	60.0	2.604
11.0	1.892	30.0	2.846					40.0	2.498	80.0	2.836
12.0	1.975							45.0	2.621	70.0	3.008
13.0	2.059							60.0	2.746		
14.0	2.142										
15.0	2.226										

positive. Theorem B shows that the integration with respect to time introduces an additional operator  $p$  in the denominator to give

$$\bar{Q}_{(p)} = \frac{[I_0(\sqrt{p} R) K_1(\sqrt{p}) - K_1(\sqrt{p} R) I_0(\sqrt{p})]}{p^{3/2} [K_1(\sqrt{p} R) I_0(\sqrt{p}) + I_1(\sqrt{p} R) K_0(\sqrt{p})]} \quad (VII-4)$$

In order to apply Mellin's inversion formula, the first consideration is the roots of the denominator of this equation

which indicate the poles. Since the modified Bessel functions for positive real arguments are either increasing or decreasing, the bracketed term in the denominator does not indicate any poles for positive real values for  $p$ . At the origin of the plane of Fig. 2 a pole exists and this pole we shall have to investigate first. Thus, the substitution of small and real values for  $z$  (Eqs. VI-12 and VI-13) in Eq. VII-4, gives

$$\bar{Q}_{(p)} \underset{p \rightarrow 0}{\approx} \frac{(R^2 - 1)}{2p}$$

TABLE IV — Constant Terminal Rate Case Radial Flow Pressure at Exterior Radius Constant

R = 1.5 $\lambda_1 = 8.4029$ $\lambda_2 = 6.6267$		R = 2.0 $\lambda_1 = 1.7840$ $\lambda_2 = 4.8021$		R = 2.5 $\lambda_1 = 1.2426$ $\lambda_2 = 8.2265$		R = 3.0 $\lambda_1 = 0.9696$ $\lambda_2 = 2.4372$		R = 3.5 $\lambda_1 = 0.7652$ $\lambda_2 = 1.9624$	
t	P <sub>(1)</sub>	t	P <sub>(1)</sub>	t	P <sub>(1)</sub>	t	P <sub>(1)</sub>	t	P <sub>(1)</sub>
5.0(10) <sup>-2</sup>	0.250	2.0(10) <sup>-1</sup>	0.424	3.0(10) <sup>-1</sup>	0.502	5.0(10) <sup>-1</sup>	0.617	5.0(10) <sup>-1</sup>	0.820
7.5 "	0.240	2.2 "	0.441	3.5 "	0.535	5.5 "	0.640	6.0 "	0.665
10.0 "	0.249	2.4 "	0.457	4.0 "	0.554	6.0 "	0.662	7.0 "	0.705
15.0 "	0.256	2.6 "	0.472	4.5 "	0.569	7.0 "	0.702	8.0 "	0.741
20.0 "	0.262	2.8 "	0.485	5.0 "	0.578	8.0 "	0.738	9.0 "	0.774
25.0 "	0.267	3.0 "	0.498	5.5 "	0.588	9.0 "	0.770	1.0 "	0.804
30.0 "	0.271	3.5 "	0.527	6.0 "	0.599	1.0 "	0.799	1.2 "	0.858
35.0 "	0.275	4.0 "	0.552	7.0 "	0.606	1.2 "	0.850	1.4 "	0.901
40.0 "	0.278	4.5 "	0.573	8.0 "	0.728	1.4 "	0.892	1.6 "	0.945
45.0 "	0.281	5.0 "	0.591	9.0 "	0.755	1.6 "	0.927	1.8 "	0.981
50.0 "	0.284	5.5 "	0.606	1.0 "	0.778	1.8 "	0.955	2.0 "	1.013
55.0 "	0.287	6.0 "	0.619	1.2 "	0.815	2.0 "	0.980	2.2 "	1.041
60.0 "	0.289	6.5 "	0.630	1.4 "	0.812	2.2 "	1.000	2.4 "	1.055
65.0 "	0.291	7.0 "	0.639	1.6 "	0.861	2.4 "	1.016	2.6 "	1.077
70.0 "	0.292	7.5 "	0.647	1.8 "	0.876	2.6 "	1.030	2.8 "	1.100
75.0 "	0.293	8.0 "	0.651	2.0 "	0.887	2.8 "	1.042	3.0 "	1.123
80.0 "	0.294	8.5 "	0.650	2.2 "	0.895	3.0 "	1.051	3.5 "	1.158
85.0 "	0.295	9.0 "	0.646	2.4 "	0.900	3.5 "	1.069	4.0 "	1.187
90.0 "	0.295	9.5 "	0.649	2.6 "	0.905	4.0 "	1.086	5.0 "	1.245
95.0 "	0.296	1.0 "	0.673	2.8 "	0.908	4.5 "	1.087	6.0 "	1.282
1.0 "	0.296	1.2 "	0.682	3.0 "	0.910	5.0 "	1.091	7.0 "	1.312
1.1 "	0.297	1.4 "	0.688	3.5 "	0.913	5.5 "	1.094	8.0 "	1.347
1.2 "	0.297	1.6 "	0.690	4.0 "	0.916	6.0 "	1.096	9.0 "	1.380
1.3 "	0.298	1.8 "	0.692	4.5 "	0.919	6.5 "	1.097	10.0 "	1.411
1.4 "	0.298	2.0 "	0.692	5.0 "	0.916	7.0 "	1.097	12.0 "	1.452
1.5 "	0.299	2.5 "	0.693	5.5 "	0.918	8.0 "	1.098	14.0 "	1.494
1.6 "	0.299	3.0 "	0.693	6.0 "	0.916	10.0 "	1.099	16.0 "	1.534

TABLE IV — Continued

R = 4.0 $\lambda_1 = 0.6370$ $\lambda_2 = 1.6369$		R = 6.0 $\lambda_1 = 0.4205$ $\lambda_2 = 1.0050$		R = 8.0 $\lambda_1 = 0.8090$ $\lambda_2 = 0.7250$		R = 10 $\lambda_1 = 0.2448$ $\lambda_2 = 0.5726$		R = 12 $\lambda_1 = 0.1516$ $\lambda_2 = 0.4772$	
t	P <sub>(1)</sub>	t	P <sub>(1)</sub>	t	P <sub>(1)</sub>	t	P <sub>(1)</sub>	t	P <sub>(1)</sub>
1.0	0.802	4.0	1.275	7.0	1.499	10.0	1.651	20.0	1.960
1.2	0.857	4.5	1.320	7.5	1.527	12.0	1.730	25.0	2.141
1.4	0.905	5.0	1.361	8.0	1.554	14.0	1.798	30.0	2.318
1.6	0.941	5.5	1.398	8.5	1.680	16.0	1.855	35.0	2.487
1.8	0.966	6.0	1.432	9.0	1.604	18.0	1.907	40.0	2.648
2.0	1.029	6.5	1.462	9.5	1.627	20.0	1.952	45.0	2.806
2.2	1.052	7.0	1.490	10.0	1.648	25.0	2.043	50.0	2.958
2.4	1.080	7.5	1.516	12.0	1.724	30.0	2.111	55.0	3.109
2.6	1.109	8.0	1.549	14.0	1.796	35.0	2.169	60.0	3.251
2.8	1.130	8.5	1.561	16.0	1.857	40.0	2.197	65.0	3.386
3.0	1.152	9.0	1.580	18.0	1.879	45.0	2.221	70.0	3.516
3.2	1.171	10.0	1.615	20.0	1.914	50.0	2.245	75.0	3.643
3.4	1.187	12.0	1.667	22.0	1.913	55.0	2.260	80.0	3.768
3.6	1.206	14.0	1.701	24.0	1.967	60.0	2.271	85.0	3.892
3.8	1.221	16.0	1.736	26.0	1.980	65.0	2.277	90.0	4.014
4.0	1.239	18.0	1.773	28.0	2.002	70.0	2.285	10.0(10) <sup>2</sup>	4.135
4.2	1.255	20.0	1.802	30.0	2.016	75.0	2.290	15.0 "	4.257
4.4	1.271	22.0	1.821	35.0	2.040	80.0	2.293	20.0 "	4.379
4.6	1.287	24.0	1.837	40.0	2.055	90.0	2.297	25.0 "	4.501
4.8	1.303	26.0	1.851	45.0	2.064	10.0(10) <sup>2</sup>	2.300	30.0 "	4.623
5.0	1.317	28.0	1.861	50.0	2.070	11.0 "	2.304	35.0 "	4.745
5.2	1.332	30.0	1.867	60.0	2.076	12.0 "	2.307	40.0 "	4.867
5.4	1.347	35.0	1.889	70.0	2.078	13.0 "	2.307	45.0 "	4.989
5.6	1.360	40.0	1.891	80.0	2.079	14.0 "	2.307	50.0 "	5.111
5.8	1.375	50.0	1.892			16.0 "	2.308	60.0 "	5.233



and by the application of Mellin's inversion formula applied at the origin, then

$$\frac{1}{2\pi i} \oint_{\lambda=0}^{\lambda_1} e^{\lambda t} \frac{1}{2} \frac{(R^2-1)}{\lambda} d\lambda = \frac{R^2-1}{2} \quad \text{VII-5}$$

An investigation of the integration along the negative real "cut" both for the upper and lower portions, Fig. 2, reveals that Eq. VII-4 is an even function for which the integration along the paths is zero. However, poles are indicated along the negative real axis and these residuals together with Eq. VII-5 make up the solution for the constant terminal pressure case for the limited radial system. The residuals are estab-

lished by the Mellin's inversion formula by letting  $\lambda = u'e^{i\pi}$ , then by Eq. VI-18

$$\frac{1}{2\pi i} \oint_{\lambda_1, \lambda_2, \text{etc.}} e^{\lambda t} \bar{Q}(\lambda) d\lambda =$$

$$\frac{1}{\pi i} \int_{a_1, a_2, \text{etc.}} e^{-u't} \frac{[J_1(uR) Y_1(u) - Y_1(uR) J_1(u)] du}{u^2 [J_1(uR) Y_2(u) - Y_2(uR) J_2(u)]} \quad \text{VII-6}$$

where  $a_1, a_2$  and  $a_n$  are the roots of

$$[J_1(a_n R) Y_2(a_n) - Y_2(a_n R) J_2(a_n)] = 0 \quad \text{VII-7}$$

and the poles are represented on the negative real axis by  $\lambda_n = -a_n^2$ , Fig. 3. The residuals of Eq. VII-6 are the series expansion

TABLE IV — Continued

R = 20 $\lambda_1 = 0.1208$ $\lambda_2 = 0.2788$		R = 25 $\lambda_1 = 0.09448$ $\lambda_2 = 0.2228$		R = 30 $\lambda_1 = 0.08032$ $\lambda_2 = 0.1840$		R = 40 $\lambda_1 = 0.06010$ $\lambda_2 = 0.1394$		R = 50 $\lambda_1 = 0.04613$ $\lambda_2 = 0.1108$	
t	P(t)	t	P(t)	t	P(t)	t	P(t)	t	P(t)
30.0	2.448	60.0	2.380	70.0	2.651	12.0(10 <sup>2</sup> )	2.813	20.0(10 <sup>2</sup> )	3.064
35.0	2.219	65.0	2.434	80.0	2.618	14.0 "	2.855	22.0 "	3.111
40.0	2.282	70.0	2.478	90.0	2.672	16.0 "	2.933	24.0 "	3.154
45.0	2.338	75.0	2.614	10.0(10 <sup>2</sup> )	2.723	18.0 "	3.011	26.0 "	3.193
50.0	2.388	80.0	2.650	12.0 "	2.812	20.0 "	3.053	28.0 "	3.229
60.0	2.478	85.0	2.682	14.0 "	2.856	22.0 "	3.102	30.0 "	3.263
70.0	2.547	90.0	2.814	16.0 "	2.950	24.0 "	3.152	35.0 "	3.339
80.0	2.609	95.0	2.843	18.0 "	2.968	26.0 "	3.191	40.0 "	3.405
90.0	2.658	100.0	2.871	17.5 "	2.979	28.0 "	3.228	45.0 "	3.461
10.0(10 <sup>2</sup> )	2.707	105.0	2.897	17.5 "	2.992	30.0 "	3.259	50.0 "	3.512
10.5 "	2.728	110.0(10 <sup>2</sup> )	2.721	18.0 "	3.003	35.0 "	3.331	55.0 "	3.554
11.0 "	2.747	12.0 "	2.707	20.0 "	3.054	40.0 "	3.391	60.0 "	3.595
11.5 "	2.764	14.0 "	2.761	25.0 "	3.160	45.0 "	3.446	65.0 "	3.630
12.0 "	2.781	16.0 "	2.838	30.0 "	3.219	50.0 "	3.482	70.0 "	3.661
12.5 "	2.796	18.0 "	2.904	35.0 "	3.268	55.0 "	3.514	75.0 "	3.688
13.0 "	2.810	20.0 "	3.024	40.0 "	3.306	60.0 "	3.545	80.0 "	3.713
13.5 "	2.823	22.0 "	3.057	45.0 "	3.332	65.0 "	3.568	85.0 "	3.735
14.0 "	2.835	24.0 "	3.085	50.0 "	3.351	70.0 "	3.588	90.0 "	3.751
14.5 "	2.846	28.0 "	3.107	60.0 "	3.378	80.0 "	3.619	95.0 "	3.771
15.0 "	2.857	28.0 "	3.126	70.0 "	3.387	90.0 "	3.640	10.0(10 <sup>2</sup> )	3.787
16.0 "	2.874	30.0 "	3.142	80.0 "	3.394	10.0(10 <sup>2</sup> )	3.656	12.0 "	3.833
18.0 "	2.906	35.0 "	3.171	90.0 "	3.397	12.0 "	3.672	14.0 "	3.862
20.0 "	2.929	40.0 "	3.189	10.0(10 <sup>2</sup> )	3.399	14.0 "	3.681	16.0 "	3.881
24.0 "	2.958	45.0 "	3.200	12.0 "	3.401	16.0 "	3.685	18.0 "	3.892
28.0 "	2.978	60.0 "	3.207	14.0 "	3.401	18.0 "	3.687	20.0 "	3.903
30.0 "	2.989	80.0 "	3.214			20.0 "	3.688	22.0 "	3.901
40.0 "	2.992	70.0 "	3.217			25.0 "	3.689	24.0 "	3.907
50.0 "	2.995	80.0 "	3.218					26.0 "	3.909
		90.0 "	3.219					28.0 "	3.910

TABLE IV — Continued

R = 60		R = 70		R = 80		R = 90		R = 100	
t	P(t)	t	P(t)	t	P(t)	t	P(t)	t	P(t)
3.0(10 <sup>2</sup> )	3.257	5.0(10 <sup>2</sup> )	3.512	6.0(10 <sup>2</sup> )	3.603	8.0(10 <sup>2</sup> )	3.747	1.0(10 <sup>3</sup> )	3.850
4.0 "	3.401	6.0 "	3.602	7.0 "	3.680	9.0 "	3.801	1.2 "	3.910
5.0 "	3.512	7.0 "	3.680	8.0 "	3.747	1.0(10 <sup>3</sup> )	3.858	1.4 "	4.026
6.0 "	3.602	8.0 "	3.746	9.0 "	3.803	1.2 "	3.949	1.6 "	4.072
7.0 "	3.678	9.0 "	3.803	10.0 "	3.857	1.4 "	3.988	1.8 "	4.130
8.0 "	3.739	10.0 "	3.854	12.0 "	3.946	1.6 "	4.025	2.0 "	4.200
9.0 "	3.792	12.0 "	3.937	14.0 "	4.019	1.8 "	4.058	2.5 "	4.303
10.0 "	3.832	14.0 "	4.003	15.0 "	4.051	1.8 "	4.141	3.0 "	4.379
12.0 "	3.908	16.0 "	4.054	16.0 "	4.060	2.0 "	4.192	3.5 "	4.431
14.0 "	3.959	18.0 "	4.095	18.0 "	4.130	2.5 "	4.285	4.0 "	4.478
16.0 "	3.996	20.0 "	4.127	20.0 "	4.171	3.0 "	4.348	4.5 "	4.510
18.0 "	4.023	25.0 "	4.181	25.0 "	4.246	3.5 "	4.394	5.0 "	4.531
20.0 "	4.043	30.0 "	4.211	30.0 "	4.297	4.0 "	4.428	5.5 "	4.552
25.0 "	4.071	35.0 "	4.228	35.0 "	4.328	4.5 "	4.448	6.0 "	4.565
30.0 "	4.084	40.0 "	4.237	40.0 "	4.347	5.0 "	4.464	6.5 "	4.578
35.0 "	4.090	45.0 "	4.242	45.0 "	4.350	5.0 "	4.482	7.0 "	4.583
40.0 "	4.092	50.0 "	4.245	50.0 "	4.350	6.0 "	4.491	7.5 "	4.588
45.0 "	4.093	55.0 "	4.247	60.0 "	4.356	7.0 "	4.498	8.0 "	4.593
50.0 "	4.094	60.0 "	4.247	70.0 "	4.378	8.0 "	4.504	8.5 "	4.598
55.0 "	4.094	65.0 "	4.248	80.0 "	4.381	9.0 "	4.508	9.0 "	4.601
		70.0 "	4.248	90.0 "	4.382	10.0 "	4.509	10.0 "	4.604
		75.0 "	4.248	10.0(10 <sup>3</sup> )	4.382	12.0 "	4.500	12.5 "	4.604
		80.0 "	4.248	11.0 "	4.382	14.0 "	4.500	15.0 "	4.605

and by the application of Mellin's inversion formula applied at the origin, then

$$\frac{1}{2\pi i} \oint_{\lambda=0} e^{\lambda t} \frac{1}{2} \frac{(R^2-1)}{\lambda} d\lambda = \frac{R^2-1}{2} \quad \text{(VII-5)}$$

An investigation of the integration along the negative real "cut" both for the upper and lower portions, Fig. 2, reveals that Eq. VII-4 is an even function for which the integration along the paths is zero. However, poles are indicated along the negative real axis and these residuals together with Eq. VII-5 make up the solution for the constant terminal pressure case for the limited radial system. The residuals are e-tab-

lished by the Mellin's inversion formula by letting  $\lambda = u'e^{i\theta}$ , then by Eqs. VI-18

$$\frac{1}{2\pi i} \oint_{\lambda_1, \lambda_2, \text{etc.}} e^{\lambda t} \bar{Q}(\lambda) d\lambda = \frac{1}{\pi i} \int_{a_1, a_2, \text{etc.}} e^{-u't} \frac{[J_0(uR) Y_0(u) - Y_0(uR) J_0(u)] du}{u^2 [J_0(uR) Y_0(u) - Y_0(uR) J_0(u)]} \quad \text{(VII-6)}$$

where  $a_1, a_2,$  and  $a_n$  are the roots of

$$[J_0(a_n R) Y_0(a_n) - Y_0(a_n R) J_0(a_n)] = 0 \quad \text{(VII-7)}$$

and the poles are represented on the negative real axis by  $\lambda_n = -a_n^2$ , Fig. 3. The residuals of Eq. VII-6 are the series expansion

TABLE IV—Continued

R = 20 $\lambda_1 = 0.1208$ $\lambda_2 = 0.3788$		R = 25 $\lambda_1 = 0.00848$ $\lambda_2 = 0.2228$		R = 30 $\lambda_1 = 0.08032$ $\lambda_2 = 0.1849$		R = 40 $\lambda_1 = 0.06010$ $\lambda_2 = 0.1884$		R = 50 $\lambda_1 = 0.04813$ $\lambda_2 = 0.1108$	
t	P(t)	t	P(t)	t	P(t)	t	P(t)	t	P(t)
20.0	2.148	60.0	2.390	70.0	2.651	12.0(10) <sup>2</sup>	2.814	20.0(10) <sup>2</sup>	2.064
25.0	2.218	65.0	2.434	80.0	2.618	14.0 "	2.485	23.0 "	2.111
30.0	2.282	70.0	2.478	90.0	2.672	16.0 "	2.053	24.0 "	2.154
35.0	2.338	75.0	2.514	10.0(10) <sup>2</sup>	2.723	18.0 "	2.011	26.0 "	2.183
40.0	2.388	80.0	2.550	12.0 "	2.812	20.0 "	2.053	28.0 "	2.220
45.0	2.475	85.0	2.583	14.0 "	2.883	22.0 "	2.102	30.0 "	2.263
50.0	2.547	90.0	2.614	16.0 "	2.950	24.0 "	2.152	35.0 "	2.330
60.0	2.609	95.0	2.643	18.0 "	2.968	26.0 "	2.191	40.0 "	2.405
70.0	2.658	10.0(10) <sup>2</sup>	2.671	17.0 "	2.979	28.0 "	2.228	45.0 "	2.461
80.0	2.707	12.0 "	2.697	15.0 "	2.992	30.0 "	2.259	50.0 "	2.512
90.0	2.728	14.0 "	2.721	20.0 "	3.008	35.0 "	2.331	55.0 "	2.554
10.0(10) <sup>2</sup>	2.747	16.0 "	2.747	25.0 "	3.054	40.0 "	2.391	60.0 "	2.593
10.5	2.764	18.0 "	2.778	30.0 "	3.160	45.0 "	2.448	65.0 "	2.630
11.0	2.781	20.0 "	2.808	35.0 "	3.219	50.0 "	2.492	70.0 "	2.661
11.5	2.798	22.0 "	2.838	40.0 "	3.269	55.0 "	2.514	75.0 "	2.684
12.0	2.810	24.0 "	2.865	45.0 "	3.308	60.0 "	2.545	80.0 "	2.713
12.5	2.823	26.0 "	2.895	50.0 "	3.332	65.0 "	2.568	85.0 "	2.735
13.0	2.836	28.0 "	2.925	55.0 "	3.351	70.0 "	2.588	90.0 "	2.751
13.5	2.848	30.0 "	2.957	60.0 "	3.378	80.0 "	2.619	95.0 "	2.771
14.0	2.861	32.0 "	2.985	65.0 "	3.387	90.0 "	2.640	10.0(10) <sup>2</sup>	2.787
14.5	2.874	34.0 "	3.012	70.0 "	3.394	10.0(10) <sup>2</sup>	2.656	12.0 "	2.803
15.0	2.887	36.0 "	3.038	80.0 "	3.407	12.0 "	2.672	14.0 "	2.816
16.0	2.906	38.0 "	3.063	90.0 "	3.408	14.0 "	2.681	16.0 "	2.822
18.0	2.929	40.0 "	3.088	10.0(10) <sup>2</sup>	3.401	16.0 "	2.686	18.0 "	2.822
20.0	2.948	45.0 "	3.107	12.0 "	3.401	18.0 "	2.687	20.0 "	2.820
24.0	2.978	50.0 "	3.126	14.0 "	3.401	20.0 "	2.688	24.0 "	2.821
28.0	2.989	55.0 "	3.142			24.0 "	2.689	26.0 "	2.820
30.0	2.992	60.0 "	3.157					28.0 "	2.818
40.0	2.995	65.0 "	3.171						
50.0		70.0 "	3.180						
		75.0 "	3.189						
		80.0 "	3.196						
		85.0 "	3.200						
		90.0 "	3.207						
		95.0 "	3.214						
		100.0 "	3.217						
			3.218						
			3.219						

TABLE IV—Continued

R = 60		R = 70		R = 80		R = 90		R = 100	
t	P(t)	t	P(t)	t	P(t)	t	P(t)	t	P(t)
3.0(10) <sup>2</sup>	3.257	6.0(10) <sup>2</sup>	3.512	6.0(10) <sup>2</sup>	3.603	8.0(10) <sup>2</sup>	3.747	1.0(10) <sup>3</sup>	3.859
4.0 "	3.401	8.0 "	3.603	7.0 "	3.680	9.0 "	3.801	1.2 "	3.910
5.0 "	3.512	9.0 "	3.680	8.0 "	3.747	1.0(10) <sup>3</sup>	3.854	1.4 "	4.028
6.0 "	3.602	10.0 "	3.746	9.0 "	3.803	1.2 "	3.949	1.6 "	4.072
7.0 "	3.678	11.0 "	3.803	10.0 "	3.857	1.3 "	3.988	1.8 "	4.150
8.0 "	3.739	12.0 "	3.854	12.0 "	3.946	1.4 "	4.025	2.0 "	4.200
9.0 "	3.792	13.0 "	3.907	14.0 "	4.019	1.5 "	4.056	2.2 "	4.303
10.0 "	3.833	14.0 "	4.003	15.0 "	4.051	1.6 "	4.144	2.4 "	4.379
12.0 "	3.908	16.0 "	4.054	16.0 "	4.080	2.0 "	4.192	2.6 "	4.431
14.0 "	3.959	18.0 "	4.095	18.0 "	4.130	2.5 "	4.255	3.0 "	4.478
16.0 "	3.996	20.0 "	4.127	20.0 "	4.171	3.0 "	4.349	3.5 "	4.510
18.0 "	4.023	25.0 "	4.181	25.0 "	4.246	3.5 "	4.394	4.0 "	4.511
20.0 "	4.043	30.0 "	4.211	30.0 "	4.297	4.0 "	4.426	4.5 "	4.522
25.0 "	4.071	35.0 "	4.228	35.0 "	4.328	4.5 "	4.448	5.0 "	4.565
30.0 "	4.084	40.0 "	4.237	40.0 "	4.347	5.0 "	4.464	5.5 "	4.579
35.0 "	4.090	45.0 "	4.242	45.0 "	4.356	6.0 "	4.482	6.0 "	4.582
40.0 "	4.092	50.0 "	4.245	50.0 "	4.360	7.0 "	4.487	7.0 "	4.583
45.0 "	4.093	55.0 "	4.247	55.0 "	4.364	8.0 "	4.491	7.8 "	4.583
50.0 "	4.094	60.0 "	4.247	60.0 "	4.378	9.0 "	4.498	8.0 "	4.593
55.0 "		65.0 "	4.248	65.0 "	4.380	10.0 "	4.499	9.0 "	4.598
		70.0 "	4.248	70.0 "	4.381	10.9 "	4.499	10.0 "	4.601
		75.0 "	4.248	75.0 "	4.382	11.0 "	4.499	12.5 "	4.604
		80.0 "	4.248	80.0 "	4.382	12.0 "	4.500	15.0 "	4.605
				85.0 "	4.382	14.0 "	4.500		
				90.0 "					
				95.0 "					
				100.0 "					

$$-2 \sum_{\substack{\alpha_1, \alpha_2 \\ \text{etc.}}}^{\infty} \frac{e^{-\alpha_1 t} [J_1(\alpha_1 R) Y_1(\alpha_1) - Y_1(\alpha_1 R) J_1(\alpha_1)]}{\alpha_1^2 \lim_{u \rightarrow \alpha_1} \frac{d}{du} [J_1(uR) Y_1(u) - Y_1(uR) J_1(u)]} \quad (VII-8)$$

since  $J_1'(z) = J_0(z) - J_1(z)/z$  (VII-9)

and  $J_1'(z) = -J_1(z)$

which are recurrence formulae for both first and second kind of Bessel functions, W.B.F., p. 45 and p. 66, then by the identities of Eqs. VII-7 and VI-23, the relation VII-8 reduces to

$$-2 \sum_{\alpha_1, \alpha_2 \text{ etc.}}^{\infty} \frac{e^{-\alpha_1 t} J_1^2(\alpha_1 R)}{\alpha_1^2 [J_1^2(\alpha_1) - J_1^2(\alpha_1 R)]}$$

Therefore, the solution for Q(t) is expressed by *Carroll*

$$Q_{(t)} = \frac{R^2 - 1}{2} - 2 \sum_{\alpha_1, \alpha_2 \text{ etc.}}^{\infty} \frac{e^{-\alpha_1 t} J_1^2(\alpha_1 R)}{\alpha_1^2 [J_1^2(\alpha_1) - J_1^2(\alpha_1 R)]} \quad (VII-10)$$

This is essentially the solution developed in an earlier work,\* but Eq. VII-10 is more rapidly convergent than the solution previously reported.

The values of Q(t) for the constant terminal pressure case for a limited reservoir have been calculated from Eq. VII-10 for R = 1.5 to 10 and are tabulated in Table 2. A reproduction of a portion of these data is given in Fig. 5. As Eq. VII-10 is rapidly convergent for t greater than a given value, only two

TABLE IV—Continued

R = 200		R = 300		R = 400		R = 500		R = 600	
t	P(t)	t	P(t)	t	P(t)	t	P(t)	t	P(t)
1.5(10) <sup>2</sup>	4.061	6.0(10) <sup>2</sup>	4.784	1.5(10) <sup>2</sup>	5.212	2.0(10) <sup>2</sup>	5.336	6.0(10) <sup>2</sup>	5.703
2.0 "	4.205	8.0 "	4.898	2.0 "	5.356	2.5 "	5.468	8.0 "	5.762
2.5 "	4.317	10.0 "	5.010	3.0 "	5.556	3.0 "	5.556	9.0 "	5.814
3.0 "	4.404	12.0 "	5.101	4.0 "	5.689	3.5 "	5.636	10.0 "	5.904
3.5 "	4.465	14.0 "	5.177	5.0 "	5.781	4.0 "	5.702	12.0 "	5.979
4.0 "	4.552	16.0 "	5.242	6.0 "	5.845	4.5 "	5.750	14.0 "	6.041
5.0 "	4.663	18.0 "	5.299	7.0 "	5.889	5.0 "	5.810	16.0 "	6.094
6.0 "	4.751	20.0 "	5.348	8.0 "	5.920	6.0 "	5.854	18.0 "	6.139
7.0 "	4.820	24.0 "	5.420	9.0 "	5.942	7.0 "	5.880	20.0 "	6.210
8.0 "	4.894	28.0 "	5.491	10.0 "	5.957	8.0 "	5.913	24.0 "	6.263
9.0 "	4.949	30.0 "	5.517	11.0 "	5.967	9.0 "	5.935	28.0 "	6.296
10.0 "	4.996	40.0 "	5.606	12.0 "	5.976	10.0 "	5.958	30.0 "	6.348
12.0 "	5.072	50.0 "	5.652	12.5 "	5.977	12.0 "	6.035	35.0 "	6.374
14.0 "	5.129	60.0 "	5.678	13.0 "	5.980	14.0 "	6.164	40.0 "	6.387
16.0 "	5.171	70.0 "	5.694	14.0 "	5.983	16.0 "	6.183	45.0 "	6.392
18.0 "	5.203	80.0 "	5.698	15.0 "	5.985	18.0 "	6.195	50.0 "	6.395
20.0 "	5.227	90.0 "	5.700	16.0 "	5.990	20.0 "	6.202	60.0 "	6.397
25.0 "	5.264	10.0(10) <sup>2</sup>	5.702	18.0 "	5.991	25.0 "	6.211		
30.0 "	5.282	12.0 "	5.703	20.0 "	5.991	30.0 "	6.214		
35.0 "	5.290	14.0 "	5.704	24.0 "		35.0 "			
40.0 "	5.294	15.0 "	5.704	26.0 "		40.0 "			

TABLE IV—Continued

R = 700		R = 800		R = 900		R = 1000		R = 1200	
t	P(t)	t	P(t)	t	P(t)	t	P(t)	t	P(t)
5.0(10) <sup>2</sup>	5.814	7.0(10) <sup>2</sup>	5.983	5.0(10) <sup>2</sup>	6.046	1.0(10) <sup>3</sup>	6.161	2.0(10) <sup>3</sup>	6.307
6.0 "	5.905	8.0 "	6.046	6.0 "	6.108	1.2 "	6.232	3.0 "	6.404
7.0 "	5.982	9.0 "	6.108	7.0 "	6.161	1.4 "	6.328	4.0 "	6.533
8.0 "	6.048	10.0 "	6.160	8.0 "	6.211	1.6 "	6.396	5.0 "	6.618
9.0 "	6.105	12.0 "	6.249	9.0 "	6.257	1.8 "	6.453	6.0 "	6.675
10.0 "	6.156	14.0 "	6.322	10.0 "	6.292	2.0 "	6.503	7.0 "	6.713
12.0 "	6.239	16.0 "	6.382	12.0 "	6.447	2.5 "	6.605	8.0 "	6.731
14.0 "	6.305	18.0 "	6.432	14.0 "	6.494	3.0 "	6.681	9.0 "	6.746
16.0 "	6.357	20.0 "	6.474	16.0 "	6.537	3.5 "	6.738	10.0 "	6.767
18.0 "	6.398	25.0 "	6.551	18.0 "	6.582	4.0 "	6.781	12.0 "	6.786
20.0 "	6.430	30.0 "	6.609	20.0 "	6.629	4.5 "	6.818	14.0 "	6.805
25.0 "	6.484	35.0 "	6.650	25.0 "	6.761	5.0 "	6.857	16.0 "	6.828
30.0 "	6.514	40.0 "	6.650	30.0 "	6.766	5.5 "	6.854	18.0 "	6.849
35.0 "	6.530	45.0 "	6.653	35.0 "	6.777	6.0 "	6.858	19.0 "	6.859
40.0 "	6.540	50.0 "	6.671	40.0 "	6.785	7.0 "	6.853	20.0 "	6.860
45.0 "	6.548	55.0 "	6.678	45.0 "	6.784	8.0 "	6.855	21.0 "	6.860
50.0 "	6.548	60.0 "	6.678	50.0 "	6.783	9.0 "	6.851	22.0 "	6.860
60.0 "	6.550	70.0 "	6.682	60.0 "	6.800	10.0 "	6.854	23.0 "	6.860
70.0 "	6.551	80.0 "	6.684	70.0 "	6.801	12.0 "	6.857	24.0 "	6.860
80.0 "	6.551	100.0 "	6.684	10.0(10) <sup>3</sup>		14.0 "	6.857		
						16.0 "	6.858		

17

terms of the expansion are necessary to give the accuracy needed in the calculations.

Likewise from the foregoing work it can be easily shown that the transform of the pressure drop at any point in the formation in a limited reservoir for the constant terminal rate case, is expressed by

$$\bar{P}_{(r,p)} = \frac{[K_1(\sqrt{p} R) I_0(\sqrt{p} r) + I_1(\sqrt{p} R) K_0(\sqrt{p} r)]}{p^{3/2} [I_1(\sqrt{p} R) K_1(\sqrt{p} r) - K_1(\sqrt{p} R) I_1(\sqrt{p} r)]} \quad (VII-11)$$

An examination of the denominator of Eq. VII-11 indicates that there are no roots for positive values of p. However, a double pole exists at p = 0. This can be determined by expanding K<sub>0</sub>(z) and K<sub>1</sub>(z) to second degree expansions for small values of z and third degree expansions for I<sub>0</sub>(z) and I<sub>1</sub>(z), and substituting in Eq. VII-11. It is found for small values of p, Eq. VII-11 reduces to

$$\bar{P}_{(r,p)} = \frac{1}{p} \left\{ \frac{R^2}{(R^2-1)} \log \frac{R}{r} - \frac{(R^2-r^2)}{2(R^2-1)} + \frac{R^2 \log R}{(R^2-1)} - \frac{(R^2+1)}{4(R^2-1)} \right\} + \frac{1}{p^2} \frac{2}{(R^2-1)} \quad (VII-12)$$

This equation now indicates both a single and double pole at the origin, and it can be shown from tables or by applying Cauchy's theorem to the Mellin's formula that the inversion of Eq. VII-12 is

$$P_{(r,t)} = \frac{2}{(R^2-1)} \left[ \frac{r^2}{4} + t \right] \frac{R^2}{(R^2-1)} \log r - \frac{(3R^2-4R^2 \log R - 2R^2-1)}{4(R^2-1)} \quad (VII-13)$$

which holds when the time, t, is large.

As in the preceding case, there are poles along the negative real axis, Fig. 3, and the residuals are determined as before by letting λ = u<sup>2</sup> e<sup>iπ</sup>; and Eqs. VI-18 give

TABLE IV — Continued

R = 1400		R = 1600		R = 1800		R = 2000		R = 2200	
t	P <sub>(t)</sub>	t	P <sub>(t)</sub>	t	P <sub>(t)</sub>	t	P <sub>(t)</sub>	t	P <sub>(t)</sub>
2.0(10) <sup>2</sup>	6.807	2.5(10) <sup>2</sup>	6.819	3.0(10) <sup>2</sup>	6.810	4.0(10) <sup>2</sup>	6.834	5.0(10) <sup>2</sup>	6.866
2.5 "	6.819	3.0 "	6.810	4.0 "	6.854	5.0 "	6.906	6.0 "	7.013
3.0 "	6.700	3.5 "	6.787	5.0 "	6.965	6.0 "	7.056	7.0 "	7.097
3.5 "	6.783	4.0 "	6.853	6.0 "	7.054	7.0 "	7.132	8.0 "	7.167
4.0 "	6.849	5.0 "	6.902	7.0 "	7.126	8.0 "	7.196	9.0 "	7.256
5.0 "	6.950	6.0 "	7.046	8.0 "	7.188	9.0 "	7.251	10.0 "	7.299
6.0 "	7.028	7.0 "	7.114	9.0 "	7.238	10.0 "	7.298	11.0 "	7.341
7.0 "	7.082	8.0 "	7.167	10.0 "	7.280	12.0 "	7.374	12.0 "	7.374
8.0 "	7.123	9.0 "	7.210	15.0 "	7.407	14.0 "	7.431	14.0 "	7.431
9.0 "	7.154	10.0 "	7.244	20.0 "	7.459	16.0 "	7.474	16.0 "	7.474
10.0 "	7.177	15.0 "	7.334	30.0 "	7.489	18.0 "	7.506	18.0 "	7.506
15.0 "	7.229	20.0 "	7.364	40.0 "	7.498	20.0 "	7.530	20.0 "	7.530
20.0 "	7.241	25.0 "	7.373	50.0 "	7.498	25.0 "	7.556	25.0 "	7.556
25.0 "	7.243	30.0 "	7.376	60.0 "	7.495	30.0 "	7.564	30.0 "	7.564
30.0 "	7.244	35.0 "	7.377	80.0 "	7.493	35.0 "	7.567	35.0 "	7.567
31.0 "	7.244	40.0 "	7.378	85.0 "	7.493	40.0 "	7.567	40.0 "	7.567
32.0 "	7.244	42.0 "	7.378	84.0 "	7.493	50.0 "	7.560	50.0 "	7.560
33.0 "	7.244	44.0 "	7.378	86.0 "	7.493	60.0 "	7.561	60.0 "	7.561
						64.0 "	7.561	70.0 "	7.566
								80.0 "	7.566

TABLE IV — Continued

R = 2400		R = 2600		R = 2800		R = 3000	
t	P <sub>(t)</sub>	t	P <sub>(t)</sub>	t	P <sub>(t)</sub>	t	P <sub>(t)</sub>
6.0(10) <sup>2</sup>	7.007	7.0(10) <sup>2</sup>	7.134	8.0(10) <sup>2</sup>	7.201	1.0(10) <sup>3</sup>	7.312
7.0 "	7.134	8.0 "	7.201	9.0 "	7.260	1.2 "	7.403
8.0 "	7.201	9.0 "	7.250	10.0 "	7.312	1.4 "	7.489
9.0 "	7.250	10.0 "	7.312	12.0 "	7.403	1.6 "	7.565
10.0 "	7.310	12.0 "	7.401	14.0 "	7.512	1.8 "	7.622
12.0 "	7.398	14.0 "	7.475	20.0 "	7.644	2.0 "	7.661
14.0 "	7.526	16.0 "	7.534	24.0 "	7.719	2.4 "	7.734
20.0 "	7.611	18.0 "	7.585	28.0 "	7.775	2.8 "	7.784
24.0 "	7.674	20.0 "	7.631	30.0 "	7.797	3.0 "	7.806
28.0 "	7.706	24.0 "	7.690	35.0 "	7.813	3.5 "	7.811
30.0 "	7.720	28.0 "	7.745	40.0 "	7.820	4.0 "	7.814
35.0 "	7.745	30.0 "	7.765	50.0 "	7.825	4.8 "	7.815
40.0 "	7.760	35.0 "	7.780	60.0 "	7.822	5.0 "	7.815
50.0 "	7.775	40.0 "	7.824	70.0 "	7.820	6.0 "	7.815
60.0 "	7.780	50.0 "	7.845	80.0 "	7.814	7.0 "	7.815
70.0 "	7.782	60.0 "	7.856	90.0 "	7.812	8.0 "	7.815
80.0 "	7.783	70.0 "	7.860	10.0(10) <sup>3</sup>	7.812	9.0 "	7.815
90.0 "	7.783	80.0 "	7.862	12.0 "	7.812	10.0 "	7.815
		90.0 "	7.862	15.0 "	7.812	12.0 "	7.815
		10.0(10) <sup>3</sup>	7.863			15.0 "	7.815

$$\frac{1}{2\pi i} \int_{\lambda_0, \lambda_1, \dots} e^{u^2 t} \frac{d\lambda}{\lambda^2} \left[ J_0(\lambda R) Y_0(\lambda r) - Y_0(\lambda R) J_0(\lambda r) \right] \quad (VII-14)$$

where  $\beta_n, \beta_{2n}, \dots$  are roots of

$$[J_0(\beta_n R) Y_0(\beta_n) - J_0(\beta_n) Y_0(\beta_n R)] = 0 \quad (VII-15)$$

with  $\lambda_n = -\beta_n^2$ . The residuals at the poles in Eq. VII-14 give the series

$$2 \sum_{\beta_n, \beta_{2n}, \dots} \frac{e^{-\beta_n^2 t} [J_0(\beta_n R) Y_0(\beta_n r) - Y_0(\beta_n R) J_0(\beta_n r)]}{\beta_n \lim_{u \rightarrow \beta_n} \frac{d}{du} [J_0(uR) Y_0(u) - J_0(u) Y_0(uR)]} \quad (VII-16)$$

By the recurrence formulae Eqs. VII-9, the identity VII-15, and Eq. VI-23, this series simplifies to

$$\sum_{\beta_n, \beta_{2n}, \dots} \frac{e^{-\beta_n^2 t} J_0(\beta_n R) [J_0(\beta_n) Y_0(\beta_n r) - Y_0(\beta_n) J_0(\beta_n r)]}{\beta_n [J_0^2(\beta_n R) - J_0^2(\beta_n)]} \quad (VII-17)$$

Therefore, the sum of all residuals, Eqs. VII-13 and VII-17 is the solution for the cumulative pressure drop at any point in the formation for the constant terminal rate case in a limited reservoir, or

$$P_{(t)} = \frac{2}{(R^2-1)} \left( \frac{r^2}{4} + t \right) - \frac{R^2}{(R^2-1)} \log r - \frac{(3R^2-4R^2 \log R - 2R^2-1)}{4(R^2-1)^2} + \sum_{\beta_n, \beta_{2n}} \frac{e^{-\beta_n^2 t} J_0(\beta_n R) [J_0(\beta_n) Y_0(\beta_n r) - Y_0(\beta_n) J_0(\beta_n r)]}{\beta_n [J_0^2(\beta_n R) - J_0^2(\beta_n)]} \quad (VII-18)$$

which is essentially the solution given by Muskat, now developed by the Laplace Transformation. Finally, for the cumulative pressure drop for a unit rate of production at the well bore,  $r = 1$ , this relation simplifies to

$$P_{(t)} = \frac{2}{(R^2-1)} \left( \frac{1}{4} + t \right) - \frac{(3R^2-4R^2 \log R - 2R^2-1)}{4(R^2-1)^2} + 2 \sum_{\beta_n, \beta_{2n}} \frac{e^{-\beta_n^2 t} J_0^2(\beta_n R)}{\beta_n [J_0^2(\beta_n R) - J_0^2(\beta_n)]} \quad (VII-19)$$

The calculations for the constant terminal rate case for a reservoir of limited radial extent have been determined from Eq. VII-19. The summary data for  $R = 1.5$  to  $10$  are given in Table 3. An illustrative graph is shown in Fig. 6. The effect of the limited reservoir is quite pronounced as it is shown that producing the reservoir at a unit rate increases the pressure drop at the well bore much faster than if the reservoir were infinite, as the constant withdrawal of fluid is reflected very soon in the productive life by the constant rate of drop in pressure with time.

**Pressure Fixed at Exterior Boundary**

As a variation on the condition that  $\left( \frac{dP}{dr} = 0 \right)_{r=R}$ , we may assume that the pressure at  $r = R$  is constant. In effect, this assumption helps to explain approximately the pressure history of flowing a well at a constant rate when, upon opening, the bottom hole pressure drops very rapidly and then levels out to become constant with time. The case has been developed by Hurst using a cylinder source and by Muskat using a joint source solution.

When developing the solution by means of the Laplace transformation, it is assumed that the exterior boundary  $r = R$ ,  $P(R, p) = 0$ , which fixes the pressure at the exterior boundary as constant. Since the above-quoted references contain complete details, the final solutions are only quoted here for completeness' sake.

Cylindrical source:

$$P_{(t)} = \log R - 2 \sum_{\lambda_n} \frac{e^{-\lambda_n^2 t} J_0^2(\lambda_n R)}{\lambda_n^2 [J_0^2(\lambda_n) - J_0^2(\lambda_n R)]} \quad (VII-20)$$

where  $\lambda_n$  is the root established from

$$J_0(\lambda_n) Y_0(\lambda_n R) - Y_0(\lambda_n) J_0(\lambda_n R) = 0 \quad (VII-21)$$

Point source:

$$P_{(t)} = \log R - \frac{2}{R^2} \sum_{\lambda_n} \frac{e^{-\lambda_n^2 t} J_0(\lambda_n)}{\lambda_n^2 J_0^2(\lambda_n R)} \quad (VII-22)$$

where the root  $\lambda_n$  is determined from  $J_0(\lambda_n R) = 0$ , W.B.F., p. 748. Table 4 is the summary of the calculated  $P(t)$  employing Eq. VII-20 for  $R = 1.5$  to  $50$ , the cylinder source solution, which applies for small as well as large times. The data given for  $R = 60$  to  $3,000$  are calculated from the point source solution Eq. VII-22. Plots of these data are given in Fig. 7.

**SPECIAL PROBLEMS**

The work that has gone before shows the facility of the Laplace transformation in deriving analytical solutions. Not yet shown is the versatility of the Laplace transformation in arriving at solutions which are not easily foreseen by the orthodox methods. One such solution derived here has shown to be of value in the analysis of flow tests.

When making flow tests on a well, it is often noticed that the production rates, as measured by the fluid accumulating in the stock tanks, are practically constant. Since it is desired to obtain the relation between flowing bottom hole pressure and the rate of production from the formation, it is necessary to correct the rate of production as measured in the flow tanks for the amount of oil obtained from the annulus between casing and tubing. To arrive at the solution for this problem, we use the basic equation for the constant terminal rate case given by Eq. IV-11, where  $q_{(r)}$  is the constant rate of fluid produced at the stock tank corrected to reservoir conditions, but  $P_{(t)}$  is a pseudo pressure drop which is adjusted mathematically for the unloading of the fluid from the annulus to give the pressure drop occurring in the formation.

It is assumed that the unloading of the annulus is directly reflected by the change in bottom hole pressure as exerted by a hydrostatic head of oil column in the casing. Therefore, the rate of unloading of the annulus  $q_{A(r)}$ , expressed in cc. per second corrected to reservoir conditions, is equal to

$$q_{A(r)} = C \frac{d\Delta P}{dt} \quad (VIII-1)$$

where  $C$  is the volume of fluid unloaded from the annulus per atmosphere bottom hole pressure drop per unit sand thickness. The rate of fluid produced from the formation is then given by  $q_{(r)} - q_{A(r)}$ . As the bottom hole pressure is continuously changing, the problem becomes one of a variable rate. The substitution of the form of Eq. IV-11 in the superposition theorem, Eq. IV-16, gives

$$\Delta P = \frac{\mu}{2\pi K} \int_0^t [q(t') - q_A(t')] P'_{(t-t')} dt' \quad (VIII-1)$$

and from Eq. VIII-1

$$\Delta P = \frac{\mu}{2\pi K} \int_0^t \left[ q(t') - C \frac{d\Delta P}{dt'} \right] P'_{(t-t')} dt' \quad (VIII-2)$$

Since  $T = f\mu c R_w^2 / K$ , and the unit rate of production at the surface corrected to reservoir conditions is  $\bar{q}_{(t)} = \frac{q_{(t)}\mu}{2\pi K}$ , Eq. VIII-2 becomes

$$\Delta P = \int_0^t \left[ q_{(t')} - \bar{C} \frac{d\Delta P}{dt'} \right] P'_{(t-t')} dt' \quad (VIII-3)$$

where  $\bar{C} = C/2\pi f c R_w^2$ .

Eq. VIII-3 presents a unique situation and we are confronted with determination of  $\Delta P$ , the actual pressure drop, appearing both in the integrand and to the left side of the equation. The Laplace transformation offers a means of solving for  $\Delta P$  which, by orthodox methods, would be difficult to accomplish.

It will be recognized that Theorem D, from Chapter V, is applicable. Therefore, if Eq. VIII-3 can be changed to a Laplace transformation,  $\Delta P$  can be solved explicitly. If we express the transform of the constant rate  $q_{(t)}$  as  $q/p$ , the transform of  $P'_{(t)}$  as  $p\bar{P}_{(p)}$ , and the transform of  $\Delta P$  as  $\Delta\bar{P}$ , so that the transform for  $d\Delta P/dt$  is  $p\Delta\bar{P}$ , then it follows that

$$\Delta\bar{P} = \left[ \frac{q}{p} - \bar{C} p\Delta\bar{P} \right] p \bar{P}_{(p)} \quad (VIII-4)$$

and on solution gives

$$\Delta\bar{P} = \frac{q \bar{P}_{(p)}}{[1 + \bar{C} p \bar{P}_{(p)}]} \quad (VIII-5)$$

Since  $q = q_{(t)}\mu/2\pi K$ , then the term  $\frac{\bar{P}_{(p)}}{[1 + \bar{C} p \bar{P}_{(p)}]}$  in Eq.

VIII-5 can be interpreted as the transform of the pseudo pressure drop for the unit rate of production at the stock tank.

No mention has been made as to what value can be substituted for  $\bar{P}_{(p)}$ . If we wish to apply the cylinder source, Eq. VI-4 applies, namely,

$$\bar{P}_{(p)} = \frac{K_o(\sqrt{p})}{p^{3/2} K_i(\sqrt{p})} \quad (VIII-6)$$

However, from the previous discussion it has been shown that for wells,  $\tau$  is usually large since the well radius is small, and the point source solution of Lord Kelvin's applies, namely,

$$P_{(t)} = \frac{1}{2} \int_0^{\infty} \frac{e^{-u^2}}{u^{3/2}} du \quad (VI-16)$$

the E-function. Therefore, to apply this expression in Eq. VIII-5, it is necessary to obtain the Laplace transform of the point source solution of Eq. VI-16. By an interchange of variables, this equation becomes

$$P_{(t)} = \frac{1}{2} \int_0^{\infty} \frac{e^{-t u}}{u} dt \quad (VIII-7)$$

and it will be recognized from Campbell and Foster, Eq. 920.1,

that the integrand is the transform for  $K_o(\sqrt{p})$ . Further, the integration with respect to time follows from Theorem B, Chapter V, so that the transform of Eq. VIII-7 is the relation

$$\bar{P}_{(p)} = \frac{K_o(\sqrt{p})}{p} \quad (VIII-8)$$

The same result can be gleaned from Eq. VIII-6 since for  $\tau$  large,  $p$  is small and  $K_o(\sqrt{p}) = 1/\sqrt{p}$ . Substitution of this approximation in Eq. VIII-6 yields Eq. VIII-8. Therefore,

introducing the expression for  $\bar{P}_{(p)}$  in Eq. VIII-5 gives

$$\Delta\bar{P} = \frac{q K_o(\sqrt{p})}{p [1 + \bar{C} p K_o(\sqrt{p})]} \quad (VIII-9)$$

for which it is necessary only to find the inverse of

$$\frac{K_o(\sqrt{p})}{p [1 + \bar{C} p K_o(\sqrt{p})]} \quad (VIII-10)$$

to obtain values for  $P_{(t)}$ , the cumulative pressure drop for unit rate of production in the stock tank which automatically takes cognizance of the unloading of the annulus.

The inverse of the form of VIII-10 by the Mellin's inversion formula can be determined by the path described in Fig. 2. The analytical determination is identical with the constant terminal rate case given in Section VI. Therefore, the cumulative pressure drop in the well bore, for a unit rate of production at the surface, corrected for the unloading of the fluid in the casing, is the relation

$$P_{(t)} = \int_0^{\infty} \frac{(1 - e^{-u^2}) J_o(u) du}{u [(1 + u^2 \bar{C} \frac{\pi}{2} Y_o(u))^2 + (u^2 \bar{C} \frac{\pi}{2} J_o(u))^2]} \quad (VIII-11)$$

Fig. 8 presents a plot of the computed values for  $P_{(t)}$  corresponding to  $\bar{C}$  from 1,000 to 75,000. It can be observed that the greater the unloading from the casing, the smaller the actual pressure drop is in a formation due to the reduced rate of fluid produced from the sand. For large times, however, all curves become identified with the point source solution which is the envelope of these curves. After a sufficient length of time, the change in bottom hole pressure is so slow that the rate of production from the formation is essentially that produced by the well, and the point source solution applies.

#### ACKNOWLEDGMENTS

The authors wish to thank the Management of the Shell Oil Co., for permission to prepare and present this paper for publication. It is hoped that this information, once available to the industry, will further the analysis and understanding of the behavior of oil reservoirs.

The authors acknowledge the help of H. Rainbow of the Shell Oil Co., whose suggestions on analytic development were most helpful, and of Miss L. Patterson, who contributed the greatest amount of these calculations with untiring effort.

#### REFERENCES

1. "Water Influx into a Reservoir and Its Application to the Equation of Volumetric Balance," William Hurst, *Trans. AIME*, 1943.



implies a vanishing compressibility; or it must have pressures fixed with time such that the time-derivative vanishes. Evidently, strict steady-state conditions are virtually impossible to attain, since these provisions are abstractions of the mind and not properties of physical systems. From a practical standpoint, however, this fact does not exclude application of steady-state mechanics, because in many situations Eq. 1 is closely approximated.<sup>3-5</sup>

The significant physical properties that determine the extent of transient behavior in spherical reservoir systems are exhibited by the so-called readjustment time which is approximated by:

$$t_r = \frac{\phi c r_p^2}{2k/\mu} \dots \dots \dots (2)$$

These factors are the size of the system, its compressibility and its mobility. When they combine to yield a large readjustment time, unsteady-state mechanics should be used unless pressures are invariant.<sup>3,5</sup>

**ENGINEERING APPLICATIONS**

When a water drive field is characterized by bottom-water encroachment, the hydrocarbon accumulation usually fills only a portion of the total thickness of the reservoir formation and is entirely underlain by water. Flow of water into the pay zone results from a gradual and uniform rise of the underlying water.

Of particular interest to the reservoir engineer are methods, formally independent of material balance principles, for determining the water influx into bottom-water drive fields. First, these methods afford determination of a number of reservoir properties through an analysis of the past reservoir history by an adjunctive use with other relations. Secondly, by independently yielding the water influx they provide means of predicting future reservoir performance. Many bottom-water drive fields lend themselves to the imposition of spherical geometry; hence, solutions of the fundamental flow equations appropriate to this symmetry can be used to analytically determine the water influx for any class of reservoir.<sup>4,6</sup>

Although many wells are completed after the drill has penetrated entirely through the pay formation, some are purposely completed after only partial penetration has been entered. Sometimes such wells are completed after the top surface of the reservoir is merely cased by the drill, in which case they are termed nonpenetrating wells.

Non-penetrating wells that occur in a relatively thick formation can be treated as spherical systems. They can be analytically investigated by using appropriate solutions of the fundamental flow equations corresponding to spherical symmetry. These investigations include flow calculations, analysis of drawdown and build-up tests, determination of static bottom-hole pressure, productivity indices, effective permeabilities and evaluation of

damaged sand conditions. Also, although the analytical solutions strictly apply only to the single-phase flow of compressible liquids, the results can sometimes be used (with proper interpretation) the flow of gases when pressure drops are small, and to the simultaneous flow of oil and gas upon imposition of drastic assumptions.<sup>3,4,7</sup>

**THEORETICAL CONSIDERATIONS**

**FUNDAMENTAL DIFFERENTIAL EQUATION**

The fundamental differential equation governing the dynamics of the flow of compressible liquids through spherical reservoir systems can be written as:

$$\frac{\partial^2 p}{\partial r^2} + \frac{2}{r} \frac{\partial p}{\partial r} = \frac{\phi c \mu}{k} \frac{\partial p}{\partial t} \dots \dots \dots (3)$$

where the porosity, compressibility and mobility are interpreted as fixed averages, and where the effects of gravity are neglected. Define a dimensionless length ratio, time ratio and pressure-drop ratio, respectively, as follows:

$$r_D = \frac{r}{r_w} \dots \dots \dots (4)$$

$$t_D = \frac{k t}{\phi \mu c r_w^2} \dots \dots \dots (5)$$

$$p_D = p_D(r_D, t_D) = \frac{p_i - p(r_D, t_D)}{p_i - p(1, t_D)} \dots \dots \dots (6)$$

Introduction of these relations into Eq. 3 permits it to be rewritten as:

$$\frac{\partial^2 p_D}{\partial r_D^2} + \frac{2}{r_D} \frac{\partial p_D}{\partial r_D} = \frac{\partial p_D}{\partial t_D} \dots \dots \dots (7)$$

which represents the fundamental differential equation in dimensionless form appropriate to reservoir systems characterized by spherical symmetry.<sup>2-5,8</sup>

**AVERAGE SPHERICAL PERMEABILITY**

Available evidence indicates that the permeability of porous media constituting reservoir systems is not isotropic in character. As a rule the vertical permeability is less than the horizontal and in some instances the difference is profound. Since spherical symmetry embraces a three-dimensional geometric space, it was felt necessary to include the effects of this anisotropy here. The radial permeability in a spherical porous medium characterized by uniform vertical and horizontal permeability components can be analytically described by:

$$\frac{1}{k_r} = \frac{1}{k_h} \sin^2 a + \frac{1}{k_v} \cos^2 a \dots \dots \dots (9)$$

The average spherical permeability can then be obtained with the volume integral:



$$\bar{k}_r = k_r = \frac{(2/3) \pi (r_e^3 - r_w^3)}{\int_0^\pi \int_0^\pi \int_{r_w}^{r_e} \frac{r^2}{k_r} \sin a \, dr \, d\alpha \, d\theta} \dots (9)$$

which, upon evaluation, gives:

$$k = \frac{3k_b k_v}{k_b + 2k_v} \dots (10)$$

the average spherical permeability.

**APPLICATION OF THE LAPLACE TRANSFORMATION**

The fundamental differential equation for a spherical reservoir system has been expressed in dimensionless form by Eq. 7. Define the product:

$$b = r_D p_D \dots (11)$$

Then Eq. 7 can be written in the alternative form:

$$\frac{\partial^2 b}{\partial r_D^2} = \frac{\partial b}{\partial t_D} \dots (12)$$

The Laplace transform of *b* is given by the definite integral:

$$\bar{b} = \int_0^\infty b \exp(-s t_D) dt_D \dots (13)$$

Multiplication by the nucleus of the transform and integration over all time converts Eq. 12 from a partial to the ordinary differential equation:

$$\frac{d^2 \bar{b}}{dr_D^2} = s \bar{b} \dots (14)$$

The general solution of this subsidiary equation can be written at once:

$$\bar{b} = C_1 \exp(-r_D \sqrt{s}) + C_2 \exp(r_D \sqrt{s}) \dots (15)$$

where *C<sub>n</sub>* is an arbitrary constant.<sup>2,9-11</sup> Particular solutions to the subsidiary equation corresponding to specifically imposed boundary conditions are obtained upon appropriate evaluation of the constants that appear in its general solution. These particular solutions would represent the Laplace transforms of the required particular solutions to Eq. 12. The latter are determined by effecting the inverse transformations of their Laplace transforms. This procedure will be used to develop the particular solutions of interest.

**SELECTION OF PARTICULAR SOLUTIONS**

Reduction of Eq. 3 to the dimensionless form depicted by Eq. 7 was effected, because the complete dimensionlessness of Eq. 7 renders the numerical values associated with its particular solutions entirely independent of the actual magnitudes of the physical properties of any given reservoir

system. But due to the generality introduced, it becomes necessary to relate certain physical quantities associated with absolute units of measurement to functions of the dimensionless variables in Eq. 7.<sup>2,5</sup>

The macroscopic radial velocity at the internal boundary of a spherical reservoir system is given by Darcy's law:<sup>2-4</sup>

$$u = -\frac{k}{\mu} \left( \frac{\partial p}{\partial r} \right)_{r_w} \dots (16)$$

Introduction of the relations defined by Eqs. 4 through 6 yields:

$$u = \frac{k}{\mu r_w} \Delta p(r_w, t) \left( \frac{\partial p_D}{\partial r_D} \right)_1 \dots (17)$$

which relates the actual velocity with the dimensionless function  $(\partial p_D / \partial r_D)_1$ . The rate of fluid influx at the internal boundary is given by:<sup>3,4</sup>

$$e = - \int_0^\pi \int_0^\pi r^2 u \sin a \, d\alpha \, d\theta = 2\pi r_w^2 \frac{k}{\mu} \left( \frac{\partial p}{\partial r} \right)_{r_w} \dots (18)$$

Then, introduction of Eqs. 4 through 6 yields:

$$e = -2\pi r_w \frac{k}{\mu} \Delta p(r_w, t) \left( \frac{\partial p_D}{\partial r_D} \right)_1 \dots (19)$$

which relates the actual fluid influx rate with the dimensionless function  $(\partial p_D / \partial r_D)_1$ .

The cumulative fluid influx at the internal boundary up to any time *t* is given by:<sup>2</sup>

$$F = \int_0^t e \, dt = 2\pi r_w^2 \frac{k}{\mu} \int_0^t \left( \frac{\partial p}{\partial r} \right)_{r_w} dt \dots (20)$$

Similarly, introduction of Eqs. 4 through 6 yields:

$$F = -2\pi \phi c r_w^3 \Delta p(r_w, t) \int_0^{t_D} \left( \frac{\partial p_D}{\partial r_D} \right)_1 dt_D \dots (21)$$

which relates the actual cumulative fluid influx with the time integral of the dimensionless function  $(\partial p_D / \partial r_D)_1$ . Upon proper interpretation, Eqs. 17, 19 and 21 can be used to determine the fluid flow and pressure behavior in a spherical reservoir system, and also to indicate the appropriate choice of particular solutions to Eq. 7. Two distinct cases arise: the so-called pressure and rate cases.<sup>2,5</sup>

*The Pressure Case*

The pressure case presumes knowledge of the pressure conditions at the internal boundary of a reservoir system and permits determination of the fluid flow behavior. Consider a spherical reservoir system characterized by dimensionless properties. Let this system be charged to a unit dimensionless pressure, and at zero time let the pressure at the internal boundary vanish and remain zero. This

condition represents the distinctive feature of the pressure case. The problem then remains to determine the dimensionless rate and cumulative fluid influx at the internal boundary as functions of dimensionless time. This dimensionless description of the fluid flow behavior and its translation into absolute units of measurement constitutes the pressure case.<sup>2,5</sup>

Under the precepts of the pressure case, the dimensionless fluid influx rate is defined by:

$$e_D = e_D(1, t_D) = - \left( \frac{\partial p_D}{\partial r_D} \right)_1 \dots \dots \dots (22)$$

and the dimensionless cumulative fluid influx by:

$$F_D = F_D(1, t_D) = - \int_0^{t_D} \left( \frac{\partial p_D}{\partial r_D} \right)_1 dt_D \dots \dots \dots (23)$$

Symbolically, the actual velocity, rate and cumulative fluid influx may now be expressed in terms of  $e_D$  and  $F_D$  as follows:

$$u = u(r_w, t) = - \frac{k}{\mu r_w} \Delta p(r_w, 0) e_D(1, t_D) \dots (24)$$

$$e = e(r_w, t) = 2\pi r_w \frac{k}{\mu} \Delta p(r_w, 0) e_D(1, t_D) \dots (25)$$

$$F = F(r_w, t) = 2\pi \phi c r_w^3 \Delta p(r_w, 0) F_D(1, t_D) \dots (26)$$

Eqs. 24 through 26 express the facts of fluid flow behavior in terms of field data and the dimensionless functions  $e_D$  and  $F_D$ . By application of the superposition principle (Duhamel's theorem) these functions can also be used to treat time-varying pressure histories.

*The Rate Case*

The rate case presumes knowledge of the fluid flow conditions at the internal boundary and permits determination of the pressure behavior. Consider a dimensionless spherical reservoir system charged to unit dimensionless pressure, and from zero-time constant, a unit dimensionless fluid influx rate be imposed. This condition, which expressed analytically is:

$$- \left( \frac{\partial p_D}{\partial r_D} \right)_1 = 1 \dots \dots \dots (27)$$

For all time  $t_D$ , represents the distinctive feature of the rate case. The problem here is to determine the dimensionless pressure drop distribution in the system, and the pressure drop at the internal boundary under the conditions prescribed by Eq. 27. This dimensionless description of pressure behavior and its translation into absolute units of measurement constitutes the rate case.<sup>2,5</sup>

Under the precepts of the rate case, the actual pressure distribution in the system is given by:

$$p(r, t) = p_i - \frac{e \mu}{2\pi k r_w} p_D(r_D, t_D) \dots \dots \dots (28)$$

Similarly, the actual pressure at the internal boundary is given by:

$$p = p(r_w, t) = p_i - \frac{e \mu}{2\pi k r_w} p_D(1, t_D) \dots \dots \dots (29)$$

These symbolic relations express the pressure behavior in terms of field data and the dimensionless functions  $p_D(t_D, r_D)$  and  $p_D(1, t_D)$ . Likewise, by application of the superposition principle, these functions can be used to treat time-varying rate histories.

DESCRIPTION OF PARTICULAR SOLUTIONS

UNLIMITED SYSTEM

By definition the external boundary of an unlimited system continuously recedes from the internal boundary without reaching a geometric limit. Under these conditions the product  $r_D p_D$  vanishes and Eq. 15 becomes:

$$\bar{b} = C_1 \exp(-r_D \sqrt{s}) \dots \dots \dots (30)$$

The precepts of the pressure case require that a dimensionless pressure drop of unity be maintained at the internal boundary, and since the Laplace transform of unity is  $1/s$ , it follows that:

$$\bar{b} = \frac{1}{s} \exp[-\sqrt{s} (r_D - 1)] \dots \dots \dots (31)$$

which is the subsidiary equation appropriate to the pressure case for an unlimited system. The dimensionless fluid influx rate  $e_D$  can be rewritten in terms of  $b$ :

$$e_D = - \left( \frac{\partial p_D}{\partial r_D} \right)_1 = - \left( \frac{\partial b}{\partial r_D} - b \right)_1 \dots \dots \dots (32)$$

Then the Laplace transform of  $e_D$ , utilizing Eqs. 31 and 32, is:

$$\bar{e}_D = \frac{1}{\sqrt{s}} + \frac{1}{s} \dots \dots \dots (33)$$

whose inverse transformation can be written at once as:

$$e_D = 1 + (\pi t_D)^{-1/2} \dots \dots \dots (34)$$

which is the dimensionless fluid influx rate of an unlimited system. The Laplace transform of  $F_D$  (dimensionless cumulative fluid influx) is simply:

$$\bar{F}_D = \frac{\bar{e}_D}{s} = \frac{1}{s^{3/2}} + \frac{1}{s^2} \dots \dots \dots (35)$$

whose inverse transformation can likewise be

written at once as:

$$F_D = t_D + 2 \left( \frac{t_D}{u} \right)^{1/2} \quad (36)$$

which is the dimensionless cumulative fluid influx of an unlimited system. 9, 11, 13, 14

The precepts of the rate case require that a dimensionless rate of unity be maintained at the internal boundary, which can be written in terms of  $b$  as:

$$-\left( \frac{\partial p_D}{\partial r_D} \right)_1 = -\left( \frac{\partial b}{\partial r_D} - b \right)_1 = 1 \quad (37)$$

Using Eq. 30 it follows that:

$$b = \frac{\exp[-\sqrt{s}(r_D - 1)]}{s(1 + \sqrt{s})} \quad (38)$$

which is the subsidiary equation appropriate to the rate case for an unlimited system. The inverse transformation is available from integral transform tables. This result divided by  $r_D$  yields:

$$p_D(r_D, t_D) = \frac{1}{r_D} \left[ \operatorname{erfc} \left( \frac{r_D - 1}{2\sqrt{t_D}} \right) - \exp(t_D + r_D - 1) \operatorname{erfc} \left( \frac{r_D - 1}{2\sqrt{t_D}} + \sqrt{t_D} \right) \right] \quad (39)$$

which is the dimensionless pressure-drop distribution of an unlimited system. Upon placing  $r_D$  at unity, Eq. 39 reduces to:

$$p_D = 1 - \exp(t_D) \operatorname{erfc}(t_D^{1/2}) \quad (40)$$

which is the dimensionless pressure drop at the internal boundary of an unlimited system. 2, 9, 11, 13, 14

At this juncture some significant observations can be made. First, the least upper bound of the dimensionless pressure drop is unity. Consequently, under the conditions of constant rate the pressure drop at the internal boundary of an unlimited spherical system can never exceed a fixed finite value. Secondly, the greatest lower bound of the dimensionless rate is also unity. Hence, the rate engendered by a single pressure drop imposed at zero time at the internal boundary of an unlimited spherical system can never be less than a fixed non-vanishing value. In either situation, it appears that an unlimited spherical reservoir system approaches steady-state conditions as dimensionless time assumes excessively large values. This property, strangely enough, is not enjoyed by unlimited linear or cylindrical (radial) systems. 2, 5

LIMITED SYSTEM WITH CLOSED EXTERNAL BOUNDARY

In a limited reservoir system the external boundary eventually coincides with a geometric

limit. At this limit, a system with a closed external boundary can sustain no fluid flow across it. Hence, the normal pressure derivative there must vanish. Introduction of this condition into Eq. 15 gives:

$$\bar{b} = C_1 \left[ \exp(-r_D \sqrt{s}) + \left( \frac{r_D' \sqrt{s} + 1}{r_D' \sqrt{s} - 1} \right) \exp \sqrt{s}(r_D - 2r_D') \right] \quad (41)$$

Under the precepts of the pressure case and by subsequent conversion to hyperbolic functions, Eq. 41 becomes:

$$\bar{b} = \frac{\sinh[\sqrt{s}(r_D' - r_D)] - \sqrt{s} r_D' \cosh[\sqrt{s}(r_D' - r_D)]}{s \{ \sinh[\sqrt{s}(r_D' - 1)] - \sqrt{s} r_D' \cosh[\sqrt{s}(r_D' - 1)] \}} \quad (42)$$

which is the subsidiary equation appropriate to the pressure case for a closed limited system. The Laplace transform of  $e_D$ , using Eqs. 32 and 42, is:

$$\bar{e}_D = \frac{\sqrt{s}(r_D' - 1) \cosh[\sqrt{s}(r_D' - 1)] + (s r_D' - 1) \sinh[\sqrt{s}(r_D' - 1)]}{s \{ \sqrt{s} r_D' \cosh[\sqrt{s}(r_D' - 1)] - \sinh[\sqrt{s}(r_D' - 1)] \}} \quad (43)$$

The inverse transformation of the relation may be obtained with the aid of Mellin's inversion theorem, and is given by the following integral in the complex plane:

$$e_D = \frac{1}{2\pi i} \lim_{\delta \rightarrow \infty} \int_{\gamma - i\delta}^{\gamma + i\delta} \exp(z t_D) \bar{e}_D dz \quad (44)$$

which for the function at hand may be evaluated by converting it to a closed contour integral and then applying the calculus of residues. Thus, by virtue of Cauchy's integral formula:

$$\frac{1}{2\pi i} \lim_{\delta \rightarrow \infty} \int_{\gamma - i\delta}^{\gamma + i\delta} e^{z t_D} \bar{e}_D dz = \frac{1}{2\pi i} \int_C e^{z t_D} \bar{e}_D dz = R_0 + \sum_{n=1}^{\infty} R_n \quad (45)$$

where  $R_0$  is the residue corresponding to the singularity at the origin and  $R_n$  the residues corresponding to the other singular points. Evaluation of Eq. 45 yields the dimensionless fluid influx rate for a closed limited spherical system, as follows:

$$e_D = \frac{2}{(r_D' - 1)} \sum_{n=1}^{\infty} \frac{w_n^2 r_D'^2 + (r_D' - 1)^2}{w_n^2 r_D'^2 - (r_D' - 1)^2} \exp \left[ \frac{w_n^2 t_D}{(r_D' - 1)} \right] \quad (46)$$

where  $w_n$  are the roots of the equation:

$$\tan w_n = \frac{r_D'}{w_n (r_D' - 1)} \quad (47)$$

The Laplace transform of  $F_D$  is:

$$\bar{F}_D = \frac{\bar{e}_D}{s} = \frac{\sqrt{s}(r_D'-1)\cosh\sqrt{s}(r_D'-1) + (sr_D'-1)\sinh\sqrt{s}(r_D'-1)}{s^2[\sqrt{s}r_D'\cosh\sqrt{s}(r_D'-1) - \sinh\sqrt{s}(r_D'-1)]} \quad (48)$$

By virtue of previous arguments, the inverse transformation of Eq. 48 yields the dimensionless cumulative fluid influx for a closed limited system:

$$\bar{F}_D = R_0 + \sum_{n=1}^{\infty} R_n = \frac{1}{3} (r_D'^3 - 1) - 2(r_D'-1) \sum_{n=1}^{\infty} \frac{1}{w_n^2} \left[ \frac{w_n^2 r_D' + (r_D'-1)^2}{w_n^2 r_D' - (r_D'-1)} \right] e^{-\frac{w_n^2 r_D'}{(r_D'-1)^2}} \quad (49)$$

where  $w_n$  are also the roots of Eq. 47.2,10,11,13-18

Under the precepts of the rate case, Eq. 41 becomes, upon conversion to hyperbolic functions:

$$\bar{b} = \frac{\sqrt{s}r_D'\cosh\sqrt{s}(r_D'-r_D) - \sinh\sqrt{s}(r_D'-r_D)}{s[\sqrt{s}(r_D'-1)\cosh\sqrt{s}(r_D'-1) + (sr_D'-1)\sinh\sqrt{s}(r_D'-1)]} \quad (50)$$

which is the subsidiary equation appropriate to the rate case for a closed limited system. As before, the inverse transformation of Eq. 50 is given by the sum of the residues, and since  $b$  is  $r_D'p_D$ , there follows:

TABLE 1 — UNLIMITED SYSTEM

Dimensionless Time ( $r_D$ )	Dimensionless Rate ( $e_D$ )	Dimensionless Influx ( $F_D$ )	Dimensionless Pressure-Drop ( $p_D$ )	Dimensionless Time ( $r_D$ )	Dimensionless Rate ( $e_D$ )	Dimensionless Influx ( $F_D$ )	Dimensionless Pressure-Drop ( $p_D$ )
0.001	18.84124	0.03668	0.03471				
0.002	13.61566	0.05246	0.04853	60.0	1.07284	68.7	0.92595
0.003	11.30065	0.06480	0.05892	70.0	1.06743	79.4	0.93103
0.004	9.92062	0.07536	0.06755	80.0	1.06308	90.1	0.93512
0.005	8.97885	0.08479	0.07504	90.0	1.05947	100.7	0.93851
0.006	8.28366	0.09340	0.08174	100.0	1.05642	111.0	0.94139
0.007	7.74336	0.10141	0.08782	200.0	1.03989	216.0	0.95703
0.008	7.30783	0.10893	0.09343	300.0	1.03257	320.0	0.96408
0.009	6.94708	0.11605	0.09865	400.0	1.02821	423.0	0.96835
0.01	6.64190	0.12284	0.10354	500.0	1.02523	525.0	0.97131
0.02	4.98942	0.17958	0.14152	600.0	1.02303	628.0	0.97352
0.03	4.25735	0.22544	0.16894	700.0	1.02132	730.0	0.97526
0.04	3.82095	0.26568	0.19098	800.0	1.01995	832.0	0.97668
0.05	3.52313	0.30231	0.20962	900.0	1.01881	934.0	0.97787
0.06	3.30329	0.33640	0.22588	1,000.0	1.01784	1,036.0	0.97888
0.07	3.13244	0.36854	0.24036	2,000.0	1.01262	2,050.0	0.98453
0.08	2.99471	0.39915	0.25345	3,000.0	1.01030	3,062.0	0.98714
0.09	2.88063	0.42851	0.26540	4,000.0	1.00892	4,071.0	0.98874
0.10	2.78412	0.45682	0.27642	5,000.0	1.00798	5,080.0	0.98984
0.20	2.26157	0.70463	0.35621	6,000.0	1.00728	6,087.0	0.99067
0.30	2.03006	0.91804	0.40798	7,000.0	1.00674	7,094.0	0.99132
0.40	1.87206	1.11365	0.44639	8,000.0	1.00631	8,101.0	0.99185
0.50	1.79788	1.29788	0.47684	9,000.0	1.00595	9,107.0	0.99229
0.60	1.72837	1.47404	0.50198	10,000.0	1.00564	10,113.0	0.99257
0.70	1.67434	1.64407	0.52330	20,000.0	1.00399	20,160.0	0.99473
0.80	1.63078	1.80925	0.54175	30,000.0	1.00326	30,195.0	0.99566
0.90	1.59471	1.97047	0.55798	40,000.0	1.00282	40,226.0	0.99623
1.0	1.56419	2.12838	0.57242	50,000.0	1.00252	50,252.0	0.99662
2.0	1.39894	3.59577	0.66380	60,000.0	1.00230	60,276.0	0.99690
3.0	1.32574	4.95441	0.71266	70,000.0	1.00213	70,299.0	0.99713
4.0	1.28209	6.25676	0.74460	80,000.0	1.00199	80,319.0	0.99731
5.0	1.25231	7.52313	0.76765	90,000.0	1.00188	90,339.0	0.99746
6.0	1.23033	8.76395	0.78534	100,000.0	1.00178	100,357.0	0.99759
7.0	1.21324	9.98541	0.79946	200,000.0	1.00126	200,505.0	0.99829
8.0	1.19947	11.19154	0.81109	300,000.0	1.00103	300,618.0	0.99860
9.0	1.18806	12.38514	0.82088	400,000.0	1.00089	400,714.0	0.99878
10.0	1.17841	13.56825	0.82927	500,000.0	1.00080	500,798.0	0.99891
20.0	1.12616	25.04626	0.87624	600,000.0	1.00073	600,874.0	0.99900
30.0	1.10301	36.18039	0.89770	700,000.0	1.00067	700,944.0	0.99908
40.0	1.08921	47.13650	0.91060	800,000.0	1.00063	801,009.0	0.99914
50.0	1.07979	57.97885	0.91943	900,000.0	1.00059	901,070.0	0.99919
				1,000,000.0	1.00056	1,001,128.0	0.99923

$p(r_D, t_D) =$

$$\frac{(3r_D' + (r_D' - 1)^2) \left[ \frac{1}{6} (r_D' - 1)^2 (2r_D' + r_D) + r_D' t_D \right] - \frac{1}{2} (r_D' - 1)^2 \left[ \frac{1}{5} (r_D' - 1)^2 + r_D' \right] r_D}{(r_D' - 1) \left[ \frac{1}{3} (r_D' - 1)^4 + 2r_D' (r_D' - 1)^2 + 3r_D'^2 \right] r_D} - \frac{2(r_D' - 1)^2}{r_D} \sum_{n=1}^{\infty} \frac{\left[ \frac{r_D' w_n}{r_D' - 1} \cos \left( w_n \frac{r_D' - r_D}{r_D' - 1} \right) - \sin \left( w_n \frac{r_D' - r_D}{r_D' - 1} \right) \right] e^{-\frac{w_n^2 t_D}{(r_D' - 1)^2}}}{w_n^2 [w_n r_D' \cos w_n + (r_D'^2 + 1) \sin w_n]} \dots (51)$$

where  $w_n$  are here the roots of:

$$\frac{\cot w}{w} - \frac{1}{w^2} = \frac{r_D'}{(r_D' - 1)^2} \dots (52)$$

The expression embodied by Eq. 51 represents the dimensionless pressure-drop distribution for a closed limited spherical system. Upon placing  $r_D$  at unity and simplifying, there follows at once the dimensionless pressure-drop at the internal boundary:

$$p_D = \frac{[(r_D' - 1)^2 + 3r_D'] \left[ \frac{1}{6} (r_D' - 1)^2 (2r_D' + 1) + r_D' \right] - \frac{1}{2} (r_D' - 1)^2 \left[ \frac{1}{5} (r_D' - 1)^2 + r_D' \right]}{(r_D' - 1) \left[ \frac{1}{3} (r_D' - 1)^4 + 2(r_D' - 1)^2 r_D' + 3r_D'^2 \right]} - 2(r_D' - 1) \sum_{n=1}^{\infty} \frac{[w_n^2 r_D'^2 + (r_D' - 1)^2]}{w_n^2 [w_n^2 r_D'^2 + (r_D'^2 + r_D' + 1)(r_D' - 1)^2]} \times e^{-\frac{w_n^2 t_D}{(r_D' - 1)^2}} \dots (53)$$

where  $w_n$  are still the roots of Eq. 52.

**LIMITED SYSTEM WITH OPEN EXTERNAL BOUNDARY**

It will be recalled that a limited reservoir system is characterized by the arrestment of growth of the external boundary when the latter coincides with the geometric limit of the system. For the case of an open boundary it is presumed that at this limit ( $r_D$ ) the system suffers no pressure drop. Introduction of this condition into Eq. 15 gives:

$$\bar{b} = C_1 [\exp(-r_D \sqrt{s}) - \exp(r_D - 2r_D) \sqrt{s}] \dots (54)$$

Under the precepts of the pressure case and conversion to hyperbolic functions, Eq. 54 becomes:

$$\bar{b} = \frac{\sinh \sqrt{s} (r_D' - r_D)}{s [\sinh \sqrt{s} (r_D' - 1)]} \dots (55)$$

which is the subsidiary equation appropriate to the pressure case for an open limited system. The Laplace transform of  $e_D$  using Eq. 55, is:

$$\bar{e}_D = \frac{1}{s} + \frac{\cosh \sqrt{s} (r_D' - 1)}{\sqrt{s} [\sinh \sqrt{s} (r_D' - 1)]} \dots (56)$$

The inverse transformation is available from integral tables in the form:

$$e_D = 1 + \frac{1}{(r_D' - 1)} \theta_4 \left[ \frac{1}{2} \left| \frac{i \pi t_D}{(r_D' - 1)^2} \right| \right] \dots (57)$$

and upon expanding the Theta function this becomes:

$$e_D = \frac{r_D'}{r_D' - 1} + \frac{2}{r_D' - 1} \sum_{n=1}^{\infty} \exp \left[ -\frac{\pi^2 n^2 t_D}{(r_D' - 1)^2} \right] \dots (58)$$

which is the dimensionless rate for an open limited system. As before, the Laplace transforms of  $F_D$  is:

$$\bar{F}_D = \frac{\bar{e}_D}{s} = \frac{1}{s^2} + \frac{\cosh \sqrt{s} (r_D' - 1)}{s^2 [\sinh \sqrt{s} (r_D' - 1)]} \dots (59)$$

whose inverse transformation was obtained with the aid of the Faltung convolution theorem as:

$$F_D = \frac{r_D' t_D}{r_D' - 1} + \frac{1}{3} (r_D' - 1) - \frac{2(r_D' - 1)}{\pi^2} \sum_{n=1}^{\infty} \frac{1}{n^2} \exp \left[ -\frac{\pi^2 n^2 t_D}{(r_D' - 1)^2} \right] \dots (60)$$

the dimensionless cumulative fluid influx for an open limited system.<sup>9-11, 13-20</sup>

Under the precepts of the rate case, Eq. 54 becomes:

$$\bar{b} = \frac{\sinh \sqrt{s} (r_D' - r_D)}{s [\sqrt{s} \cosh \sqrt{s} (r_D' - 1) + \sinh \sqrt{s} (r_D' - 1)]} \dots (61)$$

which is the subsidiary equation appropriate to the rate case for a limited system with a fixed pressure at the external boundary. The inverse transformation of Eq. 61 was again obtained by Mellin's inversion theorem, as previously explained. Thus, the pressure-drop distribution is given by:

TABLE 2 — LIMITED SYSTEMS  
Closed External Boundary

Dimensionless Functions				Dimensionless Functions			
Time ( $t_D$ )	Rate ( $e_D$ )	Influx ( $F_D$ )	Pressure Drop ( $p_D$ )	Time ( $t_D$ )	Rate ( $e_D$ )	Influx ( $F_D$ )	Pressure Drop ( $p_D$ )
Dimensionless External Radius $r_D = 2$				Dimensionless External Radius $r_D = 5$			
0.07	3.1324	0.3685	0.2404	1.0	1.5642	2.128	0.5724
0.08	2.9947	0.3992	0.2534	2.0	1.3986	3.596	0.6638
0.09	2.8806	0.4285	0.2654	3.0	1.3216	4.953	0.7133
0.10	2.7839	0.4568	0.2764	4.0	1.2673	6.246	0.7479
0.20	2.2411	0.7040	0.3567	5.0	1.2203	7.490	0.7764
0.30	1.9342	0.9120	0.4120	6.0	1.1766	8.688	0.8024
0.40	1.6358	1.0927	0.4591	7.0	1.1348	9.843	0.8273
0.50	1.4713	1.2503	0.5033	8.0	1.0946	10.958	0.8518
0.60	1.2844	1.3879	0.5467	9.0	1.0558	12.033	0.8761
0.70	1.1212	1.5080	0.5897	10.0	1.0184	13.070	0.9004
0.80	0.9788	1.6128	0.6326	20.0	0.7103	21.621	1.1424
0.90	0.8544	1.7044	0.6755	30.0	0.4954	27.585	1.3843
1.0	0.7459	1.7843	0.7184	40.0	0.3455	31.744	1.6262
2.0	0.1916	2.1921	1.1469	50.0	0.2410	34.646	1.8682
3.0	0.0491	2.2970	1.5755	60.0	0.1680	36.669	2.1101
4.0	0.0127	2.3240	2.0041	70.0	0.1172	38.080	2.3520
5.0	0.0033	2.3309	2.4327	80.0	0.0818	39.064	2.5940
6.0	0.0008	2.3327	2.8612	90.0	0.0570	39.751	2.8359
7.0	0.0002	2.3332	3.2898	100.0	0.0398	40.230	3.0778
8.0	0.0001	2.3333	3.7184	200.0	0.0000	41.333	5.5068
9.0	0.0000	2.3333	4.1469				
10.0	0.0000	2.3333	4.5755				
Dimensionless External Radius $r_D = 3$				Dimensionless External Radius $r_D = 6$			
0.2	2.2616	0.7046	0.3562	2.0	1.3989	3.596	0.6638
0.3	2.0301	0.9180	0.4080	3.0	1.3255	4.954	0.7127
0.4	1.8920	1.1136	0.4464	4.0	1.2807	6.256	0.7449
0.5	1.7972	1.2978	0.4769	5.0	1.2477	7.520	0.7687
0.6	1.7261	1.4739	0.5021	6.0	1.2201	8.753	0.7881
0.7	1.6688	1.6435	0.5236	7.0	1.1951	9.961	0.8051
0.8	1.6199	1.8079	0.5425	8.0	1.1714	11.144	0.8207
0.9	1.5764	1.9677	0.5595	9.0	1.1487	12.304	0.8356
1.0	1.5363	2.1233	0.5750	10.0	1.1265	13.441	0.8501
2.0	1.2114	3.4891	0.7012	20.0	0.9283	23.683	0.9903
3.0	0.9586	4.5692	0.8171	30.0	0.7650	32.123	1.1298
4.0	0.7586	5.4239	0.9325	40.0	0.6304	39.078	1.2693
5.0	0.6004	6.1004	1.0479	50.0	0.5195	44.810	1.4089
6.0	0.4751	6.6356	1.1633	60.0	0.4281	49.534	1.5484
7.0	0.3760	7.0591	1.2787	70.0	0.3528	53.426	1.6879
8.0	0.2975	7.3944	1.3941	80.0	0.2907	56.634	1.8275
9.0	0.2354	7.6598	1.5095	90.0	0.2396	59.277	1.9570
10.0	0.1863	7.8698	1.6249	100.0	0.1974	61.455	2.0665
20.0	0.0180	8.5899	2.7787	200.0	0.0285	70.191	3.5019
30.0	0.0017	8.6593	3.9325	300.0	0.0041	71.453	4.8972
40.0	0.0002	8.6659	5.0864	400.0	0.0006	71.636	6.2926
50.0	0.0000	8.6666	6.2402	500.0	0.0001	71.662	7.6879
60.0	0.0000	8.6667	7.3941	600.0	0.0000	71.666	9.0833
				700.0	0.0000	71.666	10.4786
				800.0	0.0000	71.667	11.8740
Dimensionless External Radius $r_D = 4$				Dimensionless External Radius $r_D = 7$			
0.7	1.6743	1.644	0.5233	3.0	1.3257	4.95	0.7127
0.8	1.6308	1.809	0.5418	4.0	1.2820	6.26	0.7446
0.9	1.5946	1.970	0.5580	5.0	1.2519	7.52	0.7678
1.0	1.5640	2.128	0.5724	6.0	1.2289	8.76	0.7857
2.0	1.3869	3.592	0.6655	7.0	1.2099	9.98	0.8004
3.0	1.2755	4.921	0.7234	8.0	1.1933	11.18	0.8131
4.0	1.1780	6.147	0.7734	9.0	1.1780	12.37	0.8244
5.0	1.0878	7.279	0.8216	10.0	1.1636	13.54	0.8348
6.0	1.0049	8.325	0.8693	20.0	1.0354	24.52	0.9255
7.0	0.9283	9.291	0.9170	30.0	0.9223	34.30	1.0133
8.0	0.8576	10.184	0.9646	40.0	0.8216	43.01	1.1010
9.0	0.7922	11.008	1.0122	50.0	0.7318	50.76	1.1887
10.0	0.7318	11.770	1.0599	60.0	0.6518	57.68	1.2765
20.0	0.3311	16.822	1.5361	70.0	0.5806	63.83	1.3642
30.0	0.1498	19.110	2.0122	80.0	0.5172	69.31	1.4519
40.0	0.0678	20.144	2.4884	90.0	0.4607	74.20	1.5396
50.0	0.0307	20.613	2.9646	100.0	0.4104	78.55	1.6273
60.0	0.0139	20.825	3.4408	200.0	0.1290	102.86	2.5045
70.0	0.0063	20.921	3.9170	300.0	0.0408	110.31	3.3817
80.0	0.0028	20.964	4.3932	400.0	0.0127	112.91	4.2598
90.0	0.0013	20.984	4.8694	500.0	0.0040	115.66	5.1361
100.0	0.0006	20.993	5.3456	600.0	0.0012	113.90	6.0133
200.0	0.0000	21.000	10.1076	700.0	0.0004	113.97	6.8905
				800.0	0.0001	113.99	7.7677
				900.0	0.0000	114.00	8.6449
				1,000.0	0.0000	114.00	9.5221

TABLE 2—LIMITED SYSTEMS (continued)

Dimensionless Functions				Dimensionless Functions			
Time (t <sub>D</sub> )	Rate (r <sub>D</sub> )	Influx (F <sub>D</sub> )	Pressure Drop (p <sub>D</sub> )	Time (t <sub>D</sub> )	Rate (r <sub>D</sub> )	Influx (F <sub>D</sub> )	Pressure Drop (p <sub>D</sub> )
Dimensionless External Radius r <sub>D</sub> = 8				Dimensionless External Radius r <sub>D</sub> = 70			
4.0	1.2821	6.26	0.7446	30.0	1.1030	36.2	0.8977
5.0	1.2523	7.52	0.7678	40.0	1.0892	47.1	0.9106
6.0	1.2302	8.76	0.7854	50.0	1.0796	58.0	0.9199
7.0	1.2128	9.98	0.7996	60.0	1.0724	68.7	0.9270
8.0	1.1983	11.19	0.8115	70.0	1.0664	79.4	0.9329
9.0	1.1859	12.38	0.8216	80.0	1.0611	90.1	0.9378
10.0	1.1747	13.56	0.8306	90.0	1.0562	100.7	0.9423
20.0	1.0860	24.85	0.8971	100.0	1.0516	111.2	0.9465
30.0	1.0078	35.31	0.9561	200.0	1.0088	214.2	0.9881
40.0	0.9354	45.02	1.0148	300.0	0.9681	313.0	1.0229
50.0	0.8681	54.04	1.0735	400.0	0.9291	407.9	1.0604
60.0	0.8056	62.40	1.1322	500.0	0.8916	498.9	1.0979
70.0	0.7477	70.17	1.1910	600.0	0.8557	586.2	1.1354
80.0	0.6939	77.37	1.2497	700.0	0.8212	670.1	1.1729
90.0	0.6440	84.06	1.3084	800.0	0.7881	750.5	1.2104
100.0	0.5976	90.26	1.3671	900.0	0.7563	827.7	1.2479
200.0	0.2832	132.37	1.9542	1,000.0	0.7259	901.8	1.2854
300.0	0.1342	152.34	2.5412	2,000.0	0.4810	1,496.9	1.6604
400.0	0.0637	161.80	3.1283	3,000.0	0.3187	1,891.2	2.0355
500.0	0.0302	166.29	3.7154	4,000.0	0.2111	2,152.4	2.4105
600.0	0.0143	168.41	4.3025	5,000.0	0.1400	2,325.7	2.7856
700.0	0.0068	169.42	4.8896	6,000.0	0.0929	2,440.5	3.1606
800.0	0.0032	169.90	5.4767	7,000.0	0.0616	2,516.7	3.5357
900.0	0.0015	170.13	6.0638	8,000.0	0.0408	2,567.1	3.9107
1,000.0	0.0007	170.24	6.6508	9,000.0	0.0270	2,600.6	4.2858
2,000.0	0.0000	170.33	12.5218	10,000.0	0.0179	2,622.7	4.6608
Dimensionless External Radius r <sub>D</sub> = 9				Dimensionless External Radius r <sub>D</sub> = 30			
5.0	1.2523	7.52	0.7676	80.0	1.0631	90.1	0.9351
6.0	1.2303	8.76	0.7853	90.0	1.0595	100.7	0.9385
7.0	1.2132	9.99	0.7995	100.0	1.0564	111.3	0.9414
8.0	1.1993	11.19	0.8112	200.0	1.0381	215.9	0.9600
9.0	1.1877	12.38	0.8211	300.0	1.0254	319.1	0.9724
10.0	1.1776	13.57	0.8296	400.0	1.0133	421.0	0.9840
20.0	1.1094	24.98	0.8848	500.0	1.0014	521.7	0.9954
30.0	1.0539	35.70	0.9271	600.0	0.9895	621.3	1.0068
40.0	1.0015	46.04	0.9684	700.0	0.9780	719.7	1.0179
50.0	0.9518	55.83	1.0096	800.0	0.9665	816.9	1.0290
60.0	0.9045	65.11	1.0508	900.0	0.9552	913.0	1.0401
70.0	0.8596	73.92	1.0920	1,000.0	0.9439	1,007.9	1.0512
80.0	0.8169	82.30	1.1332	2,000.0	0.8388	1,898.3	1.1623
90.0	0.7763	90.27	1.1745	3,000.0	0.7453	2,689.4	1.2735
100.0	0.7378	97.84	1.2157	4,000.0	0.6622	3,392.4	1.3846
200.0	0.4433	155.64	1.6278	5,000.0	0.5884	4,017.0	1.4957
300.0	0.2663	190.37	2.0398	6,000.0	0.5228	4,572.0	1.6068
400.0	0.1600	211.24	2.4519	7,000.0	0.4646	5,065.2	1.7179
500.0	0.0962	223.79	2.8640	8,000.0	0.4128	5,503.4	1.8290
600.0	0.0578	231.32	3.2761	9,000.0	0.3668	5,892.7	1.9401
700.0	0.0347	235.85	3.6882	10,000.0	0.3259	6,238.6	2.0513
800.0	0.0209	238.57	4.1003	20,000.0	0.1000	8,153.6	3.1624
900.0	0.0125	240.21	4.5124	30,000.0	0.0307	8,739.1	4.2736
1,000.0	0.0075	241.19	4.9245	40,000.0	0.0094	8,919.7	5.3847
2,000.0	0.0000	242.67	9.0455	50,000.0	0.0029	8,975.1	6.4959
Dimensionless External Radius r <sub>D</sub> = 10				Dimensionless External Radius r <sub>D</sub> = 40			
6.0	1.2303	8.76	0.7853	100.0	1.0564	111.0	0.9414
7.0	1.2132	9.99	0.7995	200.0	1.0398	216.0	0.9570
8.0	1.1995	11.19	0.8112	300.0	1.0320	320.0	0.9653
9.0	1.1880	12.38	0.8210	400.0	1.0262	422.0	0.9715
10.0	1.1783	13.57	0.8295	500.0	1.0210	525.0	0.9769
20.0	1.1196	25.02	0.8797	600.0	1.0160	627.0	0.9820
30.0	1.0783	36.01	0.9124	700.0	1.0110	728.0	0.9871
40.0	1.0398	46.60	0.9427	800.0	1.0060	829.0	0.9922
50.0	1.0027	56.81	0.9728	900.0	1.0011	929.0	0.9972
60.0	0.9669	66.66	1.0028	1,000.0	0.9962	1,029.0	1.0019
70.0	0.9325	76.15	1.0329	2,000.0	0.9485	2,001.0	1.0488
80.0	0.8992	85.31	1.0629	3,000.0	0.9031	2,927.0	1.0957
90.0	0.8672	94.14	1.0929	4,000.0	0.8598	3,808.0	1.1425
100.0	0.8362	102.66	1.1229	5,000.0	0.8184	4,647.0	1.1894
200.0	0.5816	172.78	1.4232	6,000.0	0.7794	5,446.0	1.2363
300.0	0.4045	221.56	1.7235	7,000.0	0.7421	6,207.0	1.2832
400.0	0.2813	255.48	2.0238	8,000.0	0.7066	6,931.0	1.3301
500.0	0.1956	279.07	2.3241	9,000.0	0.6727	7,620.0	1.3769
600.0	0.1361	295.49	2.6244	10,000.0	0.6405	8,277.0	1.4238
700.0	0.0947	306.90	2.9247	20,000.0	0.3920	13,339.0	1.8926
800.0	0.0659	314.85	3.2250	30,000.0	0.2400	16,436.0	2.3613
900.0	0.0458	320.37	3.5253	40,000.0	0.1472	18,332.0	2.8301
1,000.0	0.0319	324.22	3.8256	50,000.0	0.0901	19,496.0	3.2988
2,000.0	0.0008	332.77	6.8287	60,000.0	0.0552	20,208.0	3.7676
3,000.0	0.0000	332.99	9.8317	70,000.0	0.0338	20,644.0	4.2363
4,000.0	0.0000	333.00	12.8347	80,000.0	0.0207	20,911.0	4.7051
				90,000.0	0.0127	21,075.0	5.1739
				100,000.0	0.0078	21,175.0	5.6426
				200,000.0	0.0000	21,333.0	10.3302

TABLE 2—LIMITED SYSTEMS (continued)

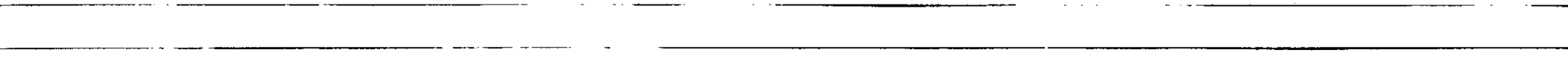
Dimensionless Functions				Dimensionless Functions			
Time ( $t_D$ )	Rate ( $F_D$ )	Inflow ( $F_D$ )	Pressure Drop ( $p_D$ )	Time ( $t_D$ )	Rate ( $F_D$ )	Inflow ( $F_D$ )	Pressure Drop ( $p_D$ )
Dimensionless External Radius $r_D = 50$				Dimensionless External Radius $r_D = 80$			
200.0	1.0399	216.0	0.9570	900.0	1.0188	934.0	0.9779
300.0	1.0325	320.0	0.9641	1,000.0	1.0178	1,036.0	0.9791
400.0	1.0280	423.0	0.9693	2,000.0	1.0108	2,050.0	0.9875
500.0	1.0246	525.0	0.9733	3,000.0	1.0047	3,057.0	0.9944
600.0	1.0217	628.0	0.9765	4,000.0	0.9987	4,059.0	1.0009
700.0	1.0190	730.0	0.9795	5,000.0	0.9927	5,055.0	1.0068
800.0	1.0164	831.0	0.9823	6,000.0	0.9868	6,045.0	1.0127
900.0	1.0139	933.0	0.9854	7,000.0	0.9809	7,028.0	1.0185
1,000.0	1.0113	1,034.0	0.9880	8,000.0	0.9750	8,006.0	1.0244
2,000.0	0.9865	2,033.0	1.0120	9,000.0	0.9692	8,978.0	1.0302
3,000.0	0.9622	3,007.0	1.0360	10,000.0	0.9634	9,945.0	1.0361
4,000.0	0.9383	3,958.0	1.0600	20,000.0	0.9073	19,295.0	1.0947
5,000.0	0.9155	4,884.0	1.0840	30,000.0	0.8545	28,102.0	1.1513
6,000.0	0.8930	5,789.0	1.1080	40,000.0	0.8048	36,396.0	1.2119
7,000.0	0.8710	6,671.0	1.1320	50,000.0	0.7579	44,207.0	1.2705
8,000.0	0.8496	7,531.0	1.1560	60,000.0	0.7138	51,564.0	1.3291
9,000.0	0.8287	8,370.0	1.1800	70,000.0	0.6723	58,493.0	1.3877
10,000.0	0.8083	9,188.0	1.2040	80,000.0	0.6331	65,018.0	1.4463
20,000.0	0.6301	16,344.0	1.4440	90,000.0	0.5963	71,163.0	1.5049
30,000.0	0.4912	21,921.0	1.6840	100,000.0	0.5616	76,950.0	1.5634
40,000.0	0.3828	26,269.0	1.9240	200,000.0	0.3081	119,176.0	2.1494
50,000.0	0.2984	29,658.0	2.1640	300,000.0	0.1697	142,333.0	2.7353
60,000.0	0.2324	32,299.0	2.4040	400,000.0	0.0933	155,096.0	3.3213
70,000.0	0.1818	34,357.0	2.6440	500,000.0	0.0512	162,112.0	3.9072
80,000.0	0.1418	35,967.0	2.8840	600,000.0	0.0281	165,967.0	4.4931
90,000.0	0.1106	37,272.0	3.1240	700,000.0	0.0155	168,084.0	5.0791
100,000.0	0.0862	38,201.0	3.3640	800,000.0	0.0085	169,248.0	5.6650
200,000.0	0.2072	41,378.0	5.7641	900,000.0	0.0047	169,887.0	6.2510
300,000.0	0.0004	41,642.0	8.1641	1,000,000.0	0.0026	170,238.0	6.8369
400,000.0	0.0000	41,664.0	10.5641	2,000,000.0	0.0000	170,666.0	12.6963
500,000.0	0.0000	41,666.0	12.9641				
Dimensionless External Radius $r_D = 60$				Dimensionless External Radius $r_D = 90$			
30.0	1.0326	320.0	0.9641	1,000.0	1.0178	1,036.0	0.9789
40.0	1.0282	423.0	0.9684	2,000.0	1.0119	2,050.0	0.9864
500.0	1.0252	525.0	0.9717	3,000.0	1.0075	3,060.0	0.9914
600.0	1.0228	628.0	0.9743	4,000.0	1.0033	4,065.0	0.9955
700.0	1.0209	730.0	0.9765	5,000.0	0.9991	5,066.0	1.0006
800.0	1.0192	832.0	0.9784	6,000.0	0.9949	6,063.0	1.0047
900.0	1.0176	934.0	0.9801	7,000.0	0.9907	7,056.0	1.0088
1,000.0	1.0160	1,035.0	0.9818	8,000.0	0.9866	8,045.0	1.0129
2,000.0	1.0015	2,044.0	0.9969	9,000.0	0.9824	9,029.0	1.0170
3,000.0	0.9872	3,038.0	1.0117	10,000.0	0.9783	10,010.0	1.0212
4,000.0	0.9732	4,019.0	1.0256	20,000.0	0.9381	19,590.0	1.0523
5,000.0	0.9594	4,985.0	1.0395	30,000.0	0.8995	28,776.0	1.1025
6,000.0	0.9457	5,937.0	1.0533	40,000.0	0.8625	37,585.0	1.1444
7,000.0	0.9323	6,876.0	1.0672	50,000.0	0.8270	46,031.0	1.1858
8,000.0	0.9190	7,802.0	1.0811	60,000.0	0.7930	54,129.0	1.2259
9,000.0	0.9060	8,714.0	1.0950	70,000.0	0.7603	61,895.0	1.2651
10,000.0	0.8931	9,614.0	1.1089	80,000.0	0.7291	69,341.0	1.3092
20,000.0	0.7779	17,935.0	1.2478	90,000.0	0.6991	76,480.0	1.3504
30,000.0	0.6706	25,143.0	1.3867	100,000.0	0.6703	83,326.0	1.3915
40,000.0	0.5811	31,393.0	1.5256	200,000.0	0.4402	138,050.0	1.8331
50,000.0	0.5036	36,808.0	1.6645	300,000.0	0.2890	173,987.0	2.2146
60,000.0	0.4363	41,499.0	1.8034	400,000.0	0.1905	197,575.0	2.6261
70,000.0	0.3780	45,564.0	1.9422	500,000.0	0.1253	213,137.0	3.0376
80,000.0	0.3275	49,086.0	2.0811	600,000.0	0.0824	223,370.0	3.4491
90,000.0	0.2838	52,137.0	2.2200	700,000.0	0.0541	230,097.0	3.8607
100,000.0	0.2458	54,781.0	2.3589	800,000.0	0.0356	234,519.0	4.2722
200,000.0	0.0590	67,879.0	2.7478	900,000.0	0.0234	237,425.0	4.6837
300,000.0	0.0141	71,014.0	3.1367	1,000,000.0	0.0154	239,335.0	5.0952
400,000.0	0.0034	71,764.0	3.5256	2,000,000.0	0.0000	243,000.0	9.7104
500,000.0	0.0008	71,943.0	3.9145				
600,000.0	0.0002	71,986.0	4.3034				
700,000.0	0.0000	71,996.0	4.6923				
800,000.0	0.0000	72,000.0	5.0812				
Dimensionless External Radius $r_D = 70$				Dimensionless External Radius $r_D = 100$			
700.0	1.0213	730.0	0.9753	1,000.0	1.0178	1,036.0	0.9789
800.0	1.0198	832.0	0.9769	2,000.0	1.0123	2,050.0	0.9853
900.0	1.0185	934.0	0.9785	3,000.0	1.0090	3,061.0	0.9894
1,000.0	1.0174	1,036.0	0.9799	4,000.0	1.0058	4,068.0	0.9930
2,000.0	1.0079	2,048.0	0.9906	5,000.0	1.0028	5,073.0	0.9954
3,000.0	0.9989	3,052.0	1.0005	6,000.0	0.9997	6,074.0	1.0000
4,000.0	0.9899	4,046.0	1.0093	7,000.0	0.9967	7,072.0	1.0038
5,000.0	0.9811	5,032.0	1.0180	8,000.0	0.9936	8,067.0	1.0070
6,000.0	0.9723	6,008.0	1.0268	9,000.0	0.9904	9,059.0	1.0098
7,000.0	0.9638	6,976.0	1.0355	10,000.0	0.9874	10,048.0	1.0128
8,000.0	0.9550	7,936.0	1.0443	20,000.0	0.9578	19,775.0	1.0430
9,000.0	0.9465	8,884.0	1.0530	30,000.0	0.9290	29,208.0	1.0720
10,000.0	0.9380	9,829.0	1.0618	40,000.0	0.9010	38,358.0	1.1020
20,000.0	0.8575	18,800.0	1.1492	50,000.0	0.8739	47,232.0	1.1320
30,000.0	0.7838	27,002.0	1.2367	60,000.0	0.8476	55,839.0	1.1620
40,000.0	0.7165	34,498.0	1.3241	70,000.0	0.8221	64,187.0	1.1920
50,000.0	0.6549	41,351.0	1.4116	80,000.0	0.7974	72,283.0	1.2220
60,000.0	0.5987	47,615.0	1.4991	90,000.0	0.7733	80,136.0	1.2520
70,000.0	0.5472	53,341.0	1.5865	100,000.0	0.7501	87,753.0	1.2820
80,000.0	0.5002	58,575.0	1.6740	200,000.0	0.5525	152,377.0	1.5820
90,000.0	0.4572	63,359.0	1.7615	300,000.0	0.4068	199,972.0	1.8820
100,000.0	0.4179	67,732.0	1.8489	400,000.0	0.2995	235,018.0	2.1820
200,000.0	0.1701	95,294.0	2.7236	500,000.0	0.2210	260,815.0	2.4820
300,000.0	0.0692	104,570.0	3.5982	600,000.0	0.1633	279,849.0	2.7820
400,000.0	0.0280	111,168.0	4.4728	700,000.0	0.1203	293,918.0	3.0820
500,000.0	0.0113	113,042.0	5.3473	800,000.0	0.0887	304,287.0	3.3820
600,000.0	0.0045	113,607.0	6.2219	900,000.0	0.0653	311,978.0	3.6820
700,000.0	0.0018	114,118.0	7.0968	1,000,000.0	0.0482	317,558.0	3.9820
800,000.0	0.0007	114,245.0	7.9714	2,000,000.0	0.0000	333,333.0	6.9820
900,000.0	0.0003	114,297.0	8.8460				
1,000,000.0	0.0001	114,318.0	9.7207				
2,000,000.0	0.0000	114,333.0	18.4627				



C

○

○



the unlimited system were computed first over the dimensionless time range 0.001 to 1,000,000. Then tables of the trigonometric relations described by Eqs. 47, 52 and 63 were developed from which the roots  $w$  (with  $n = 6$ ) were obtained. Finally, numerical values of the functions for limited systems were computed over the range of external radii ( $r_D$ ) 2 to 100. The range of dimensionless time ( $t_D$ ) for these functions was chosen to begin with the points of divergence from the unlimited system envelope and to end with steady-state values. These numerical results are included in tabular form to foster practical application of this work.

### NOMENCLATURE

$C_1, C_2$  = arbitrary constants  
 $F$  = cumulative fluid influx  
 $F_D$  = dimensionless cumulative fluid influx  
 $\bar{F}_D$  = Laplace transform of  $F_D$   
 $R_0$  = residue of singularity at origin  
 $R_n$  = residues of singularities at  $z_n$   
 $b$  = dimensionless product of pressure drop and radial distance  
 $\bar{b}$  = Laplace transform of  $b$   
 $c$  = compressibility  
 $e$  = rate of fluid influx or fluid rate  
 $e_D$  = dimensionless rate of fluid influx  
 $\bar{e}_D$  = Laplace transform of  $e_D$   
 $k$  = permeability  
 $k_b$  = horizontal permeability  
 $k_r$  = radial permeability in spherical system  
 $k_v$  = vertical permeability  
 $n$  = element of domain of positive integers  
 $p$  = pressure  
 $p_i$  = initial pressure  
 $p_D$  = dimensionless pressure drop  
 $r$  = radial distance, length of radius vector of sphere  
 $r_e$  = radius of external boundary  
 $r_w$  = radius of internal boundary  
 $r_D$  = dimensionless radial distance  
 $r_D'$  = dimensionless radius of external boundary  
 $s$  = Laplace transform parameter, a complex variable  
 $t$  = time  
 $t_r$  = readjustment time  
 $t_D$  = dimensionless time  
 $t'$  = maximum time  
 $u$  = macroscopic velocity in porous media  
 $w$  = arbitrary real variable  
 $z$  = complex variable  
 $\alpha$  = colatitude angle, spherical coordinates  
 $\gamma$  = abscissa of convergence  
 $\delta$  = arbitrary parameter  
 $\theta$  = longitudinal angle, spherical coordinates  
 $\theta_4$  = Jacobian theta function, also denoted by  $\theta_0$  or  $\theta$

33

$\mu$  = viscosity

$\phi$  = porosity

$\Delta p$  = cumulative pressure drop

### ACKNOWLEDGMENTS

Grateful acknowledgment is made to A. S. Odeh of Mobil Oil Co.'s Field Research Laboratories who reviewed this work, critically checked the mathematics and offered some valuable criticisms. The author wishes to express his appreciation to Deno Ladas of IBM Corp. for his help in programming the analytic functions and to William Chichester for his help in their computation. Thankful acknowledgment is also made to H. L. Smith of the U. S. Corps of Engineers for his practical suggestions and encouragement to publish this paper.

### REFERENCES

- Hurst, W.: "Water Influx into a Reservoir and Its Application to the Equation of Volumetric Balance", *Trans., AIME* (1943) Vol. 151, 57.
- Hurst, W. and van Everdingen, A. F.: "The Application of the Laplace Transformation to Flow Problems in Reservoirs", *Trans., AIME* (1949) Vol. 186, 305.
- Muskat, M.: *The Flow of Homogeneous Fluids Through Porous Media*, J. W. Edwards, Ann Arbor (1946).
- Muskat, M.: *Physical Principles of Oil Production*, McGraw-Hill Book Co., New York, N. Y. (1949).
- Chatas, A. T.: "A Practical Treatment of Nonsteady-State Flow Problems in Reservoir Systems", *Pet. Eng.* (May, June and Aug., 1953) 25.
- Muskat, M.: "The Performance of Bottom-Water Drive Reservoirs", *Trans., AIME* (1947) Vol. 170, 81.
- Hurst, W.: "The Skin Effect and Its Impediment to Fluid Flow into a Wellbore", *Pet. Eng.* (Oct., 1953) Vol. 25, B-6.
- Eisenhart, L. P.: *An Introduction to Differential Geometry with the Use of the Tensor Calculus*, Princeton U. Press, Princeton, N. J. (1947).
- Churchill, R. V.: *Modern Operational Mathematics in Engineering*, McGraw-Hill Book Co., New York, N. Y. (1944).
- Widder, D. V.: *The Laplace Transform*, Princeton U. Press, Princeton, N. J. (1946).
- Carlsaw, H. S. and Jaeger, J. C.: *Operational Methods in Applied Mathematics*, Dover, New York (1963).
- Bush, V.: *Operational Circuit Analysis*, John Wiley & Sons, Inc., New York, N. Y. (1929).
- Abramowitz, M. and Stegun, I. A.: *Handbook of Mathematical Functions*, U. S. Government Printing Office, Washington, D. C. (1964).
- Erdelyi, A. et al.: *Tables of Integral Transforms*, McGraw-Hill Book Co., New York, N. Y. (1954) Vol. I.
- Hildebrand, F. B.: *Advanced Calculus for Engineers*, Prentice-Hall, Inc., Englewood Cliffs, N. J. (1948).
- Murnaghan, F. D.: *Introduction to Applied Mathematics*, Dover, New York (1963).
- Churchill, R. V.: *Introduction to Complex Variables and Applications*, McGraw-Hill Book Co., New York, N. Y. (1948).
- Korn, G. A. and Korn, T. M.: *Mathematical Handbook for Scientists and Engineers*, McGraw-Hill Book Co., New York, N. Y. (1961).
- Erdelyi, A. et al.: *Higher Transcendental Functions*, McGraw-Hill Book Co., New York, N. Y. (1953) Vol. II.
- Carlsaw, H. S. and Jaeger, J. C.: *Conduction of Heat in Solids*, Oxford U. Press, Oxford, England (1959).

# THEORY OF UNSTEADY-STATE INFLUX OF WATER IN LINEAR RESERVOIRS\*

By FRANK G. MILLER†

### Symbols

- $x$  = distance from oil reservoir (measured in aquifer)
- $L$  = length of aquifer
- $b$  = width of aquifer
- $h$  = thickness of aquifer
- $u$  = microscopic velocity
- $\bar{u}$  = average microscopic velocity
- $Q$  = volumetric rate of flow
- $A$  = bulk cross-sectional area transverse to direction of flow
- $q$  = macroscopic velocity
- $\phi$  = fractional porosity
- $s$  = distance
- $\theta$  = time
- $\gamma$  = mass density
- $k$  = absolute permeability
- $\mu$  = viscosity
- $P$  = pressure
- $\Delta P$  = pressure drop
- $\bar{P}$  = mean pressure
- $T$  = absolute temperature
- $\tau$  = unit length
- $\sigma = \frac{k}{\phi \mu c}$
- $\phi$  = a function of  $x$  and  $\theta$

### Dimensionless Quantities (defined in text)

- $\Delta P$  = dimensionless pressure drop
- $t$  = dimensionless time
- $Q_D$  = dimensionless volumetric rate of flow
- $Q_C$  = dimensionless cumulative influx
- $\left(\frac{\Delta P}{Q_D}\right)$  = dimensionless pressure function
- $\left(\frac{Q_C}{\Delta P}\right)$  = dimensionless flow function
- $F(Q)$  = function of  $Q$

## INTRODUCTION

This report describes the theoretical behaviour of linear systems of oil reservoirs and adjoining high-pressure aquifers under conditions of transient flow of fluids. The present work augments that of van Everdingen and Hurst<sup>1</sup> and Chata<sup>2</sup>. They dealt almost entirely with radial flow, giving little attention to linear flow.

The structure or configuration of oil reservoir-aquifer systems is seldom, if ever, known with a high degree of precision. Geological evidence would indicate generally that the geometry is neither strictly radial nor strictly linear. If it is one or the other the equations developed either in the cited work or in this paper would describe the flow behaviour without qualification. Although the true performance of

systems of mixed geometry can usually be estimated better with ideal radial-flow equations than with ideal linear-flow equations, there are many instances when the latter are the more appropriate. Of further importance, the linear equations would be expected to yield the more conservative estimates of oil recover.

Van Everdingen and Hurst, with regard to linear systems, indicate briefly a method of solving problems pertaining to infinite aquifers. They do not treat linear aquifers of finite length. Chata's work on linear systems also relates only to aquifers of infinite length. He offers solutions to four problems which differ from one another by the boundary conditions at the outflow end of the aquifer adjacent to the oil reservoir: constant pressure, constant volumetric rate of flow, pressure an arbitrary function of time, and volumetric rate of flow an arbitrary function of time. In all four the pressure initially is uniformly high throughout the aquifer. No numerical examples are presented.

An excellent review of steady and unsteady-state flow in reservoirs has been published recently.<sup>3</sup> It summarizes the status of knowledge on the subject and provides an extensive bibliography. This review includes unsteady-state compressible-liquid flow. The treatment does not go beyond that given by the foregoing investigators, however.

In the present study the concept of unsteady-state fluid flow in porous media is discussed. Problems on the unsteady-state flow of water in linear aquifers of both finite and infinite length are solved. The pressure distribution within finite and infinite aquifers is determined as a function of time for conditions of a constant pressure or a constant volumetric rate of flow at the outflow end, which is represented by the original plane of contact of the water in the aquifer and the oil in the oil reservoir. The relationship at this terminal plane between volumetric rate of flow and time is determined for the constant and variable pressure cases. The relationship between pressure and time is determined for the constant and variable rate cases. For convenience in application, results are plotted in dimensionless form where practicable. Numerical examples are offered.

The present work is intended to fill a need in petroleum literature for further data on the theoretical flow behaviour of linear systems of oil reservoirs and adjoining high-pressure aquifers.

\* MS received 21 February 1962. † Dept of Petroleum Engineering, Stanford University, Stanford, California.



is indicated by the arrow tangent to the path of flow. Microscopic velocities are true velocities. They apply to all points within the fluid occupying the pore space. Their values at arbitrarily selected points cannot be



FIG 3

PATH OF A FLUID PARTICLE IN A MACROSCOPICALLY-LINEAR FLOW SYSTEM

When particle is at X its microscopic velocity is  $u_x$

calculated, however, without mathematical definition of the geometry of the pore channels. Even if such definition could be developed, it would probably be so complicated as to make calculation of the microscopic velocity impractical.

Macroscopic velocities, in contrast to microscopic velocities, are not true velocities. They are of great practical importance, however, and can be calculated without knowledge of pore-channel geometry. Macroscopic velocity is defined as the volumetric rate of flow per unit of bulk area transverse to the macroscopic direction of flow and is referred to a point in the system. The macroscopic direction of flow is the statistical average direction of movement of the fluid particles in the neighbourhood of the point in question.

Referring again to Fig 2, the total bulk cross-sectional area perpendicular to the plane of the paper would be uniform in the direction of the axis because the flow is specified to be macroscopically linear. Therefore, in the sense of macroscopic flow behaviour, all sections transverse to the X axis are equipotential surfaces. If the flow is from left to right as shown and if  $Q$  is the volumetric rate at  $x$ , then by definition  $Q/A$  is the macroscopic velocity  $q$  at this section. This velocity would have the same magnitude and direction at all points of the transverse area. The direction would be parallel to and in the positive direction of the X axis. Generally, in non-linear systems the macroscopic velocity is not the same at all points of equipotential surfaces. It is defined more precisely therefore as  $Q/A$ .

In accordance with the described concept of macroscopic flow, the solid matrix of the porous medium and the fluid occupying the pore channels are envisioned together as a composite conductor of fluids, the rate of flow being proportional at any point to the gradient in the flow potential. This is the concept underlying Darcy's law.

Macroscopic and microscopic velocities may be related. The microscopic velocity  $u_x$  (Fig 1) would have components  $u_x$ ,  $u_y$ , and  $u_z$  in the directions of

the co-ordinate axes. If the section at  $x$  is a statistically average section the area presented to flow would be  $A\phi$ . As the net flow is in the positive X direction only, the mean value of  $u_x$ , designated  $\bar{u}_x$ , would be equal to  $u_x$  itself at all fluid-occupied points.

No net flow normal to the X axis means also that  $\bar{u}_y$  and  $\bar{u}_z$  would each be zero. All components of  $u_x$  in the negative directions of the Y and Z axes would cancel respectively all components in the positive directions of these axes. Thus the volumetric rate of flow  $Q$ , at  $x$ , would be  $A\phi\bar{u}_x$ . From the definition of macroscopic velocity the volumetric rate of flow at  $x$  is equivalent to  $q_x A$ . Hence,

$$q = \bar{u}\phi \quad \dots \quad (1)$$

in which the subscript  $x$  has been dropped.

*Distinction of States of Fluid Motion*

A moving single-phase fluid would be in a state of steady motion if its properties and the forces acting on it at any given point in the flow system are independent of time. Otherwise it would be in a state of unsteady motion.

Considering streamline motion as is the case in Darcy-law flow, the fluid-particle velocity  $u$ , would be a function of the distance along the path of flow  $s$  and time  $\theta$ . A small change in  $u$ , may be expressed therefore by the equation

$$du = \left(\frac{\partial u}{\partial s}\right)_\theta ds + \left(\frac{\partial u}{\partial \theta}\right)_s d\theta$$

in which the subscript of  $u$  has been dropped. Dividing through by  $d\theta$  and noting that  $ds/d\theta$  and  $u$  are equivalent yields the following expression for the total acceleration  $du/d\theta$  of the fluid particle

$$\frac{du}{d\theta} = u \left(\frac{\partial u}{\partial s}\right)_\theta + \left(\frac{\partial u}{\partial \theta}\right)_s \quad \dots \quad (3)$$

The first term on the right is the convectational acceleration. It pertains to the rate of change of velocity with distance at a particular instant. The second term on the right is the local acceleration. It pertains to the rate of change of velocity with time at a particular place. The sum of these two terms is the total acceleration at a particular instant and place.

Fundamentally, the flow is steady if the local acceleration is zero and unsteady if the local acceleration is not zero. The convectational acceleration may be zero or finite for either state of flow.

Considering the macroscopic point of view, mass velocity may be defined as macroscopic velocity times fluid density,  $\rho q$ , or as mass per unit area per unit time referred to a point. Thus mass rate is  $A\rho q$  in a rectilinear flow system. It would be a function of  $x$ , and  $\theta$  and could be treated in the same manner as  $u$  in equation (3). The velocity indicated by  $dx/d\theta$  would

is from right to left in all problems investigated. The same values are assigned to the constants pertaining to the aquifer sand and water in all numerical examples presented here and in subsequent sections. These values are  $k = 500$  mD,  $\phi = 0.200$ ,  $\mu = 0.300$  cP, and  $c = 3.60 \times 10^{-6}$  (vol/vol)/psi.

In the mathematical analyses the coefficient  $\frac{k}{\phi\mu c}$  (equation (9)) is for convenience set equal to the single factor  $a$ .

**Constant-rate Case—Infinite Aquifer**

This problem may be stated

$$\frac{\partial P}{\partial t} = a \frac{\partial^2 P}{\partial x^2} \dots \dots \dots (10)$$

$$\theta = 0: \left. \begin{array}{l} P = P_f \quad ; \quad x \geq 0 \\ \frac{\partial P}{\partial x} = \frac{Q\mu}{bhk} \quad ; \quad x = 0 \\ \lim_{x \rightarrow \infty} P(x, \theta) = P_f \quad ; \quad x \rightarrow \infty \end{array} \right\} (11)$$

Equation (10) describes the flow at any point in the aquifer. Relations (11) express the initial and boundary conditions. Volumetric rate of flow  $Q$  in the present instance is a constant.

Setting  $P = P_f - \psi(x, \theta)$  and then expressing the statement of the problem in terms of  $\psi$  instead of  $P$  causes it to take the form of a heat-conduction problem which has been solved with the Laplace-transform method to determine temperature as a function of distance and time.<sup>4</sup> The result applied to the present fluid-flow problem states pressure as a function of distance and time:

$$P = P_f - \frac{Q\mu}{bhk} \left[ 2\sqrt{\frac{a\theta}{\pi}} \exp\left(-\frac{x^2}{4a\theta}\right) - x \operatorname{erfc}\left(\frac{x}{2\sqrt{a\theta}}\right) \right] (12)$$

in which  $\exp$  symbolizes exponential and  $\operatorname{erfc}$  complementary error function; thus,

$$\left. \begin{array}{l} \exp y = e^y \\ \operatorname{erfc} y = 1 - \operatorname{erf} y \\ \operatorname{erf} y = \frac{2}{\sqrt{\pi}} \int_0^y e^{-y^2} dy \end{array} \right\} (13)$$

where  $\operatorname{erf}$  symbolizes error function.<sup>4</sup> Equation (12) is the pressure-distribution equation sought. Data for plotting Fig 3 were obtained with it by setting the initial pressure  $P_f$  equal to 4200 psia, and the constant water-influx rate,  $Q/A$ , equal to  $1.00 \times 10^{-2}$  (bd)/sq ft. The equation then was solved for three different values of  $\theta$ : 1, 20, and 50 years. Numerical values of the complementary error function were obtained from tables.<sup>4</sup>

**Constant-rate Case—Finite Aquifer**

The initial and boundary conditions for this problem may be stated

$$\theta = 0: \left. \begin{array}{l} P = P_f \quad ; \quad x \geq 0 \\ \frac{\partial P}{\partial x} = \frac{Q\mu}{bhk} \quad ; \quad x = 0 \\ \frac{\partial P}{\partial x} = 0 \quad ; \quad x = L \end{array} \right\} (14)$$

The solution may be developed by the separation-of-variables method or by the Laplace-transform method.<sup>4</sup> Utilizing the first of these a new variable  $\psi(x, \theta)$  is introduced such that

$$P = \psi - \frac{Q\mu}{bhkL} \left[ \frac{(L-x)^2}{2} + a\theta \right] (15)$$

In terms of  $\psi$  the differential equation is the same as equation (10) except  $P$  is replaced with  $\psi$ . The initial and boundary conditions are

$$\theta = 0: \left. \begin{array}{l} \psi = P_f + \frac{Q\mu}{bhkL} \frac{(L-x)^2}{2} \quad ; \quad x \geq 0 \\ \frac{\partial \psi}{\partial x} = 0 \quad ; \quad x = 0 \\ \frac{\partial \psi}{\partial x} = 0 \quad ; \quad x = L \end{array} \right\} (16)$$

After the solution developed in terms of  $\psi$  is transformed back into terms of  $P$ , through equation (15), it becomes the desired pressure-distribution equation:

$$P = P_f - \frac{Q\mu}{bhk} \left[ \frac{(L-x)^2}{2L} - \frac{L}{6} + \frac{a\theta}{L} \right] + \frac{2Q\mu L}{bhk\pi^2} \sum_{n=1}^{\infty} \left( \frac{1}{n^2} \right) \exp\left(-\frac{n^2\pi^2 a\theta}{L^2}\right) \cos \frac{n\pi x}{L} (17)$$

The pressure distribution curves of Fig 4 were plotted using equation (17) and the same numerical values for the initial pressure and constant water-influx rate as were used in Fig 3. In contrast to Fig 3 the curves pertain to times of 0.5, 1.0, 2.5, and 5.0 years, respectively. The length of the aquifer is specified as 10 miles.

**Constant-pressure Case—Infinite Aquifer**

The initial and boundary conditions for this problem may be stated

$$\theta = 0: \left. \begin{array}{l} P = P_f \quad ; \quad x \geq 0 \\ P = P_c = \text{constant} \quad ; \quad x = 0 \\ \lim_{x \rightarrow \infty} P = P_f \quad ; \quad x = \infty \end{array} \right\} (18)$$

If a new variable  $\psi(x, \theta)$  is introduced such that

$$P = P_c + (P_f - P_c)\psi (19)$$

the statement of the problem in terms of  $\psi$  takes the form of a heat-conduction problem that has been

MILLER: THEORY OF UNSTEADY-STATE INFLUX OF

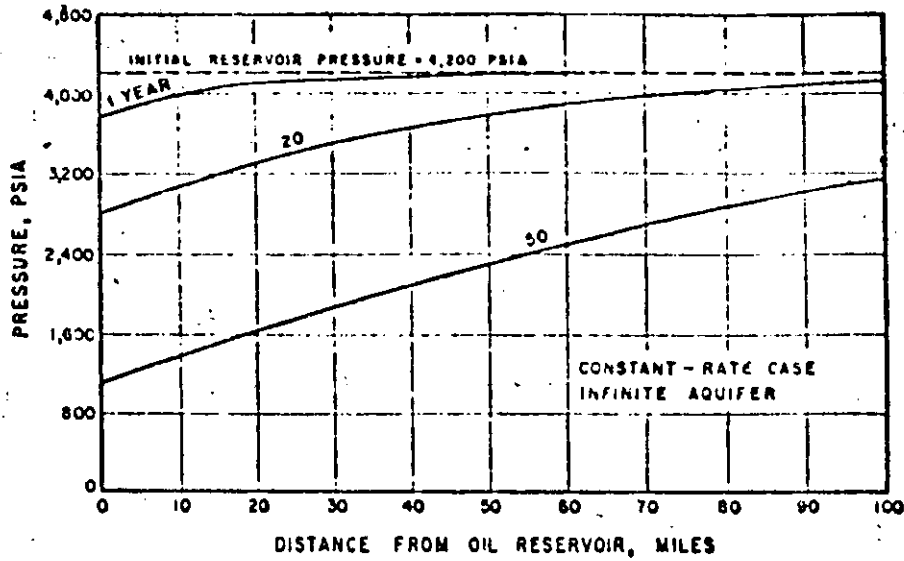


Fig 3

PRESSURE DISTRIBUTION IN THE AQUIFER AT VARIOUS TIMES FOR A CONSTANT VOLUMETRIC RATE OF WATER INFLUX AT BOUNDARY OF OIL RESERVOIR AND AN INFINITE AQUIFER

Permeability: 500 mD Porosity: 0.200 Viscosity of water: 0.300 cP  
 Compressibility of water:  $3.60 \times 10^{-6}$  (vol/vol)/psi  
 Influx rate:  $1.00 \times 10^{-8}$  (bd)/sq ft of cross-section at boundary of oil reservoir

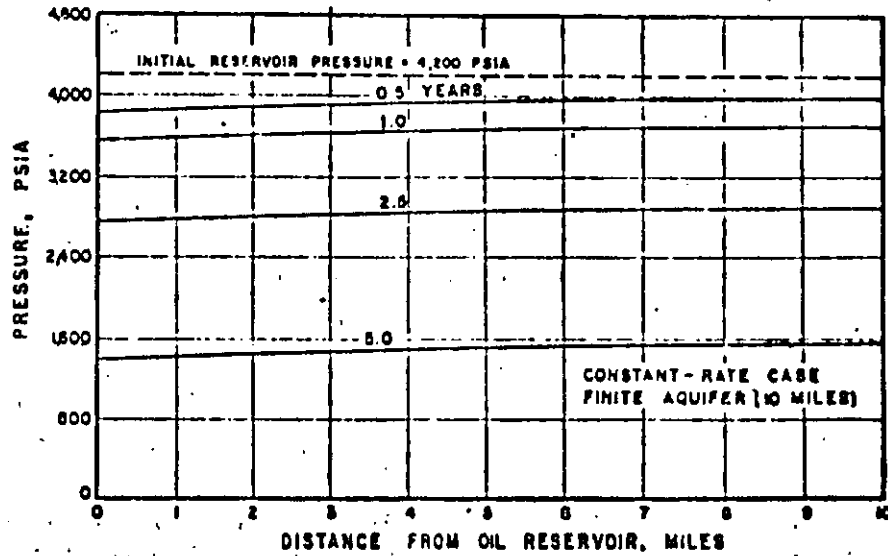


Fig 4

PRESSURE DISTRIBUTION IN THE AQUIFER AT VARIOUS TIMES FOR A CONSTANT VOLUMETRIC RATE OF WATER INFLUX AT BOUNDARY OF OIL RESERVOIR AND AN AQUIFER 10.0 MILES LONG

Permeability: 500 mD Porosity: 0.200 Viscosity of water: 0.300 cP  
 Compressibility of water:  $3.60 \times 10^{-6}$  (vol/vol)/psi  
 Influx rate:  $1.00 \times 10^{-8}$  (bd)/sq ft of cross-section at boundary of oil reservoir

solved through application of Fourier integrals to determine temperature as a function of time and distance.<sup>7</sup> In terms of the present fluid-flow problem and the original variables, the pressure-distribution equation would be

$$P = P_e + (P_f - P_e) \operatorname{erf} \frac{x}{2\sqrt{a\theta}} \quad (20)$$

Fig 5 was plotted using the same numerical values for  $P_f$  and  $a$  as in the foregoing cases. The constant pressure at  $x = 0$  was specified as 1050 psia. The curves represent distributions for  $\theta = 1, 10,$  and 50 years, respectively.

original variables, the pressure-distribution equation would be

$$P = P_e + (P_f - P_e) \frac{4}{\pi} \sum_{n=1}^{\infty} \left( \frac{1}{2n-1} \right) \exp \left[ -\frac{(2n-1)^2 \pi^2 a \theta}{4L^2} \right] \sin \frac{(2n-1)\pi x}{L} \quad (22)$$

Fig 6 was plotted using the same numerical values for  $P_f, P_e,$  and  $a$  as were used in plotting Fig 5. The length of the aquifer,  $L,$  was specified to be 10.0 miles. The curves represent values of  $\theta$  of 1, 3, 6, and 12 months respectively.

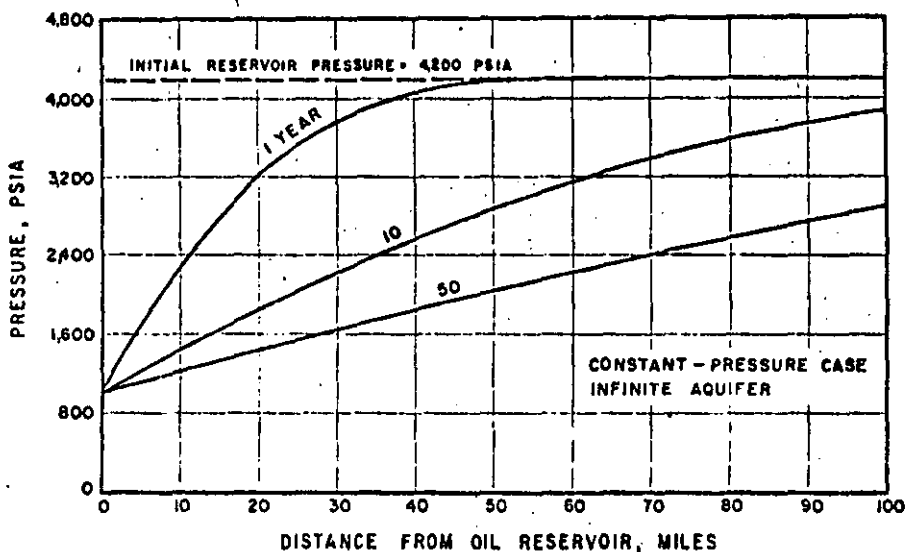


Fig 5

PRESSURE DISTRIBUTION IN THE AQUIFER AT VARIOUS TIMES FOR A CONSTANT PRESSURE AT BOUNDARY OF OIL RESERVOIR AND AN INFINITE AQUIFER

Permeability: 500 md    Porosity: 0.200    Viscosity of water: 0.300 cP  
 Compressibility of water:  $3.60 \times 10^{-6}$  (vol./vol./psi)  
 Constant pressure: 1050 psi at boundary of oil reservoir

Constant-pressure Case—Finite Aquifer

The initial and boundary conditions of the problem may be

$$\begin{aligned} 0 = 0: & \quad P = P_f & ; & \quad x \geq 0 \\ & \quad \left\{ \begin{array}{l} P = P_e = \text{constant} \\ \frac{\partial P}{\partial x} = 0 \end{array} \right. & ; & \quad x = 0 \\ 0 > 0: & & & \quad x = L \end{aligned} \quad (21)$$

If the variable  $\psi$  as defined by equation (10) is introduced, the statement of the problem when expressed in terms of  $\psi$  takes the form of a heat-conduction problem which has been solved with the separation-of-variables method to determine the relationship of temperature, distance, and time.<sup>7</sup> Expressed in terms of the present fluid-flow problem and the

DIMENSIONLESS PRESSURE AND FLOW FUNCTIONS

Definitions

The properties of the aquifer sand and water symbolized by  $k, \phi, \mu,$  and  $c$  change from system to system. A very great deal of graphing would be necessary to show their effects individually on unsteady state flow behaviour. This difficulty, plus that which would be brought about by showing in addition the effect of changes in boundary conditions and time, have led to the adoption of dimensionless groups of variables for graphing purposes.<sup>3</sup>

In the present work the groups used are the same as those of the cited reference:



- Dimensionless pressure differential,  $\Delta P = \frac{P_i - P_e}{P_i}$
- Dimensionless time,  $t = \frac{a^2}{x_e^2}$
- Dimensionless volumetric rate of flow,  $Q_D = \frac{Q_e}{hkP_i}$
- Dimensionless cumulative influx,  $Q_e = \int_0^t Q_D dt$
- Dimensionless pressure function,  $\Delta P/Q_D$
- Dimensionless flow function,  $Q_e/\Delta P$

time zero and  $P_i$  at times greater than zero. If the water influx rate  $Q$  is fixed,  $P_e$  must decrease with time. In the constant-rate cases  $\Delta P$  is considered therefore as a dimensionless cumulative drop in pressure and its determination is of primary concern. If  $P_e$  is a constant for time  $0 > 0$ ,  $\Delta P$  would also be fixed. The influx rate would decrease continuously. Hence, in the constant-pressure cases the cumulative influx is the element to be determined.

The dimensionless ratio  $\Delta P$  is not to be misconstrued as pertaining in any way to a pressure differential over a length of porous medium. Instead, it is to be recognized as pertaining to the time rate of change of the difference between initial and final pressures at a particular place, namely, at  $x = 0$ .

The constant-rate-case curves of Fig 7 show

The quantity  $x_e$  in the expression for dimensionless time  $t$  represents unit length. It is introduced merely to make the expression dimensionless.

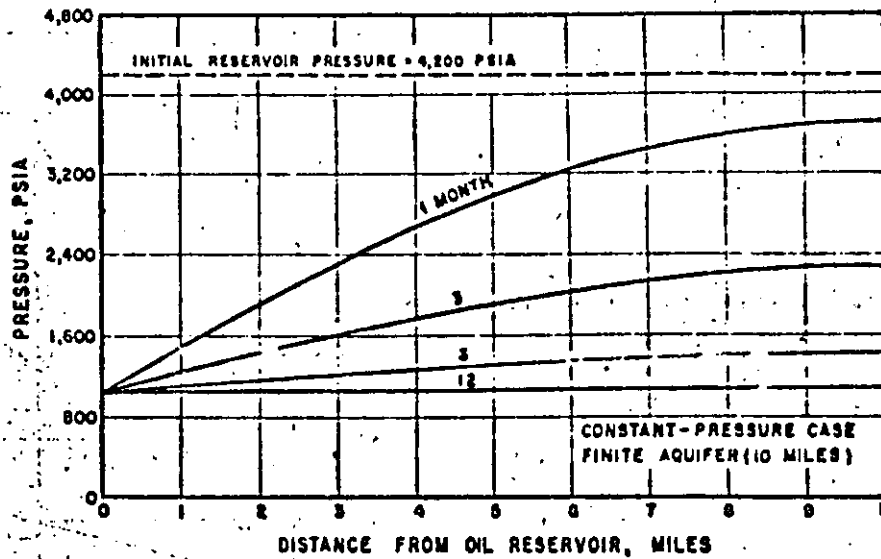


Fig 6  
 PRESSURE DISTRIBUTION IN THE AQUIFER AT VARIOUS TIMES FOR A CONSTANT PRESSURE AT BOUNDARY OF OIL RESERVOIR AND AN AQUIFER 10.0 MILES LONG  
 Permeability: 500 mD Porosity: 0.200 Viscosity of water: 0.300 cP  
 Compressibility of water:  $3.60 \times 10^{-4}$  (vol/vol)/psi

Relationships with Dimensionless Time

Graphical Representation. Considering the foregoing constant-rate cases, practical considerations indicate that desired information on oil-reservoir performance could be gained if a relationship is established between volumetric rate of influx of water, oil-reservoir pressure, time, and length of aquifer. A relationship of this kind based on the above-defined dimensionless groups and applicable to all constant-rate-case linear systems would be of major importance in simplifying their analysis. A similar relationship applicable to all constant-pressure-case linear systems would be of equal importance.

All the curves of Fig 7 refer in their entirety to conditions at the water-influx boundary ( $x = 0$ , Fig 1). The fluid pressure at this boundary is  $P_e$  at

dimensionless cumulative pressure drop per unit dimensionless volumetric rate,  $\Delta P/Q_D$ , plotted on log-log graph paper, as a function of dimensionless time  $t$  for aquifers of different length. It is a simple matter to estimate for any particular system the reduction in oil-reservoir pressure corresponding to a given fixed rate of oil production and a given time of operation, assuming, of course, that the time is short enough for the calculated reduction to be less than the initial pressure minus the pre-assigned final pressure.

The maximum cumulative influx of water or cumulative oil production (assuming enough oil is available for displacement) is limited by the minimum value specified for  $P_e$ . The bubble-point pressure of the liquid reservoir oil at reservoir temperature would probably be selected as this minimum. If the minimum is used in calculating  $\Delta P/Q_D$  and the result

entered on Fig 7, the corresponding dimensionless time  $t$  may be read off directly. The product of this time and the dimensionless flow rate is the maximum cumulative influx.

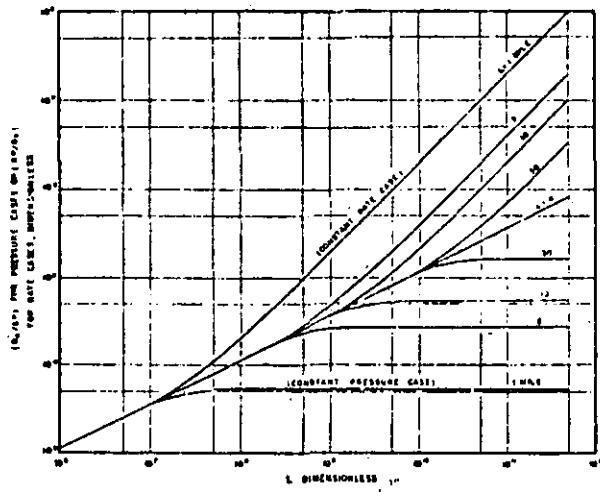


FIG 7

VARIATION OF PRESSURE FUNCTION AND FLOW FUNCTION WITH DIMENSIONLESS TIME FOR AQUIFERS OF DIFFERENT LENGTH

Evidently the slopes of the constant-rate curves relating to finite aquifers become and remain equal to unity when  $t$  is large enough. Under these conditions  $\frac{d(\Delta P)}{dt} = \text{const.}$ , or  $\frac{d(Q_c)}{dt} = \text{const.}$ . As  $P_f$  is fixed, this leads to the foregoing obvious result, namely, that  $Q_c$  attains its maximum magnitude when  $P_c$  attains its minimum.

The constant-pressure-case curves of Fig 7 show dimensionless cumulative influx of water per unit dimensionless pressure drop,  $Q_c/\Delta P$ , plotted as a function of dimensionless time  $t$  for aquifers of different length. For any particular system these curves may be used to estimate the cumulative influx corresponding to a fixed pre-assigned pressure maintained at the water-influx boundary over a given period of time.

All the constant-pressure-case curves except the one for which  $L = \infty$  eventually become and remain horizontal. When they are horizontal  $\frac{d(Q_c)}{dt} = 0$  or  $Q_b = 0$ . When  $Q_b = 0$  the fluid pressure must be the same at all points of the aquifer and equal to fixed pressure  $P_f$  at  $x = 0$ . Thus the minimum value of  $t$  required for the maximum cumulative influx is the value of  $t$  at which the curve becomes horizontal.

The curve representing  $L = \infty$  applies to both the constant-rate and constant-pressure families of curves. Its equation, as well as the equations of the other curves of both families, are derived in the next part of this paper.

As indicated by the figure, aquifers of finite length

behave the same as aquifers of infinite length during the early stages of water influx regardless of whether the pressure or the rate is constant at  $x = 0$ . If the aquifer is 10.0 miles long, for example, it will behave the same as an infinite aquifer, for either type of boundary condition, until dimensionless time  $t$  exceeds about  $1.00 \times 10^9$ .

Fig 8 shows the constant-rate-case family of curves of Fig 7 plotted on ordinary arithmetic graph paper. Fig 9 shows the constant-pressure-case curves plotted similarly. It also includes curves for  $L = 20.0, 50.0, 80.0,$  and  $120$  miles.

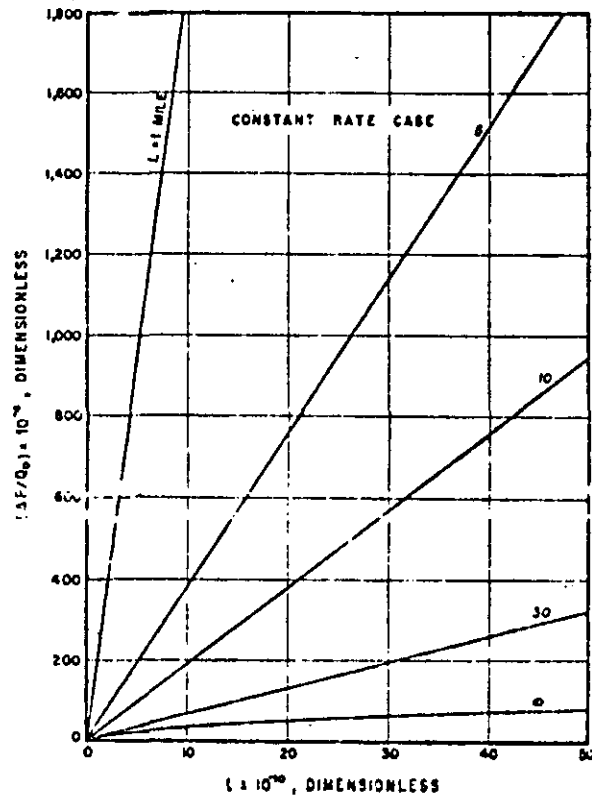


FIG 8

VARIATION OF PRESSURE FUNCTION WITH DIMENSIONLESS TIME FOR AQUIFERS OF DIFFERENT LENGTH—CONSTANT-RATE CASE

*Equations of Constant-rate Cases.* When  $P_c$  is substituted for  $P$  and zero for  $x$ , equation (12) pertaining to infinite aquifers takes the form

$$P_c = P_f - \frac{Q_c \mu}{bhk} \left( 2\sqrt{\frac{at}{\pi}} \right) \quad (23)$$

In terms of the dimensionless pressure function and dimensionless time this may be written

$$\frac{\Delta P}{Q_b} = \frac{2x_c}{b} \sqrt{\frac{t}{\pi}} \quad (24)$$

Equation (24) is the equation of the curve representing  $L = \infty$  on Figs 7 and 8;  $x_c$  and  $b$  are each unity in this equation and in subsequent equations.

In the constant-rate cases  $Q_b = Q_c/t$ . If this substitution is made for  $Q_b$ , equation (24) becomes

$$\frac{\Delta P}{Q_c} = \frac{2x_c}{b\sqrt{\pi a}} \quad (25)$$

When  $P_z$  is substituted for  $P$  and zero for  $x$ , equation (17) pertaining to finite aquifers takes the form

$$P_z = P_f - \frac{Q_c}{bhk} \left( \frac{L}{3} + \frac{a^2}{L} \right) + \frac{2Q_c L}{bhk} \sum_{n=1}^{\infty} \frac{1}{n^2} \exp \left( -\frac{n^2 \pi^2 a^2 t}{L^2} \right) \quad (26)$$

In terms of the dimensionless pressure function and dimensionless time this may be written

$$\frac{\Delta P}{Q_c} = \frac{1}{b} \left( \frac{L}{3} + \frac{x_c^2}{L} \right) - \frac{2L}{\pi^2 b} \sum_{n=1}^{\infty} \left( \frac{1}{n^2} \right) \exp \left( -\frac{n^2 \pi^2 x_c^2 t}{L^2} \right) \quad (27)$$

or

$$\frac{\Delta P}{Q_c} = F(t) \quad (28)$$

which is the equation of the constant-rate-case curves in Figs 7 and 8 for finite aquifers. Equation (28) in terms of  $Q_c$  may be written

$$\frac{\Delta P}{Q_c} = \frac{F(t)}{t} \quad (29)$$

**Equations of Constant-pressure Cases.** Equations expressing the relationship of the dimensionless flow function and dimensionless time are necessary in order to plot the constant-pressure-case curves of Figs 7 and 9. Derivation of such equations begins with differentiation of the pressure-distribution equation to determine  $\left( \frac{\partial P}{\partial x} \right)_{x=0}$  for substitution in Darcy's law.

Differentiating equation (20) with respect to  $x$  and then setting  $x$  equal to zero gives for infinite aquifers:

$$\left( \frac{\partial P}{\partial x} \right)_{x=0} = \frac{P_f - P_z}{\sqrt{\pi a t}} \quad (30)$$

According to Darcy's law the left-hand member of equation (30) is equal to  $\left( \frac{Q_c}{bh} \right)$ . Hence,

$$\frac{Q_c}{bh} = \frac{k(P_f - P_z)}{\mu \sqrt{\pi a t}} \quad (31)$$

or in terms of the dimensionless quantities  $Q_b$ ,  $\Delta P$ , and  $t$

$$Q_b = \frac{b \cdot \Delta P}{x_c \sqrt{\pi a}} \quad (32)$$

Integrating over dimensionless time  $t$ , this becomes a relationship between the dimensionless flow function and dimensionless time,

$$\frac{Q_c}{\Delta P} = \frac{2b}{x_c} \sqrt{\frac{t}{\pi}} \quad (33)$$

Equation (33) is the equation of the curve representing  $L = \infty$  on Figs 7 and 9. As  $b$  and  $x_c$  are each unity, the right-hand member is the same numerically

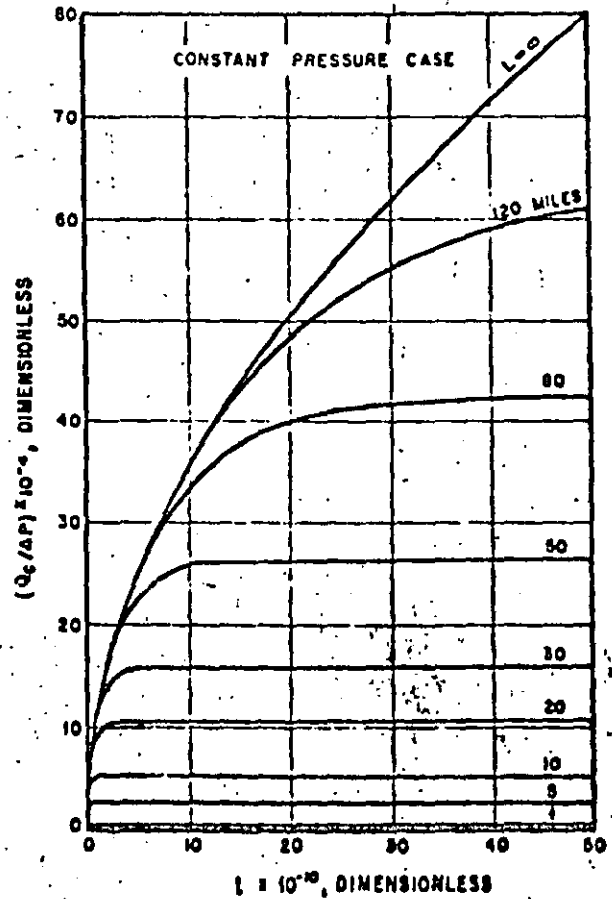


FIG 9

VARIATION OF FLOW FUNCTION WITH DIMENSIONLESS TIME FOR AQUIFERS OF DIFFERENT LENGTH—CONSTANT PRESSURE CASE

as the right-hand member of equation (24). For this reason the  $L = \infty$  curve of Fig 7 applies to both the constant-rate and constant-pressure cases.

Transformation of equation (33) back to the original variables gives the cumulative influx per unit of bulk area transverse to the direction of flow at  $x = 0$ :

$$\left( \frac{1}{bh} \right) \int_0^t Q_c dt = 2\phi k(P_f - P_z) \sqrt{\frac{a t}{\pi}} \quad (34)$$

Differentiating equation (22) with respect to  $x$  and then setting  $x$  equal to zero gives

$$\left( \frac{\partial P}{\partial x} \right)_{x=0} = \frac{2(P_f - P_z)}{L} \sum_{n=1}^{\infty} \exp \left( -\frac{n^2 \pi^2 a^2 t}{L^2} \right) \quad (35)$$

Considering Darcy's law this may be written

$$\left(\frac{Q}{bh}\right) = \frac{2k(P_L - P_s)}{\mu L} \sum_{n=1,3,5}^{\infty} \exp\left(-\frac{n^2\pi^2 a_0}{4L^2}\right) \quad (36)$$

or in terms of  $Q_D$ ,  $\Delta P$ , and  $t$ ,

$$\left(\frac{Q_D}{\Delta P}\right) = \frac{2b}{L} \sum_{n=1,3,5}^{\infty} \exp\left(-\frac{n^2\pi^2 x_c^2 t}{4L^2}\right) \quad (37)$$

Integrating term by term, over dimensionless time  $t$  results in

$$\int_0^t Q_D dt = \frac{8bL \cdot \Delta P}{\pi^2 x_c^2} \left[ \sum_{n=1,3,5}^{\infty} \left(\frac{1}{n^2}\right) - \sum_{n=1,3,5}^{\infty} \left(\frac{1}{n^2}\right) \exp\left(-\frac{n^2\pi^2 x_c^2 t}{4L^2}\right) \right] \quad (38)$$

The first summation within the brackets on the right

is equivalent<sup>1</sup> to  $\frac{\pi^2}{8}$  and the left-hand member is equivalent to  $Q_c$ . Therefore, in terms of the dimensionless flow function, equation (38) may be written

$$\left(\frac{Q_c}{\Delta P}\right) \frac{bL}{x_c^2} \left[ 1 - \frac{8}{\pi^2} \sum_{n=1,3,5}^{\infty} \left(\frac{1}{n^2}\right) \exp\left(-\frac{n^2\pi^2 x_c^2 t}{4L^2}\right) \right] \quad (39)$$

Equation (39) is the equation of the constant-pressure-case curves of Figs 7 and 9 relating to finite aquifers. Transformation of this equation back to the original variables gives the cumulative influx per unit of bulk area transverse to the direction of flow at  $x = 0$ :

$$\frac{1}{bh} \int_0^t Q d\theta = \phi c L (P_f - P_s) \left[ 1 - \frac{8}{\pi^2} \sum_{n=1,3,5}^{\infty} \left(\frac{1}{n^2}\right) \exp\left(-\frac{n^2\pi^2 a_0}{4L^2}\right) \right] \quad (40)$$

**Applications**

Oil-reservoir performance curves are shown in Figs 10-13. They could be developed through application of Figs 7-9 or through direct substitution in the foregoing equations.

Equation (23) is the equation of the pressure-decline curves of Fig 10:  $P_f$  is 4200 psia, and the constant values of  $\left(\frac{Q}{bh}\right)$  are  $0.500 \times 10^{-2}$ ,  $0.750 \times 10^{-2}$ , and  $1.00 \times 10^{-2}$  (bbl)/ft<sup>2</sup>. The cumulative-influx curves were developed by plotting  $\left(\frac{Q_D}{bh}\right)$  expressed in (bbl/ft<sup>2</sup>) against  $\theta$  expressed in years. The maximum-influx rate has been chosen arbitrarily to correspond to  $P_s = 0$ .

Equation (26) is the equation of the pressure-decline curves of Fig 11. The initial pressure, final pressure, and constant rates are the same as those used in Fig 10, and the cumulative-influx curves were plotted in the same manner.

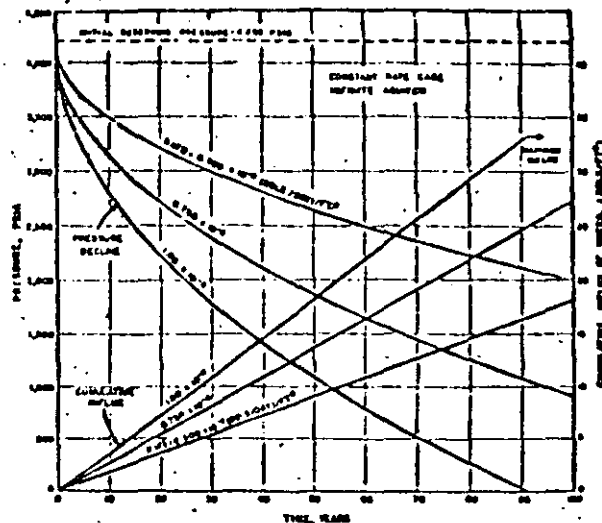


FIG 10

RESERVOIR PRESSURE AND CUMULATIVE INFLOW OF WATER AS FUNCTIONS OF TIME FOR VARIOUS CONSTANT RATES AND AN INFINITE AQUIFER

Permeability: 500 mD  
Porosity: 0.20  
Viscosity of water: 0.300 cP  
Compressibility of water:  $3.60 \times 10^{-6}$  (vol/vol)/psi

Equation (31) is the equation of the rate curves of Fig 12:  $P_f$  is 4200 psia, and the constant values of  $P_s$  are 2000, 2900, and 3600 psia. The cumulative-influx curves were developed by plotting  $\left(\frac{1}{bh}\right) \int_0^t Q d\theta$  as determined from equation (34), expressed in (bbl/ft<sup>2</sup>), against  $\theta$  expressed in years.

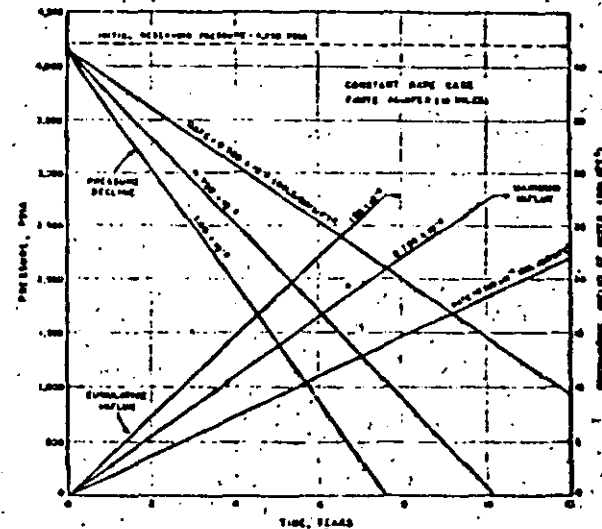


FIG 11

RESERVOIR PRESSURE AND CUMULATIVE INFLOW OF WATER AS FUNCTIONS OF TIME FOR VARIOUS CONSTANT RATES OF INFLOW AND AN AQUIFER 10.0 MILES LONG

Permeability: 500 mD  
Porosity: 0.20  
Viscosity of water: 0.300 cP  
Compressibility of water:  $3.60 \times 10^{-6}$  (vol/vol)/psi

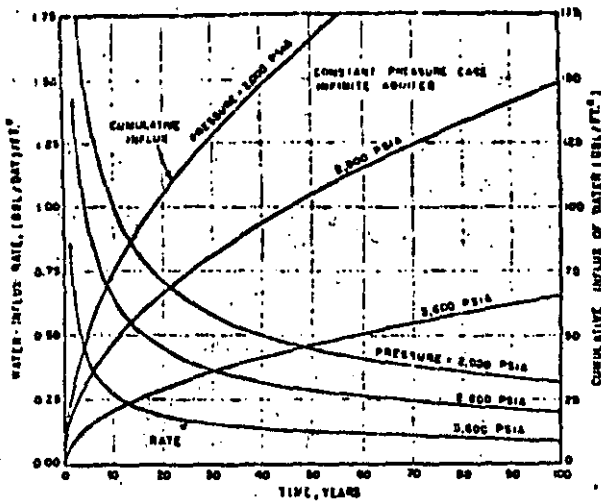


FIG 12

RATE OF INFLUX OF WATER AND CUMULATIVE INFLUX OF WATER AS FUNCTIONS OF TIME FOR VARIOUS CONSTANT PRESSURES AT THE BOUNDARY OF THE OIL RESERVOIR AND FOR AN INFINITE AQUIFER

Permeability: 500 mD  
 Porosity: 0.200  
 Viscosity of water: 0.300 cP  
 Compressibility of water:  $3.60 \times 10^{-6}$  (vol/vol)/psi

Equation (30) is the equation of the rate curves of Fig 13. The initial pressures,  $P_i$ , and the three constant values of  $P_e$  are the same as those used in Fig 12. The cumulative influx curves were developed by plotting  $\left(\frac{1}{bh}\right) \int_0^t Q dt$  as determined from equation (40), expressed in (bbl/ft<sup>2</sup>), against  $t$  expressed in years.

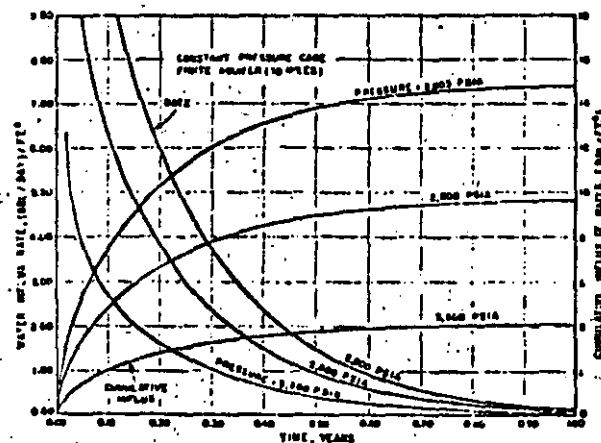


FIG 13

RATE OF INFLUX OF WATER AND CUMULATIVE INFLUX OF WATER AS FUNCTIONS OF TIME FOR VARIOUS CONSTANT PRESSURES AT THE BOUNDARY OF THE OIL RESERVOIR AND FOR AN AQUIFER 10.0 MILES LONG

Permeability: 500 mD  
 Porosity: 0.200  
 Viscosity of water: 0.300 cP  
 Compressibility of water:  $3.60 \times 10^{-6}$  (vol/vol)/psi

EFFECT OF WATER-INFLUX RATE ON CUMULATIVE OIL RECOVERY

Constant-rate Cases

If equations (24) and (25) are combined and  $t$  eliminated, the resulting relationship between  $Q_c$ ,  $Q_D$ , and  $\Delta P$ , for infinite aquifers, is found to be

$$Q_c = \frac{\pi b^2 (\Delta P)^2}{4 x_e^2 Q_D} \quad (41)$$

A pre-assigned initial pressure  $P_i$  at time zero and final pressure  $P_e$  at time  $t_M$ , at  $x = 0$ , cause the resulting relationship of  $Q_c$  and  $Q_D$  to apply only at

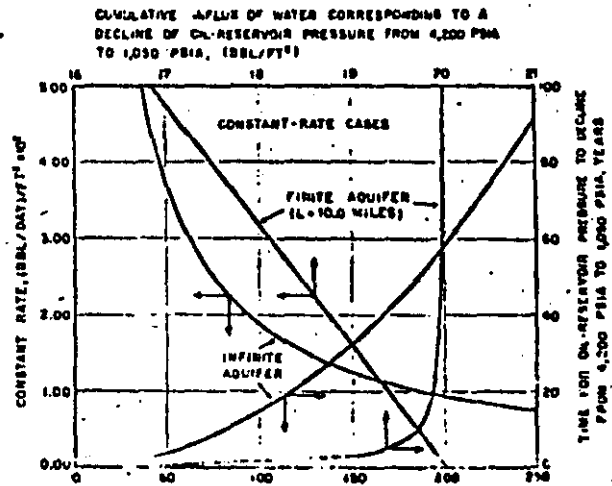


FIG 14

EFFECT OF RATE OF INFLUX OF WATER ON THE CUMULATIVE INFLUX OF WATER CORRESPONDING TO A DECLINE OF OIL RESERVOIR PRESSURE FROM 4,200 psia TO 1,050 psia FOR SYSTEMS HAVING 10.0 MILES AND INFINITE AQUIFERS

Permeability: 500 mD  
 Porosity: 0.200  
 Viscosity of water: 0.300 cP  
 Compressibility of water:  $3.60 \times 10^{-6}$  (vol/vol)/psi

the instant  $t = t_M$ . At this instant  $Q_c$  would be greater for a relatively low constant rate  $Q_D$  than for a relatively high one. The instant in question is variable. Equation (24) with  $t = t_M$  results if  $Q_c$  in equation (41) is replaced with  $Q_D t_M$ . Thus one finds that reductions in  $Q_D$  cause  $t_M$  to be greater and increases in  $Q_D$  cause  $t_M$  to be smaller.

The infinite-aquifer curve of Fig 14 depicting the relationship between constant rate of influx and cumulative influx, for a fixed pre-assigned cumulative pressure drop, was developed from equation (41) after it was transformed back to the original variables.

The curve shows  $\left(\frac{Q}{bh}\right)$  as a function of  $\left(\frac{Q_0}{bh}\right)$  for  $P_i = 4200$  psia and  $P_e = 1050$  psia. The infinite-aquifer curve portraying the relationship between time and cumulative influx, for the same pre-assigned

fixed cumulative pressure drop, was developed from equation (25) after  $t$  was replaced by  $t_M$  and it was transformed back to the original variables.

These curves indicate that the cumulative influx from infinite aquifers, corresponding to a fixed cumulative pressure drop, may be increased markedly by reducing the constant rate. If, for example, the rate is decreased from  $1.62 \times 10^{-2}$  to  $1.15 \times 10^{-2}$  bbl/ft<sup>2</sup>, the cumulative influx, according to the figure, would increase from about 117 to 165 bbl/ft<sup>2</sup>. The required time would be increased, however, from 20 to 40 years. In this instance a 29 per cent reduction in the rate would cause a 41 per cent increase in the cumulative and a 100 per cent increase in the time.

This phenomenon may be explained theoretically. Constant rate  $Q_D$  determines the pressure distribution in the aquifer at any time. The distribution existing at time  $t_M$  when final pressure  $P_e$  is approached at  $x = 0$  reflects the volume of water that has crossed the section at  $x = 0$  and entered the oil reservoir. At that time pressure  $P$  at some particular transverse section, at  $x_0$ , back in the aquifer would approach pressure  $P_f$ . If the mean value of the pressure over the distance from  $x = 0$  to  $x = x_0$  is represented by  $\bar{P}$ , and if the isothermal coefficient of compressibility of the water, represented by  $\frac{1}{\gamma} \left( \frac{\partial \gamma}{\partial P} \right)_T$ , is essentially constant over the pressure range from  $P_e$  to  $P_f$ , the cumulative influx would be given by  $bhx_0 \Delta P \left[ e^{(\bar{P}-P_e)/\gamma} - 1 \right]$ . Thus the cumulative influx would increase with increasing  $x_0$  and with decreasing  $\bar{P}$ . The foregoing analysis pertaining to Fig 14 reveals that relatively low constant rates of influx either cause  $x_0$  to increase or  $\bar{P}$  to decrease, or both. Tests of individual problems may be made with equation (12).

It can be shown readily that the summation term of equation (26) is negligible if  $L \geq 10.0$  miles and  $\theta \geq 1.00$  years. When these conditions are specified the dimensionless time as determined from equation (27) would be given by

$$t = \left( \frac{b \cdot \Delta P}{Q_D} - \frac{L}{3} \right) \frac{L}{x_0^2} \quad (42)$$

Substitution of  $Q_C/Q_D$  for  $t$  in this equation yields the following relationship between  $Q_C$ ,  $Q_D$ , and  $\Delta P$ :

$$Q_C = \frac{bL \cdot \Delta P}{x_0^2} - \frac{L^2 Q_D}{3x_0^2} \quad (43)$$

Cumulative pressure drop  $\Delta P$  is fixed by the pre-assigned value of  $P_e$  at  $x = 0$  at time  $t = t_M$ . Hence  $Q_C$  would be greater at this time for relatively low values of  $Q_D$ , than for relatively high ones, and the relationship between the two would be linear. The finite-aquifer curve of Fig 14 showing the relationship between cumulative influx and rate of influx, for a given  $\Delta P$ , was developed from equation (43) after transforming it back to the original variables. As in

the case of the infinite aquifer this curve shows  $\left( \frac{Q_C}{b\bar{h}} \right)$  as a function of  $\left( \frac{Q_D}{b\bar{h}} \right)$  for  $P_f = 4200$  psia and  $P_e = 1050$  psia.

As the summation term in equation (27) may be neglected, equation (29) with  $t$  replaced by  $t_M$  can be put in the form

$$Q_C = \frac{3bL \cdot \Delta P \cdot t_M}{L^2 + 3x_0^2 t_M} \quad (44)$$

which also would have been obtained as a result of letting  $t = t_M$  in equation (42) and then dividing through by  $t_M$ . The resulting equation, after being transformed back to the original variables, was used to plot the finite-aquifer relationship portrayed on Fig 14 between time and cumulative influx, for a fixed cumulative pressure drop.

The finite-aquifer curves of Fig 14 disclose that relatively small reductions in the rate of influx in the range from  $5.00 \times 10^{-2}$  to about  $1.00 \times 10^{-2}$  (bd) ft<sup>2</sup> are quite effective in increasing the cumulative influx, for the fixed cumulative pressure drop. Reductions in rate below about  $1.00 \times 10^{-2}$  (bd)/ft<sup>2</sup> cause no significant change in the cumulative influx. If the time taken for the pressure at  $x = 0$  to drop from 4200 to 1050 psia is increased from 20 to 100 years, the increase in cumulative influx approximates only about 4 per cent.

#### Constant-pressure Cases

If equations (32) and (33) are combined and  $t$  eliminated, the resulting relationship between  $Q_C$ ,  $Q_D$ , and  $\Delta P$  for the infinite aquifer is found to be

$$Q_C = \frac{2L^2(\Delta P)^2}{x_0^2 \cdot Q_D} \quad (45)$$

In this case  $\Delta P$  is a fixed constant independent of time. The relationship between  $Q_C$  and  $Q_D$  applies therefore at all times  $0 \leq t \leq t_M$ .

The relationship between  $Q_D$  and  $t$  expressed by equation (32) is also established by the choice of  $\Delta P$ . Thus there can be only one  $Q_C$  and  $t_M$ . This line of reasoning applies equally well to finite aquifers. One concludes that in the constant-pressure cases the cumulative influx and the corresponding required time are fixed by the choice of  $\Delta P$ .

## SUPERPOSITION CONCEPT

### Principles

Physically, it is not feasible or perhaps even possible to drop the pressure instantaneously and substantially at  $x = 0$  and then maintain the lower pressure over a long period of time. Thus the theoretical constant-pressure cases have no real oilfield

counterpart. Similarly, it is not feasible to effect instantaneously and thereafter maintain a constant volumetric rate of influx so that the theoretical constant-rate cases also have no field counterpart.

Under normal oilfield conditions the pressure and volumetric rate at  $x = 0$  would change gradually. The superposition concept or theorem provides the means for mathematical analysis of changing-pressure or changing-rate cases, through utilization of the equations already developed.

Let the ratio  $\left(\frac{P_i}{P_j}\right)$  be the ratio of the pressure  $P_i$  at  $x = 0$  at dimensionless time  $t$  to the pressure  $P_j$  at this section at time zero. Consider that this ratio is a continuously decreasing function of  $t$  when plotted over the interval  $0 \leq t \leq t_M$ . Consider further that the  $t$  axis (abscissa) is divided into  $M$  equal increments, the time being  $t_1$  at the end of the first increment,  $t_2$  at the end of the second, and so on to  $t_M$  at the end of the  $M$ th increment.

To apply the superposition concept the continuous relationship of  $\left(\frac{P_i}{P_j}\right)$  and  $t$  must be replaced by a matching step-function relationship of these two variables. For this purpose assume that the pressure ratio is reduced by an amount  $\Delta P_0$  at time zero and maintained at the lower value to  $t_1$ . Let  $(1 - \Delta P_0)$  be equivalent to the average pressure ratio as determined from the true pressure ratio-time curve, over the first increment of time ( $t_1 - 0$ ). Similarly, let the pressure ratio be further reduced at time  $t_1$  by an amount  $\Delta P_1$  and let  $(1 - \Delta P_0 - \Delta P_1)$  be equivalent to the average pressure ratio over the time increment  $(t_2 - t_1)$ . If this process is continued until it includes the last increment of time  $(t_M - t_{M-1})$ , and if the equal increments of time are small enough, the resulting step function will match closely the true pressure ratio-time curve.

The pressure decrement  $\Delta P_0$  imposed at time zero affects the flow over the time interval  $(t_M - 0)$ . Similarly,  $\Delta P_1, \Delta P_2, \dots, \Delta P_{M-1}$  are effective over the intervals  $(t_M - t_1), (t_M - t_2), \dots, (t_M - t_{M-1})$ , respectively. The constant pressure-case equations developed earlier (equations (33) and (39)), expressing cumulative influx as a function of time, may be put in the form

$$Q_c = \Delta P \cdot f(t) \quad (40)$$

Considering equation (40) and the foregoing step function, the superposition concept indicates that the cumulative influx obtained under conditions of continuously decreasing pressure at  $x = 0$  would be given by

$$Q_c = \Delta P_0 f(t_M) + \Delta P_1 f(t_M - t_1) + \Delta P_2 f(t_M - t_2) + \dots + \Delta P_{M-1} f(t_M - t_{M-1}) \quad (47)$$

Since  $\Delta t = t_1 - 0 = t_2 - t_1 = \dots = \text{constant}$  and

$$\left. \begin{aligned} t_M - t_1 &= (M - 1)\Delta t \\ t_M - t_2 &= (M - 2)\Delta t \\ \dots &\dots \dots \dots \\ t_M - t_{M-1} &= [M - (M - 1)]\Delta t \end{aligned} \right\} \quad (48)$$

the cumulative influx would be given by

$$Q_c = \Delta P_0 f(t_M) + \sum_{\tau=1}^{M-1} \Delta P(\tau) f(t_M - \tau) \quad (49)$$

Noting that

$$\Delta P(\tau) = \frac{\Delta P(\tau)}{\Delta \tau} \Delta \tau \quad (50)$$

and letting  $\Delta \tau \rightarrow 0$ , equation (49) may be written in the integral form

$$Q_c = \Delta P_0 f(t_M) + \int_0^{t_M} \frac{dP}{d\tau} f(t_M - \tau) d\tau \quad (51)$$

Equation (51) is one form of Duhamel's integral.\*

Suppose dimensionless volumetric rate of flow instead of dimensionless pressure ratio is treated in the foregoing manner. Let  $Q_D$  be an increasing function of  $t$  and again let the  $t$  axis be divided into  $M$  equal increments, each equal to  $\Delta t$ . The constant-rate case equations (equations (24) and (28)) indicate that the cumulative pressure drop as a function of time may be put in the form

$$\Delta P = Q_D f(t) \quad (52)$$

It follows that the changing-rate case equation parallel to equation (47) for the changing-pressure case would be, according to the superposition concept,

$$\Delta P = Q_{D0} f(t_M) + \Delta Q_{D1} f(t_M - t_1) + \Delta Q_{D2} f(t_M - t_2) + \dots + (\Delta Q_D)_{M-1} f(t_M - t_{M-1}) \quad (53)$$

in which  $Q_{D0}$  is the initial rate,  $\Delta Q_{D1}$  the increase in rate at  $t_1$ ,  $\Delta Q_{D2}$  the increase in rate at  $t_2$ , and so on to the final increase  $(\Delta Q_D)_{M-1}$  at  $t_{M-1}$ , effective over the last increment of time,  $(t_M - t_{M-1})$ . Equation (53) may be put in the form

$$\Delta P = Q_{D0} f(t_M) + \sum_{\tau=1}^{M-1} \Delta Q_D(\tau) f(t_M - \tau) \quad (54)$$

or in the form of a Duhamel integral

$$\Delta P = Q_{D0} f(t_M) + \int_0^{t_M} \frac{dQ_D}{d\tau} f(t_M - \tau) d\tau \quad (55)$$

*Numerical Example*

Referring to Fig 15, the rate-time relationship was imposed. The initial rate  $Q_0$  is  $0.250 \times 10^{-2}$  (bd)/ft<sup>2</sup>, and at the beginning of each of the next 12 quarters (30) this rate is increased by an amount equal to the initial value. Therefore, if  $Q_0$  is expressed in (brl/qtr)/ft<sup>2</sup> the cumulative influx at the end of the  $n$ th quarter,

expressed in brl/ft<sup>2</sup>, would be  $\sum_{m=1}^n m Q_0 \Delta t$ . The

Unsteady-State Linear Flow Equations

constant Flow Rate

$$\Delta p_{i-o} = \frac{\alpha q \mu L}{k b h} F_{1/2}(t_D) \quad \text{Acuifero Infinito}$$

$$\Delta p_{i-o} = \frac{\alpha q \mu L}{k b h} F_1(t_D) \quad \text{Acuifero finito limitado en frontera impermeable}$$

$$\Delta p_{i-o} = \frac{\alpha q \mu L}{k b h} F_0(t_D) \quad \text{Acuifero finito con linderos externos a presión constante}$$

$\alpha$  = Factor de conversión de unidades.

Darcy	5.1	Inglis
$\alpha = 1$	$\alpha = 1$	887.2
$\beta = 1$	$\beta = 1$	0.00633

$$t_D = \frac{\beta k t}{\phi \mu c L^2}$$

constant Pressure

$$W_e = \phi b h L c_e \Delta p F_{1/2}(t_D) \quad \text{Acuifero infinito}$$

$$W_e = \phi b h L c_e \Delta p F_0(t_D) \quad \text{Acuifero finito en frontera impermeable}$$

$$W_e = \phi b h L c_e \Delta p F_1(t_D) \quad \text{Acuifero finito con frontera externa a presión constante}$$

$$F_0(t_D) = 1 - \frac{8}{\pi^2} \sum_{n \text{ odd}}^{\infty} \left( \frac{1}{n^2} \right) \exp\left(-\frac{n^2 \pi^2 t_D}{4}\right)$$

$$F_{1/2}(t_D) = 2 \sqrt{\frac{t_D}{\pi}}$$

$$F_1(t_D) = \left(t_D + \frac{1}{3}\right) - \frac{2}{\pi^2} \sum_{n=1}^{\infty} \left(\frac{1}{n^2}\right) \exp\left(-\frac{n^2 \pi^2 t_D}{4}\right)$$



cumulative-influx curve therefore may be plotted readily.

The figure pertains to a finite aquifer. The constant-rate case equation is equation (26), but as the rate is increasing this equation must be used with equation (53) to calculate the pressure at any time.

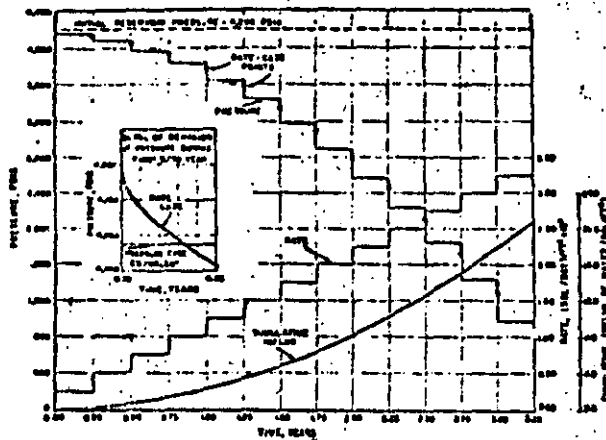


FIG 15

OIL RESERVOIR PERFORMANCE DETERMINED THROUGH APPLICATION OF THE SUPERPOSITION CONCEPT

The rate-time step function was pre-assigned and the corresponding cumulative-influx relationship calculated. This relationship was then used in determining both the rate-case and pressure-case pressure-time functions. Length of aquifer 100 miles.

- Permeability: 500 md
- Porosity: 0.200
- Viscosity of water: 0.300 cP
- Compressibility of water:  $3.00 \times 10^{-6}$  (vol/vol)/psi

Since the increases in rate ( $Q_1 - Q_0$ ) at  $t_1$ , ( $Q_2 - Q_1$ ) at  $t_2$ , ( $Q_3 - Q_2$ ) at  $t_3$  and so on to ( $Q_{n-1} - Q_{n-2}$ ) at  $t_{n-1}$  are each equal to  $Q_0$ , the pressure  $P_M$  at time  $t_M$  may be calculated with the equation

$$P_M = P_j - \frac{Q_0 \mu}{bhk} \left[ \frac{ML}{3} + \sum_{m=1}^M m \cdot \Delta t \right] - \frac{2L}{\pi^2} \sum_{n=1}^{\infty} \sum_{m=1}^{\infty} \left( \frac{1}{n^2} \right) \exp \left( - \frac{n^2 m \pi^2 \alpha \cdot \Delta t}{L^2} \right) \quad (50)$$

Pressure-time data calculated with equation (50) are shown as small circles on Fig 15 and are identified as "rate-case points." The detailed behaviour of the "rate-case" curve that would join two such points, e.g. the ones for  $t = 0$  and  $t = 0.25$  years, is shown in the inset on the figure.

Data for the pressure-case equivalent or pressure-step-function was determined through application of equation (40), and the known cumulative influx at the end of each quarter as fixed by the initially imposed rate-time relationship.

If the bracketed term of equation (40) is symbolized by  $f(t)$  or  $f(n \cdot \Delta t)$ , that equation leads to the expression

$$\left( \frac{1}{bh} \right) \int_0^{n \Delta t} Q dt = \frac{2cL}{\pi^2} \sum_{m=0}^{\infty} \Delta P_m f[(n-m)\Delta t] \quad (57)$$

The pressure drop  $\delta P_0$  for the first increment of time may be calculated directly by setting  $n = 1$ . When this pressure drop is known, the drop for the second increment,  $\delta P_1$ , may be calculated by setting  $n = 2$ . Continuation of this process until it includes the last increment of time provides necessary data for plotting the pressure step-function.

A fundamental consequence of the superposition concept is that actual oilfield water-drive problems involving continuous changes in rate and pressure may be treated on an established theoretical basis.

CONCLUSION

States of single-phase fluid motion in porous media are examined in this report. The theory of unsteady state influx of water in linear systems of oil reservoirs and fluid-connected aquifers is described in detail. Aquifers of both finite and infinite length are treated. Constant-rate-case and constant-pressure-case problems are stated analytically and solved. Results are plotted in easily usable graphical form, and numerical examples are worked out where ver practicable. The superposition concept in its relation to the problems discussed is explained. Its applicability to oilfield problems is indicated.

This paper should fill a need in petroleum literature for a theoretical dissertation on the subject of water influx in linear reservoirs. It should find application in engineering analysis of such reservoirs. Finally, it should be useful to practicing engineers and researchers studying this subject.

ACKNOWLEDGMENTS

The author wishes to express his appreciation to the management of Socony-Mobil Oil Co. Inc. for permission to publish this paper. Helpful discussions with many engineers of Mobil Oil Co. de Venezuela during the period 1 July 1939 to 1 March 1960 are gratefully acknowledged. Special thanks are due to Carlos F. Gonzalez for his assistance with the calculations.

References

- 1 van Everdingen, A. F., and Hurst, W. *Petrol. Trans. Amer. Inst. Min. Engrs.* 1940, 156, 303.
- 2 Chatain, A. T. *Petrol. Engr.* 1933, 25 (3), B42; 25 (6), B35; 25 (9), B44.
- 3 Katz, D. L., et al. "Handbook of Natural Gas Engineering," p. 403.
- 4 Churchill, R. V. "Modern Operational Mathematics in Engineering." New York: McGraw-Hill, 1944, p. 107.
- 5 "Tables of the Error Function and Its Derivative." Washington: U.S. Dept. of Commerce, National Bureau of Standards, Applied Mathematics, Series 41, 22 Oct 1954.
- 6 Carslaw, H. S., and Jaeger, J. C. "Conduction of Heat in Solids," second edn. London: Oxford University Press, 1939, p. 112.
- 7 Churchill, R. V. "Fourier Series and Boundary Value Problems." New York: McGraw-Hill, 1941, p. 111, 123.
- 8 von Karman, T., and Biot, M. A. "Mathematical Methods in Engineering." New York: McGraw-Hill, 1940, p. 320, 403.

# The Flow of Real Gases Through Porous Media

R. AL-HUSSAINY  
JUNIOR MEMBER AIME  
H. J. RAMEY, JR.\*  
P. B. CRAWFORD  
MEMBERS AIME

TEXAS A&M U.  
COLLEGE STATION, TEX.

## ABSTRACT

The effect of variations of pressure-dependent viscosity and gas law deviation factor on the flow of real gases through porous media has been considered. A rigorous gas flow equation was developed which is a second order, non-linear partial differential equation with variable coefficients. This equation was reduced by a change of variable to a form similar to the diffusivity equation, but with potential-dependent diffusivity. The change of variable can be used as a new pseudo-pressure for gas flow which replaces pressure or pressure-squared as currently applied to gas flow.

Substitution of the real gas pseudo-pressure has a number of important consequences. First, second degree pressure gradient terms which have commonly been neglected under the assumption that the pressure gradient is small everywhere in the flow system, are rigorously handled. Omission of second degree terms leads to serious errors in estimated pressure distributions for tight formations. Second, flow equations in terms of the real gas pseudo-pressure do not contain viscosity or gas law deviation factors, and thus avoid the need for selection of an average pressure to evaluate physical properties. Third, the real gas pseudo-pressure can be determined numerically in terms of pseudo-reduced pressures and temperatures from existing physical property correlations to provide generally useful information. The real gas pseudo-pressure was determined by numerical integration and is presented in both tabular and graphical form in this paper. Finally, production of real gas can be correlated in terms of the real gas pseudo-pressure and shown to be similar to liquid flow as described by diffusivity equation solutions.

Application of the real gas pseudo-pressure to radial flow systems under transient, steady-state or approximate pseudo-steady-state injection or production have been considered. Superposition of the linearized real gas flow solutions to generate variable rate performance was investigated and found satisfactory. This provides justification for pressure build-up testing. It is believed that the concept of the real gas pseudo-pressure will lead to improved interpretation of results of current gas well testing procedures, both steady and unsteady-state in nature, and improved forecasting of gas production.

## INTRODUCTION

In recent years a considerable effort has been directed

to the theory of isothermal flow of gases through porous media. The present state of knowledge is far from being fully developed. The difficulty lies in the non-linearity of partial differential equations which describe both real and ideal gas flow. Solutions which are available are approximate analytical solutions, graphical solutions, analogue solutions and numerical solutions.

The earliest attempt to solve this problem involved the method of successions of steady states proposed by Muskat.<sup>1</sup> Approximate analytical solutions<sup>2</sup> were obtained by linearizing the flow equation for ideal gas to yield a diffusivity-type equation. Such solutions, though widely used and easy to apply to engineering problems, are of limited value because of idealized assumptions and restrictions imposed upon the flow equation. The validity of linearized equations and the conditions under which their solutions apply have not been fully discussed in the literature. Approximate solutions are those of Heatherington *et al.*,<sup>3</sup> MacRoberts<sup>4</sup> and Janicek and Katz.<sup>5</sup> A graphical solution of the linearized equation was given by Cornell and Katz.<sup>6</sup> Also, by using the mean value of the time derivative in the flow equation, Rowan and Clegg<sup>7</sup> gave several simple approximate solutions. All the solutions were obtained assuming small pressure gradients and constant gas properties. Variation of gas properties with pressure has been neglected because of analytic difficulties, even in approximate analytic solutions.

Green and Wilts<sup>8</sup> used an electrical network for simulating one-dimensional flow of an ideal gas. Numerical methods using finite difference equations and digital computing techniques have been used extensively for solving both ideal and real gas equations. Aronofsky and Jenkins<sup>9</sup> and Bruce *et al.*<sup>10</sup> gave numerical solutions for linear and radial gas flow. Douglas *et al.*<sup>11</sup> gave a solution for a square drainage area. Aronofsky<sup>12</sup> included the effect of slippage on ideal gas flow. The most important contribution to the theory of flow of ideal gases through porous media was the conclusion reached by Aronofsky and Jenkins<sup>13</sup> that solutions for the liquid flow case<sup>14</sup> could be used to generate approximate solutions for constant rate production of ideal gases.

An equation describing the flow of real gases has been solved for special cases by a number of investigators using numerical methods. Aronofsky and Ferris<sup>15</sup> considered linear flow, while Aronofsky and Porter<sup>16</sup> considered radial gas flow. Gas properties were permitted to vary as linear functions of pressure. Recently, Carter<sup>17</sup> proposed an empirical correlation by which gas well behavior can be estimated from solutions of the diffusivity equation using instantaneous values of pressure-dependent gas

Original manuscript received in Society of Petroleum Engineers office June 23, 1965. Revised manuscript of SPE 1242A received Feb. 18, 1966. Paper was presented at SPE Annual Fall Meeting held in Denver, Colo., Oct. 3-6, 1965.

\*Presently on the faculty at Stanford U.

References given at end of paper.

properties evaluated at an average pressure also defined empirically. Carter gave a limited number of numerical solutions as a basis, and suggested some relations which might give a better correlation. However, the proposed relations were not evaluated in the mentioned work. Solutions have been presented by Eilerts *et al.*<sup>11,12</sup> for flow of gas-condensate fluids in linear and radial systems.

It has been observed that as the gas flow velocity increases, departure from Darcy's law occurs.<sup>13</sup> Such flow is termed non-Darcy, or turbulent flow. Flow is transitional, and not truly turbulent. A gas flow equation including a quadratic velocity term to account for turbulence near the producing well has been solved by Swift and Kiel<sup>14</sup> and Tek *et al.*<sup>15</sup> for ideal gases. Eilerts *et al.*<sup>11,12</sup> and Carter<sup>10</sup> also included non-Darcy flow in their solutions for real gases. An approximate solution including non-Darcy flow has been presented by Rowan and Clegg.<sup>16</sup>

Two other calculational procedures appear in the works of Roberts<sup>17</sup> and Kidder<sup>18</sup> for solving the one-dimensional flow equation for an ideal gas. Roberts used a stepwise forward integration in time by joining together a sequence of solutions for linearized differential equations. Kidder, applying perturbation technique and using the well-known Boltzmann transformation in the theory of diffusion, gave an exact analytic solution for gas flow in a semi-infinite porous medium. Kidder's solution is very similar to a more general one reported by Poluharinoва-Kochina<sup>19</sup> on the movement of ground water.

In summary, only a limited number of solutions for flow of real gases are available, and these are not of general utility. Furthermore, methods of analyzing gas reservoir performance in current use are generally based on solutions for the flow of ideal gases under the assumption of small pressure gradients. These methods fail to describe the behavior of low permeability and high pressure reservoirs.

FLOW OF REAL GASES

The following concerning the flow of real gases through porous media is drawn from an analogy with the theory of heat conduction in solids.<sup>20</sup> Variation of gas physical properties with the pressure correspond to that of temperature-dependent properties in the theory of heat conduction.

The mechanism of fluid flow through a porous medium is governed by the physical properties of the matrix, geometry of flow, PVT properties of the fluid and pressure distribution within the flow system. In deriving the flow equations and establishing the solutions, the following assumptions are made. The medium is homogeneous, the flowing gas is of constant composition and the flow is laminar and isothermal. Assumption of laminar flow can be removed, but will be used to simplify the presentation.

The principle of conservation of mass for isothermal fluid flow through a porous medium is expressed by the well-known continuity equation:

$$\nabla \cdot (\rho v) = \phi \frac{\partial \rho}{\partial t} \quad (1)$$

The velocity vector in Eq. 1 is given by Darcy's law for laminar flow as:

$$v = -\frac{k(p)}{\mu(p)} \nabla p \quad (2)$$

Substituting Eq. 2 in Eq. 1 yields:

$$\nabla \cdot \left[ \frac{k(p)}{\mu(p)} \nabla p \right] = \phi \frac{\partial \rho}{\partial t} \quad (3)$$

For real gases:

$$\rho = \frac{M}{RT} \left[ \frac{p}{z(p)} \right] \quad (4)$$

Density can be eliminated from Eq. 3 to yield:

$$\nabla \cdot \left[ \frac{k(p)}{\mu(p) z(p)} p \nabla p \right] = \phi \frac{\partial}{\partial t} \left[ \frac{p}{z(p)} \right] \quad (5)$$

Eq. 5 is one form of the fundamental non-linear partial differential equation describing isothermal flow of real gases through porous media.

The pressure-dependent permeability for gas was expressed by Klinkenberg<sup>21</sup> as:

$$k(p) = k_l \left( 1 + \frac{b}{p} \right) \quad (6)$$

where  $k_l$  = effective permeability to liquids; and  $b$  = the slope of a linear plot of  $k(p)$  vs.  $\frac{1}{p}$ .

However, the dependency of permeability on pressure is usually negligible for pressure conditions associated with gas reservoirs, as pointed out by Aronofsky.<sup>22</sup> In a subsequent paper, Aronofsky and Ferris<sup>23</sup> indicated that variations of gas properties with pressure are more important than variations of permeability with pressure. Therefore, liquid permeability can be used for gas flow, and the following equation is correct for all practical purposes:

$$\nabla \cdot \left[ \frac{p}{\mu(p) z(p)} \nabla p \right] = \frac{\phi}{k} \frac{\partial}{\partial t} \left[ \frac{p}{z(p)} \right] \quad (7)$$

Eq. 7 can be expanded to many different forms. For example, Eq. 7 can be rearranged to point out explicitly the real gas diffusivity

$$\frac{k}{\phi \mu(p) z(p)}$$

Since

$$p \nabla p = \frac{1}{2} \nabla p^2 \quad (8)$$

Eq. 7 becomes, after some rearrangement:

$$\nabla^2 p^2 = \frac{d(\ln \mu(p) z(p))}{dp^2} (\nabla p^2)^2 = \frac{2 \phi \mu(p) z(p)}{k} \frac{\partial}{\partial t} \left[ \frac{p}{z(p)} \right] \quad (9)$$

From the definition of the isothermal compressibility of gas:

$$c_g(p) = \frac{1}{p} \frac{dp}{dp} = \frac{z(p)}{p} \frac{d}{dp} \left( \frac{p}{z(p)} \right) = \frac{1}{p} - \frac{1}{z(p)} \frac{dz(p)}{dp} \quad (10)$$

Thus:

$$\frac{\partial}{\partial t} \left[ \frac{p}{z(p)} \right] = \frac{pc_g(p)}{z(p)} \frac{\partial p}{\partial t} \quad (11)$$

Combining Eqs. 9 and 11:

Permeability can be considered an important function of pressure for a wet condensate gas as used by Eilerts.<sup>11,12</sup> This case can be handled, as will be shown later in this paper.

$$\nabla^2 p = \frac{d[\ln \mu(p)z(p)]}{dp} (\nabla p)^2 + \frac{\phi \mu(p) c_s(p)}{k} \frac{\partial p}{\partial t} \quad (12)$$

If it is assumed that viscosity and gas law deviation factors change slowly with pressure change, the pressure differential of  $[\ln \mu(p)z(p)]$  becomes negligible. On the other hand, the assumption that pressure gradients are small will permit omission of terms of order  $(\nabla p)^2$ . In either event, Eq. 12 can be simplified to:

$$\nabla^2 p = \frac{\phi \mu(p) c_s(p)}{k} \frac{\partial p}{\partial t} \quad (13)$$

Eq. 13 is similar in form to the diffusivity equation. However, the diffusivity is a function of pressure, even for a perfect gas. In this form, the close analogy with liquid flow found by Jenkins and Aronofsky<sup>10</sup> is emphasized. However, the assumption that pressure gradients are small everywhere in the flow system cannot be justified in many important cases. The assumption of small pressure gradients is implicit in all of the pressure build-up and drawdown methods currently in use which are based upon ideal gas flow solutions or liquid flow analogies. We return, then, to the rigorous Eq. 7.

Eq. 7 can be transformed to a form similar to that of Eq. 13 without assuming small pressure gradients, by making a scale change in pressure. Define a new pseudo-pressure  $m(p)$  as follows:

$$m(p) = 2 \int_{p_w}^p \frac{p}{\mu(p)z(p)} dp \quad (14)$$

where  $p_w$  is a low base pressure. The variable  $m(p)$  has the dimensions of pressure-squared per centipoise. Since  $\mu(p)$  and  $z(p)$  are functions of pressure alone for isothermal flow, this is a unique definition of  $m(p)$ . It follows that:

$$\frac{\partial m(p)}{\partial t} = \frac{\partial m(p)}{\partial p} \frac{\partial p}{\partial t} = \left( \frac{2p}{\mu(p)z(p)} \right) \frac{\partial p}{\partial t} \quad (15)$$

and

$$\frac{\partial m(p)}{\partial x} = \left( \frac{2p}{\mu(p)z(p)} \right) \frac{\partial p}{\partial x} \quad (16)$$

with similar expressions for  $\frac{\partial m(p)}{\partial y}$  and  $\frac{\partial m(p)}{\partial z}$ .

Therefore, Eq. 7 can be rewritten in terms of the variable  $m(p)$  using the definition of  $c_s(p)$  given by Eq. 10 as:

$$\nabla \cdot [\nabla m(p)] = \frac{\phi \mu(p) c_s(p)}{k} \frac{\partial m(p)}{\partial t} \quad (17)$$

or

$$\nabla^2 m(p) = \frac{\phi \mu(p) c_s(p)}{k} \frac{\partial m(p)}{\partial t} \quad (18)$$

Comparison of Eqs. 13 and 18 shows that the form of the diffusivity equation is preserved in terms of the new variable  $m(p)$ . However, Eq. 18 is still non-linear because diffusivity is a function of potential. The gas law deviation factor  $z$  does not appear in the equation, but is involved in  $m(p)$  and  $c_s(p)$ . Eq. 18 does not involve the assumptions of small pressure gradients, nor that of slow variation of  $[\mu(p)z(p)]$ .

The importance of Eq. 18 deserves emphasis. It is a fundamental partial differential equation which describes the flow of real gases. To the authors' knowledge, this

equation has not been presented previously in connection with gas flow. Equations of this type have been called quasi-linear flow equations.<sup>11,12</sup> The real importance lies in the extreme utility of this form of the equation. As will be shown, the form of the equation suggests a powerful engineering approach to the flow of real gases.

To solve Eq. 18, it is necessary to convert the usual initial and boundary conditions into terms of the new pseudo-pressure  $m(p)$ . Important considerations are as follows.

The gas mass flux is:

$$\vec{q}_p = \frac{q}{A} p = - \frac{Mk}{RT} \frac{p}{\mu(p)z(p)} \nabla p \quad (19)$$

In terms of  $m(p)$ , the mass flux is:

$$\frac{q}{A} p = - \frac{Mk}{2RT} \nabla m(p) \quad (20)$$

The usual boundary conditions are either specification of pressure or the gas flux across bounding surfaces. When pressure is fixed,  $m(p)$  can be determined from Eq. 14. If flux is specified, the boundary conditions can be determined from Eq. 20. If the outer boundary is impermeable, then:

$$\frac{dm(p)}{dn} = 0 \quad (21)$$

where  $n$  is the direction normal to the boundary.

Steady-state flow occurs when pressure distribution and fluid velocity are independent of time. Eq. 18 reduces to:

$$\nabla^2 m(p) = 0 \quad (22)$$

which is Laplace's equation. Thus, previous solutions of the Laplace equation can be used if  $m(p)$  is used as the potential.

Steady-state flow can rarely be obtained in reality because gas wells usually produce gas from a limited, finite reservoir or drainage volume. There can be no flow across the outer boundary. Thus, pressure must decline as production continues. True steady-state would require pressure to remain constant at the outer boundary, which implies flow across the outer boundary. Production of a bounded reservoir at constant production is an important problem, which will be considered later in this paper.

### REAL GAS PSEUDO-PRESSURE

To obtain generally useful solutions for Eq. 18, the proper physical properties for natural gases must be specified. Fortunately, all required physical properties have been correlated as functions of pseudo-reduced pressures and temperatures for many gases met in field work. It should be emphasized that the concept of the real gas pseudo-pressure is not limited to use of specific gas property correlations. Pseudo-reduced pressure and temperature are defined, respectively, as:

$$p_{pr} = \frac{p}{p_r} \quad (23)$$

and

$$T_{pr} = \frac{T}{T_r} \quad (24)$$

where  $p_r$  is the pseudo-critical pressure and  $T_r$  is the pseudo-critical temperature. Real gas law deviation factors  $z(p)$  have been presented by Standing and Katz.<sup>13</sup> Vis-

coefficients of natural gases have been correlated by Carr *et al.*<sup>10</sup> as the ratio of viscosity at any pressure to that at one atmosphere. Thus:

$$\frac{\mu(p)}{\mu_1} = f(p_{pr}, T_{pr}) \dots \dots \dots (25)$$

Compressibilities of natural gases have been correlated by Trube<sup>11</sup> as reduced compressibilities, the product of compressibility and pseudo-critical pressure. That is:

$$c_{pr} = c_r(p) \cdot p_{pr} = f(p_{pr}, T_{pr}) \dots \dots \dots (26)$$

Substitution of Eqs. 23 to 25 in Eq. 14 yields:

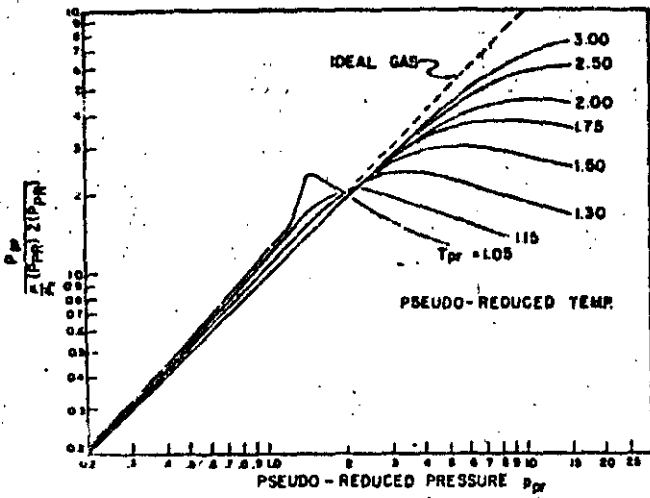


FIG. 1 RATIO OF PSEUDO-REDUCED PRESSURE TO VISCOSITY-GAS LAW DEVIATION FACTOR PRODUCT VS PSEUDO-REDUCED PRESSURE.

$$m(p) = \frac{2(p_{pr})^2}{\mu_1} \int_{(p_{pr})_0}^p \frac{p_{pr}}{(p_{pr})^2 Z(p_{pr})} dp_{pr} \dots \dots \dots (27)$$

The integral can be evaluated generally from reduced properties correlations.

EVALUATION OF REAL GAS PSEUDO-PRESSURE

To establish the relationship between  $p_{pr}$  and  $m(p)$ , the integral must be evaluated numerically for various isotherms. The lower limit of the integration  $(p_{pr})_0$  can be set arbitrarily. A value of 0.20 was chosen. Selected isotherms from pseudo-reduced temperatures of 1.05 to 3.0 were used.

Fig. 1 presents the argument of the integral in Eq. 27 vs pseudo-reduced pressure for various pseudo-reduced temperatures. The dashed line represents the ideal gas case with both viscosity ratio and gas law deviation factor equal to unity. The magnitude of gross variations of gas properties with pressure and temperature is apparent.

Fig. 2 presents  $m(p)$  integrals as functions of pseudo-reduced pressures and temperatures. The integrals were evaluated by means of the Trapezoidal rule using an IBM 709 digital computer. Values of the integrals are also presented in Table 1. Interpolation between the curves or between the values presented in the table can be performed easily.

Use of Fig. 2 or Table 1 is limited to gases containing small amounts of contaminants for which changes in viscosity and gas law deviation factor can be handled by appropriate changes in the pseudo-critical properties, as suggested by Carr *et al.*<sup>10</sup> However, useful charts can be prepared for gases containing large amounts of contaminants if complete properties are known. See Robinson

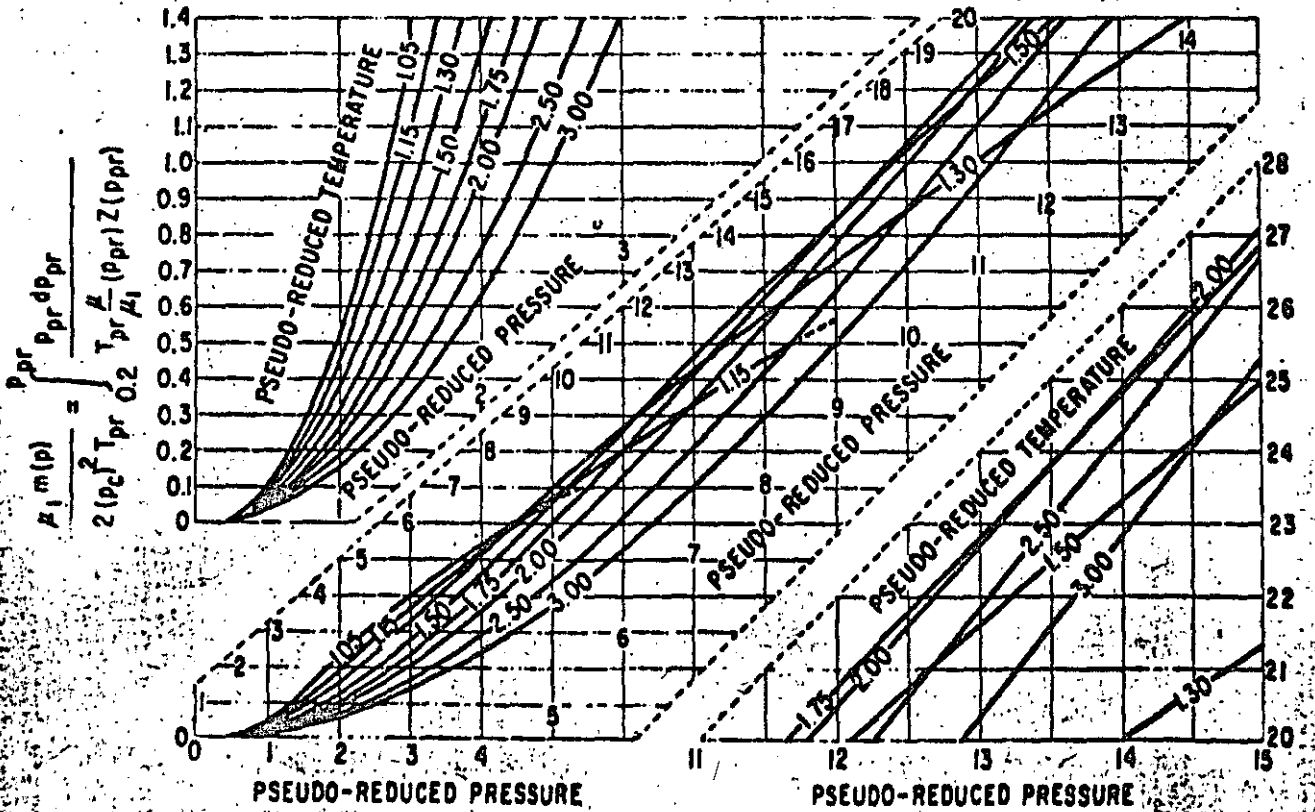


FIG. 2 REAL GAS PSEUDO-PRESSURE INTEGRALS VS PSEUDO-REDUCED PRESSURE.

of  $m(p)$  for density data for gases containing large amounts of contaminants.

In general, it is useful to prepare a chart of  $m(p)$  in units of psi-squared per centipoise vs pressure in psi for any given reservoir to aid engineering use of the real gas pseudo-pressure. The  $m(p)$  can be computed readily for any specific gas and reservoir temperature if density and viscosity are known as functions of pressure. The integration can be performed using the Trapezoidal rule or graphical integration. More sophisticated integrations are usually not required.

The  $m(p)$  values in Fig. 2 and Table 1 are presented as a convenience because it is necessary to assume many gases do follow the existing correlations because of lack of specific data. It is emphasized that the concept of the real gas potential is *general* and is *not* limited to use of the  $m(p)$  values presented herein. If viscosity and density data are available for a specific gas, it should be used in preference to Fig. 2 and Table 1 to prepare  $m(p)$  plots

for the specific gas.

TRANSIENT FLOW

CONSTANT-RATE PRODUCTION

As has been described in the introduction of this paper, Eq. 7 has been solved for specific flow cases under appropriate boundary and initial conditions by a number of authors using finite difference solutions. We seek a general solution which can be used for engineering purposes without the aid of a digital computer. Eq. 18 and the work of Aronofsky and Jenkins<sup>11</sup> provide a basis for an approach. For radial flow of *ideal* gas, the continuity equation leads to:

$$\frac{\partial^2 p^2}{\partial r^2} + \frac{1}{r} \frac{\partial p^2}{\partial r} = \frac{\phi \mu c_g(p)}{k} \frac{\partial p^2}{\partial t} \quad (28)$$

where  $c_g(p)$  for an ideal gas is the reciprocal of the pressure. Several features of Eq. 28 are noteworthy. First,

TABLE 1 —  $\int_{p_i}^{p_e} \frac{p_e \mu_e}{p_i} \frac{dp_e}{(p_e)^2} Z(p_e)$

Values of Integral for Pseudo-Reduced Temperature  $T_{pr}$  of

Pseudo-Reduced Pressure	1.05	1.15	1.30	1.50	1.75	2.00	2.50	3.00
0.30	0.0257	0.0229	0.0198	0.0170	0.0145	0.0126	0.0100	0.0083
0.40	0.0623	0.0553	0.0477	0.0409	0.0348	0.0303	0.0241	0.0200
0.50	0.1102	0.0971	0.0839	0.0716	0.0609	0.0530	0.0421	0.0349
0.60	0.1698	0.1485	0.1283	0.1091	0.0927	0.0807	0.0640	0.0532
0.70	0.2418	0.2105	0.1810	0.1532	0.1303	0.1132	0.0898	0.0747
0.80	0.3264	0.2835	0.2419	0.2037	0.1734	0.1505	0.1194	0.0993
0.90	0.4236	0.3678	0.3111	0.2608	0.2221	0.1927	0.1529	0.1271
1.00	0.5326	0.4631	0.3889	0.3246	0.2763	0.2397	0.1902	0.1580
1.10	0.6546	0.5691	0.4755	0.3954	0.3358	0.2915	0.2312	0.1920
1.20	0.7903	0.6855	0.5707	0.4734	0.4004	0.3483	0.2761	0.2292
1.30	0.9484	0.8126	0.6734	0.5579	0.4702	0.4058	0.3248	0.2695
1.40	1.1444	0.9503	0.7838	0.6484	0.5432	0.4758	0.3773	0.3129
1.50	1.3671	1.0980	0.9020	0.7449	0.6255	0.5461	0.4335	0.3594
1.60	1.5878	1.2546	1.0277	0.8473	0.7114	0.6209	0.4932	0.4090
1.70	1.7924	1.4191	1.1606	0.9558	0.8025	0.7001	0.5566	0.4616
1.80	1.9959	1.5883	1.3001	1.0703	0.8983	0.7840	0.6235	0.5173
1.90	2.1926	1.7595	1.4457	1.1906	0.9988	0.8724	0.6940	0.5760
2.00	2.3821	1.9221	1.5966	1.3164	1.1042	0.9653	0.7679	0.6378
2.10	2.5649	2.1071	1.7526	1.4474	1.2146	1.0624	0.8454	0.7025
2.20	2.7424	2.2841	1.9138	1.5838	1.3298	1.1636	0.9264	0.7701
2.30	2.9147	2.4619	2.0791	1.7253	1.4498	1.2687	1.0111	0.8407
2.40	3.0823	2.6399	2.2471	1.8712	1.5744	1.3777	1.0994	0.9143
2.50	3.2464	2.8172	2.4186	2.0214	1.7034	1.4904	1.1912	0.9907
2.60	3.4055	2.9932	2.5935	2.1758	1.8370	1.6068	1.2862	1.0700
2.70	3.5633	3.1683	2.7710	2.3341	1.9731	1.7268	1.3844	1.1522
2.80	3.7169	3.3401	2.9504	2.4957	2.1169	1.8504	1.4844	1.2373
2.90	3.8679	3.5094	3.1320	2.6612	2.2676	1.9778	1.5915	1.3252
3.00	4.0163	3.6764	3.3153	2.8308	2.4123	2.1091	1.6998	1.4159
3.10	4.1788	4.0876	3.7771	3.2685	2.8038	2.4334	1.9849	1.6550
3.20	4.3278	4.4874	4.2400	3.7223	3.2178	2.8178	2.2896	1.9112
3.30	4.4753	4.8766	4.7052	4.1897	3.6504	3.2016	2.6119	2.1844
3.40	4.6218	5.2579	5.1693	4.6678	4.0997	3.6049	2.9516	2.4731
3.50	4.7674	5.6367	5.6277	5.1539	4.5638	4.0248	3.3077	2.7782
3.60	4.9124	6.0088	6.0822	5.6459	5.0406	4.4643	3.6788	3.0994
3.70	5.0567	6.3697	6.5308	6.1413	5.5280	4.9203	4.0649	3.4357
3.80	5.2006	6.7235	6.9714	6.6377	6.0234	5.3860	4.4664	3.7865
3.90	5.3441	7.0706	7.4044	7.1355	6.5252	5.8621	4.8825	4.1511
4.00	5.4874	7.4124	7.8304	7.6343	7.0326	6.3472	5.3130	4.5266
4.10	5.6306	7.7495	8.2497	8.1338	7.5449	6.8412	5.7575	4.9194
4.20	5.7737	8.0821	8.6632	8.6336	8.0622	7.3442	6.2150	5.3241
4.30	5.9167	8.4099	9.0711	9.1326	8.5836	7.8531	6.6844	5.7413
4.40	6.0596	8.7330	9.4731	9.6297	9.1085	8.3739	7.1643	6.1699
4.50	6.2024	9.0520	9.8703	10.1249	9.6364	8.8993	7.6544	6.6104
4.60	6.3451	9.3670	10.2635	10.6185	10.1665	9.4298	8.1543	7.0633
4.70	6.4877	9.6786	10.6531	11.1091	10.6973	9.9647	8.6633	7.5283
4.80	6.6302	9.9874	11.0398	11.5957	11.2279	10.5034	9.1808	8.0049
4.90	6.7726	10.2936	11.4223	12.0794	11.7587	11.0452	9.7064	8.4921
5.00	6.9149	10.5963	11.7998	12.5615	12.2897	11.5897	10.2398	8.9884
5.10	7.0571	10.8961	12.1731	13.0416	12.8211	12.1377	10.7813	9.4932
5.20	7.2000	11.1933	12.5433	13.5194	13.3532	12.6897	11.3308	10.0062
5.30	7.3428	—	12.9102	13.9939	13.8858	13.2440	11.8872	10.5281
5.40	7.4856	—	13.2735	14.4644	14.4187	13.7993	12.4497	11.0583
5.50	7.6283	—	13.6240	14.9322	14.9513	14.3558	13.0182	11.5962
5.60	7.7711	—	13.9925	15.3980	15.4834	14.9120	13.5926	12.1421
5.70	7.9138	—	14.3483	15.8609	16.0146	15.4700	14.1700	12.6952
5.80	8.0565	—	14.7011	16.3205	16.5447	16.0274	14.7499	13.2545
5.90	8.1992	—	15.0596	16.7813	17.0730	17.1463	15.3178	13.8233
6.00	8.3419	—	16.0892	17.2412	17.6030	18.2662	17.0928	15.5560
6.10	8.4846	—	16.7703	17.7012	18.1330	19.3931	18.2738	16.7372
6.20	8.6273	—	17.4427	18.1612	18.6630	20.5120	19.4614	17.9315
6.30	8.7700	—	18.1069	18.6212	19.1930	21.6135	20.6575	19.1388
6.40	8.9127	—	18.7642	19.0812	19.7240	22.7156	21.8627	20.3556
6.50	9.0554	—	19.4147	19.5412	20.2550	23.8144	23.0724	21.5838
6.60	9.1981	—	20.0588	20.0012	20.7860	24.9057	24.2820	22.8246
6.70	9.3408	—	20.7067	20.4612	21.3170	25.9948	25.4964	24.0719
6.80	9.4835	—	21.3318	20.9212	21.8480	27.0862	26.7197	25.3268

the second degree pressure gradient term  $(\partial p/\partial r)^2$  does not appear for an ideal gas. Second, Eq. 28 has the form of the diffusivity equation, but the diffusivity is proportional to pressure. Viscosity is a function of temperature, but not of pressure for an ideal gas. Aronofsky and Jenkins found that for constant rate production of an ideal gas from a closed radial system, the pressure at the producing well could be correlated as a function of a dimensionless time based on a compressibility evaluated at the initial pressure. The correlation was slightly sensitive to the production rate, but not sensitive enough to affect engineering accuracy.

Aronofsky and Jenkins demonstrated that production of ideal gas from a closed radial system could be approximated very closely from the solutions for transient liquid flow of van Everdingen and Hurst.<sup>10</sup> Matthews<sup>11</sup> later pointed out the application of this conclusion to pressure build-up analysis for gas wells as a liquid case analog.

For radial flow of a real gas, Eq. 18 becomes:

$$\frac{\partial^2 m(p)}{\partial r^2} + \frac{1}{r} \frac{\partial m(p)}{\partial r} = \frac{\phi \mu(p) c_r(p)}{k} \frac{\partial m(p)}{\partial t} \quad (29)$$

The close analogy between Eqs. 28 and 29 suggests that the real gas pseudo-pressure  $m(p)$  should correlate as a function of a dimensionless time based on viscosity and compressibility evaluated at the initial pressure, if the variation of the viscosity-compressibility product with  $m(p)$  for a real gas is similar to the variation of compressibility for an ideal gas  $(1/p)$  with pressure squared. Fig. 3 shows the comparison.

In view of the close resemblance between  $(\mu c_r)$  vs  $m(p)$  for the real gas, and  $p'$  vs  $p^2$  for the ideal gas, it is reasonable to expect solutions for the flow of real gases to correlate as functions of a dimensionless time based on initial values of viscosity and compressibility. That is, let:

$$t_D = \frac{kt}{\phi(\mu c_r)_i r_w^2} \quad (30)$$

Further, define a dimensionless real gas pseudo-pressure drop  $m_D(r_D, t_D)$ :

$$m_D(r_D, t_D) = \frac{\pi khT_w [m(p_i) - m(r, t)]}{q_i p_i T} \quad (31)$$

where  $r_D = r/r_w$ . The dimensionless real gas pseudo-

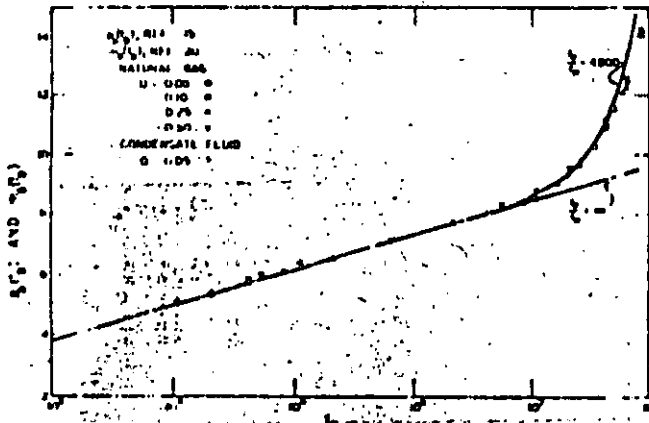


FIG. 3 PRESSURE-DEPENDENT DIFFUSIVITY TERMS VS POTENTIAL FOR IDEAL AND REAL GAS FLOW.

pressure drop is thus analogous to the van Everdingen-Hurst<sup>10</sup> dimensionless pressure drop  $p_D(r_D, t_D)$ .

Fig. 4 shows the comparison between  $p_D(t_D)$  for the liquid flow solutions and  $m_D(t_D)$  obtained from Eilerts *et al.*<sup>12</sup> solutions for the radial flow of natural gases. The solid line represents the liquid case, while points shown are computed from the Eilerts *et al.* solutions. As can be seen, the comparison is excellent for the entire range of flow considered by Eilerts *et al.* for both natural gases and condensate gases. The transient flow data computed by Carter<sup>13</sup> correlate just as well. The Eilerts *et al.* data are a severe test of the linearization of the real gas flow equation, because production included a ten-fold range in production rate, and almost complete depletion over a pressure range from 10,000 to 1,000 psi. Carter's results covered a range from 4,700 to 1,180 psia, and a more restricted range of flow rate.

The  $m_D(t_D)$  correlation (Fig. 4) is actually not as good as it appears. Although it is quite good at times before the boundary effect is felt, at long times there may be a considerable difference between  $m_D(t_D)$  and  $p_D(t_D)$  values

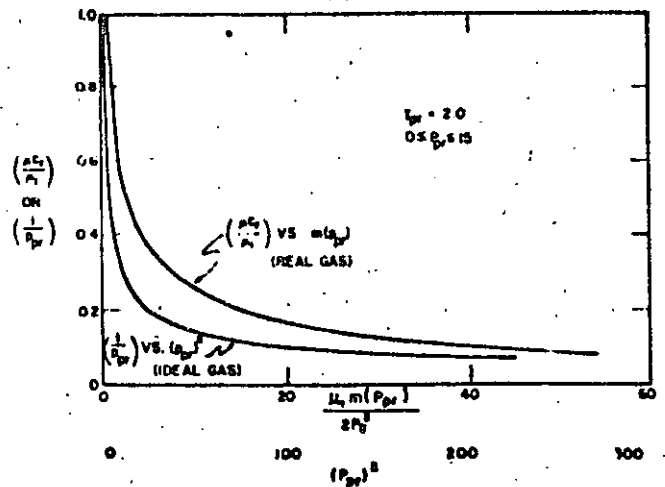


FIG. 4— $p_D(t_D)$  AND  $m_D(t_D)$  VS  $t_D$  FOR A CLOSED RADIAL RESERVOIR PRODUCED AT CONSTANT RATE.

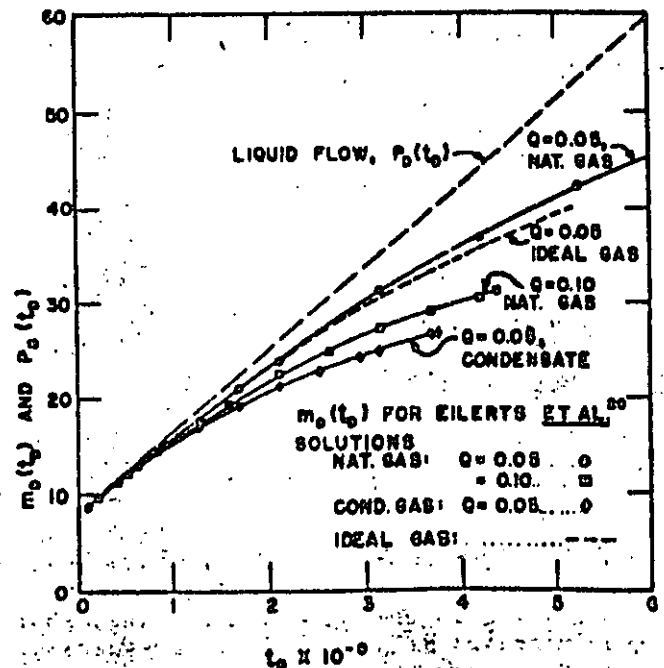


FIG. 5  $m_D(t_D)$  AND  $p_D(t_D)$  VS  $t_D$  FOR RADIAL FLOW OF LIQUID, IDEAL GAS AND REAL GASES.

(Fig. 5). Also shown on Fig. 5 are the Aronofsky-Jenkins<sup>10</sup> ideal gas flow results. It is clear that both the ideal and real gas cases lead to dimensionless pressure drops which are lower than the liquid case—and which are flow-rate dependent. Another important difference is illustrated by the case  $Q = 0.05$ . The ideal gas line terminates at the point where the well pressure is zero. The real gas solutions terminate at a well pressure of 10 per cent of the initial pressure. Although not shown on Fig. 5, the production times for the real gas cases to reach a limiting production pressure are about two and a half times that required for the ideal gas flow cases. Clearly, production forecasts based on the ideal gas solutions will be far too conservative.

Another important observation can be made from Fig. 5 by comparing the real gas solutions for natural gas and condensate for a flow rate  $Q$  of 0.05. Although the natural gas line is close to the liquid case, the condensate line is far below the liquid case line. The terminal producing pressure is reached earlier for the condensate line than for the natural gas line. This indicates the importance of gas property variations upon the results. That is, no single set of  $m_i(t_w)$  correlations could be expected to apply to all real gases at long production times. It is also clear from Fig. 5 that the real gas results tend to approach the liquid case results as flow rate decreases, and at small production times.

Aronofsky and Jenkins introduced the concept of a transient drainage radius  $r_w$ . This term should not be confused with the dimensionless radial coordinate  $r_w$ . From the Aronofsky-Jenkins definition of the transient drainage radius, we write for real gas flow:

$$\ln \frac{r_w}{r_e} = \frac{\pi khT_w}{q_w p_w T} [m(\bar{p}) - m(p_w)] = m_i(p_w) - m_i(\bar{p}) \quad (32)$$

The Eilerts *et al.*<sup>10</sup> results can also be correlated as transient drainage radii vs dimensionless time. The results are presented in Fig. 6, and agree with the Aronofsky-Jenkins results and the liquid flow results almost exactly. Actually, the correlation of the real gas flow solutions in terms of the transient drainage radius (Fig. 6) is a much better correlation than the correlation in terms of  $m_i(t_w)$  (Figs. 4 and 5). The drainage radius correlation is excellent for all values of production time. Thus, Eq. 32 provides the most useful engineering approach to the transient flow of real gases. As recommended by Jenkins and Aronofsky for ideal gas flow, the transient drainage radius for real gas flow can be found from:

$$\ln \frac{r_w}{r_e} = p_d(t_w) - 2t_w \left( \frac{r_w}{r_e} \right)^2 \quad (33)$$

and the  $m(\bar{p})$  can be found from the materials balance:

$$\left( \frac{p}{z} \right) - \left( \frac{\bar{p}}{\bar{z}} \right) = \frac{T p_w q_w}{\pi h r_w^2 \phi T_w} = \frac{1}{2} \int_{m(\bar{p})}^{m(p_w)} (\mu c_w)_{avg} dm(p) \approx \frac{(\mu c_w)_{avg}}{2} [m(p_w) - m(\bar{p})] \quad (34)$$

Eqs. 32 through 34 are not strictly a solution to Eq. 18. They represent an excellent engineering approximation which applies for a wide range of conditions. The method appears to be every bit as good as the Jenkins-Aronofsky result for ideal gas flow.

Fig. 6 shows that at long production times  $r_w$  takes the constant value 0.472  $r_e$ . This is similar to the Aronofsky-

Jenkins finding for ideal gas. Substitution of long-time values for  $p_w(t_w)$  in Eq. 33 also leads to this conclusion. Thus, Eq. 32 becomes similar in form to the liquid case pseudo-steady-state equation, at times long enough that the outer boundary effect is controlling. The fact that  $r_w$  eventually becomes constant at 0.472  $r_e$  does not mean the physical drainage radius stabilizes about half-way out in the reservoir. The entire reservoir volume is being drained, as can be seen by inspection of any of the Eilerts *et al.*<sup>10</sup> production figures.

The Eilerts *et al.* solutions have provided an excellent set of information to test the linearization of the real gas flow solutions for production. Eilerts *et al.* specified that the effective permeability was a function of pressure (assuming pressure drop would result in condensation and reduction of effective permeability). Effective permeability can thus be taken within the  $m(p)$  integral. Correlations in Figs. 4 through 6 do include a pressure-dependent permeability. Thus, if an approximation of the effect of pressure drop upon liquid condensation and reduction in permeability near the wellbore can be made, the performance can be estimated from:

$$\ln \frac{r_w}{r_e} = \frac{\pi h T_w}{q_w p_w T} [m'(\bar{p}) - m'(p_w)] \quad (35)$$

where

$$m'(p) = 2 \int_{p_w}^p \frac{k p dp}{\mu z} \quad (36)$$

and  $k$  is a known function of pressure.

The usefulness of considering  $k$  a function of pressure to handle condensate flow might be open to question. Nevertheless, it is clearly indicated that variation of  $k$  as a function of pressure can be included in the real gas pseudo-pressure.

Correlation of the Eilerts *et al.*<sup>10</sup> data presented previously involves calculation of  $m(p)$  and determination of relationships between the Eilerts *et al.* nomenclature and that used in this paper. (Necessary relationships are in the Appendix).

Eilerts *et al.*<sup>10</sup> also determined performance with a steady-state, non-Darcy flow region near the producing well. As a result, a steady-state skin effect can also be introduced to yield the following approximation for the radial flow of real gases during production:

$$\frac{\pi khT_w [m(\bar{p}) - m(p_w)]}{q_w p_w T} = \ln \frac{r_w}{r_e} + s + Dq_w \quad (37)$$

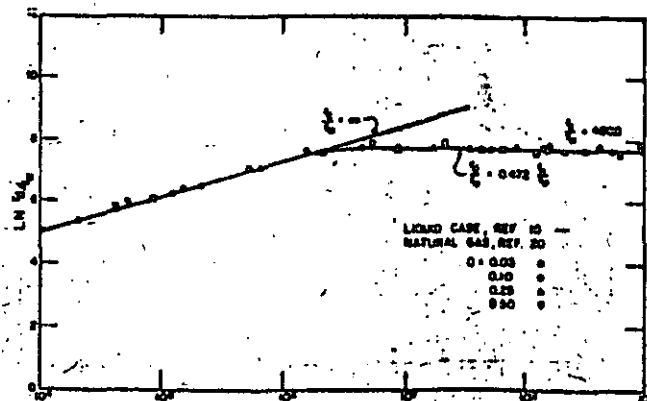


FIG. 6—JENKINS-ARONOFSKY DRAINAGE RADIUS VS  $t_w$  FOR A CLOSED-RADIAL RESERVOIR PRODUCED AT CONSTANT RATE.



where  $\alpha$  is the skin effect and  $D$  is the non-Darcy flow coefficient.

CONSTANT RATE INJECTION

All of the preceding discussion of real and ideal gas transient flow deals with *production* only. Injection results, as was clearly shown by Aronofsky and Jenkins<sup>27</sup> for radial ideal gas flow, cannot be linearized in as simple a fashion. Aronofsky and Jenkins correlated injection well pressures for radial flow of an ideal gas as functions of a dimensionless time based on gas compressibility evaluated at the initial formation pressure before injection. The dimensionless pressure rise at a given dimensionless time was generally greater than that for a liquid case, and increased with injection rate. Aronofsky and Jenkins showed that injection case results were very close to the liquid case for low injection rates. Although injection is of practical importance in itself, the major utility of injection case correlations is in application of the principle of superposition to generate variable rate production cases, including the important pressure build-up case.

Superposition, as it has been applied in gas well testing, requires that dimensionless times for both injection and production be based on the same gas physical property evaluation. Although superposition could be based on different dimensionless times for injection and production, the added complexity of such a case does not appear justified. Thus, an obvious question is: will injection solutions correlate closer to the liquid case if dimensionless time are based on physical properties evaluated at a pressure above the initial, low formation pressure?

We rule out the scheme of using a point evaluation at the existing injection pressure because this would yield a result not usable for forecasting. That is, it would be necessary to know the injection pressure-time history before it could be calculated. An obvious possibility is to evaluate physical properties at the final, elevated injection pressure, or in the case of superposition applied to reservoir production or build-up, at the initial formation pressure before production was started. This idea is fundamentally the basis for all gas well pressure build-up applications currently in use.

In brief, correlations for injection based on an elevated pressure are no better (or worse) than those based on physical properties evaluated at the initial, low formation pressure. This is true for both the ideal and real gas flow cases. Fig. 7 presents the dimensionless real gas potential rise for the Eilerts *et al.*<sup>28</sup> injection case (their Fig. 8) correlated vs dimensionless times based on both the initial, low formation pressure and the final injection pressure. The dashed line presents the liquid flow solution. Two facts are apparent, the slopes of the correlations are similar, and correlations based on final injection pressure are no worse than those based on initial, low formation pressure. From the Jenkins-Aronofsky studies of ideal gas flow, we can also conclude that the difference between the injection case correlations and the liquid case become smaller as injection rate decreases; in any case, the differences aren't large.

Fig. 7 can lead to another idea. Correlation based on a dimensionless time evaluated with physical properties about half-way between the extremes might be quite good. This idea follows immediately from the *theorem of the mean*. That is, if flowing fluid physical properties vary monotonically with potential, the proper result is limited by those evaluated at the extreme values of physical properties. Friedmann<sup>29</sup> proved that results must lie between those evaluated at the extremes of physical

properties whether physical properties are monotonic functions or not. The injection problem has been the subject of much investigation in the fields of heat transmission and ground-water movement (Friedmann,<sup>29</sup> Storm<sup>30</sup> and Polubarinova-Kochina<sup>31</sup>). As has been shown by these authors, it cannot always be assumed that evaluation at an average property will yield good results. Sometimes the answer will vary from one extreme to the other.

SUPERPOSITION OF LINEARIZED SOLUTIONS

Superposition is rigorously correct only for linear partial differential equations. Nevertheless, the extremely close check between the linearized real gas solutions correlated on the basis of the  $m_D(t_D)$ , as given by Eq. 31, and a  $t_D$  given by Eq. 30, and the liquid flow solutions of van Everdingen and Hurst, indicates the possibility that superposition might be quite good for matching an increasing rate production schedule. An increasing rate

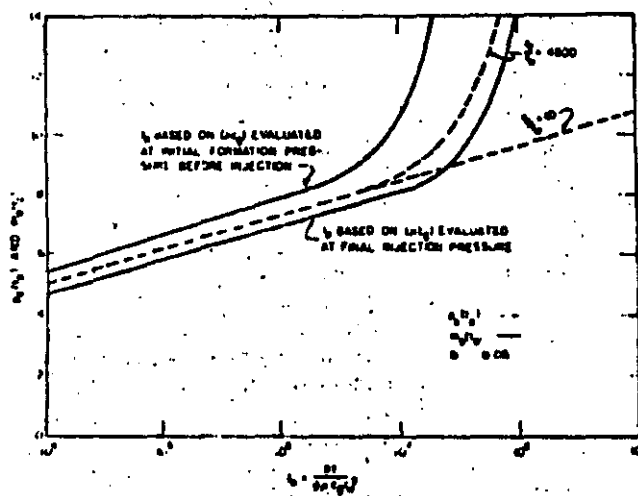


FIG. 7.  $m_D(t_D)$  vs  $t_D$  FOR INJECTION OF A REAL GAS (CORRELATION OF EILERTS *et al.*<sup>28</sup> DATA).

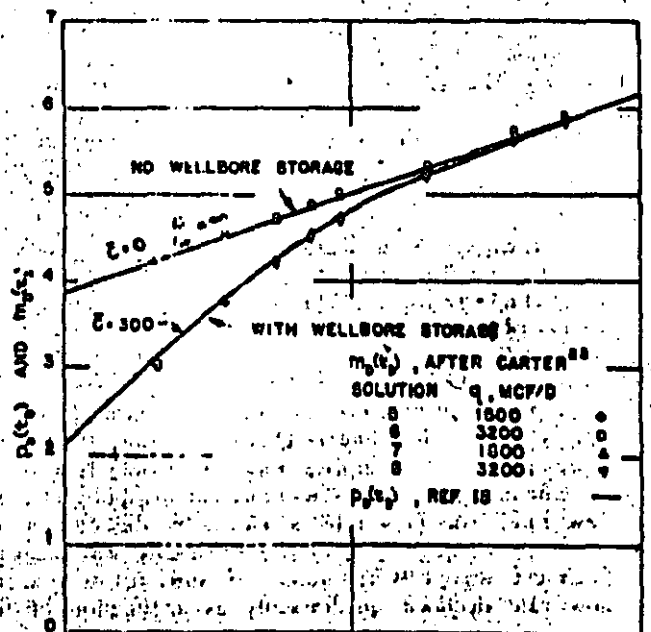


FIG. 8.  $p_D(t_D)$  AND  $m_D(t_D)$  vs  $t_D$  FOR CONSTANT RATE PRODUCTION WITH WELLBORE STORAGE.

schedule would require superposition of positive incremental rates. However, the real gas flow solutions do depend slightly upon production rate. Thus, the only way that the application of the principle of superposition (as an acceptable approximation) to real gas flow can be established is by comparison with finite-difference solutions of variable-rate, real gas flow problems.

Such a comparison can be made for an increasing production rate schedule from data for real gas flow published by Carter.<sup>22</sup> Carter studied the effect of wellbore storage on gas production. For his solutions, it was assumed that the surface flow rate was held constant, but 0.02965 Mcf was withdrawn from the wellbore per psi pressure drop in the wellbore. This resulted in the sand face flow rate increasing as a function of time toward the constant surface flow rate. This case is almost exactly analogous to the wellbore unloading case presented by van Everdingen and Hurst<sup>23</sup> in their Eq. VIII-11. The wellbore storage constant  $\bar{C}$  for Carter's solutions can be determined from Eq. 6 presented by Ramey.<sup>24</sup> The value of  $\bar{C}$  for Carter's solutions does vary slightly with pressure, but a value of 300 is quite good. Fig. 8 presents a comparison between the  $m_e(t_n)$  obtained from Carter's solutions, both with and without wellbore storage, and the van Everdingen-Hurst  $p_e(t_n)$  solutions for the liquid flow case. As can be seen, the comparison with constant rate liquid flow *without* storage is excellent. This was previously shown for the Eilerts *et al.*<sup>25</sup> solutions. Of more interest, the comparison between the liquid flow case *with* wellbore storage and Carter's two solutions with wellbore storage are also excellent. This establishes that superposition of the linearized real gas flow solutions for an increasing flow rate should be a very good approximation—at least before outer boundary effects are controlling.

Although superposition in an increasing production rate schedule appears quite good, it is not apparent that a *decreasing* rate schedule is susceptible to superposition. This results because the dimensionless real gas injection pressure increases do not correlate with the liquid case as well as do production data. Even for transient injection of an ideal gas,<sup>26</sup> the resulting dimensionless pressure rise appears to depend upon injection rate, but does approach the liquid case solution as injection rate decreases. The fact that injection results do approach the liquid case as injection rate approaches zero suggests that superposition of small *positive* incremental rates (injections) would be feasible. Again, the possibility can only be checked by comparison with finite-difference solutions.

Fortunately, both Carter<sup>22</sup> and Dykstra<sup>27</sup> have presented finite-difference solutions for decreasing flow-rate production. Dykstra's data provide an excellent set for comparison of finite-difference solutions with superposition of the linearized solutions. Fig. 9 presents a comparison of Dykstra's computed flowing pressures with those obtained by superposition of linearized real gas flow solutions. The line is Dykstra's result, while points represent results of superposition using only four or five incremental rate changes to represent a rapidly changing flow rate. The flow rate is shown by the dashed line. For the example shown, the permeability was 0.25 md, thickness was 179 ft, initial pressure 6,150 psia and flow rate declined quadratically as a function of time from 6,556 to 2,500 Mcf/D by 50 days' producing time. Superposition was accomplished using dimensionless times based on the *initial* pressure and the  $m_e(t_n)$  taken equal to the liquid case  $p_e(t_n)$  values. The maximum difference between Dykstra's result and those computed by super-

position was 20 psi out of a drawdown of 2,150 psi—a difference of 0.9 per cent. The 50-day production period was long enough that initial rate changes were influenced by the outer boundary. Thus, we conclude that superposition can be used to reproduce variable-rate drawdown data with acceptable accuracy.

The previous remarks concerning superposition of incremental rate *increases* are, of course, directly applicable to pressure build-up testing. Although insufficient comparisons between finite-difference build-up solutions and superposition solutions for the real gas flow case have been made to completely explore this problem, it does appear that build-up theory can be used with good accuracy. An interesting test of pressure build-up can be made by comparison of Dykstra's<sup>27</sup> solutions with superposition solutions. Because Dykstra's cases involved a variable-rate production period, permeability was low and pressure gradients high, it is believed that a fairly extreme test results. Fig. 10 presents the build-up following the drawdown of Fig. 9. As can be seen, the

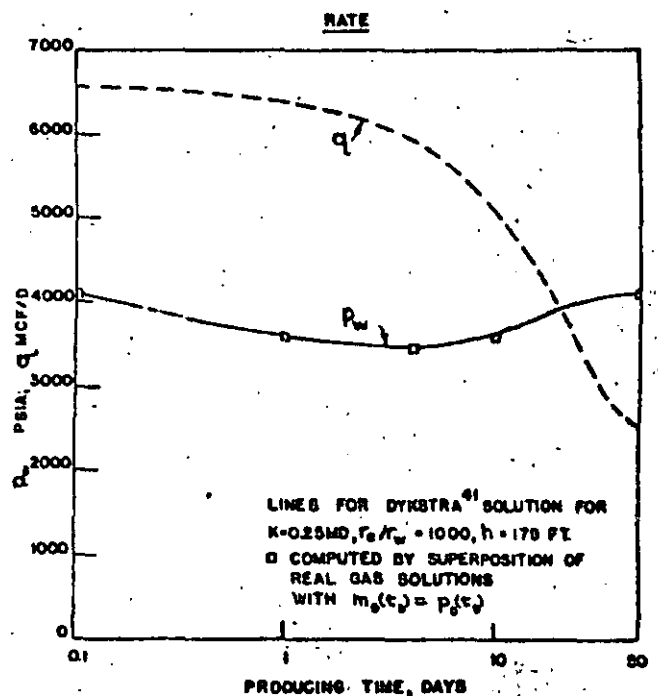


FIG. 9 COMPARISON OF FINITE DIFFERENCE AND SUPERPOSITION FLOWING PRESSURES FOR A DECREASING PRODUCTION RATE.

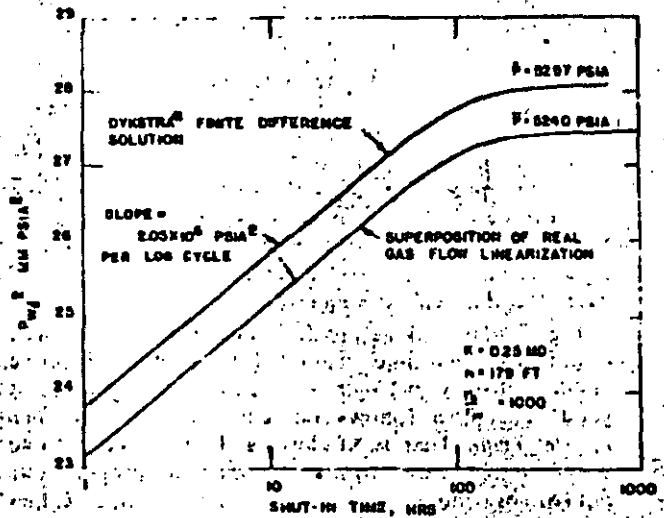


FIG. 10 COMPARISON OF FINITE DIFFERENCE AND SUPERPOSITION BUILD-UP PRESSURES FOR A REAL GAS.

superposition result yields a similar build-up curve of identical slope, but about 60 psi below Dykstra's finite-difference solutions. Again, the percentage difference is small; the final static pressure is about 1.1 per cent too low. It appears that superposition of the real gas flow linearization will always yield a pressure build-up static pressure that is too low, but as good or better than results of current methods. Furthermore, field application would be to the field measured data—the real solution—which would tend to correct for this error. We conclude that pressure-build-up analysis based on superposition can be done for real gas flow with acceptable accuracy, but that further study of pressure build-up for real gas flow is desirable.

**STEADY-STATE AND PSEUDO-STEADY-STATE FLOW**

Radial gas flow at constant production rate will be considered. A horizontal homogeneous porous medium of constant thickness  $h$  with impermeable upper and lower boundary, and a well of radius  $r_w$  located in the center of a radial reservoir, constitutes the flow system. The outer radius  $r_e$  represents either the real boundary or the radius of drainage. Two cases will be considered: (1) constant pressure at  $r_e$ , and (2) no flow across  $r_e$ .

**CONSTANT PRESSURE AT OUTER BOUNDARY**

The steady-state equation for a real gas in axisymmetrical coordinates can be written from Eq. 22 as:

$$\frac{1}{r} \frac{d}{dr} \left[ r \frac{dm(p)}{dr} \right] = 0 \quad (38)$$

The boundary conditions for two concentric cylinders of radii  $r_e$  and  $r_w$  are:

$$r = r_e : m(p) = m(p_e) \quad (39)$$

$$r = r_w : m(p) = m(p_w) \quad (40)$$

Integrating Eq. 38 and using the boundary conditions, the steady-state pressure distribution in the system is:

$$m(p) = m(p_e) + \frac{q \cdot p_e \cdot T}{\pi k h T_{sc}} \left( \ln \frac{r}{r_e} \right) \quad (41)$$

Eq. 41 can be evaluated for  $p = p_w$  at  $r = r_w$  and rearranged to provide an equation analogous to the normal radial flow equation:

$$q = \frac{\pi k h T_{sc} [m(p_e) - m(p_w)]}{T p_e \ln \frac{r_e}{r_w}} \quad (42)$$

Both Eqs. 41 and 42 are in darcy, or cgs units. Thus, the  $m(p)$  have the units of sq atm/cp.

**NO FLOW ACROSS OUTER BOUNDARY**

As was shown previously by Eq. 32 and Fig. 6, at long times, a flow equation for the closed outer boundary, constant mass rate production, radial flow case can be written:

$$\ln \frac{r_e}{r_w} = \ln \frac{0.472 r_e}{r_w} + \frac{\pi k h T_{sc}}{q \cdot p_e \cdot T} [m(\bar{p}) - m(p_e)] \quad (43)$$

Since the  $m(\bar{p})$  values were determined from a materials balance, the  $\bar{p}$  argument represents the average pressure which would yield the proper average density, or the

static pressure following a complete pressure build-up. It is *not* a volumetric average pressure. Eq. 43 coupled with the normal material balance for a bounded drainage volume provides a useful means to couple production rate and gas recovery.

In the case of liquid flow, an equation similar to Eq. 43 can be derived using the concept of pseudo-steady-state flow. That is, a condition is eventually reached for constant rate liquid production when the rate of pressure decline becomes constant everywhere in the reservoir. This condition is expressed mathematically by setting the Laplacian of the pressure equal to a constant (other than zero). Although it can be shown that the Laplacian of pressure-squared for an ideal gas, or the Laplacian of the real gas pseudo-pressure cannot be equal to a constant rigorously, a flow condition similar to pseudo-steady-state does appear to exist for both ideal and real gas flow, for all practical purposes. The existence of such a condition is suggested by Eq. 43. Fig. 11 presents an interesting inspection of the pressure behavior during the period that Eq. 43 applies for one of the Eilerts *et al.* cases. Also shown is the  $p_e(t_e)$  for comparison with the liquid case. As was seen previously in Fig. 5, the  $m_e(t_e)$  does not change at a constant rate during this period. Although it matches the liquid case solution at early times, eventually the  $m_e(t_e)$  drops below the liquid case solution. The most interesting feature of Fig. 11, however, is that the  $m_e(r_w, t_e)$  for all radial locations are essentially parallel. Thus, the  $m(p)$  profile is essentially independent of time. This condition can be described approximately by setting the Laplacian of  $m(p)$  equal to a constant. As shown in Refs. 39 and 42, this leads to an equation similar to Eq. 32, but in terms of an average  $\bar{m}(p)$  rather than  $m(p)$ . Although it can be shown that these two averages tend to be equivalent for practical ranges of conditions, it does not appear worthwhile to show the development here. In any event, Eq. 32 describes the long-time flow behavior of closed radial systems with remarkable accuracy.

Another consequence of inspection of Fig. 11 is that the  $m(p)$  distribution can be obtained readily. For ex-

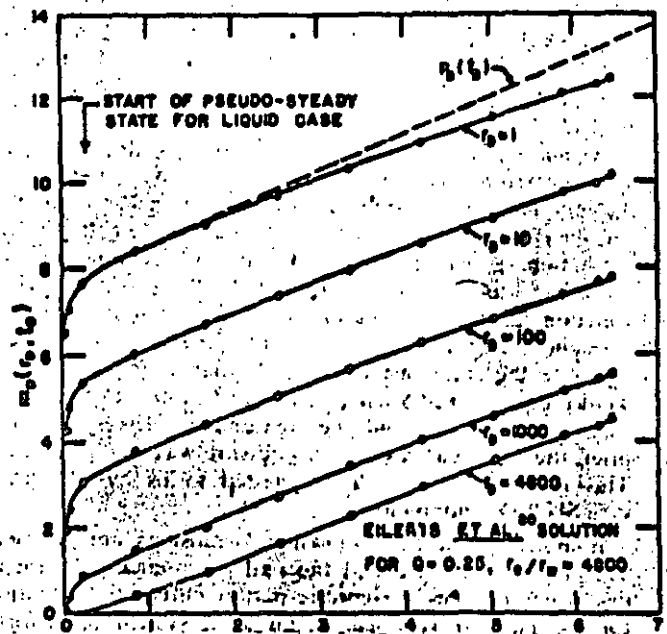


Fig. 11  $m_e(r_w, t_e)$  vs  $\ln \frac{r}{r_w}$  FOR CONSTANT RATE PRODUCTION OF A REAL GAS FROM A CLOSED RADIAL RESERVOIR.

ample, the following equation also describes flow reasonably well:

$$\ln\left(\frac{0.0016 r_e}{r_w}\right) = \frac{2khT}{q \mu z} [m(p_e) - m(p_w)] \quad (44)$$

## DISCUSSION AND CONCLUSIONS

The purpose of the preceding was to describe fundamental considerations which can be used successfully to analyze the flow of real gases. The concept of the real gas pseudo-pressure promises a considerable simplification and improvement in all phases of gas well testing analysis and gas reservoir calculations. Such applications will be described in useful engineering form in a companion paper.

Several remarks concerning the real gas pseudo-pressure are in order. No claim of originality can be made for the substitution we have called the *real gas pseudo-pressure*. Carslaw and Jaeger<sup>10</sup> reviewed application of a similar transformation which was used in solution of heat conduction problems as early as 1894 and the early 1930's. Recently, McMoradie<sup>11</sup> pointed out the utility of this sort of transformation in heat conduction problems. There have even been numerous mentions of the use of a transformation similar to the  $m(p)$  function in connection with flow through porous media. In 1949, Muskat<sup>12</sup> used the same transformation in a discussion of the theory of potentiometric models. In 1953, Leibenzon<sup>13</sup> used the transformation, and Russian authors refer to it as the Leibenzon transformation. In 1951, Fay and Prats<sup>14</sup> discussed use of a similar transformation in connection with transient liquid flow. In 1955, Atkinson and Crawford<sup>15</sup> evaluated numerically a similar function but with constant viscosity. In 1962, Carter<sup>16</sup> used a gas mobility term  $M(p)$ , which was defined as:

$$M(p) = \frac{khp}{T\mu z}$$

Clearly, the  $m(p)$  function is proportional to the pressure integral of Carter's  $M(p)$ . In 1963, Hurst *et al.*<sup>17</sup> used a similar integral, but with constant viscosity. To our knowledge, however, this paper represents the first application of the real gas pseudo-pressure to linearization of transient real gas flow. Perhaps the most surprising fact is that the realization of the utility of this concept has been so long in coming.

In the original draft of this paper and the companion paper,<sup>16</sup> we called the  $m(p)$  function the *real gas potential*. It was stated in those papers that the  $m(p)$  transformation was not a true potential. Carslaw and Jaeger<sup>10</sup> termed a similar substitution in heat conduction an *effective potential*, while Muskat<sup>12</sup> called the transformation a *potential* as a matter of convenience. We feel that the  $m(p)$  transformation will be an important function in gas reservoir engineering, and it is important that the function be given a suitable name. If we were to name the transformation as Russian authors have, we would call it the Muskat transformation. In the belief that the name should be reasonably descriptive and brief, the term real gas pseudo-pressure was finally selected. This name was originally suggested to us by M. Prats, with Shell Development Co.

It appears that the following conclusions are justified. The transformation called the real gas pseudo-pressure in this paper reduces a rigorous partial differential equation for the flow of real gas in an ideal system to a form similar to the diffusivity equation, but with potential-dependent diffusivity. Because the variation of the dif-

fusivity of real gas with pressure was similar to that of an ideal gas, it was possible to correlate finite difference solutions for the ideal radial production of real gas from a bounded system with the liquid flow solutions of van Everdingen and Hurst, and the ideal gas solutions of Aronofsky and Jenkins. This correlation avoids the assumption of small pressure gradients in the reservoir and offers generally useful solutions for the radial flow of real gas.

An investigation of the injection of real gas into a bounded radial system also gave a reasonable correlation—but not as good a correlation as production data. The correlation was as good as, or better than, the correlation of ideal gas flow results made by Aronofsky and Jenkins.

An investigation of the possibility of superposition of the linearized results indicated that superposition can be used as an acceptable engineering approximation to generate variable rate flow of real gases in a radial system. Pressure build-up for real gas flow was thus justified for the first time. (No justification for pressure build-up for the non-linear problem of ideal gas flow has yet been presented.)

Accurate and simple equations can be written to describe unsteady flow of real gases which properly consider variation of gas physical properties.

## NOMENCLATURE

- $\nabla$  = grad
- $\nabla \cdot$  = divergence
- $\nabla^2$  = Laplacian operator
- $A$  = area, sq cm
- $b$  = slope of a straight line in a plot of  $k(p)$  vs  $1/p$
- $c_g(p)$  = real gas compressibility defined by Eq. 10
- $h$  = thickness, cm
- $k(p)$  = effective permeability, darcies
- $M$  = molecular weight
- $m(p)$  = real gas pseudo-pressure defined by Eq. 14
- $p$  = pressure, atm
- $q$  = flow rate, cm<sup>3</sup>/sec
- $r$  = radius, cm
- $R$  = gas constant
- $t$  = time, sec
- $T$  = temperature, °K
- $v$  = velocity, cm/sec
- $V$  = pore volume, cm<sup>3</sup>
- $x, y, z$  = direction notation
- $z(p)$  = gas deviation factor, a function of pressure at constant temperature
- $\rho$  = density, gm/cm<sup>3</sup>
- $\mu(p)$  = real gas viscosity, a function of pressure at constant temperature, cp
- $\mu_a$  = viscosity at atmospheric pressure, cp
- $n$  = normal distance scale
- $\phi$  = hydrocarbon porosity, fraction

## SUBSCRIPTS

- $e$  = external boundary
- $l$  = liquid
- $pc$  = pseudo-critical
- $r$  = radius
- $sc$  = standard conditions
- $w$  = internal boundary, the well

## ACKNOWLEDGMENTS

The authors wish to acknowledge financial support of the Texas A&M U., the Texas Engineering Experiment Station of Texas A&M and the Texas Petroleum Research Committee. This paper represents a composite of research effort conducted over a period of time by several agencies. Crawford first evaluated the  $m(p)$  function during the past decade. Use of the  $m(p)$  function and a more recent evaluation of the function were described by Al-Hussainy.<sup>2</sup> The authors also wish to acknowledge the encouragement in the course of this study by R. L. Whiting. Portions of this work were done by Al-Hussainy in partial fulfillment of graduate degree requirements in petroleum engineering at Texas A&M U. Finally, and sincerely, the authors wish to acknowledge the numerous helpful suggestions made by the reviewers of the original draft of this paper.

## REFERENCES

- Muskat, M.: *The Flow of Homogeneous Fluids*, J. E. Edwards, Inc., Ann Arbor, Mich. (1946).
- Katz, D. L., Correll, D., Kobayashi, R., Poettman, F., Vary, J. A., Elenbaas, J. R. and Weinung, C. F.: *Handbook of Natural Gas Engineering*, McGraw-Hill Book Co. Inc., New York, N. Y. (1959).
- Heatherington, C. R., MacRoberts, D. T. and Huntington, R. L.: "Unsteady Flow of Gas Through Porous Media", *Trans., AIME* (1912) 146, 166.
- MacRoberts, D. T.: "Effect of Transient Conditions in Gas Reservoirs", *Trans., AIME* (1919) 186, 36.
- Jameck, J. D. and Katz, D. L.: "Applications of Unsteady State Gas Flow Calculations", paper presented at Research Conference on Flow of Natural Gas Reservoirs, U. of Michigan Ann Arbor, Mich. (June 30, 1955).
- Correll, D. and Katz, D. L.: "Pressure Gradients in Natural Gas Reservoirs", *Trans., AIME* (1953) 198, 61.
- Rowan, G. and Clegg, M. W.: "An Approximate Method for Transient Radial Flow", *Soc. Pet. Eng. Jour.* (Sept., 1962) 225.
- Green E. and Wilt, C. H.: "Non-steady Flow of Gas Through a Porous Wall", *Proc., First U. S. National Congress Applied Mechanics*, J. E. Edwards, Inc., Ann Arbor, Mich. (1962) 777.
- Aronofsky, J. S. and Jenkins, R.: "Unsteady Flow of Gas Through Porous Media: One-dimensional Case", *Proc., First U. S. National Congress Applied Mechanics*, J. E. Edwards, Inc., Ann Arbor, Mich. (1952) 763.
- Jenkins, R. and Aronofsky, J. S.: "Unsteady Radial Flow of Gas Through Porous Media", *Jour. Appl. Mech.* (1951) 20, 210.
- Huey, C. D., Peaceman, D. W., Rachford, H. H. and Rice, J.: "Calculations of Unsteady-State Gas Flow Through Porous Media", *Trans., AIME* (1953) 198, 79.
- Douglas, J., Jr., Peaceman, D. W. and Rachford, H. H.: "Calculation of Unsteady-State Gas Flow in a Square Reservoir", *Trans., AIME* (1955) 204, 190.
- Aronofsky, J. S.: "Effect of Gas Slip on Unsteady Flow of Gas Through Porous Media", *Jour. Appl. Phys.* (1954) 25, 48.
- Aronofsky, J. S. and Jenkins, R.: "A Simplified Analysis of Unsteady Radial Gas Flow", *Trans., AIME* (1954) 201, 149.
- van Everdingen, A. F. and Hurst, W.: "The Application of the Laplace Transformation to Flow Problems in Reservoirs", *Trans., AIME* (1949) 186, 305.
- Aronofsky, J. S. and Ferris, O. D.: "Transient Flow of Non-ideal Gases in Porous Media—One dimensional Case", *Jour. Appl. Phys.* (1951) 23, 289.
- Aronofsky, J. S. and Potter, J. D.: "Unsteady Radial Flow of Gas Through Porous Media: Variable Viscosity and Compressibility", *Jour. Appl. Mech.* (1956) 23, 128.
- Carter, R. D.: "Solutions of Unsteady-State Radial Gas Flow", *Jour. Pet. Tech.* (May, 1962) 549.
- Elliott, C. K.: "Integration of Partial Differential Equation for Transient Linear Flow of Gas-Condensate Fluids in Porous Structures", *Soc. Pet. Eng. Jour.* (Dec., 1964) 291.
- Elliott, C. K., Sumner, E. F. and Potts, N. L.: "Integration of Partial Differential Equation for Transient Radial Flow of Gas-Condensate Fluids in Porous Structures", *Soc. Pet. Eng. Jour.* (June, 1965) 141.
- Swift, G. W. and Kiel, O. G.: "The Prediction of Gas Well Performance Including the Effect of Non-Darcy Flow", *Jour. Pet. Tech.* (July, 1962) 791.
- Tek, M. H., Coats, K. H. and Katz, D. L.: "The Effect of Turbulence on the Flow of Natural Gas Through Porous Reservoirs", *Jour. Pet. Tech.* (July, 1962) 799.
- Carter, R. D.: Supplemental Appendix to "Determination of Stabilized Gas Well Performance from Short Flow Tests", *API Doc. No. 7471*, Library of Congress, Washington, D. C.
- Rowan, G. and Clegg, M. W.: "An Approximate Method for Non-Darcy Radial Gas Flow", *Soc. Pet. Eng. Jour.* (June, 1964) 96.
- Roberts, R. C.: "Unsteady Flow of Gas Through a Porous Medium", *Proc., First U. S. National Congress Applied Mechanics*, J. E. Edwards, Inc., Ann Arbor, Mich. (1952) 773.
- Kiddler, R. E.: "Unsteady Flow of Gas Through a Semi-Infinite Porous Medium", *Jour. Appl. Mech.* (1957) 24, 329.
- Polubarinova-Kochina, P. Ya.: *Theory of Ground Water Movement*, Princeton U. Press, Princeton, N. J. (1962).
- Carlaw, H. S. and Jaeger, J. C.: *Conduction of Heat in Solids*, 2nd Ed., Oxford U. Press, London, England (1959) 11.
- Klinkenberg, L. J.: "The Permeability of Porous Media to Liquids and Gases", *Drill. and Prod. Prac.*, API (1941) 200.
- Fay, C. H. and Prats, M.: "The Application of Numerical Methods to Cycling and Flooding Problems", *Proc., Third World Petroleum Congress*, Section II (1951) 555.
- Standing, M. B. and Katz, D. L.: "Density of Natural Gases", *Trans., AIME* (1912) 146, 130.
- Carr, N. I., Kobayashi, R. and Burrows, D. H.: "Viscosity of Hydrocarbons Under Pressure", *Trans., AIME* (1951) 201, 264.
- Trube, A. S.: "Compressibility of Natural Gases", *Trans., AIME* (1957) 210, 69.
- Robinson, D. B., Macrygeorgas, C. A. and Govier, G. W.: "The Volumetric Behavior of Natural Gases Containing Hydrogen Sulfide and Carbon Dioxide", *Trans., AIME* (1960) 219, 51.
- Matthews, C. S.: "Analysis of Pressure Build-Up and Flow Test Data", *Jour. Pet. Tech.* (Sept., 1961) 862.
- Friedmann, N. E.: "Quasilinear Heat Flow", *Trans., ASME* (April, 1958) 635.
- Storm, M. L.: "Heat Conduction in Simple Metals", *Jour. Appl. Phys.* (July, 1951) 22, No. 7, 192.
- McMurdie, R. K.: "Steady-State Conduction With Variable Thermal Conductivity", *Trans., ASME* (Feb., 1962) 92.
- Al-Hussainy, R.: "Flow of Real Gases Through Porous Media", MS Thesis, Texas A&M U. (Jan., 1965).
- Ramey, H. J., Jr.: "Non-Darcy Flow and Wellbore Storage Effects in Pressure Buildup and Drawdown of Gas Wells", *Jour. Pet. Tech.* (Feb., 1965) 22A.
- Dykstra, H.: "Calculated Pressure Build-up for a Low Permeability Gas-Condensate Well", *Jour. Pet. Tech.* (Nov., 1961) 1131.
- Al-Hussainy, R., Ramey, H. J., Jr. and Crawford, P. B.: "The Theory of the Real Gas Potential", Paper No. 1243-A, presented at SPE Annual Fall Meeting, Denver, Colo. (Oct. 3-6, 1965).
- Muskat, M.: "The Theory of Potentiometric Models", *Trans., AIME* (1919) 179, 216.
- Lilientzon, L. S.: "Subsurface Hydraulics of Water, Oil and Gas", *Publ. Acad. Sci., collected works, U.S.S.R.* (1953) 2.
- Atkinson, D. O. and Crawford, P. B.: "Generalized Pressure Distribution and Gas Mass in Pipe Lines", *Pet. Prod. Tech.*, AIME Conference Proc. of 1956, Miscellaneous Publication of the Texas Engineering Experiment Station (Sept., 1956) 59.
- Hurst, W., Goodson, W. C. and Leesor, R. E.: "Aspects of Gas Deliverability", *Jour. Pet. Tech.* (June, 1963) 668.
- Al-Hussainy, R. and Ramey, H. J., Jr.: "Application of the Real Gas Potential", Paper No. 1243-B, presented at the SPE Annual Fall Meeting, Denver, Colo. (Oct. 3-6, 1965).

APPENDIX

CORRELATION OF EILERTS *ET AL.* SOLUTIONS

Eilerts *et al.* solved the following equation numerically (in their nomenclature):

$$\frac{\partial}{\partial t} \left[ W(P) \frac{\partial P}{\partial t} \right] = \frac{\partial}{\partial r} \left[ \frac{r}{Z(P)} \right] \quad (A-1)$$

where

$$P = \frac{p}{p_i}, K(P) = \frac{k(p)}{k(p_i)}, z(P) = \frac{z(p)}{z(p_i)}, \rho(P) = \frac{\rho(p)}{\rho(p_i)}, w(P) = \frac{w(p)}{w(p_i)}, k(P)/\rho(P)z(P)$$

and

$$w(P) = w(p_i)W(P) \quad (A-2)$$

Dimensionless time is defined as:

$$H = \frac{\rho k(p_i)}{2\phi\mu(p_i)r_w^2} t \quad (A-3)$$

and the dimensionless radius:

$$U = \ln \frac{r}{r_w} \quad (A-4)$$

In terms of the  $m(p)$  function, and using the dimensionless variables Eq. A-2, the flow equation takes the form:

$$\frac{\partial}{\partial U} \left[ \frac{\partial m(P)}{\partial U} \right] = \frac{\phi_i \rho_i p_i^2 K(P) z(P)}{\rho k(p_i) K(P)} \frac{\partial m(P)}{\partial U} \quad (A-5)$$

where

$$m(P) = 2 \int_0^U PW(P)dP \quad (A-6)$$

Let the coefficient on the left side of Eq. A-5 be evaluated at the initial conditions, and define:

$$C = \frac{\phi_i \rho_i p_i^2}{\rho k(p_i) K(P)} \quad (A-7)$$

$$C_K(P) = \frac{2H}{C K(P)} \left( \frac{r_w}{r} \right)^2 \quad (A-8)$$

Notice that  $\rho(P)$  and  $K(P)$  are equal to one at the initial  $P$ . Hence, Eq. A-5 takes the form:

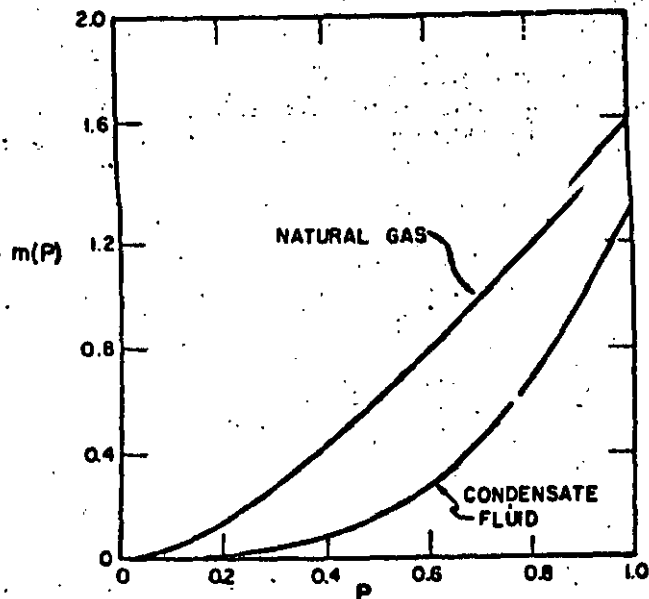


FIG. 12.  $m(P)$  VS  $P$  FOR THE EILERTS *ET AL.* GASES.

$$\frac{1}{r_w} \frac{\partial}{\partial r_w} \left[ r_w \frac{\partial m(P)}{\partial r_w} \right] = \frac{\partial m(P)}{\partial t_w} \quad (A-9)$$

The flow rate at the producing face as given by Eilerts *et al.* is:

$$Q = 2H(P) \frac{\partial P}{\partial U} = 2 \frac{\partial m(P)}{\partial U} \quad (A-10)$$

and the closed boundary:

$$\frac{\partial m(P)}{\partial U} = 0 \quad (A-11)$$

Thus, in terms of the dimensionless real gas pseudo-pressure drop:

$$m_w(r_w, t_w) = \frac{2}{Q} \Delta m(P) \quad (A-12)$$

The  $m(P)$  for the Eilerts *et al.* natural gas and condensate fluid are shown in Fig. 12. The large difference between physical properties of the two fluids is apparent.

\*\*\*

Appendix A

## Solutions for Radial Flow of Fluids of Small and Constant Compressibility

### Constant Rate, Infinite Reservoir Case

The initial value problem represented by this case is presented in Chapter 2. In summary, the mathematical problem which we must solve is:

$$\frac{\partial^2 p}{\partial r^2} + \frac{1}{r} \frac{\partial p}{\partial r} = \frac{\phi \mu c}{k} \frac{\partial p}{\partial t} \quad \dots \quad (A.1)$$

Boundary and initial conditions:

- (1)  $p = p_i$  at  $t = 0$  for all  $r$ .
- (2)  $\left( r \frac{\partial p}{\partial r} \right)_{r_w} = \frac{q \mu}{2 \pi k h}$  for  $t > 0$ .
- (3)  $p \rightarrow p_i$  as  $r \rightarrow \infty$  for all  $t$ .

As mentioned in the text, several slightly different approaches to the solution of this problem have appeared in the literature. We have chosen to present the approach of Polubarinova-Kochina<sup>1</sup> because it is quite straightforward. We are indebted to H. J. Ramey, Jr., for calling this approach to our attention.

To develop the solution, we first replace the second boundary condition by the condition

$$\lim_{r \rightarrow 0} r \frac{\partial p}{\partial r} = \frac{q \mu}{2 \pi k h}, \text{ for } t > 0.$$

This boundary condition is the "line-source" approximation to the original boundary condition. It has been shown to yield identical results (from a practical standpoint) with those obtained from solution of the problem with the original, less-tractable condition (see Mueller and Witherspoon<sup>2</sup>).

Fundamental to the solution is the use of the Boltzmann Transformation,

$$y = \frac{\phi \mu c r^2}{4 k t} \quad \dots \quad (A.2)$$

Substitution of Eq. A.2 into the differential Eq. A.1 and accompanying boundary conditions gives

$$y \frac{d^2 p}{dy^2} + \frac{dp}{dy} (1 + y) = 0, \quad \dots \quad (A.3)$$

with

$$(1) \quad p \rightarrow p_i \text{ as } y \rightarrow \infty,$$

$$(2) \quad \lim_{y \rightarrow 0} 2y \frac{dp}{dy} = \frac{q \mu}{2 \pi k h}.$$

To solve Eq. A.3 let  $p' = \frac{dp}{dy}$ .

Then Eq. A.3 becomes

$$y \frac{dp'}{dy} + (1 + y) p' = 0. \quad \dots \quad (A.4)$$

Separation of the variables and integration yield

$$\ln p' = - \ln y - y + C$$

or

$$p' = \frac{dp}{dy} = \frac{C_1}{y} e^{-y}. \quad \dots \quad (A.5)$$

$C$  and  $C_1$  are constants of integration.

From boundary condition (2) above,

$$\lim_{y \rightarrow 0} 2y \frac{dp}{dy} = \frac{q \mu}{2 \pi k h}.$$

Comparison of this expression with Eq. A.5 shows that

$$\lim_{y \rightarrow 0} 2y \frac{dp}{dy} = \frac{q \mu}{2 \pi k h} = \lim_{y \rightarrow 0} 2C_1 e^{-y}.$$

Thus,

$$C_1 = \frac{q \mu}{4 \pi k h} \quad \dots \quad (A.6)$$

Eq. A.5 now becomes

$$\frac{dp}{dy} = \frac{q \mu}{4 \pi k h} \frac{e^{-y}}{y},$$

which can be integrated to yield

$$p = \frac{q \mu}{4 \pi k h} \int \frac{e^{-y}}{y} dy + C_2 \quad \dots \quad (A.7)$$

The lower limit of the integral in Eq. A.7 can be assigned arbitrarily. We choose  $y = \infty$  and obtain

ed drainage volume with a centrally located well which produces at constant rate. We must now obtain the inverse Laplace transform of Eq. A.15.

Examination of Eq. A.15 in the complex plane indicates that there is a pole of order two at the origin and simple poles along the negative real axis. These are the only singularities of the function.

We first determine the behavior of  $\bar{P}$  at small values of  $s$ . Inversion of this equation will give the behavior of  $\Delta p_D$  at large values of  $t_{Dw}$ . The behavior at small values of  $s$  is established by introducing small argument, asymptotic expansions for the Bessel functions and examining Eq. A.15 in the limit as  $s \rightarrow 0$ . The details of this manipulation are somewhat tedious; however, the final result is

$$\lim_{s \rightarrow 0} \bar{P} = \frac{1}{s} \left\{ \frac{r_{eD}^2}{r_{eD}^2 - 1} \ln \frac{r_{eD}}{r_D} - \frac{r_{eD}^2 - r_D^2}{2(r_{eD}^2 - 1)} + \frac{r_{eD}^2 \ln r_{eD}}{(r_{eD}^2 - 1)^2} - \frac{(r_{eD}^2 + 1)}{4(r_{eD}^2 - 1)} \right\} + \frac{1}{s^2} \frac{2}{r_{eD}^2 - 1} \quad \dots \quad (A.16)$$

Consultation of standard Laplace transform tables shows that the inverse of Eq. A.16 is

$$\Delta p_D = \frac{2}{r_{eD}^2 - 1} \left[ \frac{r_D^2}{4} + t_{Dw} \right] - \frac{r_{eD}^2}{r_{eD}^2 - 1} \ln r_D - \frac{3r_{eD}^4 - 4r_{eD}^2 \ln r_{eD} - 2r_{eD}^2 - 1}{4(r_{eD}^2 - 1)^2} \quad \dots \quad (A.17)$$

Eq. A.17 is valid for large values of time,  $t_{Dw}$ . This equation is the "long-time behavior" section of Eq. 2.34 of the text.

To find the behavior for early values of time, we must apply the Cauchy Residue Theorem. The version of that theorem which we shall apply here is as follows.

Denote by  $F(s)$  the Laplace Transform of  $f(t)$ . Let

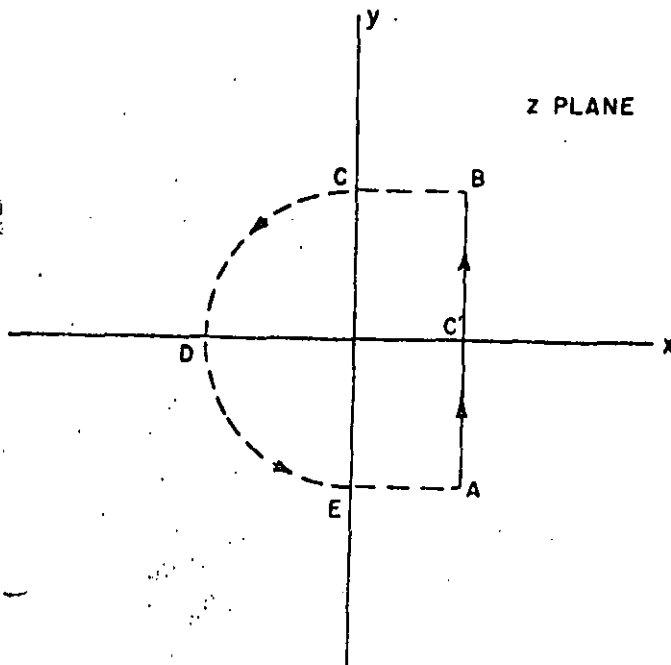


Fig. A.1 Integration path in complex plane.

**66**  $F(z)$  be the corresponding function of a complex variable. Suppose that  $F(z)$  is analytic except for a finite number of poles, all of which are to the left of some line  $x = C'$ . Also, suppose that  $F(z)$  tends uniformly to zero along the semi-circle CDE and the segments BC and EA of Fig. A.1. Then  $f(t) = \sum \text{Residue} (e^{st} F(z); a_n)$  where the points  $a_n$  are the poles of  $F(z)$ .

Since we have already found the contribution of the double pole at the origin, we must determine the residues at the poles along the negative real axis. We set  $z = u^2 e^{i\pi}$ . From Eq. A.15 we obtain

$$\text{Res} \left\{ e^{t u^2 e^{i\pi}} \bar{P}(z) \right\} = \frac{1}{2\pi i} \oint e^{t u^2 e^{i\pi}} \bar{P}(z) dz = \frac{1}{\pi i} \int \frac{e^{-u^2 t} \{ J_1(ur_{eD}) Y_0(ur_D) - Y_1(ur_{eD}) J_0(ur_D) \}}{u^2 [J_1(ur_{eD}) Y_1(u) - J_1(u) Y_1(ur_{eD})]} du \quad \dots \quad (A.18)$$

The singularities (poles) are the roots  $\alpha_n$  of the denominator of Eq. A.18, or

$$J_1(\alpha_n r_{eD}) Y_1(\alpha_n) - J_1(\alpha_n) Y_1(\alpha_n r_{eD}) = 0 \quad \dots \quad (A.19)$$

The residues at the  $\alpha_n$  are given by

$$2 \sum_{n=1}^{\infty} \frac{e^{-\alpha_n^2 t}}{\alpha_n^2} \lim_{u \rightarrow \alpha_n} \frac{d}{du} \left[ \frac{J_1(\alpha_n r_{eD}) Y_0(\alpha_n r_D) - Y_1(\alpha_n r_{eD}) J_0(\alpha_n r_D)}{J_1(ur_{eD}) Y_1(u) - J_1(u) Y_1(ur_{eD})} \right] \quad \dots \quad (A.20)$$

or

$$\pi \sum_{n=1}^{\infty} \left[ \left( e^{-\alpha_n^2 t} J_1^2(\alpha_n r_{eD}) [J_1(\alpha_n) Y_0(\alpha_n r_D) - Y_1(\alpha_n) J_0(\alpha_n r_D)] \right) \div \left( \alpha_n [J_1^2(\alpha_n r_{eD}) - J_1^2(\alpha_n)] \right) \right] \quad \dots \quad (A.21)$$

By adding these exponential terms (which die out at large values of time) to the large time solution, Eq. A.17, we obtain the complete solution given below.

$$p(r, t) = p_i - \frac{q_i h}{2\pi k h} \left\{ \frac{2}{r_{eD}^2 - 1} \left( \frac{r_D^2}{4} + t_{Dw} \right) - \frac{r_{eD}^2 \ln r_D}{r_{eD}^2 - 1} - \frac{(3r_{eD}^4 - 4r_{eD}^2 \ln r_{eD} - 2r_{eD}^2 - 1)}{4(r_{eD}^2 - 1)^2} + \pi \sum_{n=1}^{\infty} \frac{e^{-\alpha_n^2 t} J_1^2(\alpha_n r_{eD}) [J_1(\alpha_n) Y_0(\alpha_n r_D) - Y_1(\alpha_n) J_0(\alpha_n r_D)]}{\alpha_n [J_1^2(\alpha_n r_{eD}) - J_1^2(\alpha_n)]} \right\} \quad \dots \quad (A.22)$$

which is Eq. 2.34 of the text. Note that we used the definition of  $\Delta p_D$  (Eq. A.10) in obtaining Eq. A.22.



Constant Rate, Constant Pressure  
Outer Boundary Case

The mathematical statement of this problem is as follows.

$$\frac{\partial^2 p}{\partial r^2} + \frac{1}{r} \frac{\partial p}{\partial r} = \frac{\phi \mu c}{k} \frac{\partial p}{\partial t},$$

with

- (1)  $p = p_i = p_e$  at  $t = 0$ , for all  $r$ .
- (2)  $\left( r \frac{\partial p}{\partial r} \right)_{r=r_e} = \frac{q \mu}{2 \pi k h}$ , for  $t > 0$ .
- (3)  $p|_{r=0} = p_i$ , for all  $t$ .

If we recast the problem in terms of the dimensionless variables of Eq. A.10, we obtain

$$\frac{\partial^2 \Delta p_D}{\partial r_D^2} + \frac{1}{r_D} \frac{\partial \Delta p_D}{\partial r_D} = \frac{\partial \Delta p_D}{\partial t_{Dw}},$$

with

- (1)  $\Delta p_D = 0$ , at  $t_{Dw} = 0$  for all  $r_D$ .
- (2)  $\left. \frac{\partial \Delta p_D}{\partial r_D} \right|_1 = -1$ , for  $t_{Dw} > 0$ .
- (3)  $\Delta p_D = 0$  at  $r_D = r_{eD}$ , for all  $t_{Dw}$ .

Application of the Laplace transform to the above gives

$$\frac{d^2 \bar{P}}{dr_D^2} + \frac{1}{r_D} \frac{d\bar{P}}{dr_D} = s \bar{P}, \quad \dots \quad (A.23)$$

with

- (1)  $\frac{d\bar{P}}{dr_D} = -\frac{1}{s}$
  - (2)  $\bar{P}|_{r_{eD}} = 0$
- (A.24)

Again, Eq. A.14 is a general solution of the differential equation and the conditions (Eq. A.24) must be used to evaluate the constants  $A$  and  $B$ . In this case

$$A \sqrt{s} I_1(\sqrt{s}) - B \sqrt{s} K_1(\sqrt{s}) = -\frac{1}{s},$$

$$A I_0(r_{eD} \sqrt{s}) + B K_0(r_{eD} \sqrt{s}) = 0.$$

Solving for  $A$  and  $B$  and substituting into Eq. A.14 yields

$$\bar{P} = \frac{I_0(r_{eD} \sqrt{s}) K_0(r_D \sqrt{s}) - K_0(r_{eD} \sqrt{s}) I_0(r_D \sqrt{s})}{s^{3/2} [I_1(\sqrt{s}) K_0(r_{eD} \sqrt{s}) + K_1(\sqrt{s}) I_0(r_{eD} \sqrt{s})]}, \quad \dots \quad (A.25)$$

which is the transformed solution to our problem.

Proceeding as with the bounded circular reservoir

case we find that the only singularities of Eq. A.25 in the complex plane are simple poles at the origin and along the negative real axis. At the origin

$$\bar{P} = \frac{1}{s} (\ln r_{eD} - \ln r_D) \quad \dots \quad (A.26)$$

and, therefore, for large time

$$\Delta p_D = \ln r_{eD} - \ln r_D \quad \dots \quad (A.27)$$

To obtain the complete solution we again need to find the singularities along the negative real axis. Those interested in the details are referred to Carslaw and Jaeger.<sup>4</sup>

Finally, we obtain the following expression for the pressure behavior at the well.

$$p_{wf} = p_i - \frac{q \mu}{2 \pi k h} \left[ \ln r_{eD} - 2 \sum_{n=1}^{\infty} \frac{e^{-\beta_n^2 t_{Dw}} J_0^2(\beta_n r_{eD})}{\beta_n^2 [J_1^2(\beta_n) - J_0^2(\beta_n r_{eD})]} \right], \quad \dots \quad (A.28)$$

where  $\beta_n$  is a root of

$$J_1(\beta_n) Y_0(\beta_n r_{eD}) - Y_1(\beta_n) J_0(\beta_n r_{eD}) = 0.$$

Eq. A.28 is identical with Eq. 2.38 of the text.

In Ref. 4 of Chapter 8 a slightly different form of Eq. A.28 is employed to provide a basis for pressure fall-off analysis prior to reservoir fillup in the unit mobility ratio case. This form is based on the vanishingly small wellbore radius ( $r_w \rightarrow 0$ ) assumption. The pressure fall-off equation which is obtained is of the form

$$p_{ws} = p_i + b_1 e^{-\beta_1 \Delta t}.$$

Since only the first term in the series expansion has been retained, this expression is valid for large values of shut-in time only.

References

1. Polubarinova-Kochina, P. Ya.: *Theory of Ground Water Movement*, Translated from the Russian by J. M. R. DeWeist, Princeton University Press, Princeton, N.J. (1962) 549.
2. Collins, R. E.: *Flow of Fluids Through Porous Materials*, Reinhold Publishing Corp., New York (1961).
3. van Everdingen, A. F. and Hurst, W.: "The Application of the Laplace Transformation to Flow Problems in Reservoirs", *Trans., AIME* (1949) 186, 305-324.
4. Carslaw, H. S. and Jaeger, J. C.: *Conduction of Heat in Solids*, Oxford at the Clarendon Press (1959) 89.
5. Mueller, Thomas D. and Witherspoon, Paul A.: "Pressure Interference Effects Within Reservoirs and Aquifers", *J. Pet. Tech.* (April, 1965) 471-474.



**DIVISION DE EDUCACION CONTINUA  
FACULTAD DE INGENIERIA U.N.A.M.**

**CURSO: "INGENIERIA DE YACIMIENTOS GEOTERMICOS"  
13 DE MARZO AL 18 DE MAYO DE 1984**

**FLUJO DE FLUIDOS Y CALOR EN POZOS  
GEOTERMICOS**

**ING. MARIO CESAR SUAREZ ARRIAGA  
2-13 de abril**

# INGENIERIA DE YACIMIENTOS GEOTERMICOS 1984

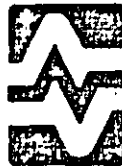
Duración total: 300 horas

Lugar: La Teoría en el Palacio de Minería, Calle de Tacuba No. 5, México, D.F. C.P. 06000 y

Las Prácticas en el Campo Geotérmico "Los Azufres" en el Estado de Michoacán, México.

Fechas: Del 7 de febrero al 13 de abril de 1984.

Coordinadores: Dr. Heber Cinco Ley y Dr. Eduardo Iglesias Rodríguez.



INSTITUTO DE  
INVESTIGACIONES  
ELÉCTRICAS



TEMA V : FLUJO DE FLUIDOS Y CALOR EN POZOS GEOTERMICOS.

MARIO CÉSAR SUÁREZ ARRIAGA

COMISIÓN FEDERAL DE ELECTRICIDAD.

GERENCIA DE PROYECTOS GEOTERMOELÉCTRICOS.

DEPARTAMENTO DE EVALUACIÓN Y YACIMIENTOS.



2.2.-	Discusión del Balance de Momento en la dirección del flujo .....	24
2.3.-	Factor de Fricción .....	25
2.4.-	Flujo Permanente .....	26
V.3.-	BALANCE DE ENERGIA EN POZOS GEOTERMICOS .....	26
3.1.-	Caso general .....	26
V.4.-	FLUJO MONOFASICO EN POZOS GEOTERMICOS .....	28
4.1.-	Deducción de la ecuación de flujo para el caso de vapor seco saturado o sobrecalentado .....	28
Vi.5.-	FLUJO BIFASICO EN POZOS GEOTERMICOS .....	34
	Introducción .....	34
	FLUJO HOMOGENEO. ECUACIONES EQUIVALENTES .....	36
	REGIMENES DE FLUJO .....	40
V.6.-	CORRELACIONES EMPIRICAS PARA CAIDA DE PRESION EN FLUJO BIFASICO .....	52
	CORRELACION DE GRIFFITH Y WALLIS .....	53
	CORRELACION DE HAGEDRON Y BROWN .....	55
	CORRELACION DE ORKISZEWSKI .....	56
	CORRELACION DE ROS .....	58
	TRANSFERENCIA DE CALOR .....	60
A.P E N D I C E A .....		80
	EL MODELO NUMERICO VSTEAM .....	80
BIBLIOGRAFIA .....		85
FIGURAS Y TABLAS.....		86
ARTICULOS COMPLEMENTARIOS .....		87
1.-	VERTICAL TWO-PHASE STEAM-WATER FLOW IN GEOTHERMAL WELLS .....	
2.-	PREDICTING TWO-PHASE PRESSURE DROPS IN VERTICAL PIPE.	
3.-	EXPERIMENTAL STUDY OF PRESSURE GRADIENTS OCCURRING DURING CONTINUOUS TWO-PHASE FLOW IN SMALL-DIAMETER VERTICAL CONDUITS.	
4.-	WELLBORE HEAT TRANSMISSION.	
5.-	OVER-ALL HEAT TRANSFER COEFFICIENTS IN STEAM AND HOT WATER INJECTION WELLS.	

---

- . N O M E N C L A T U R A . -

---

V	volumen
S	superficie
m	masa
$\rho$	densidad
dV	volumen diferencial
$\frac{d}{dt}$	derivada total
$\partial$	derivación parcial
$\nabla$	gradiente
$\vec{v}$	vector velocidad
J	determinante jacobiano
div $\vec{v}$	divergencia vectorial
$\vec{n}$	vector normal
v	volumen específico
D	dominio espacial
$\partial D$	frontera de un dominio
$\sigma$ o $\Sigma$	tensor de esfuerzos
$\sigma_{ij}$	componente del tensor esfuerzos
K	energía cinética interna
U	energía potencial interna
$W_e$	trabajo
Q	energía calorífica
u	energía potencial específica
r	radiación específica
tr A	traza de un tensor
D	tensor de tasas de deformación
P	presión
I	tensor unitario
$\lambda$	coeficiente viscoso de volumen
$\mu$	coef. viscoso cortante
$\vec{q}$	vector flujo de calor
T	temperatura
K	coef. conductividad térmica
e	energía total específica
$\Sigma_v$ , $\tau$	tensor de esfuerzos viscosos
h	entalpía específica
$\Delta$	laplaciano

---

## V.O.- PRELIMINARES.-

### INTRODUCCIÓN.-

El objetivo de este tema es el de hacer adquirir los conceptos indispensables así como las herramientas teóricas necesarias para la comprensión del comportamiento mecánico y termodinámico del fluido geotérmico dentro del pozo. Asimismo se describen las relaciones empíricas que pueden emplearse para resolver efectivamente el problema así planteado.

Entre las varias opciones posibles para presentar la teoría básica del flujo unidimensional (monofásico o bifásico), hemos escogido, por razones didácticas, la más general.

En una primera parte planteamos las grandes leyes de conservación de la mecánica del medio continuo, tanto en forma integral como diferencial, para un material arbitrario. En una segunda etapa describimos la ley de comportamiento de un fluido newtoniano, a partir de la cual deducimos la forma de las leyes anteriores para este caso particular.

De esta forma los balances de masa, momento y energía que tienen lugar en un pozo geotérmico, se obtienen fácilmente por una simple proyección de las ecuaciones precedentes, sobre el eje a lo largo del cual ocurre el flujo. Así se aprecia de inmediato cuales son las hipótesis simplificadoras que requiere el planteamiento numérico del problema.

La presentación de las diferentes correlaciones empíricas para el análisis numérico del flujo, la hacemos de manera puramente descriptiva, complementando con la publicación original.

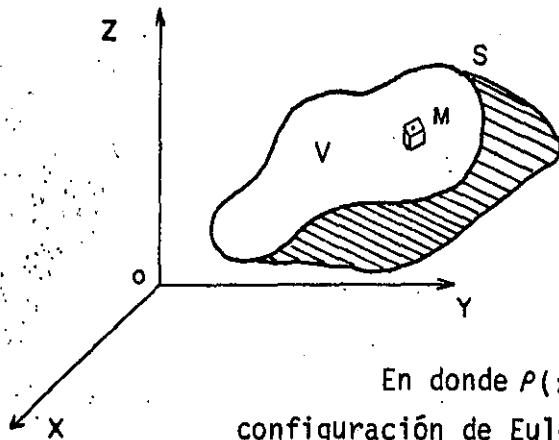
Por último, en las aplicaciones, mencionamos las utilidades que pueden obtenerse del análisis del flujo de energía y materia a través de los pozos geotérmicos.

## 0.1.- LAS GRANDES LEYES DE CONSERVACION DE LA MECANICA DEL CONTINUO.-

**OBJETIVO:** Adquirir las técnicas y herramientas analíticas suficientes para construir leyes mecánicas de conservación.

### 0.1.1.- LEY DE CONSERVACION DE LA MASA.-

Consideremos un medio material continuo cualquiera, por ejemplo un fluido, que ocupa un volumen  $V$  del espacio y encerrado por una superficie  $S$ . Por el momento, la forma de este volumen y la extensión de su superficie, son arbitrarias.



La masa total contenida en  $V$  es:

$$M = \int_{V_0} \rho \, dV = \int_{V_0} \rho_0 \, dV_0$$

En donde  $\rho(x, y, z, t)$  es la densidad en la configuración de Euler (el medio ya inició su movimiento), y  $\rho_0$  la densidad del mismo medio en la configuración de Lagrange (antes de iniciar el movimiento). Asimismo  $dV$  y  $dV_0$  son los elementos diferenciales de volumen en las configuraciones respectivas.



Sea  $M$  una partícula de  $V$ , sus coordenadas:  $\vec{OM} = (x, y, z, t)$ , en donde cada coordenada depende a su vez del tiempo. Entonces:

$$d\vec{M} = (dx, dy, dz, dt)$$

La derivada total de  $\rho$  con respecto al tiempo es entonces:

$$\frac{d\rho}{dt} = \vec{\nabla} \rho \cdot \frac{d\vec{M}}{dt} = \frac{\partial \rho}{\partial x} \frac{dx}{dt} + \frac{\partial \rho}{\partial y} \frac{dy}{dt} + \frac{\partial \rho}{\partial z} \frac{dz}{dt} + \frac{\partial \rho}{\partial t} \frac{dt}{dt}$$

Es decir:

$$\frac{d\rho}{dt} = \vec{v} \cdot \vec{\nabla} \rho + \frac{\partial \rho}{\partial t} \quad (1)$$

en donde  $\vec{v}$  es la velocidad de la partícula de masa  $\rho dV$ .

Por otra parte, esta partícula  $M$  en la configuración no deformada, tiene coordenadas:

$$\vec{OM} = (a, b, c)$$

La relación funcional entre ambas configuraciones es del tipo:

$$dV = J dV_0 \quad (2)$$

en donde:

$$J = \det \begin{pmatrix} \frac{\partial x}{\partial a} & \frac{\partial x}{\partial b} & \frac{\partial x}{\partial c} \\ \frac{\partial y}{\partial a} & \frac{\partial y}{\partial b} & \frac{\partial y}{\partial c} \\ \frac{\partial z}{\partial a} & \frac{\partial z}{\partial b} & \frac{\partial z}{\partial c} \end{pmatrix}$$

Puesto que por hipótesis:

$$x(a, b, c)$$

$$y(a, b, c)$$

$$z(a, b, c)$$

De donde deducimos que:

$$\frac{dJ}{dt} = J \operatorname{div} \vec{v} \quad (3)$$

Si la masa se conserva entonces  $\frac{dm}{dt} = 0$ . Es decir:

$$\begin{aligned} \frac{dm}{dt} &= \frac{d}{dt} \int_V \rho dV = \int_{V_0} \frac{d}{dt} (\rho J) dV_0 = \int_{V_0} \left( \frac{d\rho}{dt} J + \rho \frac{dJ}{dt} \right) dV_0 = \\ &= \int_{V_0} \left( \frac{d\rho}{dt} + \rho \operatorname{div} \vec{v} \right) J dV_0 = \int_V \left( \frac{d\rho}{dt} + \rho \operatorname{div} \vec{v} \right) dV = 0 \end{aligned}$$

Obtenemos finalmente:

$$\int_V \left( \frac{d\rho}{dt} + \rho \operatorname{div} \vec{v} \right) dV = 0 \quad (4)$$

que es la forma integral de la ecuación de la masa. Como el volumen  $V$  es arbitrario entonces:

$$\frac{d\rho}{dt} + \rho \operatorname{div} \vec{v} = 0 \quad (5)$$

o empleando (1):

$$\frac{\partial \rho}{\partial t} + \vec{v} \cdot \vec{\nabla} \rho + \rho \operatorname{div} \vec{v} = 0 \quad (6)$$

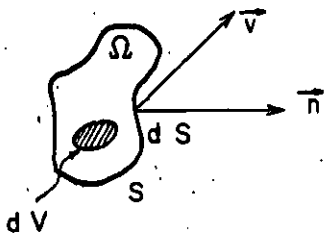
o también:

$$\frac{\partial \rho}{\partial t} + \operatorname{div} (\rho \vec{v}) = 0 \quad (7)$$

(5), (6) y (7) son tres formas equivalentes que traducen en ecuaciones diferenciales parciales, el principio de conservación de la masa localmente, o sea, en el volumen  $dV$ .

### 0.1.2.- NOTA SOBRE EL PRINCIPIO DE CONSERVACION DE LA MASA.

Imaginemos un medio fluido  $\Omega$  de frontera  $S$ . - su masa total es:



$$m = \int_{\Omega} \rho \, dV, \quad \rho \text{ densidad, } V \text{ volumen.}$$

Como anteriormente, si calculamos la variación de esta masa en el tiempo:

$$\frac{dm}{dt} = \int_{\Omega} \frac{d}{dt} (\rho \, dV) = \int_{\Omega} \frac{\partial \rho}{\partial t} \, dV + \int_{\Omega} \text{div}(\rho \vec{v}) \, dV \quad (8)$$

si utilizamos el teorema de la divergencia al revés:

$$\int_{\Omega} \text{div}(\rho \vec{v}) \, dV = \int_S \rho \vec{v} \cdot \vec{n} \, dS \quad (9)$$

La ecuación (8) representa la variación, en función del tiempo, de la masa fluida contenida en  $\Omega$ , dominio de volumen variable, limitado por la superficie -- móvil  $S$ . Si  $\frac{dm}{dt} = 0$  entonces  $\Omega$  contiene siempre la misma masa; el término  $\vec{v} \cdot \vec{n}$  representa la velocidad normal de una partícula sobre la superficie  $S$ , o sea que también - representa la velocidad de desplazamiento de la superficie  $S$ .

Por otra parte, al derivar parcialmente con -- respectó al tiempo  $\frac{\partial \rho}{\partial t}$  se están manteniendo constantes los componentes espaciales, entonces:

$$\int_{\Omega} \frac{\partial \rho}{\partial t} dV = \frac{\partial}{\partial t} \int_{\Omega} \rho dV = - \int_S \rho \vec{v} \cdot \vec{n} dS \quad (10)$$

el integrando  $\rho \vec{v} \cdot \vec{n} dS$  tiene unidades de  $\frac{kg}{s}$ , es decir un gasto a través S. Por consiguiente (10) se interpreta: la variación temporal de una masa fluida contenida en un dominio fijo del espacio, es igual a la resultante de los gastos que entren al dominio a través de su superficie.

Nótese también que en la ecuación diferencial de la densidad:

$$\frac{\partial \rho}{\partial t} + \text{div}(\rho \vec{v}) = 0$$

puede reemplazarse:  $\frac{d\rho}{dt} = \frac{\partial \rho}{\partial t} + \vec{v} \cdot \nabla \rho$

Lo cual implica:  $\frac{d\rho}{dt} = -\rho \text{div} \vec{v}$ . Sea  $\nu = \frac{1}{\rho}$

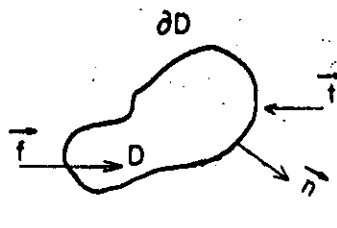
$$\Rightarrow \boxed{\text{div} \vec{v} = \frac{1}{\nu} \frac{d\nu}{dt}}$$

La divergencia de la velocidad de las partículas del fluido es la variación instantánea relativa del volumen específico para esas partículas. También se

dice que  $\text{div} \vec{v}$  representa la velocidad de dilatación cúbica (o volumétrica) del volumen diferencial rodeando a esa partícula.

### 0.1.3.- CONSERVACION DEL MOMENTO LINEAL.-

La ley fundamental de la dinámca de medios continuos se escribe:



$$\int_D \rho \bar{a} dV = \int_D \bar{f} dV + \int_{\partial D} \bar{t} dS \quad (\text{resultante})$$

$$\int_D \rho \bar{x} \times \bar{a} dV = \int_D \bar{x} \times \bar{f} dV + \int_{\partial D} \bar{x} \times \bar{t} dS \quad (\text{momento})$$

Con D un dominio material de frontera  $\partial D, \bar{x} \in DU \partial D$ ;  $\bar{f}$  es la fuerza por unidad de volumen de acción a distancia,  $\bar{t}$  es la fuerza superficial de contacto,  $\rho$  densidad del medio,  $\bar{a}$  y  $\bar{v}$  aceleración y velocidad respectivamente de las partículas que componen D.

La hipótesis de Cauchy presupone que:  $\bar{t} = \Sigma \cdot \bar{n}$ ; en donde  $\bar{n}$  es la normal unitaria exterior a D y  $\Sigma$  es el tensor de esfuerzos intrínsecos:

$$\Sigma = (\sigma_{ij}) = \begin{pmatrix} \sigma_{11} & \sigma_{12} & \sigma_{13} \\ \sigma_{21} & \sigma_{22} & \sigma_{23} \\ \sigma_{31} & \sigma_{32} & \sigma_{33} \end{pmatrix}$$

Tenemos pues, utilizando el teorema de Green:

$$\int_{\partial D} \bar{t} dS = \int_{\partial D} \Sigma \cdot \bar{n} dS = \int_D \text{div} \Sigma dV; (\text{div} \Sigma = \partial_j \sigma_{ij})$$

De donde la resultante se puede escribir:

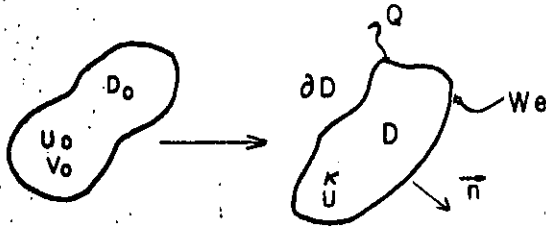
$V D \subset C D$ :  $\int_{D_0} \rho \bar{a} dV = \int_{D_0} (\bar{f} + \text{div} \Sigma) dV$ , y por tanto los integra dos coinciden:

$$\rho \bar{a} = \bar{f} + \text{div} \Sigma \quad \text{o} \quad \rho a_i = f_i + \partial_j \sigma_{ij}$$

que traduce el momento lineal o ley de la dinámca de medios continuos.

### 0.1.4.- CONSERVACION DE LA ENERGIA POTENCIAL.-

Consideremos nuevamente un medio continuo material  $D$  sujeto a diversas interacciones con el medio externo a él.



La ley de la termodinámica del medio continuo establece que el cambio en la energía interna -- del sistema  $D$ ,  $K+U$  es de la misma magnitud que el trabajo externo realizado sobre él y añadido a la cantidad

de calor intercambiada:

$$K - K_0 + U - U_0 = W_e + Q \quad (1T)$$

$$\text{En } t > 0 \text{ tenemos: } K = \int_D \frac{1}{2} \rho \vec{v} \cdot \vec{v} dV, \quad U = \int_D \rho u dV$$

con:

$\rho$  = densidad del medio.

$\vec{v}$  = velocidad de las partículas.

$u$  = energía interna específica por unidad de masa.

$K$  -- es debida al movimiento relativo de las moléculas de  $D$ .

$U$  -- es la energía potencial debida a las interacciones entre las moléculas de  $D$ .

La potencia del sistema es por definición:  $\frac{dK}{dt} + \frac{dU}{dt} \Rightarrow$

$$\frac{dK}{dt} = \frac{d}{dt} \int_D \frac{1}{2} \rho \vec{v} \cdot \vec{v} dV = \int_D (\rho \vec{v} \cdot \vec{a} + \frac{1}{2} \frac{d\rho}{dt} \vec{v} \cdot \vec{v} + \frac{1}{2} \rho \text{div} \vec{v} \cdot \vec{v}) dV$$

$$\frac{dU}{dt} = \frac{d}{dt} \int_D \rho u dV = \int_D \left[ \left( \frac{d\rho}{dt} + \rho \text{div} \vec{v} \right) u + \rho \frac{du}{dt} \right] dV$$

De donde:

$$\frac{dK}{dt} + \frac{dU}{dt} = \int_D \left[ \left( \frac{d\rho}{dt} + \rho \text{div} \vec{v} \right) \left( \frac{1}{2} \vec{v} \cdot \vec{v} + u \right) + \rho \vec{v} \cdot \vec{a} + \rho \frac{du}{dt} \right] dV$$

Además:

$$\frac{dW_e}{dt} = \int_D \vec{f} \cdot \vec{v} dV + \int_{\partial D} \vec{t} \cdot \vec{v} dS = \int_D [\vec{f} \cdot \vec{v} + \text{div}(\sum \vec{v})] dV$$

$$y: \frac{dQ}{dt} = \int_D \rho r dV - \int_{\partial D} \vec{q} \cdot \vec{n} dS = \int_D (\rho r - \text{div} \vec{q}) dV$$

Con  $\vec{f}$ ,  $\vec{t}$  y  $\sum$  definidos como antes;  $r$  la radiación específica por unidad de la masa (debida a fuentes de calor accionando a distancia, tales como ondas electromagnéticas, rayo laser, ondas nucleares, etc.) y  $\vec{q}$  el flujo de calor instantáneo a través la frontera  $\partial D$ .

La ecuación (1T) queda entonces:

$$\int_D (\cancel{\rho \vec{v} \cdot \vec{v}} + \rho \frac{du}{dt}) dV = \int_D [(\cancel{\vec{f} + \text{div} \sum}) \cdot \vec{v} + \sum : \text{grad} \vec{v} + \rho r - \text{div} \vec{q}] dV$$

y si todas las funciones involucradas son continuas se tiene:

$$\boxed{\rho \frac{du}{dt} = \sum : \text{grad} \vec{v} + \rho r - \text{div} \vec{q}}$$

que es la ecuación diferencial que describe la conservación de la energía interna de un medio material.

El término:  $\sum : \text{grad} \vec{v} = \text{tr}(\sum \text{grad} \vec{v})$  con  $\text{grad} \vec{v} = (\frac{\partial v_i}{\partial x_j})$  es una matriz. La traza de una matriz  $A$  se define mediante:

$$\text{tr} A = \text{tr} \begin{pmatrix} Q_{11} & Q_{12} & Q_{13} \\ Q_{21} & Q_{22} & Q_{23} \\ Q_{31} & Q_{32} & Q_{33} \end{pmatrix} = Q_{11} + Q_{22} + Q_{33}$$

Las ecuaciones de conservación de la masa, del momento y de la energía, son leyes universales válidas para toda la materia continua sin que importe su naturaleza íntima.

### 0.1.5.- CONSERVACION DE LA ENERGIA CINETICA.-

Consideremos nuevamente la ley deducida en ---

0.1.3.:

$$\rho \frac{d\vec{v}}{dt} = \vec{f} + \text{div } \Sigma$$

multiplicando ambos miembros escalarmente por  $\vec{v}$  :

$$\rho \vec{v} \cdot \frac{d\vec{v}}{dt} = \vec{f} \cdot \vec{v} + \text{div} (\Sigma) \cdot \vec{v}$$

Integrando ahora sobre V:

$$\int_V \rho \frac{d}{dt} \left( \frac{\vec{v} \cdot \vec{v}}{2} \right) dV = \int_V \vec{f} \cdot \vec{v} dV + \int_V \text{div } \Sigma \cdot \vec{v} dV$$

Empleando el principio de conservación de la -- masa, y el teorema de Green, la ecuación integral anterior es equivalente a:

$$\textcircled{K} \dots \frac{d}{dt} \int_V \rho \frac{v^2}{2} dV = \underbrace{\int_V \vec{f} \cdot \vec{v} dV}_{\text{Potencia de esfuerzos - exteriores - de volumen.}} + \underbrace{\int_S (\Sigma \cdot \vec{v}) \cdot \vec{n} dS}_{\text{Potencia de esfuerzos - superficiales.}} - \underbrace{\int_V \text{tr} (\Sigma \nabla \vec{v}) dV}_{\text{Potencia de esfuerzos - internos a - V.}}$$

Si la fuerza volumétrica  $\vec{f}$  deriva de un potencial de esfuerzos F, entonces:  $\vec{f} = -\rho \nabla F$ , con F-- independiente del tiempo.

Nótese que:  $\frac{dF}{dt} = \frac{\partial F}{\partial t} + \vec{v} \cdot \nabla F$ , pero  $\frac{\partial F}{\partial t} = 0$ , luego:  $\vec{f} \cdot \vec{v} = -\rho \vec{v} \cdot \nabla F = -\rho \frac{dF}{dt}$

De donde:

$$\frac{d}{dt} \int_V \left( \frac{\rho v^2}{2} + \rho F \right) dV = \int_S (\Sigma \cdot \vec{v}) \cdot \vec{n} dS - \int_V \text{tr} (\Sigma \nabla \vec{v}) dV$$



## 0.2.- FLUIDOS NEWTONIANOS.

OBJETIVO: Definir la forma matemática que tiene el --- fluido geotérmico, y construir las diferentes ecuaciones que lo gobiernan.

### 0.2.1.- LEY DE COMPORTAMIENTO DEL FLUIDO NEWTONIANO.

Consideremos ahora un fluido compresible, viscoso y eventualmente, conductor del calor.

Debido a que las velocidades de deformación de un fluido son mucho mayores que las de los sólidos, introducimos un tensor que relaciona deformación con velocidad y definido así:

$$D = (D_{ij}) \quad \text{con} \quad D_{ij} = \frac{1}{2} \left( \frac{\partial v_i}{\partial x_j} + \frac{\partial v_j}{\partial x_i} \right)$$

Las ecuaciones de comportamiento se escriben entonces:

$$\Sigma = - p \Pi + \lambda \text{tr } D \Pi + 2 \mu D$$

con el flujo de calor a través del fluido dado por:

$$\vec{q} = - K \vec{\nabla} T$$

$p$  es la presión hidrodinámica,  $\lambda$  y  $\mu$  los coeficientes de viscosidad,  $T$  la temperatura y  $K$  la conductividad térmica del fluido.

En particular si el fluido es un gas como el ---  
aire, entonces los coeficientes  $\lambda, \mu = 0$  y obtenemos las-  
ecuaciones de la aerodinámica:

$$\Sigma = - p \Pi$$

Las ecuaciones precedentes son la base de todas-  
las Ingenierías que estudian el comportamiento de fluidos  
newtonianos.

### 0.2.2.- DISCUSION DE LA ENERGIA TOTAL PARA UN FLUIDO NEWTONIANO.

En la sección 0.1.4 se ha establecido una ecua --  
ción que proporciona la evolución de la energía interna -  
potencial específica  $u$ . De forma análoga puede deducirse  
una ecuación diferencial para la energía total interna:

Sea  $e = u + \frac{v^2}{2}$  la energía total interna de una -  
partícula.

$$\begin{aligned} \frac{d}{dt} \int_D \rho e dv &= \int_{D_0} \frac{d}{dt} (\rho e J) dv_0 = \int_D \left[ \frac{\partial}{\partial t} (\rho e) + \text{div}(\rho e \vec{v}) \right] dv = \\ &= \int_D \left[ \vec{f} \cdot \vec{v} + \text{div} (\Sigma \cdot \vec{v}) \right] dv - \int_D \text{div} \vec{q} dv \end{aligned}$$

o sea que localmente:

$$\frac{\partial}{\partial t} (\rho e) = - \text{div} (\rho e \vec{v}) + \vec{f} \cdot \vec{v} + \text{div} (\Sigma \cdot \vec{v}) - \text{div} \vec{q}$$

Supongamos un fluido newtoniano, cuya ley de com-  
portamiento es:

$$\Sigma = - p I + \Sigma v$$

con  $\Sigma_v = \lambda \text{tr}(D)I + 2 \mu D$  el tensor de esfuerzos viscosos.

Supongamos una ley de tipo Fourier para la transmisión del calor:

$$\vec{q} = - K \vec{\nabla} T$$

entonces:

$$\frac{d}{dt} (\rho e) = - \rho e \text{div } \vec{v} + \vec{f} \cdot \vec{v} - \text{div} (P\vec{v}) + \text{div} (\Sigma_v \vec{v}) + K \Delta T \dots (E)$$

variación instantánea de energía interna total.	energía de dilatación volumétrica.	potencia de esfuerzos exteriores.	trabajo total de las fuerzas de presión.	trabajo total de esfuerzos viscosos.	energía calorífica (distribución).
---	------------------------------------	-----------------------------------	--	--------------------------------------	------------------------------------

Los términos convectivos significan respectivamente:

$-\text{div} (P\vec{v}) = P \text{div } \vec{v} - \vec{v} \cdot \vec{\nabla} P$	$;$	$\text{div} (\Sigma_v \vec{v}) = \text{div} (\Sigma_v) \cdot \vec{v} + \Sigma_v \cdot \vec{\nabla} \vec{v}$
trabajo de las fuerzas de presión durante la deformación (dilatación o compresión).		trabajo de las fuerzas de presión durante el desplazamiento.
		trabajo de las fuerzas de viscosidad durante el desplazamiento.
		trabajo de viscosidad durante la deformación.

Aquí los términos trabajo y energía se entiende que son instantáneos y tienen unidades de potencias por unidad de volumen.

### 0.2.3.- ENTALPIA TOTAL.-

Nótese que en términos de la entalpía específica:  $h = \mu + \frac{P}{\rho}$ , la ecuación (E) se escribe:

$$\frac{d}{dt} \left[ \rho \left( h + \frac{v^2}{2} \right) \right] = \frac{dP}{dt} - \left[ \rho \left( h + \frac{v^2}{2} \right) - P \right] \operatorname{div} \bar{v} + \bar{f} \cdot \bar{v} - \operatorname{div} (P \bar{v}) + \operatorname{div} (\Sigma \bar{v}) + K \Delta T$$

Al término:  $\rho \left( h + \frac{v^2}{2} \right)$  se le llama entalpía - específica total.

---

### 0.2.4.- LAS ECUACIONES DE NAVIER-STOKES.-

Utilicemos la ecuación del movimiento deducida en 0.1.3., válida para todo medio continuo:

$$\rho \frac{d\bar{v}}{dt} = \bar{f} + \operatorname{div} \Sigma$$

Supongamos un fluido newtoniano cuya ley de comportamiento es de la forma:

$$\Sigma = -P I + \lambda D_{jj} I + 2\mu D$$

$$\text{Calculando: } \operatorname{div} \Sigma = -\bar{\nabla} P + \lambda \bar{\nabla} D_{jj} + 2\mu \operatorname{div} D$$

$$\text{Pero: } D_{jj} = \partial_j v_j \Rightarrow \bar{\nabla} D_{jj} = (\partial_{ij} v_j)$$

Asimismo:

$$D_{ij} = \frac{1}{2} (\partial_j v_i + \partial_i v_j) \Rightarrow \partial_j D_{ij} = \frac{1}{2} (\partial_{jj} v_i + \partial_{ij} v_j)$$

Por tanto la ecuación del movimiento para un fluido newtoniano es:

$$\rho \frac{dv_i}{dt} = f_i - \partial_i P + (\lambda + \mu) \partial_{ij} v_j + \mu \partial_{jj} v_i, \quad \text{o también:}$$

$$\rho \frac{d\vec{v}}{dt} = \rho \left[ \frac{\partial \vec{v}}{\partial t} + \vec{v} \cdot \nabla \vec{v} \right] = \vec{f} - \nabla P + (\lambda + \mu) \nabla (\text{div } \vec{v}) + \mu \Delta \vec{v}$$

Estas son las ecuaciones de Navier-Stokes, bastante difíciles de tratar debido a los términos no-lineales.

Para el caso de un fluido perfecto en que  $\lambda = \mu = 0$ :

$$\frac{d\vec{v}}{dt} = \frac{1}{\rho} \vec{f} - \frac{1}{\rho} \nabla P$$

### 0.2.5.- LA ECUACION DE BERNOULLI.-

Como se ha visto en 0.1.5., la ecuación que describe el cambio instantáneo de energía cinética en forma integral es:

$$\frac{d}{dt} \int_V \left( \rho \frac{v^2}{2} + \rho F \right) dV = \int_S (\rho \vec{v}) \cdot \vec{n} dS - \int_V \text{tr} (\sigma \nabla \vec{v}) dV$$

Sea  $e = \frac{v^2}{2} + F$ , y supongamos un fluido-newtoniano cuyo comportamiento es descrito por:  $\sigma = -PI + \tau$  con  $\tau = \lambda D_{jj} + 2\mu D$  el tensor de viscosidades. Podemos entonces escribir:

$$\begin{aligned} \frac{d}{dt} \int_V \rho e dV &= \int_{V_0} \frac{d}{dt} (\rho e J) dV_0 = \int_{V_0} \left[ \frac{d}{dt} (\rho e J) + \rho e \frac{dJ}{dt} \right] dV_0 = \\ &= \int_V \left[ \frac{\partial}{\partial t} (\rho e) + \vec{v} \cdot \nabla (\rho e) + \rho e \text{div } \vec{v} \right] dV = \\ &= \int_V \frac{\partial}{\partial t} (\rho e) dV + \int_V \text{div} (\rho e \vec{v}) dV \end{aligned}$$

Además:

$$\int_S (\sigma \cdot \vec{v}) \cdot \vec{n} ds = - \int_S P \vec{v} ds + \int_S (\tau \cdot \vec{v}) \cdot \vec{n} ds$$

$$\int_V \text{tr}(\sigma \nabla \vec{v}) dV = - \int_V P \text{tr}(\nabla \vec{v}) dV + \int_V \text{tr}(\tau \nabla \vec{v}) dV$$

De lo cual deducimos:

$$\begin{aligned} \int_V \frac{\partial}{\partial t} \left[ \rho \frac{v^2}{2} + \rho F \right] dV + \int_S \left( \rho \frac{v^2}{2} + \rho F + P \right) \vec{v} \cdot \vec{n} ds = \\ = \int_S (\tau \cdot \vec{v}) \cdot \vec{n} ds + \int_V P \text{div} \vec{v} dV - \int_V \text{tr}(\tau \nabla \vec{v}) dV \quad \text{----- (B)} \end{aligned}$$

Esta ecuación conocida como fórmula de COTTON-FORTIER, es la ecuación general de Bernoulli, que traduce la conservación de la energía cinética para un fluido newtoniano sobre el cual se ejerce un potencial de es - fuerzas volumétricos F.

Escalarmente los términos de disipación energética debida al frotamiento se interpretan como sigue:

$$\int_S (\tau \cdot \vec{v}) \cdot \vec{n} ds = \int_S n_i \tau_{ij} v_j ds \quad \text{Potencia disipada por -- frotamiento superficial-- durante el desplazamiento.}$$

$$- \int_V \text{tr}(\tau \nabla \vec{v}) dV = - \int_V \tau_{ij} \frac{\partial v_i}{\partial x_j} dV \quad \text{Potencia disipada por -- frotamiento durante la - deformación.}$$

Como casos particulares de la ecuación (B) --- tenemos los siguientes:

1).- El fluido es incompresible  $\Rightarrow \text{div} \vec{v} = 0$  y el término correspondiente desaparece.

2).- El fluido es incompresible y las fuerzas de viscosidad despreciables:

$$\int_V \frac{\partial}{\partial t} \left( \rho \frac{v^2}{2} + \rho F \right) dV + \int_S \left( \rho \frac{v^2}{2} + \rho F + P \right) \vec{v} \cdot \vec{n} ds = 0$$

Como el flujo es no-permanente entonces:

$$\int_V \left\{ \frac{\partial}{\partial t} \left( \rho \frac{v^2}{2} + \rho F \right) + \operatorname{div} \left[ \left( \frac{\rho v^2}{2} + \rho F + P \right) \vec{v} \right] \right\} dV = 0$$

Integrando continuo sobre un volumen arbitrario --  
V implica:

$$\frac{\partial}{\partial t} \left( \rho \frac{v^2}{2} \right) + \frac{\partial}{\partial t} (\rho F) + \operatorname{div} \left[ \left( \frac{\rho v^2}{2} + \rho F + P \right) \vec{v} \right] = 0$$

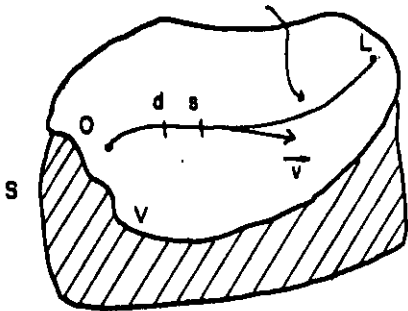
pero:

$$\operatorname{div} \left[ \left( \frac{\rho v^2}{2} + \rho F + P \right) \vec{v} \right] = \left( \frac{\rho v^2}{2} + \rho F + P \right) \underbrace{\operatorname{div} \vec{v}}_0 + \vec{v} \cdot \nabla \left( \frac{\rho v^2}{2} + \rho F + P \right)$$

Luego:

$$\frac{\partial}{\partial t} \left( \rho \frac{v^2}{2} \right) + \frac{\partial}{\partial t} (\rho F) + \vec{v} \cdot \nabla \left( \frac{\rho v^2}{2} + \rho F + P \right) = 0 \quad \text{----- (B1)}$$

TRAYECTORIA O  
LINEA DE CORRIENTE



Un resultado interesante se obtiene al integrar la ecuación anterior sobre una línea de corriente. --  
Nótese primero que el vector velocidad es tangente, en cada punto, a la trayectoria.

Por consiguiente:

$$\frac{1}{v} \cdot \nabla \left( \frac{\rho v^2}{2} + \rho F + P \right) = \frac{\partial}{\partial s} \left( \rho \frac{v^2}{2} + \rho F + P \right)$$

es la derivada en la dirección de la trayectoria -  
del término entre paréntesis.

Luego:

$$\int_0^L \frac{1}{v} \frac{\partial}{\partial t} \left( \rho \frac{v^2}{2} \right) ds + \int_0^L \frac{1}{v} \frac{\partial}{\partial t} (\rho F) ds + \int_0^L \frac{\partial}{\partial s} \left( \rho \frac{v^2}{2} + \rho F + P \right) ds = 0$$

es decir:

$$\int_0^L \frac{1}{v} \frac{\partial}{\partial t} \left( \rho \frac{v^2}{2} \right) ds + \int_0^L \frac{1}{v} \frac{\partial}{\partial t} (\rho F) ds + \left( \frac{\rho v^2}{2} + \rho F + P \right) \Big|_0^L = \left( \frac{\rho v^2}{2} + \rho F + P \right) \Big|_0^L = \text{constante}$$

(B2)...

3).- Fuerzas de viscosidad nulas, fluido incompresible y homogéneo. El potencial de fuerzas es debido al campo gravitatorio;

$$\frac{\partial p}{\partial t} = 0, \quad F = gz,$$

z    Coordenada vertical de la partícula.  
g    Aceleración gravitacional.

La ecuación (B2) deviene:

$$\rho \int_0^L \frac{\partial v}{\partial t} ds + \left( \frac{\rho v^2}{2} + \rho gz + P \right)_L = \left( \frac{\rho v^2}{2} + \rho gz + P \right)_0 \quad \text{-----} \quad (B3)$$

4).- Flujo permanente y fluido incompresible. En este caso, el más simple, tendremos de (B1):

$$\vec{v} \cdot \vec{\nabla} \left( \frac{\rho v^2}{2} + \rho F + P \right) = 0$$

Hay tres posibilidades:

i).-  $\vec{v} = \vec{0} \implies$  no hay flujo. Caso estático que descartamos.

ii).-  $\vec{\nabla} \left( \frac{\rho v^2}{2} + \rho F + P \right) = 0 \implies \frac{\rho v^2}{2} + \rho F + P = \text{constante.}$

iii).- La velocidad y el gradiente son ortogonales y como su producto escalar representa la derivada de la cantidad entre paréntesis -- sobre una trayectoria, entonces:

$$v \frac{\partial}{\partial s} \left( \frac{\rho v^2}{2} + \rho F + P \right) = 0 \implies \frac{\rho v^2}{2} + \rho F + P = \text{constante}$$

sobre una línea de corriente.

En conclusión para que (ii) o (iii) sean satisfechas, es suficiente que:

$$(B4) \text{-----} \quad \frac{\rho v^2}{2} + \rho F + P = \text{constante,}$$

sobre cada trayectoria.



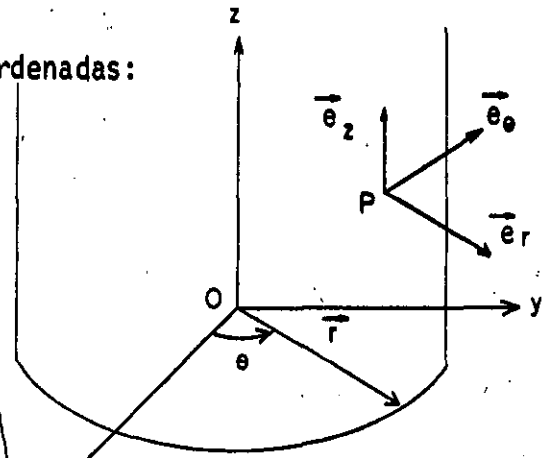
Las fórmulas (B1), (B2), (B3) y (B4) son casos particulares de la ecuación de Bernoulli general (B).

### 0.3.- OPERADORES DIFERENCIALES EN COORDENADAS CILINDRICAS.

El estudio del flujo dentro de dominios espaciales con simetría radial, que es el caso de los pozos, se simplifica convenientemente si las ecuaciones generales que acabamos de desarrollar son planteadas en una base de coordenadas cilíndricas.

Sea P un punto del espacio de coordenadas:

$$\vec{OP} = \begin{pmatrix} x \\ y \\ z \end{pmatrix} = \begin{pmatrix} r \cos \theta \\ r \sin \theta \\ z \end{pmatrix}$$



Definimos los vectores unitarios:

$$\vec{e}_r = \frac{\partial \vec{OP}}{\partial r} = (\cos \theta, \sin \theta, 0)$$

$$\vec{e}_\theta = \frac{1}{r} \frac{\partial \vec{OP}}{\partial \theta} = (-\sin \theta, \cos \theta, 0)$$

$$\vec{e}_z = \frac{\partial \vec{OP}}{\partial z} = (0, 0, 1)$$

$$\Rightarrow \vec{OP} = r\vec{e}_r + \theta\vec{e}_\theta + z\vec{e}_z$$

De donde, para una cantidad  $u(r, \theta, z)$ , y un vector  $\vec{v} = v_r \vec{e}_r + v_\theta \vec{e}_\theta + v_z \vec{e}_z$ :

(1) Gradiente:  $\vec{\nabla}u = \frac{\partial u}{\partial r} \vec{e}_r + \frac{1}{r} \frac{\partial u}{\partial \theta} \vec{e}_\theta + \frac{\partial u}{\partial z} \vec{e}_z$

(2) Laplaciano:  $\Delta u = \frac{\partial^2 u}{\partial r^2} + \frac{1}{r} \frac{\partial u}{\partial r} + \frac{1}{r^2} \frac{\partial^2 u}{\partial \theta^2} + \frac{\partial^2 u}{\partial z^2}$

(3) Divergencia vectorial:  $\text{div } \vec{v} = \vec{\nabla} \cdot \vec{v} = \frac{\partial v_r}{\partial r} + \frac{1}{r} \frac{\partial v_\theta}{\partial \theta} + \frac{\partial v_z}{\partial z}$

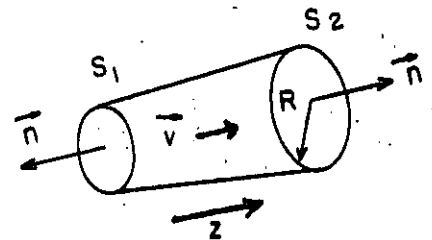
(4) Divergencia tensorial:

$$\operatorname{div} \vec{\tau} = \begin{pmatrix} \partial_r \tau_{rr} + \frac{1}{r} \partial_\theta \tau_{r\theta} + \partial_z \tau_{rz} \\ \partial_r \tau_{\theta r} + \frac{1}{r} \partial_\theta \tau_{\theta\theta} + \partial_z \tau_{\theta z} \\ \partial_r \tau_{zr} + \frac{1}{r} \partial_\theta \tau_{z\theta} + \partial_z \tau_{zz} \end{pmatrix} = \begin{pmatrix} \zeta_r \\ \zeta_\theta \\ \zeta_z \end{pmatrix}$$

V.1.- BALANCE DE MASA EN POZOS GEOTERMICOS.-

**OBJETIVO:** Deducir la forma particular de la ecuación de conservación de la masa dentro del pozo para flujo permanente y no-permanente.

Consideremos la tubería de un pozo geotérmico de sección  $S(z)$  variable. Ya hemos visto que la forma integral de la ecuación de conservación de la masa (10) puede escribirse:



$$\frac{\partial}{\partial t} \int_V \rho dV = - \int_S \rho \vec{v} \cdot \vec{n} ds$$

El campo de velocidades, al interior del pozo, tiene la forma :  $\vec{v} = \begin{pmatrix} 0 \\ 0 \\ v \end{pmatrix}$  con  $v(r, z, t)$ .

Es decir:  $v_r = v_\theta = 0$ . La entrada y salida de masa del volumen  $V$ , limitado por las paredes del tubo, solo ocurre a través de  $S_1$  y  $S_2$ , en la dirección normal:

$$\vec{n} = (0, 0, \pm 1)$$

Entonces la ecuación integral anterior equivale a:

$$\frac{\partial}{\partial t} \iiint_{\text{pozo}} \rho r dr d\theta dz = - \int_S \rho v ds \text{ -----(1)}$$

### V.1.1.- FLUJO NO-PERMANENTE.-

La densidad del fluido dentro del pozo, varía con el tiempo. Supondremos además que ésta sólo depende espacialmente de la coordenada vertical  $\rho(z, t)$ :

$$\frac{\partial}{\partial t} \int_{R_1}^{R_2} r \, dr \cdot \int_0^{2\pi} d\theta \cdot \int_{z_1}^{z_2} \rho \, dz = - \left[ \int_{S_1} -\rho v \, ds + \int_{S_2} \rho v \, ds + \int_{\text{tubo}} \rho v \, ds = 0 \right]$$

Por lo tanto:

$$\pi(R_2^2 - R_1^2) \frac{\partial}{\partial t} \int_{z_1}^{z_2} \rho \, dz = \rho_1 \bar{v}_1 S_1 - \rho_2 \bar{v}_2 S_2 \quad \text{-----}(2)$$

en donde  $\bar{v}_i = \frac{1}{S_i} \int_{S_i} v \, ds$ , es la velocidad media del fluido al atravesar la sección de área  $S_i$  ( $i = 1, 2$ ).

La ecuación (2), traduce en términos matemáticos, el balance de masa para flujo transitorio entre dos secciones- $S_1$  y  $S_2$  de un pozo geotérmico.

### V.1.2.- FLUJO PERMANENTE.-

Por definición, esto ocurre cuando  $\frac{\partial}{\partial t} = 0$ , y entonces (2) deviene:

$$\rho_1 \bar{v}_1 S_1 = \rho_2 \bar{v}_2 S_2 \quad \text{-----}(3)$$

es decir:

$$\rho \bar{v} S = \text{constante} \quad \text{-----}(4)$$

Como  $\bar{v}$  representa a la velocidad media en la sección S, entonces si  $v(r, z)$  se tendrá:

$$\bar{v} S = \int_S v ds = \int_0^{2\pi} d\theta \int_0^R v r dr = 2\pi \int_0^R v r dr \quad \text{-----(5)}$$

La ecuación (3), (o la 4), constituye el balance de masa en un pozo geotérmico para flujo permanente.

## V.2.- BALANCE DE MOMENTO EN POZOS GEOTERMICOS.-

**OBJETIVO:** Aplicar la conservación del momento lineal al flujo dentro de un pozo.

En la sección 0.2.4., observamos que la ecuación del movimiento combinada con una ley de comportamiento newtoniano engendra a la ecuación de Navier-Stokes que describe vectorialmente la dinámica del fluido geotérmico. Esta ecuación la escribiremos:

$$\rho \left[ \frac{\partial \vec{v}}{\partial t} + \vec{v} \cdot \nabla \vec{v} \right] = \vec{f} - \nabla P + \text{div } \tau \quad \text{-----(1)}$$

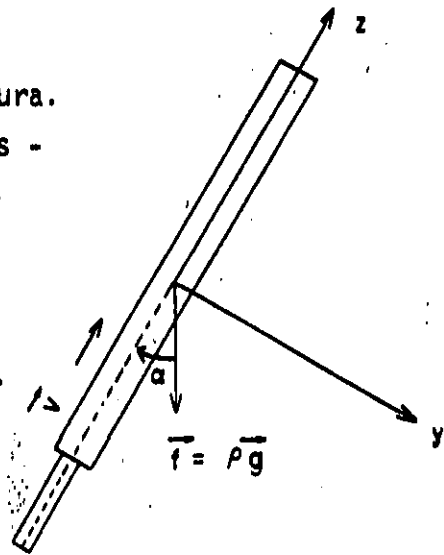
en donde  $\tau = \lambda \text{ div } \vec{v} \cdot \mathbf{I} + 2\mu D$ , es el tensor de viscosidades discutidos en 0.2.4.

### V.2.1.- CONSERVACION DEL MOMENTO TOTAL EN COORDENADAS CILINDRICAS.

El flujo unidimensional dentro del pozo, se-

muestra esquemáticamente en la figura.  
 Suponiendo el perfil de velocidades -  
 planteado en V.1.:

$$v = \begin{pmatrix} v_r \\ v_\theta \\ v_z \end{pmatrix} = \begin{pmatrix} 0 \\ 0 \\ v \end{pmatrix}, v(r, z, t).$$



y con:

$$\vec{f} = (f_x \vec{e}_x + f_y \vec{e}_y + f_z \vec{e}_z)$$

Pero como:  $\vec{e}_x = \cos \theta \vec{e}_r - \sin \theta \vec{e}_\theta$ ,  
 $\vec{e}_y = \sin \theta \vec{e}_r + \cos \theta \vec{e}_\theta$  y además:  $f_x = 0$ ,  $f_y = \rho g \sin \alpha$ ,  
 $f_z = -\rho g \cos \alpha$ .

Entonces en cilíndricas, las componentes del --  
 campo de fuerzas volumétricas es:

$$\vec{f} = \rho g \sin \alpha (\sin \theta \vec{e}_r + \cos \theta \vec{e}_\theta) - \rho g \cos \alpha \vec{e}_z \quad \text{-----}(2)$$

La ecuación de Navier-Stokes, con estas hipóte-  
 sis, se escribe entonces:

$$\frac{\rho \partial}{\partial t} \begin{pmatrix} 0 \\ 0 \\ v \end{pmatrix} + \rho \begin{pmatrix} 0 & 0 & 0 \\ 0 & 0 & 0 \\ \frac{\partial v}{\partial r} & \frac{1}{r} \frac{\partial v}{\partial \theta} & \frac{\partial v}{\partial z} \end{pmatrix} \begin{pmatrix} 0 \\ 0 \\ v \end{pmatrix} = \rho g \begin{pmatrix} \sin \alpha \sin \theta \\ \sin \alpha \cos \theta \\ -\cos \alpha \end{pmatrix} - \begin{pmatrix} \frac{\partial P}{\partial r} \\ \frac{1}{r} \frac{\partial P}{\partial \theta} \\ \frac{\partial P}{\partial z} \end{pmatrix} + \text{div } \tau$$

con la  $\text{div } \tau$  dada por la ecuación (4) de la sección 0.3.

La variación de presión sobre cada componente-  
 cilíndrica será entonces:

$$\frac{\partial P}{\partial r} = \rho g \operatorname{sen} \alpha \operatorname{sen} \theta + \tau_r \text{ -----(3)}$$

$$\frac{\partial P}{\partial \theta} = r \rho g \operatorname{sen} \alpha \cos \theta + r \tau_\theta \text{ -----(4)}$$

$$\frac{\partial P}{\partial z} = -\rho \frac{\partial v}{\partial t} - \rho v \frac{\partial v}{\partial z} - \rho g \cos \alpha + \tau_z \text{ -----(5)}$$

Estas tres ecuaciones constituyen el balance del momento total debido a todas las fuerzas actuantes dentro de un pozo geotérmico.

### V.2.2.- DISCUSION DEL BALANCE DE MOMENTO EN LA DIRECCION DEL FLUJO.-

Para velocidades de flujo suficientemente altas, podemos considerar que la pérdida de presión principal ocurre sobre Oz y que la única componente no nula del tensor de viscosidades es precisamente  $\tau_{rz}$ . Obtendremos entonces:

$$\frac{\partial P}{\partial z} = -\rho \frac{\partial v}{\partial t} - \rho v \frac{\partial v}{\partial z} - \rho g \cos \alpha + \frac{\partial \tau_{rz}}{\partial z} \text{ -----(6)}$$

caída total de presión.      cambio de presión por variación instantánea de velocidad.      pérdida de presión por aceleración.      pérdida de presión por gravedad.      pérdida de presión por fricción.

Esta última ecuación (6), es sobre la que se realiza usualmente el análisis numérico de la caída total de presión en un pozo.

### V.2.3.- FACTOR DE FRICCIÓN.-

La variación del esfuerzo cortante viscoso -- dentro del tubo, se considera proporcional a la energía cinética del fluido, es decir:

$$\frac{\partial \tau_{rz}}{\partial z} = \gamma \frac{\rho v^2}{2} \text{-----}(7)$$

en donde  $\gamma$  es un factor de proporcionalidad que tiene unidades de  $\frac{1}{m}$ .

Este coeficiente depende tanto de las dimensiones como de la geometría y de la rugosidad del tubo. Su naturaleza es complicada y solo puede determinarse de manera empírica. Usualmente se expresa en función de las dimensiones del tubo y del factor de fricción mediante la relación experimental:

$$\gamma = \frac{P}{4S} f$$

en donde P es el perímetro interno del tubo, S su área seccional y f el factor de fricción de Moody. Entonces (7) se escribe:

$$\frac{\partial \tau_{rz}}{\partial z} = - \frac{Pf}{4S} \frac{\rho v^2}{2} \text{-----}(8)$$

La expresión más común para la variación lineal del esfuerzo cortante se hace en términos del diámetro efectivo del tubo, el cual puede variar de sección en sección. Si R es el radio interno, entonces  $D = 2R$ , y como  $S = \pi R^2$  y  $P = 2\pi R \Rightarrow 4S/P = 2R = D$ .

Por tanto:

$$\frac{\partial \tau_{rz}}{\partial z} = - \frac{f}{D} \frac{\rho v^2}{2} \text{-----}(9)$$

Reemplazando (9) en (6):

$$\frac{\partial P}{\partial z} = - \rho \frac{\partial v}{\partial t} - \rho v \frac{\partial v}{\partial z} - \rho g \cos \alpha - \frac{f}{D(z)} \frac{\rho v^2}{2} \text{-----}(10)$$

Esta última ecuación es la que se usa comúnmente en la simulación numérica del pozo.

#### V.2.4.- FLUJO PERMANENTE.-

Si el movimiento del fluido es permanente: --

$\frac{\partial v}{\partial t} = 0$  y la ecuación (10), deviene:

$$\frac{\partial P}{\partial z} = - \rho v \frac{\partial v}{\partial z} - \rho g \cos \alpha - \frac{f}{D(z)} \frac{\rho v^2}{2} \text{-----}(11)$$

#### V.3.- BALANCE DE ENERGIA EN POZOS GEOTERMICOS.

**OBJETIVO:** Escribir explícitamente la conservación de la energía total dentro de un pozo geotérmico.

##### V.3.1.- CASO GENERAL.-

Reconsideremos la ecuación desarrollada en --

o.2.2.:



$$\frac{\partial}{\partial t} (\rho e) + \text{div} (\rho e \vec{v}) = \vec{f} \cdot \vec{v} - \text{div} (P \vec{v}) + \text{div} (\tau \cdot \vec{v}) - \text{div} \vec{q} \dots$$

Bajo hipótesis análogas a las de secciones anteriores, sobre el campo de velocidades y las fuerzas actuantes, cada término se traduce en lo siguiente:

$$\vec{f} \cdot \vec{v} = \rho g \begin{pmatrix} \text{sen} \alpha \text{ sen} \theta \\ \text{sen} \alpha \text{ cos} \theta \\ -\text{cos} \alpha \end{pmatrix} \cdot \begin{pmatrix} 0 \\ 0 \\ v \end{pmatrix} = - \rho g \text{ cos} \alpha$$

$$\text{div} (P \vec{v}) = \frac{\partial}{\partial z} (P v) ; \quad \tau \cdot \vec{v} = \begin{pmatrix} \tau_{rz} \cdot v \\ \tau_{\theta z} \cdot v \\ \tau_{zz} \cdot v \end{pmatrix}$$

Siendo  $\text{div} (\tau \vec{v})$ , el trabajo total de los esfuerzos viscosos lo representaremos mediante  $-\frac{\partial W}{\partial z}$ . Asimismo tomaremos  $\text{div} \vec{q} = \frac{\partial q}{\partial z}$  solamente.

Como además la entalpía específica es  $h = u + \frac{P}{\rho}$

deducimos finalmente:

$$\frac{\partial}{\partial t} \left( \rho u + \frac{\rho v^2}{2} \right) + \frac{\partial}{\partial z} \left[ \rho v \left( h + \frac{v^2}{2} \right) \right] = - \rho g v \text{ cos} \alpha - \frac{\partial}{\partial z} (q + W) \dots (1)$$

La ecuación (1), se interpreta como el balance de energía total del fluido dentro del pozo geotérmico. En el caso de flujo permanente, el término  $\frac{\partial}{\partial t}$  desaparece.

#### V.4.- FLUJO MONOFASICO EN POZOS GEOTERMICOS.-

OBJETIVO: Adquirir las técnicas de resolución del problema de flujo en una fase para los casos que se presentan en los pozos geotérmicos, líquido y vapor, ambos en una sola fase.

Las ecuaciones que dedujimos en V.1, V.2 y V.3 consideran el flujo del fluido en una sola fase, por consiguiente, todo lo hasta aquí desarrollado corresponde a flujo monofásico. A continuación presentamos un algoritmo desarrollado por el Ing. Héctor Gutiérrez Puente (Ref. 1), que permite calcular la caída de presión en un pozo dentro del cual fluye solo vapor.

##### V.4.1.- DEDUCCION DE LA ECUACION DE FLUJO PARA EL CASO DE VAPOR SECO SATURADO O SOBREALENTADO FLUYENDO A TRAVES DE UNA TUBERIA VERTICAL.

ECUACION DE CONTINUIDAD.- 
$$\int_V \frac{\partial \rho}{\partial t} dV = \int_{sc} \bar{\rho} \bar{v} \cdot ds$$

para estado permanente: 
$$-\int_{sc} \bar{\rho} \bar{v} ds = 0$$

Integrando a lo largo de un tubo de corriente de sección transversal conocida.

$$\rho_1 \bar{v}_1 S_1 = \rho_2 \bar{v}_2 S_2 = \text{CTE.} \quad \text{-----(1)}$$

##### ECUACION DE FUERZAS.-

$$\frac{\partial (\bar{v}^2/2)}{\partial z} + f \frac{1}{D} \frac{\bar{v}^2}{2} + \frac{1}{\rho} \frac{\partial p}{\partial z} = 0 \quad \text{-----(2)}$$

### ECUACIÓN DE ENERGÍA.-

$$q_H + p_1/\rho_1 + gz_1 + \frac{\bar{V}_1^2}{2} + u_1 = W_s + p_2/\rho_2 + gz_2 + \frac{\bar{V}_2^2}{2} + u_2 \text{ -----(3)}$$

La determinación de las caídas de presión a lo largo de la tubería consiste en resolver las tres expresiones anteriores, para lo cual se hacen las siguientes consideraciones:

- a).- El flujo de gas ocurre en régimen permanente.
- b).- No existe intercambio de calor entre el fluido y las paredes del pozo ( $dq_H = 0$ ).
- c).- No se efectúa trabajo por o sobre el fluido ( $dW_s = 0$ ).

Las tres ecuaciones anteriores quedarán como:

### ECUACIÓN DE CONTINUIDAD.-

$$\dot{m} = \rho_1 \bar{V}_1 A_1 = \rho_2 \bar{V}_2 A_2 \text{ -----(1')}$$

### ECUACIÓN DE FUERZAS.-

$$\frac{\bar{V}_1^2}{2} - \frac{\bar{V}_2^2}{2} + f \frac{\bar{V}_1^2}{2D} (Z_1 - Z_2) + \frac{1}{\rho} dp \text{ -----(2')}$$

### ECUACIÓN DE ENERGÍA.-

$$h_1 + \frac{\bar{V}_1^2}{2} + gz_1 = h_2 + \frac{\bar{V}_2^2}{2} + gz_2 \text{ -----(3')}$$

Si hacemos la hipótesis (generalmente aceptada), de que el flujo de vapor dentro del pozo ocurre mediante un proceso isoentálpico, e introduciendo la ecuación de estado a partir de los calores específicos del vapor;

$$\left(\frac{k}{k-1}\right) \frac{p_1}{\rho_1} = \left(\frac{k}{k-1}\right) \frac{p_2}{\rho_2} \quad \text{-----(4)}$$

Entonces, la ecuación (3') puede ser escrita como:

$$\frac{\bar{v}^2}{2} + gz_2 = \frac{\bar{v}_1^2}{2} + gz_1$$

$$\bar{v}_2^2 = \bar{v}_1^2 + 2g(z_1 - z_2) \quad \text{-----(5)}$$

de la ecuación (3), para entalpía constante:

$$\frac{p_1}{\rho_1} = \frac{p_2}{\rho_2} = \text{CTE}$$

$$\frac{1}{\rho} = \frac{\text{CTE}}{p} \quad \text{-----(6)}$$

Sustituyendo (5) y (6) en (2') y haciendo  $z_1 - z_2 = \Delta z$

$$\frac{\bar{v}_1^2}{2} - \frac{\bar{v}_1^2 + 2g \cdot \Delta z}{2} + \frac{f}{2} \frac{\bar{v}_1^2}{2} \Delta z + \text{CTE} \frac{dp}{\rho} = 0 \quad \text{-----(7)}$$

Integrando entre dos profundidades dadas de la línea de flujo y multiplicando por 2:

$$\bar{v}_1^2 - \bar{v}_1^2 + 2g\Delta z + \frac{f}{D} \bar{v}^2 \Delta z + 2 \cdot \text{CTE} \quad [ \text{Ln } p_2 - \text{Ln } p_1 ] = 0 \quad \text{-----(8)}$$

$$- 2g \Delta z - \frac{f}{D} v^2 \Delta z + 2 \text{CTE} \ln p_1 = 2 \text{CTE} \ln p_2 \quad \text{-----}(9)$$

como  $\Delta z = z_1 - z_2$ , pero siempre  $z_1 < z_2$  para un pozo en consecuencia, cambiamos el signo de  $\Delta z$  y tomamos solo el valor absoluto de la longitud del intervalo en que sea dividida la línea de flujo.

$$\frac{2g \Delta z + \frac{f}{D} v^2 \Delta z + 2 \text{CTE} \ln p_1}{2 \text{CTE}} = \ln p_2 \quad \text{-----}(10)$$

haciendo:

$$A = 2g \Delta z + \frac{f}{D} v^2 \Delta z \quad \text{-----}(11)$$

$$B = 2 \text{CTE} \quad \text{-----}(12)$$

$$- \frac{A + 2 B \ln p_1}{2B} = \ln p_2$$

Finalmente:

$$p_2 = e^{\frac{A}{2B} + \ln p_1} \quad \text{-----}(13)$$

H. Gutiérrez propuso un algoritmo para la determinación de las caídas de presión en un pozo geotérmico fluyendo vapor saturado o sobrecalentado.

En la determinación de las caídas de presión en un pozo de vapor se utiliza generalmente datos de producción del pozo tales como: Gasto de vapor producido (másico), presión en la cabeza del pozo (fluyendo), temperatura del vapor en la cabeza del pozo (fluyendo), entalpía del vapor medida a condiciones de flujo.

Datos del pozo tales como: Profundidad del horizonte --- expuesto a producción, diámetros de las tuberías de producción, rugosidad relativa ( $\xi/D$ ) de las tuberías de producción, profundidades de los cambios de diámetro.

Con los datos anteriores el procedimiento propuesto es:

- a).- Elegir el número de intervalos en que se quiera dividir la profundidad del pozo. ( $\Delta z$ )
- b).- Calcular el área de la sección transversal de la tubería de producción a la primera profundidad.

$$S = \frac{\pi D^2}{4}$$

- c).- Con la temperatura del vapor en la superficie, determinar su viscosidad.

$$\mu = 0.407 \times 10^{-7} T + 80.4 \times 10^{-7}$$

- d).- Con la presión y la entalpía en la superficie determinar la densidad del vapor en la superficie.

Esto se puede realizar mediante las tablas de vapor o --- bién utilizando alguna correlación ya calibrada para este fin.

- e).- Calcular la velocidad del vapor en la boca del pozo.

$$\bar{v} = \frac{\dot{w}}{\rho S}$$

- f).- Calcular el número de Reynolds.
- g).- Determinar el coeficiente de fricción mediante el diagrama de Moody o bién resolviendo la ecuación propuesta por Colebrook;

$$\frac{1}{\sqrt{f}} = 4.0 \log (D/\xi) + 2.28 - 4 \log \left( 1 + \frac{4.67 D/\xi}{Re \sqrt{f}} \right)$$

h).- Con los datos anteriores podremos calcular la presión de fondo fluyendo en el intervalo siguiente, mediante la expresión;

$$p_2 = e^{\frac{A}{2B}} + \ln p_1$$

en donde:

$$A = 2g \Delta z + \frac{f}{D} v^2 \Delta z$$

$$B = 2 CTE = 2 p/\rho$$

i).- Con el valor de la presión en el punto 2, repetir ---  
pasos d, e y h hasta alcanzar la presión de fondo ---  
fluyendo final.

## V.5.- FLUJO BIFASICO EN POZOS GEOTERMICOS.-

### INTRODUCCIÓN.-

Por flujo polifásico se entiende el movimiento simultáneo de varias fases de un mismo fluido compuesto por una sola sustancia química. Las fases pueden ser líquida, gaseosa o sólida. En el caso de pozos geotérmicos el flujo puede ser trifásico (gas, vapor, líquido). Nosotros consideraremos en lo que sigue, la manera en que puede analizarse el flujo bifásico del agua, es decir, el movimiento simultáneo de líquido y vapor dentro del pozo.

Todas las ecuaciones deducidas en secciones anteriores, -- gobiernan también al flujo en dos fases; su uso requiere sólo una --- ligera complicación con respecto al flujo monofásico. Existen sin em--- bargo varios métodos para analizar el flujo bifásico empleando las --- ecuaciones fundamentales:

- 1).- Ecuaciones diferenciales parciales: A partir de las leyes diferenciales de V.1, V.2 y V.3, se calcula numéricamente la caída de presión y la velocidad.
- 2).- Ecuaciones integrales: Con condiciones de frontera y simplificaciones adecuadas, se supone cierta distribución de velocidades en el tubo, escribiendo las ecuaciones básicas en forma integral a la cual se le aplica algún método numérico de resolución.
- 3).- Modelos analíticos: Estos se plantean al simplificar lo más posible las ecuaciones de flujo mediante hipótesis que eliminan los detalles del comportamiento real del fluido.- Esto permite encontrar una solución exacta para las ecuaciones así escritas.





### 3.2 Flow Equation From First Law

The flow equation can also be derived directly from the First Law of Thermodynamics if the proper assumptions are made.

#### Energy

$$\frac{dQ}{dL} - \frac{dW}{dL} = \frac{d}{dL} \left( H + \frac{v^2}{2} + gz \right) \quad (3.4)$$

Two important relationships are then used:

1.  $dH = Tds + vdp$  ( $v = 1/\bar{\rho}$ )

2.  $\int Tds = Q + F$   
 $Tds = dQ + dF$

where  $F$  is the frictional loss

Substituting these expressions into (3.4) yields

$$-\frac{dW}{dL} = \frac{1}{\bar{\rho}} \frac{dp}{dL} + v \frac{dv}{dL} + g \frac{dz}{dL} + \frac{dF}{dL} \quad (3.5)$$

Assuming no work done on or by the system yields the familiar form

$$-\frac{dp}{dL} = \bar{\rho} g \sin \theta + \bar{\rho} \frac{dF}{dL} + \rho v \frac{dv}{dL} \quad (3.6)$$

### 3.3 Friction Term

The friction term in (3.3) is more easily interpreted than that in (3.5). The wall shear stress exerted by the fluid is assumed to be given by the proportion

$$\tau_w \propto \frac{\bar{\rho} v^2}{2} \quad (3.7)$$

The friction gradient then takes the form

$$\left(\frac{dp}{dL}\right)_f = C_f \frac{2\bar{\rho} v^2}{g_c d} \quad (3.8)$$

where  $C_f$  = influence coefficient of proportionality.

This is by definition the Fanning friction relation. In terms of the Moody or Darcy-Weisbach friction factor,  $f_m = 4C_f$ .

It has been determined experimentally that the friction factor is related to the Reynolds number and relative pipe roughness ( $k/d$ ). The standard Moody chart is included. The Reynolds number is a standard dimensionless group given by the relationship:

$$N_{Re} = \frac{\rho v d}{\mu} \quad (3.9)$$

where  $\rho$  = density, lb/ft<sup>3</sup>  
 $\mu$  = viscosity, lb/ft/sec  
 $v$  = velocity, ft/sec  
 $d$  = diameter, ft

For gas flow, this number is conveniently evaluated in field units by the expression

$$N_{Re} = 20.0 \frac{q_G \gamma_G}{\mu d}$$

where  $q_G$  = flow, Mscf/d  
 $\gamma_G$  = gas gravity  
 $\mu$  = viscosity in centipoise  
 $d$  = diameter, inches

### 3.4 Modification for Two-Phase Flow

In two-phase flow the mixture is nearly always assumed to be homogeneous from the viewpoint of flow equation derivation. Given this assumption and neglecting the acceleration terms, corrections need only be made to the head term and friction term to account for deviations from homogeneity.

The head term is usually assumed to be accounted for through a volume weighted mixture density in the form:

$$\bar{\rho} = \rho_L \epsilon_L + \rho_G (1 - \epsilon_L) \quad (3.11)$$

The term  $\epsilon_L$  is the in-situ volume fraction liquid accounting for slip and is the subject of empirical correlation efforts.

The friction term is usually assumed to be accounted for through the friction factor in the form:

$$f_{tp} = R_c f_{ns} \quad (3.12)$$

The term  $R_c$  is empirically correlated while  $f_{ns}$  is the non-slip friction factor depending upon a particular correlation. For many vertical flow correlations,  $R_c$  is assumed to be 1.0 with all corrections in the head term.

### 3.5 Flow Regimes

Determination of flow regimes for a steam water mixture is not necessarily an easy task. It is not clear that two-component immiscible charts will apply to single-component systems. In any case, the flow regime types will be the same.

Figure 1 shows a typical geothermal wellbore with all of the possible flow regimes in diagrammatic form. Figure 2 shows the flow regime map for an air-water system using the Ros velocity numbers:

$$N_G = v_{SG} (\rho_L / g\sigma)^{1/4} \quad (3.13)$$

$$\begin{aligned} N_L &= v_{SL} (\rho_L / g\sigma)^{1/4} \quad (3.14) \\ &= 1.938 v_{SL} (\rho_L / \sigma)^{1/4} \end{aligned}$$

Since the physical property group of both numbers is the same, the coordinates represent principally the superficial velocity of each phase at in-situ conditions.

In order to examine this map, take  $N_L = 1.0$  and vary  $N_G$  from 0.1 to 1000. This will traverse the map horizontally through three distinct flow regime classifications:

1. Liquid Phase Continuous (bubble flow);
2. Alternating Phases (slug and froth flow);
3. Gas Phase Continuous (annular and mist flow).

As steam is generated in a geothermal well during flow from bottom to top, the fluid normally passes through each of the flow regimes in the order listed above.

Griffith shows that the slug to annular regime change occurs at higher quality with higher pressure. This indicates that, for efficient operations, a relatively high backpressure should be maintained at the wellhead: if the wellhead pressure is lowered too much, then the well will tend to shift into the annular flow regime and the mass rate delivered from the reservoir will not be as great.

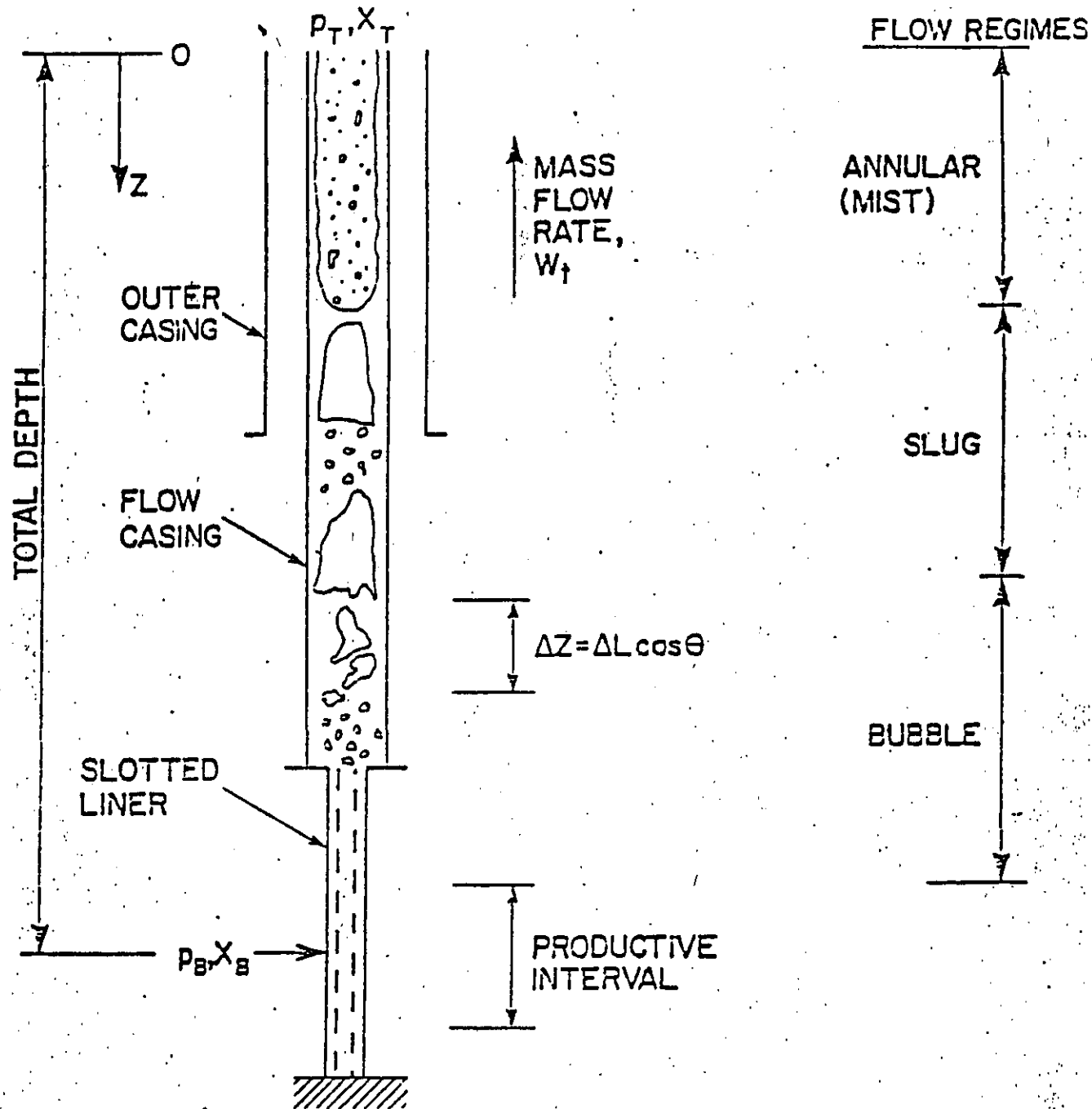


FIGURE 1. TYPICAL COMPLETION CHARACTERISTICS FOR A GEOTHERMAL STEAM/WATER PRODUCTION WELL





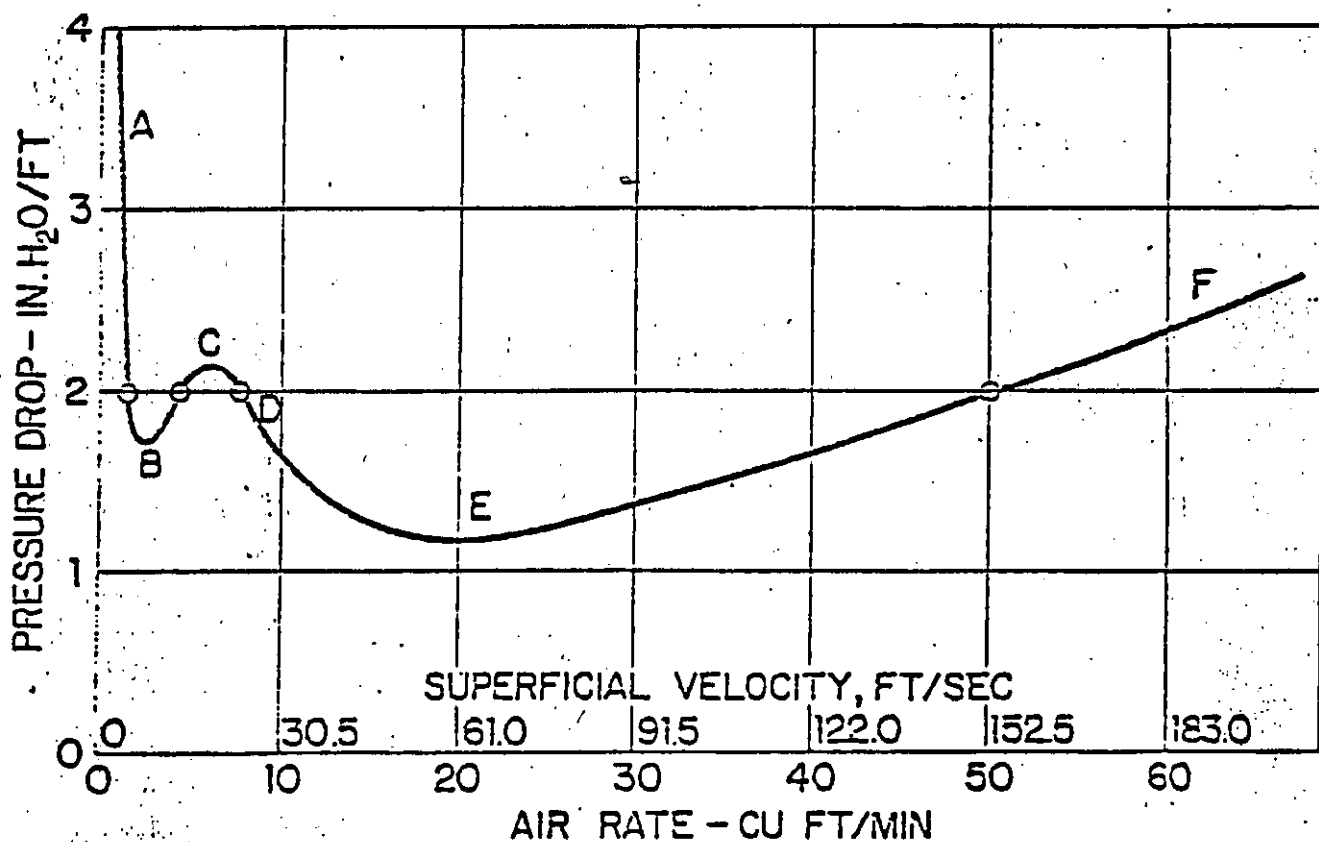
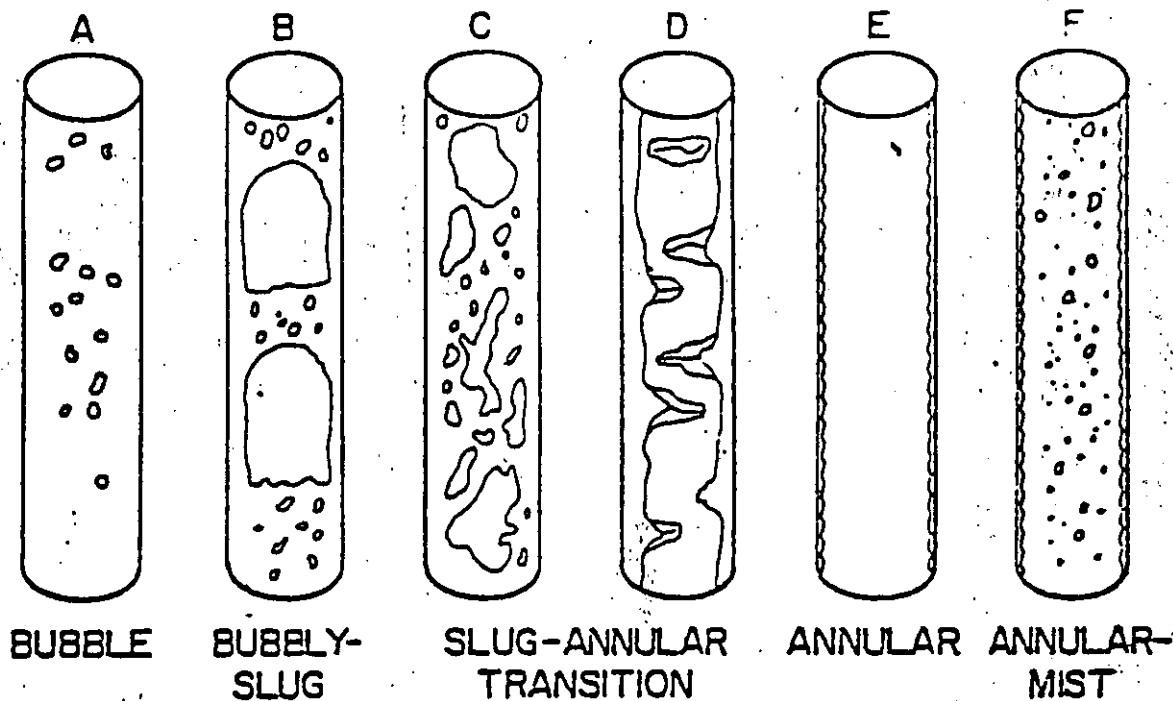


FIGURE 3. FLOW PATTERNS IN COCURRENT VERTICAL TWO-PHASE FLOW AND A PLOT OF PRESSURE DROP VERSUS AIR RATE IN A 1" I.D. TUBE

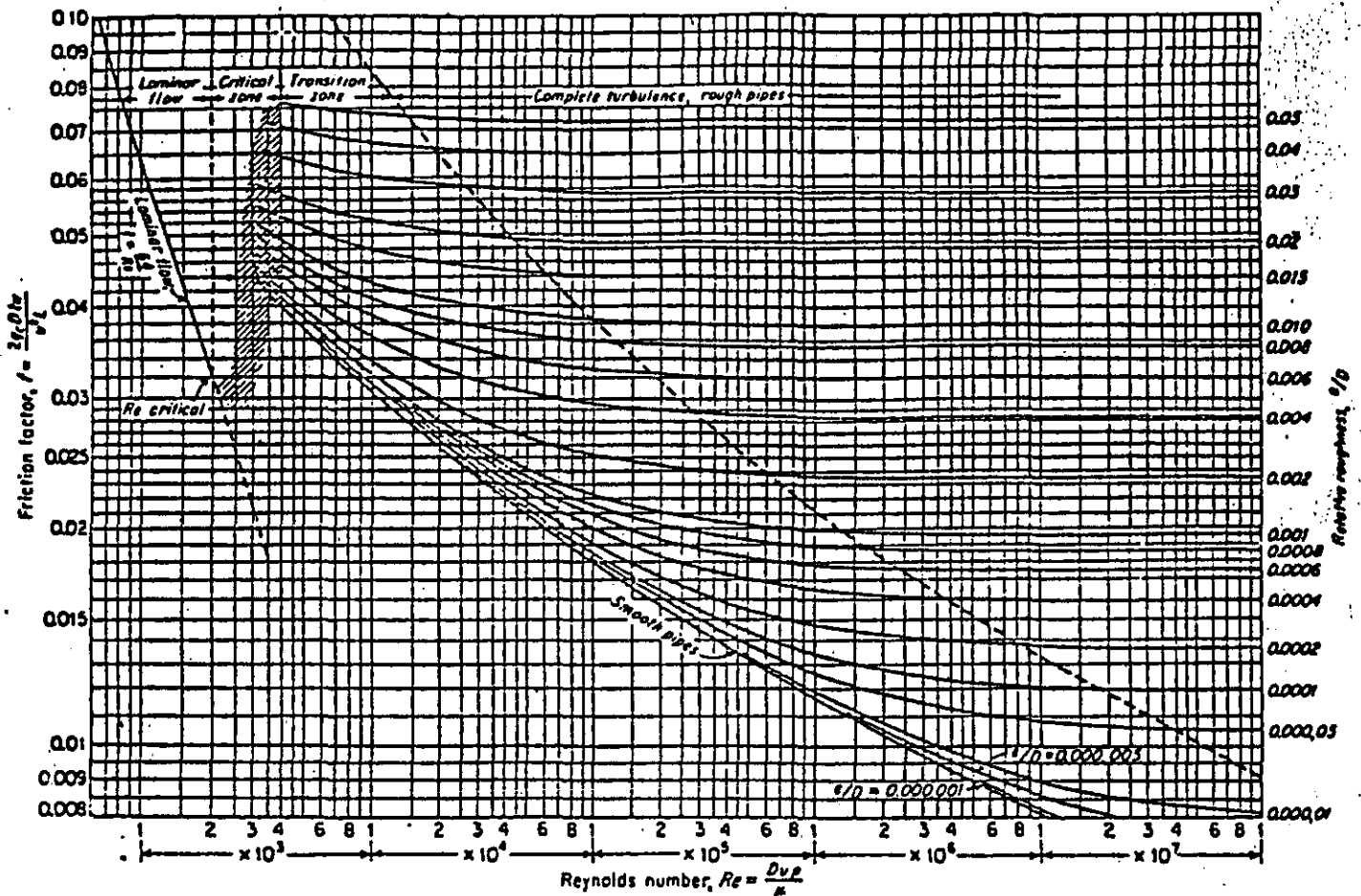


Fig. 7-3. Friction factor for flow of fluids in pipe. (Moody, 7-25. Courtesy ASME.)

Fig. 7-4. Friction factor at completely turbulent flow as function of roughness.

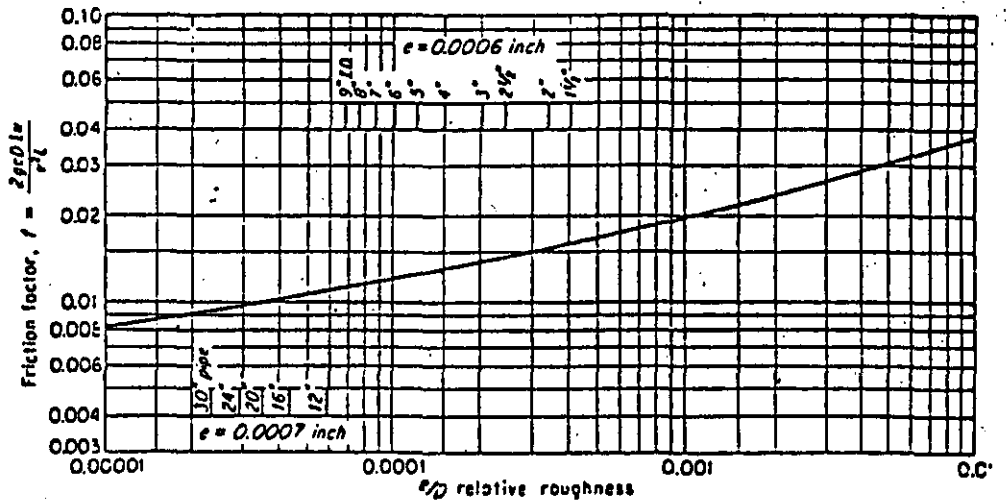
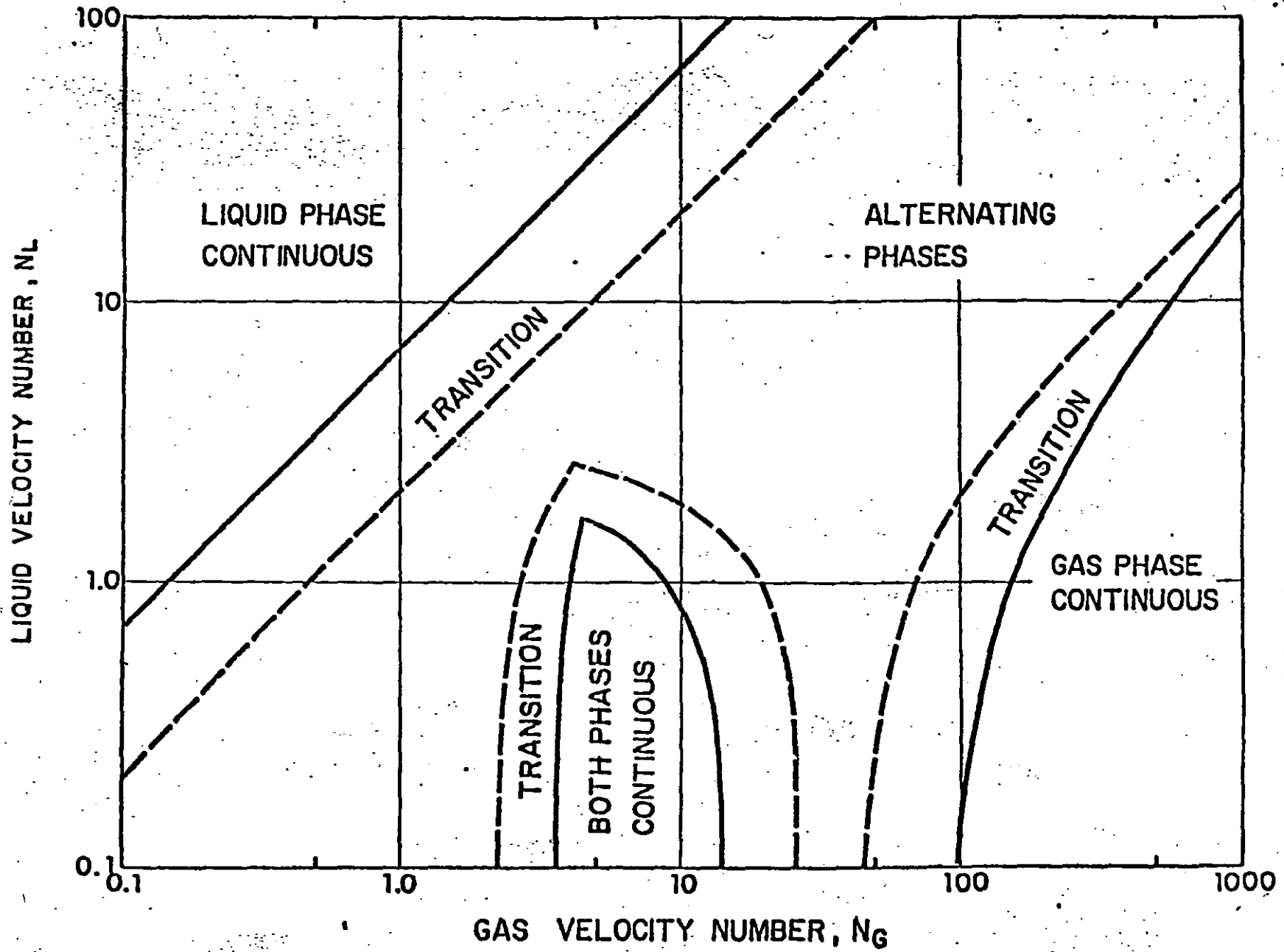


FIGURA 4.



FLOW REGIME MAP FOR VERTICAL TWO-COMPONENT FLOW IN A 1" PIPE

FIGURA 5.

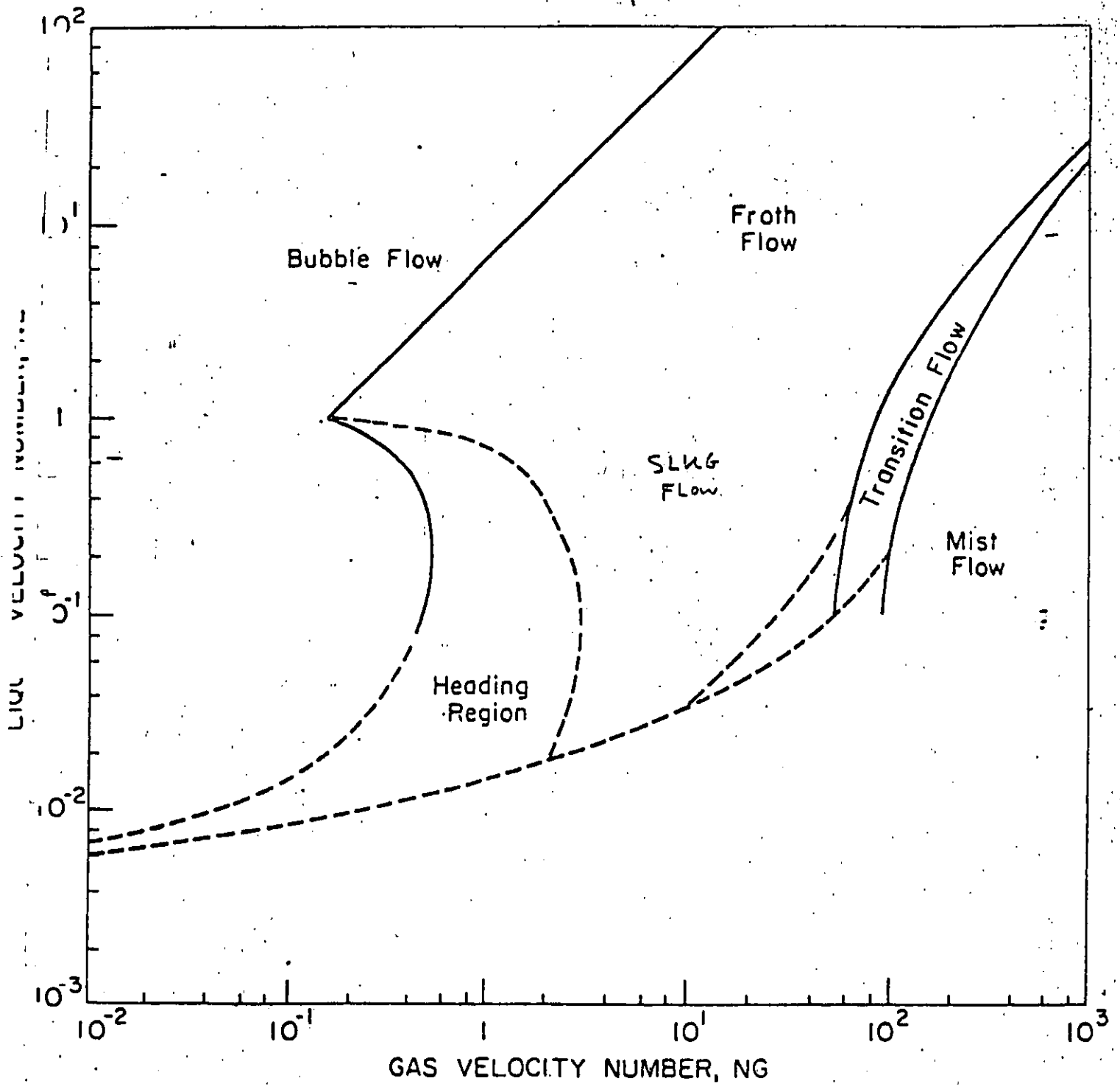
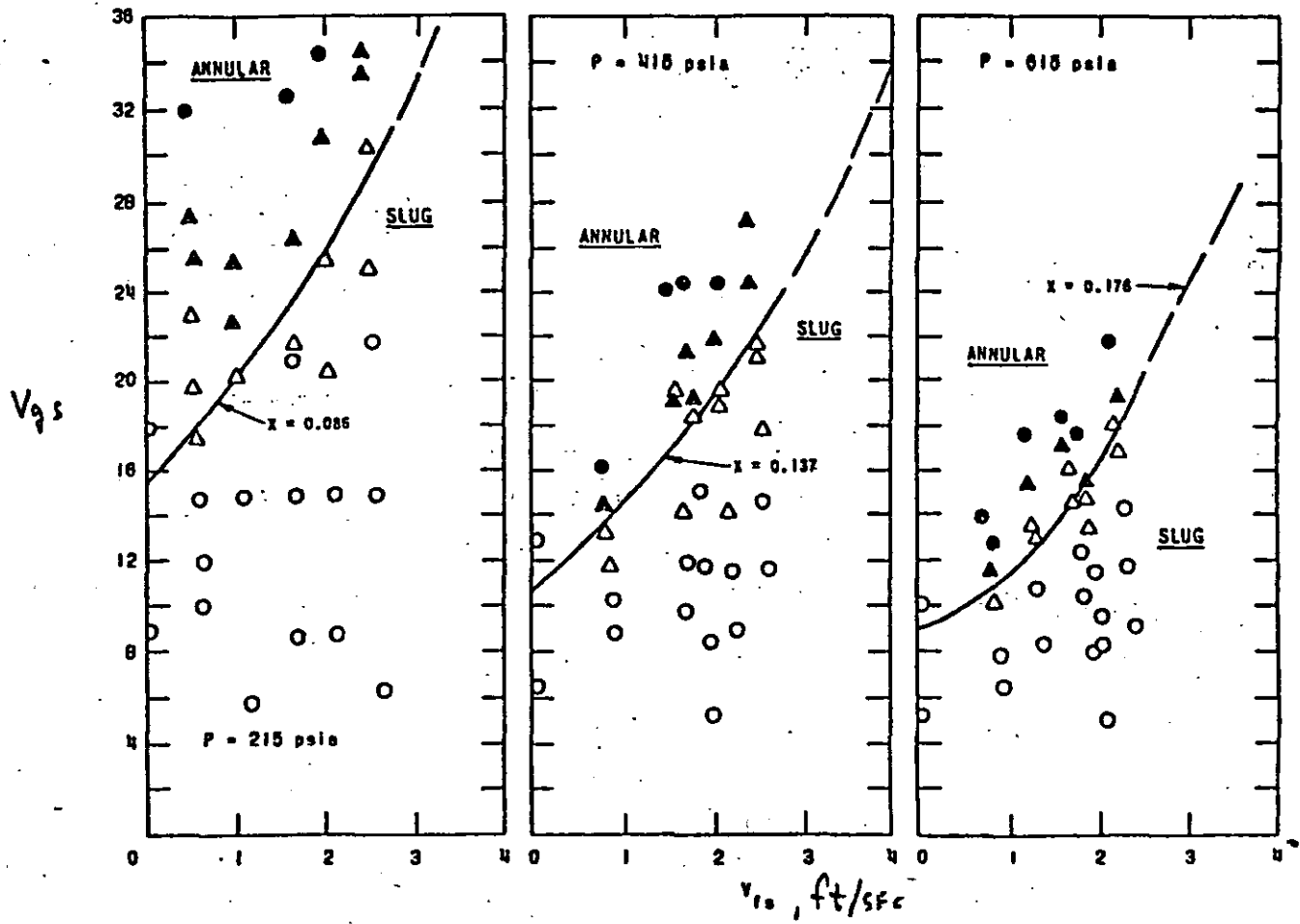


FIGURA 6.

Extended Flow Regime Map

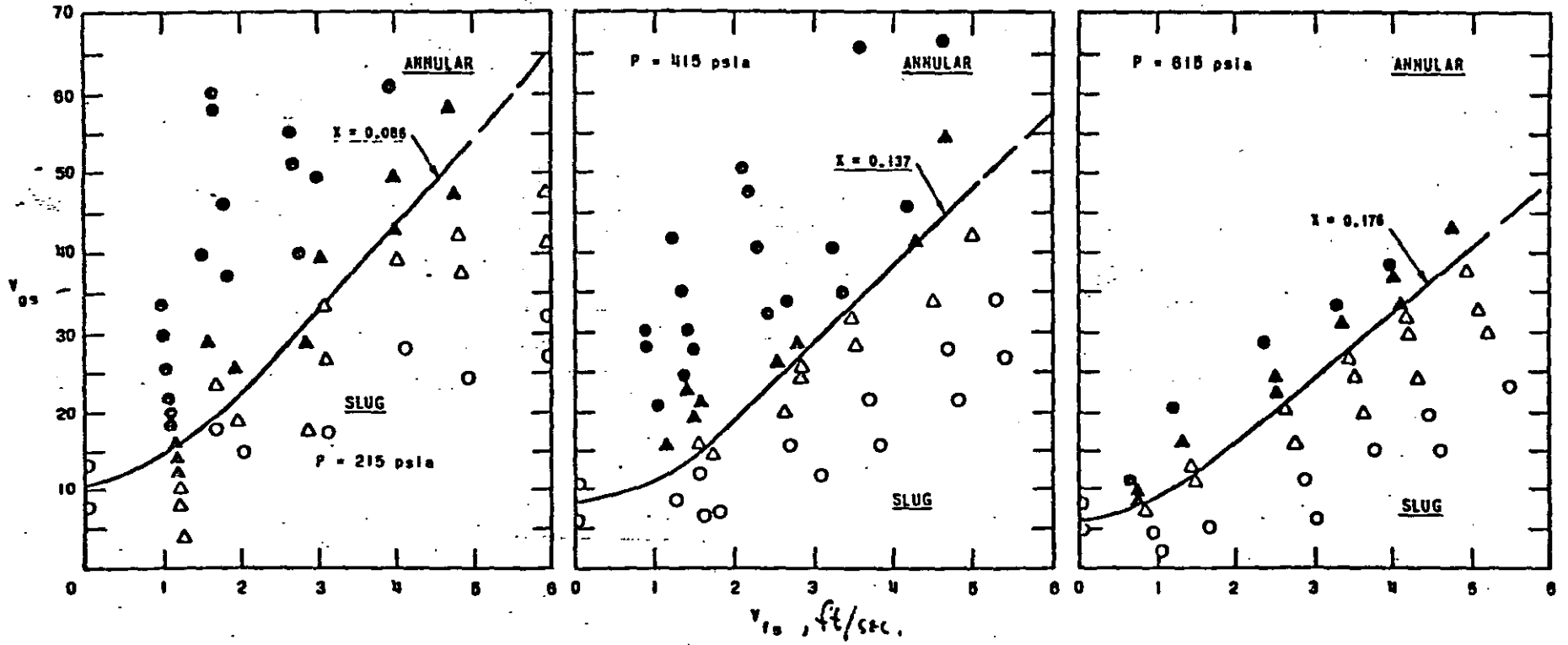


Figs. 6, 7, and 8. Flow Regime Maps (Using Top Probe) for 0.875-in. Pipe (steam-water)

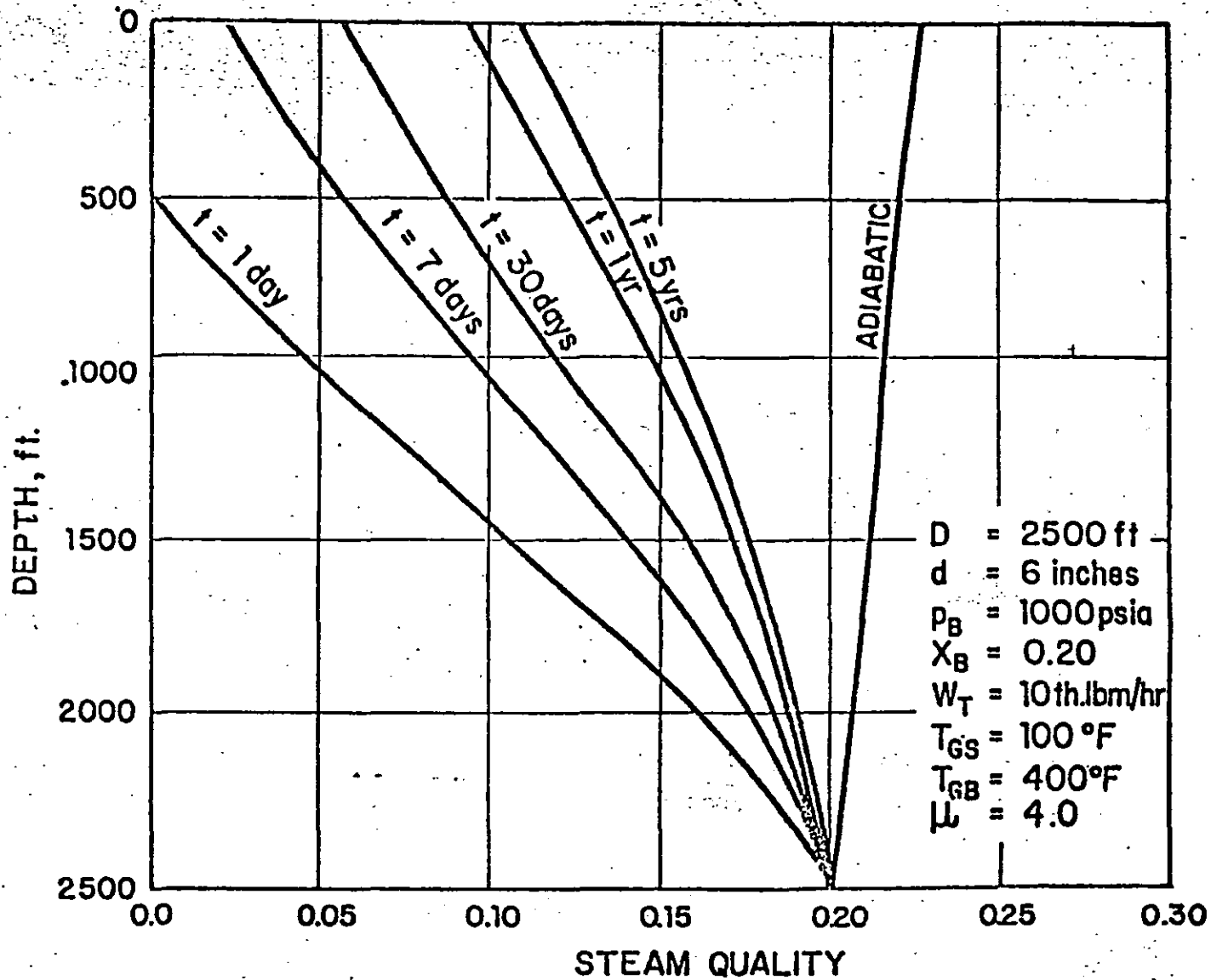
- pure ANNULAR
- △ ? transition
- slug

FIGURA 7.

FIGURA 8.



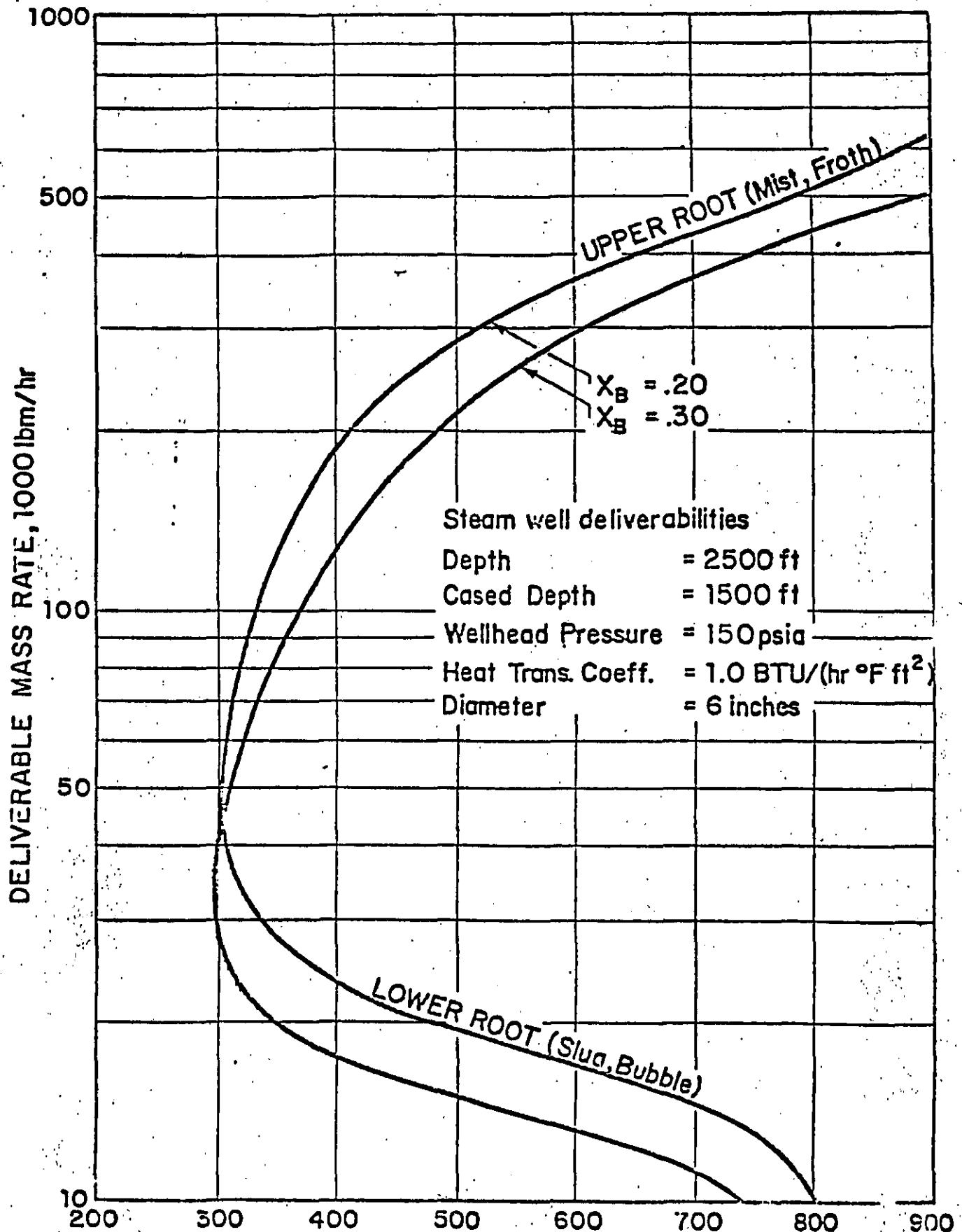
Figs. 9, 10, and 11. Flow Regime Maps (Using Top Probe) for 0.625-in. Pipe (steam-water)



VARIATION OF FLOWING QUALITY PROFILE WITH TIME

FIGURA 9.

FIGURA 10.



DELIVERABILITY FUNCTION SHOWING BOTH UPPER AND LOWER ROOTS



**6.- CORRELACIONES EMPIRICAS PARA  
CAIDA DE PRESION EN FLUJO BIFASICO.**

### 3.6 Griffith and Wallis Correlation

For the regime of liquid phase continuous or bubble flow, the Griffith and Wallis correlation is used most often in the literature. The vapor void fraction is derived directly from the drift flux concept and has the form

$$\alpha = 1/2 [1 + v_T/v_\infty - \sqrt{(1 + v_T/v_\infty)^2 - 4 v_{SG}/v_\infty}] \quad (3.15)$$

where  $\alpha$  = vapor void fraction

$v_T$  = total velocity

$v_\infty$  = bubble rise velocity

The bubble rise velocity is correlated by Griffith and Wallis for the regime of "plug" flow, or large bullet shaped bubbles. The correlation shows the rise velocity to be function of diameter.

In the liquid phase continuous regime, the flow velocity is higher than plug flow with the result that small bubbles tend to coalesce and large bubbles tend to break up due to turbulence. Harmathy<sup>43</sup> presents a correlation that accounts for this process:

$$v_\infty = 0.79 \left[ \frac{\sigma_D (\rho_L - \rho_G)}{\rho_L^2} \right]^{1/4} \quad (3.16)$$

where  $\sigma_D$  is the surface tension, dynes/cm.

For an air-water system,  $v_\infty$  equals 0.81 ft/sec. For a steam-water system, the surface tension is not well defined and the value of  $v_\infty$  is not therefore very accurate. However, the bubble flow regime does not usually occupy much pipe length due to rapid flashing in a typical wellbore.

Having developed Eqs. (3.15) and (3.16) for gas hold-up, we can write down the equations for  $\rho_{AV}$  and  $\tau_f$  in the bubble-plug flow regime:

$$\rho_{AV} = (1 - \alpha) \rho_L + \alpha \rho_G \quad (3.17)$$

$$\tau_f = \frac{f_m \rho_{AV} v_T}{2 g_c d} \quad (3.18)$$

Notice that the Moody friction factor based on the liquid Reynolds number is used here for  $\tau_f$ , since the flow regime is, by definition, liquid phase continuous. Under these conditions, the Moody friction factor has little effect on the overall pressure gradient, since the head term dominates.

### 3.7 Hagedorn and Brown Correlation

The correlation was developed originally for all flow regimes and is based on data from two-component air-water and gas-oil data. In this work the correlation has been restricted to the alternating phase region only (slug-froth flow). Separated correlations have been used for each of the other regions.

The mixture density is determined according to Eq. (3.11) with the hold-up fraction  $\epsilon_L$  computed from an empirical correlation that uses two dimensionless groups in addition to the Ros numbers:

$$N_d = 120.87 d \sqrt{\rho_L / \sigma_L} \quad (3.19)$$

$$N_\mu = 0.1573 \mu_L [1 / \rho_L \sigma^3]^{1/4} \quad (3.20)$$

The correlation takes the form of

$$\epsilon_L / \psi = f \left[ \left( \frac{N_L}{N_G} \right)^{0.575} \left( \frac{P}{P_A} \right)^{0.1} \left( \frac{C^*}{N_d} \right) \right] \quad (3.21)$$

where  $C^*$  is correlated with  $N$

$$\psi \text{ is correlated with } \left( \frac{N_G N_\mu^{0.38}}{N_d^{2.14}} \right)$$

Turn to the corresponding figures to see how the correlations interact. After determining  $C^*$  and  $\psi$ , then  $\epsilon_L$  is directly computed.

The friction factor is computed from a standard Moody chart using a two-phase Reynolds number where the hold-up fraction enters only through the viscosity.

$$\mu_m = \mu_L \epsilon_L + \mu_g (1 - \epsilon_L) ?$$

### 3.8 Orkiszewski Correlation

In order to develop his correlation for the alternating phase region, Orkiszewski had to introduce a new parameter,  $\Gamma$ , called the "liquid distribution function". He found that " $\Gamma$  correlates with total fluid velocity and liquid viscosity. The scatter of data may be attributable to such additional parameters as liquid velocity, GOR (gas-oil ratio) and interfacial tension". It is again not clear that a two-component correlation such as this would work at all for steam-water flow. If sufficient field data were available, it would certainly be worthwhile to re-correlate  $\Gamma$  for steam-water systems.

The Orkiszewski correlation for  $\rho_{AV}$  and  $\tau_f$  can then be written as follows:

$$\rho_{AV} = \frac{W_T + \rho_L v_b A}{q_T + v_b A} + \Gamma \rho_L \quad (3.22)$$

$$\tau_f = \frac{f_m \rho_L v_T^2}{2 g_c d} \left[ \frac{q_L + v_b A}{q_T + v_b A} + \Gamma \right] \quad (3.23)$$

In the above equations,  $v_b$  is the "bubble rise velocity" as correlated by Griffith and Wallis:

$$v_b = C_1 C_2 \sqrt{g d} \quad (3.24)$$

where  $C_1$  and  $C_2$  are functions of bubble and liquid Reynolds numbers. The liquid distributions function,  $\Gamma$ , is constrained by

$$\Gamma \geq -0.065 v_T \quad (3.25)$$

and

$$\Gamma \geq \frac{-v_b A}{q_T + v_b A} \left( 1 - \frac{\rho_{AV}}{\rho_L} \right) \text{ for } v_T > 10 \quad (3.26)$$

### 3.9 Ros Correlation

This correlation applies to the flow regime classified here as gas phase continuous. There has been a great deal of analytical and empirical work done on this flow regime. In fact, a book by Hewitt and Hall-Taylor, Annular Two-Phase Flow, was recently published. This regime is particularly important in steam-water systems where heat and mass transfer is occurring in the presence of two-phase flow.

For the hold-up correlation in this regime, Ros suggests that there is virtually no slip in annular-mist flow. This leads to the relationship that  $\epsilon_G = \alpha$ . However, the data of Govier and others have shown that, during annular flow, there is a great deal of slip. Consequently, the actual gas fraction in annular flow would be much less than that predicted by the assumption of no slip. On this basis, the author prefers the Turner relation as re-correlated by Wallis:

$$\frac{J_G^*}{1 - 3.1 \epsilon_L} - \frac{J_L^*}{3.1 \epsilon_L} = 1.0 \quad (3.27)$$

where,

$$J_G^* = v_{SG} \left[ \frac{\rho_G}{g d (\rho_L - \rho_G)} \right]^{1/2} \quad (3.28)$$

$$J_L^* = v_{SL} \left[ \frac{\rho_L}{g d (\rho_L - \rho_G)} \right]^{1/2} \quad (3.29)$$

Solving Eq. (3.27) for the hold-up,  $\epsilon_L$ , allows the calculation of average mixture density by Eq. (3.11). The relation for hold-up, Eq. (3.27), is only valid in the annular flow regime below a drop entrainment of about 20 percent. Above this value of entrainment, the hold-up should approach the...

non-slip fraction. Unfortunately, there is no available field data in oil, gas or geothermal wells that could test this proposal. Only laboratory data has been used to develop Eq. (3.27).

For the friction gradient in annular-mist flow, Rosin suggests that the superficial gas velocity be used with the friction factor based on this velocity and an empirically determined roughness ratio,  $\epsilon/d$ , to account for liquid on the walls.

$$\tau_f = \frac{f_m \rho_G v_{SG}^2}{2 g_c d} \quad (3.30)$$

The standard Moody chart is used to compute the friction factor.

## 4. HEAT BALANCE

### 4.1 Heat Transfer

The equations describing the heat conduction into a solid by a pipe flowing fluid are well established. The first step is to write a heat balance on the fluid flowing through the selected pipe increment. This is summarized by Ramey for single-phase flow. In two-phase flow, the kinetic energy is usually negligible, but is included in the following equation:

$$H_i = H_{i-1} - Q + \frac{g}{g_c} \frac{\Delta z}{J} + \frac{\Delta v_T^2}{2g_c J} \quad (4.1)$$

The heat balance nomenclature is summarized on Figure 3. The potential energy term in this equation is added because  $z$  is measured downwards. The total enthalpy is a function of the enthalpies of each phase ( $H_G$  and  $H_L$ ) and the flowing steam quality ( $x_i$ ):

$$H_i = H_G x_i + H_L (1 - x_i) \quad (4.2)$$

Assuming a pressure increment, the pressure is known at  $i$  and since the fluid is saturated, the temperature and enthalpy of each phase can be found in the steam tables. Using Eq. (4.1) to calculate  $H_i$ , Eq. (4.2) can be used to calculate the flowing quality  $x_i$ .

The heat transfer to the surroundings is given by the standard heat conduction formula in terms of an overall efficient,  $U$

$$Q = \frac{U \pi d \Delta L (T_{av} - T_g)}{w_T} \quad (4.3)$$



$T_{av}$  = average temperature of the increment,  
 $T_g$  = ground temperature at depth  $z$ ,  
 $w_T$  = total mass flow rate.

The overall heat transfer coefficient is a combination of convection in the casing-tubing annulus and conduction into the formation. Willhite<sup>21</sup> gives a good development of the equations. The final result is as follows:

$$U = \frac{hk}{(hr_t f(t) + k)} \quad (4.4)$$

where  $k$  = thermal conductivity  
 $h$  = convective coefficient  
 $r_t$  = tubing radius

If the wellbore completion is convection heat transfer controlled, then the time function gets cancelled out of Eq. (4.4). The time dependency function has been found to be accurate at times greater than a week for most reservoir problems. This function implies a radiation boundary condition that probably is not accurate at shorter times.

$$\text{where } f(t) = -\ln \left( \frac{r_c}{2\sqrt{\alpha t}} \right) - 0.290 \quad (4.5)$$

$\alpha$  = thermal diffusivity of the earth,  
 $r_c$  = casing outer radius,  
 $t$  = time since well opened for flow,

The film coefficient is usually negligible. In applications for which it is important, it should be noted that this coefficient is a function of flow regime.

## 4.2 Effects of Slip

It has been proposed that Eq. (4.2) be adjusted to account for the presence of excess liquid due to slip. There are thermodynamic arguments to the reverse.

This is an interesting point for current discussion. There is some field data that would be better matched if slip were included.

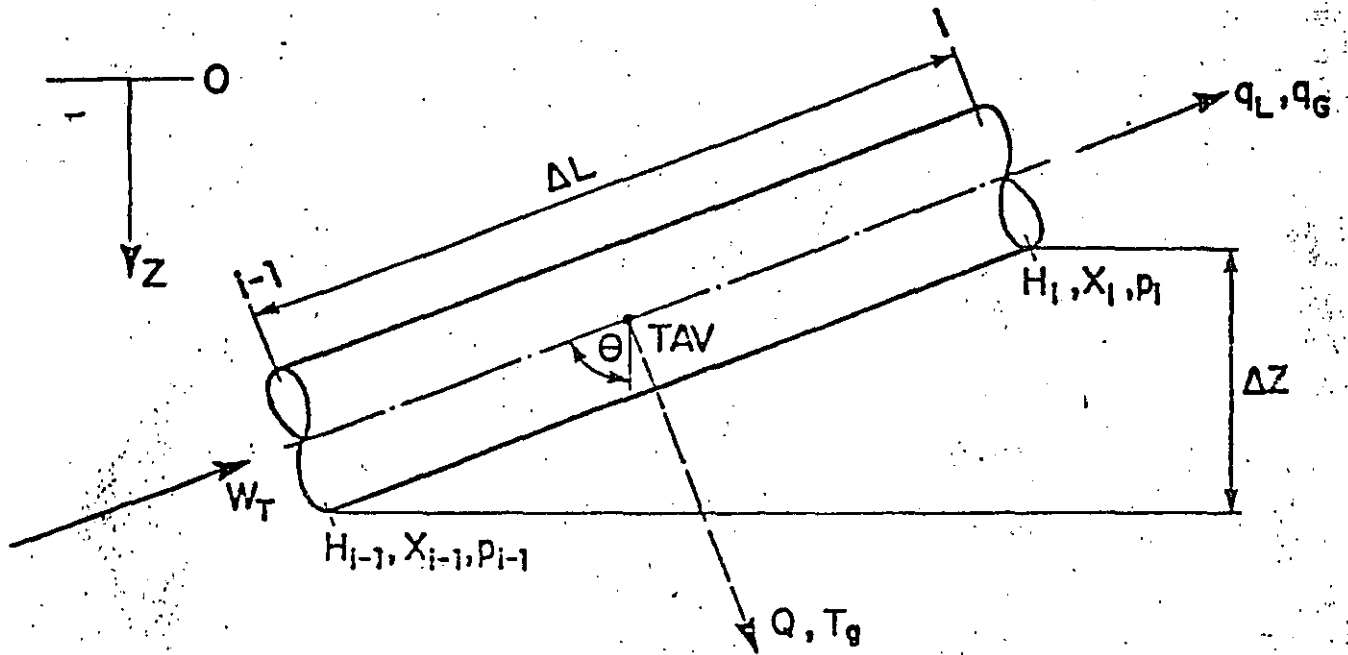
## 4.3 Transient Rock Temperatures

In many cases, such as short term well tests, the time function of Eq. (4.5) is insufficient. In addition, the time function approach does not easily allow for applications involving variable or reversed flow.

In order to account for this, a simple one-dimensional transient heat flux calculation is usually applied. The equation is written in radial coordinates as:

$$k \left( \frac{\partial^2 T}{\partial r^2} + \frac{1}{r} \frac{\partial T}{\partial r} \right) = \rho C_p \frac{\partial T}{\partial t} \quad (4.6)$$

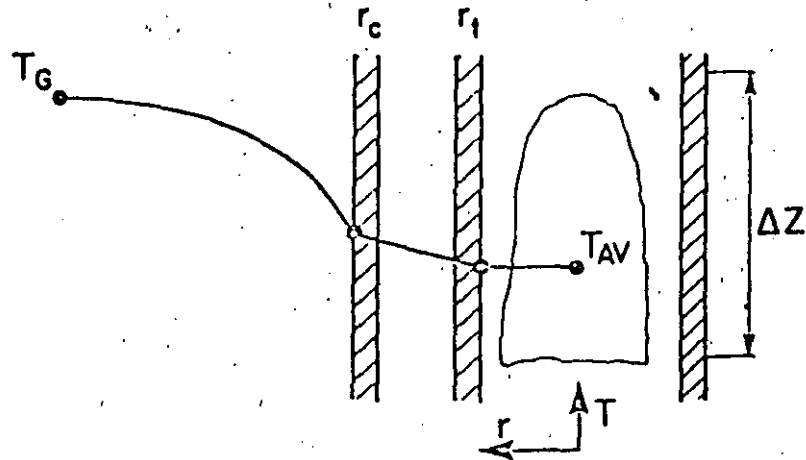
The use of this form of the heat flux calculation allows for variable rate with time by applying a fixed flux or temperature over the timestep. In addition, the system can be layered vertically with good results.



SCHMATIC OF HEAT TRANSFER NOMENCLATURE

FIGURA 11.

FIGURA 12.



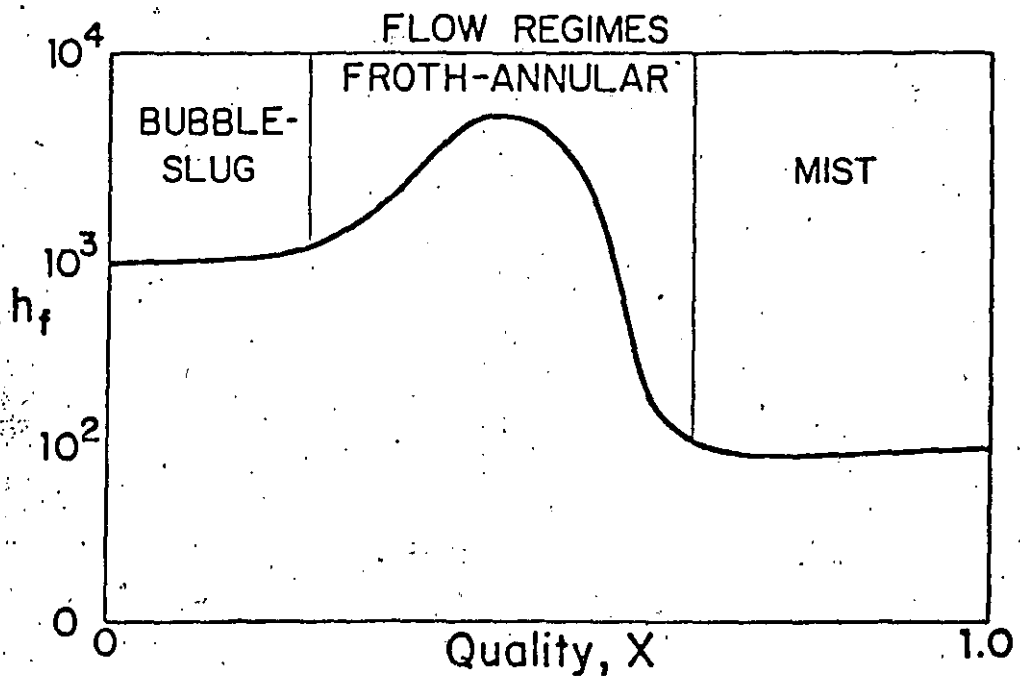
$$\frac{1}{U} = \frac{1}{k_G} + \frac{1}{h_c} + \frac{1}{h_f}$$

$U$  = overall heat transfer coefficient,  
BTU/(hr sq.ft °F)

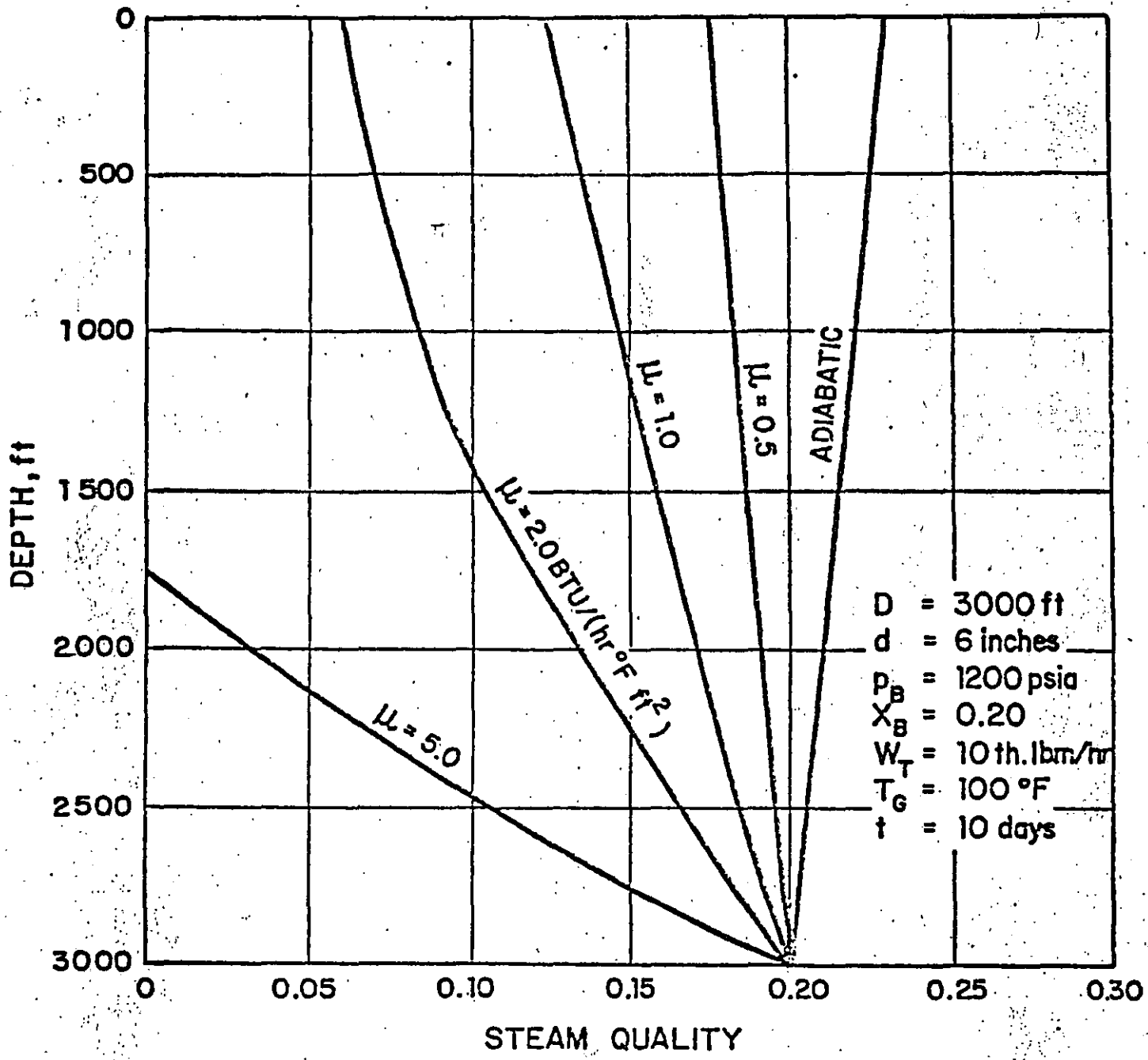
$h_f$  = boiling/condensing coefficient

$h_c$  = effective tubing/casing coefficient

$k_G$  = thermal conductivity of the ground



HEAT TRANSFER COEFFICIENTS



VARIATION OF FLOWING QUALITY PROFILE WITH HEAT TRANSFER COEFFICIENT AT RELATIVELY LOW FLOW RATE

FIGURA 13.

## 5. COUPLED EQUATIONS

### 5.1 Algorithms

It is important to couple the pressure drop equations to the heat transfer equations. Each of these depends upon the other. The pressure drop algorithm consists of a set of subroutines, one for each flow regime, that are called from a control routine. The heat transfer calculations have been imbedded in the control routine in order to iterate on pressure drop. The steam tables are entered in vector form so that any table variable can be determined knowing the value of one other. The specific enthalpy of each phase can be calculated knowing pressure or temperature.

The lengths in Eqs. (4.1) and (4.3) are not known at the beginning of an increment calculation. Using the pressure drop correlations and Eq. (3.6), an estimate of  $\Delta L$  can be calculated knowing the average quality. The quality determines the non-slip flow rates. Eqs. (4.1) and (4.3) determine the dependence of steam quality on  $\Delta L$ . An iterative procedure is then used for each increment in order to converge quality and pressure gradient. The calculations are completed when the sum of  $\Delta L$  equals the total length.

Of course an alternate scheme exists under which the length is specified. The equations would then be worked in reverse order and converged iteratively.

### 5.2 Analytical Methods

Ramey has shown how the heat and momentum balances can be coupled for single phase fluids with constant heat capacities. Refer to the enclosed paper and work out an example using this analytical solution.

### 5.3 Computed Results

Using the coupled equations, a number of interesting sensitivity calculations can be made. Figure 10 shows how the overall heat transfer coefficient affects the flowing quality profile. Figure 11 shows how the time function affects quality profiles. In general, the quality produced should improve with time.

Figure 12 shows the wellbore deliverability against fixed wellhead and bottomhole pressures. Cross plotting the formation deliverability will yield the expected system operating conditions.

TABLE 1. SATURATION TEMPERATURES

Temp F f	Abs Press.	Specific Volume			Enthalpy			Entropy			Temp F f
	lb Sq in. p	Sat. Liquid v <sub>f</sub>	Evap v <sub>fg</sub>	Sat. Vapor v <sub>g</sub>	Sat. Liquid h <sub>f</sub>	Evap h <sub>fg</sub>	Sat. Vapor h <sub>g</sub>	Sat. Liquid s <sub>f</sub>	Evap s <sub>fg</sub>	Sat. Vapor s <sub>g</sub>	
32	0.08854	0.01602	3308	3308	0.00	1075.8	1075.8	0.0000	2.1877	2.1877	32
35	0.09995	0.01602	2947	2947	3.02	1074.1	1077.1	0.0061	2.1709	2.1770	35
40	0.12170	0.01602	2444	2444	8.05	1071.3	1079.3	0.0162	2.1435	2.1597	40
45	0.14752	0.01602	2036.4	2036.4	13.06	1068.4	1081.5	0.0262	2.1167	2.1429	45
50	0.17811	0.01603	1703.2	1703.2	18.07	1065.6	1083.7	0.0361	2.0903	2.1264	50
60	0.2563	0.01604	1206.6	1206.7	28.06	1059.9	1088.0	0.0555	2.0393	2.0948	60
70	0.3631	0.01608	867.8	867.9	38.04	1054.3	1092.3	0.0745	1.9902	2.0647	70
80	0.5069	0.01608	633.1	633.1	48.02	1048.6	1096.6	0.0932	1.9428	2.0360	80
90	0.6982	0.01610	468.0	468.0	57.99	1042.9	1100.9	0.1115	1.8972	2.0087	90
100	0.9492	0.01613	350.3	350.4	67.97	1037.2	1105.2	0.1295	1.8531	1.9826	100
110	1.2748	0.01617	265.3	265.4	77.94	1031.6	1109.5	0.1471	1.8108	1.9577	110
120	1.6924	0.01620	203.25	203.27	87.92	1025.8	1113.7	0.1645	1.7694	1.9339	120
130	2.2225	0.01625	157.32	157.34	97.90	1020.0	1117.9	0.1816	1.7296	1.9112	130
140	2.8886	0.01629	122.99	123.01	107.89	1014.1	1122.0	0.1984	1.6910	1.8894	140
150	3.718	0.01634	97.06	97.07	117.89	1008.2	1126.1	0.2149	1.6537	1.8685	150
160	4.741	0.01639	77.27	77.29	127.89	1002.3	1130.2	0.2311	1.6174	1.8485	160
170	5.992	0.01645	62.04	62.06	137.90	996.3	1134.2	0.2472	1.5822	1.8293	170
180	7.510	0.01651	50.21	50.23	147.92	990.2	1138.1	0.2630	1.5480	1.8109	180
190	9.339	0.01657	40.94	40.96	157.95	984.1	1142.0	0.2785	1.5147	1.7932	190
200	11.528	0.01663	33.62	33.64	167.99	977.9	1145.9	0.2938	1.4824	1.7762	200
210	14.123	0.01670	27.80	27.82	178.05	971.6	1149.7	0.3090	1.4508	1.7598	210
212	14.896	0.01672	26.78	26.80	180.07	970.3	1150.4	0.3120	1.4448	1.7568	212
220	17.186	0.01677	23.13	23.15	188.13	965.2	1153.4	0.3239	1.4301	1.7440	220
230	20.780	0.01684	19.365	19.382	198.23	958.8	1157.0	0.3387	1.3901	1.7288	230
240	24.969	0.01692	16.308	16.323	208.34	952.2	1160.5	0.3531	1.3609	1.7140	240
250	29.825	0.01700	13.804	13.821	218.48	945.5	1164.0	0.3675	1.3323	1.6998	250
260	35.429	0.01709	11.746	11.763	228.64	938.7	1167.3	0.3817	1.3043	1.6860	260
270	41.858	0.01717	10.044	10.061	238.84	931.8	1170.6	0.3958	1.2769	1.6727	270
280	49.203	0.01726	8.628	8.645	249.06	924.7	1173.8	0.4096	1.2501	1.6597	280
290	57.556	0.01735	7.444	7.461	259.31	917.5	1176.6	0.4234	1.2238	1.6472	290
300	67.013	0.01745	6.449	6.466	269.59	910.1	1179.7	0.4369	1.1980	1.6350	300
320	89.66	0.01765	4.896	4.914	290.28	894.9	1185.2	0.4637	1.1478	1.6115	320
340	118.01	0.01787	3.770	3.788	311.13	879.0	1190.1	0.4900	1.0992	1.5891	340
360	153.04	0.01811	2.939	2.957	332.18	862.2	1194.4	0.5158	1.0519	1.5677	360
380	195.77	0.01836	2.317	2.335	353.45	844.6	1198.1	0.5413	1.0059	1.5471	380
400	247.31	0.01864	1.8447	1.8633	374.97	826.0	1201.0	0.5664	0.9608	1.5272	400
420	308.83	0.01894	1.4811	1.5000	396.77	806.3	1203.1	0.5912	0.9168	1.5078	420
440	381.59	0.01926	1.1979	1.2171	418.90	785.4	1204.3	0.6158	0.8730	1.4887	440
460	466.9	0.0196	0.9748	0.9944	441.4	763.2	1204.6	0.6402	0.8298	1.4700	460
480	566.1	0.0200	0.7972	0.8172	464.4	739.4	1203.7	0.6645	0.7868	1.4513	480
500	680.8	0.0204	0.6545	0.6749	487.8	713.9	1201.7	0.6887	0.7438	1.4325	500
520	812.4	0.0209	0.5365	0.5594	511.9	686.4	1198.2	0.7130	0.7006	1.4136	520
540	982.5	0.0215	0.4434	0.4649	536.6	656.6	1193.2	0.7374	0.6568	1.3942	540
560	1133.1	0.0221	0.3647	0.3868	562.2	624.2	1186.4	0.7621	0.6121	1.3742	560
580	1325.8	0.0228	0.2969	0.3217	588.9	588.4	1177.3	0.7872	0.5659	1.3532	580
600	1542.9	0.0236	0.2432	0.2668	617.0	548.5	1165.5	0.8131	0.5176	1.3307	600
620	1786.6	0.0247	0.1955	0.2201	646.7	503.6	1150.3	0.8398	0.4664	1.3062	620
640	2059.7	0.0260	0.1538	0.1798	678.6	452.0	1130.5	0.8679	0.4110	1.2789	640
660	2365.4	0.0278	0.1165	0.1442	714.2	390.2	1104.4	0.8987	0.3485	1.2472	660
680	2708.1	0.0305	0.0810	0.1115	757.3	309.9	1067.2	0.9351	0.2719	1.2071	680
700	3093.7	0.0369	0.0362	0.0761	823.3	172.1	995.4	0.9905	0.1484	1.1389	700
705.4	3206.2	0.0503	0	0.0503	902.7	0	902.7	1.0580	0	1.0580	705.4



TABLE 2. SATURATION PRESSURES

Abs Press.		Specific Volume		Enthalpy			Entropy			Internal Energy			Abs Press.	
lb Sq In. P	Temp F t	Sat. Liquid v <sub>f</sub>	Sat. Vapor v <sub>g</sub>	Sat. Liquid h <sub>f</sub>	Evap h <sub>fg</sub>	Sat. Vapor h <sub>g</sub>	Sat. Liquid s <sub>f</sub>	Evap. s <sub>fg</sub>	Sat. Vapor s <sub>g</sub>	Sat. Liquid u <sub>f</sub>	Evap u <sub>fg</sub>	Sat. Vapor u <sub>g</sub>	lb Sq In. P	lb Sq In. P
1.0	101.74	0.01614	333.6	69.70	1036.3	1106.0	0.1326	1.8456	1.9782	69.70	974.6	1044.3	1.0	1.0
2.0	126.08	0.01623	173.73	93.99	1022.2	1116.2	0.1749	1.7451	1.9200	93.98	957.9	1051.9	2.0	2.0
3.0	141.48	0.01630	118.71	109.37	1013.2	1122.6	0.2008	1.6855	1.8863	109.36	947.3	1056.7	3.0	3.0
4.0	152.97	0.01636	90.63	120.86	1006.4	1127.3	0.2198	1.6427	1.8625	120.85	939.3	1060.2	4.0	4.0
5.0	162.24	0.01640	73.52	130.13	1001.0	1131.1	0.2347	1.6094	1.8441	130.12	933.0	1063.1	5.0	5.0
6.0	170.06	0.01645	61.98	137.96	996.2	1134.2	0.2472	1.5820	1.8292	137.94	927.5	1065.4	6.0	6.0
7.0	176.85	0.01649	53.64	144.76	992.1	1136.9	0.2581	1.5580	1.8167	144.74	922.7	1067.4	7.0	7.0
8.0	182.86	0.01653	47.34	150.79	988.5	1139.3	0.2674	1.5383	1.8057	150.77	918.4	1069.2	8.0	8.0
9.0	188.28	0.01656	42.40	156.22	985.2	1141.4	0.2759	1.5203	1.7962	156.19	914.6	1070.8	9.0	9.0
10	193.21	0.01659	38.42	161.17	982.1	1143.3	0.2835	1.5041	1.7876	161.14	911.1	1072.2	10	10
14.696	212.00	0.01672	26.80	180.07	970.3	1150.4	0.3120	1.4446	1.7566	180.02	897.5	1077.5	14.696	14.696
15	213.03	0.01672	26.29	181.11	969.7	1150.8	0.3135	1.4415	1.7549	181.06	898.7	1077.8	15	15
20	227.96	0.01683	20.089	196.16	960.1	1156.3	0.3356	1.3962	1.7319	196.10	885.8	1081.9	20	20
30	250.33	0.01701	13.746	218.82	945.3	1164.1	0.3680	1.3313	1.6993	218.73	869.1	1087.8	30	30
40	267.25	0.01715	10.498	236.03	933.7	1169.7	0.3919	1.2844	1.6763	235.90	856.1	1092.0	40	40
50	281.01	0.01727	8.515	250.09	924.0	1174.1	0.4110	1.2474	1.6585	249.93	845.4	1095.3	50	50
60	292.71	0.01738	7.175	262.09	915.5	1177.6	0.4270	1.2168	1.6438	261.90	836.0	1097.9	60	60
70	302.92	0.01748	6.206	272.61	907.9	1180.6	0.4409	1.1906	1.6315	272.38	827.8	1100.2	70	70
80	312.03	0.01757	5.472	282.02	901.1	1183.1	0.4531	1.1676	1.6207	281.76	820.3	1102.1	80	80
90	320.27	0.01766	4.896	290.56	894.7	1185.3	0.4641	1.1471	1.6112	290.27	813.4	1103.7	90	90
100	327.81	0.01774	4.432	298.40	888.8	1187.2	0.4740	1.1286	1.6026	298.08	807.1	1105.2	100	100
120	341.25	0.01789	3.728	312.44	877.9	1190.4	0.4916	1.0962	1.5878	312.05	795.6	1107.6	120	120
140	353.02	0.01802	3.220	324.82	868.2	1193.0	0.5069	1.0682	1.5751	324.35	785.2	1109.6	140	140
160	363.53	0.01815	2.834	335.93	859.2	1195.1	0.5204	1.0436	1.5640	335.39	775.8	1111.2	160	160
180	373.06	0.01827	2.532	346.03	850.8	1196.9	0.5325	1.0217	1.5542	345.42	767.1	1112.5	180	180
200	381.79	0.01839	2.288	355.36	843.0	1198.4	0.5435	1.0018	1.5453	354.68	759.0	1113.7	200	200
250	400.95	0.01865	1.8438	376.00	825.1	1201.1	0.5675	0.9588	1.5263	375.14	740.7	1115.8	250	250
300	417.33	0.01890	1.5433	393.84	809.0	1202.8	0.5879	0.9225	1.5104	392.79	724.3	1117.1	300	300
350	431.72	0.01913	1.3260	409.69	794.2	1203.9	0.6056	0.8910	1.4966	408.45	709.6	1118.0	350	350
400	444.59	0.0193	1.1613	424.0	780.5	1204.5	0.6214	0.8630	1.4844	422.6	695.9	1118.5	400	400
450	456.28	0.0195	1.0320	437.2	767.4	1204.6	0.6356	0.8378	1.4734	435.5	683.2	1118.7	450	450
500	467.01	0.0197	0.9278	449.4	755.0	1204.4	0.6487	0.8147	1.4634	447.6	671.0	1118.6	500	500
550	476.93	0.0199	0.8424	460.8	743.1	1203.9	0.6608	0.7934	1.4542	458.8	659.4	1118.2	550	550
600	486.21	0.0201	0.7698	471.6	731.6	1203.2	0.6720	0.7734	1.4454	469.4	648.3	1117.7	600	600
700	503.10	0.0205	0.6554	491.5	709.7	1201.2	0.6925	0.7371	1.4296	488.8	627.5	1116.3	700	700
800	518.23	0.0209	0.5867	509.7	688.9	1198.6	0.7108	0.7045	1.4153	506.6	607.8	1114.4	800	800
900	531.98	0.0212	0.5006	526.6	668.8	1195.4	0.7275	0.6744	1.4020	523.1	589.0	1112.1	900	900
1000	544.61	0.0216	0.4456	542.4	649.4	1191.8	0.7430	0.6467	1.3897	538.4	571.0	1109.4	1000	1000
1100	556.31	0.0220	0.4001	557.4	630.4	1187.8	0.7575	0.6205	1.3780	552.9	553.5	1106.4	1100	1100
1200	567.22	0.0223	0.3619	571.7	611.7	1183.4	0.7711	0.5956	1.3667	566.7	536.3	1103.0	1200	1200
1300	577.46	0.0227	0.3293	585.4	593.2	1178.6	0.7840	0.5719	1.3559	580.0	519.4	1099.4	1300	1300
1400	587.10	0.0231	0.3012	598.7	574.7	1173.4	0.7963	0.5491	1.3454	592.7	502.7	1095.4	1400	1400
1500	596.23	0.0235	0.2765	611.6	556.3	1167.9	0.8082	0.5269	1.3351	605.1	486.1	1091.2	1500	1500
2000	635.82	0.0257	0.1878	671.7	463.4	1135.1	0.8619	0.4230	1.2849	662.2	403.4	1065.6	2000	2000
2500	668.13	0.0267	0.1307	730.6	360.5	1091.1	0.9126	0.3197	1.2322	717.3	313.3	1030.8	2500	2500
3000	695.36	0.0346	0.0558	802.5	217.8	1020.3	0.9731	0.1885	1.1615	783.4	189.3	972.7	3000	3000
3206.2	705.40	0.0503	0.0503	902.7	0	902.7	1.0580	0	1.0580	872.9	0	872.9	3206.2	3206.2

TABLE 3. SUPERHEATED VAPOR

Abs Press. lb/Sq In. (Sat. Temp)		Temperature, F											
		200	300	400	500	600	700	800	900	1000	1200	1400	1600
1 (101.74)	v	392.6	452.3	512.0	571.6	631.2	690.8	750.4	809.9	869.5	988.7	1107.8	1227.0
	h	1150.4	1195.8	1241.7	1288.3	1335.7	1383.6	1432.8	1482.7	1533.5	1637.7	1745.7	1857.5
	s	2.0512	2.1153	2.1720	2.2233	2.2702	2.3137	2.3542	2.3923	2.4283	2.4952	2.5586	2.6137
5 (162.24)	v	78.16	90.25	102.26	114.22	126.16	138.10	150.03	161.95	173.87	197.71	221.6	245.5
	h	1148.8	1195.0	1241.2	1288.0	1335.4	1383.6	1432.7	1482.6	1533.4	1637.7	1745.7	1857.4
	s	1.8718	1.9370	1.9942	2.0456	2.0927	2.1361	2.1767	2.2148	2.2509	2.3178	2.3792	2.4363
10 (193.21)	v	38.85	45.00	51.04	57.05	63.03	69.01	74.98	80.95	86.92	96.84	110.77	122.69
	h	1146.6	1193.9	1240.6	1287.5	1335.1	1383.4	1432.5	1482.4	1533.2	1637.6	1745.6	1857.3
	s	1.7927	1.8595	1.9172	1.9689	2.0160	2.0596	2.1002	2.1383	2.1744	2.2413	2.3028	2.3598
14.696 (212.00)	v		30.53	34.68	38.78	42.86	46.94	51.00	55.07	59.13	67.25	75.37	83.48
	h		1192.8	1239.9	1287.1	1334.8	1383.2	1432.3	1482.3	1533.1	1637.5	1745.5	1857.3
	s		1.8160	1.8743	1.9261	1.9734	2.0170	2.0576	2.0958	2.1319	2.1989	2.2603	2.3174
20 (227.96)	v		22.36	25.43	28.46	31.47	34.47	37.46	40.45	43.44	49.41	55.37	61.34
	h		1181.6	1239.2	1286.6	1334.4	1382.9	1432.1	1482.1	1533.0	1637.4	1745.4	1857.2
	s		1.7808	1.8396	1.8918	1.9392	1.9829	2.0235	2.0618	2.0978	2.1648	2.2263	2.2834
40 (257.25)	v		11.040	12.628	14.168	15.688	17.198	18.702	20.20	21.70	24.89	27.88	30.66
	h		1186.8	1236.5	1284.8	1333.1	1381.9	1431.3	1481.4	1532.4	1637.0	1745.1	1857.0
	s		1.6994	1.7608	1.8140	1.8619	1.9058	1.9467	1.9850	2.0212	2.0883	2.1498	2.2069
60 (292.71)	v		7.259	8.357	9.403	10.427	11.441	12.449	13.452	14.454	16.451	18.446	20.44
	h		1181.6	1233.6	1283.0	1331.8	1380.9	1430.5	1480.8	1531.9	1636.6	1744.8	1856.7
	s		1.6492	1.7135	1.7678	1.8162	1.8605	1.9015	1.9400	1.9762	2.0434	2.1049	2.1621
80 (312.03)	v			6.220	7.020	7.797	8.562	9.322	10.077	10.830	12.332	13.830	15.325
	h			1230.7	1281.1	1330.5	1379.9	1429.7	1480.1	1531.3	1636.2	1744.5	1856.5
	s			1.6791	1.7348	1.7836	1.8281	1.8694	1.9079	1.9442	2.0115	2.0731	2.1303
100 (327.81)	v			4.937	5.589	6.218	6.835	7.446	8.052	8.656	9.860	11.060	12.258
	h			1227.6	1279.1	1329.1	1378.9	1428.9	1479.5	1530.8	1635.7	1744.2	1856.2
	s			1.6518	1.7085	1.7581	1.8029	1.8443	1.8829	1.9193	1.9867	2.0484	2.1056
120 (341.25)	v			4.081	4.636	5.165	5.683	6.195	6.702	7.207	8.212	9.214	10.213
	h			1224.4	1277.2	1327.7	1377.8	1428.1	1478.8	1530.2	1635.3	1743.9	1856.0
	s			1.6287	1.6869	1.7370	1.7822	1.8237	1.8625	1.8990	1.9664	2.0281	2.0854
140 (353.02)	v			3.468	3.954	4.413	4.861	5.301	5.738	6.172	7.035	7.895	8.752
	h			1221.1	1275.2	1326.4	1376.8	1427.3	1478.2	1529.7	1634.9	1743.5	1855.7
	s			1.6087	1.6683	1.7190	1.7645	1.8063	1.8451	1.8817	1.9493	2.0110	2.0683
160 (363.53)	v			3.008	3.443	3.849	4.244	4.631	5.015	5.398	6.152	6.906	7.656
	h			1217.6	1273.1	1325.0	1375.7	1426.4	1477.5	1529.1	1634.5	1743.2	1855.5
	s			1.5908	1.6519	1.7033	1.7491	1.7911	1.8301	1.8667	1.9344	1.9962	2.0535
180 (373.06)	v			2.649	3.044	3.411	3.764	4.110	4.452	4.792	5.468	6.136	6.804
	h			1214.0	1271.0	1323.5	1374.7	1426.4	1477.5	1529.1	1634.5	1743.2	1855.5
	s			1.5745	1.6373	1.6894	1.7355	1.7776	1.8167	1.8534	1.9212	1.9831	2.0404
200 (381.79)	v			2.361	2.726	3.060	3.380	3.693	4.002	4.309	4.917	5.521	6.123
	h			1210.3	1268.9	1322.1	1373.6	1424.8	1476.2	1528.0	1633.7	1742.6	1855.0
	s			1.5594	1.6240	1.6767	1.7232	1.7655	1.8048	1.8415	1.9094	1.9713	2.0287
220 (385.86)	v			2.125	2.465	2.772	3.066	3.352	3.634	3.913	4.467	5.017	5.565
	h			1206.5	1266.7	1320.7	1372.8	1424.0	1475.5	1527.5	1633.3	1742.3	1854.7
	s			1.5453	1.6117	1.6652	1.7120	1.7545	1.7939	1.8308	1.8957	1.9607	2.0181
240 (397.37)	v			1.9276	2.247	2.533	2.804	3.068	3.327	3.584	4.093	4.597	5.100
	h			1202.5	1264.5	1319.2	1371.5	1423.2	1474.8	1526.9	1632.9	1742.0	1854.5
	s			1.5319	1.6003	1.6546	1.7017	1.7444	1.7839	1.8209	1.8889	1.9510	2.0084

**Table 4. Liquid**

p (t Sat.)	0				500 (467.13)				1000 (544.75)			
t	v	u	h	s	v	u	h	s	v	u	h	s
Sat.					.019748	447.70	449.53	.64904	.021591	538.39	542.38	.74320
32	.016027	.01	.01	.00003	.015994	.00	1.49	.00000	.015967	.03	2.99	.00005
50	.016024	18.06	18.06	.03607	.015998	18.02	19.50	.03599	.015972	17.99	20.94	.03592
100	.016130	68.05	68.05	.12963	.016106	67.87	69.36	.12932	.016082	67.70	70.68	.12901
150	.016343	117.95	117.95	.21304	.016318	117.66	119.17	.21457	.016293	117.38	120.40	.21410
200	.016635	168.05	168.05	.29402	.016608	167.65	169.19	.29341	.016580	167.26	170.32	.29281
250	.017003	218.52	218.52	.36777	.016972	217.99	219.56	.36702	.016941	217.47	220.61	.36628
300	.017433	269.61	269.61	.43732	.017416	268.92	270.53	.43641	.017379	268.24	271.46	.43552
350	.018000	321.59	321.59	.50359	.017954	320.71	322.37	.50249	.017909	319.83	323.15	.50140
400	.018668	374.85	374.85	.56740	.018608	373.68	375.40	.56604	.018550	372.55	375.98	.56472
450	.019503	429.96	429.96	.62970	.019420	428.40	430.19	.62798	.019340	426.89	430.47	.62632
500	.02060	488.1	488.1	.6919	.02048	485.9	487.8	.6896	.02036	483.8	487.5	.6874
510	.02087	500.3	500.3	.7046	.02073	497.9	499.8	.7021	.02060	495.6	499.4	.6997
520	.02116	512.7	512.7	.7173	.02100	510.1	512.0	.7146	.02086	507.6	511.5	.7121
530	.02146	525.3	525.3	.7303	.02130	522.6	524.5	.7273	.02114	519.9	523.8	.7245
540	.02182	538.6	538.6	.7434	.02162	535.3	537.3	.7402	.02144	532.4	536.3	.7372
550	.02221	552.1	552.1	.7569	.02198	548.4	550.3	.7532	.02177	545.1	549.2	.7499
560	.02265	566.1	566.1	.7707	.02237	562.0	564.0	.7666	.02213	558.3	562.4	.7630
570	.02313	580.8	580.8	.7851	.02281	576.0	578.1	.7804	.02253	571.8	576.0	.7763
580					.02332	590.8	592.9	.7946	.02298	585.9	590.1	.7899
590					.02392	606.4	608.6	.8096	.02349	600.6	604.9	.8041
600									.02409	616.2	620.6	.8189
610									.02482	632.9	637.3	.8348
p (t Sat.)	1500 (596.39)				2000 (636.00)				2500 (668.31)			
t	v	u	h	s	v	u	h	s	v	u	h	s
Sat.	.023461	604.97	611.48	.80824	.025649	662.40	671.89	.86227	.028605	717.66	730.89	.91306
32	.015939	.05	4.47	.00007	.015912	.06	5.95	.00008	.015885	.08	7.43	.00009
50	.015946	17.95	22.38	.03584	.015920	17.91	23.81	.03575	.015895	17.88	25.23	.03566
100	.016058	67.53	71.99	.12870	.016034	67.37	73.30	.12839	.016010	67.20	74.61	.12808
150	.016268	117.10	121.62	.21364	.016244	116.83	122.84	.21318	.016220	116.56	124.07	.21272
200	.016554	166.87	171.46	.29221	.016527	166.49	172.60	.29162	.016501	166.11	173.75	.29104
250	.016910	216.96	221.65	.36554	.016880	216.46	222.70	.36482	.016851	215.96	223.75	.36410
300	.017343	267.58	272.39	.43463	.017308	266.93	273.33	.43376	.017274	266.29	274.28	.43290
350	.017865	318.98	323.94	.50034	.017822	318.15	324.74	.49929	.017780	317.33	325.56	.49826
400	.018493	371.45	376.59	.56343	.018439	370.38	377.21	.56216	.018386	369.34	377.84	.56092
450	.019264	425.44	430.79	.62470	.019191	424.04	431.14	.62313	.019120	422.68	431.52	.62160
500	.02024	481.8	487.4	.6853	.02014	479.8	487.3	.6832	.02004	478.0	487.3	.6813
510	.02048	493.4	499.1	.6974	.02036	491.4	498.9	.6953	.02025	489.4	498.8	.6932
520	.02072	505.3	511.0	.7096	.02060	503.1	510.7	.7073	.02048	501.0	510.4	.7051
530	.02099	517.3	523.1	.7219	.02085	514.9	522.6	.7195	.02072	512.6	522.2	.7171
540	.02127	529.6	535.5	.7343	.02112	527.0	534.8	.7317	.02098	524.5	534.2	.7292
550	.02158	542.1	548.1	.7469	.02141	539.2	547.2	.7440	.02125	536.6	546.4	.7413
560	.02191	554.9	561.0	.7596	.02172	551.8	559.8	.7565	.02154	548.9	558.8	.7536
570	.02228	568.0	574.2	.7725	.02206	564.6	572.8	.7691	.02186	561.4	571.5	.7659
580	.02269	581.6	587.9	.7857	.02243	577.8	586.1	.7820	.02221	574.3	584.5	.7785
590	.02314	595.7	602.1	.7993	.02284	591.3	599.8	.7951	.02258	587.4	597.9	.7913
600	.02366	610.4	616.9	.8134	.02330	605.4	614.0	.8086	.02300	601.0	611.6	.8043
610	.02426	625.8	632.6	.8281	.02382	620.0	628.8	.8225	.02346	615.0	625.9	.8177
620	.02498	642.5	649.4	.8437	.02443	635.4	644.5	.8371	.02399	629.6	640.7	.8315
630	.02590	660.8	668.0	.8609	.02514	651.9	661.2	.8525	.02459	644.9	656.3	.8459
640					.02603	669.6	679.4	.8697	.02530	661.2	672.9	.8610
650					.02724	690.3	700.4	.8881	.02616	678.7	690.8	.8773
660									.02729	698.4	711.0	.8954
670									.02895	722.1	735.3	.9172



**Table 7. Dynamic viscosity (micropoise)**

Pressure bars	lb/in <sup>2</sup>	Temp. °C °F	0	50	100	150	200	250	300	350	375
			32	122	212	302	392	482	572	662	707
1	14.504		17500	5440	121.1	141.5	161.8	182.2	202.5	223	233
5	72.52		17500	5440	2790	1810	160.2	181.4	202.3		234
10	145.04		17500	5440	2790	1810	158.5	180.6	202.2		234
25	362.6		17500	5440	2800	1820	1340	177.8	201.6		236
50	725.2		17500	5450	2800	1820	1350	1070	200.6		240
75	1087.8		17500	5450	2800	1830	1350	1080	199.2		244
100	1450.4		17500	5450	2810	1830	1360	1080	905		249
125	1813.0		17500	5460	2810	1840	1360	1090	911		254
150	2176		17400	5460	2820	1840	1370	1100	917		262
175	2538		17400	5460	2820	1850	1380	1100	924		273
200	2901		17400	5460	2830	1860	1380	1110	930	735	291
225	3263		17400	5460	2830	1860	1390	1120	936	747	491
250	3626		17400	5470	2840	1870	1390	1120	943	760	597
275	3989		17400	5470	2840	1870	1400	1130	949	772	633
300	4351		17400	5470	2850	1880	1400	1130	955	785	657
350	5076		17300	5480	2860	1890	1420	1150	968	805	693
400	5802		17300	5480	2870	1900	1430	1160	981	825	721
450	6527		17300	5490	2880	1910	1440	1170	993	837	743
500	7252		17200	5490	2890	1920	1450	1180	1010	850	762
550	7977		17200	5500	2900	1930	1460	1200	1020	860	780
600	8702		17200	5500	2910	1940	1480	1210	1030	870	795
650	9427		17200	5510	2920	1960	1490	1220	1040	882	809
700	10153		17100	5510	2930	1970	1500	1230	1060	895	822
750	10878		17100	5520	2940	1980	1510	1240	1070	905	835
800	11603		17100	5520	2950	1990	1520	1260	1080	915	846

Pressure bars	lb/in <sup>2</sup>	Temp. °C °F	400	425	450	475	500	550	600	650	700
			752	797	842	887	932	1022	1112	1202	1292
1	14.504		243	253	264	274	284	304	325	345	365
5	72.52		244	254	264	274	284	305	325	345	366
10	145.04		244	255	265	275	285	305	326	346	366
25	362.6		246	256	266	276	287	307	327	347	367
50	725.2		250	259	269	279	289	309	329	349	369
75	1087.8		253	263	273	282	292	312	332	352	372
100	1450.4		258	267	276	286	295	315	334	354	374
125	1813.0		263	271	280	289	299	318	337	357	376
150	2176		269	276	285	294	302	321	340	359	379
175	2538		276	282	290	298	307	324	343	362	381
200	2901		286	289	296	303	311	328	346	365	384
225	3263		299	298	302	309	316	332	350	368	386
250	3626		321	309	310	315	321	336	353	371	389
275	3989		367	324	320	322	327	341	357	374	392
300	4351		458	345	331	330	334	346	361	377	395
350	5076		573	416	363	351	349	357	369	385	401
400	5802		628	503	411	379	369	369	379	392	408
450	6527		664	565	468	415	393	383	389	401	415
500	7252		693	609	521	456	421	400	401	410	423
550	7977		716	643	564	497	453	418	414	420	431
600	8702		736	670	600	534	485	439	428	430	439
650	9427		754	693	629	567	516	460	442	441	448
700	10153		770	713	654	596	545	482	458	453	458
750	10878		784	732	676	621	572	504	474	466	468
800	11603		798	748	695	644	596	526	491	478	478

**Conversion Factors for Viscosity**

10<sup>6</sup> micropoise = 0.0020885 lbf × sec/ft<sup>2</sup>  
 = 0.067197 lb/(ft × sec)

= 241.91 lb/(hr × ft)  
 = 0.58015 × 10<sup>-4</sup> lbf × hr/ft<sup>2</sup>

= 0.1 kg/(m × sec)

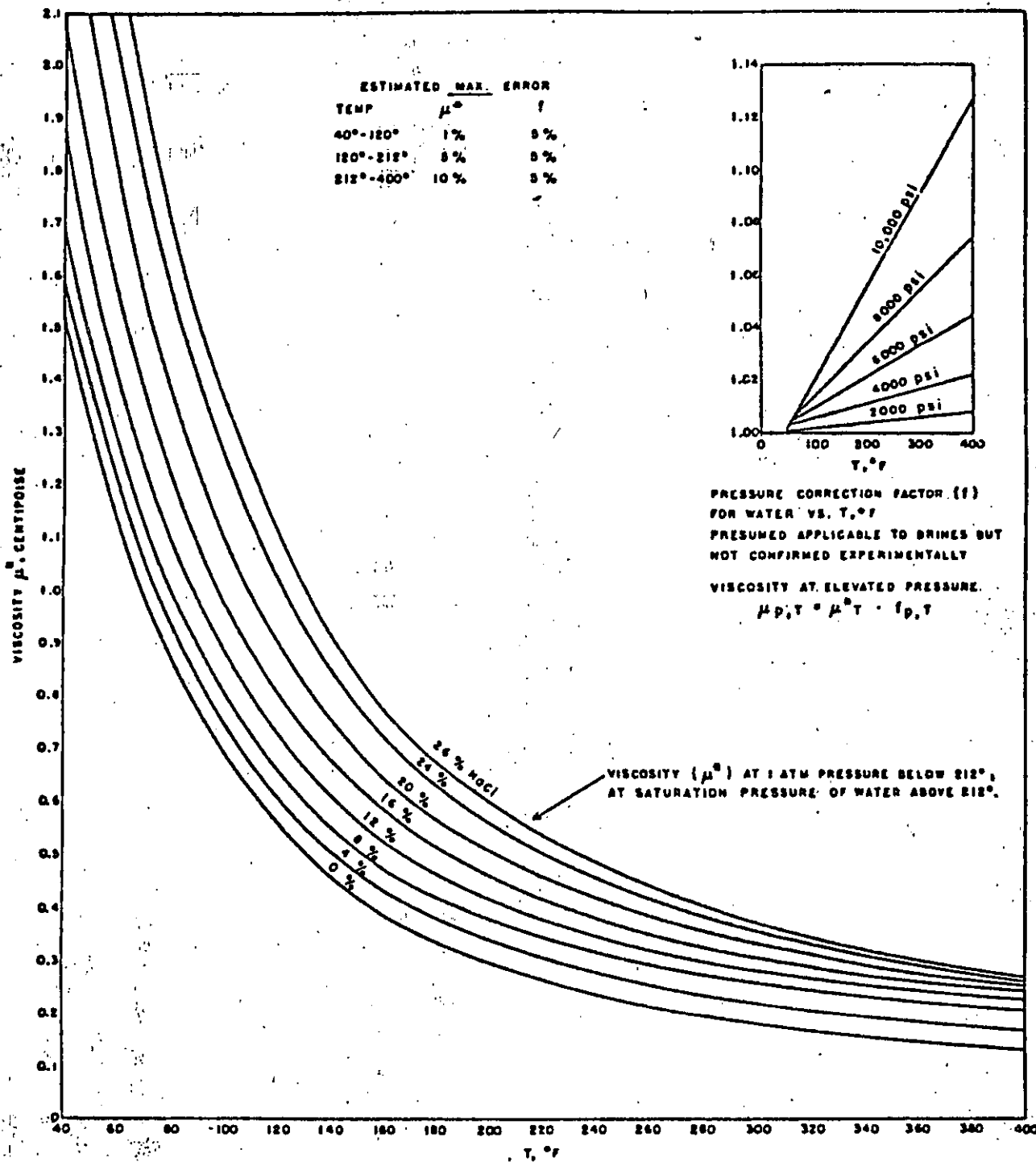
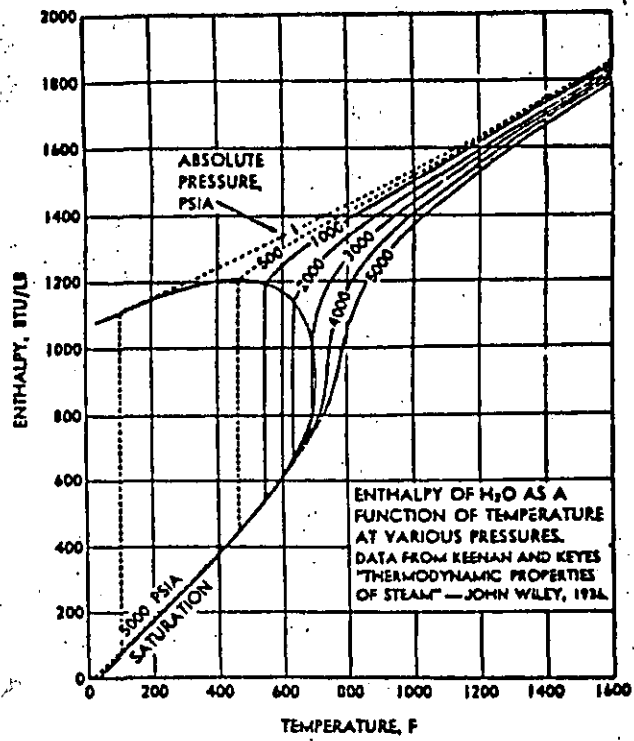
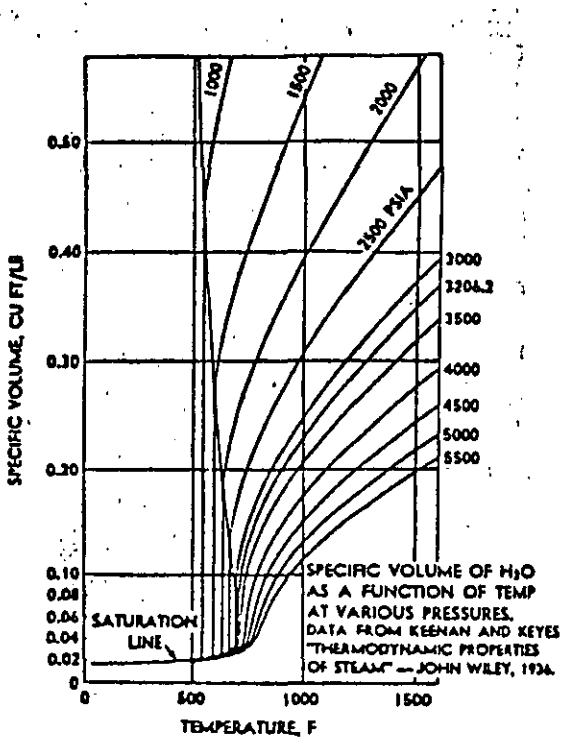


Fig. G.4 Water viscosities for various salinities and temperatures. From Chesnut, unpublished, Shell Development Co.

FIGURA 14:

## Some Thermodynamic Properties of H<sub>2</sub>O in the Subcritical and Supercritical Regions



In Fig. 22-16 is shown the difference between the FVF of gas-saturated water and the FVF of pure water. To get the FVF of pure water saturated with gas, this difference is added to the FVF of pure water from Fig. 22-15.

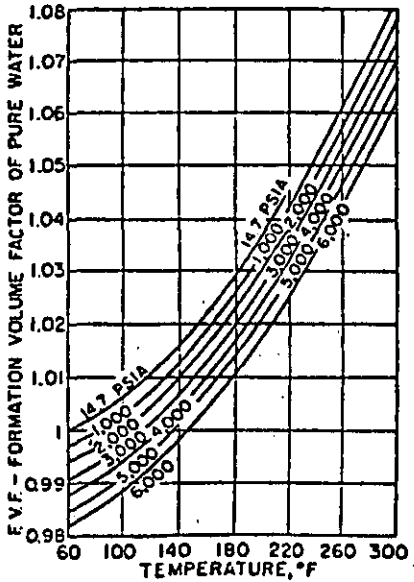


FIG. 22-15. Formation volume factor of pure water. (Calculated from data of Keenan and Keyes.)

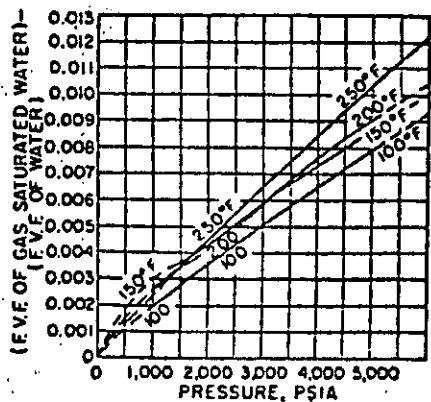


FIG. 22-16. Difference in formation volume factor of gas-saturated pure water and of pure water.

FIGURA 15.

# MOLLIER CHART

ENTROPY, BTU/LB, F

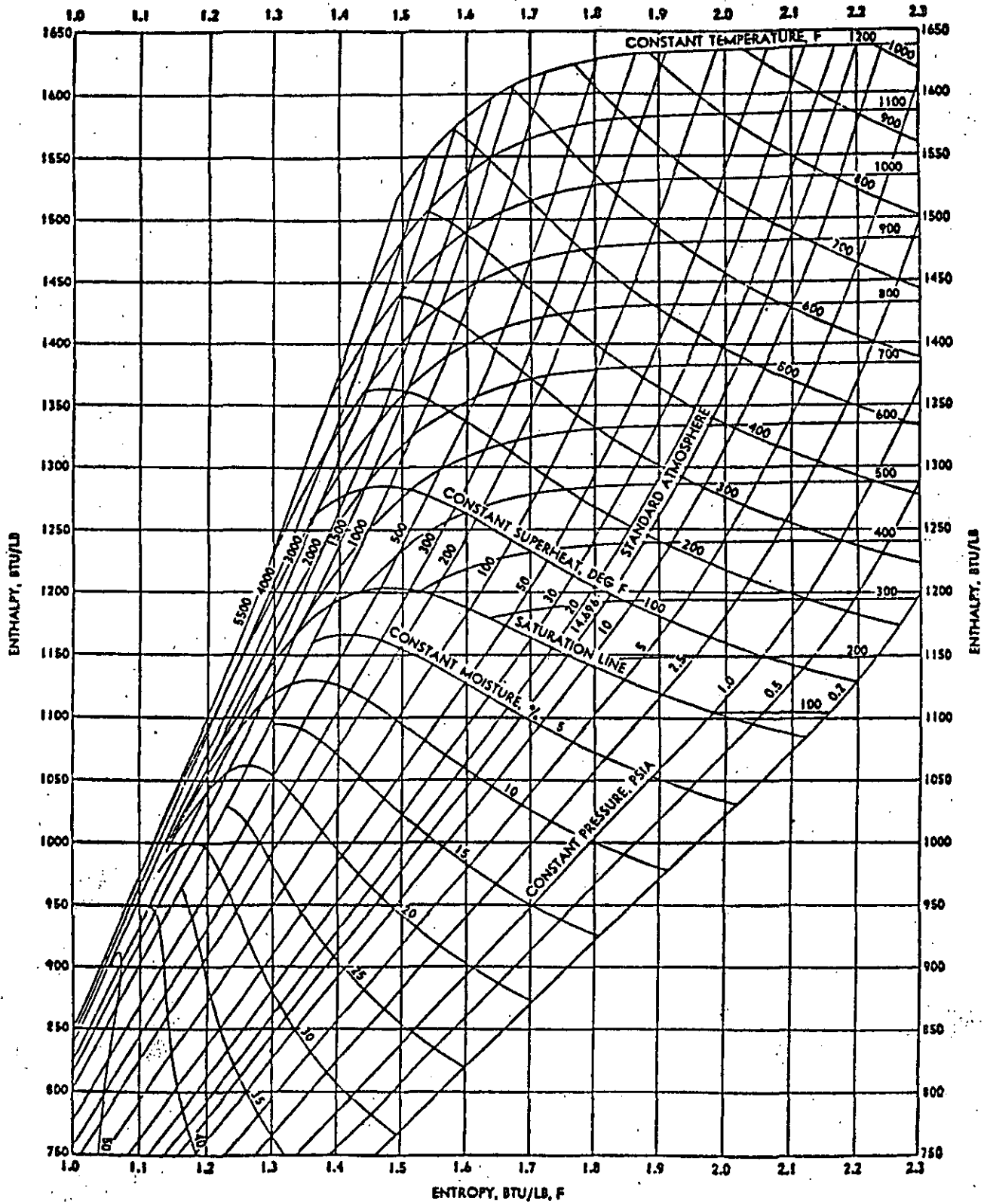
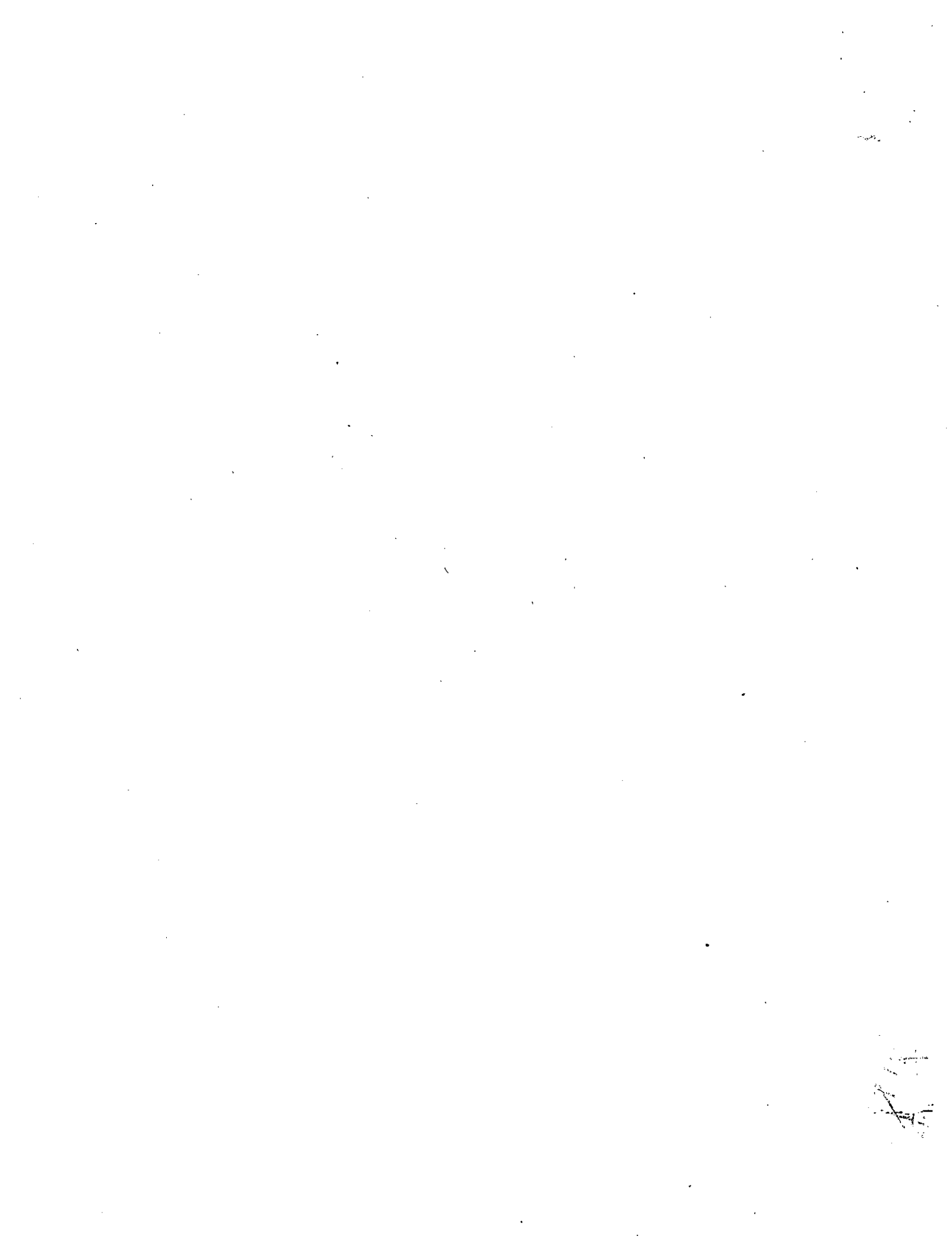


FIGURA 16.



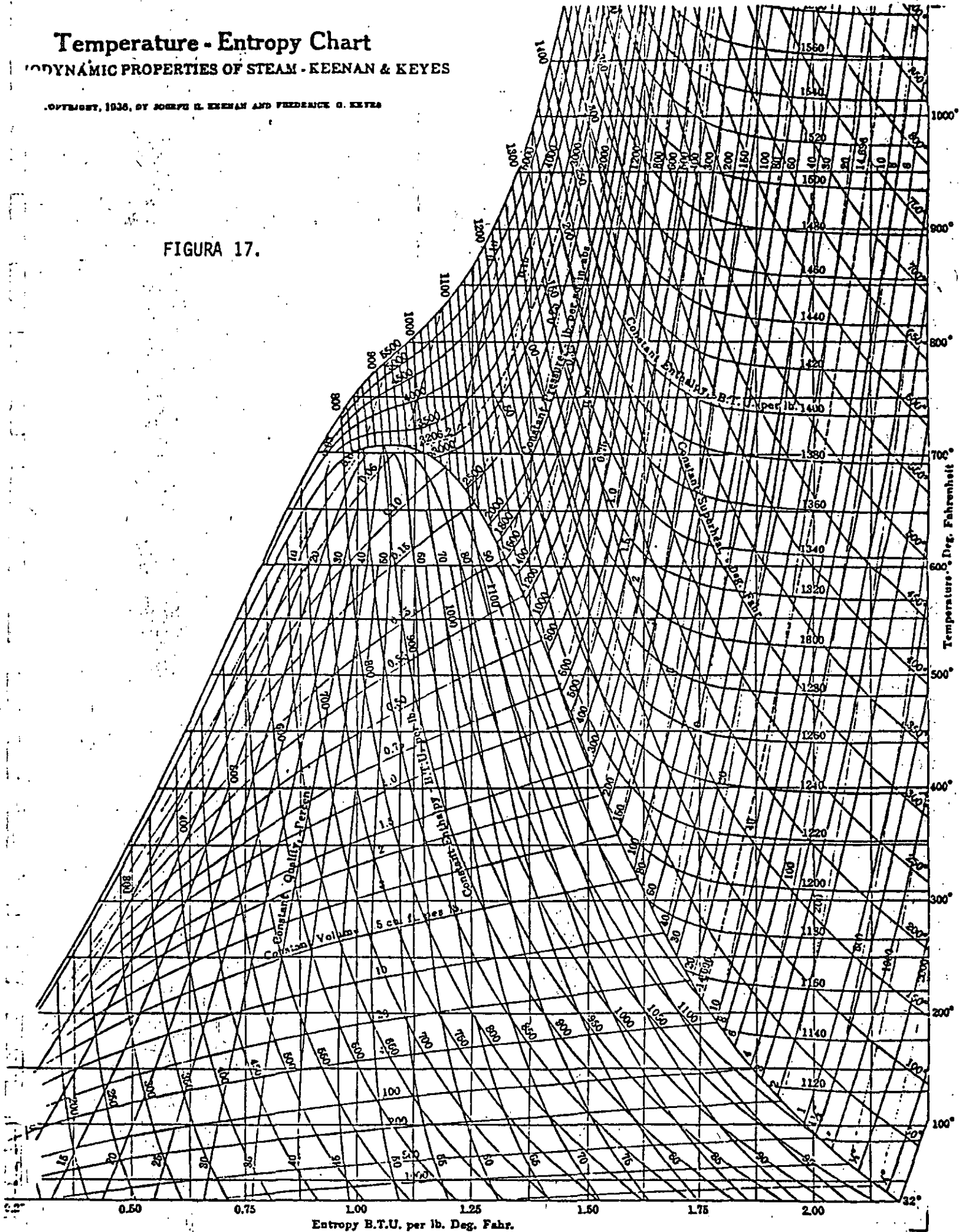


# Temperature - Entropy Chart

TERMO-DYNAMIC PROPERTIES OF STEAM - KEENAN & KEYES

Copyright, 1936, by JOSEPH H. KEENAN AND FREDERICK G. KEYES

FIGURA 17.



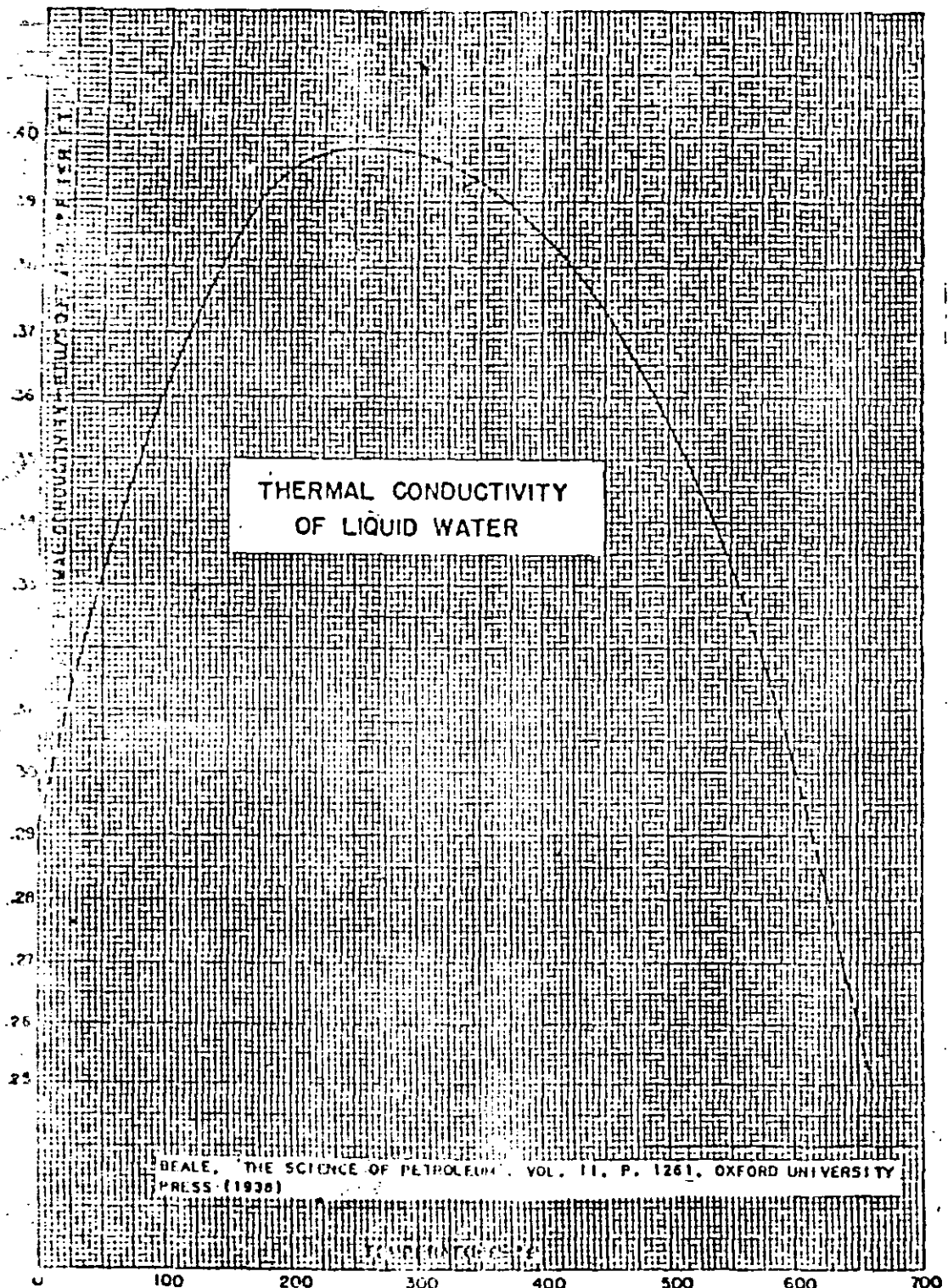


Fig. 7. (a) Prandtl number of liquid water below 1000 lb/lin.<sup>2</sup>; (b) Prandtl number of superheated water vapor.

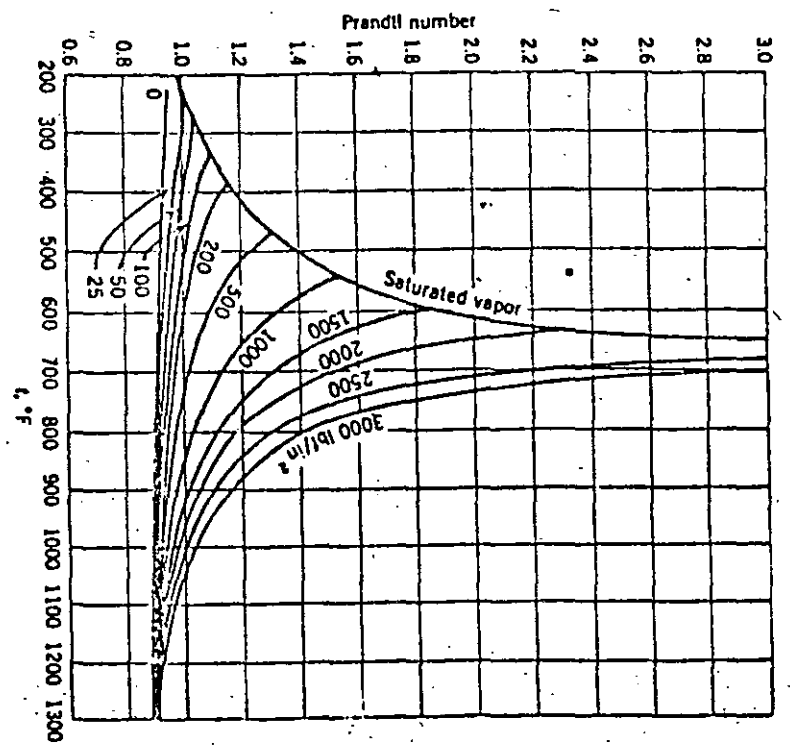
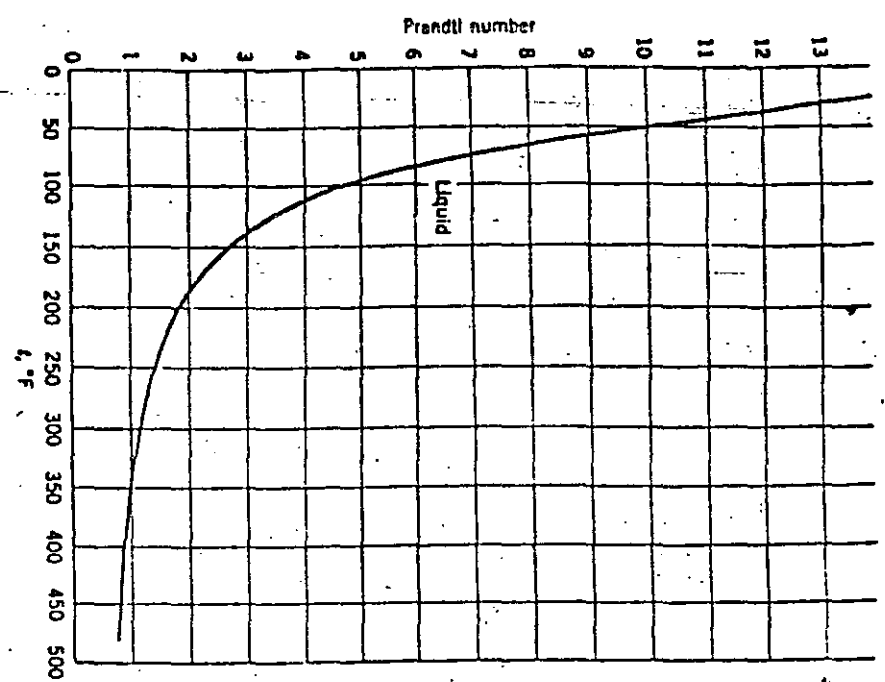


FIGURA 18.

# LABORATORY MEASUREMENT OF 98.7% METHANE GAS SOLUTION IN DISTILLED WATER (Culberson and McKetta, 1951)

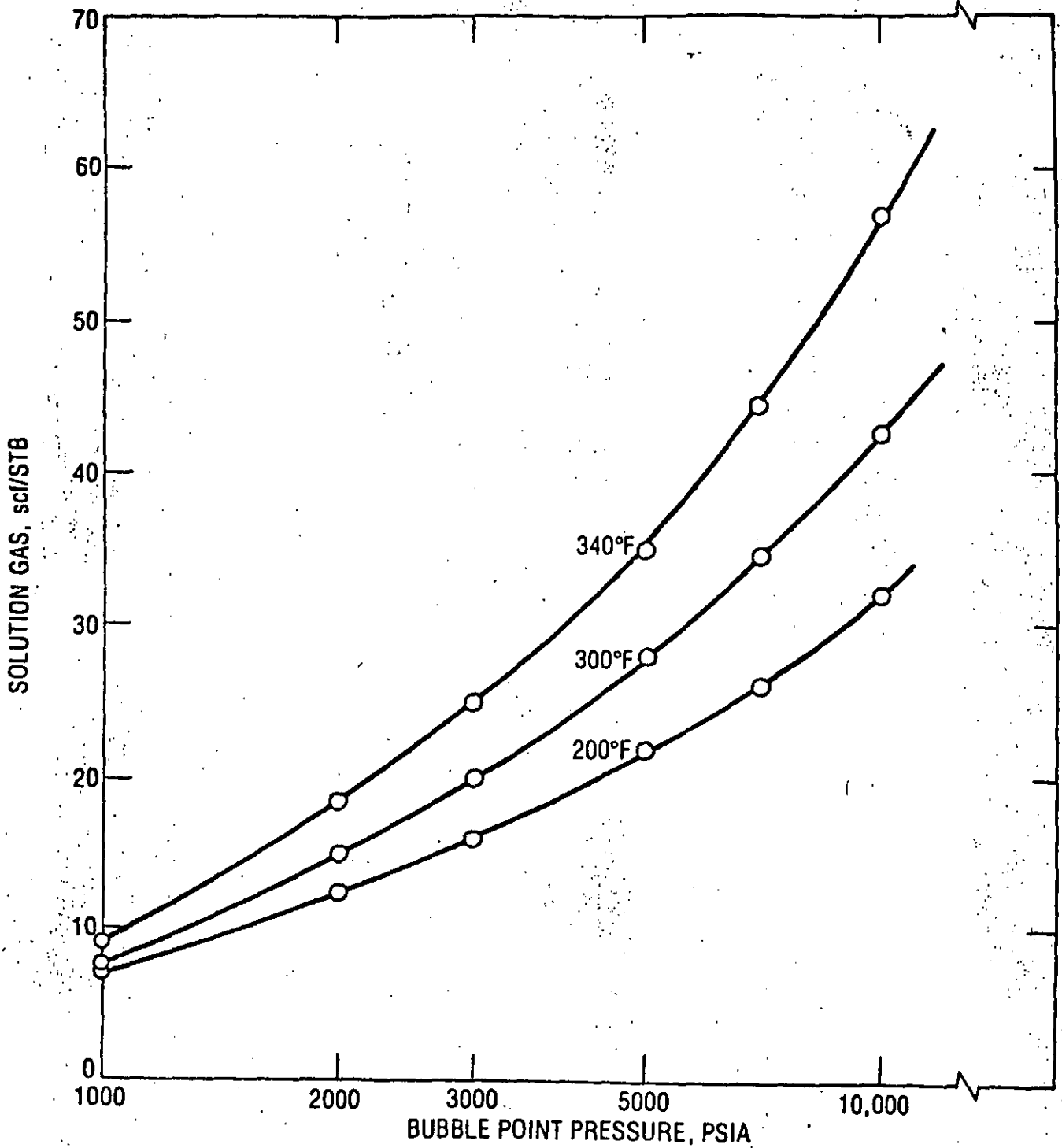


FIGURA 19.

# APPENDIX A

## VSTEAM NUMERICAL MODEL

---

The basic equations that make up this numerical model consist of "flow equations" and "heat transfer equations." These equations are coupled numerically in the model through a heat balance on each pipe increment. A detailed discussion of this procedure is given in the following.

Figure 1 shows a typical geothermal well with hot water under pressure being produced by the formation. In addition to single-phase steam or water, the fluid may encounter the flow regimes of bubble, slug, transition and mist in a single pipe. If single-phase water is present, the procedure must be able to compute the flash point. If single-phase steam is present, it is by definition superheated.

### FLOW EQUATIONS

The equations describing the flow characteristics of a two-phase system are almost always written from a pressure drop point of view. The common approach is to begin with a momentum balance and the continuity equation for steady homogeneous one-dimensional two-phase flow in a pipe. The combined equation has been presented by Ros and others.<sup>9,13,15</sup>

$$\frac{dp}{dL} = -\rho_{av} \frac{g}{g_c} \cos \theta - \frac{f_m \bar{\rho} v_T^2}{2g_c d} - \rho_{av} \frac{V_T}{g_c} \frac{dv_T}{dL} \quad (1)$$

Where

$\rho_{av}$	=	mixture density
$\bar{\rho}$	=	representative density depending on author.
$f_m$	=	Moody friction factor
$v_T$	=	total velocity
$L$	=	length of pipe

From this form of the equation it can be easily recognized that the total pressure gradient is made up of three individual gradients:<sup>15</sup>

1. gravitational gradient (head),
2. friction gradient,  $\tau_f$ ,
3. acceleration gradient,  $A_c$ .

Proper calculation of each gradient should yield the total pressure drop. Under conditions where the acceleration gradient is negligible, Figure 2 shows a plot of the two-phase pressure drop as a function of gas rate at a constant liquid rate. As more gas enters the pipe, the velocity and therefore friction increases. Likewise, the higher the gas/liquid ratio becomes then the mixture density should decrease, causing the head to decrease.

However, this development assumes homogeneity of the mixture. This assumption implies that there are no flow regime effects and that both phases travel at the same velocity (no slip). In reality, this is not true. Figure 3 from Calvert<sup>2</sup> shows each of the possible flow regimes that may occur in two-phase flow and their effect on the total pressure gradient. What must be emphasized for steam-water production wells is that all of these flow regimes can coexist in the same pipe. In addition, unless the liquid is completely entrained as a mist in the gas, there is always slip occurring between the phases. The gas travels faster than the liquid resulting in a "liquid holdup."

From the above discussion, it is recognized that flow regimes must be detected point by point through the pipe. Furthermore, Equation (1) does not have a direct analytical solution since the right hand side is an empirical function of pressure and other variables. The solution of this equation lends itself then to finite difference approximation in which the pipe is segmented. This allows for the flexibility of varying the flow regimes by segments. Rearranging Equation (1) in finite difference form as shown by several authors<sup>8,9,13</sup> yields:

$$\Delta P = \Delta L \frac{\rho_{av} \frac{g}{g_c} \cos \theta + \tau_f}{144(1 - A_c)} \quad (2)$$

where  $\rho_{av}$  = mixture density  
 $\tau_f$  = friction term  
 $A_c$  = acceleration term

Notice that Equation (2) has been rearranged in terms of the pressure increment. That is, in this model the length increment will be specified and the corresponding pressure increment calculated. When the sum of the  $\Delta L$  increments equals the depth, the wellbore pressure drop has been determined.

After calculating the two-phase pressure drop for an increment  $\Delta L$ , the fluid pressure is known and the enthalpies and densities of each phase can be directly determined from the steam tables. This of course assumes that phase equilibrium has been established in each increment. The determination of the flowing quality of the increment becomes an iterative procedure with the heat transfer calculations as shown in the next section.

Knowing the physical properties of the increment, the geometry, and the mass rate, we are in a position to determine flow regimes and each of the three empirical terms of Equation (2). These three terms correspond to the three gradients in Equation (1). Each of these terms has several variations depending upon flow regime and author. In general, the mixture density term is presented as follows:

$$\rho_{av} = \rho_L H_L + \rho_G (1 - H_L) \quad (3)$$

Where  $\rho_L, \rho_G$  = liquid and gas densities

$H_L$  = volumetric liquid fraction actually occurring in the increment, termed "liquid holdup."

If the non-slip volumetric liquid fraction,  $\lambda_L$ , is given by:

$$\lambda_L = q_L/q_T, \quad (4)$$

Then, since gas always "slips" past the liquid in vertical upflow except in fully entrained mist flow, the holdup is related to  $\lambda_L$  by:

$$H_L \geq \lambda_L \quad (5)$$

The essence of every two-phase flow empirical correlation is to determine the relationship between  $H_L$  and  $\lambda_L$  for the flow regime, geometry, and flow parameters of the system.

The friction term,  $\tau_f$ , is usually slightly different with each author, but in the general form:

$$\tau_f = \frac{f_m \bar{\rho} \bar{V}_T^2}{2g_c d} \quad (6)$$

The friction factor in turn is dependent on a representative two-phase Reynolds number:

$$N_{RE} = \frac{\bar{\rho} \bar{V}_T d}{\bar{\mu}} \quad (7)$$

The values used for  $\bar{\rho}$ ,  $\bar{V}_T$ , and  $\bar{\mu}$  have a direct bearing on the holdup. Most investigators assume a friction gradient and then back correlate a holdup function that yields a match of the measured two-phase pressure drop. Therefore, the friction and holdup correlations are usually tied together in vertical two-phase flow. Since they are not independent, it would not in general be good practice to generate "hybrid correlations" by mixing terms.

The acceleration term,  $A_C$ , has been shown by Wallis<sup>20</sup> to represent the two-phase Mach number squared,  $M^2$ . Each author again presents his own definition of the term. In general  $A_C$  is much less than 1. However, at high flow rates and low pressures, as usually occur near the wellhead of geothermal wells, this term is important.

It is beyond the scope of this appendix to present the complete slip correlation for every flow regime, as they are published elsewhere.<sup>1,8,9,13,20,19</sup>

## HEAT TRANSFER EQUATIONS

The equations describing the heat conduction into a solid by a pipe flowing fluid are well established.<sup>14,3</sup> The first step is to write a heat balance on the fluid flowing through the selected pipe increment. This is summarized by Ramey<sup>14</sup> for single-phase flow. In two-phase flow, the kinetic energy is usually negligible, but is included in the following equation:

$$H_i = H_{i-1} - \alpha + \frac{g}{g_c} \frac{\delta z}{J} + \frac{\delta v_T^2}{2g_c J} \quad (8)$$

The heat balance nomenclature is summarized on Figure 7. The potential energy term in this equation is added because  $z$  is measured downwards. The total enthalpy is a function of the enthalpies of each phase ( $H_G$  and  $H_L$ ) and the flowing steam quality ( $x_i$ ):

$$H_i = H_G x_i + H_L (1 - x_i) \quad (9)$$

Assuming a pressure increment, the pressure is known at  $i$  and since the fluid is saturated, the temperature and enthalpy of each phase can be found in the steam tables. Using Equation (8) to calculate  $H_i$ , Equation (9) can be used to calculate the flowing quality  $x_i$ .

The heat transfer to the surroundings is given by the standard heat conduction formula with a time dependency factor:

$$Q = \frac{U \pi d \delta L (T_{av} - T_g)}{W_T f(t)} \quad (10)$$

$$\text{Where } f(t) = -\ln \frac{r_c}{2\sqrt{\alpha t}} - 0.290 \quad (11)$$

- $U$  = overall heat transfer coefficient,
- $\alpha$  = thermal diffusivity of the earth,
- $r_c$  = casing outer radius.
- $t^c$  = time since well opened for flow,
- $T_{av}$  = average temperature of the increment,
- $T_g$  = ground temperature at depth  $z$ ,
- $W_T$  = total mass flow rate.

The time dependency function has been found<sup>14</sup> to be accurate at times greater than a week for most reservoir problems. This function implies a radiation boundary condition that probably is not accurate at shorter times.

The overall heat transfer coefficient is a combination of convection in the casing-tubing annulus and conduction into the formation. Willhite<sup>21</sup> gives a good development of the equations. The final result is as follows:



$$U = \frac{hk}{(hr_t^2(t) + k)} \quad (12)$$

Where  $k$  = thermal conductivity  
 $h$  = convective coefficient  
 $r_t$  = tubing radius

If the wellbore completion is convection heat transfer controlled, then the time function gets cancelled out of Equation (10).

### NUMERICAL MODEL

It is important to couple the pressure drop equations to the heat transfer equations. Each of these depends upon the other. The pressure drop algorithm consists of a set of subroutines, one for each flow regime, that are called from a control routine. The heat transfer calculations have been imbedded in the control routine in order to iterate on pressure drop. The steam tables are entered in vector form so that any table variable can be determined knowing the value of one other. The specific enthalpy of each phase can be calculated knowing pressure or temperature.

The lengths in Equations (8) and (10) are not known at the beginning of an increment calculation. Using the pressure drop correlations and Equation (2), an estimate of  $\Delta L$  can be calculated knowing the average quality. The quality determines the non-slip flow rates. Equations (8) and (10) determine the dependence of Steam Quality on  $\Delta L$ . An iterative procedure is then used for each increment in order to converge quality and pressure gradient. The calculations are completed when the sum of  $\Delta L$  equals the total length.

In addition to two-phase flow, there are the two special cases of compressed liquid and superheated steam. Wells that produce compressed liquid at the sandface and flash to two-phase in the tubing are very common in the western U.S. The flash point can be predicted from an enthalpy balance and the saturation pressure versus temperature curve. It is very important to get an accurate calculation of liquid compressibility with pressure and temperature so that the compressed liquid gradient is correct.

Wells producing superheated steam can be found in many parts of the world. Knowing the pressure in a particular increment and the enthalpy of the fluid, the temperature can be determined from the steam tables. Specific volume varies with pressure and temperature and the calculation becomes iterative until the physical properties and heat balance converge.

## BIBLIOGRAFIA

- 1.- Gutierrez, P. H.: "DETERMINACION DE CAIDAS DE PRESION EN POZOS FLUYENTES, LOCALIZADOS EN YACIMIENTOS DE GAS- Y GEOTERMICOS DE FASE VAPOR DOMINANTE".  
Tesis (Inédita, en revisión), Facultad de Ingeniería, UNAM, México, 1984.
  - 2.- Wallis, G.: "ONE DIMENSIONAL TWO-PHASE FLOW".  
Ed MacGraw-Hill, New York, 1969.
  - 3.- Gould, T. : "STEAM-WATER FLOW IN WELLS".  
Intercomp R. D. E., Ing. Oklahoma, 1976.
  - 4.- Lowe, H. C.: "FLUID MECHANICS".  
The MacMillan Press, Londres, 1979.
  - 5.- Comolet, R.: "MECANIQUE EXPERIMENTALE DES FLUIDES".  
Vol. II. Ed Masson, Paris, 1973.
  - 6.- Custodio, E.: "HIDROLOGIA SUBTERRANEA".  
Vol, I., Ed Omega, Barcelona, 1975.
-

-. FIGURAS Y TABLAS .-

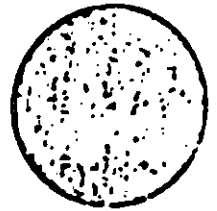
<u>No.</u>	<u>FIGURA</u>	<u>página</u>
1	Características típicas de terminación para un pozo geotérmico productor de agua/vapor .....	42
2	Caída de presión del flujo bifásico como combinación de gradientes gravitatorio y de fricción .....	43
3	Patrones de flujo vertical bifásico .....	44
4	Factor de Fricción de Moody .....	45
5	Carta del régimen de flujo bifásico vertical en tuberías .....	46
6	Carta del régimen de flujo ampliada .....	47
7	Cartas de régimen de flujo en tubería de 0.875 plg. ....	48
8	Cartas de régimen de flujo en tubería de 0.625 plg. ....	49
9	Variación temporal del perfil de calidad de flujo .....	50
10	Función de Disponibilidad .....	51
11	Esquema de la nomenclatura para transferencia de calor .....	63
12	Coefficientes de transferencia de calor .....	64
13	Variación del perfil de calidad de flujo con el coeficiente de transferencia de calor .....	65
14	Viscosidad del agua salina .....	74
15	Algunas propiedades termodinámicas del agua .....	75
16	Carta de Mollier .....	76
17	Carta Temperatura-Entropía .....	77
18	Número de Prandtl y conductividad térmica del agua .....	78
19	Mediciones de laboratorio de 98.7 % de gas metano disuelto en agua destilada .....	79

<u>No.</u>	<u>TABLA</u>	<u>página</u>
1	Temperatura de Saturación .....	68
2	Presiones de Saturación .....	69
3	Vapor Sobrecalentado .....	70
4	Líquido Comprimido .....	71
7	Viscosidad Dinámica .....	73

**ARTICULOS COMPLEMENTARIOS.**

BIBLIOTECA

NO. DE REGISTRO		10 P 10-61	
F. III		10 SET. 1973	



# Vertical Two-Phase Steam-Water Flow In Geothermal Wells

Thomas L. Gould, SPE-AIME, INTERCOMP Resource Development and Engineering, Inc.

## Introduction

The current examination of our country's energy resources has resulted in new and greater interest in geothermal power. There are geothermal installations in New Zealand, Italy, California, Mexico, Japan, U.S.S.R., and elsewhere. Many of these operations have long been producing power from reservoirs that are principally vapor-dominated systems, where essentially dry steam is produced at the wellhead and used directly for power generation. Unfortunately, vapor-dominated systems are relatively rare and current geothermal projects in the U. S. propose to use aquifers that produce hot water or a steam-water mixture.<sup>1</sup> New Zealand is the leader in developing the technology required to operate these two-phase steam-water systems.

A typical aquifer, when first discovered, will produce undersaturated water at the wellbore sand-face. As the fluid flows up the wellbore and pressure is lost, the fluid eventually flashes, producing a steam-water mixture in the well. The two-phase mixture is usually separated at the wellhead, with the steam being used directly to generate power.<sup>2,3,4</sup> More advanced designs<sup>5</sup> call for the fluid heat to be transferred to a secondary fluid, such as freon or isobutane, thereby using the potential of both steam and hot-water fractions. The secondary fluid is used to generate power and the condensed water is reinjected into the formation. This approach reduces environmental problems and makes more efficient use of the available thermal energy. The reinjected water maintains aquifer pres-

sure and prolongs the producing life of the field. As production continues over a period of months, the aquifer pressure will usually drop to the saturation point, and fully developed two-phase steam-water flow will be produced by the formation at the sand-face. The two-phase mixture then flows towards the surface, experiencing pressure drop and heat transfer. In many applications, minerals are deposited on the wellbore casing where the mixture is flashing.

The design, analysis, and operation of geothermal systems requires sophisticated applications of the principles of fluid mechanics, heat transfer, and flow through porous media. The mathematical equations that describe a geothermal wellbore will be presented in this paper. The simulation of the combined effects of heat transfer and two-phase flow in wells has not previously been fully presented. Various portions of the technology have been published, but in a piecemeal fashion. The aim of this work is to develop an integrated approach to the problem, an adequate treatment of which must account for the following effects:

1. Two-phase pressure drop,
2. Flow regime change,
3. Phase change (fluid miscibility),
4. Relative steam-water velocity (slip),
5. Heat transfer from the fluid.

All these effects are interrelated. For example, the pressure drop cannot be calculated unless the flow

*The efficient design and operation of a geothermal wellbore requires an understanding of the complex interactions of heat transfer, fluid flow, phase change, flow regime change, and steam-water slip. The equations and concepts presented here account for those interactions and are used in simulating two-phase steam-water flow in a wellbore.*

regime, phase change, and slip are known. The phase change and slip cannot be determined unless the enthalpy and pressure of the fluid are known, and these in turn require heat-transfer and pressure-drop calculations.

The problem of two-phase flow in an essentially isothermal system has been well studied by several authors.<sup>1,2,3,4,5,6,7,8,9,10,11,12</sup> The concepts that have been developed allow for the coexistence of several flow regimes in the same pipe. Fig. 1 shows a typical geothermal well with hot water under pressure being produced by the formation. The fluid may encounter the flow regimes of bubble, slug, transition, and mist in a single pipe. To date, the equations governing two-phase flow have been empirical, but good success has been achieved in accounting for the effects of important variables. The equations governing heat transfer to a wellbore have also been published.<sup>9,10,11,12</sup> These equations, originally developed for the injection of steam into oil reservoirs to improve recovery,

can be applied to steam production from geothermal aquifers. It therefore remains only to combine this technology into an integrated simulation procedure for calculating flowing bottom-hole pressure, knowing the wellhead pressure, well geometry, mass flow rate, and wellhead steam quality.

### Flow Equations

The equations describing the flow characteristics of a two-phase system are almost always written from a pressure-drop point of view. The common approach is to begin with a momentum balance and the continuity equation for steady homogeneous one-dimensional two-phase flow in a pipe. The combined equation has been presented by Ros and others.<sup>9,10,11</sup>

$$\frac{dp}{dL} = -\bar{p} \frac{g}{g_c} \cos \theta - \frac{f_m \rho v_T^2}{2g_c d} - \bar{p} \frac{v_T}{g_c} \frac{dv_T}{dL} \quad (1)$$

From this form of the equation, it can be easily recognized that the total pressure gradient is made up of three individual gradients<sup>13</sup>:

- I. Gravitational gradient (head),
- II. Friction gradient,  $\tau_f$ ,
- III. Acceleration gradient,  $A_e$ .

Proper calculation of each gradient should yield the total pressure drop.

This development assumes homogeneity of the mixture, which implies that there are no flow regime effects and that both phases travel at the same velocity (no slip). In reality, this is not true. Calvert<sup>3</sup> showed that each of the following possible flow regimes may occur in two-phase flow, and he discussed their effect on the total pressure gradient: bubble, bubbly-slug, slug-annular transition, annular, and annular-mist. For steam-water production wells, all these flow regimes can coexist in the same pipe. In addition, unless the liquid is completely entrained as a mist in the gas, there is always slip occurring between the phases. The gas phase travels faster than the liquid, resulting in a "liquid holdup."

### Flow Regimes

Since flow regimes are critically important to two-phase flow calculations, we must be able to predict them as a function of the flow parameters. Ros<sup>14</sup> has developed a set of flow regime coordinates that have proved to be consistent over a range of conditions in vertical two-phase, two-component flow. These dimensionless numbers are

Gas velocity number,

$$N_{gv} = v_{gs} (\rho_l / g\sigma)^{1/4} \quad (2)$$

Liquid velocity number,

$$N_{lv} = v_{ls} (\rho_l / g\sigma)^{1/4} \quad (3)$$

Since the physical property group of both numbers is the same, the coordinates represent principally the superficial velocity of each phase at in-situ conditions. Fig. 2 shows the flow regime map<sup>14</sup> used in this study. To examine this map, take  $N_{lv} = 1.0$  and vary

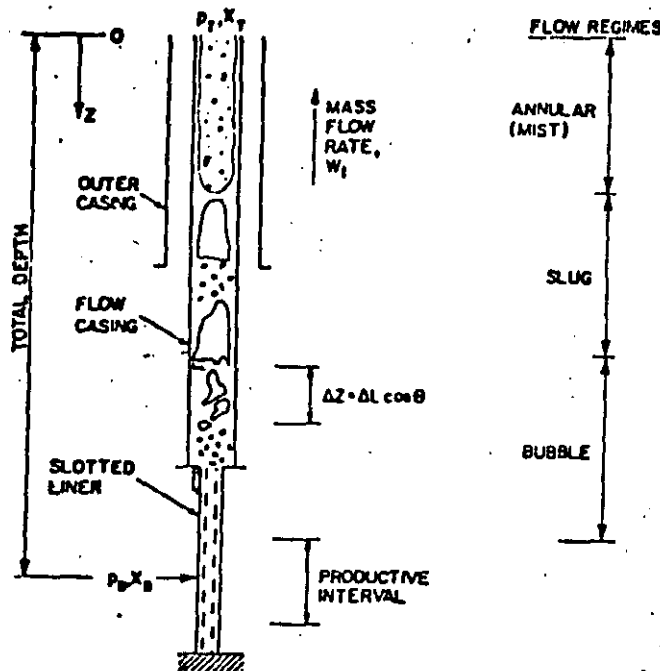


Fig. 1—Typical completion characteristics for a geothermal steam-water production well.

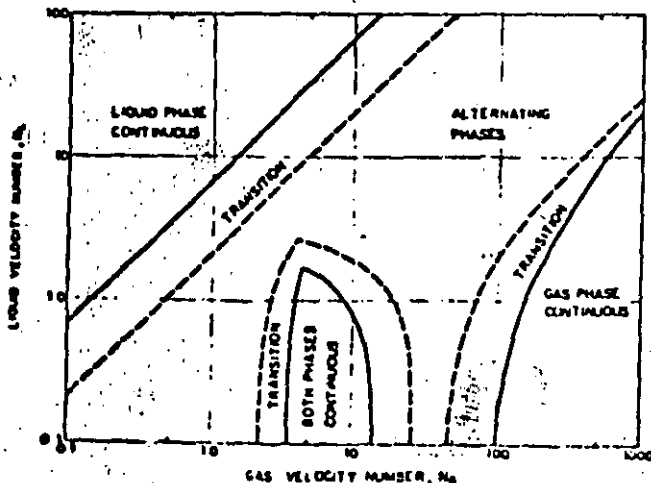


Fig. 2—Flow regime map for vertical two-component flow in a 1-in. pipe.

$N_{re}$  from 0.1 to 1,000. This will traverse the map horizontally through three distinct flow regime classifications:

1. Liquid-phase continuous (bubble flow);
2. Alternating phases (slug and froth flow);
3. Gas-phase continuous (annular and mist flow).

As steam is generated in a geothermal well during flow from bottom to top, the fluid normally passes through each of the flow regimes in the order listed above.

Fig. 2 was developed using two-component data. Research on one-component steam-water flow regimes is currently being conducted.<sup>20</sup> Wells that produce a steam-water mixture at the sand-face will usually experience both slug flow and annular-mist flow in the wellbore. Bennett *et al.*<sup>21</sup> showed that the change from slug to annular flow regime occurs at lower quality as the mass flux increases. This is significant because it is usually preferable to operate in the slug flow regime from the point of view of minimum pressure drop for the most flow rate.

Griffith shows that the change from slug to annular flow occurs at higher quality with higher pressure. This indicates that, for efficient operations, a relatively high backpressure should be maintained at the wellhead. If the wellhead pressure is lowered too much, the well will tend to shift into the annular flow regime and the mass rate of delivery from the reservoir will not be as great.

#### Pressure-Drop Model

As the foregoing discussion implies flow regimes must be detected point by point through the pipe. Furthermore, Eq. 1 does not have a direct analytical solution since the right-hand side is an empirical function of pressure and other variables. The solution of this equation lends itself then to finite-difference approximation in which the pipe is segmented. This allows flexibility for varying the flow regimes by segments. Rearranging Eq. 1 in finite-difference form as shown by several authors<sup>8, 9, 11</sup> yields

$$\Delta L = \Delta p \left[ \frac{144(1 - A_c)}{\bar{\rho} \frac{g}{g_c} \cos \theta + \tau_f} \right] \dots \dots \dots (4)$$

Notice that Eq. 4 has been rearranged in terms of the length increment. That is, in this model the pressure increment will be specified and the corresponding length increment calculated. When the sum of the  $\Delta L$  increments equals the depth, the wellbore pressure drop has been determined.

It would be intuitively easier to divide the wellbore into length increments. However, this approach would yield additional calculation complexities. By specifying the pressure increment, the fluid pressure is known and the enthalpies and densities of each phase can be determined directly from the steam tables. This, of course, assumes that phase equilibrium has been established in each increment. The determination of the flowing quality of the increment becomes an iterative procedure with the heat transfer calculations, as shown in the next section.

Knowing the physical properties of the fluid, the geometry, and the mass rate, one can determine flow regimes and each of the three empirical terms of Eq. 4. These three terms correspond to the three gradients in Eq. 1. Each term has several variations, depending upon flow regime and author. In general, the mixture density is presented in terms of the actual volumetric liquid fraction in the increment (holdup) as follows:

$$\bar{\rho} = \rho_l H_l + \rho_g (1 - H_l) \dots \dots \dots (5)$$

In a two-phase mixture, the specific volume of each phase is available in the steam tables. If the nonslip volumetric liquid fraction,  $\lambda_l$ , is given by

$$\lambda_l = \frac{q_l}{(q_l + q_g)} \dots \dots \dots (6)$$

then, since gas always "slips" past the liquid in vertical upflow except in fully entrained mist flow, the holdup is related to  $\lambda_l$  by

$$H_l \geq \lambda_l \dots \dots \dots (7)$$

The essence of every two-phase flow empirical correlation is to determine the relationship between  $H_l$  and  $\lambda_l$  for the flow regime, geometry, and flow parameters of the system.

The friction term,  $\tau_f$ , is usually slightly different with each author, but in the general form,

$$\tau_f = \frac{f_M \rho_r v_{rr}^2}{2g_c d} \dots \dots \dots (8)$$

The friction factor ( $f_M$ ) in turn is dependent on a representative two-phase Reynolds number:

$$N_{Re} = \frac{\rho_r v_{rr} d}{\mu_r} \dots \dots \dots (9)$$

The values used for  $\rho_r$ ,  $v_{rr}$  and  $\mu_r$  have a direct bearing on the holdup. Most investigators assume a friction gradient and then back-correlate a holdup function that yields a match of the measured two-phase pressure drop. Therefore, the friction and holdup correlations are usually tied together in vertical two-phase flow. Since they are not independent, it would not in general be good practice to generate "hybrid correlations" by mixing correlations.

The acceleration term,  $A_c$ , has been shown by Wallis<sup>20</sup> to represent the two-phase Mach number squared,  $M^2$ . Each author again presents his own definition of the term. In general,  $A_c$  is much less than 1. However, at high flow rates and low pressures, as usually occur near the wellhead of geothermal wells, this term is important.

There are many correlations in the literature that account for slip in vertical two-phase two-component flow. The most familiar of them were developed on the basis of air-water or natural gas-oil data. The pressure-drop model used in this work will attempt to use these two-component slip correlations for the one-component steam-water system. It is beyond the scope of this paper to present the complete slip correlations for each flow regime, as they are published elsewhere.<sup>1, 8, 9, 11, 12, 20</sup> However, in a later discussion several correlations will be compared with field data.

The correlations quoted here are for vertical flow only. Eq. 4 allows for modification of the head gradient with inclination, but this is valid for only slight deviations from vertical. Highly deviated wells must also include the variation of holdup with angle of inclination.

### Heat-Transfer Equations

The equations describing the conduction of heat into a solid by a pipe flowing fluid are well established.<sup>3,10</sup> The first step is to write a heat balance on the fluid flowing through the selected pipe increment. This is summarized by Ramey<sup>14</sup> for single-phase flow. In two-phase flow, the kinetic energy is usually negligible, but is included in the following equation:

$$H_i = H_{i-1} - Q + \frac{g}{g_r} \frac{\Delta Z}{J} + \frac{\Delta v_r^2}{2g_r J} \quad (10)$$

A heat balance schematic is shown in Fig. 3. The potential energy term in this equation is added because  $Z$  is measured downwards. The total enthalpy is a function of the enthalpies of each phase,  $h_g$  and  $h_l$ , and the flowing steam quality,  $x_i$ :

$$H_i = h_g x_i + h_l (1 - x_i) \quad (11)$$

Assuming a pressure increment, the pressure is known at  $i$ , and since the fluid is saturated, the temperature and enthalpy of each phase can be found in the steam tables. Eq. 10 is used to calculate  $H_i$ , and Eq. 11 can be used to calculate the flowing quality,  $x_i$ .

The heat transfer to the surroundings is given by the standard heat-conduction formula with a time dependency factor:

$$Q = \frac{U_{nd} \Delta L (\bar{T} - T_p)}{w_{rf}(t)} \quad (12)$$

where

$$f(t) = -\ln \left( \frac{r_c}{2\sqrt{at}} \right) - 0.290 \quad (13)$$

The time dependency function has been found<sup>14</sup> to be accurate at times greater than a week for most reservoir problems. This function implies a radiation boundary condition that probably is not accurate at shorter times. The ground or rock temperature ( $T_p$ ) does not change linearly with depth and this information must be available for an accurate heat-loss calculation.

The over-all heat-transfer coefficient is a combina-

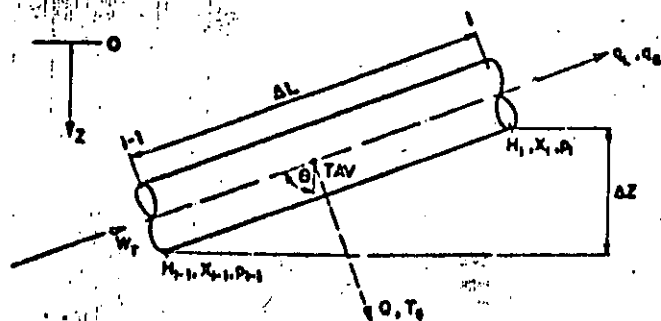


Fig. 3—Schematic of heat-transfer nomenclature.

tion of convection in the casing-tubing annulus and conduction into the formation. Willhite<sup>21</sup> gives a good development of the equations. The final result is as follows:

$$U = \frac{hk}{[hr_f(t) + k]} \quad (14)$$

If the wellbore completion is controlled by convection heat transfer, then the time function cancels out of Eq. 12. In this work, a single uniform heat-transfer coefficient will be used for the entire wellbore. Since rock properties and wellbore geometry vary with depth, this coefficient should also vary with depth when sufficient data are available.

### Numerical Model

It is necessary to couple the equation for pressure drop with that for heat transfer since each depends upon the other. For example, the pressure gradient is dependent on the quality of the mixture. The quality is dependent upon specific enthalpies of each phase, which are in turn dependent on pressure. A coupling of these two equations should yield a simultaneous calculation of both pressure and temperature profiles. The coupling algorithm discussed below uses the length of the increment under consideration as an intermediate parameter between the two equations.

The lengths in Eqs. 10 and 12 are not known at the beginning of an increment calculation. Using a selected pressure-drop correlation and Eq. 4, an estimate of  $\Delta L$  can be calculated, knowing the average quality. The quality determines the nonslip flow rates. Eq. 12 couples  $\Delta L$  to the heat-loss calculation, which in turn affects the steam quality through Eqs. 10 and 11. Steam tables are used to determine the specific enthalpies of each phase. An iterative procedure is then used for each increment to converge quality and pressure gradient. The calculations are completed when the sum of  $\Delta L$  increments equals total length.

When compressed liquids are flowing at the sandface, the density of the liquid must be calculated accurately to determine the correct pressure drop. The variation of water formation volume factor,  $B_w$ , with temperature and pressure is given graphically by Frick.<sup>22</sup> An approximate correlation for this property is given by the following:

$$B_w = 1.0 + 1.2 \times 10^{-4} T_p + 1.0 \times 10^{-6} T_p^2 - 3.33 \times 10^{-9} p \quad (15)$$

The actual water density at any particular pressure, temperature, and water gravity,  $\gamma_w$ , is given by

$$\rho_l = \frac{62.4 \gamma_w}{B_w} \quad (16)$$

The water gravity can be determined from the salt concentration. It should be noted that the water gravity of a flushing brine will change with depth as the salt concentration in the liquid varies. In addition, the steam tables used for specific enthalpies are for fresh water only; they should be applied to saline waters with caution.

The pressure-drop calculation for compressed liquid flow is straightforward. In many such wells,



however, the liquid flashes near the surface as the pressure is lowered. The flash point can be predicted from the enthalpy balance and the curve of steam saturation pressure vs temperature.

Wells that produce single-phase steam are by definition "superheated." Wells of this type are not very common, but examples exist in many parts of the world. The numerical model becomes more complicated for this type of well since the pressure and temperature are no longer related by saturation as before. If the pressure and enthalpy of a particular increment are known, the temperature can be determined from the steam tables. The specific volume also varies with pressure and temperature, so that the calculation of each increment becomes iterative until the physical properties and heat balance converge.

### Investigation of the Model

As discussed above, the simulation model consists of a pressure-drop calculation coupled with the heat-transfer calculations for the wellbore. To date, the published data for flowing pressure and temperature drops in producing steam-water wells are very limited. More of such data are needed to establish the validity of calculation techniques that have been and will be developed for the geothermal wellbore. The data used in this study came from well tests performed in the Wairakei<sup>17</sup> and the Broadlands<sup>18</sup> geothermal fields of New Zealand. The data are divided into two groups, with the first set taken during 1967 and the second set taken during 1969. The New Zealand Ministry of Works has been most helpful in providing both qualitative and quantitative information. A comparison with the well data from the U. S. Bureau of Reclamation<sup>23</sup> well Mesa 6-1 is also shown.

To test the vertical slip correlations for two-phase flow, four cases were considered. Each case consists of a different set of correlations, which are included in the references. For identification, the sets are listed here by correlation author and flow regime (slug/annular-mist):

1. Hagedorn and Brown/Ros,
2. Hagedorn and Brown/Turner-Ros,
3. Aziz/Turner-Ros,
4. Orkiszewski/Turner-Ros.

For the bubble flow regime, the Griffith and Wallis

correlation was used exclusively. The flow regime boundaries in Fig. 2 were used to distinguish which correlation should be used under specified conditions.

### Field Data

Table 1 gives the completion characteristics and other information for each well test in the 1967 data. The reference depth is the point of pressure measurement and not necessarily the total well depth. Thermal fluid enters the wellbore over a large interval through a slotted liner. The liner is attached to the production casing at the "cased depth." Table 2 shows the measured pressure drop for each well and the corresponding calculated pressure drop for the last three cases. This table also shows the flow regimes encountered in each well test.

Some comments are appropriate here concerning the nature of each case and certain well tests. The first and second cases differ only in the slip correlation used for mist flow. The well test BR-7 is the only pressure drop that consists entirely of annular-mist flow. The first correlation case uses the Ros assumption of no slip in annular-mist flow. The second case uses the Turner correlation<sup>20</sup> to estimate the slip. Using slip, Case 2 calculated within 10 percent of the measured pressure drop. Case 1 predicts less than half the pressure drop for BR-7. On this basis, the Turner-Ros model for annular-mist flow will be considered in all further analyses. This conclusion is based on only one well test and should be verified when more data become available.

Because the wells are all producing at high rates, none of the available 1967 well test data include results in the bubble flow regime. Also because of high rates, these pressure-drop calculations were relatively insensitive to heat-transfer coefficient. A heat-transfer coefficient of 1.0 Btu/(hr °F sq ft) was assumed. The pressure drops were sensitive to the roughness assumed for the slotted liner. A value of 0.0054 in. was used for the liner and 0.0018 in. was used for the casing. Many of the 1967 data were read from graphs and therefore may not be so accurate as needed for true calibration of the model. It is not clear whether or not all the bottom-hole pressures were measured under flowing conditions.

Table 3 shows the 1969 New Zealand data from well tests in Broadlands Wells 11 and 13. The data

TABLE 1—WELL DATA FROM BROADLANDS AND WAIRAKEI, NEW ZEALAND (1967)

Well Test	Reference Depth (ft)	Cased Depth (ft)*	Steam Rate (1,000 lb <sub>m</sub> /hr)	Water Rate (1,000 lb <sub>m</sub> /hr)	Wellhead Quality	Wellhead Pressure (psig)	Bottom-hole Pressure (psig)	Measured Pressure Drop (psi)
BR-2	2,486	1,367	195	400	0.328	200	775	575
BR-3	2,480	1,538	120	250	0.324	145	475	330
BR-7	2,504	1,766	60	23	0.723	150	350	200
BR-8	2,491	1,458	190	205	0.481	155	720	565
BR-9	2,500	1,500	44**	96**	0.314	155	320	165
BR-13	2,450	1,700**	70	220	0.241	145	475	330
WK-27A	2,010	1,390	85	525	0.139	165	360†	195
WK-27B	2,010	1,390	58	500	0.104	245	410†	165
WK-27C	2,010	1,390	35	425	0.076	320	470†	150

\*Diameter = 7.825 ID to cased depth, and slotted liner below = 5.836.

\*\*Estimated.

†Diameter = 7.825 ID to cased depth, and slotted liner below = 5.836.

consist of measured flowing pressure profiles at different test conditions. Table 3 shows only selected pressure drops rather than each measured value. All the measurements were made within the slotted liner. These calculations do not account for any additional two-phase pressure drop that might be attributed to the fittings used in the diameter change from slotted liner to casing.

At the time of these tests, BR-11 was completed with 7.825-in.-ID casing from the wellhead to 1,582 ft. A slotted liner was used from this point to a depth of 2,487 ft. Well BR-13 used 7.825-in.-ID casing from the wellhead to 1,459 ft. A casing of 6.969 in. ID was used from 1,459 to 2,602 ft, and at this point a slotted liner was used to 3,534 ft. The slotted liner used in both wells had an inside diameter of 5.921 in., with 16 slots ( $2 \times \frac{3}{4}$  in.) per foot.

The wellhead qualities ranged from 0.05 to 0.29. The calculations showed all these well tests to be in the slug flow regime. The roughness used was 0.0018 in. The heat-transfer coefficient made some difference in these runs. A value of 30 Btu/(hr °F sq ft)

was used for both wells. The rock temperatures used in the calculations were based on the shut-in stabilized temperature profiles in each well.

Fig. 4 shows the results of a well test performed recently on the well Mesa 6-1. Unfortunately, the flow rate from this well was not accurately determined but was estimated at 50,000 lb<sub>m</sub>/hr. The well produces compressed liquid from the formation through a slotted liner set at 7,292 ft. The bottom-hole was selected as 7,000 ft for these calculations at a flowing pressure of 1,275 psig. Since bottom-hole measurements were available in this case, the calculations were performed from bottom to top in the direction of flow.

Fig. 4 shows that the calculated flash point agrees very well with the observed position. Eq. 16 was used to correct the single-phase pressure gradient. Without the density correction, large errors in the flash-point prediction occur. Using the measured rock temperature profile, a heat-transfer coefficient of 10 Btu/(hr °F sq ft) matched the observed temperature profile in the single-phase region. The Case 2 model,

TABLE 2—COMPARISON OF 1967 FIELD DATA WITH CALCULATED RESULTS

Well Test	Total Mass Rate (1,000 lb <sub>m</sub> /hr)	Predicted Flow Regimes*	$\Delta p_w$	Case 2**		Case 3		Case 4	
				$\Delta p_w$ (psi)	Percent Difference†	$\Delta p_w$ (psi)	Percent Difference	$\Delta p_w$ (psi)	Percent Difference
BR-2	595	M, T, S	575	592	2.9	1,075	87.	719	24.9
BR-3	370	M, T, S	330	368	11.6	739	124.	440	33.2
BR-7	83	M	200	184	- 8.5	184	- 8.5	184	- 8.5
BR-8	395	M, T, S	565	507	-10.3	1,040	84.	649	14.8
BR-9	140	T, S	165	166	0.7	377	128.	231	39.9
BR-13	290	T, S	330	247	-25.3	492	49.	258	- 21.8
WK-27A	610	S	195‡	187	- 4.1	289	48.	117	- 40.
WK-27B	558‡	S	165‡	151	- 5.4	227	27.	111	- 32.7
WK-27C	460	S	150‡	137	- 8.7	202	35.	111	- 26.
				Average	- 5.2		+ 64		- 1.8

\*M = Mist  
T = Transition  
S = Slug  
B = Bubble

\*\*Slotted liner roughness = 0.0054 in.

$$\dagger \text{Percent Difference} = \frac{(\Delta p_w - \Delta p_w) (100)}{\Delta p_w}$$

‡Taken over top 1,100 ft.

TABLE 3—COMPARISON OF 1969 FIELD DATA WITH CALCULATED RESULTS

Test Number	Depth to Pressure (ft)	Total Mass Rate (1,000 lb <sub>m</sub> /hr)	Wellhead Enthalpy (Btu/lb <sub>m</sub> )	Wellhead Pressure (psig)	$\Delta p_w$ (psi)	Case 2		Case 4	
						$\Delta p_w$ (psi)	Percent Difference*	$\Delta p_w$ (psi)	Percent Difference*
11-1A	1,800	280	540	380	153	153	0	115	- 24.8
11-1B	2,400	280	540	380	218	231	+ 5.9	187	- 14.2
11-2	2,400	375	560	338	237	276	+ 16.3	252	+ 6.3
11-3A	1,600	120	465	400	125	135	+ 8.0	319	-
11-3B	2,400	120	465	400	241	215	- 10.8	497	+ 106
11-4	2,000	220	505	440	172	176	+ 2.3	155	- 9.9
11-5	2,000	311	510	385	206	198	- 3.9	161	- 21.8
11-6	2,000	386	505	350	227	223	- 1.8	183	- 19.4
13-7	3,400	260	585	156	252	285	+ 13.1	296	+ 17.5
13-8	3,400	245	570	215	308	274	- 11.0	287	- 6.8
13-12A	3,000	246	574	215	242	222	- 8.2	230	- 4.9
13-12B	3,400	246	574	215	304	274	- 9.9	289	- 4.9
					Average		- 0.01		+ 2.1

$$* \text{Percent Difference} = \frac{(\Delta p_w - \Delta p_w) (100)}{\Delta p_w}$$

which included all flow regimes from bubble to mist, was used for the two-phase pressure drop. Although the pressure calculation was very good in the two-phase portion of the wellbore, small differences in pressure caused significant differences in the calculated temperature profile. Over all, the calculated results appear to match the observed values quite well.

Tables 2 and 3 indicate that Case 2 matched the data fairly well. Because of the small size of the data sample and the uncertainties mentioned above, the conclusion that Case 2 is the best set of correlations for steam-water two-phase flow is tentative at best. However, as more data are gathered, these and other slip correlations can be tested again to improve the prediction performance. Fig. 5 compares all the results for Case 2. The data cover a relatively narrow range of pressure drops, but this is because the test wells are shallow. Deeper wells will, of course, produce higher pressure-drop systems. The horizontal bars drawn around each data point indicate the estimated accuracy of each pressure-drop measurement. Fig. 6 shows the results for Case 4 on the 1967 New Zealand data. There is more scattering of the results than on Fig. 5.

### Temperature Profiles

The three well tests that were available from the Wairakei field<sup>17</sup> were in the form of measured flowing temperature profiles. Fig. 7 compares the Case 2 model with the measured data. In the fully developed two-phase region, the model matches the data quite well. In the range from 1,200 to 1,400 ft the temperature rises sharply and all three tests approach the same value. In this well, a liner was set at 1,390 ft.

It is probable that under these test conditions, the formation is producing undersaturated thermal water. The tubing was inspected after the data were taken

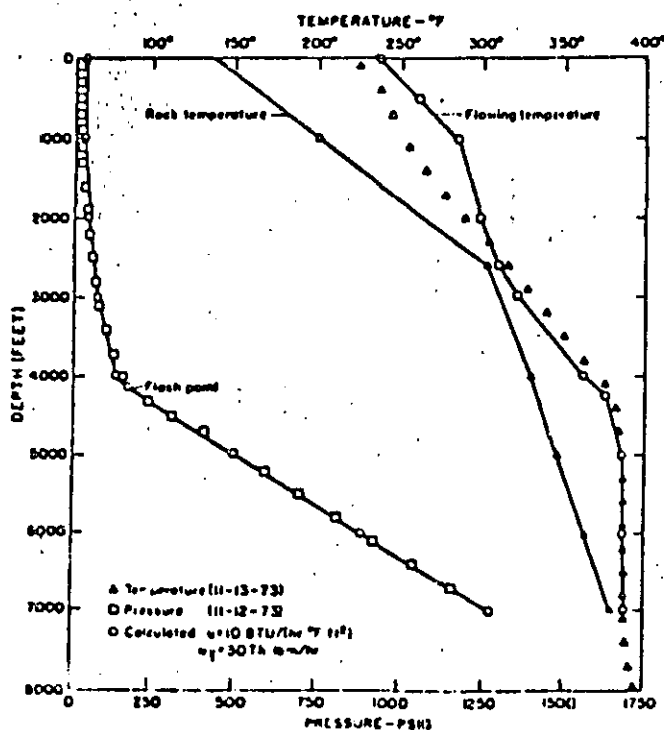


Fig. 4—Temperature and pressure in Well Mesa 6-1, Imperial Valley, Calif.

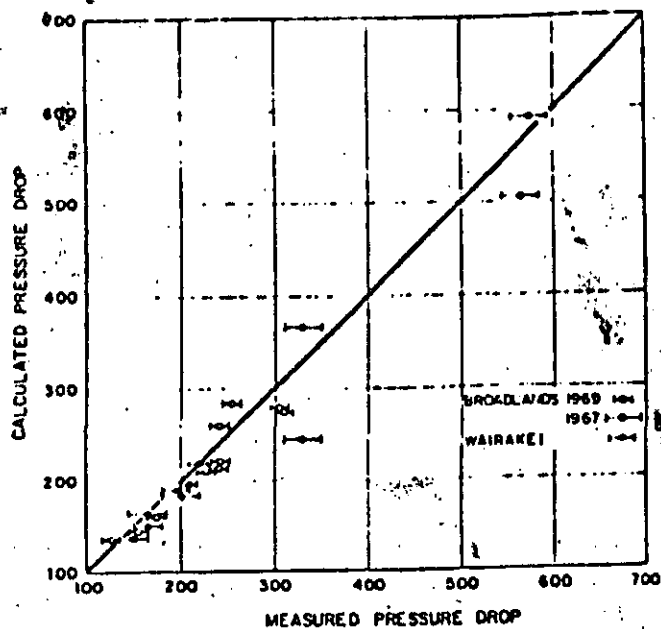


Fig. 5—New Zealand data compared with the Hagedorn and Brown/Turner-Ros model.

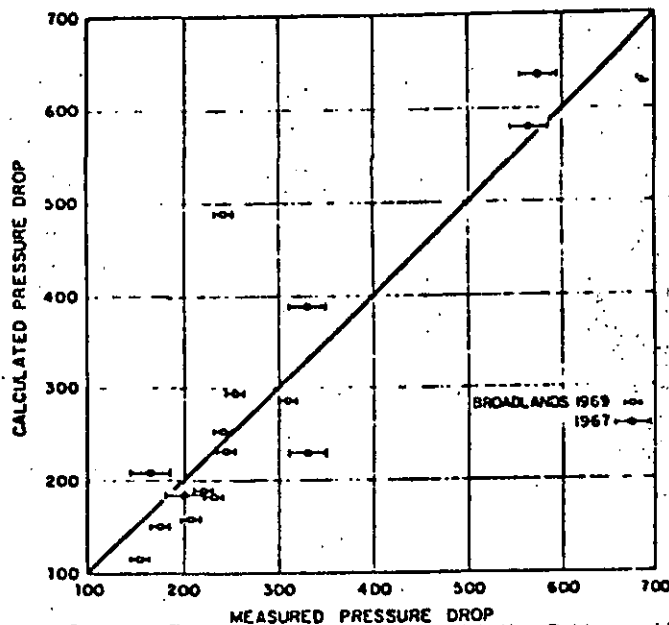


Fig. 6—New Zealand data compared with the Orkiszewski (gas-water)/Turner-Ros model.

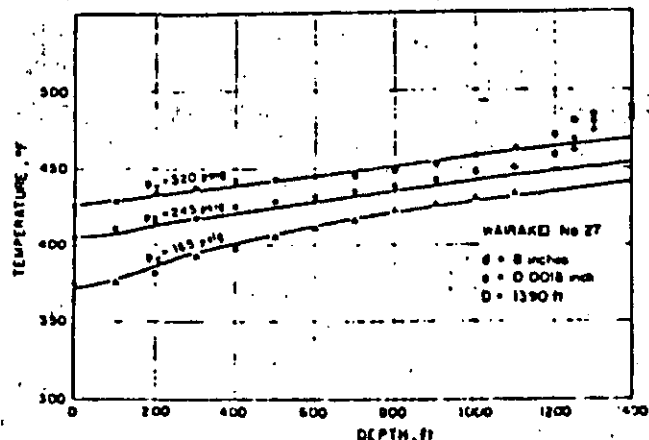


Fig. 7—Comparison of measured temperature and temperature calculated by Hagedorn and Brown.



nished for any of the important system parameters.

This leads to the determination of wellbore deliverability, which often controls the performance of geothermal steam reservoirs. The deliverability is a function of many variables and is defined as follows: The deliverability of a steam-water wellbore is the total mass rate that will flow for a given wellbore geometry (diameters, depth), wellhead pressure, bottom-hole pressure, and bottom-hole quality. The calculation of deliverability is an iterative problem based upon pressure profiles.

The discussion of Eqs. 1 and 4 showed that the pressure drop has been empirically correlated with holdup and friction factors. The flow rates of each phase are included in these correlations, but in an implicit form. It follows that the calculation of deliverability is a trial-and-error procedure. The convergence scheme used is discussed in detail in Ref. 8. The first step consists of an interval search to find the feasible range of mass rates for the given data. Once the range is known, a *regula-falsi* algorithm is used to converge on the deliverability.

Fig. 12 shows typical curves of steam well deliverability vs flowing bottom-hole pressure for a fixed wellhead pressure. The curves demonstrate one of the interesting numerical problems encountered in this study: If the wellhead pressure is fixed and the bottom-hole pressure is fixed, there are two mass flow rates that will satisfy the total pressure drop in the system. Intuitively, this does not make much sense. However, the explanation lies in the combination of head and friction gradients to make up a total pressure gradient. At a constant liquid rate, the head gradient will decrease and the friction gradient will increase as more and more gas is flowing in the wellbore. This causes the total pressure gradient to show a minimum with respect to total mass rate. Note that Fig. 12 shows a minimum pressure drop where no flow can exist at the diameter used.

When the pressure drop is specified, the resulting two mass rates will be referred to as the "upper" and "lower" roots of the deliverability. The upper root is the higher-rate root and tends to occur in annular-mist or froth flow. The majority of commercial steam-water production wells are the upper root type. If a wellbore performs at the lower root, it is usually shut in as uneconomical. The reservoir also has a deliverability as a function of bottom-hole pressure. The intersection of these two deliverabilities will yield the total deliverability of a geothermal system.

### Summary

1. The heat-transfer relationships have been coupled with two-phase flow in the wellbore.
2. Several two-component vertical two-phase-flow pressure-drop correlations have been compared with existing field data for one-component steam-water wells.
3. For steam-water flow in a geothermal wellbore, the Griffith and Wallis/Hagedorn and Brown/Turner-Ros pressure-drop model appears, on the basis of the limited data, to be the most consistent.
4. The calculation of flowing pressure and tem-

perature profiles in geothermal wells can have many useful applications; for example in defining and determining deliverability.

### Nomenclature

- $A_e$  = acceleration gradient, dimensionless
- $B_w$  = water formation volume factor (FVF)
- $C$  = conversion factor
- $d$  = inside pipe diameter, ft
- $f_M$  = Moody friction factor
- $f(t)$  = time varying function
- $g$  = gravitational acceleration, ft/sec<sup>2</sup>

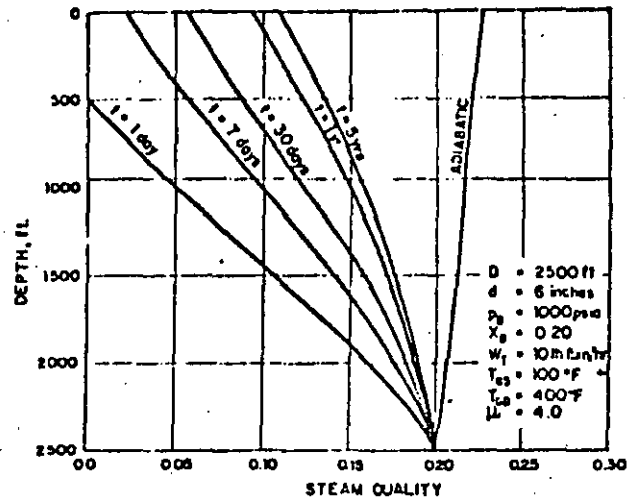


Fig. 11—Variation of flowing quality profile with time.

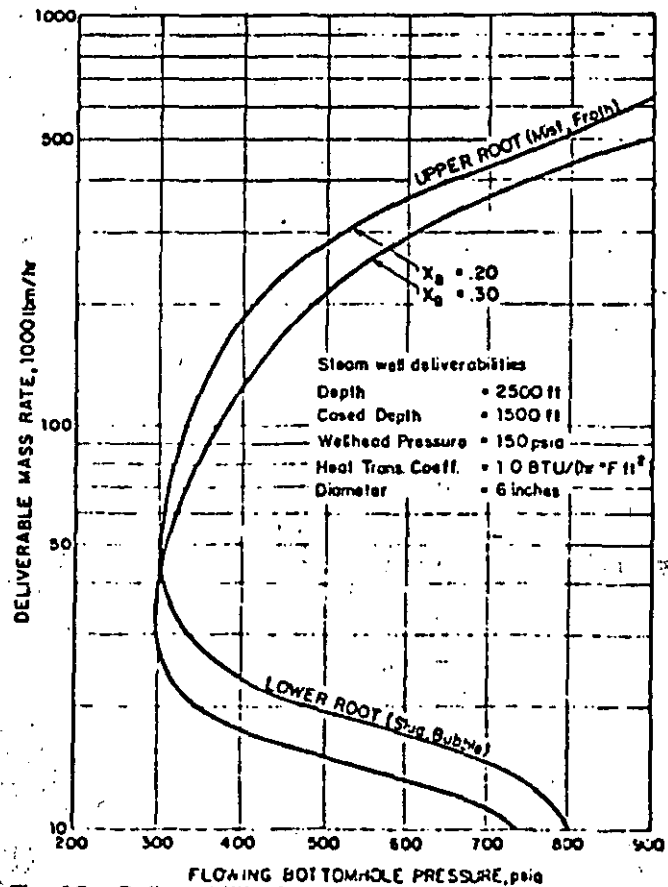


Fig. 12—Deliverability function, showing both upper and lower roots.

$h$  = convective heat-transfer coefficient, Btu/(hr °F sq ft)  
 $h_g, h_l$  = specific enthalpies of each phase at  $(\bar{p}, \bar{T})$ , Btu/lb<sub>m</sub>  
 $H_i$  = total enthalpy of the  $i$ th increment, Btu/lb<sub>m</sub>  
 $H_l$  = volumetric liquid fraction, holdup fraction  
 $J$  = mechanical equivalent of heat, 778 ft-lb<sub>f</sub>/Btu  
 $k$  = thermal conductivity, Btu/(hr ft °F)  
 $L$  = length of pipe, ft  
 $N_{gv}, N_{lv}$  = gas and liquid velocity numbers, dimensionless  
 $N_{R_0}$  = two-phase Reynolds number, dimensionless  
 $\bar{p}$  = average pressure in a given calculation increment, psia  
 $p_b$  = flowing bottom-hole pressure, psia  
 $\Delta p_c$  = calculated pressure drop, psi  
 $\Delta p_m$  = measured pressure drop, psi  
 $q_g, q_l$  = volumetric flow rate of each phase, cu ft/sec  
 $Q$  = heat transferred to surroundings, Btu/lb<sub>m</sub>  
 $r_o$  = outer radius of the casing, ft  
 $r_i$  = inner radius of the tubing, ft  
 $t$  = time since the well was open for flow, days  
 $\bar{T}$  = average temperature in a given calculation increment, °F  
 $T_g$  = ground or rock temperature at depth  $z$ , °F  
 $T_s = \bar{T} - 60$   
 $U$  = over-all heat-transfer coefficient, Btu/(hr sq ft °F)  
 $v_{og}, v_{ol}$  = superficial gas and liquid velocities, ft/sec  
 $v_T$  = total velocity, ft/sec  
 $v_{Tr}$  = representative total velocity depending on correlation, ft/sec  
 $w_T$  = total mass flow rate, lb<sub>m</sub>/hr  
 $x$  = mass fraction of steam (quality)  
 $Z$  = depth measured downwards, ft  
 $\alpha$  = thermal diffusivity of the earth, sq ft/D  
 $\gamma_w$  = specific gravity of brine with respect to pure water  
 $\theta$  = angle of inclination from the vertical  
 $\bar{\rho}$  = average mixture density, lb<sub>m</sub>/cu ft  
 $\rho_r$  = representative density depending on correlation, lb<sub>m</sub>/cu ft  
 $\rho_g, \rho_l$  = gas and liquid in-situ densities, lb<sub>m</sub>/cu ft  
 $\mu_g, \mu_w$  = gas and liquid viscosities, cp  
 $\mu_r$  = representative viscosity depending on correlation, cp  
 $\tau_f$  = friction gradient, lb/sq ft/ft

## Acknowledgment

I appreciate the assistance of R. S. Bolton of the New Zealand Ministry of Works in providing much of the data used in this work.

## References

1. Aziz, K., Govier, G. W., and Fogarasi, M.: "Pressure Drop in Wells Producing Oil and Gas," *J. Cdn. Pet. Tech.* (Sept. 1972) 38-48.
2. Calvert, S.: "Vertical, Upward, Annular, Two-Phase Flow in Smooth Tubes," PhD thesis, U. of Michigan, Ann Arbor (1952).
3. Carslaw, H. S., and Jaeger, J. S.: *Conduction of Heat in Solids*, Oxford Press, London (1959).
4. Craft, B. C., and Hawkins, M. F., Jr.: *Applied Petroleum Reservoir Engineering*, Prentice-Hall, Inc., Englewood Cliffs, New Jersey (1959).
5. Farlougher, R. C., Jr.: "Some Practical Considerations in the Design of Steam Injection Wells," *J. Pet. Tech.* (Jan. 1969) 79-86; *Trans., AIME*, 246.
6. Elder, J. W.: "Heat and Mass Transfer in the Earth: Hydrothermal Systems," *Bull. 169*, Dept. of Science and Industrial Research, New Zealand (1966).
7. "Geothermal Energy Resources and Research," U. S. Senate Hearings for Senate Resolution 45 (June 1972) No. 92-31.
8. Gould, T. L.: "Vertical Two-Phase Flow in Oil and Gas Wells," PhD thesis, U. of Michigan, Ann Arbor (1972).
9. Hagedorn, A. R., and Brown, K. E.: "The Effect of Liquid Viscosity in Vertical Two-Phase Flow," *J. Pet. Tech.* (Feb. 1964) 203-210; *Trans., AIME*, 231.
10. Katz, D. L.; Cornell, D.; Kobayashi, R.; Poettmann, F. H.; Vary, J. A.; Elenbaas, J. R., and Weinang, C. F.: *Handbook of Natural Gas Engineering*, McGraw-Hill Book Co., Inc., New York (1959).
11. McKenzie, G. R., and Smith, J. H.: "Progress of Geothermal Energy Development in New Zealand," paper presented at World Power Conference VII, Moscow (Aug. 1968).
12. McNitt, J. R.: "Exploration and Development of Geothermal Power in California," *Report 75*, California Div. of Mines and Geology (1963).
13. Orkiszewski, J.: "Predicting Two-Phase Pressure Drop in Vertical Pipe," *J. Pet. Tech.* (June 1967) 829-838; *Trans., AIME*, 240.
14. Ramey, H. J., Jr.: "Wellbore Heat Transmission," *J. Pet. Tech.* (April 1962) 427-435; *Trans., AIME*, 225.
15. Ros, N. C. J.: "Simultaneous Flow of Gas Liquid as Encountered in Well Tubing," *J. Pet. Tech.* (Oct. 1961) 1037-1049; *Trans., AIME*, 222.
16. Satter, A.: "Heat Losses During Flow of Steam Down a Wellbore," *J. Pet. Tech.* (July 1965) 845-851; *Trans., AIME*, 234.
17. Smith, J. H.: "Production and Utilization of Geothermal Steam," N. Z. Institution of Engineers (April 1958).
18. Smith, J. H.: "Geothermal Development in New Zealand," United Nations Symposium on the Development of Geothermal Resources, Pisa, Italy (1970).
19. Scheidegger, A. E.: *The Physics of Flow Through Porous Media*, Macmillan Co., New York (1960).
20. Wallis, G. B.: *One-Dimensional Two-Phase Flow*, McGraw-Hill Book Co., Inc., New York (1969).
21. Willhite, G. P.: "Over-all Heat Transfer Coefficient in Steam and Hot Water Injection Wells," *J. Pet. Tech.* (May 1967) 607-615.
22. Frick, T. C.: *Petroleum Production Handbook*, Society of Petroleum Engineers of AIME, Dallas (1962).
23. Lundberg, E. A.: "Geothermal Resource Investigations — Special Report on Test Well Mesa 6-1," U. S. Bureau of Reclamation (Feb. 1973).
24. Bennett, A. W. et al.: "Flow Visualization Studies of Boiling at High Pressure," AERE-R 4874 (1965).

# Predicting Two-Phase Pressure Drops in Vertical Pipe

J. ORKISZEWSKI\*

ESSO PRODUCTION RESEARCH CO.  
HOUSTON, TEX.

## ABSTRACT

A method is presented which can accurately predict, with a precision of about 10 percent, two-phase pressure drops in flowing and gas-lift production wells over a wide range of well conditions. The method is an extension of the work done by Griffith and Wallis<sup>1</sup> and was found to be superior to five other published methods. The precision of the method was verified when its predicted values were compared against 148 measured pressure drops. The unique features of this method over most others are that liquid holdup is derived from observed physical phenomena, the pressure gradient is related to the geometrical distribution of the liquid and gas phase (flow regimes), and the method provides a good analogy of what happens inside the pipe. It takes less than a second to obtain a prediction on the IBM 7044 computer.

## INTRODUCTION

The problem of accurately predicting pressure drops in flowing or gas-lift wells has given rise to many specialized solutions for limited conditions, but not to any generally accepted one for broad conditions. The reason for these many solutions is that the two-phase flow is complex and difficult to analyze even for the limited conditions studied. Under some conditions, the gas moves at a much higher velocity than the liquid. As a result, the down-hole flowing density of the gas-liquid mixture is greater than the corresponding density, corrected for down-hole temperature and pressure, that would be calculated from the produced gas-liquid ratio. Also, the liquid's velocity along the pipe wall can vary appreciably over a short distance and result in a variable friction loss. Under other conditions, the liquid is almost completely entrained in the gas and has very little effect on the wall friction loss. The difference in velocity and the geometry of the two phases strongly influence pressure drop. These factors provide the basis for categorizing two-phase flow. The generally accepted categories (flow regimes) of two-phase flow are bubble, slug, (slug-annular) transition and annular-mist.<sup>2,3</sup> They are ideally depicted in Fig. 1 and briefly described as follows.

### BUBBLE FLOW (FIG. 1A)

The pipe is almost completely filled with the liquid and

the free-gas phase is small. The gas is present as small bubbles, randomly distributed, whose diameters also vary randomly. The bubbles move at different velocities depending upon their respective diameters. The liquid moves in the pipe at a fairly uniform velocity and, except for its density, the gas phase has little effect on the pressure gradient.

### SLUG FLOW (FIG. 1B)

In this regime, the gas phase is more pronounced. Although the liquid phase is still continuous, the gas bubbles coalesce and form stable bubbles of approximately the same size and shape which are nearly the diameter of the pipe. They are separated by slugs of liquid. The bubble velocity is greater than that of the liquid and can be predicted in relation to the velocity of the liquid slug.<sup>4</sup> There is a film of liquid around the gas bubble. The liquid velocity is not constant—whereas the liquid slug always moves upward (in the direction of bulk flow); the liquid in the film may move upward but possibly at a lower velocity, or it may move downward. These varying liquid velocities will result not only in varying wall friction loss but also in a "liquid holdup" which will influence flow density. At higher flow velocities, liquid can even be entrained in the gas bubbles. Both the gas and liquid phases have significant effects on the pressure gradient.

### TRANSITION FLOW (FIG. 1C)

The change from a continuous liquid phase to a continuous gas phase occurs in this region. The liquid slug between the bubbles virtually disappears, and a significant amount of liquid becomes entrained in the gas phase. Although the effects of the liquid are significant, the gas phase is more predominant.

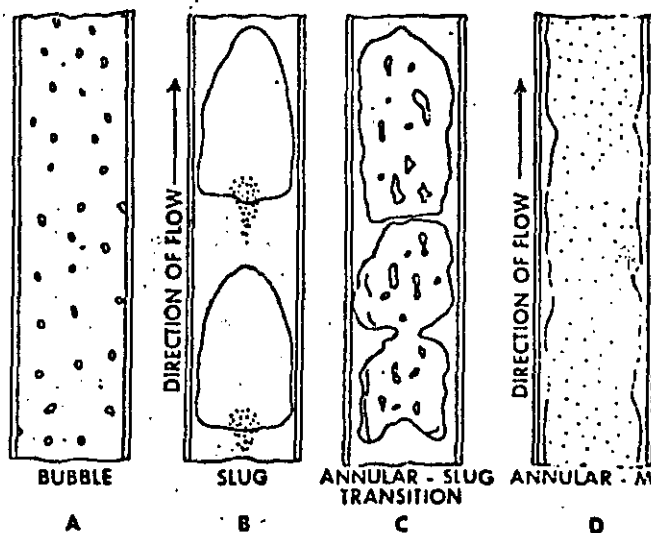


FIG. 1.—GEOMETRICAL CONFIGURATIONS IN VERTICAL FLOW.

Original manuscript received in Society of Petroleum Engineers office August 8, 1966. Revised manuscript of SPE 1546 received March 1, 1967. Paper was presented at 41st Annual Fall Meeting held in Dallas, Tex., Oct. 2-5, 1966. ©Copyright 1967 American Institute of Mining, Metallurgical, and Petroleum Engineers, Inc.

\*Presently with International Petroleum Co. Ltd., Talara, Peru.

<sup>1</sup>References given at end of paper.

<sup>2,3</sup>All four regimes could conceivably exist in the same well. An example would be a deep well producing light oil from a reservoir which is near its bubble point. At the bottom of the hole, with little free gas present, flow would be in the bubble regime. As the fluid moves up the well, the other regimes would be encountered because gas continually comes out of solution, and the pressure continually decreases. Normally, however, flow is in the slug regime and rarely in mist, except for condensate reservoirs or steam-stimulated wells.

### ANNULAR MIST FLOW (FIG. 1D)

The gas phase is continuous. The bulk of the liquid is entrained and carried in the gas phase. A film of liquid wets the pipe wall, but its effects are secondary. The gas phase is the controlling factor.

To cope with the complex problem, the many published methods were analyzed to determine whether any one method was broad enough, or had the ingredients to be broad enough, to accurately predict pressure drops over a wide range of well conditions. The methods were first categorized. Certain methods were selected from each category to predict pressure drops for two selected well cases whose flow conditions were significantly different from those originally used in developing the various methods. Finally, the predicted pressure drops using the more promising methods were compared against known values taken from 148 cases having widely varying conditions of rate, GOR, tubing size, water cut and fluid properties.

### BASIS FOR SELECTING METHODS STUDIED

Based upon similarity in theoretical concepts, the published methods were first divided into three categories. From each category certain methods were selected, based on whether they were original or unique, and were developed from a broad base of data. The discriminating features of the three categories are shown.

#### CATEGORY 1 (REFS. 1, 3, 6, 9)

Liquid holdup is not considered in the computation of the density. The density is simply the composite density of the produced (top-hole) fluids corrected for down-hole temperature and pressure. The liquid holdup and the wall friction losses are expressed by means of an empirically correlated friction factor. No distinctions are made among flow regimes.

#### CATEGORY 2 (REFS. 7, 8, 10)

Liquid holdup is considered in the computation of the density. The liquid holdup is either correlated separately or combined in some form with the wall friction losses. The friction losses are based on the composite properties of the liquid and gas. No distinctions are made among flow regimes.

#### CATEGORY 3 (REFS. 2, 11-13)

The calculated density term considers liquid holdup. Li-

quid holdup is determined from some concept of slip velocity (the difference between the gas and liquid velocities). The wall friction losses are determined from the fluid properties of the continuous phase. Four distinct flow regimes are considered.

Of the 13 methods categorized, two from each category were selected for further study. The methods of Poettmann and Carpenter,<sup>1</sup> and Tek<sup>2</sup> were picked from Category 1. Most of the methods in this category are extensions of the Poettmann-Carpenter work. In the second category, the Hughmark and Pressburg method<sup>3</sup> was selected; the Hagedorn and Brown method<sup>4</sup> was not available at the time of the initial screening, but it was included in the final detailed evaluation. There are really only two methods in Category 3. The Griffith<sup>5</sup> and the Griffith and Wallis<sup>6</sup> methods are synonymous; the Nicklin, Wilkes, and Davidson method<sup>7</sup> is for special conditions and parallels the work of Griffith-Wallis. The other method is that of Duns and Ros.<sup>8</sup>

### RESULTS OF THE COMPARISON

The five methods initially selected, whose results were hand calculated, were compared by determining the deviation between predicted and measured pressure drops for the first two well conditions listed in Table 1. Fig. 2 compares the predictions for Well 1. The results were similar for Well 2. The most accurate methods (Duns-Ros and Griffith-Wallis) were then programmed for machine computation and further tested against 148 well conditions.\*

Neither method proved accurate over the entire range of conditions used. Although the Griffith-Wallis method was reliable in the lower flow-rate range of slug flow, it was not accurate in the higher range. The Duns-Ros method exhibited the same behavior except that it was also inaccurate for the high-viscosity oils in the low flow-rate range. The Griffith-Wallis method appeared to provide the better foundation for an improved general solution although its predicted values were in greater error (21.9 percent) than Duns and Ros (2.4 percent). The heart of this method, prediction of slip velocity, is derived from physical observation. However, since friction drop was

\*The data in Table 1 are from 22 Venezuelan heavy-oil wells. In addition to the data presented in Table 1, the data used are from the publications of Poettmann and Carpenter,<sup>1</sup> Bazendell and Thomas,<sup>2</sup> Fancher and Brown,<sup>3</sup> and Hagedorn and Brown.<sup>4</sup> These represent 128 additional pieces of data.

TABLE 1—PHYSICAL CONDITIONS AND FLOW RATES OF HEAVY-OIL WELLS STUDIED

Well No.	Oil Rate (B/D)	GOR (scf/bbl)	Water Cut (%)	Oil Gravity ( <sup>o</sup> API)	Measured Depth (ft)	Wellhead Pressure (psig)	Flow String Diameter (in.)	Measured Ap (psi)
1	320	4020	30	10.3	4360	250	8.76	810
2	175	6450	17	9.5	4360	300	8.76	925
3	1065	765	—	15.1	3825	550	2.992	650
4	1300	252	—	14.6	3940	150	"	850
5	3166	1430	—	14.4	3800	700	"	550
6	1965	232	—	14.4	3720	300	"	900
7	1165	957	—	15.6	4240	700	"	850
8	1965	1500	—	13.5	4570	850	"	650
9	2700	267	—	15.6	4175	300	"	1200
10	855	185	—	12.9	4355	250	"	1450
11	2320	1565	—	13.6	4670	910	"	740
12	2480	858	—	18.6	4575	650	"	900
13	1040	472	—	18.6	4400	400	"	950
14	1490	341	—	13.0	4065	500	"	1050
15	1310	335	—	13.6	3705	500	"	950
16	1350	185	—	12.9	4160	150	"	1350
17	788	222	—	16.0	4210	350	"	1400
18	1905	962	—	14.1	4487	580	"	720
19	967	193	—	13.3	4766	250	"	1300
20	1040	385	—	12.5	4505	250	"	1100
21	1585	865	—	12.9	4692	400	"	750
22	1850	575	—	18.7	3924	700	"	600



negligible in the work, the method for predicting friction losses is an approximation and therefore open to improvement. On the other hand, the Duns and Ros work in this range (which they termed plug flow) is presented as a complex set of interrelated parameters and equations, and is therefore difficult to relate to what physically occurs inside the pipe.

The Griffith-Wallis work was extended to include the high-velocity flow range. In modifying the method, a parameter was developed to account for (1) the liquid distribution among the liquid slug, the liquid film and entrained liquid in the gas bubble and (2) the liquid holdup at the higher flow velocities. This parameter served to better approximate wall friction losses and flowing density, and was principally correlated from the earlier published data of Hagedorn and Brown.<sup>8</sup> The data from Table 1 were also used to determine the effects of pipe diameter on the parameter. The details of the parameter evaluation are given in Appendix C and a brief description of the modified Griffith-Wallis method is outlined in Appendix A.

The results of the study, summarized in Table 2, are presented as the deviations between predicted and measured values for the modified Griffith-Wallis, the Duns-Ros and the then recently published Hagedorn-Brown<sup>8</sup> methods. (The Hagedorn-Brown method was included because of the excellent accuracies reported and the broad data range presented.) Plots of the individual predicted and measured values for the three methods are shown in Figs. 3 through 5. When the three methods are compared against the various grouped data sources (Table 2), only the modified Griffith-Wallis method is sufficiently accurate (average error) and precise (standard deviation) over the entire range of conditions. None of the 148 well conditions studied were in mist flow or wholly in (annular-slug) transition. The breakdown of wells by flow regimes includes seven partly in slug and transition, 26 partly in slug and bubble, four completely in bubble and 111 completely in slug flow.

### CONCLUSIONS

For general engineering work, the modified Griffith-Wallis method will predict pressure drops with sufficient accuracy and precision over a wide range of well conditions. I recommend its use. However, the method should be used with discretion for those well conditions which were not

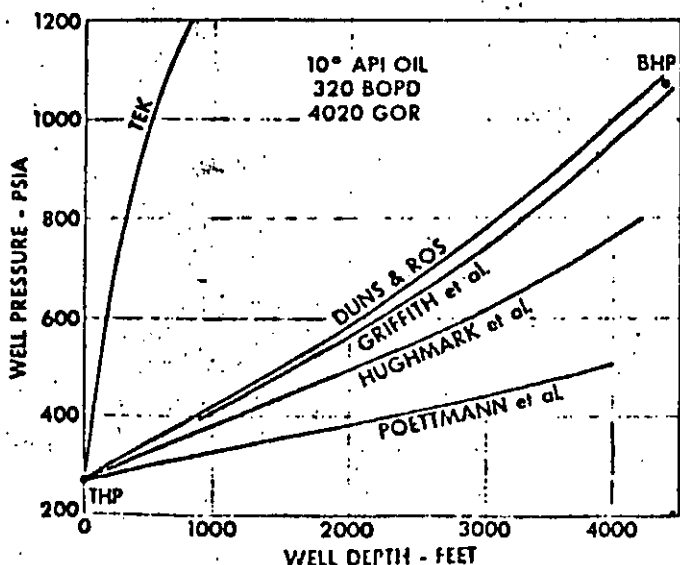


FIG. 2—COMPARISON OF PRESSURE PROFILES CALCULATED BY VARIOUS METHODS FOR WELL 1 (TABLE 1).

### MEASURED AND PREDICTED PRESSURE DROPS

	Prediction Method		
	This Method	Duns and Ros	Hagedorn and Brown
<b>Over all Results</b>			
(148 Well conditions)			
Avg. error, percent	- 0.8	+ 2.4	+ 0.7
Std. deviation, percent	10.8	27.0	24.2
<b>Results from Grouped Data Sources</b>			
<b>Table 1 — Heavy-Oil Wells</b> (22 Wells, low to medium velocities, 10 to 20° API oils)			
Avg. error, percent	- 1.2	+22.7	+16.4
Std. deviation, percent	10.4	18.7	41.4
<b>Baxendell-Thomas<sup>6</sup></b> (1 Well, 25 rates mostly high velocities, 34° API oil)			
Avg. error, percent	- 2.1	+ 2.3	+ 8.7
Std. deviation, percent	11.1	20.0	12.7
<b>Fancher-Brown<sup>8</sup></b> (1 Well, 20 rates medium to high velocities, 95 percent water cut)			
Avg. error, percent	+ 0.3	+ 1.7	+ 5.4
Std. deviation, percent	11.8	32.1	10.8
<b>Hagedorn-Brown<sup>8</sup></b> (1 Well, medium to high velocities, 16 water runs, 16 oil runs of 10 to 100 cp oil)			
Avg. error, percent	+ 0.1	-16.9	+ 1.2
Std. deviation, percent	8.2	36.6	10.3
<b>Poettmann-Carpenter<sup>1</sup></b> (49 Wells, low to medium velocities, 15 wells high water cut, rest 36 to 54° API oils)			
Avg. error, percent	- 1.0	+ 5.8	-13.0
Std. deviation, percent	12.0	12.4	22.2

sufficiently evaluated (e.g., flow in the casing annulus and in the mist-flow regime). The method's precision might be further improved if the liquid phase distribution could be more rigorously analyzed.

This method is accurate over a broader range than previous correlations. For a prediction method to be general, it must be expressed in terms of flow regime and liquid distribution. The other methods, which were not de-

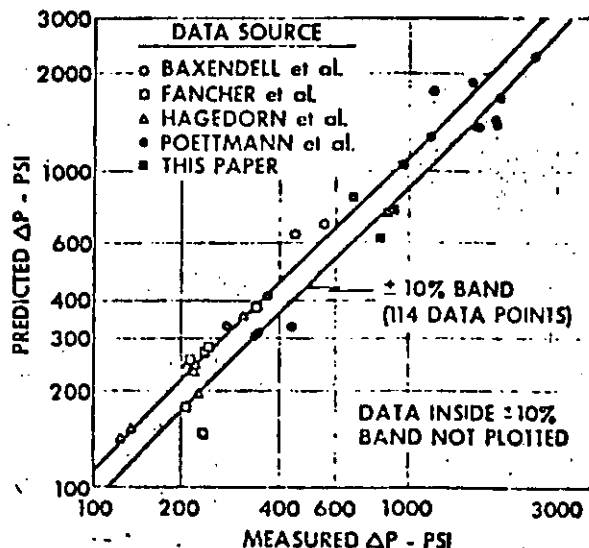


FIG. 3—THIS WORK (MODIFIED GRIFFITH AND WALLIS PREDICTION)

ped. In this manner, are only useful in the range of conditions from which they were developed.

### NOMENCLATURE

- $A_p$  = flow area of pipe, sq ft
- $B_o$  = oil formation volume factor, bbl/STB
- $C_o, C_s$  = parameters used to calculate bubble rise velocities from Eq. C-5, dimensionless, to be evaluated from Figs. 8 and 9
- $d_h$  = hydraulic pipe diameter ( $4 \times A_p$ /wetted perimeter), ft
- $D$  = depth from wellhead, ft
- $\Delta D$  = increment of depth, ft
- $f$  = Moody friction factor, dimensionless, to be evaluated from Fig. 6
- $F_g$  = flowing gas fraction, dimensionless
- $g$  = acceleration of gravity, ft/sec<sup>2</sup>
- $g_o$  = gravitational constant, ft-lb(mass)/lb(force)-sec<sup>2</sup>
- $(L)_b$  = bubble-slug boundary, dimensionless
- $(L)_m$  = transition-mist boundary, dimensionless
- $(L)_s$  = slug-transition boundary, dimensionless
- $N_b$  =  $1,488 v_b d_h \rho / \mu_o$  bubble Reynolds number, dimensionless
- $N_{no}$  =  $1,488 v D_h \rho / \mu_o$  Reynolds number, dimensionless
- $p$  = pressure, psia
- $\Delta p$  = pressure drop, psi
- $\bar{p}$  = average pressure, psia
- $p_{pc}$  = pseudo-critical pressure, psia
- $p_r$  = reduced pressure, dimensionless
- $P$  = pressure, lb/sq ft
- $q$  = volumetric flow rate, cu ft/sec
- $q_o$  = oil rate, B/D
- $R$  = produced GOR, scf/STB
- $R_s$  = solution gas, scf/STB
- $T_{pc}$  = pseudo-critical temperature, °R
- $T_r$  = reduced temperature, dimensionless
- $\bar{T}$  = average temperature, °F
- $v$  = fluid velocity, ft/sec
- $v_b$  = bubble rise velocity (velocity of rising gas bubble relative to preceding liquid slug), ft/sec
- $v_{bo}$  = base bubble rise velocity for Eq. C-9, ft/sec
- $v_s$  = slip velocity (difference between average gas and liquid velocities), ft/sec
- $v_{so}$  =  $q_o (\sqrt{\rho_l/g_o})/A_p$ , dimensionless gas velocity
- $z$  = gas compressibility factor, dimensionless
- $\gamma$  = fluid specific gravity, dimensionless

- $\Gamma$  = liquid distribution coefficient, to be evaluated from Eqs. C-11 through C-16, dimensionless
- $\mu$  = viscosity, cp
- $\xi/D$  = Moody pipe relative roughness factor (Fig. 7) and Duns-Ros mist flow factor (Eqs. C-21 and C-22), dimensionless
- $\rho$  = density, lb/cu ft
- $\bar{\rho}$  = average flowing density, lb/cu ft
- $\tau_f$  = friction-loss gradient, lb/sq ft/ft
- $\sigma$  = surface tension, lb/sec

### SUBSCRIPTS

- $g$  = gas
- $L$  = liquid
- $o$  = oil
- $t$  = total

### ACKNOWLEDGMENT

The author wishes to thank the Creole Petroleum Corp. for supplying data in Table 1 from 22 Venezuelan heavy-oil wells.

### REFERENCES

1. Poettmann, F. H. and Carpenter, P. G.: "The Multiphase Flow of Gas, Oil, and Water Through Vertical Flow Strings"; *Drill and Prod. Prac.*, API (1952) 257.
2. Duns, H., Jr., and Ros, N. C. J.: "Vertical Flow of Gas and Liquid Mixtures from Boreholes"; *Prac.*, Sixth World Pet. Congress, Frankfurt (June 19-26, 1963) Section II, Paper 22-PD6.
3. Baxendell, P. B. and Thomas, R.: "The Calculation of Pressure Gradients in High Rate Flowing Wells"; *J. Pet. Tech.* (Oct., 1961) 1023-1028.
4. Tek, M. R.: "Multiphase Flow of Water, Oil, and Natural Gas Through Vertical Flow Strings"; *J. Pet. Tech.* (Oct., 1961) 1029-1036.
5. Yocum, B. T.: "Two-Phase Flow in Well Flowlines"; *Pet. Eng.* (Nov., 1959) B-40.
6. Fancher, G. H., Jr., and Brown, K. E.: "Prediction of Pressure Gradients for Multiphase Flow in Tubing"; *Soc. Pet. Eng. J.* (March, 1963) 59-69.
7. Baker, W. J. and Keep, K. R.: "The Flow of Oil and Gas Mixtures in Wells and Pipelines: Some Useful Correlations"; *J. Inst. of Pet.* (May, 1961) 47, No. 449, 162-169.
8. Hughmark, G. A. and Pressburg, B. S.: "Hold-Up and Pressure Drop with Gas-Liquid Flow in a Vertical Pipe"; *AIChE J.* (Dec., 1961) 7, No. 4, 677-682.
9. Hagedorn, A. R. and Brown, K. E.: "The Effect of Liquid Vis-

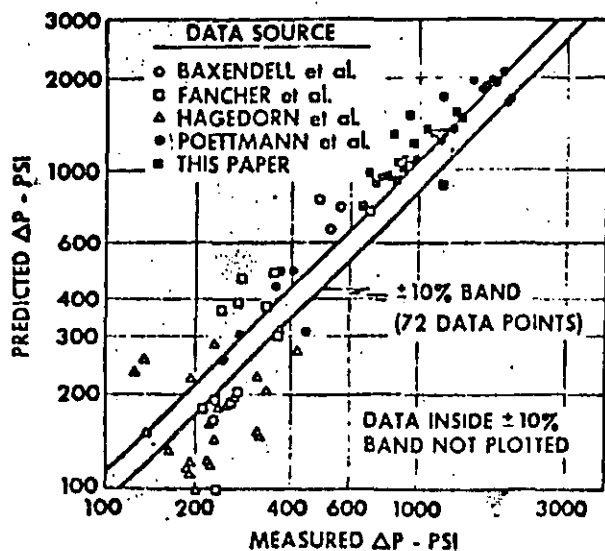


FIG. 4—DUNS AND ROS PREDICTION.<sup>9</sup>

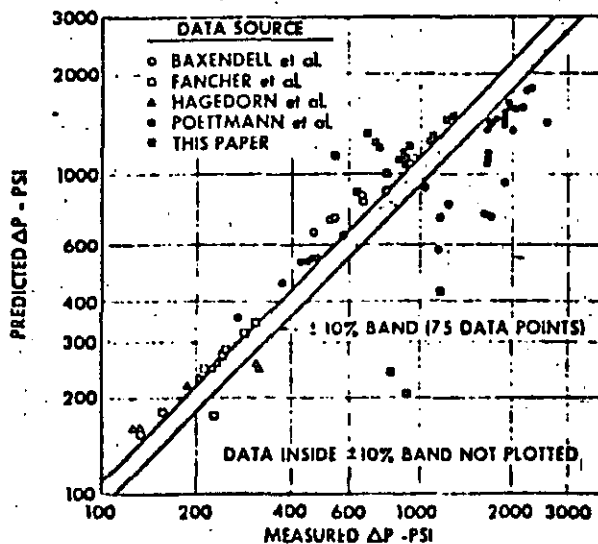


FIG. 5—HAGEDORN AND BROWN PREDICTION.<sup>10</sup>

10. Hagedorn, A. R. and Brown, K. E.: "Experimental Study of Pressure Gradients Occurring During Continuous Two-Phase Flow in Small-Diameter Vertical Conduits", *J. Pet. Tech.* (April, 1965) 475-484.

11. Griffith, P. and Wallis, G. R.: "Two-Phase Slug Flow", *J. Heat Transfer; Trans., ASME* (Aug., 1961) 307-320.

12. Griffith, P.: "Two-Phase Flow in Pipes", Special Summer Program, Massachusetts Institute of Technology, Cambridge, Mass. (1962).

13. Nicklin, D. J., Wilkes, J. O. and Davidson, J. F.: "Two-Phase Flow in Vertical Tubes", *Trans., AIChE* (1962) 40, 61-68.

14. Stadley, D. W.: "Wall Shear Stress in Two-Phase Slug Flow", MS Thesis, Massachusetts Institute of Technology, Cambridge (June, 1962).

15. Moody, L. F.: "Friction Factors in Pipe Flow", *Trans., ASME* (1944) 66, 671-684.

16. Frick, T. C.: *Petroleum Production Handbook—Vol. II, Reservoir Engineering*, McGraw-Hill, New York (1962).

w<sub>g</sub> = total gas flow rate

q<sub>g</sub> = gas volumetric flow rate, cu ft/sec.

With the above conditions and Eq. A-2, Eq. A-1 may then be expressed in a more convenient form.

$$\Delta p = \left[ \frac{1}{144} \frac{\bar{p} + \tau_f}{w_g q_g / 4.637 A_p^2 \bar{p}} \right] \Delta D \quad (A-3)$$

where for average temperature-pressure conditions at increment k,

- $\bar{p}$  = average fluid density, lb/cu ft,
- $\Delta p$  = pressure drop, psi,
- $\bar{p}$  = average pressure, psia.

Since temperature is related to depth, Eq. A-3 may be incremented by either fixing  $\Delta D$  and solving for  $\Delta p$ , or vice versa. However, since pressure usually has a greater influence on the average fluid properties than temperature,  $\Delta p$  should be fixed because the change in average fluid properties would then be more gradual in going from one increment to another. The value of  $\Delta p$  should be around 10 percent of the absolute pressure, which is known for one point in the increment, but should not be greater than 100 psi for that increment.

Pressure drops can be calculated, using Eq. A-3 in the following manner.

1. Pick a point in the flow string (e.g., wellhead or bottom-hole) where the flow rates, fluid properties, temperature and pressure are known.
2. Estimate the temperature gradient of the well.
3. Fix the  $\Delta p$  at about 10 percent of the measured or previously calculated pressure, which may be at either the top or bottom of the increment. Find average pressure of increment.
4. Assume a depth increment  $\Delta D$  and find average depth of increment.
5. From the temperature gradient, determine average temperature of increment.
6. Correct fluid properties for temperature and pressure.
7. Determine the type of flow regime from Appendix B.
8. Based on Step 7, determine the average density ( $\bar{\rho}$ ) and the friction loss gradient ( $\tau_f$ ) from Appendix C.
9. Calculate  $\Delta D$  from Eq. A-3.
10. Iterate, if necessary, starting with Step 4. until assumed  $\Delta D$  equals calculated  $\Delta D$ .
11. Determine values of  $p$  and  $D$  for that increment.
12. Repeat procedure from Step 3 until the sum of the  $\Delta D$ 's equals the total length of the flow string.

A detailed example of the above calculated procedure is given in Appendix D.

### APPENDIX A

#### DESCRIPTION OF MODIFIED GRIFFITH AND WALLIS METHOD\*

The fluid pressure drop in a vertical pipe is the sum effect of the energy lost by friction, the change in potential energy and the change in kinetic energy. This energy balance, which is basic to all pressure-drop calculations, can be generally written as

$$-dP = \tau_f dD + (g\rho/g_c) dD + (\rho v/g_c) dv \quad (A-1)$$

- where
- $P$  = pressure, lb/sq ft,
  - $\tau_f$  = friction-loss gradient, lb/sq ft/ft,
  - $D$  = depth, ft,
  - $g$  = acceleration of gravity, ft/sec<sup>2</sup>,
  - $g_c$  = gravitational constant, ft-lb(mass)/lb(force)-sec<sup>2</sup>,
  - $\rho$  = fluid density, lb/cu ft,
  - $v$  = fluid velocity, ft/sec.

The procedure was credited to Griffith and Wallis because slug flow occurred in 95 percent of the cases studied. Although the mist-flow regime could not be evaluated, the Duns-Ros method was used because it appeared to be more accurate and logical than the Martinelli method recommended by Griffith. In two-phase flow, both  $\tau_f$  and  $p$  are influenced by the flow regime type, and all three terms are functions of temperature and pressure. Therefore, to use Eq. A-1, (1) the flow string must be incremented so the fluid properties do not change markedly within any of the increments, (2) the flow regime type and corresponding variables of  $\bar{p}$  and  $\tau_f$  must be determined for each increment and (3) each increment must be evaluated by an iterative procedure.

The kinetic energy term is significant only in the mist-flow regime.<sup>2</sup> In mist flow  $v_s \ll v_g$ , the kinetic energy term may be expressed<sup>3</sup> more simply (using the gas law).

$$(\rho v/g_c) dv = - \frac{w_g q_g}{g_c A_p^2 P} dP \quad (A-2)$$

where  $A_p$  = pipe area, sq ft.

\*This method is a composite of the following:

Method	Flow Regime
Griffith <sup>11</sup>	Bubble
Griffith and Wallis <sup>11</sup>	Slug (densly term)
This work	Slug (friction gradient term)
Duns and Ros <sup>8</sup>	Transition
Duns and Ros <sup>8</sup>	Annular-mist

### APPENDIX B

#### DETERMINATION OF FLOW REGIME

Griffith and Wallis have defined the boundary between bubble and slug flow,<sup>11</sup> and Duns and Ros have defined the boundaries for the remaining three regimes.<sup>8</sup> The flow regime may be determined by testing whether the variables  $q_g/q_l$  or  $v_{gs}$  or both, fall within the limits prescribed.

<sup>11</sup>All volumetric (q) and mass (w) flow rates are those of the produced fluids that are corrected for temperature, pressure and gas solubility.

<sup>8</sup> $\Delta Z$  is taken as positive downward. The pressure should be made discontinuous with depth should the denominator approach zero, or become negative, to establish the shock front that characterizes sonic velocities.

Limits	Flow Regime
$q_g/q_t < (L)_b$	Bubble
$q_g/q_t > (L)_b, v_{gs} < (L)_s$	Slug
$(L)_s > v_{gs} > (L)_b$	Transition
$v_{gs} > (L)_s$	Mist

The above variables are defined as

$$v_{gs} = q_g(\sqrt{\rho_L g \sigma})/A_p \quad \dots \dots \dots (B-1)$$

$$(L)_b = 1.071 - (0.2218 v_{gs}^2/d_h) \text{ with the limit } (L) \geq 0.13 \quad \dots \dots \dots (B-2)$$

$$(L)_s = 50 + 36 v_{gs} q_g/q_t \quad \dots \dots \dots (B-3)$$

$$(L)_t = 75 + 84 (v_{gs} q_g/q_t)^{0.8} \quad \dots \dots \dots (B-4)$$

where  $v_{gs}$  = dimensionless gas velocity,

$v_t$  = total fluid velocity ( $q_t/A_p$ ), ft/sec,

$\rho_L$  = liquid density, lb/cu ft,

$\sigma$  = liquid surface tension, lb/sec<sup>2</sup>.

### APPENDIX C

#### EVALUATION OF AVERAGE DENSITY AND FRICTION LOSS GRADIENT

In the first four sections of this Appendix, the variables  $\bar{\rho}$  and  $\tau_f$  are defined for bubble flow, slug flow, transition and mist flow. The second section, while the most complex, is also the most important since slug flow had been encountered in over 95 percent of the gas-lift or flowing wells studied. The last section of this Appendix describes how  $\tau_f$  was developed for the slug flow regime.

#### BUBBLE FLOW (REF. 12)

The void fraction of gas ( $F_g$ ) in bubble flow can be expressed as

$$F_g = \frac{1}{2} \left[ 1 + \frac{q_g}{v_s A_p} - \sqrt{\left(1 + \frac{q_g}{v_s A_p}\right)^2 - \frac{4q_g}{v_s A_p}} \right] \quad \dots \dots \dots (C-1)$$

where  $v_s$  = slip velocity in ft/sec. Griffith suggested that a good approximation of an average  $v_s$  is 0.8 ft/sec.\* Thus, with Eq. C-1, the average flowing density can be computed as

$$\bar{\rho} = (1 - F_g) \rho_L + F_g \rho_g \quad \dots \dots \dots (C-2)$$

The friction gradient is

$$\tau_f = f_L v_L^2 / 2g d_h \quad \dots \dots \dots (C-3)$$

where

$$v_L = q_L / [A_p (1 - F_g)]$$

The friction factor  $f$  is obtained from Fig. 6 by using a Moody relative-roughness factor obtained from Fig. 7. The Reynolds number is calculated as  $N_{Re} = 1,488 \rho_L d_h v_L / \mu_L$  where  $d_h$  = hydraulic pipe diameter, ft, and  $\mu_L$  = liquid viscosity, cp.

#### SLUG FLOW (REF. 11)

The average density term is

$$\bar{\rho} = \frac{w_g + \rho_L v_s A_p}{q_g + v_s A_p} + \Gamma \rho_L \quad \dots \dots \dots (C-4)$$

where  $\Gamma$  is a coefficient correlated from oilfield data. Griffith and Wallis correlated the bubble rise velocity  $v_b$  by the relationship

$$v_b = C_1 C_2 \sqrt{g d_b} \quad \dots \dots \dots (C-5)$$

where  $C_1$  is expressed in Fig. 8 as a function of bubble Reynolds number ( $N_b = 1,488 v_b d_b \rho_L / \mu_L$ ), and  $C_2$  is expressed in Fig. 9 as a function of both  $N_b$  and liquid Reynolds number.

$$N_{Re} = 1,488 \rho_L d_h v_t / \mu_L \quad \dots \dots \dots (C-6)$$

where  $v_t$  equals total velocity of liquid and gas ( $q_t/A_p$ ), ft/sec.

Fig. 9 was extrapolated\*\* so that  $v_b$  could be evaluated at the higher Reynolds numbers. When  $C_2$  cannot be read

\*\*The parallel work of Nicklen, Wilkes and Davidson<sup>13</sup> provided the basis for the extrapolation. It showed that bubble rise velocity was independent of  $N_b$  in the Reynolds number range of  $9 \times 10^5$  to  $1 \times 10^6$ . The correlation of bubble rise velocity was found comparable to Eq. C-5 when  $N_b$  was around  $8 \times 10^5$ . The results were incorporated into the above extrapolation.

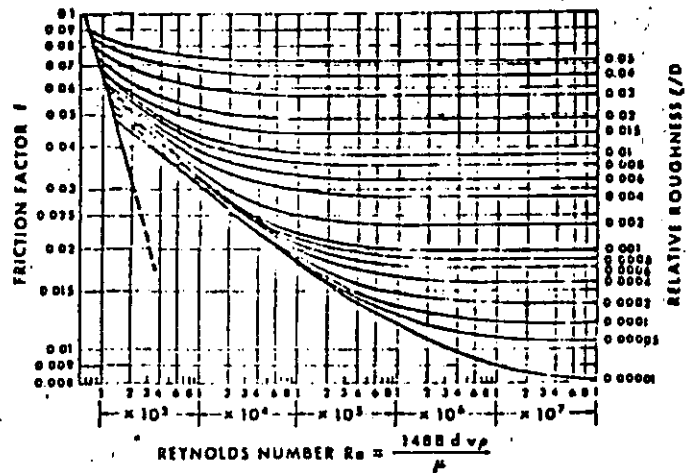


FIG. 6—MOODY FRICTION FACTOR<sup>10</sup>

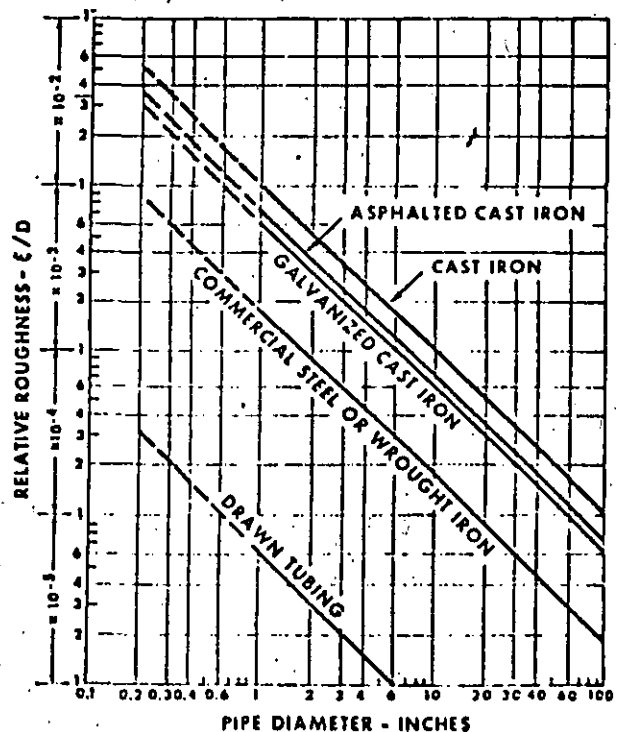


FIG. 7 EFFECT OF PIPE DIAMETER AND MATERIAL ON RELATIVE ROUGHNESS<sup>10</sup>

\*Although the method is simple, it is reasonably precise. For the four wells that were wholly in bubble flow, the standard deviation was 5.1 percent, whereas the deviation was 9.8 percent for those wells partly in bubble and slug.

from Fig. 9, the extrapolated values of  $v_s$  may be calculated from the following set of equations.

When  $N_b \leq 3,000$ ,

$$v_s = (0.546 + 8.74 \times 10^{-4} N_b) \sqrt{gd_s} \quad (C-7)$$

When  $N_b \geq 8,000$ ,

$$v_s = (0.35 + 8.74 \times 10^{-4} N_b) \sqrt{gd_s} \quad (C-8)$$

When  $3,000 < N_b < 8,000$ ,

$$v_{s1} = (0.251 + 8.74 \times 10^{-4} N_b) \sqrt{gd_s}$$

$$v_s = \frac{1}{2} v_{s1} + \sqrt{v_{s1}^2 + \frac{13.59 \mu_L}{\rho_L \sqrt{d_s}}} \quad (C-9)$$

The wall friction-loss term, which has been independently derived, is expressed as

$$\tau_f = \frac{\rho_L v_s^2}{2g_s d_s} \left[ \frac{q_L + v_s A_p}{q_f + v_s A_p} + \Gamma \right] \quad (C-10)$$

The friction factor is obtained from Fig. 6 and is a function of the Reynolds number given by Eq. C-6 and the  $\xi/D$  obtained from Fig. 7. The liquid distribution coefficient  $\Gamma$  may be determined by the equation which meets the following conditions.

Continuous Liquid Phase	$v_s$	Use Equation
Water	<10	C-11
Water	>10	C-12
Oil	<10	C-13
Oil	>10	C-14

$$\Gamma = [(0.013 \log \mu_L)/d_s^{0.25}] - 0.681 + 0.232 \log v_s - 0.428 \log d_s \quad (C-11)$$

$$\Gamma = [(0.045 \log \mu_L)/d_s^{0.25}] - 0.709 - 0.162 \log v_s - 0.888 \log d_s \quad (C-12)$$

$$\Gamma = [0.0127 \log (\mu_L + 1)/d_s^{0.25}] - 0.284 + 0.167 \log v_s + 0.113 \log d_s \quad (C-13)$$

$$\Gamma = [0.0274 \log (\mu_L + 1)/d_s^{0.25}] + 0.161 + 0.569 \log d_s - \log v_s + [0.01 \log (\mu_L + 1)/d_s^{0.25}] + 0.397 + 0.63 \log d_s \quad (C-14)$$

but is constrained by the limits

$$\Gamma \geq -0.065 v_s \quad (C-15)$$

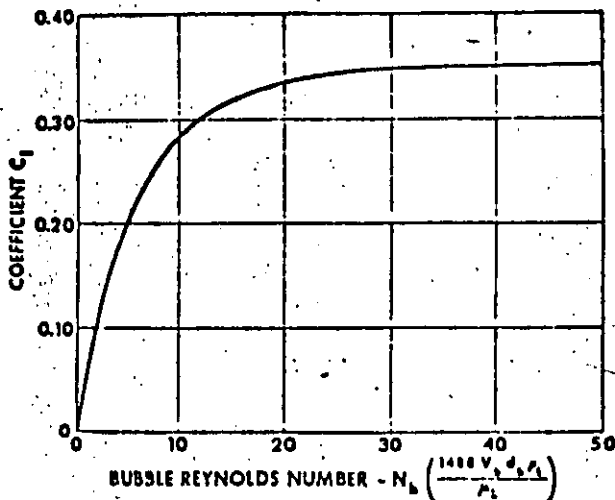


FIG. 8—GRIFFITH AND WALLIS'  $C_1$  VS BUBBLE REYNOLDS NUMBER.

and when  $v_s > 10$ .

$$\Gamma \geq - \frac{v_s A_p}{q_f + v_s A_p} \left( 1 - \frac{\bar{p}}{\rho_L} \right) \quad (C-16)$$

The above constraints eliminate pressure discontinuities between flow regimes.

### TRANSITION FLOW

Duns and Ros approximated  $\bar{p}$  and  $\tau_f$  for transition flow. The method is first to calculate these terms for both slug and mist flow, and then linearly weight each term with respect to  $v_{sD}$  and the limits of the transition zone ( $L_s$  and  $(L)_M$ ). The terms  $v_{sD}$ ,  $(L)_M$  and  $(L)_s$  are defined in Appendix B. The average density term would be

$$\bar{p} = \frac{(L)_M - v_{sD}}{(L)_M - (L)_s} \left[ \bar{p} \right]_{slug} + \frac{v_{sD} - (L)_s}{(L)_M - (L)_s} \left[ \bar{p} \right]_{mist} \quad (C-17)$$

The friction gradient term would be weighted similarly. A more accurate friction-loss prediction is claimed if the gas volumetric flow rate for mist flow is taken as

$$q_g = A_p (L)_M (\rho_L/g\sigma)^{0.5} \quad (C-18)$$

### MIST FLOW

The average flowing density for mist flow is given in Eq. C-2. Since there is virtually no slip between the phases,  $F_g$  is

$$F_g = 1/(1 + q_L/q_g) \quad (C-19)$$

Duns and Ros express the friction-loss gradient as

$$\tau_f = f \rho_L v_s^2 / 2g_s d_s \quad (C-20)$$

where  $v_s$  is the superficial gas velocity, and  $f$  is again obtained from Fig. 6 as a function of gas Reynolds number ( $N_{Re} = 1,488 p_s d_s v_s / \mu_g$ ) and a correlated form of the Moody relative roughness factor  $\xi/D$  that was developed by Duns and Ros. In their correlation, they limit  $\xi/D$  to being no smaller than  $10^{-3}$  but no greater than 0.5. Between these limits,  $\xi/D$  is determined from Eq. C-21 if  $N_{Re}$  is less than 0.005 and from Eq. C-22 if  $N_{Re}$  is greater than 0.005.

$$\xi/D = 34 \sigma / (\rho_L v_s^2 d_s) \quad (C-21)$$

$$\xi/D = 174.8 \sigma (N_{Re})^{0.25} / (\rho_L v_s^2 d_s) \quad (C-22)$$

where  $N_{Re} = 4.52 \times 10^{-4} (v_s \mu_L / \sigma)^2 \rho_L / \rho_L$ .

### DEVELOPMENT OF $\tau_f$ FOR SLUG FLOW

A new method was developed to correlate the friction-loss gradient for slug flow because neither the Griffith and Wallis method, nor the Stanley method (an outgrowth of the Griffith-Wallis work) proved accurate for the well conditions studied. (The Griffith-Wallis data were taken

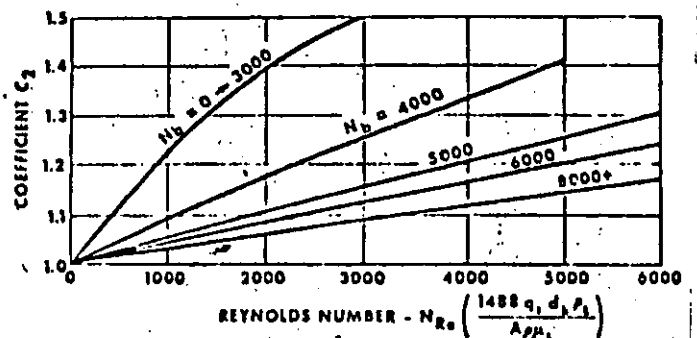


FIG. 9—GRIFFITH AND WALLIS'  $C_2$  VS BUBBLE REYNOLDS AND REYNOLDS NUMBERS.

from low-flow velocity tests in which friction losses were minor and liquid entrainment was negligible.) This new method accounted for the complex nature of friction loss in slug flow by the introduction of a correlated liquid distribution function  $\Gamma$  (Eq. C-10) which implicitly accounts for the following physical phenomena.

1. Liquid is distributed in three places: the slug, the film around the gas bubble and in the gas bubble as entrained droplets. A change in this distribution will change the net friction losses.

2. The friction loss has essentially two contributions, one from the liquid slug and the other from the liquid film.

3. The bubble rise velocity approaches zero as mist flow is approached.

Values of the liquid distribution coefficient were calculated from the data of Hagedorn and Brown<sup>9</sup> by using Eq. A-3 of Appendix A and Eqs. C-4 through C-10 of Appendix C. (These data were selected because they covered a wide range of conditions for each of the four liquids used.) These values correlate with total fluid velocity and liquid viscosity. Fig. 10 shows the results where the fluid is water, and Fig. 11 shows the results where the fluids are oil. Coefficients were also calculated for the heavy-oil wells shown in Table 1, but these values were small and scattered because  $\tau$  was small in comparison to  $\bar{p}$ . Nevertheless, the results were sufficiently grouped to show that pipe diameter ( $d_s$ ) is another independent variable.

Neither the reversal in slopes nor the data scatter as seen in Figs. 10 and 11 can be resolved without additional experimental work. It is probable, however, that the slope reversal may be due to liquid entrained in the gas phase

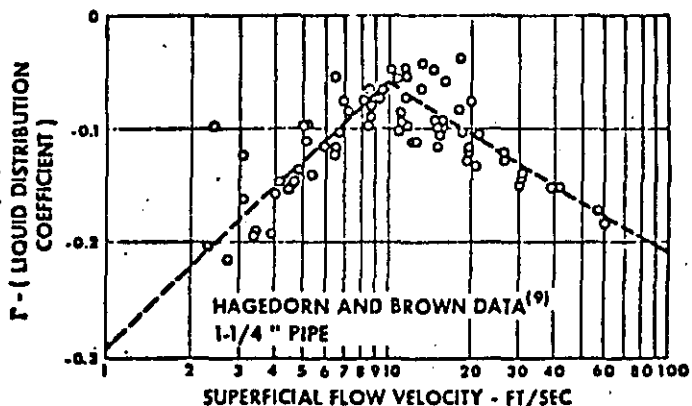


FIG. 10—EFFECT OF VELOCITY ON WATER DISTRIBUTION COEFFICIENT.

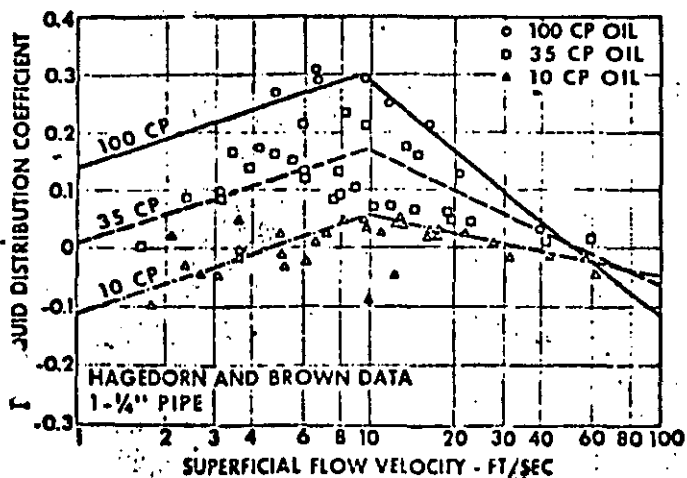


FIG. 11—OIL DISTRIBUTION COEFFICIENT AFFECTED BY BOTH VELOCITY AND VISCOSITY.

TABLE 3—FLOW RATES AND PHYSICAL CONDITIONS OF HEAVY-OIL WELL 22

Oil Rate ( $q_o$ )	1,850 STB/D	Oil Specific Gravity ( $\gamma_o$ )	0.942
Produced GOR ( $R$ )	575 scf/ STB	Gas Specific Gravity ( $\gamma_g$ )	0.75
Total depth ( $D$ )	3,890 ft	Wellhead Pressure	670 psia
Tubing diameter ( $d_s$ )	0.249 ft	Tubing Area $A_p$	0.0488 sq ft
Temperatures:		Dead Oil Viscosity:	
Wellhead	126F	at 100F	89 cp
Reservoir	150F	at 210F	8.8 cp

and that the data scatter may be attributable to such additional parameters as liquid velocity, GOR and interfacial tension.

## APPENDIX D

### EXAMPLE OF TWO-PHASE PRESSURE DROP CALCULATION

An example calculation of the modified Griffith-Wallis method is presented to illustrate the details of the procedure outlined in Appendix A. In this example we will predict the pressure drop for heavy-oil Well 22 (Table 1). The input well data required for the calculation are given in Table 3. In addition, we will need the following correlations\* that correct fluid properties for pressure and temperature:

Gas pseudo-critical properties (Katz *et al.*)  $T_{pc}, P_{pc}$ .

Gas compressibility (Brown *et al.*)  $z$ .

Live oil viscosity (Chew and Connally)  $\mu$ .

Oil formation volume factor (Standing)  $B_o$ .

Solution gas (Lasater)  $R_s$ .

For calculational convenience, the temperature-viscosity-depth data contained in Table 3 should be plotted. The temperature-depth plot is shown in Fig. 12, and log viscosity-log temperature plot is shown in Fig. 13.

The detailed procedure for the calculation of the pressure drop for the first increment ( $k = 1$ ) is as follows.

1. Based on the 670-psia wellhead pressure, fix  $\Delta p$  at 100 psi. Assume  $\Delta D$  to be 540 ft. The average pressure ( $\bar{p}$ ) and depth ( $\bar{D}$ ) of increment  $k$  is then:

$$\bar{p}_k = p_{k-1} + \frac{\Delta p_k}{2} = 670 + \frac{100}{2} = 720 \text{ psia}$$

$$\bar{D}_k = D_{k-1} + \frac{\Delta D_k}{2} = 0 + \frac{540}{2} = 270 \text{ ft.}$$

The average temperature ( $\bar{T}$ ), read from Fig. 12 is 127.5F.

\*These are conveniently found in Frick's *Petroleum Production Handbook*, Vol. II (Ref. 16).

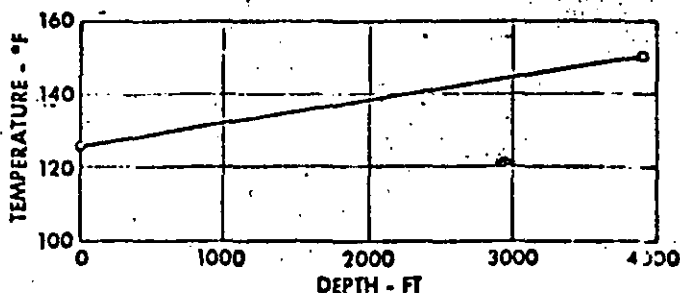


FIG. 12—TEMPERATURE VS DEPTH — WELL 22.

2. With the condition determined in Step 1, the fluid properties are corrected for temperature and pressure.

From Frick<sup>11</sup> the following values are obtained.

$$R_s = 115 \text{ scf/bbl (page 19-9).}^*$$

$$B_o = 1.073 \text{ bbl/STB (page 19-25).}$$

$$P_{sc} = 665 \text{ psia (page 17-6).}$$

$$T_{sc} = 415 \text{ R (page 17-6).}$$

$$\mu = 18 \text{ cp}^{**} \text{ (page 19-40).}$$

The gas compressibility  $c$  is determined as

$$T_c = \frac{\bar{T} + 460}{T_{sc}} = \frac{587.5}{415} = 1.42$$

$$P_c = \frac{\bar{p}}{P_{sc}} = \frac{720}{665} = 1.08,$$

and from Frick (page 17-15),

$$z = 0.875.$$

The corrected volumetric flow rates are

$$q_L = 6.49 \times 10^{-3} q_o B_o = 6.49 \times 10^{-3} (1,850) (1.073) = 0.129 \text{ cu ft/sec}$$

$$q_g = 3.27 \times 10^{-3} z q_o (R - R_s) \frac{(\bar{T} + 460)}{\bar{p}} = 3.27 \times 10^{-3} (0.875) (1,850) (575 - 115) (587.5) / 720 = 0.199 \text{ cu ft/sec}$$

$$q_L = 0.128 + 0.199 = 0.328 \text{ cu ft/sec.}$$

The corrected mass flow rates are

$$w_L = q_o (4.05 \times 10^{-3} \gamma_o + 8.85 \times 10^{-3} \gamma_o R_s) = 1,850 [4.05 \times 10^{-3} (0.942) + 8.85 \times 10^{-3} (0.75) (115)] = 7.20 \text{ lb/sec}$$

$$w_g = 8.85 \times 10^{-3} q_o \gamma_o (R - R_s) = 8.85 \times 10^{-3} (1,850) (0.75) (575 - 115) = 0.565 \text{ lb/sec}$$

$$w_s = 7.20 + 0.57 = 7.77 \text{ lb/sec.}$$

\*Parentheses indicate the page number in Frick's book<sup>11</sup>, where the various correlations are found.

\*\*Live oil viscosity. Dead oil viscosity, a parameter in the correlation, is read from Fig. 13.

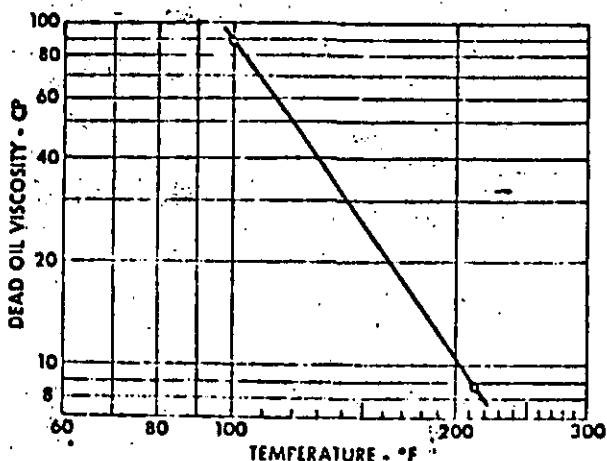


Fig. 13—DEAD OIL VISCOSITY VS TEMPERATURE—WELL 22.

The corrected densities are

$$\rho_L = w_L / q_L = 7.20 / 0.129 = 55.8 \text{ lb/cu ft}$$

$$\rho_g = w_g / q_g = 0.565 / 0.199 = 2.84 \text{ lb/cu ft.}$$

3. The variables described in Appendix B are calculated and then are tested against the boundary limits to determine the flow regime.

Test Variables:

$$v_s = q_s / A_p = 0.328 / 0.0488 = 6.72 \text{ ft/sec.}$$

$$q_s / q_L = 0.199 / 0.328 = 0.607.$$

$$v_{sp} = 0.199 \left[ \sqrt{0.534 (55.8)} \right] / 0.0488 = 9.53 \quad (\text{B-1})$$

Boundary Limits:

$$(L)_s = 1.071 - \frac{0.2218 (6.72)^2}{0.249} \dots \dots \dots (\text{B-2})$$

$$(L)_s = -22. \text{ Since } (L)_s \text{ has the limit of } 0.13,$$

$$\therefore (L)_s = 0.13.$$

$$(L)_s = 50 + 36 (9.53) (0.129) / 0.199 = 272 \dots (\text{B-3})$$

Because  $q_s / q_L > (L)_s$  and  $v_{sp} < (L)_s$ , the fluids are in slug flow.

4. The equations given in the Slug Flow section of Appendix C are used to calculate  $\bar{p}$  and  $\tau_f$ .

Determine Reynolds number, bubble Reynolds number and slip velocity ( $v_s$ ).

$$N_{Re} = 1,488 (55.8) (0.249) (6.72) / 18 = 7,720 \quad (\text{C-6})$$

Since the bubble rise velocity is a nonlinear correlation, iteration is necessary. Therefore, assuming  $v_s = 1.75$ , bubble Reynolds number is

$$N_b = 1,488 (55.8) (0.249) (1.75) / 18 = 2,010.$$

$C_s$  cannot be read from Fig. 9. Thus the extrapolation equation (Eq. C-7) is used since  $N_b < 3,000$ .

$$v_s = [0.546 + 8.74 \times 10^{-4} (7,720)] \sqrt{32.2 (0.249)} = 1.74 \text{ ft/sec.}$$

Determine liquid distribution coefficient  $\Gamma$  and friction factor  $f$ . Eq. C-13 is used to evaluate  $\Gamma$  since  $v_s < 10$ :

$$\Gamma = \left[ \frac{0.0127 \log (18 + 1)}{(0.249)^{1.04}} \right] - 0.284 + 0.167 \log 6.72 + 0.113 \log 0.249 = -0.097.$$

Test limiting  $\Gamma$  with Eq. C-15:

$$-0.097 \geq -0.065 (6.72) \geq -0.436;$$

therefore,  $\Gamma = -0.097$ .

The  $\xi/D$  value from Fig. 7 is 0.0006. With this value and the calculated  $N_{Re}$  of 7,720, a friction factor of 0.034 is read from Fig. 6.

Evaluate  $\bar{p}$  with Eq. C-4:

$$\bar{p} = \frac{7.77 + 55.8 (1.74) (0.0488)}{0.328 + 1.74 (0.0488)} + (-0.097) (55.8) = 24.9 \text{ lb/cu ft.}$$

Evaluate  $\tau_f$  with Eq. C-10:

$$\tau_f = \frac{0.034 (55.8) (6.72)^2}{64.4 (0.249)} \left[ \frac{0.129 + 1.74 (0.0488)}{0.328 + 1.74 (0.0488)} \right] = 0.097 \quad (\text{C-10})$$

$$= 2.26 \text{ lb/sq ft.}$$

5. The depth increment from Eq. A-3 is

$$\Delta D = 144 \left[ \frac{\Delta p \left( 1 - \frac{w_1 q_0}{4,637 A_w \bar{p}} \right)}{p + \tau_1} \right]$$

$$= 144 \left[ \frac{100 \left( 1 - \frac{7.77 (0.199)}{4,637 (0.0188) (720)} \right)}{24.9 + 2.3} \right] = 529 \text{ ft.}$$

The true value of  $\Delta D$ , is near 529 ft. The calculation will converge very closely to this value even when the assumed  $\Delta Z$  is off by  $\pm 10$  percent of the assumed value (540 ft) because, under these well conditions, the pressure gradient is primarily controlled by the relatively temperature-insensitive density head. However, under those circumstances where the friction gradient, which is temperature sensitive, is significant, iteration would be necessary should the calculated value of  $\Delta D$  differ from the assumed value by  $\pm 10$  percent.

6. The top of the next increment is fixed at 529 ft and 770 psi, and Steps 1 through 6 are repeated for the new conditions.

7. The procedure is continued until  $\Sigma \Delta D$  is equal to the total depth. The calculated pressure profile is compared against the measured profile in Fig. 14. \*\*\*

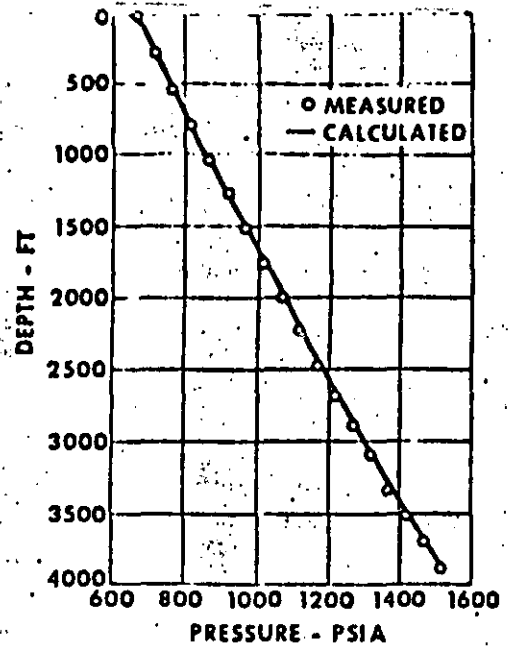


FIG. 14—CALCULATED VS MEASURED PRESSURE DROP—WELL 22.



# Experimental Study of Pressure Gradients Occurring During Continuous Two-Phase Flow in Small-Diameter Vertical Conduits

ALTON R. HAGEDORN\*  
JUNIOR MEMBER AIME  
KERMIT E. BROWN  
MEMBER AIME

THE U. OF TEXAS  
AUSTIN, TEX.

## ABSTRACT

*A 1,500-ft experimental well was used to study the pressure gradients occurring during continuous, vertical, two-phase flow through 1-in., 1¼-in. and 1½-in. nominal size tubing.*

*The test well was equipped with two gas-lift valves and four Mairhak electronic pressure transmitters as well as with instruments to measure the liquid production rate, air injection rate, temperatures and surface pressures.*

*Tests were conducted for widely varying liquid flow rates, gas-liquid ratios and liquid viscosities. From these data, an accurate pressure-depth traverse was constructed for each test in each of the three tubing sizes.*

*From the results of these tests, correlations have been developed which allow the accurate prediction of flowing pressure gradients for a wide variety of tubing sizes, flow conditions, and liquid properties. Also, the correlations and equations which are developed satisfy the necessary condition that they reduce to the relationships appropriate to single-phase flow when the flow rate of either the gas or the liquid phase becomes zero. All the correlations involve only dimensionless groups, which is a condition usually sought for in similarity analysis but not always achieved.*

*The correlations developed in this study have been used to calculate pressure gradients for pipes of larger diameter than those upon which the correlations are based. Comparisons of these calculated gradients with experimentally determined gradients for the same flow conditions obtained from the literature indicate that extrapolation to these larger pipe sizes is possible with a degree of accuracy sufficient for engineering calculations. The extent of this extrapolation can only be determined with additional data from larger pipe diameters.*

## INTRODUCTION

The accurate prediction of the pressure drop expected to occur during the multiphase flow of fluids in the flow string of a well is a widely recognized problem in the petroleum industry. The problem has been brought even more into prominence with the advent of tubingless or slim-hole completions which use small-diameter tubing. Many of the correlations which give reasonably accurate results in the larger tubing sizes are greatly in error when

applied to small-diameter conduits. Small-diameter conduits are defined as 1½-in. nominal size tubing or smaller.

The study of the pressure gradients which occur during multiphase flow of fluids in pipes is exceedingly complex because of the large number of variables involved. Further difficulties relate to the possibility of numerous flow regimes of widely varying geometry and mechanism and the instabilities of the fluid interfaces involved. Consequently, a solution to the problem by the approach normally used in classical fluid dynamics based on the formulation and solution of the Navier-Stokes equation has not been forthcoming. This is primarily the result of the nonlinearities involved and the difficulty of adequately describing the boundary conditions. As a result of the foregoing, most investigators have chosen semi-empirical or purely empirical approaches in an effort to obtain a practical solution to the problem.

Much of the previous work in this area was done in short-tube models in the laboratory. A number of problems arise, however, when attempts are made to extrapolate these laboratory results to oilfield conditions where a much longer tube is encountered. In those few studies where data taken in long tubes were utilized, the data covered only a limited range of the variables, and as a result inaccuracies are introduced when the correlations are extended outside the range of the original data. Also, as a consequence of the limited amount of data available for these studies, the effects of several important variables were overlooked.

The problem of predicting the pressure drop which occurs in multiphase flow differs from that of single-phase flow in that another source of pressure loss is introduced, namely, those pressure losses arising from slippage between the phases. This slippage is a result of the difference between the integrated average linear velocities of the two phases, which in turn is due to the physical properties of the fluids involved. In contrast to single-phase flow, the pressure losses in multiphase flow do not always increase with a decrease in the size of the conduit or an increase in production rate. This is attributed to the presence of the gas phase which tends to slip by the liquid phase without actually contributing to its lift.

Many investigators have attempted to correlate both the slippage losses and the friction losses by means of a single energy-loss factor analogous to the one used in the single-phase flow problem.<sup>1,2,3,4,5,6</sup> In an approach of this type, however, many of the important variables, such as

Original manuscript received in Society of Petroleum Engineers office Aug. 8, 1964. Revised manuscript received Feb. 23, 1965. Paper presented at SPE 29th Annual Fall Meeting held in Houston, Oct. 11-14, 1964.

\*Presently associated with Esso Production Research Co., Houston, Tex.

<sup>1</sup>References given at end of paper.

the gas-liquid ratio, the liquid viscosity and the surface tension, are not adequately accounted for. Also, the correlations are not general, and a large number of correlations would be required to cover the range of conditions encountered in oilfield practice.

Other investigators have chosen to measure the liquid holdup, i.e., the fractional volume of the conduit actually occupied by liquid, by various means.<sup>10, 11, 12, 13, 14</sup> This allowed them to correct the static gradient portion of the total gradient for the effects of slippage. The remaining losses were attributed to friction, and friction factors were calculated from the test data. These friction factors were then correlated with various groups. When these correlations are applied to data taken in a long tube, however, the calculated pressure losses are much greater than those actually observed, and, in fact, in many cases those losses calculated by the corrected static gradient alone exceed the observed total pressure losses. This would indicate that the fractional volume of the tube actually occupied by liquid is smaller for the long tube than for the short tube, or that the flow is more efficient in the long tube.

The object of the present study was to obtain data from tests conducted in a long tube and utilize these data to develop correlations which would account separately for the effects of slippage and friction.

The first logical approach would be to perform the same type study on the long tubes as was done in the case of the short-tube models, i.e., measure the liquid holdup in the long tube and correlate these measurements with known flow properties. This would present a great many experimental problems, not to mention the increased expense involved.

An alternate approach to the problem would be to determine a friction-factor correlation based on an analogy with single-phase flow. The friction losses could then be determined using these friction factors, and the difference between the measured total pressure losses and the friction losses could be attributed to the static gradient as increased by slippage between the phases. Holdup factors could then be calculated from the test data. It can be argued at this point that in an approach of this type neither the liquid holdup nor the friction losses are actually measured. However, if a reasonable friction-factor correlation can be determined, a large percentage of the pressure losses calculated by this friction factor will be due to friction. Since the other major source of pressure loss is the static gradient as increased by slippage, this loss will be reflected in the holdup-factor correlation. It is true that some friction losses might be included in the holdup correlation and vice versa. These should be small, and since these factors are experimentally determined, these losses will be accounted for. It would be virtually impossible to separate all forms of losses and develop correlations for each, but an approach of this type will separate the friction losses from those due to liquid holdup to a large degree and will also account for all other losses.

The latter approach is the one which was adopted for the present study. The purpose of the experimental work described in the next section was to obtain the necessary data from long tubes which could then be used in the development of a more generalized correlation.

## EXPERIMENTAL PROCEDURE

The experimental data were taken in a test well located Dallas, Tex. The test well was utilized to more nearly approach actual field conditions. The test well also had the advantage over an actual field well in that the liquid

to be produced could be controlled from the surface, thus allowing different liquids to be tested.

Test conditions were varied in an attempt to study the effects of all the controlling groups. A complete series of tests was run on each of three pipe sizes, namely, 1-in., 1¼-in. and 1½-in. nominal diameter tubing. These three sets of data along with the data taken by Fancher and Brown<sup>1</sup> on 2-in. nominal size tubing made it possible to study the effect of the pipe diameter on the pressure gradients.

Four liquids of widely varying viscosity were tested in the 1¼-in. tubing, and two liquids of different viscosity were tested in the 1½-in. tubing. The effects of the liquid viscosity on the pressure gradients in the 1¼-in. tubing were reported in an earlier paper by the authors.<sup>1</sup> These data were used to determine the effect of liquid properties, primarily the liquid viscosity and the liquid density, on the pressure gradients. The physical properties of these liquids are given in Table 1.

For each liquid in a given pipe size, the liquid rate was varied, and for each liquid rate the gas-injection rate was varied over the complete range made possible by the experimental equipment. These data made it possible to study the effects of the flow parameters on the pressure gradients.

The assumption was made that the amount of air which went into solution during the tests was negligible. This is certainly true in the case of water. The assumption is also believed to be valid in the case of the oils because of the low pressures encountered and the very short contact time even at the highest of these pressures. The widely differing compositions of the air and the oils also tend to decrease the amount of air going into solution. This assumption implies that there was essentially no effect of pressure on the viscosity of the oils. In the application of the correlations, however, these solubility effects are taken into account.

No attempt was made to study specifically the effect of surface tension. The surface tension is included in several of the groups, but additional experiments are needed to determine if it is sufficiently accounted for. In most oilfield situations, as in the case of this study, the surface tension will vary only approximately two-fold, whereas the viscosity of the liquid in this study varied over a hundred-fold. Since the present work is directed primarily toward oilfield conditions, the surface tension is not considered to be one of the more important variables. Nemet has also indicated that in short tubes the effects of the surface tension, density ratio, and gas introduction are more important than in long tubes.<sup>2</sup>

The quantity of data taken in an installation of this type is not as great as might be taken in a laboratory model. Nevertheless, the 475 tests run in the test well along with 106 tests reported by Fancher and Brown<sup>1</sup> provided 2,905 pressure points over a wide range of conditions. The data taken as part of this study have been reported elsewhere.<sup>3</sup>

The surface equipment utilized during these tests is shown in Fig. 1. The downhole equipment for the tests involving the 1¼-in. tubing is shown in Fig. 2. The only changes for the other tubing sizes were the locations of the

TABLE 1—PHYSICAL PROPERTIES OF LIQUIDS

Liquid	Specific Gravity	Surface Tension (dynes/cm)	Viscosity (cp @ 60°F)
Water	1.000	72.0	0.86
Oil	0.856	33.5	10.00
Oil	0.875	34.8	35.00
Oil	0.900	36.2	110.00
Oil	0.870	34.4	30.30

downhole equipment, and these locations are given in Table 2. The testing procedure has been described previously.<sup>1,2</sup>

## DEVELOPMENT OF CORRELATIONS

### THE GRADIENT EQUATION

The development of the gradient equation used in the evaluation of the data taken as part of the present study is given in the Appendix. The form of the equation used in the calculation is:

$$1.44 \frac{\Delta p}{\Delta h} = \bar{p}_w + \frac{f q_L^2 M^2}{2.9652 \times 10^{11} D^5 \bar{p}_w} + \bar{p}_w \frac{\Delta \left( \frac{v_w^2}{2g} \right)}{\Delta h} \quad (1)$$

where

$$\bar{p}_w = \bar{p}_L H_L + \bar{p}_s (1 - H_L) \quad (2)$$

The gradient equation does not neglect the contribution of the acceleration gradient to the total pressure gradient. Lubinski has cited a practical example in a discussion of Poettmann and Carpenter's paper for which the loss of pressure due to a change in kinetic energy was appreciable and could not be neglected.<sup>3</sup> Calculations made during the course of this work indicate that under conditions of high mass flow rates and low tubing pressures, the pressure losses as a result of the acceleration gradient may constitute as much as 10 per cent of the total pressure drop near the top of the well. Under these conditions, the change in kinetic energy should not be neglected.

Eqs. 1 and 2 contain two factors which must be determined—the friction factor  $f$  and the holdup factor  $H_L$ . To determine these factors, it is necessary to fix the value of one by some means, and then calculate the value for the other by using Eqs. 1 and 2 and experimental data. The approach taken by previous investigators has been to measure the liquid holdup in the laboratory and correlate it with known fluid, pipe and flow properties. The friction

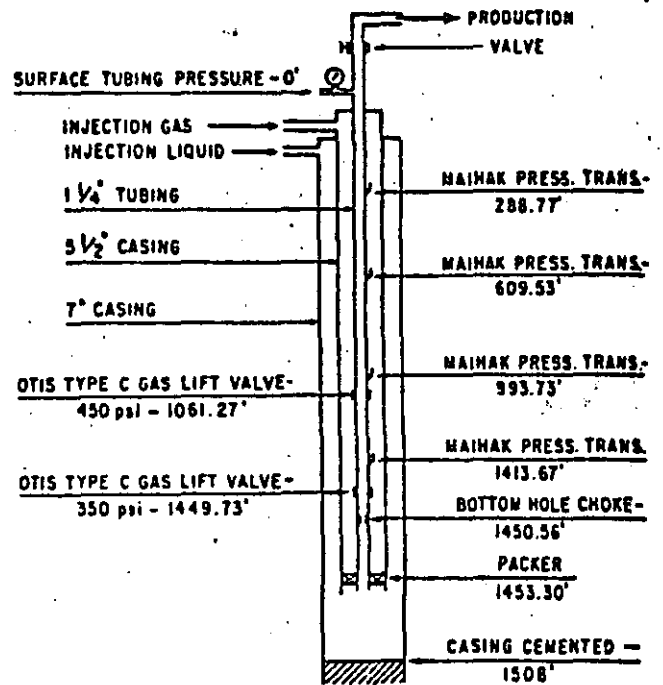


FIG. 2—OTIS EXPERIMENTAL TEST WELL WITH DOWN-HOLE EQUIPMENT.

factors could then be calculated from the experimental data. These values of the holdup, however, appear to be too high when applied to the long tubes encountered in oilfield practice, particularly for small values of the liquid holdup.

The approach used in this study was to develop a means for determining the friction factor and then use this friction factor and Eqs. 1 and 2 to calculate values of the holdup factor from the experimental data. The development of the friction-factor correlation and the holdup-factor correlation will be presented in that order.

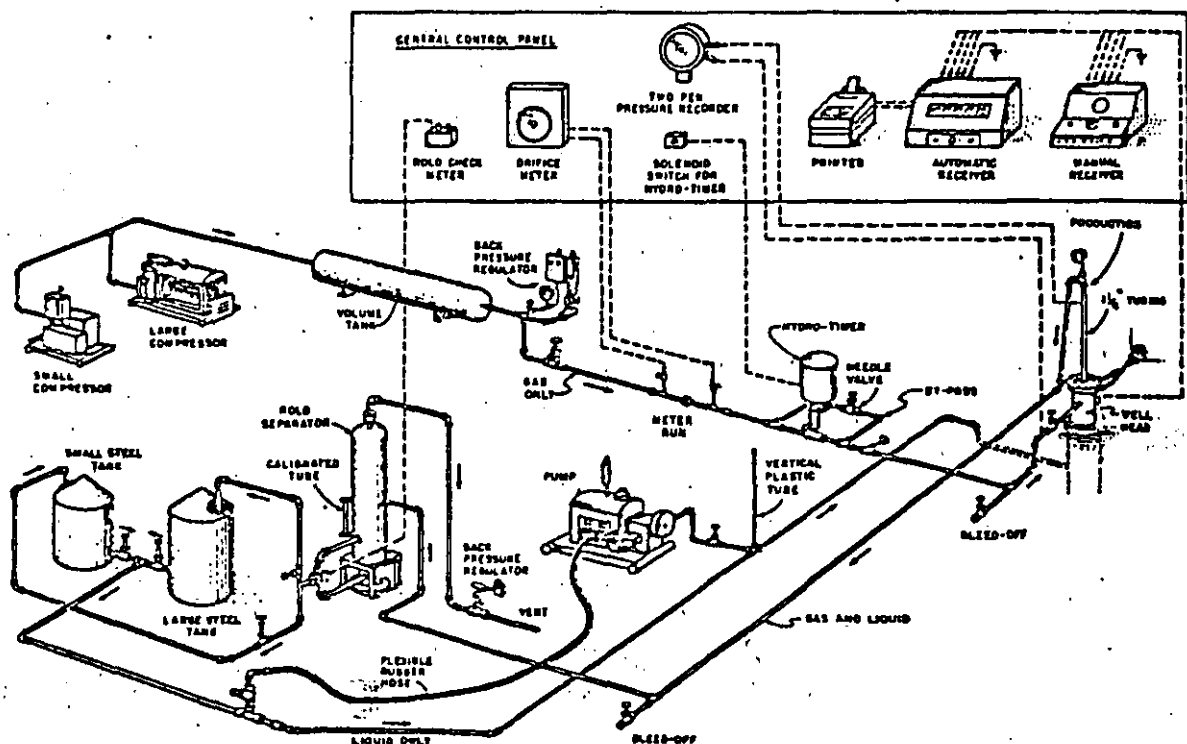


FIG. 1—SURFACE TESTING EQUIPMENT.

TABLE 2—LOCATION OF DOWN-HOLE EQUIPMENT

Tubing Size (in.)	Market Instruments				Gas-Lift Valves		Bottom-Hole Choke (in.)
	No. 1 (ft)	No. 2 (ft)	No. 3 (ft)	No. 4 (ft)	No. 1 (ft)	No. 2 (ft)	
1	398.01	450.10	1018.83	1428.06	1084.37	1443.37	1499.47
1 1/8	282.77	409.53	992.73	1413.67	1041.27	1449.73	1450.56
1 1/2	228.43	491.58	917.91	1346.56	986.79	1383.23	1417.18

**FRICTION-FACTOR CORRELATION**

The friction-factor correlation used in this work is the standard one for single-phase flow in pipes in which the friction factor  $f$  is given by

$$f = \frac{2gD \Delta W_1}{v^2 \Delta h} \dots \dots \dots (3)$$

This friction factor is commonly plotted as a function of the Reynolds number  $N_{Re}$ , with the relative roughness,  $\epsilon/D$ , as a parameter. It should be noted that the friction factor  $f$  used herein is given by the Darcy-Weisbach equation and differs from the friction factor  $f'$  in the Fanning equation by a factor of four, i.e.,  $f = 4f'$ .

Since the assumption was made that over a finite interval, the mixture of liquid and gas can be treated as a homogeneous mixture, the Reynolds number for the mixture can be written as

$$(N_{Re})_{TF} = C_1 \frac{v_m \rho_m D}{\mu_m} \dots \dots \dots (4)$$

where

$$v_m = \frac{C_2 q_L + C_3 q_G}{A_1} \dots \dots \dots (5)$$

$$= v_{GL} + v_{GO}$$

$$\rho_m = \rho_L H_L + \rho_G (1 - H_L) \dots \dots \dots (6)$$

and  $C_2$ ,  $C_3$  and  $C_1$  are the necessary conversion constants for dimensional consistency.

The problem then arises as how best to represent the viscosity of the gas-liquid mixture,  $\mu_m$ . The simplest assumption would be that the viscosities of the two components should be additive:

$$\mu_m = x\mu_1 + (1-x)\mu_2 \dots \dots \dots (7)$$

where  $\mu_1$  and  $\mu_2$  are the viscosities of the components,  $x$  has been expressed as a volume fraction, weight fraction, and molar fraction with no apparent justification for any of these. This would assume an ideal mixture, and no ideal mixtures have been found which will follow this law no matter which way the concentration is expressed.

It has been noted that in real mixtures, the viscosity-concentration curve is convex toward the concentration axis. This behavior was noted also by Uren in his work on the absolute viscosity of a gas-liquid mixture.<sup>13</sup> As the gas-liquid ratio is increased, the viscosity of the mixture rapidly decreases from the viscosity of the liquid and approaches the viscosity of the gas at very high gas-liquid ratios. A similar type of curve is observed when the viscosity of an oil is plotted as a function of the gas in solution.

It would thus seem that to represent the viscosity of a gas-liquid mixture, an equation is necessary which will produce this "sag" in the viscosity-concentration curve. A relationship which exhibits this characteristic behavior is an empirical equation proposed by Arrhenius<sup>14</sup> which appears as follows:

$$\mu_m = \mu_1' \mu_2^{1-x} \dots \dots \dots (8)$$

where the logarithms of the viscosities of the components are assumed to be additive. A comparison of this equation with the linear equation for the same component viscosities is shown in Fig. 3. The shape of the curve for Eq. 8 is similar to that for the curve determined by Uren. Eq. 8 was used to represent the viscosity of the mixture with  $\mu_1 = \mu_L$ ,  $\mu_2 = \mu_G$ , and  $x = H_L$ . In most situations encountered in oilfield practice, a deviation between the actual viscosity of the mixture and the viscosity given by Eq. 8 will not affect the friction-factor determination a great deal, since the Reynolds numbers are in the turbulent region of the friction-factor curve. Only in the case of high liquid viscosities and low liquid rates and gas-liquid ratios would the friction-factor determination be affected by any deviation between the actual and calculated viscosities of the mixture. Even here the deviation is small for most practical situations. Any deviation, however, will be included in the calculated holdup factor.

Combining Eqs. 4, 5, 6 and 8, the Reynolds number for the two-phase mixture becomes

$$(N_{Re})_{TF} = \frac{C_1 D}{\mu_L^{xL} \mu_G^{1-xL}} [\rho_L H_L + \rho_G (1 - H_L)] \frac{(C_2 q_L + C_3 q_G)}{A_1} \dots \dots \dots (9)$$

If the limit is taken of the Reynolds number for the mixture as  $H_L \rightarrow 0$ ,  $q_L \rightarrow 0$  and  $H_L \rightarrow 1$ ,  $q_G \rightarrow 0$ , it reduces to the Reynolds number for single-phase gas or single-phase liquid flow, respectively,

$$\lim_{\substack{H_L \rightarrow 0 \\ q_L \rightarrow 0}} (N_{Re})_{TF} = \lim_{\substack{H_L \rightarrow 0 \\ q_L \rightarrow 0}} \frac{C_1 D}{\mu_L^{xL} \mu_G^{1-xL}} [\rho_L H_L + \rho_G (1 - H_L)] \frac{(C_2 q_L + C_3 q_G)}{A_1} \dots \dots \dots (10)$$

$$= \frac{C_1 D \rho_G (C_3 q_G)}{\mu_G \frac{A_1}{A_1}} = C_1 \frac{v_G \rho_G D}{\mu_G} = (N_{Re})_G$$

and

$$\lim_{\substack{H_L \rightarrow 1 \\ q_G \rightarrow 0}} (N_{Re})_{TF} = \lim_{\substack{H_L \rightarrow 1 \\ q_G \rightarrow 0}} \frac{C_1 D}{\mu_L^{xL} \mu_G^{1-xL}} [\rho_L H_L + \rho_G (1 - H_L)] \frac{(C_2 q_L + C_3 q_G)}{A_1} \dots \dots \dots (11)$$

$$= \frac{C_1 D \rho_L (C_2 q_L)}{\mu_L \frac{A_1}{A_1}} = C_1 \frac{v_L \rho_L D}{\mu_L} = (N_{Re})_L$$

For the quantities and units used in the present study, the Reynolds number for the two-phase mixture becomes

$$(N_{Re})_{TF} = 2.2 \times 10^4 \frac{q_L M}{D \mu_L^{xL} \mu_G^{1-xL}} \dots \dots \dots (12)$$

The friction-factor correlation<sup>15</sup> used to determine  $f$  appears in Fig. 4. The relative roughness is also accounted for in this correlation, although the effect of the relative roughness appears to be very small in two-phase flow.

**HOLDUP-FACTOR CORRELATION**

To determine the effect of including the slippage losses in the friction factor, the friction factors for each pressure increment were calculated from the test data assuming no slippage between the phases. The value of "pseudo" hold-

up factor  $H_L$  can be calculated directly under this condition. These friction factors were then plotted vs the two-phase Reynolds number. The results for water in the 1/4-in. tubing are shown in Fig. 5.

Several interesting observations can be made on a plot of this type. First, at high values of the Reynolds number, or at high mass flow rates, the points approach the curve for single-phase flow through a pipe of the same diameter. At these high mass flow rates, most of the energy losses are the result of friction and could be correlated with the Reynolds number. Second, at the lower mass flow rates where slippage between the phases becomes significant, the points begin to deviate from the curve for single-phase flow. The deviation of the points from the solid curve was thus attributed to the increased liquid holdup as a consequence of slippage. The values of the holdup factor  $H_L$  necessary to make the friction factors determined from Fig. 4 and those calculated from Eq. 1 identical were then calculated from the experimental data.

It can be argued at this point that  $H_L$  might not represent the actual fraction of the pipe occupied by liquid. This may be true, and the only way to resolve this point would be to measure the liquid holdup in place. To do so would be quite expensive and was therefore not attempted. It is recognized, however, by most investigators in this area that the pressure losses in two-phase flow are the result of two primary causes—friction and liquid holdup. Consequently, if the friction factors as determined from Fig. 4 are a reasonable approximation of the friction losses

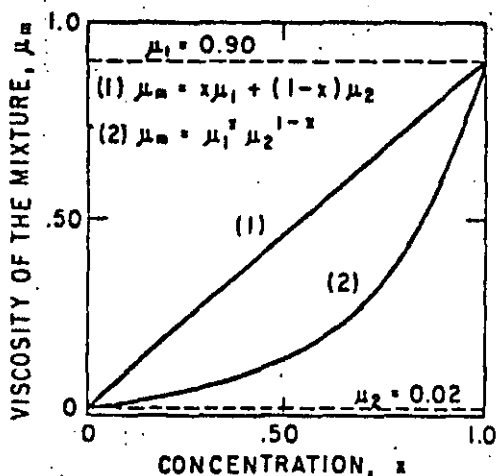


FIG. 3—COMPARISON OF RELATIONSHIPS PREDICTING VISCOSITIES OF MIXTURES.

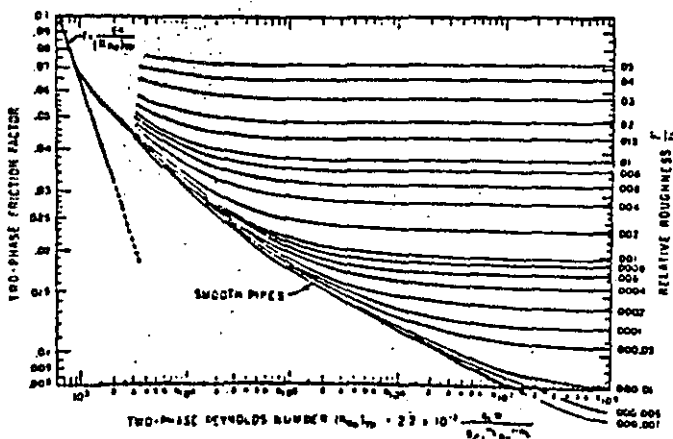


FIG. 4—FRICTION-FACTOR CORRELATION.

then a large percentage of the remaining losses are due to the increased static gradient because of slippage, and should be correlative through the use of a holdup factor.

The holdup factors calculated from the test data were then correlated with known flow, pipe and fluid properties. It can be shown by dimensional analysis<sup>10</sup> that the liquid holdup is related principally to four dimensionless parameters:

$$\left. \begin{aligned} N_{Lv} &= v_{mL} \sqrt{\rho_L / g \sigma} && \text{liquid velocity number} \\ N_{Gv} &= v_{mG} \sqrt{\rho_G / g \sigma} && \text{gas velocity number} \\ N_D &= D \sqrt{\rho_L g / \sigma} && \text{pipe diameter number} \\ N_L &= \mu_L \sqrt{R / \rho_L \sigma^3} && \text{liquid viscosity number} \end{aligned} \right\} (13)$$

For the units given in the nomenclature, these groups become

$$\left. \begin{aligned} N_{Lv} &= 1.938 v_{mL} \sqrt{\rho_L / \sigma} \\ N_{Gv} &= 1.938 v_{mG} \sqrt{\rho_G / \sigma} \\ N_D &= 120.872 D \sqrt{\rho_L g / \sigma} \\ N_L &= 0.15726 \mu_L \sqrt{1 / \rho_L \sigma^3} \end{aligned} \right\} (14)$$

The holdup factor should then be correlative with these four dimensionless groups.

The first step was to find a correlation for water in the 1/4-in. tubing. This was done to determine the effect of the flow parameters  $N_{Lv}$  and  $N_{Gv}$ . After many attempts, it was determined that the function  $N_{Lv} / N_{Gv}^\alpha$  would best correlate the holdup factor. The best value of  $\alpha$  was then determined and found to be 0.575.

It was noted that the pressure level was still having some effect on the scatter of data points so a new dimensionless parameter  $p/p_s$  was introduced and the correlating function assumed the form

$$(N_{Lv} / N_{Gv}^\alpha) (p/p_s)^\beta$$

The best value of  $\beta$  was then determined and found to be 0.1. The resulting correlation for 1/4-in. tubing is shown in Fig. 6.

This group would not, however, correlate the data for the 35-cp and 110-cp oil in the 1/4-in. tubing and for the water in the 1-in. tubing. The increased scatter noted in these cases appeared to be dependent on the liquid viscosity, the in-place gas velocity, and the pipe diameter. The observations indicate that a change in the flow pattern in the pipe might be the cause of the deviations.

Figs. 7 and 8 were then prepared for the 35-cp and the 110-cp oils, respectively. The data in Fig. 7 represent a liquid rate of 60 B/D, and the data in Fig. 8 are for a liquid rate of 54 B/D. Similar plots were prepared for other liquid rates, but only the gas velocity in place and not the liquid rates seemed to be affecting the scatter of the points. It is apparent in these figures that the curves

for the various gas rates approach some limiting curve at high pressures and low gas rates, each of which reduces in-place gas velocity, and that this limiting curve was parallel to those for water and the 10-cp oil in 1/4-in. tubing. Also, as the gas rate becomes very large or the pressure becomes very small, i.e., the in-place gas velocity becomes very large, these curves must approach zero since liquid holdup becomes very small. Consequently, these individual curves must also approach the limiting curve as the in-place gas velocity increases to very large values.

It is postulated that these deviations are the result of formation of a ring-type or annular flow pattern. As the in-place gas velocity is increased, the gas breaks through the liquid phase with the result that the liquid phase forms concentric cylinder around the gas phase. As a consequence, slippage is increased. This breakthrough of the gas would explain the rapid increase of the deviations shown in Figs. 7 and 8 as the in-place gas velocity is increased.

the gas velocity is increased even further, the thickness of the liquid cylinder diminishes until the mist flow pattern is formed, where the gas is the continuous phase with the liquid dispersed in the form of small droplets.

At this point the deviations would disappear. Cromer has served the formation of the annular flow pattern during visual studies of vertical two-phase flow in pipes.<sup>6</sup> The pattern was reportedly formed under the same conditions as described above.

The secondary correction factors  $\psi$  necessary to account for these deviations were calculated and correlated with the group

$$N_{ov} N_L^{.75} / N_D^{2.15}$$

as shown in Fig. 9. The curve is consistent with the ob-

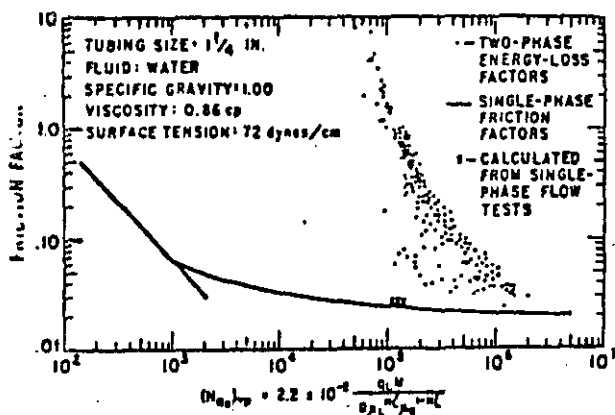


FIG. 5—COMPARISON OF TWO-PHASE ENERGY LOSS FACTORS WITH SINGLE-PHASE FRICTION FACTORS.

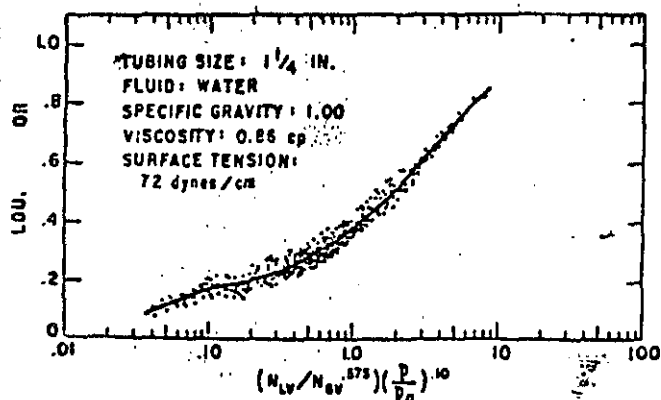


FIG. 6—HOLDUP-FACTOR CORRELATION, 1/4-IN. TUBING.

ervation that  $\psi = 1$  for all data except the three cases upon which this secondary correction factor is based.

The use of this secondary correction factor where conditions make it necessary results in a reversal of the curvature in the calculated pressure-depth traverses near the top of the well. This reversal actually appears in measured traverses,<sup>14</sup> and the correction factor  $\psi$  makes it possible to predict this reversal with a high degree of accuracy.

The curves for water in the four pipe sizes were then plotted as shown in Fig. 10 to determine the effect of pipe diameter. The curves were essentially parallel and by including the pipe diameter number,  $N_D$ , in the denominator of the correlating function, the curves were shifted the necessary amount to make them coincident.

The curves for the four liquids tested in the 1/4-in. tubing were then plotted as shown in Fig. 11 in an effort to determine the effect of the fluid properties, primarily the liquid viscosity and liquid density. It was apparent that no simple function of the viscosity number would make the correlating function independent of the viscosity number. The curves in Fig. 11 are essentially parallel, so by multiplying each curve by a constant it is possible to make them coincident. The constant, however, is a function of the viscosity number. Therefore, the term  $CN_L$  was included in the correlating function. The curve for water was arbitrarily chosen as the base curve, and  $C$  was defined to be 1 for water. The values of  $C$  necessary to shift each of the curves for the oils until they were coincident with the curve for water were then calculated. The term  $CN_L$  was then plotted as a function of  $N_L$  as shown in Fig. 12. This curve indicates that for low values

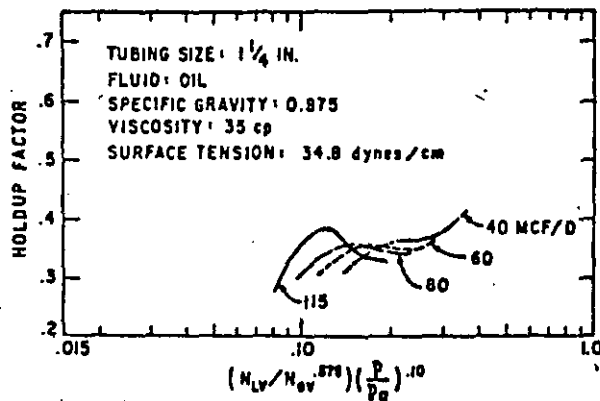


FIG. 7—EFFECT OF GAS VELOCITY ON HOLDUP FACTOR IN HIGH-VISCOSITY OIL.

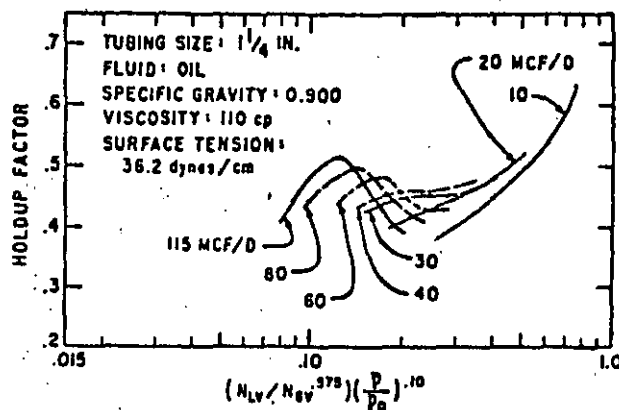


FIG. 8—EFFECT OF GAS VELOCITY ON HOLDUP FACTOR IN HIGH-VISCOSITY OIL.

of the liquid viscosity, the viscosity has very little effect. This has been noted previously by others.<sup>1,2</sup>

The final holdup-factor correlation is presented in Fig. 13. Several important features of the holdup-factor correlation should be noted. First, if the gas rate approaches zero, the value of the correlating function becomes very large, and the value of the holdup factor approaches one. Similarly, as the liquid rate approaches zero, the value of the correlating function becomes very small, and the holdup factor approaches zero. Therefore, as was previously shown, the two-phase Reynolds number becomes the Reynolds number for a single phase, and the gradient equation reduces to the gradient equation describing single-phase pressure gradients as either the liquid or the gas flow rate becomes zero. The holdup-factor correlation is thus consistent with the arguments presented during the development of the gradient equation and the friction-factor correlation.

### CALCULATIONAL PROCEDURE

To construct a pressure-depth traverse for a specific set of flow conditions, it is necessary to solve the finite-difference form of the gradient equation given by Eq. 1. The right side of this equation is a function of both the pressure and the length of the increment of the tube over which the incremental pressure drop  $\Delta p$  occurs. If it can be determined that the pressure drop due to a change in kinetic energy is negligible, the last term can be neglected and the solution is simplified to a single trial-and-error; otherwise, it is a double trial-and-error solution. The method of solution presented here is for the form of the gradient equation as it appears in Eq. 1. The step-by-step procedure is as follows:

1. Determine a suitable temperature-depth traverse. A

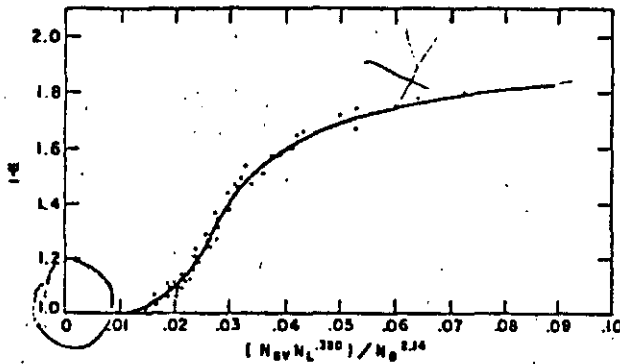


FIG. 9—CORRELATION FOR SECONDARY CORRECTION FACTOR.

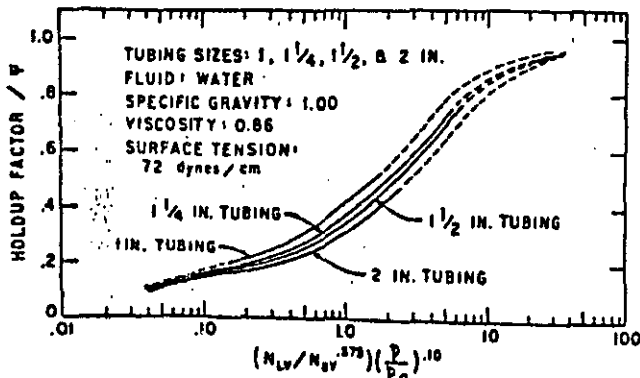


FIG. 10—EFFECT OF PIPE DIAMETER ON HOLDUP-FACTOR CORRELATION.

simplified approach assumes a straight-line relationship. A more accurate method involves the calculation of the temperature distribution in the wellbore using the method proposed by Ramey.<sup>3</sup>

2. Beginning with a known pressure and elevation, assume a value for  $\Delta p$  and a value for  $\Delta h$ .

3. Calculate the average pressure and temperature for the assumed increment, and determine  $\bar{\rho}_v$  at these conditions. Also, calculate the velocity of the mixture at both ends of the increment using the pressures at those two points and the ratio of the flow rates as measured at the out-flow end of the tube.

4. Calculate a value for  $N_L$ , and determine a value for  $CN_L$  from Fig. 12. In the calculation of  $N_L$ , the viscosity of the gas-free oil at the average temperature for the increment must be corrected for the effect of solution gas.

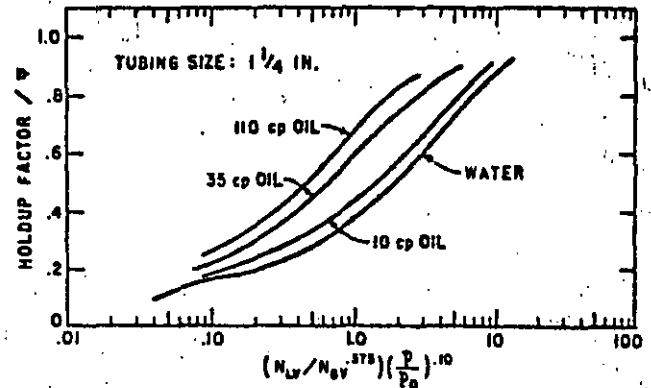


FIG. 11—EFFECT OF FLUID PROPERTIES ON HOLDUP-FACTOR CORRELATION.

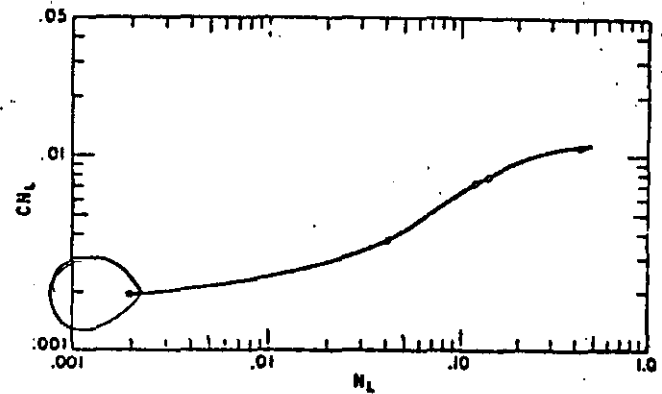


FIG. 12—CORRELATION FOR VISCOSITY NUMBER COEFFICIENT C.

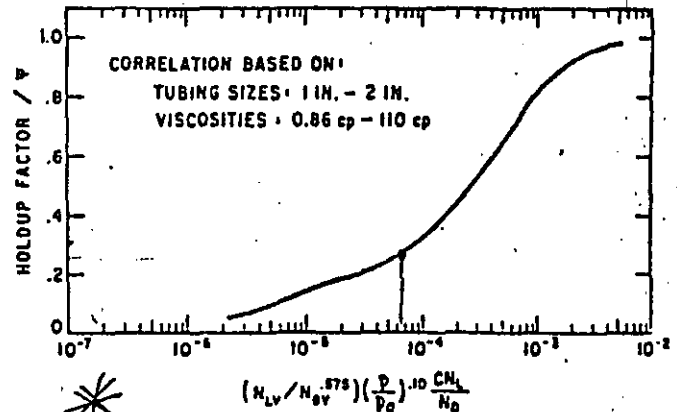


FIG. 13—HOLDUP-FACTOR CORRELATION.

If these data are not available for the specific oil, correlations such as the one developed by Chew and Connally<sup>2</sup> can be used.

5. Calculate the value of the correlating function, and determine the value of the holdup-factor/ $\psi$  from Fig. 13. When calculating the superficial liquid and gas velocities, the effect of solution gas must be accounted for. The liquid rate must be multiplied by the formation volume factor for the liquid, and the gas-liquid ratio is decreased by the amount of gas in solution at the average pressure of the increment. This must be done since only free gas should be considered in calculating the superficial gas velocity. The correlating function can be expressed in field units as follows:

$$(N_{Lv}/N_{ov}^{0.75})(p/p_o)^{-1}(CN_L/N_o) = 0.00326 \times$$

$$q_L = \frac{\left[ \left( \frac{1}{1 + \text{WOR}} \right) B_o + \left( \frac{\text{WOR}}{1 + \text{WOR}} \right) B_w \right] \bar{p}^{0.75} \sigma^{0.25} CN_L}{D^{1.75} (\bar{T} \bar{Z})^{0.75} \bar{\rho}_L^{0.25} \left[ \text{GLR} - R_s \left( \frac{1}{1 + \text{WOR}} \right) \right]^{0.75}} \quad (15)$$

6. Calculate a value for  $N_{ov} N_L^{0.25} / N_o^{0.25}$ . Obtain a value for  $\psi$  from Fig. 9 and multiply the value for the holdup-factor/ $\psi$  obtained in Step 5 by  $\psi$  to obtain the value for the holdup factor.

7. Using the holdup factor from Step 6, calculate a value for the two-phase Reynolds number and the relative roughness ratio  $\epsilon/D$  and obtain a value for the friction factor  $f$  from Fig. 4.

8. Calculate  $M$  and  $\bar{p}_w$ .

9. Calculate  $\Delta p / \Delta h$  from Eq. 1.

10. Calculate  $\Delta h$  by dividing the assumed  $\Delta p$  by the value of  $\Delta p / \Delta h$  from Step 9. If the calculated  $\Delta h$  is not the same as the originally assumed  $\Delta h$ , assume a new value and repeat Steps 3 through 10 until the two values of  $\Delta h$  agree with the required accuracy.

The pressure  $p + \Delta p$  occurs at depth  $h + \Delta h$ . A new  $\Delta p$  is then assumed, and the procedure is repeated. A pressure-depth traverse can then be plotted for the particular flow conditions, and the pressure at any depth is determined from the curve. These procedures were used to obtain the results which are discussed in the next section.

## RESULTS

To obtain a measure of the accuracy of the correlations developed in the preceding sections, a statistical analysis was performed on the results of the calculations utilizing the data obtained as part of the present study as well as those data reported by Fancher and Brown. The latter were included because the data represented higher tubing pressures and greater gas-liquid ratios than were obtainable in the test well.

All the pressure traverses measured by Baxendell<sup>3</sup> in 2 3/8-in. and 3 1/2-in. nominal size tubing, except those which appeared to be heading, were also included in the analysis. These data included production rates as high as 5,082 B/D with a gas-liquid ratio of 723 scf/bbl. Baxendell has also recorded bottom-hole pressures for 29 field wells with depths to 10,774 ft and tubing pressures to 1,000 psia. These data were included in the analysis to see if the correlations could predict the results for conditions so far removed from the test conditions from

which they were developed. The results indicate the correlations can be extrapolated to these conditions with a high degree of accuracy.

Gaither, *et al* reported pressure measurements at the ends of 1,000-ft vertical sections of 1-in. and 1 1/4-in. nominal size tubing over a wide range of flow conditions for gas and water.<sup>4</sup> The bottom-hole pressures were also calculated for the reported conditions using the correlations developed in this paper and compared with the measured bottom-hole pressures.

Since the calculation of the pressure-depth traverses involves an iteration process, any error made in one increment is carried over to all succeeding increments. The maximum error should occur, in most cases, at the deepest calculated point in the well for the particular test. All values, therefore, should be maxima. A negative per cent error indicates the calculated value is too low.

The algebraic average per cent error, or bias, as well as the standard deviation from the algebraic average per cent error were calculated for each set of data as well as for the combined data. The results are shown in Table 3.

For the data presented by Gaither, *et al* the calculated values are lower than the measured experimental values. The maximum deviations occurred in the 1-in. tubing at very high total fluid production rates. The deviations also increased with decreasing tubing pressure. The possibility exists, however, that the measured bottom-hole pressures are too high as a consequence of end effects at the point of measurement.

## CONCLUSIONS

As a result of the present work, the following conclusions have been reached:

1. Friction factors for two-phase flow can be determined from a conventional friction-factor diagram by defining a Reynolds number for two-phase flow, provided a suitable definition of the holdup factor is made.

2. It is not necessary to separate two-phase flow into the various flow patterns and develop correlations for each. The generalized correlations developed in this work in which no attempt was made to determine the flow patterns provide sufficient accuracy for engineering purposes.

3. In many instances, the pressure loss due to a change in the kinetic energy can account for an appreciable percentage of the total pressure losses, particularly near the top of the well when low tubing pressures are encountered. Under these conditions, the change in kinetic energy should be taken into consideration.

4. The correlations developed as part of this work

TABLE 3—STATISTICAL ANALYSIS OF RESULTS

Source	Pipe Diameter (in.)	Liquid	Average Per Cent Error	Standard Deviation
Hagedorn	1	Water	1.166	5.516
Hagedorn	1 1/4	Water	-2.373	6.231
Hagedorn	1 1/4	10 cp Oil	0.804	5.071
Hagedorn	1 1/4	35 cp Oil	0.767	4.591
Hagedorn	1 1/4	110 cp Oil	0.261	4.181
Hagedorn	1 1/4	Water	-2.379	5.154
Hagedorn	1 1/2	30 cp Oil	1.549	5.564
Gaither, <i>et al.</i>	1			
	1 1/4	Water	-3.782	7.531
	2	95% Water 5% Oil	0.538	3.697
Fancher & Brown				
Baxendell	2 3/8			
(test data)	3 1/2	34° API Oil	1.727	4.346
Baxendell	2 3/8			
(field data)	3 1/2	Oil	-1.373	8.801
Combined Data	All	All	-1.101	6.469
	above	above		



appear to be quite general and can be applied over a much wider range of conditions than most correlations presented previously. The correlations involve only dimensionless groups and are consistent with the requirement that the gradient equation for two-phase flow reduce to the gradient equation for single-phase flow when either the flow rate of the gas or the liquid is allowed to approach zero.

## NOMENCLATURE

- $A$  = cross-sectional area of tubing, sq ft  
 $B$  = formation-volume factor, bbl/bbl  
 $C$  = coefficient for liquid viscosity number, -  
 $D$  = pipe diameter, ft  
 $f$  = Darcy-Weisbach friction factor, -  
 $g$  = acceleration of gravity, ft/sec<sup>2</sup>  
 $g_c$  = conversion constant equal to 32.174 lb<sub>m</sub>ft/lb<sub>m</sub>sec<sup>2</sup>  
 GLR = gas-liquid ratio, scf/bbl  
 $h$  = depth, ft  
 $H_L$  = liquid-holdup factor, -  
 $M$  = total mass of oil, water and gas associated with 1 bbl of liquid flowing into and out of the flow string, lb<sub>m</sub>/bbl  
 $N_D$  = pipe diameter number, -  
 $N_{Dv}$  = gas velocity number, -  
 $N_L$  = liquid viscosity number, -  
 $N_{Lv}$  = liquid velocity number, -  
 $N_{Re}$  = Reynolds number, -  
 $p$  = pressure, psia  
 $\bar{p}$  = average pressure for increment, psia  
 $q_g$  = gas production rate, scf/day  
 $q_L$  = total liquid production rate, B/D  
 $R_s$  = solution gas-oil ratio, scf/bbl  
 $T$  = temperature, °R  
 $\bar{T}$  = average temperature for increment, °R  
 $v$  = velocity, ft/sec  
 $\bar{v}$  = average velocity at flowing conditions, ft/sec  
 $V$  = specific volume of fluid at flowing conditions, cu ft/lb<sub>m</sub>  
 $\bar{V}$  = average specific volume at flowing conditions, cu ft/lb<sub>m</sub>  
 $V_p$  = volume of pipe element, cu ft  
 $W_e$  = external work done by the flowing fluid, lb<sub>m</sub>ft/lb<sub>m</sub>  
 $W_i$  = irreversible energy losses, lb<sub>m</sub>ft/lb<sub>m</sub>  
 WOR = water-oil ratio, bbl/bbl  
 $Z$  = compressibility factor for gas, -

## SUBSCRIPTS

- $a$  = atmospheric  
 $b$  = base  
 $g$  = gas  
 $L$  = liquid  
 $m$  = mixture  
 $o$  = oil  
 $SG$  = superficial gas  
 $SL$  = superficial liquid  
 $TP$  = two-phase  
 $w$  = water

## GREEK SYMBOLS

- $\alpha$  = arbitrary constant, -  
 $\beta$  = arbitrary constant, -  
 $\gamma$  = specific gravity, -  
 $\Delta$  = difference, -  
 $\epsilon$  = absolute roughness, ft  
 $\mu$  = viscosity, cp  
 $\rho$  = density, lb<sub>m</sub>/cu ft

- $\bar{\rho}$  = integrated average density at flowing conditions, lb<sub>m</sub>/cu ft  
 $\sigma$  = surface tension of liquid-air interface, dynes/cm  
 $\psi$  = secondary correction factor, -

## ACKNOWLEDGMENTS

The authors wish to thank the management of the Otis Engineering Corp. for furnishing their experimental well in which to conduct these tests. In addition, all experimental equipment including valves, Malhak pressure transducers, wireline work, and labor to perform these operations were furnished by the Otis Engineering Corp. Particular thanks are extended to L. M. Wilhoit, M. B. Roach, P. J. Thrash, Carlos Canalizo, Carl Ivey, Don Taylor, Ray Sharp and numerous others.

Sincere thanks are also due the Gardner-Donver Co. and their representative, Tom Smith, of Dallas, Tex., for the use of the compressor units which were utilized in these tests.

## REFERENCES

1. Baxendell, P. B.: "The Calculation of Pressure Gradients in High-Rate Flowing Wells", *Jour. Pet. Tech.* (Oct., 1961) 1023.
2. Chew, J. and Connally, C. A., Jr.: "A Viscosity Correlation for Gas-Saturated Crude Oils", *Trans., AIME* (1959) 216, 23.
3. Cromer, S.: "An Investigation of the Flow of Mixtures of Water and Air in Vertical Columns", U. of Oklahoma, MS Thesis (1937).
4. Fancher, G. H., Jr. and Brown, K. E.: "Prediction of Pressure Gradients for Multiphase Flow in Tubing", *Soc. Pet. Eng. Jour.* (March, 1963) 59.
5. Gaither, O. D., Winkler, H. W. and Kirkpatrick, C. F.: "Single and Two-Phase Fluid Flow in Small Vertical Conduits Including Annular Configurations", *Jour. Pet. Tech.* (March, 1963) 308.
6. Govier, G. W. and Short, W. L.: "The Upward Vertical Flow of Air-Water Mixtures", *The Canadian Jour. Chem. Eng.* (Oct. 1958) 36, 195.
7. Hagedorn, A. R. and Brown, K. E.: "The Effect of Liquid Viscosity in Vertical Two-Phase Flow", *Jour. Pet. Tech.* (Feb., 1964) 203.
8. Hagedorn, A. R.: "Experimental Study of Pressure Gradients Occurring During Vertical Two-Phase Flow in Small-Diameter Conduits", The U. of Texas, PhD Dissertation (1964).
9. Hatcher, E.: *The Viscosity of Liquids*, G. Bell and Sons, Ltd., London (1928).
10. Hughmark, G. A.: "Holdup in Gas-Liquid Flow", *Chem. Eng.* (April, 1962) 58, 62.
11. Hughmark, G. A. and Pressburg, B. S.: "Holdup and Pressure Drop with Gas-Liquid Flow in a Vertical Pipe", *AICAE Jour.* (Dec., 1961) 7, 677.
12. Moody, L. F.: "Friction Factors in Pipe Flow", *Trans., ASME* (1944) 66, 671.
13. Moore, T. V. and Schilthuis, R. J.: "Calculation of Pressure Drops in Flowing Wells", *Petr. Dev. and Tech.*, AIME (1933) 103, 170.
14. Moore, T. V. and Wilde, H. D.: "Experimental Measurements of Slippage in Flow Through Vertical Tubes", *Petr. Dev. and Tech.*, AIME (Oct., 1930) 92, 296.
15. Nemet, A. G.: "Flow of Gas-Liquid Mixtures in Vertical Tubes", *Ind. and Engr. Chem.* (Feb., 1961) 53, 151.
16. Poettmann, F. H. and Carpenter, P. G.: "The Multiphase Flow of Gas, Oil and Water Through Vertical Flow Strings with Application to the Design of Gas-Lift Installations", *Drill. and Prod. Proc.*, API (1952) 257.
17. Ramey, H. J., Jr.: "Wellbore Heat Transmission", *Jour. Pet. Tech.* (April, 1962) 436.
18. Ros, N. C. J.: "Simultaneous Flow of Gas and Liquid as Encountered in Well Tubing", *Jour. Pet. Tech.* (Oct., 1961) 1037.
19. Streeter, V. L.: *Fluid Mechanics*, McGraw-Hill Co., Inc., New York (1958).
20. Tek, M. R.: "Multiphase Flow of Water, Oil and Natural Gas

### APPENDIX GRADIENT EQUATION

The basic flow equation in symbolic differential form based on 1 lb of the flowing fluid is

$$144 \frac{g_c}{g} V dp + dh + \frac{v dv}{g} + dW_f + dW_s = 0. \quad (A-1)$$

This equation assumes only steady flow and can be made the basis of any fluid-flow relationship.

In this study, the mixture of gas and liquid is treated as a homogeneous mixture of combined properties. Assuming no external work is done by the fluid between Points 1 and 2 of the flow string, the symbolic equation becomes

$$144 \frac{g_c}{g} V dp + dh + \frac{v dv}{g} + dW_f = 0, \quad (A-2)$$

where  $v$  is based on the ratio of fluids entering or leaving the system. By defining a two-phase friction factor similar to the one used in single-phase flow, the two-phase friction factor is given by

$$f = \frac{2gD}{v_m^3} \frac{dW_f}{dh} \quad (A-3)$$

Substituting Eq. A-3 into Eq. A-2, the basic flow equation for the mixture becomes

$$144 \frac{g_c}{g} V_m dp + dh + \frac{v_m dv_m}{g} + \frac{f v_m^3 dh}{2gD} = 0, \quad (A-4)$$

where  $v_m$  is an average velocity of the mixture whose existence is guaranteed by the theorem of the mean for integrals on the pressure range from  $p_1$  to  $p_2$ . Eq. A-4 can now be integrated from Point 1 to Point 2 to get

$$144 \frac{g_c}{g} \int_{p_2}^{p_1} V_m dp + (h_2 - h_1) + \frac{(v_{m2}^2 - v_{m1}^2)}{2g} + \frac{f v_m^3 (h_2 - h_1)}{2gD} = 0. \quad (A-5)$$

Since  $V_m$  is an approximately linear function of pressure over fairly large increments of pressure, the average integrated specific volume of the mixture,  $\bar{V}_m$ , between pressure limits  $p_1$  and  $p_2$  can be approximated by

$$\bar{V}_m = \frac{\int_{p_1}^{p_2} V_m dp}{\int_{p_1}^{p_2} dp} \quad (A-6)$$

After substitution, Eq. A-5 becomes

$$144 \frac{g_c}{g} \bar{V}_m \Delta p + \Delta h + \Delta \left( \frac{v_m^2}{2g} \right) + \frac{f \bar{v}_m^3 \Delta h}{2gD} = 0. \quad (A-7)$$

The average integrated velocity between Points 1 and 2 can be calculated from

$$\bar{v}_m = \bar{v}_{sl} + \bar{v}_{sg} \quad (A-8)$$

and the velocity of the mixture,  $v_m$ , at a point is given by

$$v_m = v_{sl} + v_{sg} \quad (A-9)$$

The following relationship for the average integrated density of the mixture between Points 1 and 2 is given by the definition of the density of the mixture

$$\bar{\rho}_m = \frac{1}{V_m} \quad (A-10)$$

By employing this substitution, Eq. A-7 becomes

$$144 \frac{g_c}{g} \frac{\Delta p}{\bar{\rho}_m} + \Delta h + \Delta \left( \frac{v_m^2}{2g} \right) + \frac{f \bar{v}_m^3 \Delta h}{2gD} = 0. \quad (A-11)$$

Eq. A-11 may be solved for the pressure gradient,  $144 \Delta p / \Delta h$ , and expressed in terms of quantities normally measured in the field as

$$144 \frac{\Delta p}{\Delta h} = \bar{\rho}_m + \frac{f q_L^2 M^2}{2.9652 \times 10^{11} D^3 \bar{\rho}_m} + \bar{\rho}_m \frac{\Delta \left( \frac{v_m^2}{2g} \right)}{\Delta h}, \quad (A-12)$$

where  $g$  is assumed numerically equal to  $g_c$  and  $\Delta p = p_1 - p_2$ . The total mass associated with each barrel of produced liquid is given by

$$M = \left( \frac{1}{1 + \text{WOR}} \right) \times (\gamma_g)(5.61 \times 62.4) + (0.0764)(\gamma_g)(\text{GLR}) + \left( \frac{\text{WOR}}{1 + \text{WOR}} \right) (\gamma_o)(5.61 \times 62.4). \quad (A-13)$$

Since the average density in-place cannot be calculated directly in view of the slippage which occurs between the phases, it is necessary to introduce the concept of a holdup factor. The holdup factor is theoretically the fractional volume of the conduit actually occupied by the liquid phase. The average density of the mixture in an element of the pipe is then described by

$$\bar{\rho}_m = \frac{\gamma_L \rho_L H_L V_L + \gamma_g \rho_{g, \text{avg}} \left( \frac{\bar{p} T_1}{p_1 T} \right) V_g (1 - H_L)}{V_m}$$

or

$$\bar{\rho}_m = \bar{\rho}_L H_L + \bar{\rho}_g (1 - H_L). \quad (A-14)$$

Eq. A-14 can be substituted into Eq. A-11 to give

$$144 \frac{\Delta p}{\Delta h} = \frac{g_c}{g} \left[ \bar{\rho}_L H_L + \bar{\rho}_g (1 - H_L) \right] \left\{ 1 + \frac{f(\bar{v}_{sl} + \bar{v}_{sg})^2}{2gD} + \frac{\Delta[(v_{sl} + v_{sg})^2]}{2g \Delta h} \right\} \quad (A-15)$$

Taking the limit as  $H_L \rightarrow 1$ ,  $\bar{v}_{sg} \rightarrow 0$ , and  $v_{sg} \rightarrow 0$ , i.e., as the gas rate becomes zero, Eq. A-15 reduces to

$$144 \frac{\Delta p}{\Delta h} = \frac{g_c}{g} \bar{\rho}_L + \frac{f \bar{\rho}_L \bar{v}_{sl}^2}{2gD} + \bar{\rho}_L \frac{\Delta \left( \frac{v_{sl}^2}{2g} \right)}{\Delta h} \quad (A-16)$$

since the superficial velocity is the real velocity when only one phase is present.

Eq. A-16 may be recognized as the equation describing the pressure gradients occurring in single-phase liquid flow. Similarly, if the limit of Eq. A-16 is taken as  $H_L \rightarrow 0$ ,  $\bar{v}_{sl} \rightarrow 0$ , and  $v_{sl} \rightarrow 0$ , i.e., as the liquid rate becomes zero, the result is the equation describing the pressure gradients which occur in the single-phase gas flow. \*\*\*

# Wellbore Heat Transmission

M. J. RAMEY, JR.  
MEMBER AIME

MOBIL OIL CO  
SANTA FE SPRINGS, CALIF.

## ABSTRACT

As fluids move through a wellbore, there is transfer of heat between fluids and the earth due to the difference between fluid and geothermal temperatures. This type of heat transmission is involved in drilling and in all producing operations. In certain cases, quantitative knowledge of wellbore heat transmission is very important.

This paper presents an approximate solution to the wellbore heat-transmission problem involved in injection of hot or cold fluids. The solution permits estimation of the temperature of fluids, tubing and casing as a function of depth and time. The result is expressed in simple algebraic form suitable for slide-rule calculation. The solution assumes that heat transfer in the wellbore is steady-state, while heat transfer to the earth will be unsteady radial conduction. Allowance is made for heat resistances in the wellbore. The method used may be applied to derivation of other heat problems such as flow through multiple strings in a wellbore.

Comparisons of computed and field results are presented to establish the usefulness of the solution.

## INTRODUCTION

During the past few years, considerable interest has been generated in hot-fluid-injection oil-recovery methods. These methods depend upon application of heat to a reservoir by means of a heat-transfer medium heated at the surface. Clearly, heat losses between the surface and the injection interval could be extremely important to this process. Not quite so obvious is the fact that every injection and production operation is accompanied by transmission of heat between wellbore fluids and the earth.

Previously, the interpretation of temperature logs<sup>1,2</sup> has been the main purpose of wellbore heat studies. The only papers dealing specifically with long-time injection operations are those of Moss and White<sup>3</sup> and Lesem, *et al.*<sup>4</sup> The purpose of the present study is to investigate wellbore heat transmission to provide engineering methods useful in both production and injection operations, and basic techniques useful in all wellbore heat-transmission problems. The approach is similar to that of Moss and White.<sup>3</sup>

## DEVELOPMENT

The transient heat-transmission problem under consideration is as follows. Let us consider the injection of a fluid down the tubing in a well which is cased to the top

of the injection interval. Assuming fluid is injected at known rates and surface temperatures, determine the temperature of the injected fluid as a function of depth and time. Consideration of the heat transferred from the injected fluid to the formation leads to the following equations. For liquid,

$$T_1(z, t) = aZ + b - aA + (T_0 + aA - b)e^{-z/A}; \quad (1)$$

and for gas,

$$T_1(z, t) = aZ + b - A \left( a + \frac{1}{778c} \right) + \left[ T_0 - b + A \left( a + \frac{1}{778c} \right) \right] e^{-z/A} \quad (1A)$$

where

$$A = \frac{Wc[k + r_1U/(t)]}{2\pi r_1 Uk} \quad (2)$$

Eqs. 1, 1A and 2 are developed in the Appendix. These equations were developed under the assumption that physical and thermal properties of the earth and wellbore fluids do not vary with temperature, that heat will transfer radially in the earth and that heat transmission in the wellbore is rapid compared to heat flow in the formation and, thus, can be represented by steady-state solutions.

Special cases of this development have been presented by Nowak<sup>5</sup> and Moss and White.<sup>3</sup> Both references are recommended for excellent background material. Nowak<sup>5</sup> presents very useful information concerning the effect of a shut-in period on subsequent temperatures.

Since one purpose of this paper is to present methods which may be used to derive approximate solutions for heat-transmission problems associated to those specifically considered here, a brief discussion of associated heat problems is also presented in the Appendix. Analysis of the derivation presented in the Appendix will indicate that many terms can be re-defined to modify the solution for application to other problems.

Before Eqs. 1, 1A and 2 can be used, it is necessary to consider the significance of the over-all heat-transfer coefficient  $U$  and the time function  $f(t)$ .

Thorough discussions of the concept of the over-all heat-transfer coefficient may be found in many references on heat transmission. See McAdams<sup>6</sup> or Jakob,<sup>7</sup> for example. Briefly, the over-all coefficient  $U$  considers the net resistance to heat flow offered by fluid inside the tubing, the tubing wall, fluids or solids in the annulus, and the casing wall. The effect of radiant heat transfer from the tubing to the casing and resistance to heat flow caused by scale or wax on the tubing or casing may also be included in the over-all coefficient. According to McAdams, on page 136 of Ref. 5,

Original manuscript received in Society of Petroleum Engineers office Aug. 24, 1961. Revised manuscript received March 6, 1962. Paper presented at 36th Annual Fall Meeting of SPE Oct. 8-11, 1961, in Dallas.  
<sup>1</sup>References given at end of paper.

$$\frac{1}{U} = \frac{dA_1}{h_1 dA_1} + \frac{x_1 dA_1}{k_1 dA_1} + \frac{dA_2}{h_2 dA_2} + \frac{dA_3}{h_3 dA_3} + \frac{x_2 dA_3}{k_2 dA_3} \quad (3)$$

The differential areas presented in Eq. 3 are perpendicular to heat flow and, thus, proportional to either radius or diameter measurements. The logarithmic mean area may be determined from

$$A_1 = \frac{A_2 - A_1}{\ln(A_2/A_1)} \quad (4)$$

where "ln" denotes the natural logarithm.

If the annulus is filled with an insulating material, the third and fourth terms in Eq. 3 should be dropped and a term similar to those for the tubing or casing wall added. Eq. 3 then becomes

$$\frac{1}{U} = \frac{dA_1}{h_1 dA_1} + \frac{x_1 dA_1}{k_1 dA_1} + \frac{x_2 dA_1}{k_2 dA_1} + \frac{x_3 dA_1}{k_3 dA_1} \quad (3A)$$

The local heat-transfer coefficients appearing in Eq. 3 ( $h_1, h_2$ ) may be found from heat-transfer correlations for the particular type of flow, i.e., turbulent, streamline, or free convection. (See pages 168, 190 and 248 of Ref. 5.) If the annulus is under vacuum, the local heat-transfer coefficient for the annulus will be negligible, but heat may be transferred from tubing to casing by radiation. An equivalent local heat-transfer coefficient for the radiation effect may be found on page 63 of Ref. 5. Radiation may be important whether the annulus is under vacuum or filled with gas. If so, the local heat-transfer coefficient for the annulus should be increased by the radiation contribution. It is also possible that any or all of the surfaces of the tubing and casing will be covered by scale and wax. This effect can be included in Eq. 3 by addition of terms similar to those for transfer through the fluid films. The corresponding area term will be the area of the surface covered by the scale or wax. Values for scale or wax coefficients are also presented by McAdams,<sup>4</sup> on page 137.

In many cases, the annulus between the casing and hole is cemented. Because the conductivity of cement may be lower than that of the surrounding earth, a term similar to that for the resistance of pipe or casing wall should appear in the over-all heat-transfer coefficient, Eq. 3. The thickness of cement-filled annulus should be used with the logarithmic mean area of the cement. In this instance, the temperature  $T_1$  will refer to the temperature of the outside surface of the cement and a corresponding radius should be used to evaluate  $f(t)$ . The conductivity of cement may be estimated from data presented by Jakob, on page 94 of Ref. 6.

For those readers not familiar with the over-all heat-transfer-coefficient concept, the following "rules of thumb" are offered for convenience.

1. The thermal resistance of pipe or casing can often be neglected since the thermal conductivity of steel is much higher than that of other materials in the wellbore or the earth.
2. The thermal resistance of liquid water or condensing steam can often be neglected since heat-transfer film coefficients are so high as to offer little resistance to heat flow (range from about 200 to 2,000 Btu/hr-sq ft-°F).
3. Gas film coefficients and thermal resistance of insulating materials in the wellbore often exert the greatest effect on the over-all coefficient. Gas film coefficients for turbulent flow are often about 2 to 5 Btu/hr-sq ft-°F.

Evaluation of the over-all heat-transfer coefficient is the most difficult step involved in wellbore heat-transmission

problems. But certain problems—for example, injection of a liquid down casing—thermal resistance in the wellbore is negligible. In this case, the over-all heat-transfer coefficient can be assumed infinite, and Eq. 2 reduces to

$$A = \frac{Wc f(t)}{2rk} \quad (2A)$$

The problem then becomes simply to find the proper time function  $f(t)$ . This case is that treated by Moss and White.<sup>1</sup>

The time function  $f(t)$  introduced in Eq. 2 may be estimated from solutions for radial heat conduction from an infinitely long cylinder. Such solutions are presented in many texts on heat transmission and are analogous to transient fluid-flow solutions used in reservoir engineering. (See Carslaw and Jaeger,<sup>1</sup> page 283.) Fig. 1 presents  $f(t)$  for a cylinder losing heat at constant temperature, a constant heat-flux line source and a cylinder losing heat under the "radiation" or convection boundary condition. As can be seen from Fig. 1 (as well as long-time solutions presented by Carslaw and Jaeger<sup>1</sup>), all three solutions eventually converge to the same line. The convergence time is on the order of one week for many reservoir problems. Thus, the line source solution will often provide a useful result if times are greater than one week. The equation for  $f(t)$  for the line source for long times is

$$f(t) = -\ln \frac{r_1'}{2\sqrt{at}} - 0.290 + O(r_1'^2/4at) \quad (5)$$

For estimation of temperatures at times before the convergence time shown on Fig. 1,  $f(t)$  should be read from the "radiation"-boundary-condition case at the proper value of  $(r_1 U/k)$ . See the Appendix.

## DISCUSSION

The preceding offers an approximate solution to the wellbore heat problem involved in injection of a hot fluid down tubing. Two assumptions appear to be of primary importance: (1) heat flows radially away from the wellbore; and (2) heat flow through various thermal resistances in the immediate vicinity of the wellbore is rapid compared to heat flow in the formation, and can be represented by steady-state solutions. Other assumptions, such as constant thermal and physical properties, appear reasonable.

To test the usefulness of the approximate solution, computed results have been compared with field data.

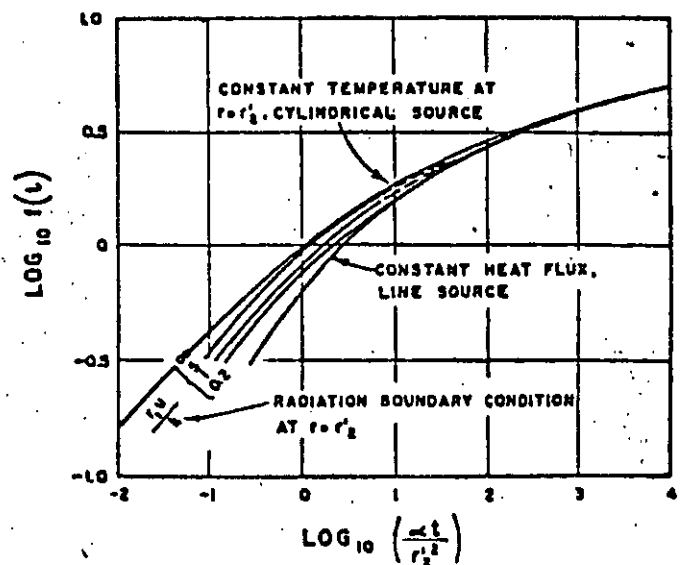


FIG. 1—TRANSIENT HEAT CONDUCTION IN AN INFINITE RADIAL SYSTEM.<sup>1</sup>

## COMPARISON OF FIELD TEMPERATURES WITH COMPUTED TEMPERATURES

Following are analyses of field data from a variety of water and gas injections.

### Cold Water Injection

Fig. 2 presents a comparison of temperatures measured in a water-injection well with temperatures computed for existing conditions. The water-injection rate at the time of the survey was 4,790 barrels per day; the well had been on injection for a period of approximately 75 days. Water-injection temperature was 58.5°F. As shown on Fig. 2, the computed temperatures were within 1.5°F of the measured temperatures. The reported accuracy of the temperature log was  $\pm 2^\circ\text{F}$ . A sample calculation for this case is presented in the Appendix.

Fig. 2 illustrates a point worth concern in certain waterflooding operations. The water entering the interval at approximately 6,500 ft is 55°F cooler than the formation temperature. An approximate calculation of the rate of the water-front advance and the cold-front advance indicates the cold front would move about half the velocity of the water front for many California water floods. Thus, recovery of residual oil behind the water front by continued flooding could be seriously affected by an increase in oil viscosity at the temperature of the cold injected water. (Formation temperature was observed to drop 50°F several hundred feet away from an injection well in a Wilmington water flood.)

### Air Injection

Fig. 3 presents a comparison of measured and computed temperatures for an air-injection well. At the time of the survey, air was being injected at 230 Mcf/D and had been injected for a period of six days. Injection temperature was 94°F. As shown on Fig. 3, computed temperatures closely agreed with measured temperatures near the top of the well, but were 8°F higher than measured temperatures at 1,500 ft. The estimated accuracy of temperature measurements was  $\pm 5^\circ\text{F}$ . The increase in temperature opposite the injection interval was caused by spontaneous reaction between air and oil which eventually resulted in ignition of the oil.

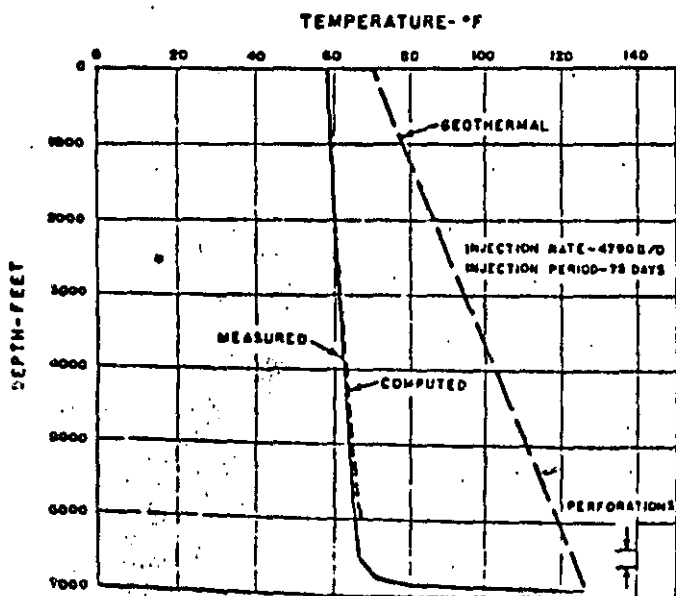


FIG. 2—MEASURED AND COMPUTED TEMPERATURES FOR A WATER-INJECTION WELL.

This case is a particularly interesting one. Air was injected in the casing annulus, and temperatures were measured in the tubing which was plugged on bottom. In addition, sufficient information was available to permit estimation of the effect of mud and cement in the annulus between the bore and casing and the effect of surface pipe on heat transmission.

### Hot Natural-Gas Injection

Fig. 4 presents a comparison of measured and computed temperatures for injection of hot natural-gas down insulated tubing. This gas-injection project provided the most complete information available for testing the approximate solution. During the year and a half this test was

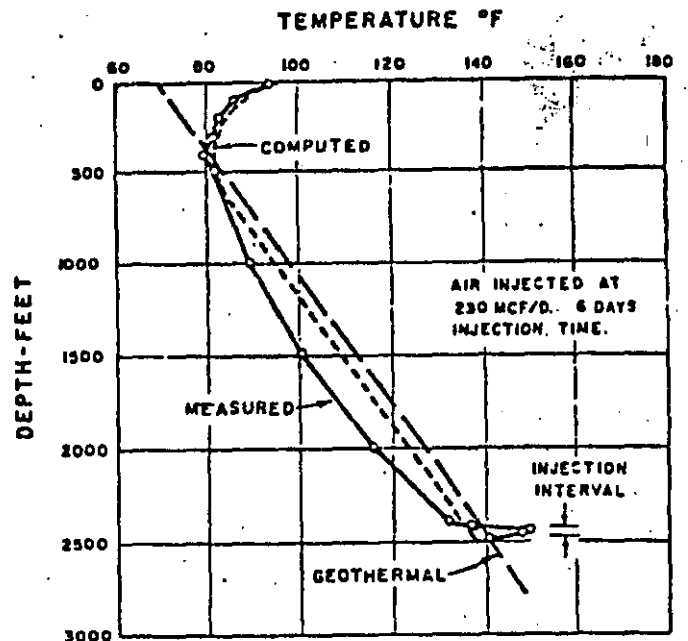


FIG. 3—MEASURED AND COMPUTED TEMPERATURES IN AN AIR-INJECTION WELL (AIR INJECTED AT 230 Mcf/D, SIX DAYS INJECTION TIME).

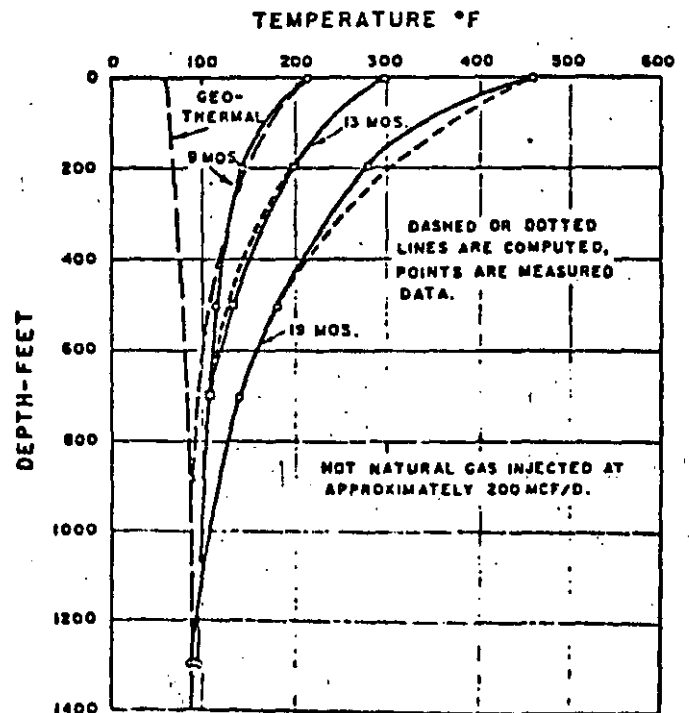


FIG. 4—MEASURED AND COMPUTED TEMPERATURES FOR HOT NATURAL-GAS INJECTION DOWN INSULATED TUBING (HOT NATURAL GAS INJECTED AT APPROXIMATELY 200 Mcf/D).

operated, the temperature of the injected gas was increased to almost 500°F, and the gas-injection rate varied from 10 to 215 Mcf/D. Gas was injected down 3-in. tubing. The annulus between the tubing and the 7-in. casing was filled with Perlite.

Measured and computed temperatures are shown on Fig. 4 for three times after start of injection—9, 13 and 19 months. The computed curves are quite similar to the measured curves. Both computed and measured temperatures are below 100°F at 1,300-ft depth throughout the test—despite the surface injection temperature of 460°F. This case illustrates the importance of wellbore heat loss during hot, noncondensable gas injection.

Other sets of field temperatures have been compared with computed temperatures, with results similar to those presented. The three cases presented were selected as representative of the widest conditions tested to date. In view of the reasonable agreement between measured and computed temperatures, it appears that the approximate solution offers a useful method for estimation of temperatures—at least over the ranges of field conditions tested. Further checks of field temperatures and computed temperatures should help define the usefulness of this solution.

#### HOT FLUID INJECTION

An interesting application of the wellbore heat-transmission problem is estimation of heat losses from the wellbore during injection of a hot fluid for recovery of oil. In addition to wellbore heat loss, vertical heat losses from the producing formation are also important. Although not treated in this paper, several authors have considered vertical heat losses from the formation.<sup>10</sup> Several field pilot tests of steam or hot water injection have been completed, or are in progress.<sup>11</sup>

Of the various heat-transport mediums available, steam or high-pressure hot water appear most attractive. Both steam and hot water have much higher specific-heat capacity than inert gases. However, several questions arise. Will wellbore heat losses be as severe as indicated by Fig. 4? Is it possible to reduce wellbore heat loss to a practical level?

To explore these questions, three cases of steam or hot-water injection have been considered. Before proceeding with these sample cases, it is informative to consider phase relationships for water. Fig. 5 presents a pressure-temperature phase diagram for water in the liquid-vapor region.<sup>12</sup>

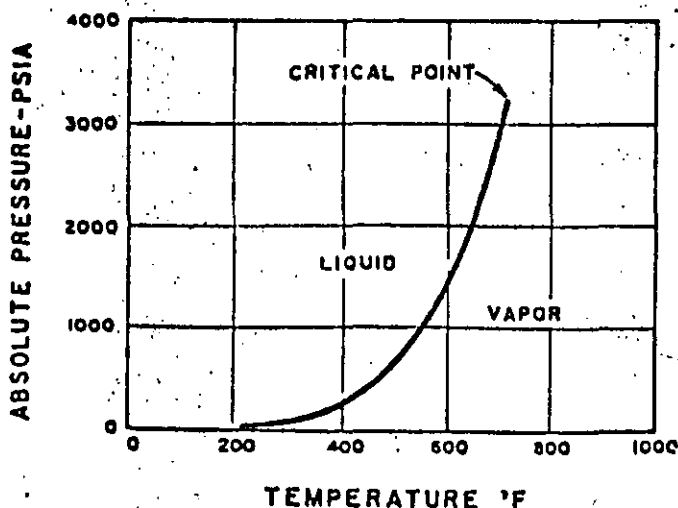


FIG. 5—PRESSURE-TEMPERATURE DIAGRAM FOR WATER.<sup>12</sup>

Assuming that it is necessary to raise formation temperature to 400°F to achieve satisfactory removal of oil, Fig. 5 indicates that the condition of the water injected will depend upon the injection pressure required. If injection pressure is less than 250 psia, it would be possible to inject steam and take benefit of the high latent-heat content. If injection pressure is above 250 psia, it will be necessary to inject liquid water.

Let us first consider the injection of 500 barrels per day of water at a temperature of 397°F down the casing of a well completed with 7 in., 23-lb casing. If injection pressure is assumed to be 1,000 psi, Fig. 5 indicates that the water will be in the liquid phase. Thus, the previous solution given by Eq. 1 may be applied directly to estimate the temperatures in the well at any time after injection and for any depth. Fig. 6 presents computed temperatures for one week of injection. As shown on Fig. 6, temperatures would decrease severely with depth, indicating a serious heat loss from the hot water.

If 500 BWPD at 397°F are injected at a pressure of 223 psi (238 psia), Fig. 5 indicates that the water may be saturated steam at 397°F. Assuming that the water is saturated steam, temperatures in the wellbore will remain nearly constant until all the steam is condensed as a result of heat loss. (Actually, there would be a slight change in temperature caused by a change in pressure with increased depth.) Fig. 6 also presents estimated temperatures for this case. Despite the fact that temperatures remain constant for this case, heat loss will be greater than for hot-water injection and will result in condensation of much of the steam.

To explore the possibility of reducing heat loss, assume that 500 barrels per day of hot, liquid water is injected at 1,000 psi down 2-in. line pipe centered inside the casing and that the annulus is filled with a granular insulating material. The insulating material has an effective thermal conductivity of 0.1 Btu/hr-ft-°F. The temperatures for this case (also presented on Fig. 6) show only a slight drop with depth, indicating a considerable improvement over injection down the casing.

Fig. 7 presents the percentage heat loss as a function of depth for each preceding case. Percentage loss was based upon heat content above a formation temperature of 150°F at 4,000 ft. Fig. 7 shows that 45 per cent of the heat had been lost from the injected steam by 4,000-ft depth, despite constant wellbore temperatures shown on

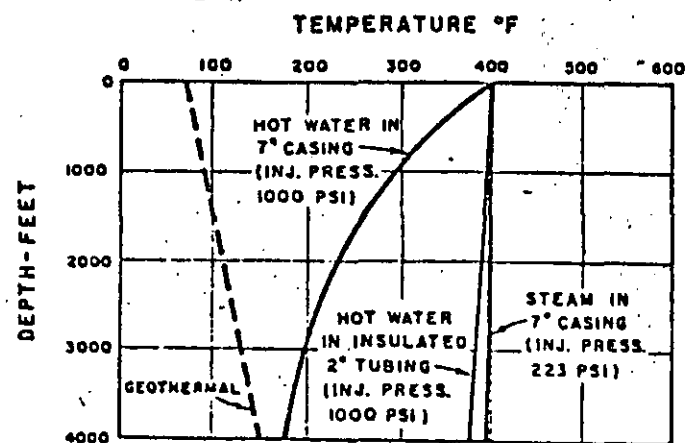


FIG. 6—COMPUTED WELLBORE TEMPERATURES RESULTING FROM INJECTION OF 500 B/D OF STEAM OR HOT WATER FOR ONE WEEK. (EARTH THERMAL CONDUCTIVITY OF 1.4 BTU/HR-FT-°F; EARTH THERMAL DIFFUSIVITY OF 0.04 SQ FT/HR.)

Fig. 6. Heat loss during liquid water injection was reduced from 89 per cent at 4,000 ft for injection down the casing to only 9 per cent at 4,000 ft by injecting down insulated 2-in. pipe.

Fig. 8 shows the change in wellbore temperatures with increased time of injection for the previous example of injection of 500 B/D of 397°F hot water down casing. As would be expected, temperatures increase with time as the earth surrounding the wellbore becomes heated. But the thermal diffusivity of the earth is such that temperatures are still changing slowly even after 10 years of injection. This is analogous to slow pressure build-up in very tight formations.

The foregoing cases were selected to illustrate the type of information which may be gained by study of wellbore heat transmission. Because of the extreme variety of conditions possible for hot fluid injection, it does not appear feasible to compute generally applicable results. But the work required for any particular case can be done rapidly with the slide rule. If the injection project has not been drilled, it may be useful to explore the effect of tubing and casing size on heat loss. Heat loss can be reduced by slim-hole completion.

Several important observations concerning use of the methods described in this report have been made which are not apparent from the examples presented. Computed temperatures can sometimes be very sensitive to the geothermal temperatures used. Because geothermal temperatures vary considerably from field to field—and even within a given field—efforts should be made to obtain the best possible estimate of earth temperatures.

Surprisingly, good results have been obtained from different geographical areas using a single value of earth conductivity—1.4 Btu/hr-ft-°F—and a single value of thermal diffusivity—0.04 sq ft/hr. Thermal conductivity for a particular location may be estimated from field temperature logs. (See Ref. 1.)

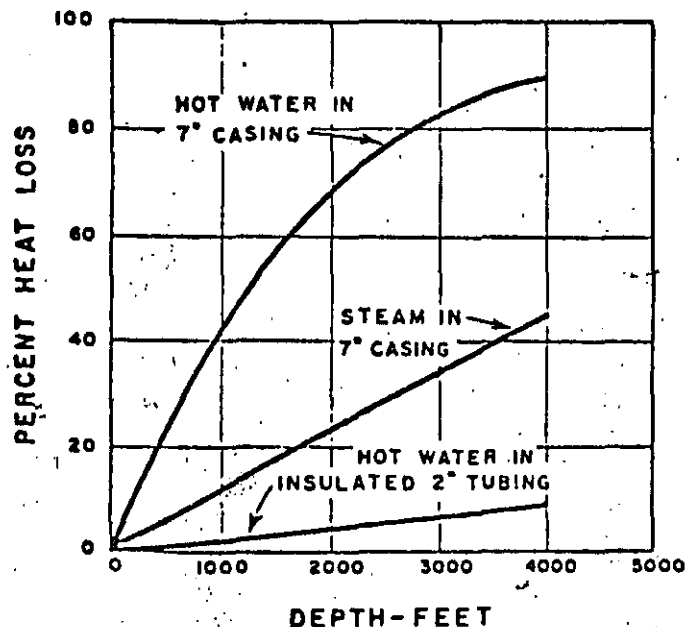


FIG. 7—COMPUTED HEAT LOSS VS DEPTH FOR INJECTION OF 500 B/D OF STEAM OR HOT WATER FOR ONE WEEK. (CONDITIONS: SURFACE INJECTION TEMPERATURE, 397°F; STEAM INJECTION PRESSURE, 223 PSI; HOT-WATER INJECTION PRESSURE, 1,000 PSI; HEAT LOSS BASED ON TEMPERATURE OF 150°F; TOTAL HEAT INJECTION RATES, 191 MILLION BTU/DAY FOR STEAM, 44.9 MILLION BTU/DAY FOR HOT WATER.)

In most cases of water or liquid injection down casing, the resistance to heat flow between the hot stream and the earth is negligible ( $U = \infty$ ). Thus, the bulk fluid temperature becomes equal to the casing temperature at that depth. (Both Nowak and Moss and White used this simplification for water-injection cases.)

Many wellbore heat problems exist which involve heat effects not considered in the subject development. Examples are: expansion of gas, heat generated by friction (an oil-well pump, for example) and latent heat effects from phase changes. Often such complications can be handled by proper modification of the solution.

In the development of Eq. 1, it was assumed that the surface temperature of the injection stream could vary with time. Because of the approximation introduced to account for heat loss to the earth,  $f(t)$ , surface temperature should not change rapidly. The effect of a rapid change can be pictured by considering the case of a long period of water injection at 400°F followed by a sudden drop in temperature to 200°F. It would be possible for the 200°F water to gain heat near the surface from the preheated surrounding earth, although the approximate solution would indicate a heat loss. Thus, computed results for rapid changes in injection temperature may be grossly in error and should be used with caution.

## CONCLUSIONS

An approximate solution to the transient heat-conduction problem involved in movement of hot fluids through a wellbore has been developed. The approximate solution considers the effect of thermal resistances in the wellbore. These thermal resistances can be very important in certain cases. Comparison of computed temperatures with those measured in a limited number of field gas- and water-injection wells indicates good agreement. The solution may be applied to a large variety of wellbore heat problems involving different types of well completions and operating methods. Solutions to more complex wellbore heat-transmission problems may be approximated in a similar fashion with the same methods and principles. Calculations involved are simple and require only slide-rule manipulation.

## NOMENCLATURE

$A$  = a time function defined by Eq. 2, ft

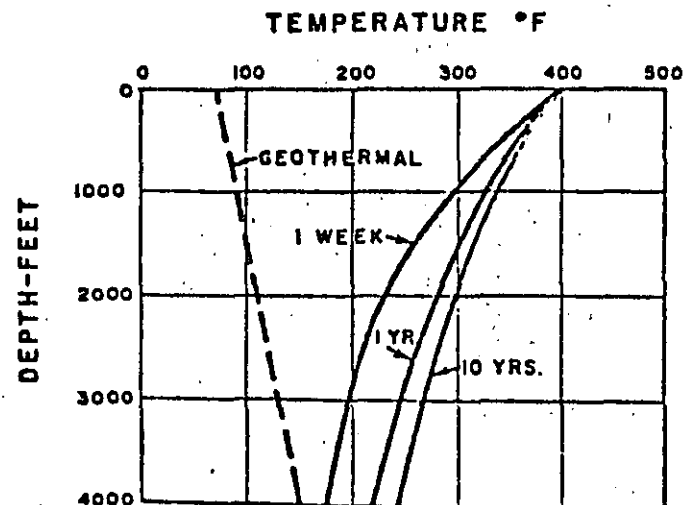


FIG. 8—COMPUTED WELLBORE TEMPERATURES RESULTING FROM INJECTION OF 500 B/D OF HOT WATER DOWN 7-IN. CASING.

$A_i$  = inside area of tubing  
 $A_m$  = log mean area of tubing  
 $A_o$  = outside area of tubing  
 $A_c$  = inside area of casing  
 $A_{cm}$  = log mean area of casing  
 $a$  = geothermal gradient, °F/ft  
 $b$  = surface geothermal temperature, °F  
 $c$  = specific heat at constant pressure of fluid, Btu/lb-°F  
 $c_p$  = specific heat of earth, Btu/lb-°F  
 $A_a$  = log mean area of annulus, or log mean of  $A_i$  and  $A_o$   
 $E$  = internal energy  
 $e$  = base of natural logarithm  
 $f(t)$  = transient heat-conduction time function for earth, dimensionless (Fig. 1)  
 $g$  = gravitational acceleration, 32.2 ft/sec<sup>2</sup>  
 $g_c$  = conversion factor, 32.2 ft-lb mass/sec<sup>2</sup>-lb force  
 $H$  = enthalpy, Btu/lb mass  
 $h_i$  = local film coefficient of heat transfer for gas or liquid inside tubing, Btu/day-sq ft-°F  
 $h_o$  = local film coefficient of heat transfer for gas or liquid in annulus  
 $J$  = mechanical equivalent of heat, 778 ft-lb force/Btu  
 $k$  = thermal conductivity of earth, Btu/day-ft-°F  
 $k_t$  = thermal conductivity of tubing material, Btu/day-ft-°F  
 $k_c$  = thermal conductivity of casing material, Btu/day-ft-°F  
 $k_a$  = effective thermal conductivity of annulus material, Btu/day-ft-°F  
 $O$  = "on the order of"  
 $P$  = absolute pressure  
 $q$  = heat-transfer rate, Btu/day  
 $Q$  = heat transferred from surrounding, Btu/lb-mass  
 $r_i$  = inside radius of tubing, ft  
 $r_c$  = inside radius of casing, ft  
 $r_o$  = outside radius of casing, ft  
 $T_e$  = temperature of earth, °F  
 $T_s$  = surface temperature of injected fluid, °F  
 $T_t$  = temperature of fluid in tubing, °F  
 $T_c$  = temperature of outside of casing, °F  
 $t$  = time from start of injection, days  
 $U$  = over-all heat-transfer coefficient between inside of tubing and outside of casing based on  $r_i$ , Btu/day-sq ft-°F  
 $U_o$  = over-all heat-transfer coefficient based on outside radius of casing, Btu/day-sq ft-°F  
 $v$  = fluid velocity  
 $V$  = specific volume  
 $W$  = fluid injection rate, lb/day  
 $W_f$  = flow work, ft-lb force/lb mass  
 $x_a$  = thickness of annulus or difference between inside radius of casing and outside radius of tubing, ft  
 $x_c$  = thickness in casing wall, ft  
 $x_t$  = thickness of tubing wall, ft  
 $Z$  = depth below surface, ft

$\alpha$  = thermal diffusivity of earth, sq ft/day ( $\alpha = k/\rho c_p$ )  
 $\rho$  = density of earth, lb/cu ft

## ACKNOWLEDGMENT

The author wishes to express his appreciation to Mobil Oil Co. for permission to publish this paper. Special thanks are offered to E. J. Couch, L. K. Strange and D. Hodges of the Socony Mobil Field Research Laboratories for their helpful comments concerning this work and for certain of the field data which were used to test the results.

## REFERENCES

- Nowak, T. J.: "The Estimation of Water Injection Profiles from Temperature Surveys", *Trans., AIME* (1953) 198, 203.
- Bird, J. M.: "Interpretation of Temperature Logs in Water and Gas Injection Wells and Gas Producing Wells", *Drill. and Prod. Prac.*, API (1954) 187.
- Moss, J. T. and White, P. D.: "How to Calculate Temperature Profiles in a Water-Injection Well", *Oil and Gas Jour.* (March 9, 1959) 57, No. 11, 174.
- Lesem, L. B., Greytak, F., Marotta, F. and McKetta, J. J.: "A Method of Calculating the Distribution of Temperature in Flowing Gas Wells", *Trans., AIME* (1957) 210, 169.
- McAdams, W. H.: *Heat Transmission*, Second Ed., McGraw-Hill Book Co., Inc., N. Y. (1942).
- Jakob, M.: *Heat Transfer*, Vol. I, John Wiley & Sons, Inc., N. Y. (1950).
- Carlsw, H. S. and Jaeger, J. C.: *Conduction of Heat in Solids*, Oxford U. Press, Amen House, London (1950).
- Lauwerier, H. A.: "The Transport of Heat in an Oil Layer Caused by the Injection of Hot Fluid", *Appl. Sci. Res.* (1955) Sec. A, 5, 145.
- Marx, J. W. and Langenheim, R. N.: "Reservoir Heating by Hot Fluid Injection", *Trans., AIME* (1959) 216, 312.
- "A Pilot Hot Water Flood", *Newsletter, Oil and Gas Jour.* (Feb. 8, 1960) 58, No. 6.
- "Steam Flooding", *Newsletter, Oil and Gas Jour.* (March 28, 1960) 58, No. 13.
- Keenan, J. H. and Keyes, F. G.: *Thermodynamic Properties of Steam*, John Wiley & Sons, Inc., N. Y. (1947).
- van Everdingen, A. F. and Hurst, W.: "The Application of the Laplace Transformation to Flow Problems in Reservoirs", *Trans., AIME* (1949) 186, 305.
- van Everdingen, A. F.: "The Skin Effect and Its Influence on the Productive Capacity of a Well", *Trans., AIME* (1953) 198, 171.

## APPENDIX

### DERIVATION OF WELLBORE HEAT-TRANSMISSION SOLUTION

Let us consider the injection of a fluid down the tubing in a well which is cased to the top of the injection interval. Assuming fluid is injected at known rates and surface temperatures, determine the temperature of the injected fluid as a function of depth and time. Fig. 9 presents a schematic diagram of the problem. Depths are measured from the surface. As shown on Fig. 9,  $W$  lb/day of fluid is injected in the tubing, at the surface at a temperature of  $T_s$ . The inside radius of the tubing is  $r_i$ , and the temperature  $T_t$  of the fluid in the tubing is a function of both depth  $Z$  and time  $t$ . The outside radius of the casing is  $r_o$ , and the temperature of the casing outer surface is  $T_c$ , also a function of depth and time.

The usual procedure for flow problems of this type is to solve the total-energy and mechanical-energy equations simultaneously to yield both temperature and pressure distributions. However, the solution may be approximated by the following considerations. The total-energy equation is



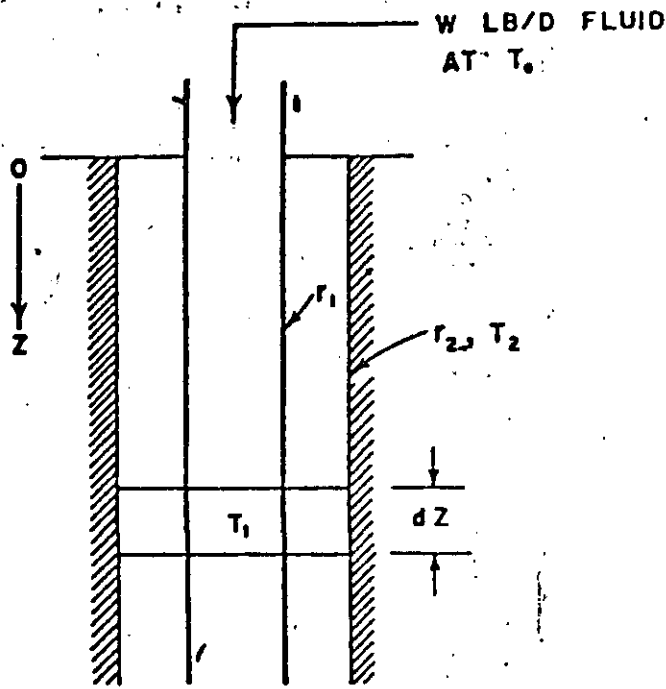


FIG. 9—SCHEMATIC OF WELLBORE HEAT PROBLEM.

$$dH + \frac{g dZ}{g.J} + \frac{udu}{g.J} = dQ - \frac{dW_i}{J} \quad (6)$$

Assuming steady flow of a single-phase fluid in a pipe, flow-work  $W_i$  is zero and Eq. 6 becomes

$$dH + \frac{g dZ}{g.J} + \frac{udu}{g.J} = dQ \quad (7)$$

LIQUID CASE

If the fluid flowing is a noncompressible liquid, the kinetic-energy term becomes zero. Thus,

$$dH + \frac{g dZ}{g.J} = dQ \quad (8)$$

But by definition, enthalpy is

$$dH = dE + \frac{d(PV)}{J} = dE + \frac{VdP}{J} \quad (9)$$

for a noncompressible liquid. Or

$$dH = cdT + \frac{VdP}{J} \quad (10)$$

Neglecting the flowing friction, the  $VdP$  term is equal to the change in fluid head, and the change in enthalpy is

$$dH \approx cdT + \frac{g dZ}{g.J} \quad (11)$$

Considering flow down the well, the increase in enthalpy due to increase in pressure is approximately equal to the loss in potential energy. Conversely, for flow up the well, the loss of enthalpy due to the decrease in pressure is approximately equal to the increase in potential energy.

As a result, the total-energy equation becomes

$$cdT \approx dQ \quad (12)$$

for a noncompressible liquid flowing vertically in a constant-diameter tube:

Assuming no phase changes, an approximate energy balance over the differential element of depth,  $dZ$ , yields: heat lost by liquid = heat transferred to casing, or

$$dq = -WcdT, = 2\pi r_1 U(T_1 - T_2)dZ \quad (13)$$

The rate of heat conduction from the casing to the surrounding formation may be expressed as

$$dq = \frac{2\pi k(T_2 - T_1)dZ}{f(t)} \quad (14)$$

Eq. 14 implies the assumption that heat transfers radially away from the wellbore. The time function  $f(t)$  depends on the conditions specified for heat conduction and will be discussed later. Assuming the geothermal temperature is a linear function\* of depth,

$$T_2 = aZ + b \quad (15)$$

Eqs. 14 and 15 may be substituted in Eq. 13 to yield

$$\frac{\partial T_1}{\partial Z} + \frac{T_1}{A} - \frac{(aZ + b)}{A} = 0, A \neq 0 \quad (16)$$

and

$$A = \frac{Wc[k + r_1 U f(t)]}{2\pi r_1 U k} \quad (17)$$

An integrating factor for Eq. 16 is  $e^{Z/A}$ . Thus,

$$T_1 e^{Z/A} = \int \frac{(aZ + b)e^{Z/A}}{A} dZ + C(t) \quad (18)$$

or

$$T_1 e^{Z/A} = (aZ - aA + b)e^{Z/A} + C(t) \quad (19)$$

or

$$T_1(Z, t) = aZ - aA + b + C(t)e^{-Z/A} \quad (20)$$

The function  $C(t)$  may be evaluated from the condition that  $T_1 = T_0(t)$  for  $Z = 0$ . Thus,

$$C(t) = T_0(t) + aA - b \quad (21)$$

And the final expression for liquid temperature as a function of depth and time is

$$T_1(Z, t) = aZ + b - aA + [T_0(t) + aA - b]e^{-Z/A} \quad (22)$$

where the time function  $A$  is defined by Eq. 17.

GAS CASE

If the fluid flowing is a perfect gas, enthalpy does not depend on pressure, and

$$dH = cdT \quad (23)$$

Thus, a potential-energy term will appear in the total energy balance. Eq. 13 then becomes for gas flow,

$$dq = -WcdT, \pm \frac{WdZ}{778} = 2\pi r_1 U(T_1 - T_2)dZ \quad (24)$$

where the plus sign on the potential-energy term is used for flow down the well and the negative sign is used for flow up the well. Simultaneous solution of Eq. 24 with Eqs. 14 and 15 yields

$$T_1(Z, t) = aZ + b - A \left( a \pm \frac{1}{778c} \right) + \left[ T_0 - b + A \left( a \pm \frac{1}{778c} \right) \right] e^{-Z/A} \quad (25)$$

The plus sign on the potential-energy term is used for flow down the well and depth taken positively increasing from the surface; the negative sign is used for flow up the well with depth taken positively increasing upward from the producing interval. Geothermal temperature must also be represented with depth increasing positively upward for flow up a well.

To apply Eqs. 22 or 25, it is necessary to evaluate the time function,  $f(t)$ . Eq. 14 can be rearranged to

$$f(t) = \frac{2\pi k(T_2 - T_1)}{dq/dZ} \quad (14A)$$

which is the definition of this time function. In this form, it is clear that the function  $f(t)$  has the same relationship to transient heat flow from a wellbore that the van Ever-

\*It is not necessary that geothermal temperature be linear with depth. Solutions may also be obtained if geothermal temperature is represented graphically as a function of depth.

dingen, Hurst" constant flux  $P(t)$  function has to transient fluid flow. In the case of the general wellbore heat problem, though, neither heat flux nor temperature at the wellbore remains constant except in special cases. A semi-rigorous treatment of transient heat conduction would involve a complex superposition at each depth. Thus, we wish to find approximate values of  $f(t)$  which will provide engineering accuracy. Success will be determined by comparison of calculated temperatures with measured field temperatures.

Fortunately, many solutions to transient heat and fluid flow exist which may be used to estimate  $f(t)$ . For example, the Moss and White' wellbore heat-transmission solution assumes that transient heat conduction to the earth can be represented by a line source losing heat at constant flux. Carslaw and Jaeger (page 283)' present graphical and analytical solutions for the cases of internal cylindrical sources losing heat at constant flux, constant temperature and under the radiation boundary condition. Fig. 1 presents the time function for several different internal boundary conditions. As can be seen from Fig. 1, the solutions presented converge at long times (approximately one week or more). This is completely analogous to pressure build-up theory that at sufficiently long times pressure is controlled by formation conditions.

For times less than a dimensionless time of 1,000 (i.e.,  $at/r_s^2 = 1,000$ ), the radiation boundary condition has been found to yield reasonable values for  $f(t)$ . The radiation inner boundary condition is

$$-k \left( \frac{\partial T}{\partial r} \right)_{r=r_s} = U_s (T_s - T_i) \dots \dots \dots (26)$$

where  $U_s = r_s U/r_s'$ . This boundary condition is analogous to the van Evertingen" skin effect, also well known in pressure build-up theory. Physically, Eq. 26 states that heat flow in the annular region between  $r_s$  and  $r_s'$  is controlled by steady-state convection, rather than conduction.

The solution for this case is presented by Carslaw and Jaeger (page 282)' and is reproduced on Fig. 1. The time function is seen to depend upon  $(r_s U/k)$ . However, the radiation boundary case does not depend strongly upon  $(r_s U/k)$  and the solution to this case approaches that of the constant-temperature cylindrical source as  $(r_s U/k)$  approaches infinity. Thus, the constant-temperature cylindrical-source solution is the recommended solution if thermal resistance in the wellbore is negligible. For times greater than those shown on Fig. 1, the line source solution as given by Eq. 5 is recommended. I am indebted to E. J. Couch for pointing out application of the radiation boundary case to evaluation of the time function.

### ASSOCIATED HEAT PROBLEMS

The solution presented by Eqs. 1, 1A and 2 also applies to wellbore heat problems other than injection down tubing. For example, injection down casing may be handled by computing the over-all coefficient including only the film coefficient at the casing wall and the resistance of the casing wall. Wellbore temperatures in a flowing well may be computed if the depth scale is referenced to the producing interval. Thus,  $T_w(t)$  becomes the producing formation temperature, and geothermal temperature should be expressed as a function of distance above the producing interval.

Other wellbore heat problems may be solved approximately by methods similar to those used for Eq. 1. That is, write heat balances over each flowing stream in the

wellbore and assume that heat loss from the wellbore may be represented by Eq. 14. If two or more flowing streams are involved, the result will be a higher-order differential equation than Eq. 16. Temperatures in each stream may be determined, if desired. Note that Eqs. 13, 14 and 15 could have been solved for  $T_s$ , the casing temperature. This problem may have significance in interpretation of temperatures measured in the annulus when fluid is flowing in the tubing. This problem is also important when considering whether temperatures will become great enough to damage cement in hot-fluid injection wells.

### SAMPLE CALCULATION FOR WATER-INJECTION WELL

For the sample calculation, the following field data will be assumed: injection rate, 4,790 B/WPD; surface water temperature, 58.5°F, casing size, 7 in.-23 lb (6.366 in. ID); casing shoe, 6,605 ft; no tubing; geothermal temperature, 70.0° + 0.0083°F/ft ( $Z$  ft); and injection period, approximately 75 days.

Film heat-transfer coefficients for water flowing vertically or horizontally in tubes are correlated as a function of the Reynolds number by McAdams on page 178 of Ref. 5. The Reynolds number for flow is

$$N_{Re} = \frac{DG}{\mu} = \frac{(6.366 \text{ in.})(4,790 \text{ B/D})}{\pi (6.366 \text{ in.})^2 (1.1 \text{ cp})} \left[ \frac{(350 \text{ lb/bbl})(12 \text{ in./ft}) + (2.42 \text{ lb/hr-ft-cp})(24 \text{ hr/day})}{(2.42 \text{ lb/hr-ft-cp})(24 \text{ hr/day})} \right] = 63,000$$

where  $D$  = inside diameter of tube, ft,

$G$  = flowing mass flux, lb/br-sq ft,

$\mu$  = viscosity at flowing conditions, lb/hr-ft, and

$N_{Re}$  = Reynolds number, dimensionless; from McAdams,' for Reynolds number of 63,000,

$$hD/k = 155(c_p/k)^{0.4}$$

where  $k$  = thermal conductivity of water, 0.339 Btu/hr-ft-°F,

$c_p$  = specific heat of water, Btu/lb-°F, and

$(c_p/k)$  = Prandtl number for water, 7.5, dimensionless (McAdams, page 414 of Ref. 5).

Thus

$$h = \frac{(155)(7.5)^{0.4}(0.339 \text{ Btu/hr-ft-°F})}{(6.366 \text{ in.})} (12 \text{ in./ft}) = 222 \text{ Btu/hr-sq ft-°F.}$$

From Eq. 3,

$$1/U = 1/h + x_s/k_s,$$

since only the resistance of the water film and casing wall is involved, and the difference in inside and outside area of casing wall is neglected. The thermal conductivity of steel is about 25 Btu/hr-ft-°F. Thus,

$$\frac{1}{U} = \frac{1}{222} + \frac{(7 - 6.366 \text{ in.})}{(2)(12 \text{ in./ft})(25 \text{ Btu/hr-ft-°F})} = 0.00451 + 0.00106 = 0.00557,$$

$$U = 180 \text{ Btu/hr-sq ft-°F}$$

$$= 4,320 \text{ Btu/day-sq ft-°F.}$$

The transient time function  $f(t)$  may be estimated from Fig. 1. The period of injection was about 75 days.

$$(at/r_i^2) = \frac{(0.04 \text{ sq ft/hr})(75 \text{ days})(24 \text{ hr/day})}{(3.5 \text{ in.}/12 \text{ in./ft})^2}$$

$$= 845$$

$$\log_e (at/r_i^2) = 2.93$$

from Fig. 1, the corresponding value of  $\log_e f(t)$  is 0.58.

Thus,

$$f(t) = 3.8$$

From Eq. 2,

$$A = \frac{Wc [k + r_i U f(t)]}{2\pi r_i U k}$$

$$= \left[ \frac{(4,790 \text{ B/D})(350 \text{ lb/bbl})}{2\pi(0.5)(6.366 \text{ in.})} \right]$$

$$\frac{(1 \text{ Btu/lb}\cdot\text{F})(12 \text{ in./ft})}{(24 \text{ hr/day})(1.4 \text{ Btu/hr}\cdot\text{ft}\cdot\text{F})(4,320 \text{ Btu/day}\cdot\text{sq ft}\cdot\text{F})}$$

$$\left[ \frac{(24 \text{ hr/day})(1.4 \text{ Btu/hr}\cdot\text{ft}\cdot\text{F})(4,320 \text{ Btu/day}\cdot\text{sq ft}\cdot\text{F})}{1.4(24) + \frac{(0.5)(6.366)}{(12)} \times (4,320)(3.8 \text{ Btu/day}\cdot\text{ft}\cdot\text{F})} \right]$$

$$A = 30,400 \text{ ft.}$$

Since the heat-transfer coefficient for water is large, a reasonable approximation would be that the value of  $U$  is infinite. This corresponds to the assumption that the temperatures of the water and casing are identical. The value of  $A$  computed for this case from Eq. 2A is 30,200 ft. Thus, the film coefficient for many water-injection cases should be high enough that assumption of an infinite overall coefficient is reasonable. This will generally not be true in the case of gas injection.

Temperatures may now be computed for any depth by means of Eq. 1.

$$T_i = aZ + b - aA + (T_o + aA - b) e^{-Z/A}$$

for 6,000 ft,

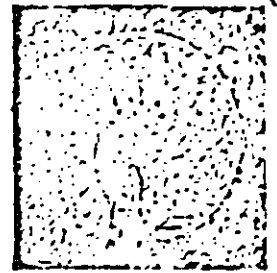
$$T_i = (0.0083^\circ\text{F/ft})(6,000 \text{ ft}) + 70^\circ\text{F}$$

$$- (0.0083^\circ\text{F/ft})(30,400 \text{ ft})$$

$$+ [58.5^\circ\text{F} + (0.0083)(30,400)^\circ\text{F} - 70^\circ\text{F}] e^{-6,000/30,400}$$

$$T_i = 65.2^\circ\text{F.}$$

\*\*\*



## Over-all Heat Transfer Coefficients in Steam And Hot Water Injection Wells

G. PAUL WILLHITE  
JUNIOR MEMBER AIME

CONTINENTAL OIL CO.  
PONCA CITY, OKLA.

### Abstract

Casing temperatures and wellbore heat losses are critical variables in steam and hot water injection wells. Several papers have been written presenting methods of estimating these parameters if the over-all heat transfer coefficient is known. The over-all heat transfer coefficient for a wellbore is developed from its component terms to promote a better understanding of the concept. Specific methods have been selected from the heat transfer literature for estimating the size of each heat transfer component. Simplified calculation procedures are suggested for determining the over-all heat transfer coefficient. Comparison of calculated and measured casing temperatures during steam injection confirms the basic formulation and applicability of the suggested procedure for engineering calculations.

### Introduction

The design of steam and hot water injection projects requires estimation of casing temperatures and wellbore heat losses. Several authors have shown that wellbore heat losses and casing temperatures can be calculated if the over-all heat transfer coefficient is known.<sup>1-3</sup> This article discusses methods of determining the over-all heat transfer coefficient from the process variables.

### Development

The steady-state rate of heat flow through a wellbore  $Q$  Btu/hour is proportional to the temperature difference between the fluid and the formation, and the cross-sectional area perpendicular to the direction of heat flow. The proportionality factor, called the over-all heat transfer coefficient, represents the net resistance of the flowing fluid, tubing, casing annulus, casing wall and cement sheath to the flow of heat. Thus, we can write

$$Q = U_o A_o \Delta T_o \quad \dots \quad (1)$$

Eq. 1 defines  $U_o$ , the over-all heat transfer coefficient based on the characteristic area  $A_o$ , and a characteristic tempera-

ture difference  $\Delta T_o$ . Subscript  $j$  in Eq. 1 identifies the surface upon which these quantities are based. In theory, any radial surface could be used to determine the characteristic area. Some choices are more convenient to work with than others. For example, if hot fluid is injected down tubing it is preferred to let  $A_o$  be the outside surface area of an incremental length of injection tubing,  $2\pi r_o \Delta L$ , and let  $\Delta T_o$  be the difference between the temperature of the flowing fluid  $T_o$  and the temperature at the cement-formation interface (the drill hole)  $T_i$ . Then  $U_o = U_{oi}$ , referring to the outside tubing surface area, and Eq. 1 would be

$$Q = 2\pi r_o U_{oi} (T_o - T_i) \Delta L \quad \dots \quad (2)$$

If the fluid is injected down the casing or casing annulus, the characteristic area could be the inside surface area of the casing, and Eq. 1 would be written as

$$Q = 2\pi r_{ci} U_{ci} (T_o - T_i) \Delta L \quad \dots \quad (3)$$

Subscript  $ci$  refers to the inside casing surface.

An expression for the over-all heat transfer coefficient for any well completion can be found by considering the heat transfer mechanisms between the flowing fluid and the cement-formation interface. A brief derivation of the over-all heat transfer coefficient is presented in the following paragraphs for the case of a hot fluid flowing through tubing insulated with a dry air annulus. Other cases can be derived easily once the basic concepts are understood. Fig. 1 shows the wellbore model which will be used to derive  $U_{oi}$ .

### Heat Transfer Mechanisms

The rate of heat transfer between the flowing fluid and inside tubing wall is given by Eq. 4.

$$Q = 2\pi r_{oi} h_i (T_o - T_{oi}) \Delta L \quad \dots \quad (4)$$

$h_i$  is defined by Eq. 4 and is the film coefficient for heat transfer based on the inside surface area of the tubing (subscript  $oi$ ) and the temperature difference between the flowing fluid and the inside tubing wall  $T_o - T_{oi}$ .

Heat flow through the tubing wall, casing wall and the cement sheath occurs by conduction. Fourier<sup>4</sup> discovered that the rate of heat flow through a body is directly proportional to the temperature gradient in the medium. The

Original manuscript received in Society of Petroleum Engineers office April 4, 1966. Revised manuscript received Jan. 20, 1967. Paper (SPE 1419) was presented at SPE Rocky Mountain Regional Meeting held in Denver, Colo., May 23-24, 1966. ©Copyright 1967 American Institute of Mining, Metallurgical, and Petroleum Engineers, Inc.

<sup>1</sup>References given at end of paper.

proportionality factor,  $k$ , is termed the thermal conductivity of the medium. In the radial system of the wellbore,

$$Q = -2\pi r k \frac{dT}{dr} \Delta L \dots \dots \dots (5)$$

Integration of Eq. 5 with  $Q$  constant gives Eqs. 6 through 8 for conduction through the tubing wall, casing wall and cement sheath.

$$\text{Tubing, } Q = \frac{2\pi k_{tu} (T_{ti} - T_{to}) \Delta L}{\ln \frac{r_{to}}{r_{ti}}} \dots \dots \dots (6)$$

$$\text{Casing, } Q = \frac{2\pi k_{ca} (T_{ci} - T_{co}) \Delta L}{\ln \frac{r_{co}}{r_{ci}}} \dots \dots \dots (7)$$

$$\text{Cement, } Q = \frac{2\pi k_{cm} (T_{co} - T_{fo}) \Delta L}{\ln \frac{r_{fo}}{r_{co}}} \dots \dots \dots (8)$$

Three modes of heat transfer are present in the casing annulus. Heat is conducted through the air contained in the annulus. Radiation and natural convection also occur. When a body is heated, radiant energy is emitted at a rate dependent on the temperature of the body. The amount of radiant energy transported between the tubing and casing depends on the view the surfaces have of each other and the emitting and absorbing characteristics of their surfaces. Heat transfer by natural convection in the annulus between the tubing and casing is caused by fluid motion resulting from the variation of density with temperature. Hot fluid near the tubing wall is less dense than the fluid in the center of the annulus and tends to rise. Similarly, the fluid near the casing wall is cooler (and denser) than in the center of the annulus and tends to fall. Fig. 2 is an interpretation of fluid motion in the casing annulus.

Radiation, natural convection and conduction are independent heat transfer mechanisms. Thus, the total heat flow in the annulus is the sum of the heat transferred by each of the above mechanisms. In practice, it is convenient to define the heat transfer rate through the annulus in terms of the heat transfer coefficients  $h$ , (natural con-

vection and conduction) and  $h_r$  (radiation). These coefficients are based on the outside surface area of the tubing ( $2\pi r_{ti} \Delta L$ ) and the temperature difference between the outside tubing surface and the inside casing surface. Thus,

$$Q = 2\pi r_{ti} (h_c + h_r) (T_{ti} - T_{ci}) \Delta L \dots \dots \dots (9)$$

We can now "assemble"  $U_{ca}$  from its component terms. Note that

$$T_{ti} - T_{fo} = (T_{ti} - T_{to}) + (T_{to} - T_{ci}) + (T_{ci} - T_{co}) + (T_{co} - T_{fo}) \dots \dots \dots (10)$$

Since heat flow in the well completion is assumed to be steady state at any particular time, the values of  $Q$  in Eqs. 4 and 6 through 9 are equal. Solving for the respective temperature differences in these equations and substituting them into Eq. 10 gives Eq. 11.

$$T_{ti} - T_{fo} = \frac{Q}{2\pi \Delta L} \left[ \frac{1}{r_{ti} h_c} + \frac{\ln \frac{r_{to}}{r_{ti}}}{k_{tu}} + \frac{1}{r_{ci} (h_c + h_r)} + \frac{\ln \frac{r_{co}}{r_{ci}}}{k_{ca}} + \frac{\ln \frac{r_{fo}}{r_{co}}}{k_{cm}} \right] \dots \dots \dots (11)$$

Comparison with Eq. 2 shows that

$$U_{ca} = \left[ \frac{r_{to}}{r_{ti} h_c} + \frac{r_{to} \ln \frac{r_{to}}{r_{ti}}}{k_{tu}} + \frac{1}{(h_c + h_r)} + \frac{r_{to} \ln \frac{r_{co}}{r_{ci}}}{k_{ca}} + \frac{r_{to} \ln \frac{r_{fo}}{r_{co}}}{k_{cm}} \right]^{-1} \dots \dots \dots (12)$$

In a similar manner, an expression for  $U_{ca}$  can be written to include the case when the injection tubing is insulated with commercial insulation of thickness  $\Delta r$  and thermal conductivity  $k_{ins}$ . Let  $r_{ins} - r_{to} = \Delta r$ . Then,

$$U_{ca} = \left[ \frac{r_{to}}{r_{ti} h_c} + \frac{r_{to} \ln \frac{r_{ins}}{r_{to}}}{k_{ins}} + \frac{r_{to} \ln \frac{r_{co}}{r_{ci}}}{k_{ca}} + \frac{r_{to}}{r_{ins} (h_c + h_r)} + \frac{r_{to} \ln \frac{r_{fo}}{r_{co}}}{k_{cm}} + \frac{r_{to} \ln \frac{r_{fo}}{r_{ins}}}{k_{ins}} \right]^{-1} \dots \dots \dots (13)$$

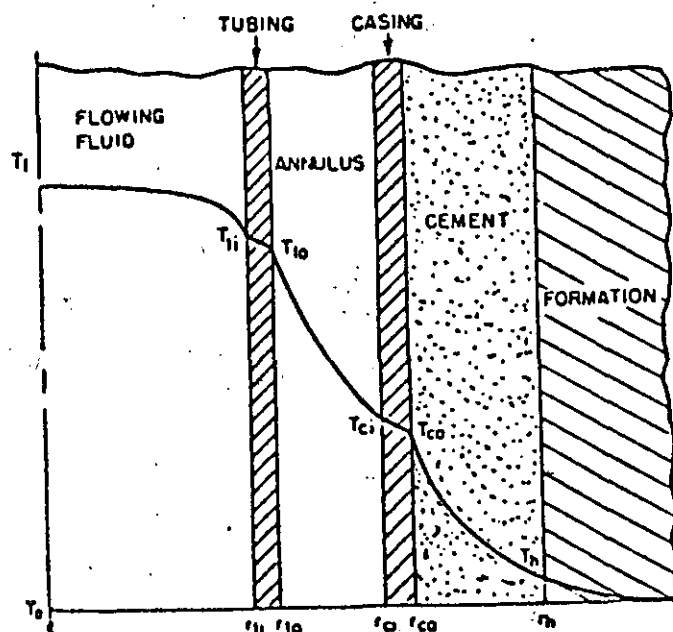


Fig. 1—Temperature distribution in an annular completion.

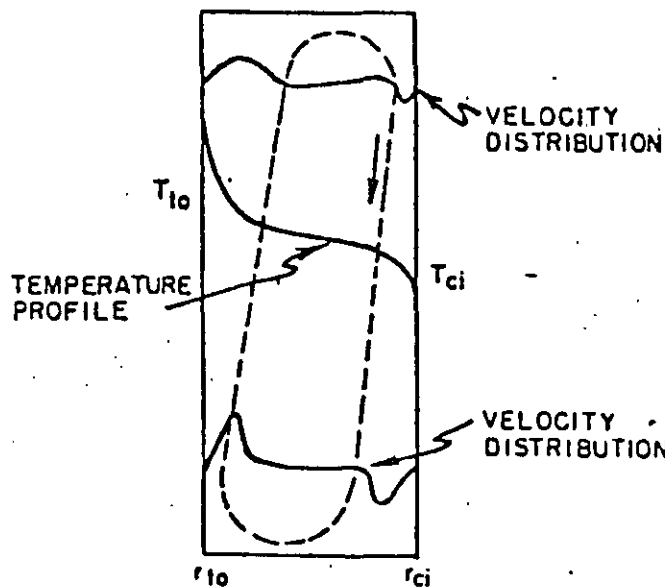


Fig. 2—Natural convection in the casing annulus.

The coefficients  $h_o'$  and  $h_i'$  in Eq. 13 are based on the surface area  $2\pi r_{oo} \Delta L$  and the temperature difference  $(T_{io} - T_{oi})$ .

$U_{oo}$  can be calculated from Eqs. 12 or 13 once  $k_{oo}$ ,  $k_{oi}$ ,  $k_{oo}$ ,  $h_o$ ,  $h_i$ , and  $h_c$  are determined. Representative values of the thermal conductivities of wellbore materials are presented in Table 1.

Table 1 shows that thermal conductivity of the tubing and casing steel is considerably higher than for the other materials in the wellbore. These terms thus constitute a small part of  $U_{oo}$  and can be deleted from Eqs. 12 and 13. This is equivalent to the assumption that  $T_{oi} = T_{oo}$  and  $T_{oo} = T_{oi}$ .

Film coefficients for water in turbulent flow are generally high enough (500 to 2,000 Btu/hour sq ft °F) that the assumption of an infinite film coefficient can be applied (i.e.,  $T_i = T_{oi}$ ). Condensation coefficients for steam are also large (500 to 4,000 Btu/hour sq ft °F). Thus, Eqs. 12 and 13 simplify to Eqs. 14 and 15.

$$U_{oo} = \frac{1}{\left( \frac{1}{h_o + h_c} + \frac{r_{oo} \ln \frac{r_o}{r_{oi}}}{k_{oo}} \right)} \quad (14)$$

$$U_{oo} = \frac{1}{\left[ \frac{r_{oi} \ln \frac{r_{io}}{r_{oi}}}{k_{oi}} + \frac{r_{oi}}{r_{oi} (h_o' + h_i')} + \frac{r_{oi} \ln \frac{r_o}{r_{oi}}}{k_{oo}} \right]} \quad (15)$$

#### Estimating $h_o$ and $h_i$

The radiant heat flux  $Q_r$  between the outer surface of the tubing at temperature  $T_{oi}$  and the inside surface of the casing at  $T_{oo}$  can be calculated from the Stefan-Boltzmann law.<sup>1</sup> That is,

$$Q_r = 2\pi r_{oi} \sigma F_{oi} (T_{oi}^* - T_{oo}^*) \Delta L \quad (16)$$

The asterisk refers to absolute temperature in °R ( $T + 460$ ) and  $\sigma$  is the Stefan-Boltzmann constant ( $1.713 \times 10^{-8}$  Btu/sq ft hour °R<sup>4</sup>).  $F_{oi}$  is the view factor representing the fraction of the radiation emitted from the external surface area of tubing  $A_{oi}$  which is intercepted by the inner casing surface area  $A_{oo}$ . This term relates the geometry of the wellbore and the emitting properties of the tubing and casing surfaces to the radiant heat flux. The emitting property of a surface is expressed in terms of its emissivity, a measure of its ability to absorb radiation. For a concentric annulus,

$$\frac{1}{F_{oi}} = \frac{1}{F_{oo}} + \left( \frac{1}{\epsilon_{oi}} - 1 \right) + \frac{A_{oo}}{A_{oi}} \left( \frac{1}{\epsilon_{oi}} - 1 \right) \quad (17)$$

In Eq. 17,  $\epsilon_{oi}$  and  $\epsilon_{oo}$  are the emissivities of the external tubing and internal casing surfaces, respectively.  $F_{oi}$  is the over-all interchange factor between the two surfaces.  $F_{oi}$  can usually be taken as 1.0 for wellbore heat transfer, and Eq. 17 reduces to

$$\frac{1}{F_{oi}} = \frac{1}{\epsilon_{oi}} + \frac{r_{oi}}{r_{oo}} \left( \frac{1}{\epsilon_{oi}} - 1 \right) \quad (18)$$

A heat transfer coefficient for radiation  $h_r$  can be defined by factoring Eq. 16 and substituting as shown in Eqs. 19 through 21.

$$Q_r = 2\pi r_{oi} h_r (T_{oi}^* - T_{oo}^*) \Delta L \quad (19)$$

$$= 2\pi r_{oi} h_r (T_{oi} - T_{oo}) \Delta L \quad (20)$$

where

$$h_r = \sigma F_{oi} (T_{oi}^* + T_{oo}^*) (T_{oi}^* + T_{oo}^*) \quad (21)$$

$h_r$  can be calculated if  $T_{oi}$  and  $T_{oo}$  are known.

#### Natural Convection ( $h_c$ )

Literature concerning natural convection coefficients indicates the difficulty of their evaluation. Although natural convection has been studied between enclosed vertical plates, little work has been done using vertical concentric cylinders. Results of vertical plate studies can be used for estimating  $h_c$  between vertical concentric cylinders if the effect of curvature is negligible.

Heat transfer by conduction and natural convection between the inside casing surface and the outside tubing surface is given by Eq. 22.

$$Q_c = \frac{2\pi k_{ac} (T_{oi} - T_{oo}) \Delta L}{\ln \frac{r_{oi}}{r_{oo}}} \quad (22)$$

where  $Q_c$  = heat transfer rate due to conduction and natural convection, Btu/hour

$k_{ac}$  = equivalent thermal conductivity of the annular fluid, Btu/hour ft °F.

When natural convection is small,  $k_{ac} = k_{oo}$ , the thermal conductivity of the fluid in the annulus. Since,

$$Q_c = 2\pi r_{oi} h_c (T_{oi} - T_{oo}) \Delta L \quad (23)$$

$$h_c = \frac{k_{ac}}{r_{oi} \ln \frac{r_{oi}}{r_{oo}}} \quad (24)$$

Dropkin and Sommerscales<sup>2</sup> measured values of  $k_{ac}$  between enclosed vertical plates. Their data were correlated as a function of the Grashof number  $Gr$  and the Prandtl number  $Pr$  of the annulus fluid. Eq. 25 is the correlation of Dropkin and Sommerscales in terms of the nomenclature of the wellbore,

$$\frac{k_{ac}}{k_{oo}} = 0.049 (GrPr)^{0.25} Pr^{0.14} \quad (25)$$

where

$$Gr = \frac{(r_{oi} - r_{oo})^3 \rho_{oo}^2 \beta (T_{oi} - T_{oo})}{\mu_{oo}} \quad (26)$$

and

$$Pr = \frac{c_{oo} \mu_{oo}}{k_{oo}} \quad (27)$$

Eq. 25 is valid for  $5 \times 10^4 < GrPr < 7.17 \times 10^6$ . The product of  $GrPr$  in wells with high-pressure gas in the annulus ranges from  $10^4$  to  $10^6$ , so the extrapolation error should not be large.

#### Calculation Procedure

Calculation of the radiation and natural convection coefficients from Eqs. 16 through 27 requires knowledge of

TABLE 1—THERMAL CONDUCTIVITY OF WELLBORE MATERIALS

Material	Thermal Conductivity (Btu/hr · ft · °F)
steel	25.0
Insulation (calcium silicate)	0.02 to 0.06
Cement:	
Wet (at completion)	0.5 to 0.6
Dry	0.2 to 0.4

the tubing and casing temperatures. Assume that the tubing temperature is known or can be calculated. This assumption will be discussed later. The casing temperature is calculated using Eq. 28, which was derived by combining Eqs. 2, 7 and 8.

$$T_{cs} = T_s + \left( \frac{\ln \frac{r_o}{r_{cs}}}{k_{ann}} + \frac{\ln \frac{r_{cs}}{r_o}}{k_{ann}} \right) r_{cs} U_{cs} (T_s - T_o) \quad (28)$$

By neglecting the thermal resistance of the film, tubing and casing, Eq. 28 reduces to Eq. 29.

$$T_{cs} = T_s + \frac{r_{cs} U_{cs} \ln \frac{r_o}{r_{cs}}}{k_{ann}} (T_{cs} - T_o) \quad (29)$$

An expression for  $T_s$  is needed to use Eq. 29. In developing the wellbore heat transfer model, the heat flow in the well completion (Eq. 2) is equated to the radial heat flow into the formation at the cement formation interface. Using Ramey's procedure<sup>1</sup> the radial flow of heat at the cement formation interface is approximated by Eq. 30.

$$Q = \frac{2\pi k_o (T_o - T_s) \Delta z}{f(t)} \quad (30)$$

Equating Eqs. 2 and 30 with  $\Delta z = \Delta L$  and then solving for  $T_s$  gives

$$T_s = \frac{T_o f(t) + \frac{k_o}{r_{cs} U_{cs}} T_{cs}}{f(t) + \frac{k_o}{r_{cs} U_{cs}}} \quad (31)$$

where  $T_o$  = undisturbed temperature of the formation at depth  $z$ , °F

$k_o$  = thermal conductivity of the formation at the depth  $z$ , Btu/hour ft °F

$f(t)$  = transient heat conduction function.

The transient heat conduction function  $f(t)$  enters into wellbore heat loss calculations because heat flow in the surrounding formation varies with time. Heat losses to these formations are large initially, but decrease with time as thermal resistance to the flow of heat builds up in the formation. Methods of evaluating  $f(t)$  have been discussed in detail by Ramey<sup>1</sup> and the reader is referred to his paper for background material.  $f(t)$  can be obtained from Table 2 for short injection times. Table 2 was prepared using the data and calculation procedure of Jessop.<sup>20</sup> It

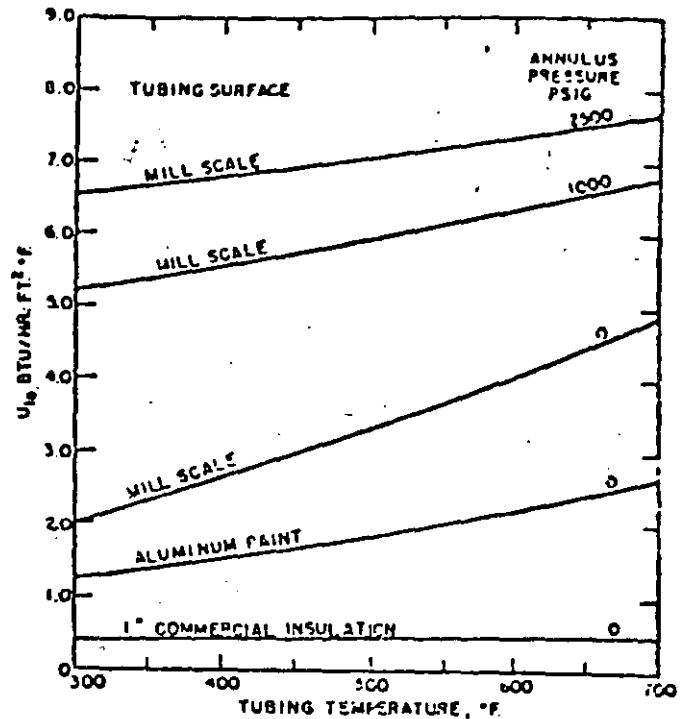


Fig. 3—Variation of  $U_{cs}$  with tubing temperature for parameters of Table 3.

is believed that values of  $f(t)$  are accurate to three significant figures. An approximate value can be calculated using Eq. 32 for longer times. Short injection time is usually considered to be less than 7 days.

$$f(t) = \ln \frac{2\sqrt{at}}{r_o} - 0.29 \quad (32)$$

Examination of Eqs. 29 and 31 shows that the casing temperature is a function of  $U_{cs}$ . As previously noted,  $T_{cs}$  is used to calculate  $h_o$  and  $h_{cs}$ , the natural convection and radiation heat transfer coefficients for the casing annulus. Hence, a trial-and-error or iterative solution is required to determine the proper combination of  $U_{cs}$  and  $T_{cs}$  when radiation and natural convection are the primary heat transfer mechanisms. The iterative solution assumes a value for  $T_{cs}$  to calculate  $U_{cs}$ . A new value of  $T_{cs}$  is calculated using this value of  $U_{cs}$  in Eqs. 29 and 31. This procedure is repeated until convergence is obtained. Normally, three calculations are sufficient to determine  $T_{cs}$  and  $U_{cs}$  for a particular tubing temperature and injection time.

The calculation procedure discussed in the preceding

TABLE 2—TIME FUNCTION  $f(t)$  FOR THE RADIATION BOUNDARY CONDITION MODEL

$\frac{r_{cs} U_{cs}}{k_o} = \frac{at}{r_o^2}$	0.01	0.02	0.05	0.1	0.2	0.5	1.0	2.0	5.0	10	20	50	100	$\infty$
0.1	0.313	0.313	0.314	0.316	0.318	0.323	0.330	0.345	0.373	0.396	0.417	0.433	0.438	0.445
0.2	0.423	0.423	0.424	0.427	0.430	0.439	0.452	0.473	0.511	0.538	0.568	0.572	0.578	0.528
0.5	0.616	0.617	0.619	0.623	0.629	0.644	0.666	0.698	0.745	0.772	0.790	0.802	0.806	0.811
1.0	0.802	0.803	0.806	0.811	0.820	0.842	0.872	0.910	0.958	0.984	1.00	1.01	1.01	1.02
2.0	1.02	1.02	1.03	1.04	1.05	1.08	1.11	1.15	1.20	1.22	1.24	1.24	1.25	1.25
5.0	1.36	1.37	1.37	1.38	1.40	1.44	1.48	1.52	1.56	1.57	1.58	1.59	1.59	1.59
10.0	1.65	1.66	1.66	1.67	1.69	1.73	1.77	1.81	1.84	1.86	1.86	1.87	1.87	1.88
20.0	1.96	1.97	1.97	1.99	2.00	2.05	2.09	2.12	2.15	2.16	2.16	2.17	2.17	2.17
50.0	2.39	2.39	2.40	2.42	2.44	2.48	2.51	2.54	2.56	2.57	2.57	2.57	2.58	2.58
100.0	2.73	2.73	2.74	2.75	2.77	2.81	2.84	2.86	2.88	2.89	2.89	2.89	2.89	2.90

paragraph was used to prepare Fig. 3, a plot of  $U_{oi}$  vs tubing temperature for several modifications of an annular completion. Steam was assumed to be injected down 2 3/8-in. tubing in 7-in. casing for 14 days. The casing was cemented to the surface in a 9 3/8-in. hole with a high-temperature resistance cement. Parameters used to calculate  $U_{oi}$  are summarized in Table 3.

The five completions presented on Fig. 3 were selected to illustrate the heat transfer mechanisms in the annuli of steam and hot water injection wells. A standard completion is 2 3/8-in. tubing (mill-scale surface) set on a packer with the annulus open to the atmosphere. Radiation is the primary heat transfer mechanism in this completion. Since radiation varies with the emitting properties of the tubing surface, the radiation heat transfer coefficient  $h_r$  can be lowered by coating the tubing surface with a highly reflective material. This is shown by the curve for aluminum paint which was assumed to have an emissivity of 0.4.

Another completion technique is to use high-pressure air or nitrogen to eliminate the down-hole packer. The radiation coefficient is nearly the same value as when a packer is used. However, the natural convection coefficient is larger by one or two orders of magnitude because the density of the gas in the annulus increases. The effect of natural convection is illustrated by comparing the curves with annulus pressures of 0, 1,000 and 2,500 psig.

Radiation and natural convection can be minimized by insulating the injection tubing. Commercial insulation has such a low thermal conductivity (0.02 to 0.06 Btu/hour ft °F) that conduction through the insulation controls wellbore heat transfer. Radiation and natural convection coefficients based on the outer surface of the insulation can be large, but their effect on  $U_{oi}$  is small since they are in series with the high thermal resistance of the commercial insulation. The lower curve on Fig. 3 was calculated for calcium silicate insulation 1 in. thick.

Fig. 3 is useful in estimating the over-all heat transfer coefficient for wells with parameters other than those in Table 3. The following procedure is suggested:

1. Select a value of  $U_{oi}$  corresponding to the temperature of the fluid or tubing from Fig. 3 for the corresponding well completion.
2. Determine  $f(t)$  from Table 2 or Eq. 32.
3. Calculate  $T_{wi}$  using Eq. 31.
4. Calculate  $T_{oi}$  from Eq. 29.
5. Then estimate  $h_c$  (Eqs. 18 and 21) and  $h_r$  (Eqs. 24 through 27).
6. Determine a new value of  $U_{oi}$  from Eqs. 14 or 15.
7. Compare the calculated value of  $U_{oi}$  with the value used in Steps 2 through 5 and repeat Steps 2 through 6 until agreement is obtained between two successive trials. Normally, three sets of calculations are sufficient. A sample calculation is presented in the Appendix.

#### Variable Tubing Temperature

Fig. 3 relates  $U_{oi}$  to the fluid or tubing temperature when the formation temperature is 80F. Fluid temperatures may vary considerably with depth when hot water or superheated steam is injected.<sup>24</sup> The over-all heat transfer coefficient will also vary with depth. In this case the depth step method discussed by Satter<sup>1</sup> can be used to determine the tubing temperature at each depth in the well. This calculation procedure involves two successive iterative solutions because both tubing and casing temperatures depend on the over-all heat transfer coefficient.

TABLE 3—PARAMETERS FOR FIG. 3

Hole size:	9.625 in.
Casing (7 in., 26 lb, J-55):	
OD	7.000 in.
ID	6.276 in.
Tubing (2 3/8 in., 6.4 lb, J-55):	
OD	2.875 in.
ID	2.441 in.
$k_c$ :	1.4 Btu/hr ft °F <sup>2</sup>
$k_{ann}$ :	0.51 Btu/hr ft °F
$k_{ins}$ :	0.0256 + (T-50) (3.67 × 10 <sup>-4</sup> ) Btu/hr ft °F
$a$ :	0.04 sq ft/hr
$\epsilon_{ms} = \epsilon_{ms}$ (mill scale):	0.9
$\epsilon_{ms}$ (aluminum paint):	0.4
$T_o$ :	80F

Wellbore heat losses and casing temperatures for the injection of wet steam are often calculated by assuming that  $T_o$ ,  $T_{wi}$  and  $T_{oi}$  are equal to the injection temperature. A single value of  $U_{oi}$  evaluated at the injection temperature and at the average formation temperature is used in these calculations.

This is an approximation because the temperature of the flowing fluid may be lower, equal to or higher than the injection temperatures. The actual value depends on the relationship between wellbore heat loss, two-phase frictional pressure drop and the pressure change due to density variations. In many projects, operating conditions are such that the difference between the sand face temperature and the injection temperature is less than 10 percent. Thus, a single value of  $U_{oi}$  may provide sufficient accuracy for engineering calculations. This can be checked by varying the fluid temperature in accordance with rough estimates of the pressure changes. If approximate calculations indicate large temperature changes, simultaneous solution of the total energy and mechanical energy equations may be required for good estimates of heat losses and casing temperatures.

#### Practical Application of the Over-all Heat Transfer Coefficient in Engineering Calculations

Casing failure is a known problem in production wells stimulated with steam. While it is not always possible to determine exactly when a casing will fail, a knowledge of the casing temperature is essential to estimate and minimize thermal stresses in the casing. Casing temperatures were calculated for the injection of steam at 650F using the parameters of Table 3. These temperatures are plotted against injection time on Fig. 4 for the five completions of Fig. 3.

The cement sheath does not remain wet at shallow depths during steam or hot water injection. As the casing temperature increases, the boiling point of water in the cement may exceed the prevailing hydrostatic pressure. The water is either superheated in situ or driven from the cement into the surrounding formation by vaporization. The latter process allows the cement sheath to dry, and its thermal conductivity will decrease to the values in Table 1. When drying occurs,  $U_{oi}$  is approximated by reducing the thermal conductivity of the cement to the lower values. Then the over-all heat transfer coefficient represents the conditions after drying for all injection times. As an example, casing temperatures for the low-pressure annulus of Fig. 4 were recalculated using 0.2 Btu/hour ft °F for the thermal conductivity of dry cement. The temperatures are shown as the dashed curve on Fig. 5. The



corresponding curve from Fig. 4 was reproduced on Fig. 5 for comparison.

Drying may also extend into the formation if the formation is porous and the temperature of the drill hole  $T_1$  exceeds the boiling point of water at formation pressure. To investigate this phenomenon, a dry zone was included in the over-all heat transfer coefficient. Fig. 6 is the dry zone heat transfer model. The radius of the dry zone  $r_d$  is defined as the point where the temperature of the dry zone  $T_d$  is equal to the boiling point of water at hydrostatic pressure. This adds another conduction term to the over-all heat transfer coefficient so that Eqs. 14 and 15 become

$$U_{10} = \left( \frac{1}{h_o + h_c} + \frac{r_{10} \ln \frac{r_b}{r_{10}}}{k_{100}} + \frac{r_{10} \ln \frac{r_d}{r_b}}{k_d} \right)^{-1} \quad (33)$$

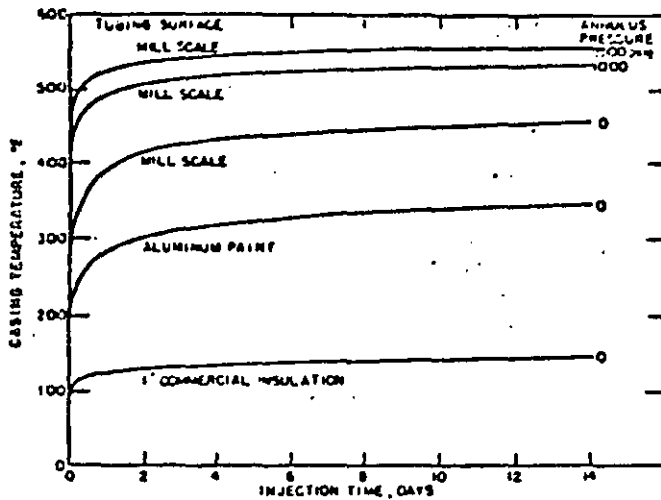


Fig. 4—Calculated casing temperatures when 650F steam is injected down tubing.

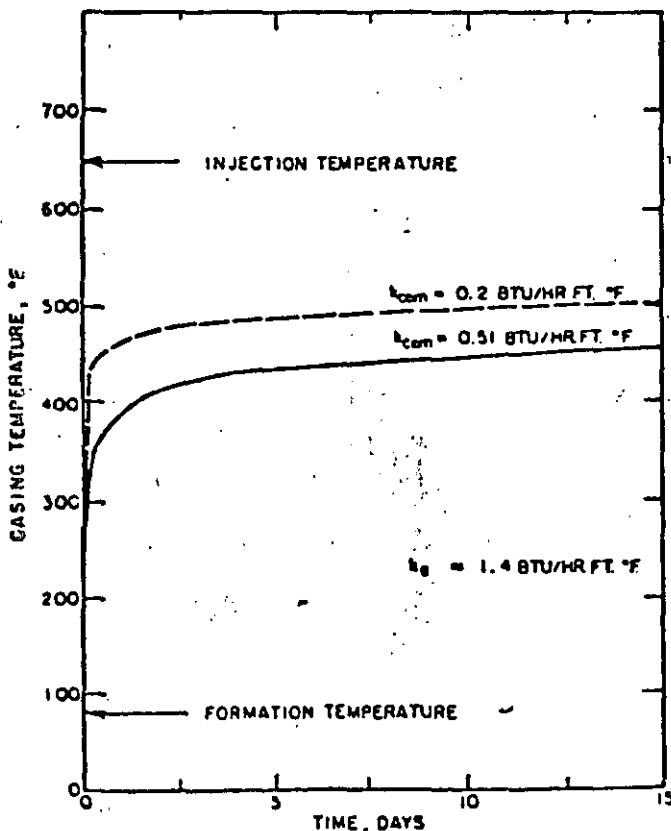


Fig. 5—Comparison of casing temperatures for dry and wet cements.

$$U_{10} = \left[ \frac{r_{10} \ln \frac{r_{10}}{r_{10}}}{k_{100}} + \frac{r_{10}}{r_{10} (h_o + h_c)} + \frac{r_{10} \ln \frac{r_b}{r_{10}}}{k_{100}} + \frac{r_{10} \ln \frac{r_d}{r_b}}{k_d} \right]^{-1} \quad (34)$$

Now the over-all heat transfer coefficient is based on the outside surface area of the tubing and the temperature difference between the injected fluid and the dry zone interface. The radius of the dry zone is substituted for  $r_b$  in the calculation of  $f(i)$  from Eq. 32 or Table 2. With these changes the equations for the casing temperature and the dry zone interface temperature are

$$T_{10} = T_1 + \left( \frac{\ln \frac{r_b}{r_{10}}}{k_{100}} + \frac{\ln \frac{r_d}{r_b}}{k_d} \right) r_{10} U_{10} (T_1 - T_d) \quad (35)$$

$$T_d = \frac{T_1 f(i) + \frac{k_s}{r_{10} U_{10}} T_s}{f(i) + \frac{k_s}{r_{10} U_{10}}} \quad (36)$$

This model assumes that the dry zone forms at time zero, although it is known that drying will not begin until the drill hole temperature  $T_1$  is at least 212F. The dry zone radius is not constant but will change with time. As a result, the model does not represent the vaporization and condensation which occurs during the formation of the dry zone. It will indicate the maximum effect of a dry zone. A numerical solution would provide a better representation if the problem is severe enough to warrant further investigation.

Calculations were made to estimate the effect of a dry zone on casing temperature. An unconsolidated sand was used as the formation because it shows the effect of a large difference between the wet and dry thermal conductivities; i.e., 1.6 Btu/hour ft °F for the wet zone and 0.152 Btu/hour ft °F for the dry. These values correspond to the data of Woodside and Cliffe<sup>17</sup> for Ottawa sand (100 lb/cu ft). Calculated casing temperatures were 50 to 75F higher than the dry cement curve of Fig. 5 when  $T_1 = 212$ F and  $r_d$  was evaluated at the maximum injection time. The value of  $r_d$  for  $T_1 = 212$ F was found by plotting calculated values of  $T_1$  against assumed values of  $r_d$ .

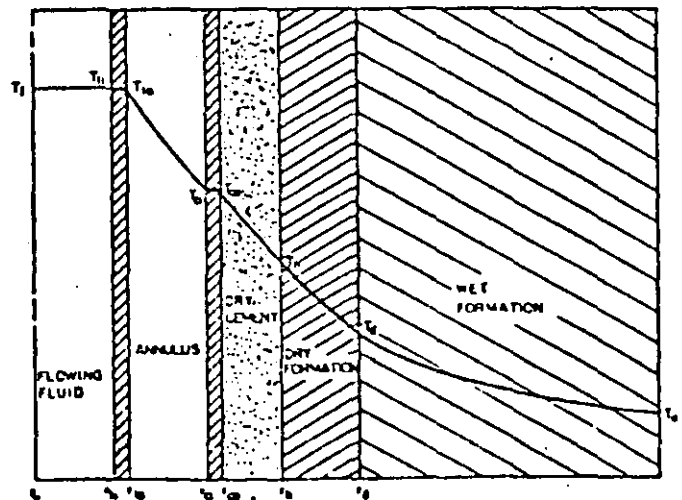


Fig. 6—Dry zone heat transfer model.

## Field Results

Casing temperatures were measured during steam injection in one of our steam injection projects. Steam was injected down tubing set on a packer in 7-in. casing. Casing temperatures were calculated for these conditions using  $k_c = 1.0$  Btu/hour ft °F,  $k_{c,m} = 0.2$  Btu/hour ft °F and a drill hole diameter of 12 in. Measured and calculated casing temperatures are compared on Fig. 7. The long-term agreement is well within the accuracy required for engineering calculations.

There was a large difference between the calculated and measured temperatures during the first 48 hours of injection, part of which was due to lower injection temperatures (50F) during this time. The remainder of the difference includes unsteady-state effects in the wellbore. It was previously stated that the wellbore model represents a quasi-steady system. That is, steady-state equations are used to describe heat transfer through the region included in the over-all heat transfer coefficient. Transient effects such as vaporization of water in the cement and surrounding formation are not included. Thus, a significant difference between calculated and measured casing temperatures should be expected during the short transient period after injection begins.

## Conclusions

It has been shown that the over-all heat transfer coefficient can be estimated from the process variables. A brief derivation was presented to indicate how various heat transfer mechanisms are included in an over-all heat transfer coefficient. A simplified calculation procedure was outlined for determining the over-all heat transfer coefficient. Comparison of predicted and field casing temperatures confirms the basic formulation and applicability of the suggested procedures for engineering calculations.

## Nomenclature

- $A_j$  = characteristic surface area, sq ft (subscript  $j$  identifies the surface)  
 $A_{i,c}$  = inside surface area of the casing, sq ft  
 $A_{o,t}$  = outside surface area of the tubing, sq ft  
 $c_{a,m}$  = heat capacity of the fluid in the annulus at the average annulus temperature, Btu/lb °F  
 $f(t)$  = transient time function, dimensionless

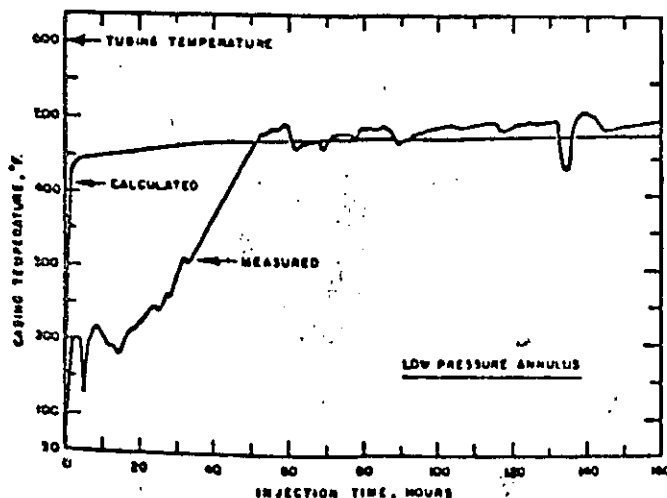


Fig. 7—Comparison of field data with calculated results.

$F_{o,i}$  = view factor based on outside tubing and inside casing surfaces, dimensionless

$\bar{F}_{o,i}$  = over-all interchange factor between the outside tubing and inside casing surfaces, dimensionless

$g$  = acceleration due to gravity,  $4.17 \times 10^8$  ft/hr<sup>2</sup>

$Gr$  = Grashof number, dimensionless

$h_c$  = heat transfer coefficient for natural convection based on the outside tubing surface and the temperature difference between the outside tubing and inside casing surfaces, Btu/hr sq ft °F

$h_c'$  = heat transfer coefficient for natural convection based on the outside insulation surface and the temperature difference between the outside insulation and inside casing surface, Btu/hr sq ft °F

$h_f$  = film coefficient for heat transfer or condensation coefficient based on inside tubing or casing surface and the temperature difference between the flowing fluid and either of these surfaces, Btu/hr sq ft °F

$h_r$  = heat transfer coefficient for radiation based on the outside tubing surface and the temperature difference between the outside tubing and inside casing surfaces, Btu/hr sq ft °F

$h_r'$  = heat transfer coefficient for radiation based on outside insulation surface and the temperature difference between the outside insulation and inside casing surfaces, Btu/hr sq ft °F

$k_{c,m}$  = thermal conductivity of the casing material at the average casing temperature, Btu/hr ft °F

$k_{c,m}$  = thermal conductivity of the cement at the average cement temperature and pressure, Btu/hr ft °F

$k_d$  = thermal conductivity of the dry zone, Btu/hr ft °F

$k_f$  = thermal conductivity of the formation, Btu/hr ft °F

$k_a$  = thermal conductivity, Btu/hr ft °F

$k_{a,m}$  = thermal conductivity of the fluid in the annulus at the average temperature and pressure of the annulus, Btu/hr ft °F

$k_{a,n}$  = equivalent thermal conductivity of the annular fluid with natural convection effects, evaluated at the average temperature and pressure of the annulus, Btu/hr ft °F

$k_{i,m}$  = thermal conductivity of the insulation at the average temperature of the insulation, Btu/hr ft °F

$k_{t,m}$  = thermal conductivity of the tubing material at the average tubing temperature, Btu/hr ft °F

$Pr$  = Prandtl number, dimensionless

$Q$  = heat flow through the wellbore, Btu/hr

$Q_c$  = heat flow in the annulus by natural convection and conduction, Btu/hr

$Q_r$  = heat flow in the annulus due to radiation, Btu/hr

$r$  = radius, ft

$r_{i,c}$  = inside radius of casing, ft

$r_{o,c}$  = outside radius of casing, ft

$r_d$  = radius of dry zone (distance where  $T_d$  is equal to the boiling point of water at formation pressure)

$r_h$  = radius of drill hole, ft

$r_{i,i}$  = radius of the outside insulation surface, ft

$r_{i,t}$  = inside radius of tubing, ft

$r_{o,t}$  = outside radius of tubing, ft

$t$  = time, hours or units consistent with  $a$

$T$  = temperature, °F

- $T^{\circ}$  = absolute temperature,  $^{\circ}R = ^{\circ}F + 460$
- $T_{av}$  = average temperature of the fluid in the annulus,  $^{\circ}F$
- $T_{is}$  = temperature of inside casing surface,  $^{\circ}F$
- $T_{os}$  = temperature of outside casing surface,  $^{\circ}F$
- $T_b$  = boiling point of water at formation pressure,  $^{\circ}F$
- $T_f$  = temperature of flowing fluid,  $^{\circ}F$
- $T_o$  = undisturbed temperature of the formation,  $^{\circ}F$
- $T_c$  = temperature at cement-formation interface,  $^{\circ}F$
- $T_{ins}$  = temperature of the outside surface of the insulation,  $^{\circ}F$
- $T_{it}$  = temperature of inside tubing surface,  $^{\circ}F$
- $T_{ot}$  = temperature of outside tubing surface,  $^{\circ}F$
- $U_{is}$  = over-all heat transfer coefficient based on the inside casing surface and the temperature difference between the fluid and cement-formation interface, Btu/hr sq ft  $^{\circ}F$
- $U_i$  = over-all heat transfer coefficient based on the characteristic surface area  $A_i$  and characteristic temperature difference  $\Delta T_i$ , Btu/hr sq ft  $^{\circ}F$
- $U_{os}$  = over-all heat transfer coefficient based on the outside tubing surface and the temperature difference between fluid and cement-formation interface, Btu/hr sq ft  $^{\circ}F$
- $z$  = depth, ft
- $\alpha$  = thermal diffusivity of the earth, sq ft/hr
- $\beta$  = thermal volumetric expansion coefficient of the

fluid in the annulus,  $^{\circ}R^{-1} = \frac{1}{T_{av}^{\circ}}$  for an ideal gas, or generally =  $-\frac{1}{P_{av}} \left( \frac{\partial P_{av}}{\partial T} \right)_P$ , where  $P$  is the annulus pressure

- $\Delta L$  = increment of tubing or casing length, ft
- $\Delta r$  = insulation thickness, ft
- $\Delta T_i$  = characteristic temperature difference related to  $U_i$  and the surface area  $A_i$ ,  $^{\circ}F$
- $\epsilon_{os}$  = emissivity of outside tubing surface, dimensionless
- $\epsilon_{is}$  = emissivity of inside casing surface, dimensionless
- $\sigma$  = Stefan-Boltzmann constant,  $1.713 \times 10^{-9}$ /sq ft hr  $^{\circ}R^4$
- $\rho_{av}$  = density of the fluid in the annulus at  $T_{av}$  and pressure  $P$ , lb/cu ft
- $\mu_{av}$  = viscosity of the fluid in the annulus at  $T_{av}$  and  $P$ , lb mass/ft hr

**Acknowledgments**

The author wishes to express his appreciation to the management of Continental Oil Co. for permission to publish this article. The comments of W. L. Martin with Continental in Ponca City, Okla., and the assistance of W. K. Dietrich with Continental in Denver in obtaining the field data are gratefully acknowledged. J. A. Sievert, Continental, Ponca City, assisted in the evaluation of  $f(t)$ .

**References**

1. Bohlenar, T.: "The Thermal Field of the Earth's Crust and Its Influence on the Ventilation of Deep and Hot Mines", *Acta Technica Acad. Scient. Hung.*, XVI Fasc 3-4, 415-427.
2. Ramey, H. J., Jr.: "Wellbore Heat Transmission", *J. Pet. Tech.* (April, 1962) 427-433.

3. Leutwyler, Kurt and Bigelow, H. L.: "Temperature Effects on Subsurface Equipment in Steam Injection Systems", *J. Pet. Tech.* (Jan., 1965) 93-101.
4. Satter, Abdul: "Heat Losses During Flow of Steam Down a Wellbore", *J. Pet. Tech.* (July, 1965) 845-851.
5. Leutwyler, Kurt: "Casing Temperature Studies in Steam Injection Wells", *J. Pet. Tech.* (Sept., 1966) 1157-1162.
6. Fourier, J. B. J.: "Theorie Analytique de la Chaleur", Gauthier-Villars, Paris (1822); English translation by Freeman, Cambridge (1878).
7. Eckert, E. R. G. and Carlson, W. D.: "Natural Convection in an Air Layer Enclosed Between Two Vertical Plates with Different Temperatures", *Int. J. Heat Mass Transfer* (1961) 2, 106-120.
8. McAdams, W. H.: *Heat Transmission*, 3rd Ed., McGraw Hill Book Co., New York (1954).
9. Dropkin, D. and Sommerscales, E.: "Heat Transfer by Natural Convection in Liquids Confined by Two Parallel Plates Inclined at Various Angles with Respect to the Horizontal", *J. Heat Transfer; Trans., ASME, Series C* (Feb., 1965) 87, 77-84.
10. Jessop, A. M.: "Heat Flow in a System of Cylindrical Symmetry", *Can. J. of Physics* (1966) 44, 677-679.
11. Personal communication.
12. Woodside, W. and Cliffe, J. E.: "Heat and Moisture Transfer in Closed Systems of Two Granular Materials", *Soil Science* (1959) 87, No. 2, 75-82.

**APPENDIX**

**Sample Calculation**

Steam at 600F is injected down 3 1/2-in. tubing set on a packer in 9 5/8-in., 53.5-lb/ft, N-80 casing. The annulus contains a stagnant gas at 14.7 psia and the casing is cemented to surface in a 12-in. hole. A temperature survey in the well indicates a mean subsurface temperature of 100F. The reservoir is at 1,000 ft. Estimate the over-all heat transfer coefficient, average casing temperature and wellbore heat loss after 21 days of continuous injection.

**Data**

- $r_{is} = 0.146$  ft
- $r_{os} = 0.355$  ft
- $r_{ca} = 0.400$  ft
- $r_b = 0.500$  ft
- $\alpha = 0.0286$  sq ft/hr
- $k_c = 1.0$  Btu/hr sq ft  $^{\circ}F/ft$
- $\epsilon_{is} = \epsilon_{os} = 0.9$
- $k_{ins} = 0.2$  Btu/hr sq ft  $^{\circ}F/ft$

Step 1—estimate  $U_{is}$  from Fig 3 for an injection temperature of 600F and the low pressure annulus:  $U_{is} = 4.05$  Btu/hr sq ft  $^{\circ}F$ .

Step 2—calculate  $f(t)$ . Since  $t = 21$  days, Eq. 32 can be

used:  $f(t) = \ln \frac{2\sqrt{(0.0286)(504)}}{0.5} - 0.29 = 2.43$ .

Step 3—calculate  $T_c$  (Eq. 31):

$$T_c = \frac{(600)(2.43) + \frac{1.0}{(0.146)(4.05)}(100)}{2.43 + \frac{1.0}{(0.146)(4.05)}} = 395F.$$

Step 4—calculate  $T_{av}$  neglecting casing and surface resistances (Eq. 29):

$$T_{av} = 395 + \frac{(0.146)(4.05)}{0.2} \ln \frac{0.5}{0.4} (600 - 395) = 530F.$$

Step 5—estimate  $h_w$  (Eqs. 18 and 21):

$$F_{w,0} = \frac{1}{\frac{1}{0.9} + \frac{0.146}{0.355} \left( \frac{1}{0.9} - 1.0 \right)} = 0.865$$

$$h_w = (0.865) (1.773 \times 10^{-7}) [(600 + 460)^2 + (530 + 460)^2] [(600 + 460) + (530 + 460)] = 6.39 \text{ Btu/hr sq ft } ^\circ\text{F}$$

estimate  $h_c$  (Eqs. 24 through 27):

$$T_{w,0} = 565\text{F}$$

$$\rho_{w,0} = 0.0388 \text{ lb/cu ft}$$

$$\mu_{w,0} = 0.069 \text{ lb mass/ft hr}$$

$$c_{w,0} = 0.245 \text{ Btu/lb } ^\circ\text{F}$$

$$k_{w,0} = 0.0255 \text{ Btu/hr sq ft } ^\circ\text{F/ft}$$

$$\beta = \frac{1}{T_{w,0}}$$

$$= 9.75 \times 10^{-4} \text{ } ^\circ\text{R}^{-1}$$

calculate Pr using Eq. 27:

$$Pr = \frac{(0.245)(0.069)}{0.0255} = 0.66$$

$$r_{w,0} L_{r,w,0} = 0.209 \text{ ft}$$

calculate Gr using Eq. 26:

$$Gr = \frac{(0.209)^3 (4.17 \times 10^7) (0.0388)^2 (9.75 \times 10^{-4}) (600 - 530)}{(0.069)^2}$$

$$= 8.26 \times 10^4$$

calculate  $k_w$  from Eq. 25:

$$\frac{k_w}{k_{w,0}} = (0.049) [(8.26 \times 10^4) (0.66)]^{0.4} = (0.66)^{0.4} = 1.81$$

$$k_w = 0.046 \text{ Btu/hr ft } ^\circ\text{F}$$

$$\text{then, } h_c = \frac{0.046}{0.146 \ln \frac{0.355}{0.146}}$$

$$= 0.36 \text{ Btu/hr sq ft } ^\circ\text{F}$$

Step 6—calculate  $U_{w,0}$  (Eq. 14):

$$U_{w,0} = \left( \frac{1}{6.39 + 0.36} + \frac{0.146 \ln \frac{0.5}{0.4}}{0.2} \right)^{-1}$$

$$= 3.22 \text{ Btu/hr sq ft } ^\circ\text{F}$$

Step 7—since the assumed and calculated values of  $U_{w,0}$  do not agree, repeat Steps 2 through 6 until agreement is obtained between two successive trials. Results of successive iterations are tabulated below.

Trial	Assumed		Calculated			
	$U_{w,0}$ (Btu/hr sq ft $^\circ\text{F}$ )	$T_w$ ( $^\circ\text{F}$ )	$T_{w,0}$ ( $^\circ\text{F}$ )	$h_c$ (Btu/hr sq ft $^\circ\text{F}$ )	$h_w$ (Btu/hr sq ft $^\circ\text{F}$ )	$U_{w,0}$ (Btu/hr sq ft $^\circ\text{F}$ )
1	4.05	395	530	6.39	0.36	3.22
2	3.22	367	487	6.00	0.42	3.15
3	3.15	364	485	5.97	0.42	3.14

The wellbore heat loss can be calculated using Eq. 2:  
 $Q = (2\pi) (0.146) (3.14) (600 - 364) (1,000) = 680,000 \text{ Btu/hr}$

\*\*\*

A BIOGRAPHICAL SKETCH AND PHOTOGRAPH OF G. PAUL WILLHITE APPEAR ON PAGE 21 OF THE JAN., 1967, ISSUE OF JOURNAL OF PETROLEUM TECHNOLOGY.